

AD-A054 427

GEORGIA INST OF TECH ATLANTA ENGINEERING EXPERIMENT --ETC F/G 17/9
RADAR DETECTION, DISCRIMINATION, AND CLASSIFICATION OF BURIED N--ETC(U)
FEB 78 J D ECHARD, J A SCHEER, E O RAUSCH DAAG53-76-C-0112

UNCLASSIFIED

| OF 6
AD
A054427

EES/GIT-A-1828-F-VOL-1

NL



ADA 054427

FOR FURTHER TRANSMISSION

UNCLASSIFIED

12
B.S.

FINAL TECHNICAL REPORT
Volume I

RADAR DETECTION, DISCRIMINATION,
AND CLASSIFICATION OF BURIED NON-
METALLIC MINES (U)

By

J. D. Echard, J. A. Scheer, E. O. Rausch, W. H. Licata,
J. R. Moore and J. A. Nestor

Prepared for

U. S. ARMY MOBILITY EQUIPMENT RESEARCH
AND DEVELOPMENT COMMAND
FT. BELVOIR, VIRGINIA 22060

Under

CONTRACT DAAG53-76-C-0112



AD No. _____

DDC FILE COPY

February 1978

GEORGIA INSTITUTE OF TECHNOLOGY

Engineering Experiment Station
Atlanta, Georgia 30332



1978



DISTRIBUTION STATEMENT A

Approved for public release;
Distribution Unlimited

UNCLASSIFIED

74

EES/GIT-A-1828-F-VOL-1

12

UNCLASSIFIED

SECURITY CLASSIFICATION OF THIS PAGE (When Data Entered)

| REPORT DOCUMENTATION PAGE | | | READ INSTRUCTIONS BEFORE COMPLETING FORM |
|--|-------------------------------------|--|---|
| 1. REPORT NUMBER <i>(6)</i> | 2. GOVT ACCESSION NO. <i>(9)</i> | 3. RECIPIENT'S CATALOG NUMBER | |
| 4. TITLE (and Subtitle) Radar Detection, Discrimination, and Classification of Buried Non-metallic Mines, Volume 1. (Final Report) | | 5. TYPE OF REPORT & PERIOD COVERED Final technical rept. March 1976 - September 1977 | |
| 6. AUTHOR(s) J. D. Echard, J. A. Scheer, E. O. Rausch, W. H. Licata, J. R. Moore, and J. A. Nestor | | 7. PERFORMING ORG. REPORT NUMBER EES/GIT-A-1828 Final | |
| 8. CONTRACT OR GRANT NUMBER(s) DAAG53-76-C-0112 | | 9. PERFORMING ORGANIZATION NAME AND ADDRESS Engineering Experiment Station Georgia Institute of Technology Atlanta, Georgia 30332 | |
| 10. CONTROLLING OFFICE NAME AND ADDRESS U.S. Army Mobility Equipment Research and Development Command Ft. Belvoir, VA 22060 | | 11. PROGRAM ELEMENT, PROJECT, TASK AREA & WORK UNIT NUMBERS 12/532P | |
| 12. MONITORING AGENCY NAME & ADDRESS (if different from Controlling Office) <i>(15) DAAG53-76-C-0112</i> | | 13. REPORT DATE 11 Feb 1978 | |
| | | 14. NUMBER OF PAGES 512 + xxiv | |
| | | 15. SECURITY CLASS. (of this report) UNLIMITED | |
| | | 16. DECLASSIFICATION/DOWNGRADING SCHEDULE | |
| 17. DISTRIBUTION STATEMENT (of this Report) DISTRIBUTION STATEMENT A Approved for public release; Distribution Unlimited | | | |
| 18. SUPPLEMENTARY NOTES <i>D D D</i> <i>R E P R I N T</i> <i>MAY 26 1978</i> <i>A</i> | | | |
| 19. KEY WORDS (Continue on reverse side if necessary and identify by block number) Radar Classification Detection Mines Discrimination | | | |
| 20. ABSTRACT (Continue on reverse side if necessary and identify by block number) The U.S. Army Mobility Equipment Research and Development Command (MERADCOM) has been involved in a program for development of an off-road mine detection system. The Georgia Institute of Technology Engineering Experiment Station (GIT/EES) was tasked to gather and analyze wideband radar spectral data to determine detection and classification potential for buried objects of interest. In particular, the portion of the spectrum which is most useful in the detection, discrimination, and classification of buried targets was (continued) <i>next page</i> | | | |

UNCLASSIFIED

SECURITY CLASSIFICATION OF THIS PAGE(When Data Entered)

to be identified.

Two sets of data were taken. Wideband CW radar data were collected by personnel of the National Bureau of Standards (NBS) in Boulder, Colorado, using a computer-driven automatic network analyzer. Wideband pulse radar data were collected by the Georgia Institute of Technology Engineering Experiment Station using a Government Furnished Equipment (GFE) short-pulse radar owned by MERADCOM. The wideband target signatures obtained using the MERADCOM short-pulse radar were used to verify the utility of the processing algorithms which were developed from wideband CW radar data.

The measurement and analysis tasks were completed, but mixed success was achieved in finding exploitable target discriminants. The performance of each processing step--detection, discrimination, and classification--was acceptable for the specified scenario when the soil was relatively dry (i.e., zero to ten percent moisture content). However, when the soil was more moist than this (e.g., ten to thirty percent), the performance of the processor deteriorated noticeably.

| | | |
|---------------------------------------|----------------------|-------------------------------------|
| ACCESSION NO. | | |
| NTIS | White Section | <input checked="" type="checkbox"/> |
| NSC | Buff Section | <input type="checkbox"/> |
| UNANNOUNCED | | |
| JUSTIFICATION <i>Pitts on file</i> | | |
| BY..... | | |
| DISTRIBUTION/AVAILABILITY CODES | | |
| B&W | AVAIL AND OR SPECIAL | |
| A | | |

UNCLASSIFIED

**FINAL TECHNICAL REPORT
VOLUME I**

**Radar Detection, Discrimination, and
Classification of Buried Non-Metallic Mines (U)**

Prepared For:

**U.S. Army Mobility Equipment Research and
Development Command
Ft. Belvoir, Virginia 22060**

Under

Contract DAAG53-76-C-0112

By

**J. D. Echard, J. A. Scheer, E. O. Rausch, W. H.
Licata, J. R. Moore and J. A. Nestor**

February 1978

**Engineering Experiment Station
Georgia Institute of Technology
Atlanta, Georgia 30332**

UNCLASSIFIED

SUMMARY

The U.S. Army Mobility Equipment Research and Development Command (MERADCOM) has been involved in a program for development of an off-road mine detection system. The Georgia Institute of Technology Engineering Experiment Station (GIT/EES) was awarded a nine-month contract to gather and analyze wideband radar spectral data to determine detection and classification potential for buried objects of interest. In particular, the portion of the spectrum which is most useful in the detection, discrimination, and classification of buried targets was to be identified. Later, the contract was modified to include additional measurement and analysis tasks and to extend the effort to 18 months.

Two sets of data were taken. Wideband CW radar data were collected by personnel of the National Bureau of Standards (NBS) in Boulder, Colorado, using a computer-driven automatic network analyzer. For the initial measurements used in this program, a pair of broadband, non-dispersive antennas was mounted on a cart and pointed at the ground. Wideband pulse radar data were collected by the Georgia Institute of Technology Engineering Experiment Station using a Government Furnished Equipment (GFE) short-pulse radar owned by MERADCOM. The wideband target signatures obtained using the MERADCOM short-pulse radar were used to verify the utility of the processing algorithms which were developed from wideband CW radar data. The MERADCOM radar is mounted on a General Electric Electro-Trak tractor with a broadband, non-dispersive antenna which is adjustable in height. The tractor-mounted radar can be easily moved from one location to another to accommodate measurements.

UNCLASSIFIED

UNCLASSIFIED

The measurement and analysis tasks were completed, but mixed success was achieved in finding exploitable target discriminants. The performance of each processing step--detection, discrimination, and classification--was acceptable for the specified scenario when the soil was relatively dry (i.e., zero to ten percent moisture content). However, when the soil was more moist than this (e.g., ten to thirty percent), the performance of the processor deteriorated noticeably.

The processing time required with a modest amount of processing equipment was determined to be about 40 milliseconds for each mine which was correctly detected, discriminated, and classified.

It is suggested that only the spectrum from 0.5 to 1.5 GHz needs to be used to adequately detect, discriminate, and classify anti-vehicular, non-metallic mines in relatively dry soil. Thus, an antenna smaller and lighter than the ones specified with the MERADCOM tractor-mounted radar can be utilized providing a more portable mine detection system.

UNCLASSIFIED

UNCLASSIFIED

PREFACE

The research on this program was conducted by the Radar Analysis Division, Radar and Instrumentation Laboratory, Engineering Experiment Station, Georgia Institute of Technology, Atlanta, Georgia, with Mr. James A. Scheer serving as Project Director, and Dr. J. D. Echard serving as Associate Project Director.

This report was prepared by the Engineering Experiment Station at the Georgia Institute of Technology for the U.S. Army Mobility Equipment Research and Development Command under Contract DAAG53-76-C-0112. The Technical Monitor was Mr. L. Mittelman, Jr. For the purposes of internal control at Georgia Tech, the effort was designated project A-1828. The measurements reported herein were conducted by Mr. G. Counas under the direction of Mr. F. Clague of the U.S. Department of Commerce, National Bureau of Standards.

The final report summarizes the work performed under this contract and gives recommendations for a follow-on program. It is divided into two volumes. Most of the work is presented in Volume I; Volume II contains a brief description of the inert mines used in the data collection phase and identifies the type A, B, and C mines referred to in Volume I. This report covers work which was performed from March 1976 through September 1977. In addition to this final report, an interim report was issued in December 1976 entitled "Spectral Characteristics of Buried Objects."

The authors are grateful to Messrs. Clague and Counas of the National Bureau of Standards for their care and perseverance in conducting the measurements, often under difficult conditions, and to Mr. Clague for supplying the photographs reproduced herein.

UNCLASSIFIED

UNCLASSIFIED

The guidance of Mr. J. L. Eaves and Dr. E. K. Reedy, Associate Director and Director, respectively, of the Radar and Instrumentation Laboratory is appreciated. We also appreciate the assistance of Mr. M. C. McGee in proofreading these two volumes and suggesting improvements to the presentation of this material. Our final appreciation goes to the Radar Analysis Division secretary, Mrs. S. A. Busby, who typed this report.

UNCLASSIFIED

UNCLASSIFIED

TABLE OF CONTENTS

| <u>Section</u> | | <u>Page</u> |
|----------------|--|-------------|
| I. | INTRODUCTION | 1 |
| II. | DATA COLLECTION | 5 |
| | - NBS MEASUREMENTS | 6 |
| | - Measurement System | 6 |
| | - Measurement Sites | 8 |
| | - Preliminary Data Measurements | 15 |
| | - Selection of the Test Matrix | 17 |
| | - Typical Data | 19 |
| | - SHORT-PULSE RADAR MEASUREMENTS | 33 |
| | - Measurement System | 36 |
| | - Selection of Test Matrix | 36 |
| | - Typical Data | 37 |
| III. | DATA REDUCTION | 45 |
| | - NBS DATA | 48 |
| | - Computer Program Development | 48 |
| | - Filter Selection | 54 |
| | - Range Gate Algorithm Development | 55 |
| | - Removal of Ground Return from Processed Data . . . | 63 |
| | - SHORT-PULSE RADAR DATA | 72 |
| | - Design and Construction of the Event Recorder . . | 75 |
| | - Generating Computer Compatible Data Tapes | 77 |
| | - Computer Processing Development | 78 |

UNCLASSIFIED

UNCLASSIFIED

TABLE OF CONTENTS
(continued)

| <u>Section</u> | | <u>Page</u> |
|----------------|---|-------------|
| IV. | MATHEMATICAL MODEL OF BURIED TARGET AND ENVIRONMENT | 81 |
| | - DEVELOPMENT OF MATHEMATICAL MODEL. | 81 |
| | - EFFECT OF WET SOIL ON TARGET RETURNS | 88 |
| | - APPLICATION TO NBS MEASUREMENTS. | 91 |
| | - APPLICATION TO SHORT-PULSE RADAR MEASUREMENTS. | 100 |
| | - COMPARISON OF PROCESSED NBS DATA AND MATHEMATICAL MODEL. | 104 |
| V. | SELECTION AND DEVELOPMENT OF DISCRIMINATION/CLASSIFICATION ALGORITHMS | 117 |
| | - CFAR ANALYSIS. | 123 |
| | - PATTERN RECOGNITION. | 139 |
| | - Data Selection | 141 |
| | - Feature Extraction | 142 |
| | - Classifier Selection | 145 |
| | - CORRELATION PROCESSING | 156 |
| VI. | DISCRIMINATION/CLASSIFICATION PERFORMANCE AND COMPARISON | 181 |
| | - PERFORMANCE CURVES | 181 |
| | - NBS DATA | 187 |
| | - Signal Attenuation and Signature Gating. | 187 |
| | - Shape of Scatterer and Radar Pulse Width | 189 |
| | - Learning Set Size. | 198 |

UNCLASSIFIED

UNCLASSIFIED

TABLE OF CONTENTS
(continued)

| <u>Section</u> | | <u>Page</u> |
|----------------|--|-------------|
| VI. | DISCRIMINATION/CLASSIFICATION PERFORMANCE AND COMPARISON (continued) | |
| | - Influence of Feature Size on Classification | 203 |
| | - Classifier Performance | 203 |
| | - SHORT-PULSE RADAR DATA. | 230 |
| VII. | HARDWARE REQUIREMENTS | 245 |
| | - SIGNAL PROCESSING ALGORITHM | 246 |
| | - SIGNAL PROCESSING EQUIPMENT | 251 |
| | - Systems Configuration | 252 |
| | - Minicomputer. | 255 |
| | - Preprocessors | 256 |
| | - High Speed Processing Equipment | 257 |
| | - Processing Requirements | 257 |
| | - Detection Processing. | 258 |
| | - Discrimination Processing | 260 |
| | - Classification Processing | 260 |
| | - Total Processing Requirements | 262 |
| | - Alternate Hardware Configurations | 262 |
| | - Signal Processing | 263 |
| VIII. | CONCLUSIONS AND RECOMMENDATIONS | 265 |
| | - RECOMMENDATIONS | 270 |

UNCLASSIFIED

UNCLASSIFIED

TABLE OF CONTENTS
(continued)

| <u>Section</u> | <u>Page</u> |
|---|-------------|
| REFERENCES | 273 |
| APPENDIX A. NBS DATA SPECTRAL AND TEMPORAL PLOTS | A-1 |
| APPENDIX B. SHORT-PULSE RADAR DATA SPECTRAL AND TEMPORAL PLOTS | B-1 |
| APPENDIX C. NBS AND SHORT-PULSE RADAR DISCRIMINATION/CLASSIFICATION CURVES | C-1 |
| APPENDIX D. HOMOMORPHIC DECONVOLUTION ANALYSIS | D-1 |

UNCLASSIFIED

UNCLASSIFIED

LIST OF ILLUSTRATIONS

| <u>Figure</u> | | <u>Page</u> |
|---------------|--|-------------|
| 1 | Two-port network | 7 |
| 2 | Test lane layout | 10 |
| 3 | Test site at NBS laboratories in Boulder | 12 |
| 4 | Test site at Gun Barrel Hill, about 15 miles from the NBS site in Boulder | 12 |
| 5 | NBS test site prepared for flooding | 13 |
| 6 | NBS site during flooding | 13 |
| 7 | Gun Barrel Hill test site just before being flooded . | 14 |
| 8 | Gun Barrel Hill site being flooded | 14 |
| 9 | Normalized weighting function, $I_1(x)/x$ | 21 |
| 10 | Measured characteristics for a type A mine at 3-inch depth | 23 |
| 11 | Measured characteristics for a metal plate at 6-inch depth | 24 |
| 12 | Measured characteristics for a rock at 3-inch depth . | 25 |
| 13 | Time response of metal plate at 6-inch depth in damp soil. | 26 |
| 14 | Time response of type A mine at 6-inch depth in dry soil. | 27 |
| 15 | Deconvolved spectrum of a metal plate | 28 |
| 16 | Deconvolved spectrum of a type A mine | 29 |
| 17 | Time domain response of shallow target in dry soil. . | 31 |
| 18 | Deconvolved spectrum of shallow target in dry soil. . | 32 |
| 19 | Vehicular-mounted mine detector radar (left-side view) | 34 |

UNCLASSIFIED

UNCLASSIFIED

LIST OF ILLUSTRATIONS
(continued)

| <u>Figure</u> | | <u>Page</u> |
|---------------|---|-------------|
| 20 | Vehicular-mounted mine detector radar (right-side view) | 35 |
| 21 | MERADCOM short-pulse radar returns from a metal plate buried 6" below ground surface in dry clay soil | 38 |
| 22 | MERADCOM short-pulse radar return from a type A non-metallic mine buried 6" below ground surface in dry clay soil | 39 |
| 23 | MERADCOM short-pulse radar returns from a type C non-metallic mine buried 6" below ground surface in dry clay soil | 40 |
| 24 | Calculated spectral response for one period of sine waveform | 42 |
| 25 | Processing of NBS data to provide temporal and spectral plots. | 46 |
| 26 | Processing of short-pulse radar data to provide temporal and spectral plots. | 47 |
| 27 | Typical temporal return from a buried land mine | 56 |
| 28 | Non-adaptive threshold algorithm. | 59 |
| 29 | Smoothed data array y | 62 |
| 30 | Time response of metal plate buried 6" below ground, 7% moisture: (a) with ground return present; (b) with ground return subtracted (GT5-65 subtracted from GT5-68) | 65 |
| 31 | Time response of type A mine buried 6" below ground, 7% moisture: (a) with ground return present; (b) with ground return subtracted (GT5-53 subtracted from GT5-56) | 66 |
| 32 | Sampling position relative to the ground return analog envelope. (a) Sampling on peak value; (b) Sampling off peak value. | 68 |

UNCLASSIFIED

UNCLASSIFIED

LIST OF ILLUSTRATIONS
(continued)

| <u>Figure</u> | | <u>Page</u> |
|---------------|--|-------------|
| 33 | Measured data. Time response of type A mine buried 6" below ground, 7% moisture--with ground return subtracted--GT5-71 subtracted from GT5-74. | 70 |
| 34 | Measured data. Time response of type A mine buried 6" below ground, 7% moisture--GT5-74. Also time response of adjacent ground without target--GT5-71. | 71 |
| 35 | Measured data. Time responses of ground without target--GT5-71 and GT5-77 (ground areas adjacent to type C mine). | 73 |
| 36 | Block diagram of event recorder | 76 |
| 37 | Byte packing on computer tape | 77 |
| 38 | Target and environment model. | 82 |
| 39 | The dielectric constant and loss tangent of water at a frequency of 3,000 mc | 87 |
| 40 | Attenuation versus depth for a metal plate target in moderately wet soil ($K = 0.5$, $\epsilon_r = 6.5$) | 93 |
| 41 | Math model of radar return from metal plate buried in a lossless medium | 94 |
| 42 | Math model of radar return from a metal plate buried 6" in a lossy medium ($K = 0.5$) | 95 |
| 43 | Math model of radar return from metal plate buried 6" in lossy soil (loss equal to that of pure water at $20^\circ C$, $K = 1.0$) | 96 |
| 44 | Math model of radar return from non-metallic mine type A buried 6" in lossless medium | 97 |
| 45 | Math model of radar return from non-metallic mine type A buried 6" in a lossy medium ($K = 0.5$) | 98 |
| 46 | Math model of radar return from non-metallic mine type A buried 6" in a lossy medium (loss equal to that of pure water at $20^\circ C$, $K = 1.0$) | 99 |

UNCLASSIFIED

UNCLASSIFIED

LIST OF ILLUSTRATIONS
(continued)

| <u>Figure</u> | | <u>Page</u> |
|---------------|---|-------------|
| 47 | Math model of radar return from non-metallic mine type C buried 6" in lossless medium. | 101 |
| 48 | Math model of radar return from non-metallic mine type C buried 6" in a lossy medium ($K = 0.5$) | 102 |
| 49 | Math model of radar return from non-metallic mine type C buried 6" in a lossy medium (loss equal to that of pure water at $20^\circ C$, $K = 1.0$). | 103 |
| 50 | Measured data--metal plate 6" below ground, 7% moisture--GT5-68 | 106 |
| 51 | Behavior of EM waves at a Boundary | 109 |
| 52 | Metal plate buried in soil | 109 |
| 53 | Non-metallic mine buried in soil | 109 |
| 54 | Metal plate, 6" depth, 7% moisture, with time distortion removed | 110 |
| 55 | Type A mine, 6" depth, 7% moisture with time distortion | 111 |
| 56 | Type A mine, 6" depth, 7% moisture, with time distortion removed | 112 |
| 57 | Type C mine, 6" depth, 7% moisture, with time distortion | 113 |
| 58 | Type C mine, 6" depth, 7% moisture, with time distortion removed | 114 |
| 59 | Three-step mine detection/classification processor . | 118 |
| 60 | Histograms of temporal data subjected to an adaptive threshold (CFAR). Sidelobes of temporal waveform are 40 dB. | 125 |
| 61 | Potential target detection - CFAR. | 126 |
| 62 | Potential target detection - CFAR. | 127 |
| 63 | Potential target detection - CFAR. | 129 |

UNCLASSIFIED

UNCLASSIFIED

**LIST OF ILLUSTRATIONS
(continued)**

| <u>Figure</u> | | <u>Page</u> |
|---------------|---|-------------|
| 64 | Potential target detection - CFAR. | 130 |
| 65 | Histograms of time data subjected to fixed threshold . | 131 |
| 66 | Potential target detection - unnormalized. | 133 |
| 67 | Potential target detection - unnormalized. | 134 |
| 68 | Potential target detection - unnormalized. | 135 |
| 69 | Potential target detection - unnormalized. | 136 |
| 70 | Histograms of time data subjected to an adaptive threshold (CFAR). Sidelobes of temporal waveform is 60 dB. | 137 |
| 71 | Histograms of time data subjected to a fixed threshold (CFAR). Sidelobes of temporal waveform is 60 dB . . . | 138 |
| 72 | Classification data processing system. | 140 |
| 73 | Frequency domain signature ensemble. | 144 |
| 74 | Fisher's Linear Discriminant classifier. | 148 |
| 75 | Normalized density distributions projected onto the \vec{w} vector | 148 |
| 76 | Space partition classifier | 152 |
| 77 | Cross-correlation processor. | 157 |
| 78 | Mathematically derived mine signature and auto-correlation function | 160 |
| 79 | Cross-correlation of ideal mine signature with measured data from a type A mine. | 161 |
| 80 | Cross-correlation of ideal mine signature with measured data from a metal plate. | 162 |
| 81 | Cross-correlation classifier | 165 |
| 82 | Cross-correlation classifier | 166 |

UNCLASSIFIED

UNCLASSIFIED

**LIST OF ILLUSTRATIONS
(continued)**

| <u>Figure</u> | | <u>Page</u> |
|---------------|--|-------------|
| 83 | Cross-correlation classifier. | 167 |
| 84 | Cross-correlation classifier. | 168 |
| 85 | Cross-correlation classifier. | 169 |
| 86 | Cross-correlation classifier. | 170 |
| 87 | Impulse-correlation circuit | 173 |
| 88 | Impulse response of impulse-correlation circuit . . . | 173 |
| 89 | Impulse-correlation classifier. | 175 |
| 90 | Impulse-correlation classifier. | 176 |
| 91 | Impulse-correlation classifier. | 177 |
| 92 | Impulse-correlation classifier. | 178 |
| 93 | Impulse-correlation classifier. | 179 |
| 94 | Impulse-correlation classifier. | 180 |
| 95 | Probability density functions for separated classes . | 182 |
| 96 | Probability plot for separated classes. | 182 |
| 97 | Probability density functions for completely overlapping classes | 182 |
| 98 | Probability plot for completely overlapping classes . | 182 |
| 99 | Probability density functions for partially overlapping classes | 182 |
| 100 | Probability plot for partially overlapping classes. . | 182 |
| 101 | Probability density functions for separated classes . | 185 |
| 102 | Probability plot for separated classes. | 185 |
| 103 | Probability density functions for completely overlapping classes | 185 |

UNCLASSIFIED

UNCLASSIFIED

**LIST OF ILLUSTRATIONS
(continued)**

| <u>Figure</u> | | <u>Page</u> |
|---------------|---|-------------|
| 104 | Probability plot for completely overlapping classes | 185 |
| 105 | Probability density functions for partially overlapping classes | 185 |
| 106 | Probability plot for partially overlapping classes | 185 |
| 107 | Nearest neighbor classifier. | 192 |
| 108 | Nearest neighbor classifier. | 193 |
| 109 | Nearest neighbor classifier. | 194 |
| 110 | Nearest neighbor classifier. | 195 |
| 111 | Nearest neighbor classifier. | 196 |
| 112 | Nearest neighbor classifier. | 197 |
| 113 | Nearest neighbor classifier. | 199 |
| 114 | Nearest neighbor classifier. | 200 |
| 115 | FLD/Bayes classifier | 201 |
| 116 | Nearest neighbor classifier. | 204 |
| 117 | Nearest neighbor classifier. | 205 |
| 118 | Nearest neighbor classifier. | 206 |
| 119 | Nearest neighbor classifier. | 207 |
| 120 | Nearest neighbor classifier. | 208 |
| 121 | Nearest neighbor classifier. | 209 |
| 122 | Nearest neighbor classifier. | 210 |
| 123 | Nearest neighbor classifier. | 211 |
| 124 | Nearest neighbor classifier. | 212 |
| 125 | Nearest neighbor classifier. | 213 |

UNCLASSIFIED

UNCLASSIFIED

LIST OF ILLUSTRATIONS
(continued)

| <u>Figure</u> | | <u>Page</u> |
|---------------|--|-------------|
| 126 | Nearest neighbor classifier. | 214 |
| 127 | Nearest neighbor classifier. | 215 |
| 128 | Nearest neighbor classifier. | 216 |
| 129 | Nearest neighbor classifier. | 217 |
| 130 | Nearest neighbor classifier. | 218 |
| 131 | Nearest neighbor classifier. | 219 |
| 132 | FLD/Bayes classifier | 221 |
| 133 | Nearest neighbor classifier. | 222 |
| 134 | Space partition classifier | 223 |
| 135 | Nearest neighbor classifier. | 224 |
| 136 | Nearest neighbor classifier. | 225 |
| 137 | Nearest neighbor classifier. | 226 |
| 138 | Nearest neighbor classifier. | 227 |
| 139 | Nearest neighbor classifier. | 228 |
| 140 | Nearest neighbor classifier. | 229 |
| 141 | Spectral and temporal responses of type A mines buried in dry soil (7% moisture in loam) from NBS measurements. Files 54, 55, and 56 represent positions -4, 0, and +4 over buried mine | 233 |
| 142 | Spectral and temporal responses of type A mines buried in dry soil from short-pulse radar measurements. Files 43, 44, and 45 represent measurement positions -4, 0, and +4 inches over buried mine | 234 |
| 143 | Spectral and temporal responses of type C mines buried in dry soil (7% moisture in loam) from NBS measurements. Files 62, 63, and 64 represent measurement positions -4, 0, and +4 inches over buried mine. | 235 |

UNCLASSIFIED

UNCLASSIFIED

**LIST OF ILLUSTRATIONS
(continued)**

| <u>Figure</u> | | <u>Page</u> |
|---------------|--|-------------|
| 144 | Spectral and temporal responses of type C mines buried in dry soil from short-pulse radar measurements. Files 46, 47, and 48 represent measurement positions -4, 0, and +4 inches over buried mine. | 236 |
| 145 | Nearest neighbor classifier. | 238 |
| 146 | Nearest neighbor classifier. | 239 |
| 147 | Nearest neighbor classifier. | 241 |
| 148 | Nearest neighbor classifier. | 242 |
| 149 | Nearest neighbor classifier. | 243 |
| 150 | Nearest neighbor classifier. | 244 |
| 151 | Flow diagram of signal processing algorithm. | 247 |
| 152 | Signal processing hardware | 253 |

UNCLASSIFIED

UNCLASSIFIED

LIST OF TABLES

| <u>Table</u> | | <u>Page</u> |
|--------------|---|-------------|
| 1 | MEASUREMENT MATRIX. | 19 |
| 2 | ACTUAL DATA MATRIX. | 19 |
| 3 | SHORT-PULSE MEASUREMENTS. | 37 |
| 4 | DOLPH-TCHEBYCHEV CONSTANTS. | 55 |
| 5 | DIELECTRIC CONSTANT OF VARIOUS TYPES OF SOIL. | 86 |
| 6 | NBS DATA PERFORMANCE MATRIX | 188 |
| 7 | SHORT-PULSE RADAR DATA PERFORMANCE MATRIX | 231 |
| 8 | MINE DETECTION SYSTEM REQUIREMENTS. | 245 |
| 9 | 1602 EXECUTION TIMES. | 255 |
| 10 | CFAR PROCESSING | 259 |
| 11 | GATE SETTING PROCESSING | 260 |
| 12 | DISCRIMINATION PROCESSING | 261 |
| 13 | CLASSIFICATION PROCESSING | 261 |
| 14 | SYSTEM CHARACTERISTICS. | 263 |

UNCLASSIFIED

Preceding Page BLANK - ^{NOT} FILMED

UNCLASSIFIED

SECTION I

INTRODUCTION

The U.S. Army Mobility Equipment Research and Development Command (MERADCOM) has been involved in a program for development of an off-road mine detection system. In March of 1976, the Georgia Institute of Technology Engineering Experiment Station (GIT/EES) began a nine-month contract to gather and analyze wideband radar spectral data to determine detection and classification potential for buried objects of interest. In particular, the portion of the spectrum which is most useful in the detection, discrimination, and classification of buried targets was to be identified. In January of 1977, the contract was modified to include additional measurement and analysis tasks and to extend the effort to 18 months. The measurement and analysis tasks were completed, but mixed success was achieved in finding exploitable target discriminants. This final report describes the work accomplished under contract DAAG53-76-C-0112.

Two sets of data were taken. The wideband radar data were collected personnel of the National Bureau of Standards (NBS) in Boulder, Colorado, using a computer-driven automatic network analyzer. The equipment is housed in a mobile van and can therefore be driven to any site accessible by vehicle; a trailer-mounted generator set augments this mobility. This equipment includes a rubber-tired cart which can be commanded by the computer to advance to any of a set of predetermined positions and to then remain stationary while the data are collected. For the initial measurements used in this program, a

UNCLASSIFIED

UNCLASSIFIED

pair of broadband, non-dispersive antennas was mounted on the cart and pointed at the ground.

Wideband pulse radar data were collected by the GIT/EES using a Government Furnished Equipment (GFE) short-pulse radar owned by MERADCOM. The wideband target signatures obtained using the MERADCOM short-pulse radar were used to verify the utility of the processing algorithms which were developed from wideband CW radar data. The MERADCOM radar is mounted on a General Electric Electro-Trak tractor with a broadband, non-dispersive antenna which is adjustable in height. The tractor-mounted radar can be easily moved from one location to another to accommodate measurements.

GIT/EES personnel analyzed the data to identify distinguishing characteristics in the temporal and spectral signatures of the targets. These distinguishing characteristics were exploited to develop detection, discrimination, and classification algorithms. The Fast Fourier Transform was used for transforming the data into the time domain or the frequency domain, as required. The analysis also included direct comparison of measured spectral and temporal data with data derived using a mathematical model.

Techniques for detecting the presence of potential targets buried in soil of various types and moistures were investigated. Discrimination algorithms to differentiate between mines and non-mine objects were employed and evaluated. In addition, classification techniques were used to distinguish the various types of mines. Each of these processes were evaluated, and performance curves were generated and are included in this report with accompanying discussions.

UNCLASSIFIED

UNCLASSIFIED

The final report summarizes the work performed under this contract and gives recommendations for a follow-on program. It is divided into two volumes. Most of the work is presented in Volume I; Volume II contains a brief description of the mines used in the data collection phase and identifies the type A, B, and C mines referred to in Volume I.

Section II of Volume I details the data collection effort with both the NBS measuring equipment and the MERADCOM short-pulse radar. The objects used in the measurement program were two types of inert non-metallic mines, a root, two rocks, and a flat metal plate, all buried in various types of soil with various degrees of moisture content.

Since one of the objectives for the mine detection program was to develop algorithms to automatically process real-time data, it was necessary to visually observe and compare the temporal and spectral responses for the various objects sensed with the measurement system. The data were processed off-line with Georgia Tech's CYBER 74 computer to provide plots of time and frequency responses. The processing equipment required for this purpose is discussed in Section III.

When the measured data were processed and examined, it was noted that radar returns from the same target at the same depth varied with soil moisture. Since consistency in target return signatures seemed lacking in the measured data, a generalized mathematical model was developed for the metal plate and the type A, B, and C targets buried in soil. This model provided an understanding of the target and the environment. The mathematical model was programmed on a general purpose computer to yield plots of the temporal and spectral characteristics of radar returns from various types of targets.

UNCLASSIFIED

UNCLASSIFIED

Parameters such as target depth and soil moisture were varied, and changes in target return characteristics were observed and compared. A discussion of the mathematical model and its describing equations are presented in Section IV.

Section V discusses the selection and development of the discrimination/classification algorithms. Section VI presents the algorithms' performance and compares the various techniques that were considered. The real-time hardware requirements for the recommended discrimination/classification techniques are discussed in Section VII. Finally, the conclusions and recommendations are given in Section VIII.

Three appendices present plots of the collected data and plots of the performance for each processing algorithm considered. A brief effort was expended on the homomorphic deconvolution approach and this is reported in Appendix D.

UNCLASSIFIED

UNCLASSIFIED

SECTION II
DATA COLLECTION

In the following paragraphs, the two measurement systems used in obtaining the radar data are briefly described, along with some of the measurements. The objects used in the measurement program were two types of inert non-metallic mines, a root, two rocks, and a flat metal plate, all buried in various types of soil with various degrees of moisture content.

The first task of the subsurface target data collection effort was to decide what and how many measurements were to be made. The decision was influenced in part by the equipment available, the nature of the obstacles of interest, and the range of soil characteristics desired; the amount of time and funds that were available for the task also influenced the decision.

Two types of GFE measuring equipment were made available. Initially, a Hewlett-Packard computer-controlled automatic network analyzer, installed in a 19-foot step van and assembled in the S-parameter configuration, was used to obtain reflectivity measurements from various types of objects buried in soil of various textures. This equipment was owned by the U.S. Army and operated by the National Bureau of Standards in Boulder, Colorado. Later the Army furnished to Georgia Tech a short-pulse radar (1.2 nanosecond pulse length) originally developed by the CALSPAN Corporation. It was used as a tool to obtain wideband target signatures for use in verifying the utility of the processing algorithms which have been developed with the network analyzer measurements. Each of these equipments will be described in more detail in the following paragraphs. In addition, typical data

UNCLASSIFIED

UNCLASSIFIED

taken from the two measurement systems will be presented.

NBS MEASUREMENTS

The NBS-operated equipment used in collecting the data will first be discussed and the measurement sites described. The selection of the test matrix and some of the data parameters will then be explained. This will be followed by a discussion of some of the salient features found in the NBS data.

Measurement System

The measurement equipment consists of a government-furnished Hewlett-Packard computer-controlled automatic network analyzer installed in a 19-foot step van for mobility. Only its salient features will be discussed. The equipment and operation thereof will be described in more detail in a manual currently being prepared by NBS personnel. [1] The data were collected by means of an automatic network analyzer whose basic function is to measure the scattering (S) parameter matrix of a two-port network (or device) at a sequence of discrete frequencies. The S-matrix is a set of four complex numbers that describe the network behavior, representing the reflection and coupling coefficients relating incident and reflected waves. [2]

Specifically, we may represent incident voltage or electric field waves injected into the two ports by a_1 and a_2 , as shown in Figure 1, and waves emerging from these ports by b_1 and b_2 . a_1 and a_2 are considered independent quantities applied externally (and simultaneously, if necessary) while b_1 and b_2 represent the resulting response. The response involves the S-parameters via the network equations

$$b_1 = S_{11} a_1 + S_{12} a_2 \quad (1)$$

$$b_2 = S_{21} a_1 + S_{22} a_2 \quad (2)$$

UNCLASSIFIED

UNCLASSIFIED

where S_{11} and S_{22} are the reflection coefficients associated with ports 1 and 2, while S_{12} and S_{21} are port-to-port transmission coefficients. In general, it requires four measurements to determine the four coefficients, but for linear, passive devices $S_{21} = S_{12}$, and only three measurements are needed. In the measurements program, identical antennas were used; hence, it was assumed that S_{22} was essentially the same as S_{11} , and only two complex quantities measured were, S_{11} and S_{21} . All four parameters can be determined by measuring b_1 and b_2 with either a_1 or a_2 set to zero.

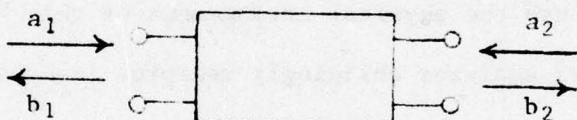


Figure 1. Two-port network.

The S-parameters are functions of frequency and the automatic network analyzer can be indexed through discrete frequencies from about 100 MHz through 4 GHz. A minicomputer with 16,000 words of memory is used to control the frequency stepping, as well as to position the antenna cart along a fixed path and to record the measured information on tape. In its factory-delivered configuration, the automatic network analyzer was restricted to a capacity of 53 frequencies due to software stored in core, but NBS personnel

UNCLASSIFIED

UNCLASSIFIED

were later able to expand this to a total of 128 frequencies. As will be discussed later, the number of frequencies must be an integral power of 2 in order to exploit the features of the Fast Fourier Transform (FFT).

The device connected to the automatic network analyzer consisted of a pair of non-dispersive, broadband antennas aimed at the ground. The input connector of one antenna became port #1 and that of the other antenna became port #2. Since the electromagnetic fields are not confined within a closed system, the environment surrounding the antennas, including antenna coupling, cable coupling, the ground, and any nearby buried obstacles, becomes an integral part of the "two-port device." The network analyzer does not know this, of course, and although the physical arrangement of this "network" is complicated, the network analyzer obligingly measures its characteristics.

The antennas were connected to the equipment inside the van by a pair of coaxial cables, each about 50 feet long and supported by a boom mounted on the van. The system had to be periodically calibrated (every half hour or so, perhaps longer under good conditions) by the substitution of standard devices for the device to be measured. These must be connected at the far end of the cables and take the form of precision short circuits, matched loads, feed-throughs and the like. The cables themselves change characteristics with changing temperature and NBS personnel have found that wrapping them with metal foil reduces their sensitivity to wind and sunlight.

Measurement Sites

The measurements were conducted on 35-foot test lanes prepared at two different sites in and near Boulder, Colorado. Three soil types were

UNCLASSIFIED

UNCLASSIFIED

represented and, with appropriate test lane flooding, at least three levels of moisture content were achieved. The first site was on U.S. Department of Commerce property in the city of Boulder and the second was on Gun Barrel Hill, located some 15 miles east and north of Boulder.

The NBS site contained two types of soil, one being a sandy loam trucked in from off the site several years ago to build up a thick layer-- perhaps 4 feet-- of homogeneous soil. The sandy loam constituted the first 20 feet of the test lane. The remaining 15 feet contained soil of essentially the same texture but interspersed with rocks and pebbles whose exact sizes and distributions are not known with certainty. Near the surface, these rocks were a few centimeters in diameter.

The soil at the Gun Barrel Hill site was a class of bentonite interspersed with small pebbles and rocks. The site had been leased by the Department of Commerce from a local farmer who had been raising crops on the land. One corner of a field had been cleared of vegetation for an unrelated experiment and NBS personnel laid out the test lane on a small section of this corner.

The same test lane layout was used at both sites. As shown in the diagram of Figure 2, seven targets consisting of both natural and man-made objects were buried 60 inches apart along a straight line. Preliminary background runs were conducted to collect reference data at closely spaced stations along two separate five-foot stretches of the test lanes before the targets were buried. After the measurement program got underway, the cart, provided with electric stepping motors controlled by the minicomputer

UNCLASSIFIED

UNCLASSIFIED

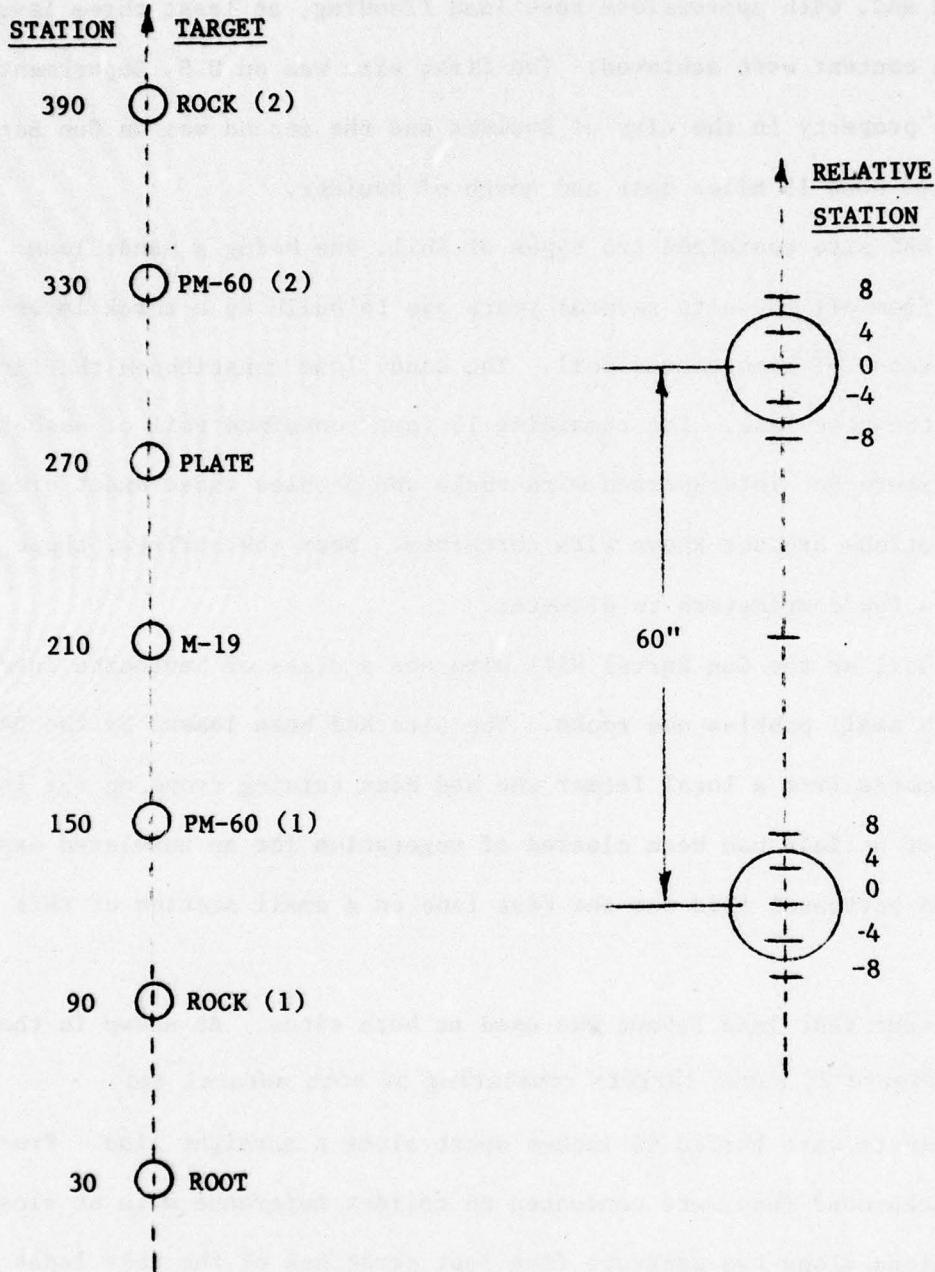


Figure 2. Test lane layout.

UNCLASSIFIED

UNCLASSIFIED

in the system, was commanded to stop at given positions over or near each target. These positions were -8, -4, 0, 4, and 8 inches from the target, and a sixth position midway between targets (i.e., 30 inches) was included for the purpose of acquiring "background" data. At each position, the frequency was indexed through 123 discrete values at which the S-parameters were measured and recorded automatically on magnetic tape. A boardwalk was laid out and leveled alongside the test lane to provide a smooth runway for the antenna cart. The cart was guided along its path by an aluminum rail pinned to the ground on one side of the boardwalk. The test target positions were carefully located by strings stretched along and across the target center-line track. These and other details of the test lanes can be seen in the photographs of Figures 3 through 8.

The moisture content of the soil was usually, but not always, determined by two different means. The most convenient method utilized a water-carbide reaction inside a sealed pressure vessel. Known amounts of soil and the carbide reagent are deposited in the container but not allowed to contact each other until the vessel has been sealed. Then the two are mixed by external agitation and the resulting chemical reaction produces acetylene, generating heat and a rise in internal pressure. A pressure gauge calibrated in per cent moisture content converts the pressure reading to moisture content. The "bomb" technique is within a percentage point in accuracy, it is claimed, and oven-drying techniques tend to support this claim, at least for soils with modest surface area to volume ratios. The oven method relies on a comparison of sample weight before and after several hours of baking

UNCLASSIFIED

UNCLASSIFIED

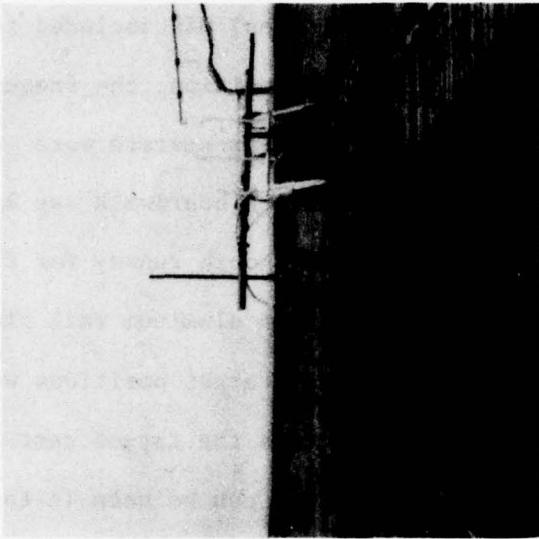


Figure 3. Test site at NBS laboratories in Boulder. Photo was taken during background runs before target burial. Aluminum guide rail can be seen at extreme right just off the edge of the boardwalk. Shed in background shelters an indoor test lane.

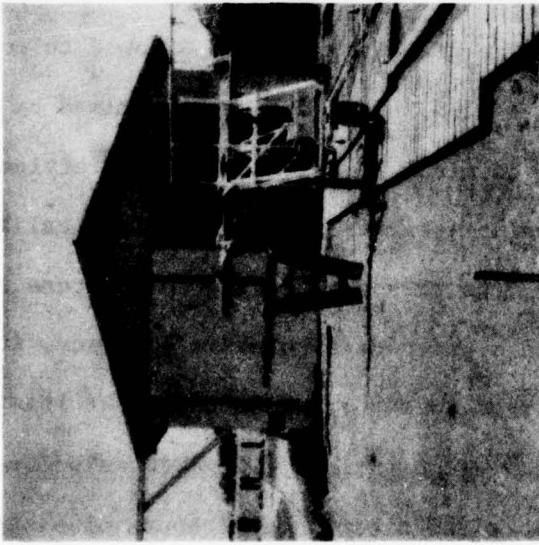


Figure 4. Test site at Gun Barrel Hill, about 15 miles from the NBS site in Boulder. Note strings tied across the test bed to mark target locations. Cables leading off to the right are connected to test gear housed inside a mobile van. The cart is propelled by stepping motors controlled by a minicomputer.

UNCLASSIFIED

UNCLASSIFIED

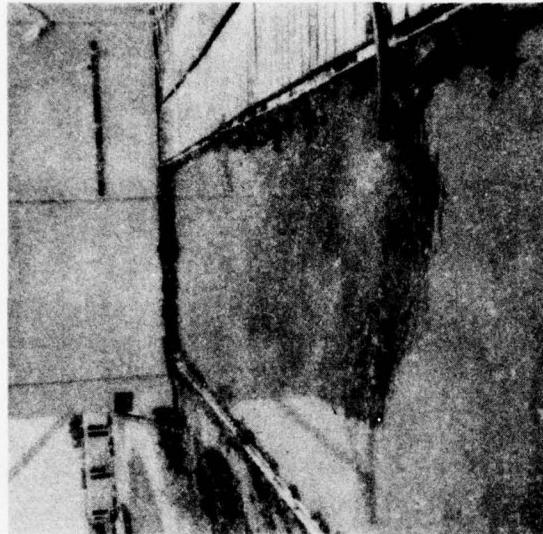
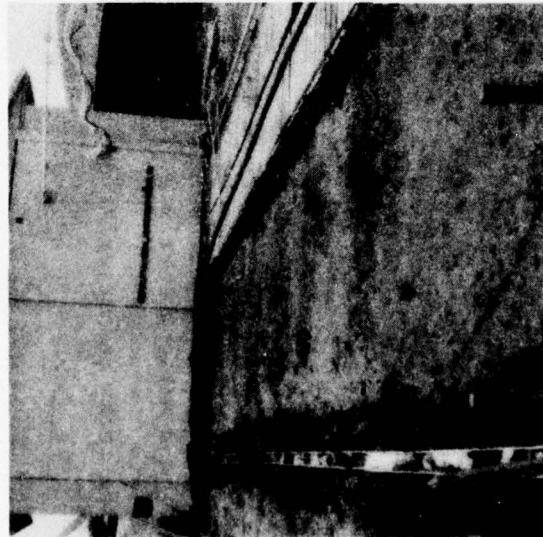


Figure 6. NBS site during flooding.
Figure 5. NBS test site prepared for flooding. It required an estimated 2500 to 3000 gallons of water to bring the moisture content up to about 17%.



UNCLASSIFIED

UNCLASSIFIED

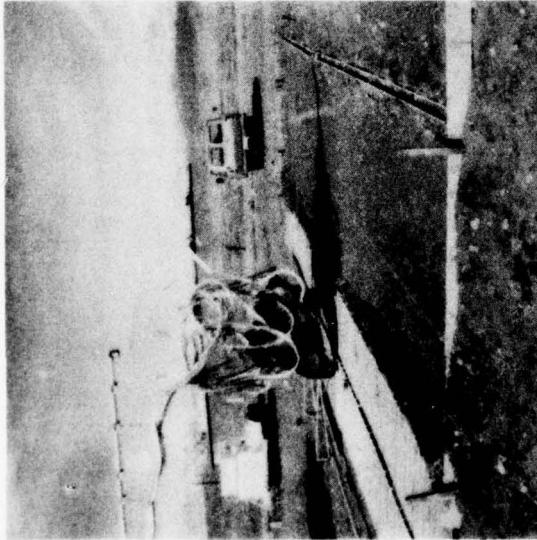
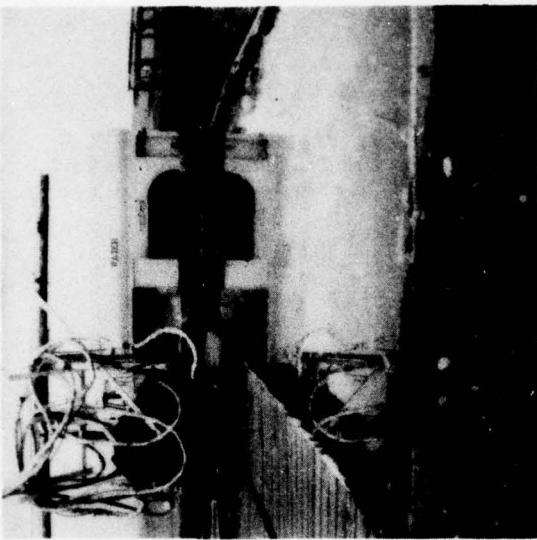


Figure 7. Gun Barrel Hill test site just before being flooded. Aluminum guide rail parallels the boardwalk at extreme left. The excess cable draped about the antenna cart was dressed prior to measurements. Note the size of the rocks characteristic of the site.

Figure 8. Gun Barrel Hill site being flooded. The soil here was relatively impermeable, hence the moisture content 12" below grade and deeper could not be raised above 25%. Nearer the surface it rose to as much as 30% before the measurements were commenced.

UNCLASSIFIED

UNCLASSIFIED

near the boiling point of water. It is considered more accurate than the bomb technique.

Moisture content was not always measured as a function of depth, but in those cases where it was, it tended to be more uniform at the NBS site than at the Gun Barrel Hill site. The soil at the NBS site was lighter than at Gun Barrel Hill and was uniform to a depth of 4 feet or more. As seen in Figure 7, Gun Barrel Hill soil appears to be thoroughly laced with small rocks and pebbles ranging up to a few centimeters in size; however, the last 15 feet of the NBS site are also impregnated with assorted small rocks and pebbles.

Preliminary Data Measurements

When the contract at Georgia Tech began, the measurement facility at the National Bureau of Standards had already been developed and was being used for similar measurements. Some preliminary data collection procedures had already been established and GIT was immediately in a position to review some of the data.

The very first data consisted of only 23 samples, starting at 240 MHz and going up to 2000 MHz, with 80 MHz increments. It was apparent that this resolution in the frequency domain was too coarse to derive a good data base. We therefore suggested that the frequency resolution be improved. The next data received contained 48 points from 120 MHz to 2000 MHz, giving a 40 MHz resolution. Considerably more detail was seen in this spectral data, suggesting that we improve the resolution even more until it was apparent that additional resolution would create a diminishing return. Initially there appeared

UNCLASSIFIED

UNCLASSIFIED

to be a software problem in storing more than 53 points; however, the memory space problem was resolved and a system capability of 128 points was achieved. The next set of data was taken using two frequency bands per target. The lower band was 105 to 1995 MHz. The higher band was 2010 to 3915 MHz. Both bands had a resolution of 15 MHz. These data gave us the capability to evaluate the deleterious effect of degraded resolution by eliminating data points during computer processing. It was apparent that the 15 MHz resolution was fully sufficient and in fact using every other point (simulating 30 MHz spacing) provided sufficient resolution. At that time, it was determined that data could be recorded from about 100 MHz to about 3 GHz without requiring recalibration of the measurement system. These observations led to the final choice of measurement range from 120 MHz to 3048 MHz in 24 MHz steps.

In addition to conventional mine data, it was suggested that some other special situations would be required. One set of data was measured for the case in which a mine was unearthed, and the hole was refilled with dirt. This data is useful in determining the difference between the undisturbed dirt and the dirt packed on top of the various targets.

Another special run was made with the bistatic pair of antenna aimed at the sky, rather than the ground, to obtain some information on the undisturbed coupling between the antennas. While the antennas were elevated, a mine was positioned 8 inches above them for one run to determine the characteristics of one of the targets of interest without the effect of clutter.

UNCLASSIFIED

UNCLASSIFIED

Selection of the Test Matrix

Early in the project it was determined that a test matrix had to be developed, representing the method for collection of all subsequent data. Early in May, some preliminary data was received, having only 23 points with a frequency spacing of 80 MHz. It was soon decided that the spectral resolution was not adequate for picking up the high rate of oscillation in the spectrum. Subsequently, data was received containing measurements from 105 MHz to 3915 MHz, in 15 MHz increments. This data certainly had enough resolution, as determined by evaluating the degradation when every other data point was deleted, providing 30 MHz resolution. This data also demonstrated that there was very little information beyond 3000 MHz because of the loss in the antennas and the loss in the ground at the higher frequencies. Consequently a measurement program was defined in which the upper frequency was held at 3048 MHz and the lower at 120 MHz, with the measurements made every 24 MHz. This provided precisely 128 frequencies, including those below 120 MHz which could not be measured and had to be artificially assigned some value, usually zero. The measurements could be carried out using a single calibration run, thereby saving time, since frequencies above (about) 3000 MHz would have required a second calibration.

There remained the problem of selecting an optimum antenna height for the measurements. It had been pointed out previously that, due to refractive effects at the ground surface, it may be possible to choose the antenna height so as to maximize the signal return due to a specular reflection from the target. Since the refraction depends on soil moisture content, the

UNCLASSIFIED

UNCLASSIFIED

optimum antenna height would be different for different moisture conditions. NBS personnel therefore carried out a sequence of measurements in which the antenna was placed 2, 4, 6, and 12 inches above the ground for both dry and damp conditions.

The "dry" soil moisture content was reported to be of the order of 2% and the "damp" about 13%. The measurements were conducted in the NBS indoor test lane and the damp condition was created by flooding the test lane with several inches of standing water. The water was permitted to percolate through the ground for several days before the measurements were made. The dry soil tests showed that a 12-inch antenna height was not as desirable as lower heights, but that the differences between the 2-, 4-, and 6-inch heights were not pronounced. Nevertheless, the target seemed to stand out a little more clearly for the 4-inch height than the others, and this was selected as the optimum. The damp soil tests were inconclusive, with no height appearing to be better than any other. Consequently, GIT recommended to NBS personnel that the antenna be fixed at 4 inches above the ground for all tests.

Upon completion of this evaluation, Table 1 was generated as a guide to direct the measurements effort at both the test sites. The selection of these parameters has proven to be acceptable in the analysis of the data. Table 2 shows the matrix of data actually collected.

UNCLASSIFIED

UNCLASSIFIED

Table 1
MEASUREMENT MATRIX

| | |
|-----------------------|--|
| Antenna polarization: | parallel to direction of travel |
| Antenna orientation: | bistatic |
| Antenna height: | 4" |
| Targets: | 3 mines, 3 false alarms, 1 metal plate |
| Positions per target: | -8", -4", 0", 4", 8", 30" |
| Target spacing | 60" |
| Depths: | 3", 6" |
| Moisture contents: | low, medium, high |
| Frequencies: | 120 MHz to 3048 MHz, 24 MHz steps |

Table 2
ACTUAL DATA MATRIX

| | |
|------------------------------|---|
| Antenna polarization: | parallel to direction of travel |
| Antenna orientation: | bistatic |
| Antenna height: | 4" nominal |
| Targets: | mine types A, B, and C; (2) rocks; (1) root, (1) metal plate |
| Positions: | -8", -4", 0", 4", 8", 30" |
| Target spacing: | 60" |
| Depths: | 3", 6" |
| Soil types/moisture content: | Loam: 7%, 17%, 18% Bentonite: 12-20%, 13-16%, 26-30%, 30% |
| Frequencies: | 120 MHz to 3048 MHz, 24 MHz steps |

Typical Data

Results of a typical measurement are presented for a type A mine, a metal plate and a rock of about the same size as the mine. At each of the

UNCLASSIFIED

UNCLASSIFIED

123 frequencies, the real and imaginary parts of the S_{12} parameter (the coupling coefficient from Port 1 to Port 2) were recorded, and the magnitude of S_{12} is displayed. The phase angle at each frequency was also calculated from the real and imaginary components and used in the FFT computations. A casual examination of the following figures shows that the spectra are complicated.

Before the line spectra were transformed to the time domain, the spectral data were weighted with a Chebychev weighting function designed to yield low (40 dB) time sidelobes. The weighting function is plotted in Figure 9 where it is normalized to the peak amplitude occurring at mid-frequency, f_0 . After the spectral data are multiplied by this weighting function, the data are ready for transformation to the time domain. The standard FFT requires that the number of samples be an integral power of 2; samples were selected for 128 frequencies, including zero frequency (DC). Since the five lowest frequency samples lie below the capability of the equipment and were not measured, zeroes were arbitrarily inserted to represent the unmeasured values.

The FFT algorithm used in the generation of the time domain signals creates an array of 256 datum points, 128 of these being the measured data for positive frequencies and the other 128 being their complex conjugates for the corresponding negative frequencies. The total time record length is the reciprocal of the frequency interval; hence, a 24 MHz sampling interval generates a time record 41-2/3 nsec long. Virtually all the signals of interest occur in the first half of this record, however; hence, only the data for the first 20-5/6 nsec are presented.

UNCLASSIFIED

UNCLASSIFIED

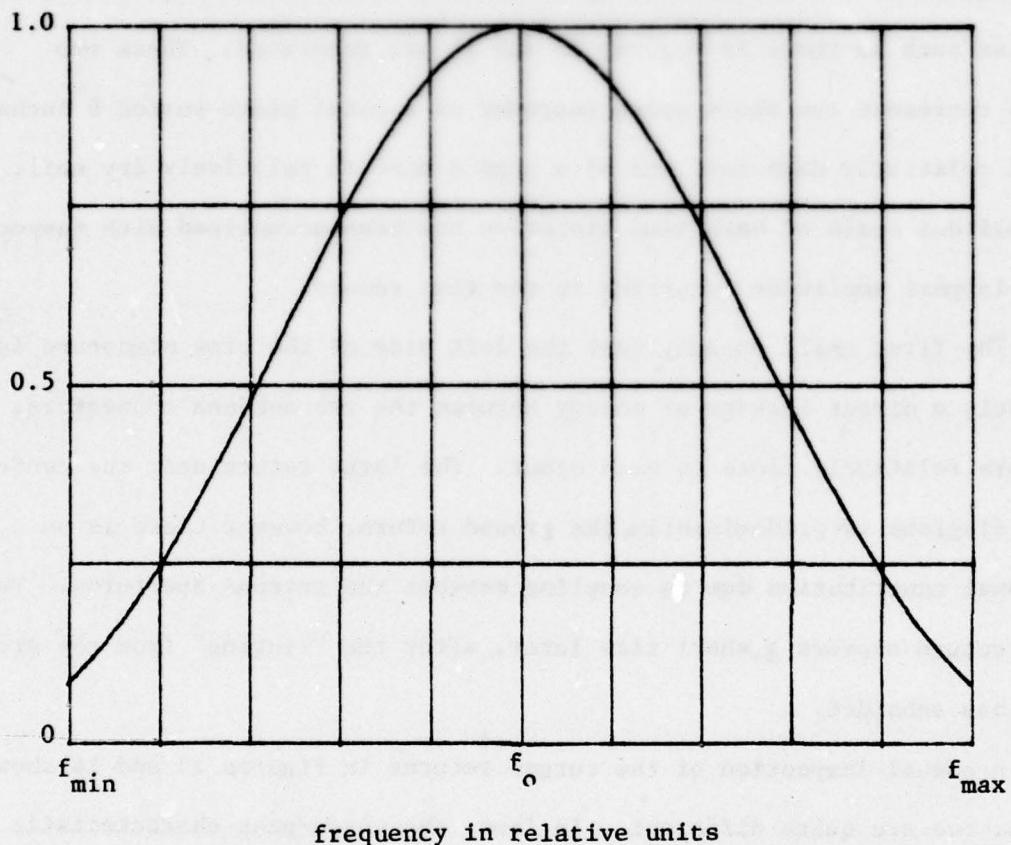


Figure 9. Normalized weighting function, $I_1(x)/x$.

UNCLASSIFIED

UNCLASSIFIED

Line spectra data such as those in Figures 10 through 12 were used to synthesize the performance of a short pulse system by means of the FFT. After weighting the data with a Dolph-Chebychev function centered on the mid-band frequencies to simulate the spectrum of a short transmitted pulse, time histories such as those in Figures 13 and 14 are generated. These two figures represent the short pulse response of a metal plate buried 6 inches deep in relatively damp soil and of a type A mine in relatively dry soil; the amplitude scale of both time histories has been normalized with respect to the largest amplitude occurring in the time record.

The first small anomaly near the left side of the time signature is apparently a direct leakage of energy between the two antenna connectors, which are relatively close to each other. The large return near the center of the diagrams is predominantly the ground return, however there is an additional contribution due to coupling between the antenna apertures. The target return appears a short time later, after the "ringing" from the ground return has subsided.

A casual inspection of the target returns in Figures 13 and 14 shows that the two are quite different. In fact, the three-peak characteristic in Figure 14 was recognizable in most of the time histories obtained for the type A mine. The spectral characteristics of the target alone can be extracted from the time histories by applying a range gate or time "window" that deletes all the returns except those from the target. Typically the window need be only a few nanoseconds wide, and the time data can be transformed back to the frequency domain using an inverse FFT. This process generates potentially useful spectral data, as shown in Figures 15 and 16.

UNCLASSIFIED

UNCLASSIFIED

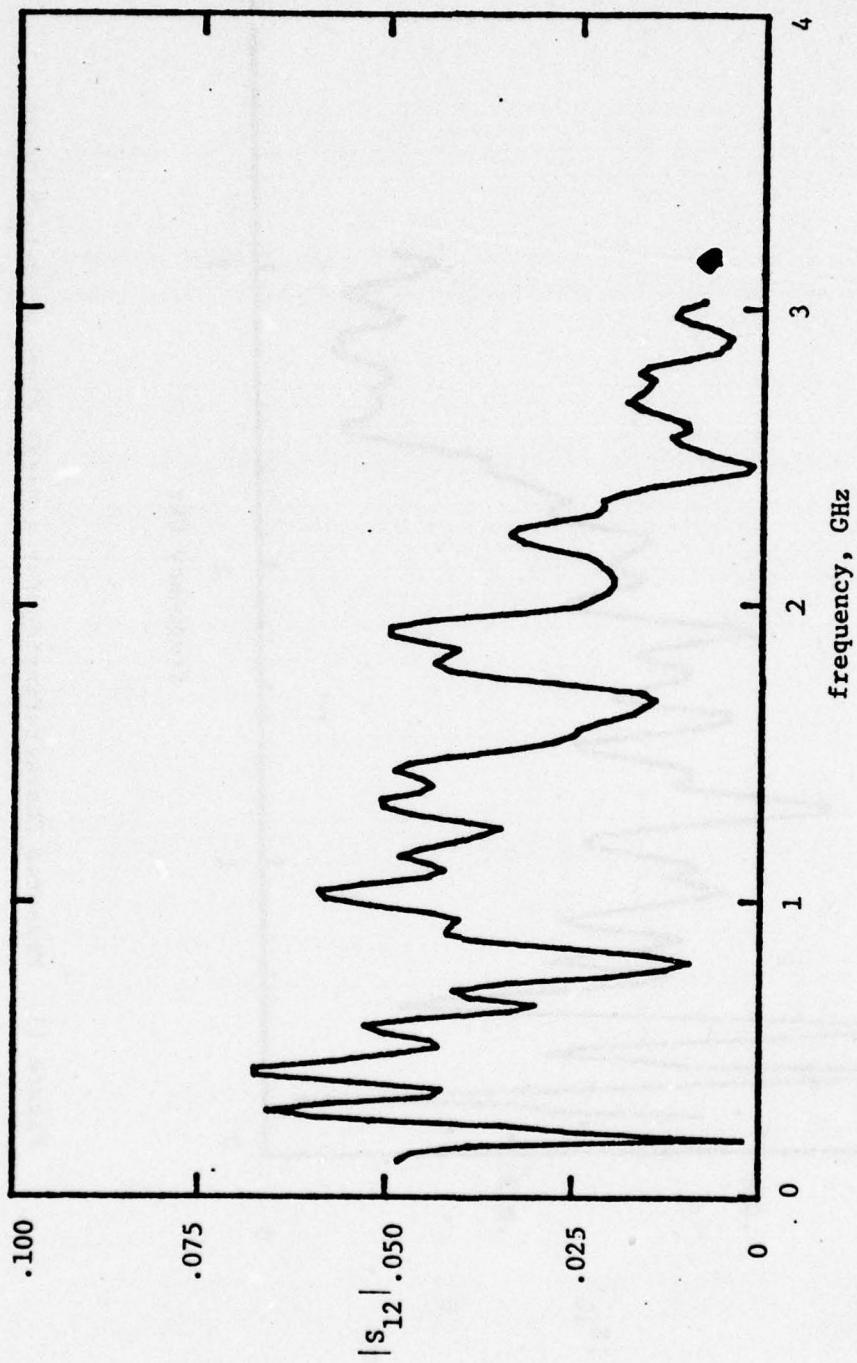


Figure 10. Measured Characteristics for a Type A Mine at 3-inch Depth.

UNCLASSIFIED

UNCLASSIFIED

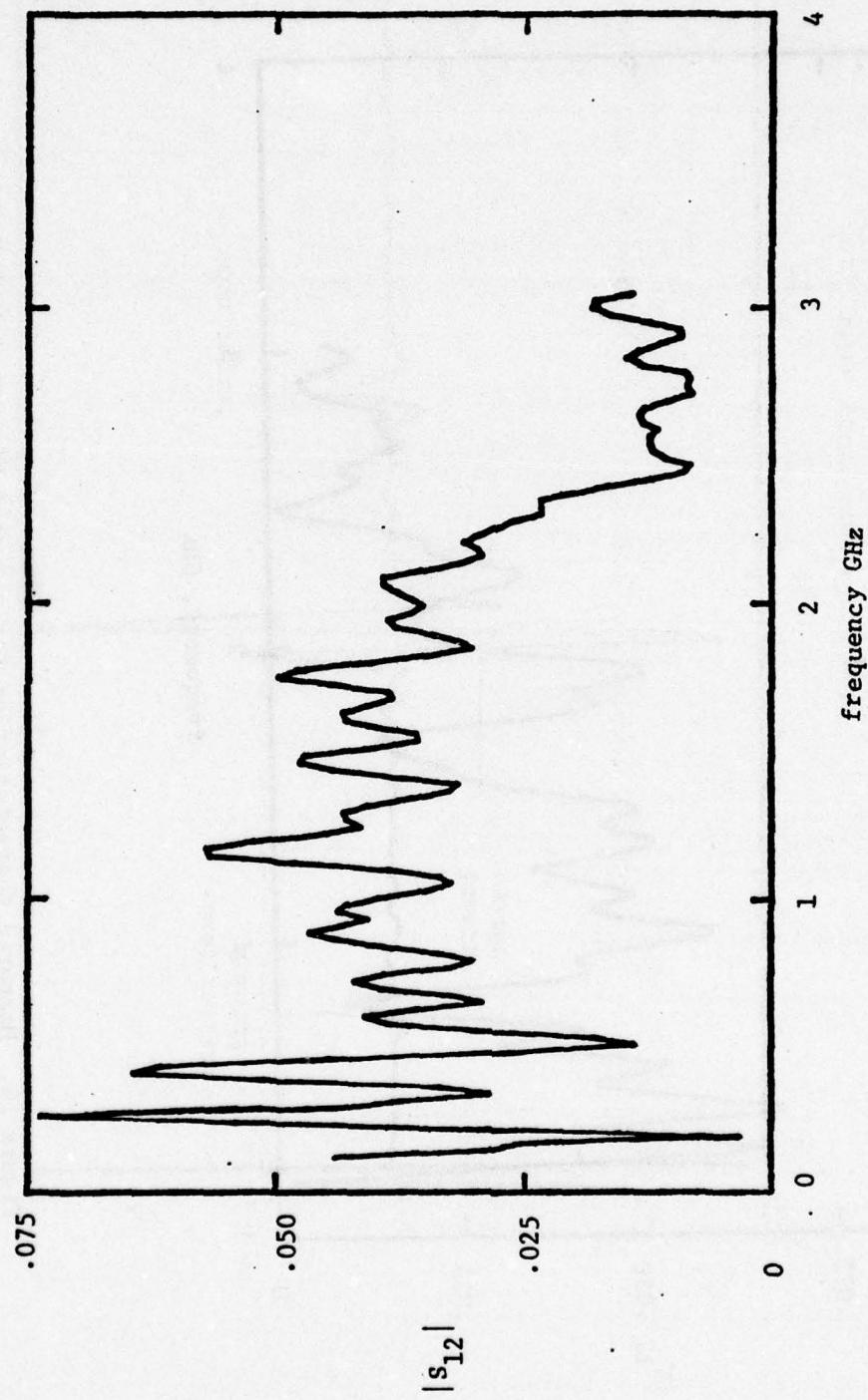


Figure 11. Measured Characteristics for a Metal Plate at 6-inch Depth.

UNCLASSIFIED

UNCLASSIFIED

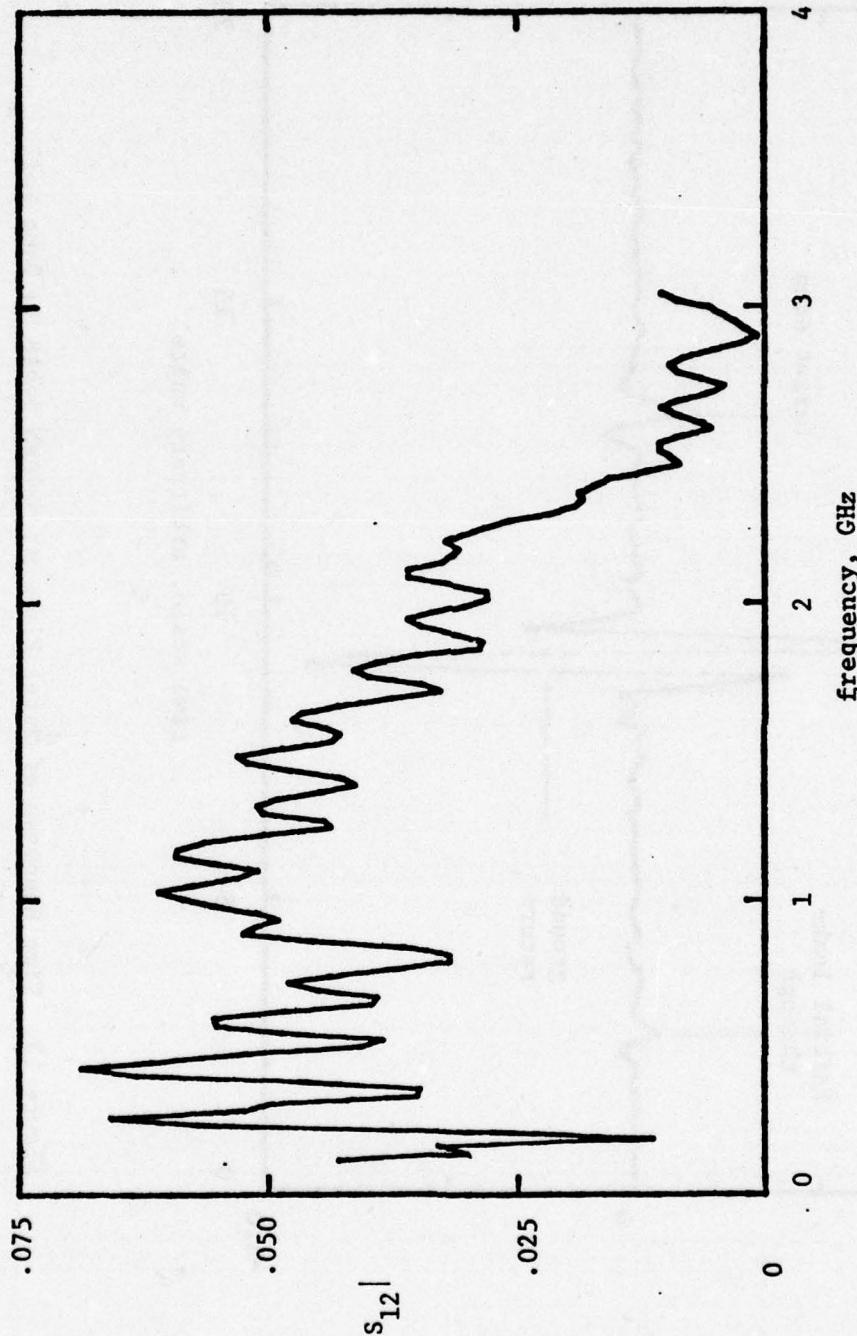


Figure 12. Measured Characteristics for a Rock at 3-inch Depth.

UNCLASSIFIED

UNCLASSIFIED

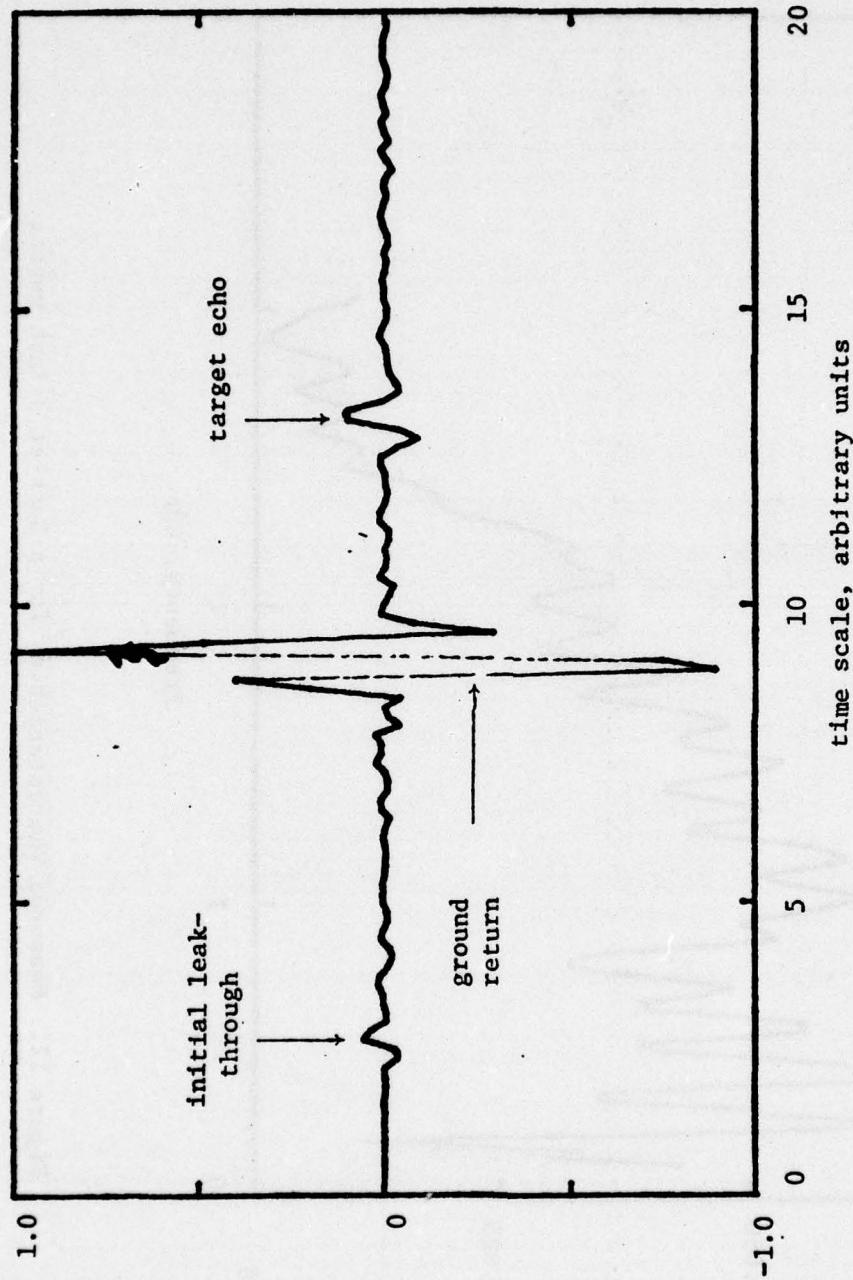


Figure 13. Time Response of Metal Plate at 6-inch Depth in Damp Soil.

UNCLASSIFIED

UNCLASSIFIED

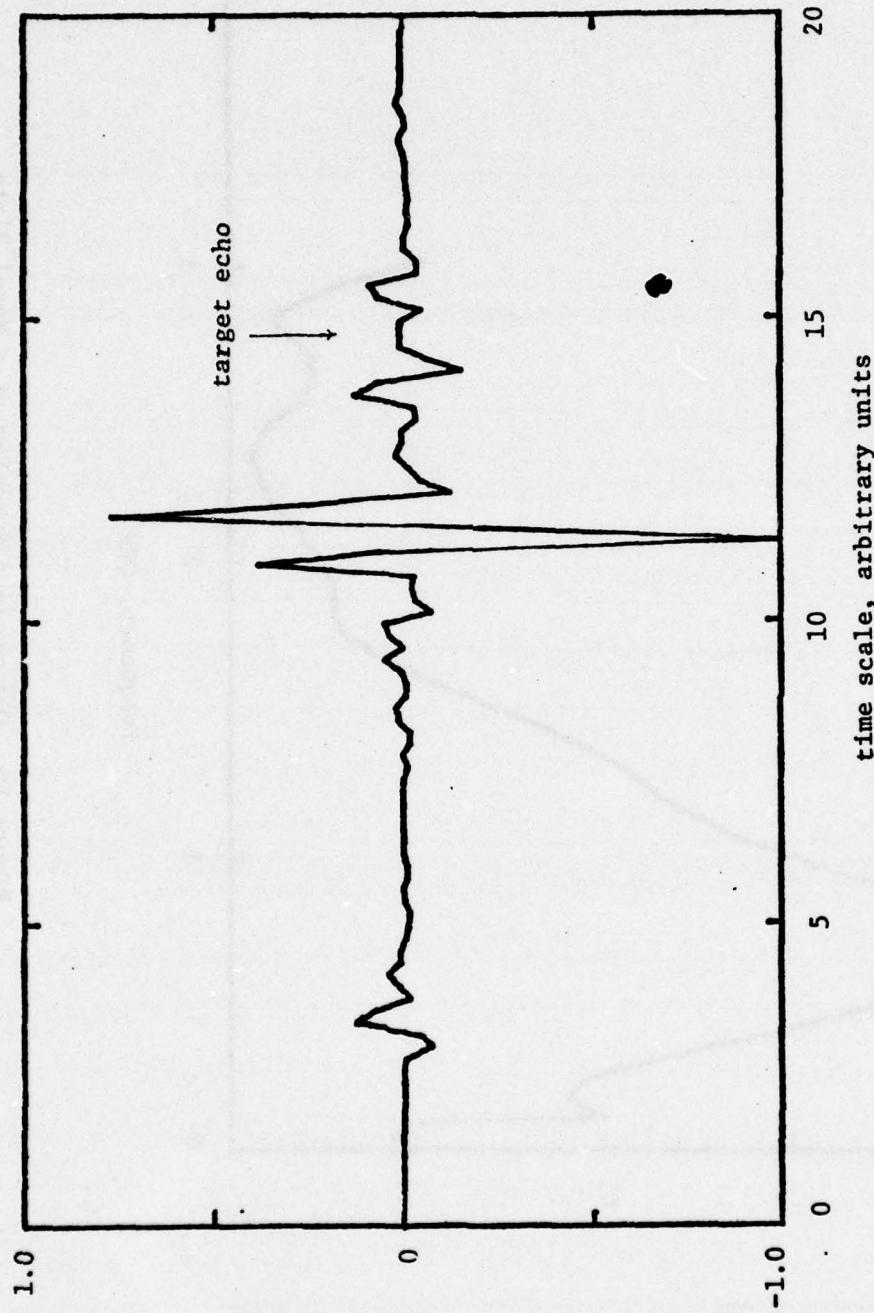


Figure 14. Time Response of Type A Mine at 6-inch Depth in Dry Soil.

UNCLASSIFIED

UNCLASSIFIED

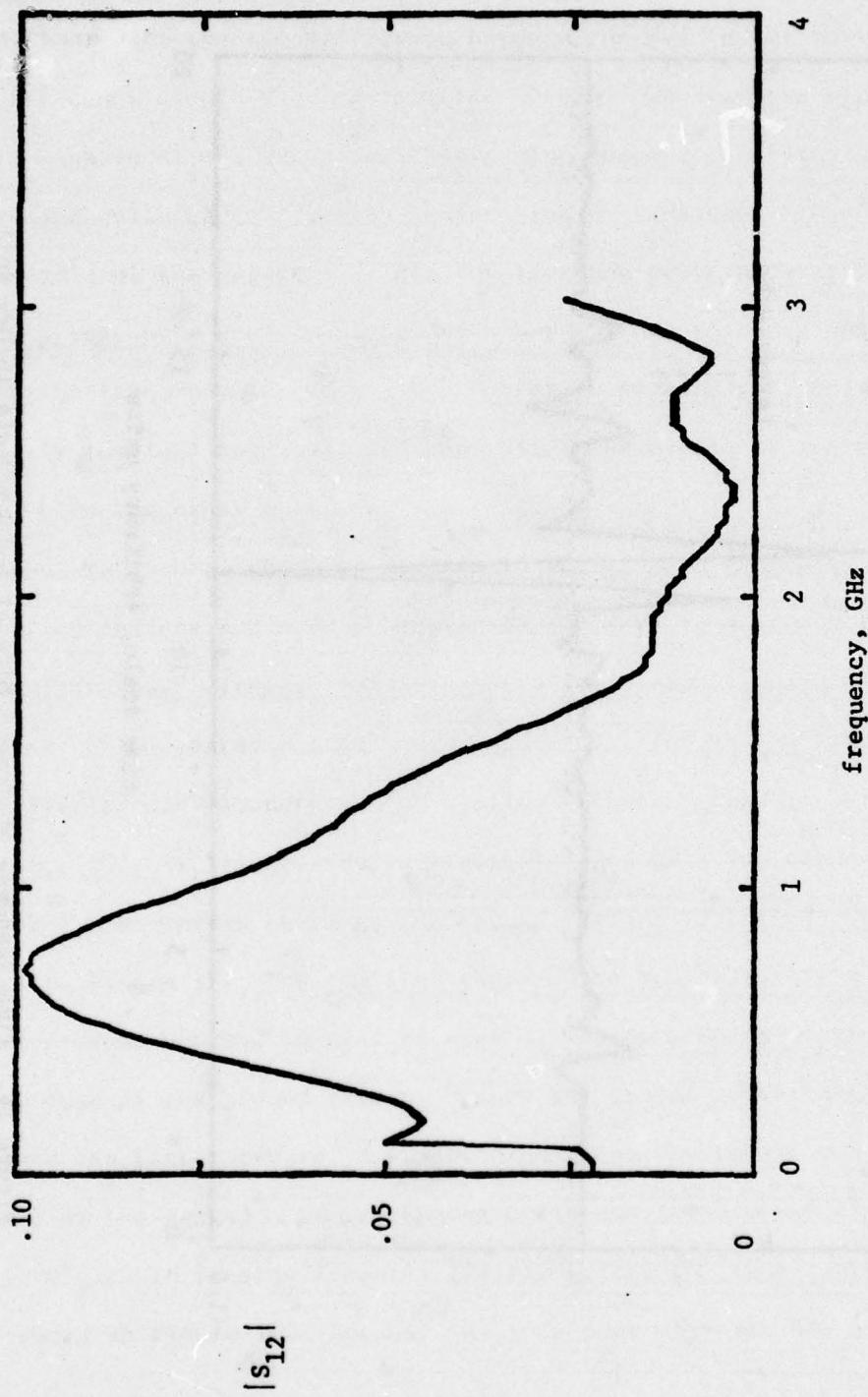


Figure 15. Deconvolved Spectrum of a Metal Plate.

UNCLASSIFIED

UNCLASSIFIED

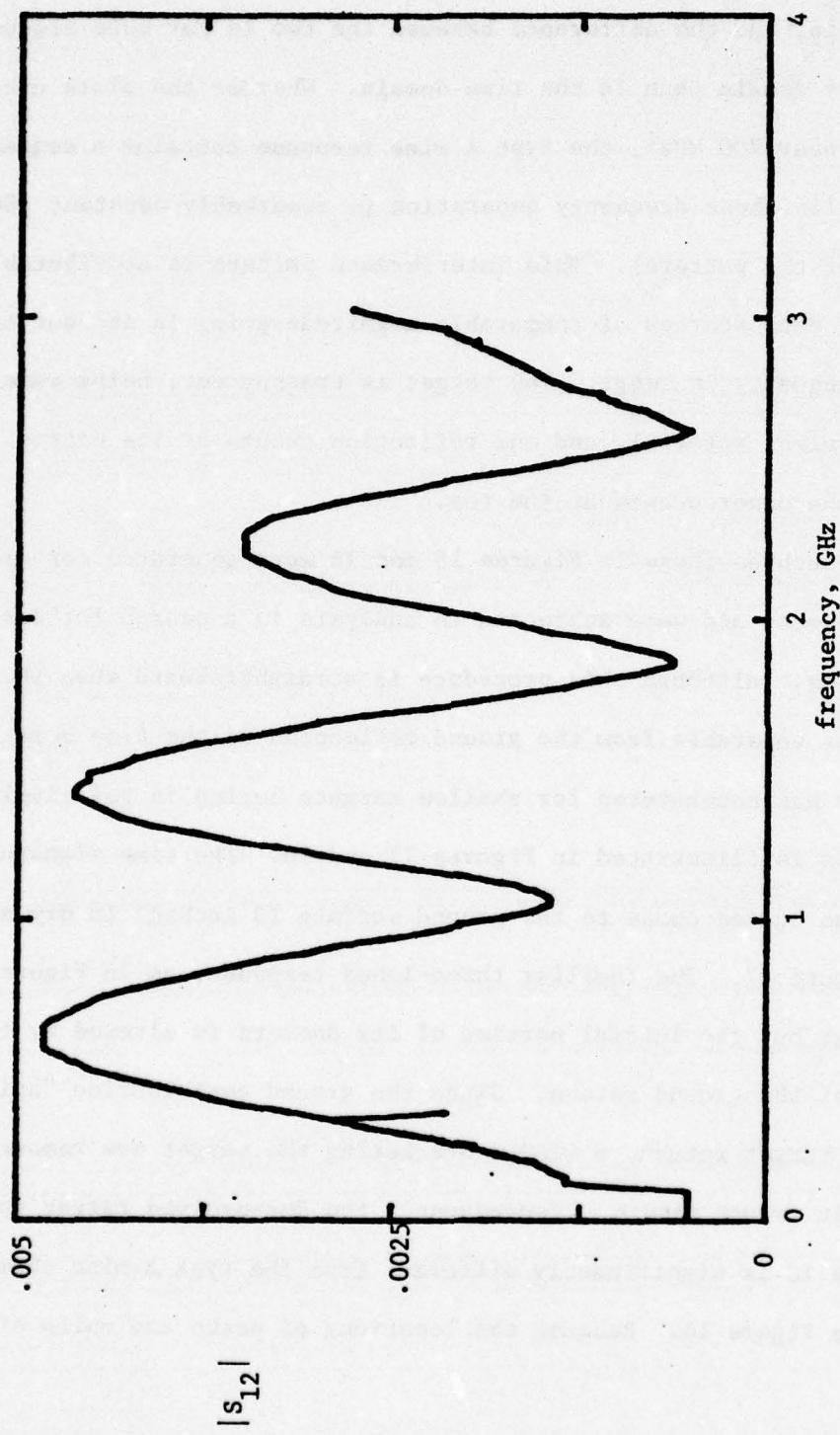


Figure 16. Deconvolved Spectrum of a Type A Mine.

UNCLASSIFIED

UNCLASSIFIED

The metal plate response is shown in Figure 15 and that of a type A mine in Figure 16, and the difference between the two is far more pronounced in the frequency domain than in the time domain. Whereas the plate exhibits a single peak (near 700 MHz), the type A mine response contains a sequence of peaks and nulls whose frequency separation is remarkably constant (800 MHz per cycle of the pattern). This interference pattern is attributable to two discrete echo sources of comparable magnitude going in and out of phase as the frequency is swept. The target is transparent, being made of essentially lossless material, and one reflection occurs at its bottom surface while the other occurs at the top.

Spectra such as those in Figures 15 and 16 were generated for all seven buried objects and were subjected to analysis in a search for discrimination features. Although this procedure is straightforward when the target return is separable from the ground reflection in the time domain, some difficulty was encountered for shallow targets buried in relatively dry soils. This is illustrated in Figures 17 and 18. The time signature of a type A mine buried close to the ground surface (3 inches) in dry soil is shown in Figure 17. The familiar three-lobed response, as in Figure 14, is still present but the initial portion of its pattern is altered by the trailing edge of the ground return. Since the ground contribution "spills over" into the target return, a window bracketing the target now removes only part of the ground return. Consequently the deconvolved target spectrum shown in Figure 18 is significantly different from the type A mine characteristics shown in Figure 16. Because the locations of peaks and nulls of these

UNCLASSIFIED

UNCLASSIFIED

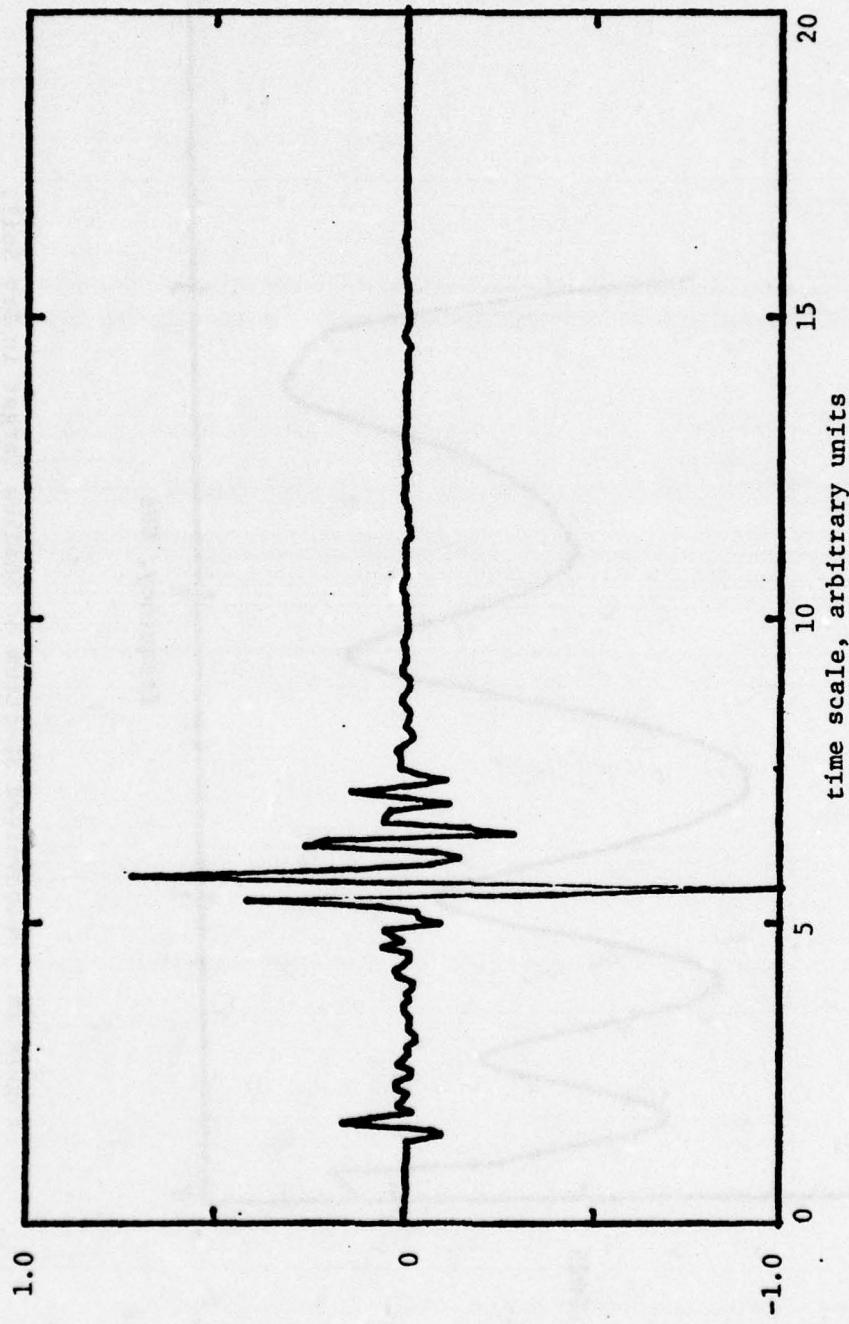


Figure 17. Time Domain Response of Shallow Target in Dry Soil.

UNCLASSIFIED

UNCLASSIFIED

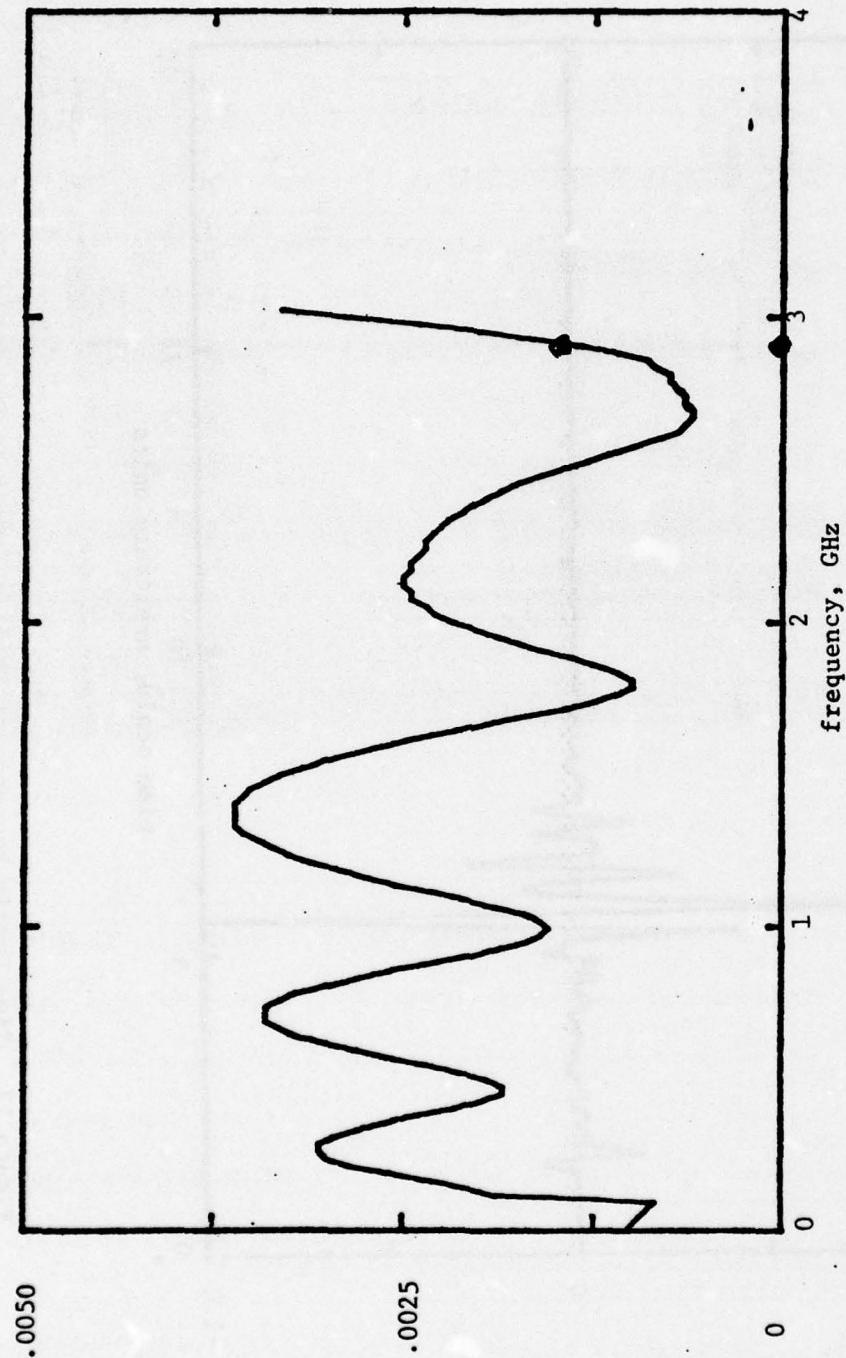


Figure 18. Deconvolved Spectrum of Shallow Target in Dry Soil.

UNCLASSIFIED

UNCLASSIFIED

spectra are different, a discrimination scheme based on Figure 16 would not necessarily classify the spectrum of Figure 18 as being that of a type A mine.

SHORT-PULSE RADAR MEASUREMENTS

The short-pulse radar system used for collecting the short-pulse data is briefly described in the following paragraphs. In addition, the condition of the site where the data was taken is reviewed. Then, the test matrix utilized is explained and some typical data collected are presented.

Measurement System

The experimental vehicular-mounted mine-detector radar system supplied by the U.S. Government and shown in Figures 19 and 20 primarily comprises three short-pulse receiver/transmitters, three wideband antennas, and a storage oscilloscope mounted on a GFE General Electric tractor (Model E-15). Some additional equipment was supplied but was not used.

The radar operates at a pulse repetition frequency of 5 MHz. This pulse repetition rate is derived by dividing down a 15 MHz crystal controlled oscillator. To avoid mutual interference, the output of the transmitter pulses are staggered so that each radar operates at a different time interval. This staggering is accomplished by shifting the phase of the 5 MHz signal to provide 0°, 120°, and 240° outputs. A fourth 5 MHz output is provided which is divided in frequency by a factor of 500 and used for synchronization of the range gates and staircase sweep generator.

Synchronization of the radar is provided by a 5 MHz sine-wave which is divided down by a factor of 500 to produce a 10 kHz clock signal. This clock

UNCLASSIFIED

UNCLASSIFIED

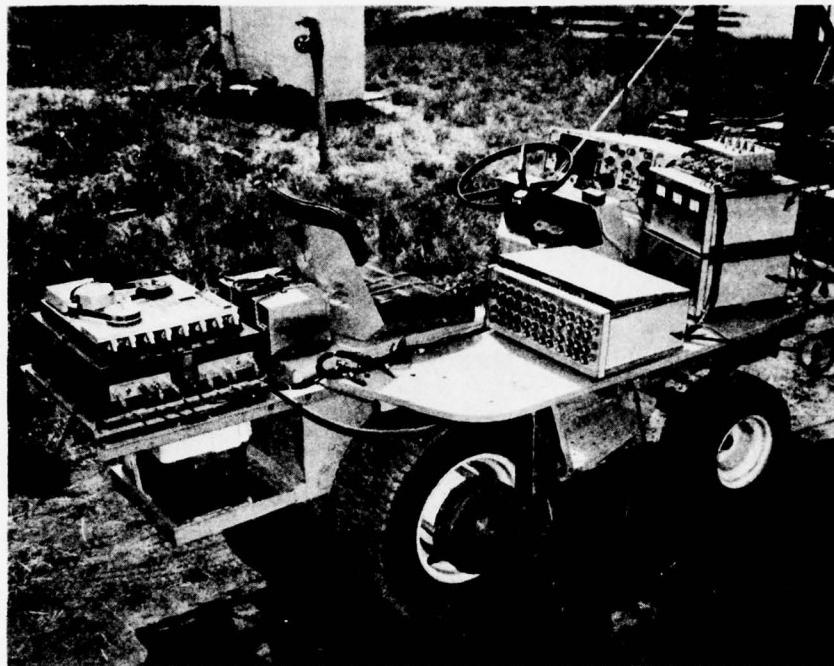


- (1) three short-pulse receiver/transmitter modules
- (9) oscilloscope monitor
- (10) audio and video alarm unit
- (11) battery box
- (12) three antenna units
- (15) recorder remote control box

Figure 19. Vehicular-mounted mine detector radar (left side view).

UNCLASSIFIED

UNCLASSIFIED



- (2) radar control console
- (3) recorder junction box
- (4) display generator
- (5) magnetic tape recorder
- (6) discriminator unit
- (7) storage oscilloscope
- (8) power junction box
- (14) position potentiometer

Figure 20. Vehicular-mounted mine detector radar (right side view).

UNCLASSIFIED

UNCLASSIFIED

signal is used to step the staircase sweep generator which moves the sampling probe progressively in time. The received signal is sampled approximately 50,000 times for each 10 ms sweep. By using the sampling receiver technique, a real-time waveform of approximately 10 nsec duration is displayed on the monitor scope in approximately 10 msec.

Measurement Sites

All of the sites for the short-pulse radar measurements were selected at random in the grounds surrounding the Georgia Tech Baker Building. The soil was dry red clay. All the mines, metal plates, and rocks were buried with their top surfaces approximately six inches beneath the soil surface. All large rocks and other debris were removed during the burying process. In most cases, the surface grass was replaced for the measurement. Only one of the three radar modules was used in data collection; the same radar was used for all measurements. The radar antenna was placed approximately four inches above the soil surface in each case.

Selection of Test Matrix

A matrix of measurements to be made with the short-pulse radar was generated and is given in Table 3. Since the major purpose of the short-pulse measurements was to verify that this measurement system is effective for target discrimination/classification, all of the measurements were made in dry soil. All objects were buried 6 inches below the soil surface in a red clay soil. The objects buried were two types of non-metallic mines, a metal plate and a rock about the same size as the mines. In addition, some data were taken in ground without buried objects and is labeled in Table 3 as

UNCLASSIFIED

UNCLASSIFIED

background data. Each object was buried in 4 different locations, and for each location three radar measurements were taken. One measurement was taken with the radar antenna centered over the object, and one measurement 4 inches on either side of the center. Thus, a total of 12 dry measurements per object were taken.

Table 3
SHORT-PULSE MEASUREMENTS

| | |
|-------------|-------------------------|
| Type A Mine | 3 measurements/object |
| Type C Mine | 4 locations |
| Metal Plate | |
| Rock | |
| BACKGROUNDS | 3 measurements/location |
| | 4 locations |

Typical Data

Some typical temporal and spectral plots of the data taken with the short-pulse radar are shown in Figure 21 and Figures 22 and 23. In each figure, six plots are shown. The center pair of plots represent the time and spectral responses of measurements taken when the antenna was centered over the buried object. The pair of plots at the top and bottom of the figures are the data taken when the antenna was centered 4" on either side of the object center. The time plots on the left span a time of zero to seven nanoseconds and the spectral plots on the right represent zero to 3.33 Ghz.

UNCLASSIFIED

UNCLASSIFIED

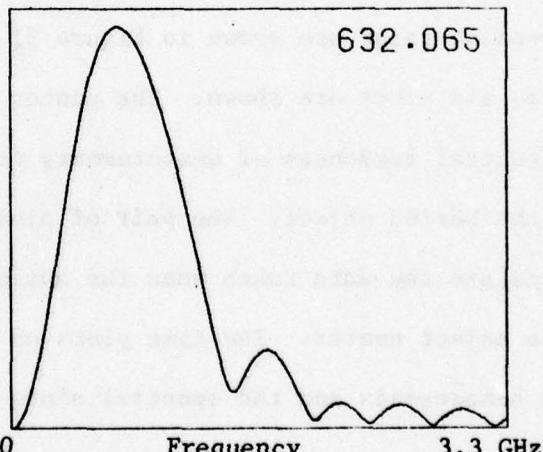
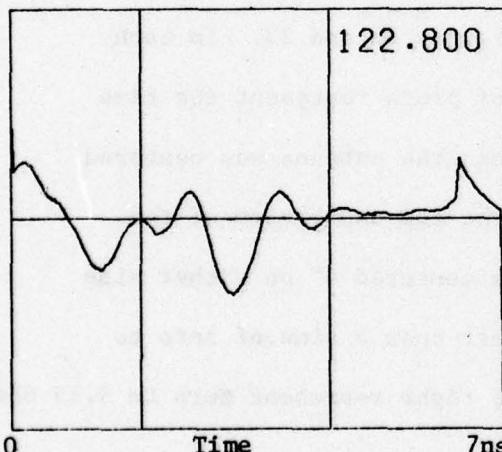
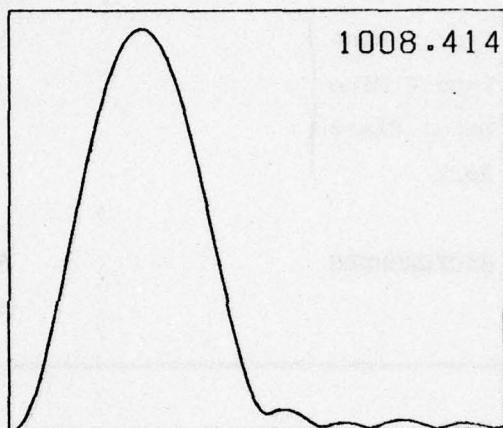
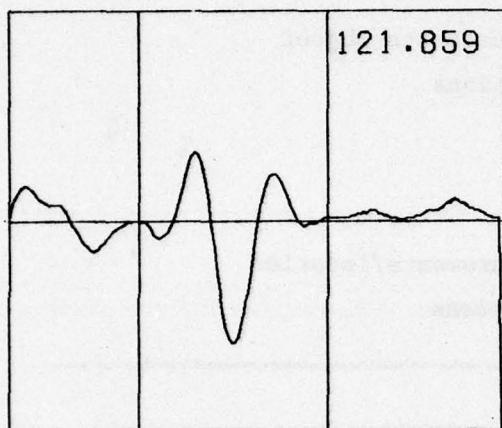
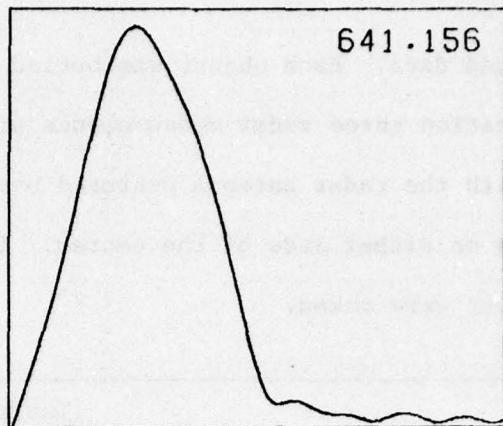
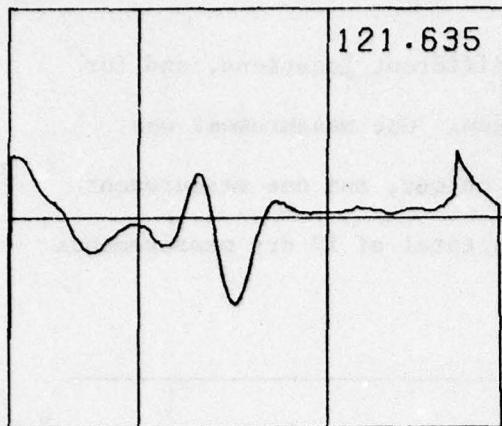
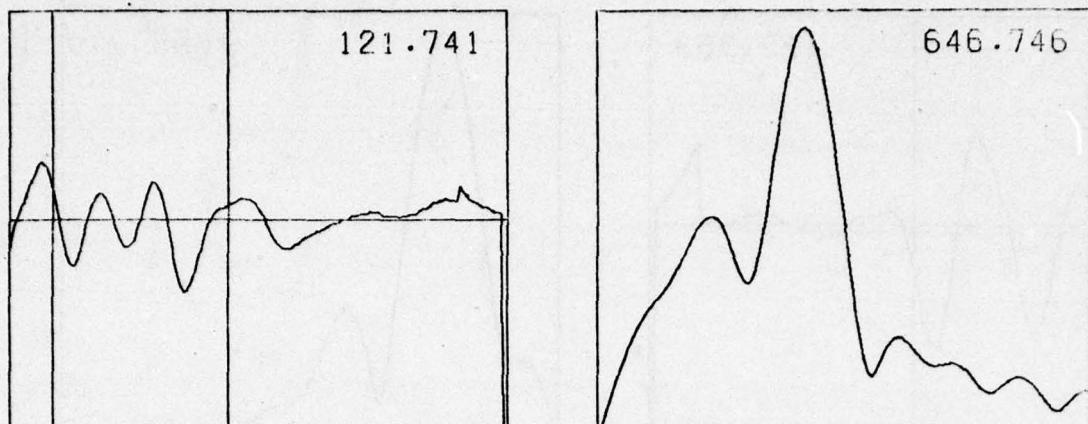


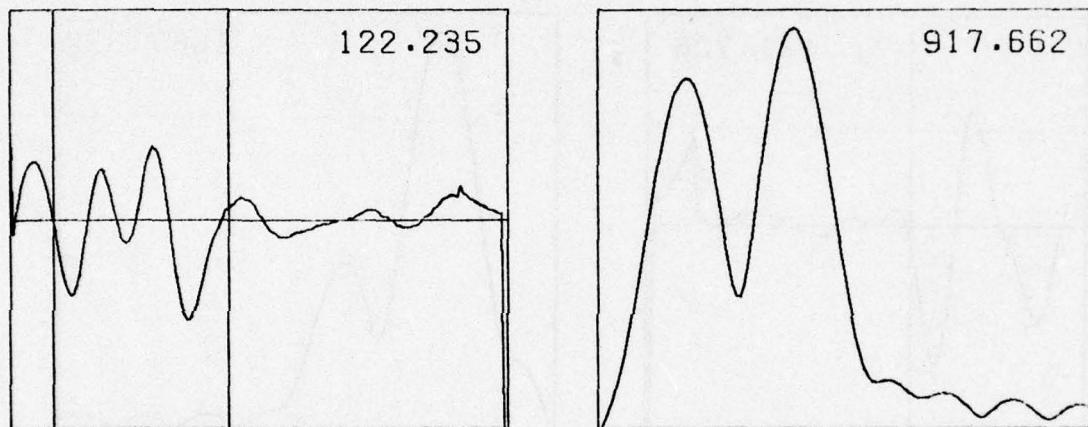
Figure 21. MERADCOM short-pulse radar returns from metal plate buried 6" below ground surface in dry clay soil.

UNCLASSIFIED

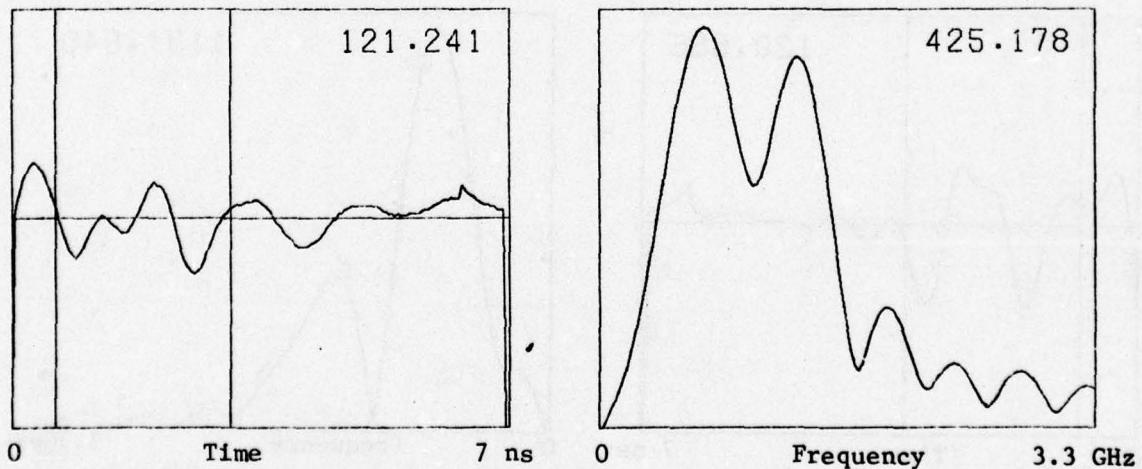
UNCLASSIFIED



43



44

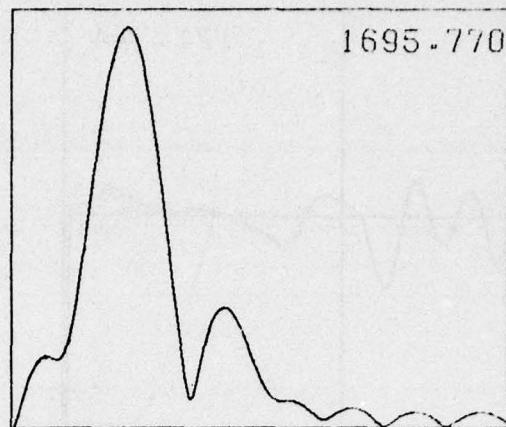
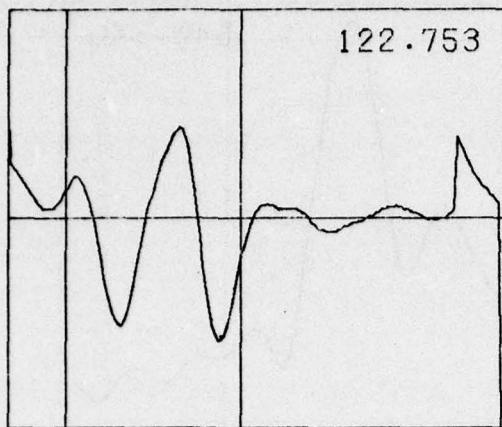


45

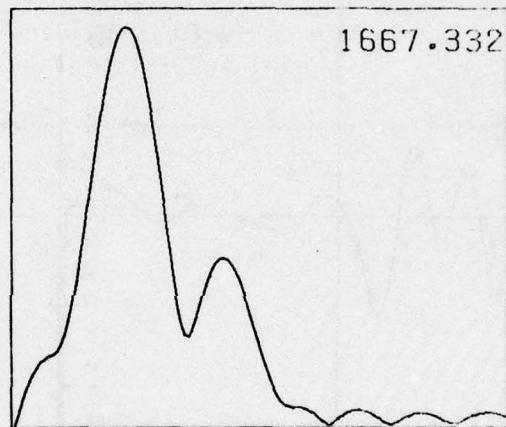
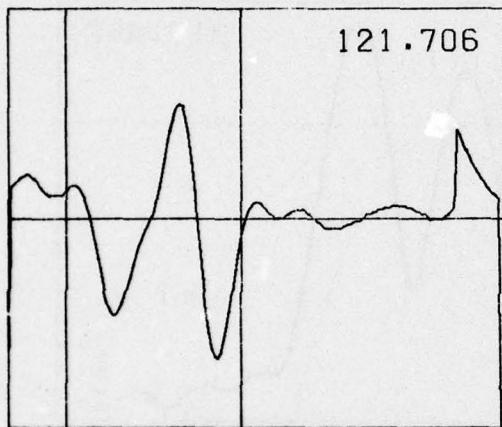
Figure 22. MERADCOM short-pulse radar return from a type A non-metallic mine buried 6" below ground surface in dry clay soil.

UNCLASSIFIED

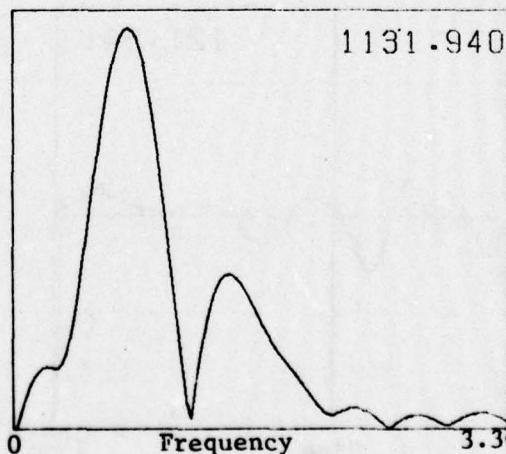
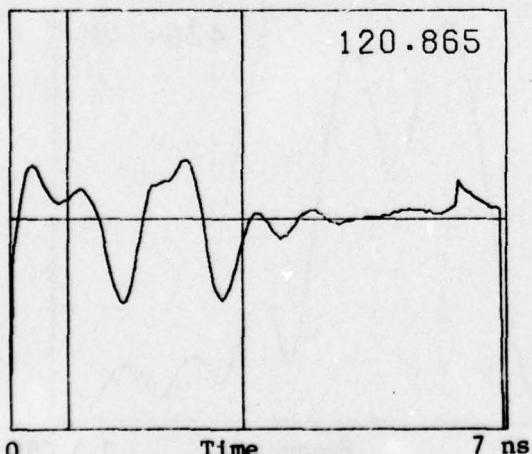
UNCLASSIFIED



64



65



66

Figure 23. MERADCOM short-pulse radar returns from a type C non-metallic mine buried 6" below ground surface in dry clay soil.

UNCLASSIFIED

UNCLASSIFIED

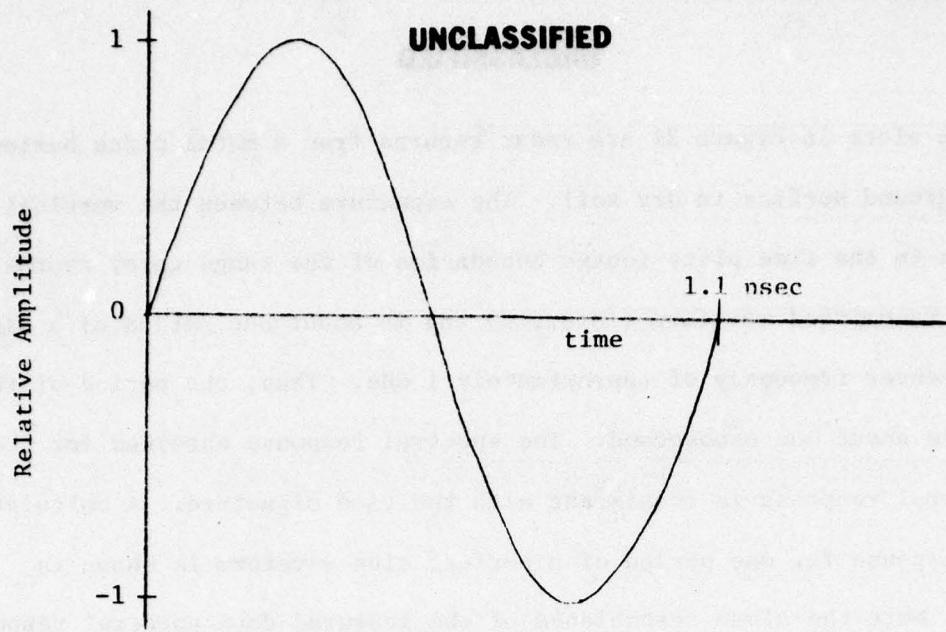
The plots in Figure 21 are radar returns from a metal plate buried 6" below the ground surface in dry soil. The signature between the vertical lines shown in the time plots (outer boundaries of the range gate) approximates the transmitted waveform (inverted) and is about one period of a sine-wave with center frequency of approximately 1 GHz. Thus, the period of the signature is about one nanosecond. The spectral response obtained for the gated temporal response is consistent with the time signature. A calculated spectral response for one period of a perfect sine waveform is shown in Figure 24. Note the close resemblance of the measured data spectral response to the calculated one.

The time response preceding the range gate is part of the ground return. The sharp peak following the gate is the edge of a 6.4 nanosecond gate built into the short-pulse radar. The beginning of this gate is at the left edge of each figure. It shows in the figures because the plots exceed 6.4 nanoseconds in time extent (i.e., 7.0 nanoseconds).

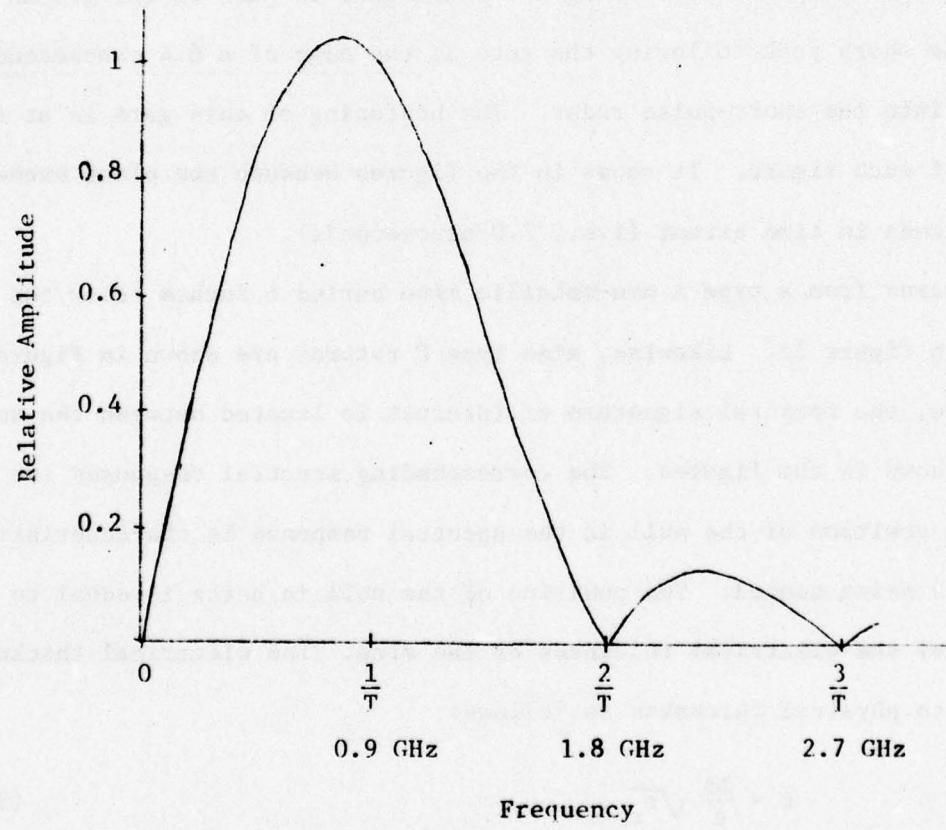
Returns from a type A non-metallic mine buried 6 inches below the soil are shown in Figure 22. Likewise, mine type C returns are shown in Figure 23. In each case, the temporal signature of interest is located between the vertical lines shown in the figures. The corresponding spectral responses are also shown. The position of the null in the spectral response is characteristic of the mines being sensed. The position of the null in hertz is equal to the reciprocal of the electrical thickness of the mine. The electrical thickness is related to physical thickness as follows:

$$t = \frac{2d}{c} \sqrt{\epsilon_r} \quad (3)$$

UNCLASSIFIED



(a) Transmitted Temporal Waveform



(b) Transmitted Waveform Spectrum

Figure 24. Calculated spectral response for one period of sine waveform.

UNCLASSIFIED

UNCLASSIFIED

where

d = physical thickness

c = velocity of light in free space

t = time

ϵ_r = the relative dielectric constant of the material

in the mine (for paraffin wax, ϵ_r = 2.25)

The type A mine is about 4.5 inches in thickness. Thus, its time thickness, t, is about 1.14 nanoseconds. The null should be at $1/t$ or 0.88 GHz. Careful measurement of the spectral plots will indicate close agreement. The type C mine is about 3.2 inches thick; therefore, t is 0.81 nanoseconds. The null is located at 1.2 GHz which it should be.

UNCLASSIFIED

UNCLASSIFIED

SECTION III

DATA REDUCTION

One of the objectives of the mine detection program is to develop algorithms to automatically process real-time data in order to detect and identify non-metallic mines buried in soil. However, before selecting and testing candidate detection and classification schemes, it was necessary to visually observe and compare the temporal and spectra responses for the various buried objects sensed with the measurement system. To provide plots of the time and frequency responses, the data were processed off-line with Georgia Tech's CYBER 74 computer as indicated in Figures 25 and 26. Figure 25 outlines the processing performed on the NBS data to provide the necessary plots, and Figure 26 shows the processing necessary to generate plots of the short-pulse radar data.

As indicated previously, the NBS data were collected with a network analyzer which is a CW device. Each CW measurement (amplitude and phase) represented one line of a line spectrum. To simulate a short-pulse return, the 128 lines representing frequencies from 0 MHz to 3.048 GHz were transformed from the frequency domain to the time domain. In addition, amplitude weighting was used to control the time sidelobes, the ground return was removed, and the remaining data were searched for the proper range gate position. An inverse Fast Fourier Transform was used to generate a "gated spectrum"--the spectrum of the suspected temporal signature. Plots of the time and frequency signatures were generated for visual inspection and comparison.

UNCLASSIFIED

UNCLASSIFIED

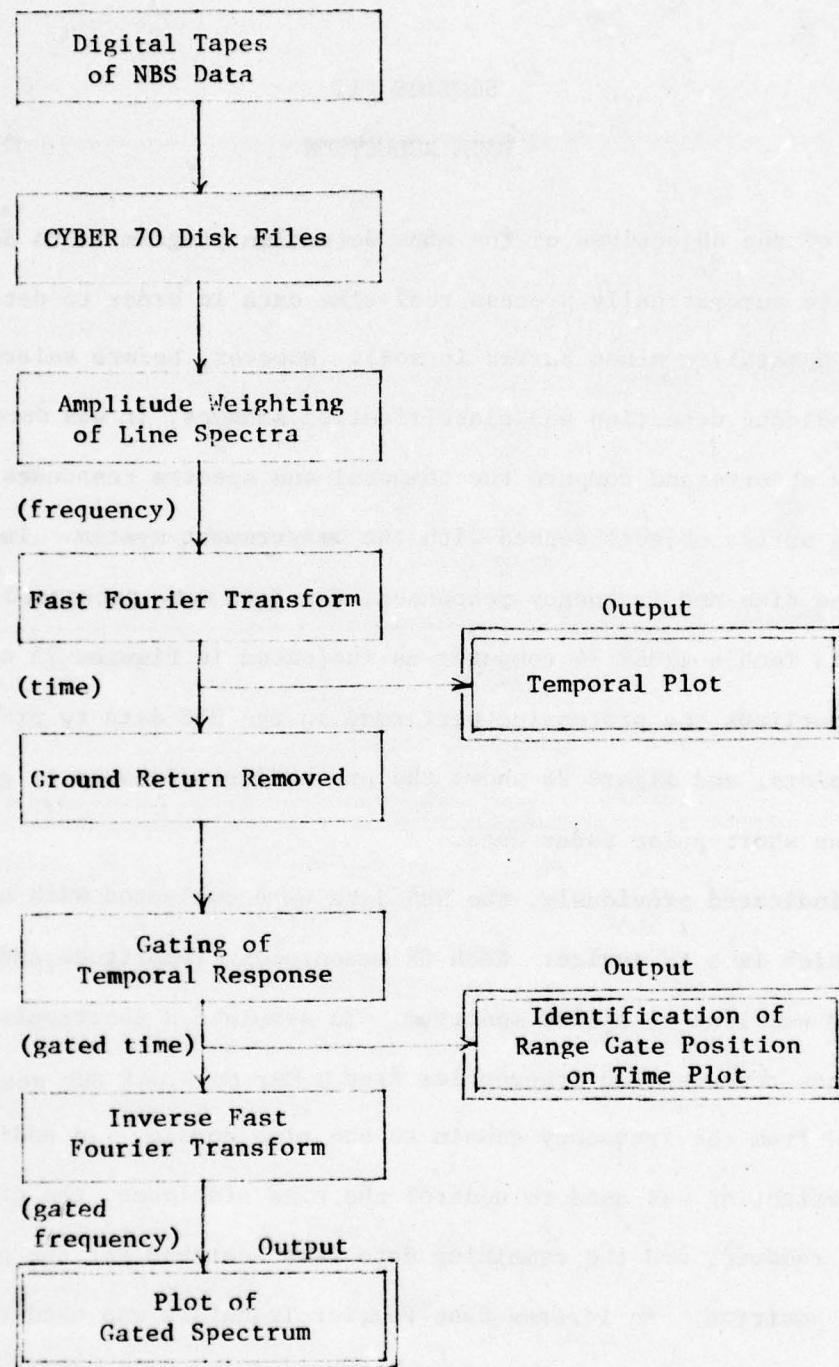


Figure 25. Processing of NBS data to provide temporal and spectral plots.

UNCLASSIFIED

UNCLASSIFIED

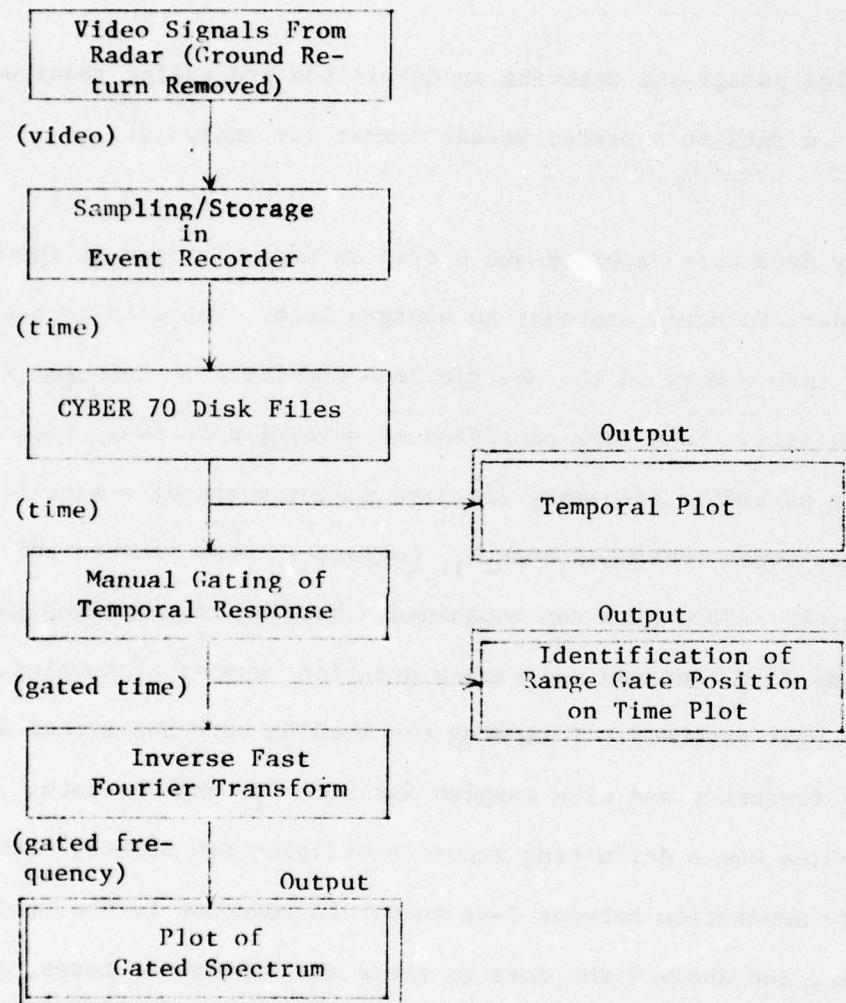


Figure 26. Processing of short-pulse radar data to provide temporal and spectral plots.

UNCLASSIFIED

UNCLASSIFIED

The short-pulse radar data were processed in a similar manner as shown in Figure 26 to provide the necessary plots; however, these data were recorded as a temporal signature. Therefore, the "forward" Fourier transform was not necessary.

The following paragraphs describe in detail the processing required to present the measured data in a proper visual format for analysis.

NBS DATA

Preliminary data were recorded and stored on magnetic tape at the NBS test site in Boulder, Colorado and sent to Georgia Tech. The data on these tapes were loaded into memory in the Georgia Tech CDC CYBER 74 computer for processing and analysis. Each tape consisted of several data runs, each containing scattering parameter frequency response measurements of a specific target. These data tapes contained both S_{11} monostatic measurements and S_{21} bistatic measurements. Each data run contained a heading record which gave such information as date, antenna and target position, number of samples, and name of the target measured. Following the heading were the actual data samples, keyed by frequency and with samples for both S_{11} and S_{21} data. Following the samples was a delimiting record containing two values, -1.0 and 0, to identify separation between data runs. In response to the need to reduce, process, and analyze the data on these and subsequent tapes, a series of analysis computer programs was developed.

Computer Program Development

The processing requirement for the data was to perform an inverse Fast Fourier Transform (FFT) on a desired spectral data run and display the

UNCLASSIFIED

UNCLASSIFIED

resulting time response data in a manner that could easily be interpreted by the user. The FFT program read either S_{11} monostatic or S_{21} bistatic data, as specified by the program user, from the data file and data run of the user's choice. The program was designed to read the header for pertinent information concerning the sampling period and adjust the data automatically to fit the power-of-two array required by the FFT. The output was in the form of a numerical print-out and a plot provided by the CALCOMP digital plotter. Verification of the inverse FFT's performance was obtained by entering test cases whose temporal responses were known. To provide a faster turnaround on plots, a plotting routine employing a Tektronix interactive graphics terminal was added to the program. This made it possible for the user to employ the program in an on-line, interactive analysis mode, as graphic output was now returned to the user immediately. It was also desired that frequency response data be displayed graphically so a CALCOMP routine to plot signal magnitude versus frequency was added.

Casual observance of the resultant time plots indicated that all useful information involving the target returns in the time response array was located within the first 20 nanoseconds of time samples. To display only this portion of the array, the plotting routines were modified to plot only one-half or one-quarter (depending on the total time length) of the time response, rather than that suggested by the sampling resolution.

Another addition to the program was the filtering subroutine which weighted the frequency response data before the FFT. Low and high frequency limits of the filter could either be set by the user during program execution

UNCLASSIFIED

UNCLASSIFIED

or by the program as the low and high sample frequencies of the data run being processed. Initially, the main lobe of a sin x/x weighting function was used, with subsequent addition of the Dolph-Tchebychev weighting for sidelobe control.

At this point, the analysis program had a variety of optional operational modes based on selection of the filtering mode, the output format, the selection of appropriate data, and others. To allow selection of these various options in an efficient manner, a system of control variables was implemented. Each option was controlled by the value of an associated integer variable. Values were assigned to these variables at the beginning of the program in one of two ways. In the first, the program interrogated the user as to the value of each control variable. A message explaining the options for each control variable was printed before each. In the second, predetermined values were assigned to each variable as part of the program flow, and the user was not interrogated.

Study of time response plots for S_{11} data revealed a "ringing" oscillation. It was concluded that this was brought about by a "spike" at 105 MHz, detected on the frequency response magnitude plot of the data. To suppress this undesirable ringing, the option of deleting data samples below 300 MHz was added to the system, made possible by the control variable system. The low frequency spike appeared to be peculiar to the S_{11} data and the low frequency deletion was not required for processing of S_{21} data associated with the bistatic arrangement of the measurement system.

Other options were added to the program, mostly pertaining to program control. Normally, the program would read and process a data run once, but

UNCLASSIFIED

UNCLASSIFIED

when specified by the user, the program could reprocess a previous data run, making it possible to study the effects of filtering and other factors in an interactive manner. In order to test transform and data accuracy, the option of varying the size of the array used in the FFT routine was added.

Data collection conforming to the suggested measurement matrix began and more comprehensive data tapes began arriving at Georgia Tech. Analysis of this data suggested new requirements, and further modifications of the program became desirable. For better reference and organization, the two CALCOMP plotting routines were consolidated to plot frequency response and time response data side-by-side on a single plot.

The range gate and forward FFT option was implemented to aid in analysis of data. This option allowed the user to specify two "range gate limits" in the temporal domain. These gates were entered by the user in units of nanoseconds, which the program converted to the proper array indices for the time response array. The program then generated a gated time response array, containing only the time response data located within the range gates. Elements of the array outside the range gates were assigned the value of zero. A forward FFT was then performed on the gated time array to produce a range-gated frequency response array. This modification made it possible for the user to specify a particular portion of the time array, such as that associated with a target, and exclude all other information thus producing a frequency response array containing only the desired target information. To display this new information, the CALCOMP plotting routine was designed to plot frequency response, time response, gated time response, and gated frequency response on one page.

UNCLASSIFIED

UNCLASSIFIED

As data from the NBS measurements site arrived, it was placed in mass storage on the CYBER 74. Although the data contained both S_{11} and S_{21} data, only S_{21} data were analyzed. Each data run contained 123 samples between and including 120 and 3048 MHz. Because of the accumulation of a large volume of data and this method of storage, disc storage costs rose considerably during this time. Also, program input was impaired by the large volume of data and the necessary ASCII to binary conversion during data read. To cut down on storage and processing costs, the data was reformatted and converted to binary code. All redundant and unnecessary information, such as the S_{11} data and the frequency, was removed. The FFT program was modified to read this reformatted data, and all files in use were reformatted.

Analysis of the Dolph-Tchebychev filter was performed. Time sidelobes of -20 dB to -80 dB were tried and target detectability and separation were evaluated. The filter parameters were subsequently set to a -40 dB sidelobe level. This filter was used for essentially all subsequent processing and analysis.

To augment the analysis of the time response data further, the Tektronix time response plotting routine was modified to implement the terminal's joystick cursor as a range finding device. When interrogated by the computer, the joystick cursor displays a set of crosshairs on the display of the terminal, controlled by the attached joystick. When the user has positioned the crosshairs in the desired position, he returns control to the program by typing a character on the keyboard. This returns the coordinates of the crosshairs to the program. The time response plotting routine employed the cursor

UNCLASSIFIED

UNCLASSIFIED

in this fashion. After the time response was plotted, the program would go into the cursor mode. To determine the range of a given feature on the time response plot, the user would position the crosshairs over that feature and request the time associated with the feature and the cursor. When the appropriate command was given, the program would return to normal processing.

As a result of analysis using the Tektronix cursor routine to determine range information, it became desirable that certain features of the time response, such as the location of the ground return, be determined automatically by the program. To satisfy this need, a subroutine was developed to locate the ground return. Extensive observation of the temporal plots suggested that the nature of the ground return was consistent and could be found by an appropriate algorithm. The subroutine located the ground return by searching for the first two positive and negative peaks associated with the ground return, which have consistent and recognizable relative amplitudes. This marked the location of the ground return. The subroutine then located each subsequent crossing of the zero axis of amplitude, and stored the locations of these crossings in an array. This subroutine became the basis of later development of an automatic range gate routine for location of the target information in the time array.

Another CALCOMP plotting routine was added for generating the plots for the first interim report. This routine plots a series of 5 data runs on an 8-1/2 by 11 inch sheet of paper. For each data run, there were three adjacent plots, each 2 by 1-1/2 inches. The first plot consisted of the raw frequency response magnitude, the time response with the range gates marked by vertical

UNCLASSIFIED

UNCLASSIFIED

lines, and the gated frequency response magnitude. Figures found in Appendix A are representative of the format in that report.

Filter Selection

To reduce the number of options from which the user had to select, it was determined that selection of an optimum filtering function had to be made. Hanning, Hamming, and Kaiser window functions were briefly considered along with $\frac{\sin x}{x}$ and various Dolph-Tchebychev filters; however, it was decided that the latter two represented enough variability to select the appropriate function.

The $\frac{\sin x}{x}$ function was used in the initial analysis efforts. The subroutine which performed the actual data weighting allowed the user to specify the center frequency and the bandwidth of the main lobe. The use of a narrower bandwidth permitted inclusion of more of the sidelobes within the frequency extent of the data, producing lower time sidelobes at the expense of time resolution.

Later the Dolph-Tchebychev weighting function was implemented. It has the form $\frac{I_1(x)}{x}$, where I_1 is the modified Bessel function of order one and the argument, x , is defined as follows:

$$x = K \left\{ 1 - \left[\frac{2(f-f_o)}{f_{\max} - f_{\min}} \right]^2 \right\}^{1/2} \quad (4)$$

The constant, K , is related to the desired time sidelobe level by

$$K = \ln(R + \sqrt{R^2 - 1}) \quad (5)$$

UNCLASSIFIED

UNCLASSIFIED

where R is the square root of the reciprocal of the sidelobe level.

Table 4 gives the value of K for the various sidelobe levels studied.

Table 4
DOLPH-TCHEBYCHEV CONSTANTS

| Sidelobe Level <u>Magnitude</u> | <u>dB</u> | <u>R</u> | <u>K</u> |
|------------------------------------|-----------|----------|----------|
| .1 | -20 | 10 | 2.9932 |
| .01 | -40 | 100 | 5.2983 |
| .001 | -60 | 1000 | 7.601 |
| .001 | -80 | 10,000 | 9.9035 |

An example of a Dolph-Tchebychev weighting function is shown in Figure 9.

Range Gate Algorithm Development

When the range gated temporal response was initially generated, the position of the range gate was entered by the computer user by typing in the range based on a priori knowledge of the target position. Subsequently, the location of the range gate was determined interactively by using the cursor mode in the Tektronix display. For large scale processing of data, an automatic range gate placement routine is desired. Several techniques for accomplishing this function were explored before a satisfactory algorithm was generated.

Figure 27 illustrates some of the general conditions which impact the problem of automatically locating the area of target return in a typical temporal plot. For the most part, the time resolution, δt , of the temporal

UNCLASSIFIED

UNCLASSIFIED

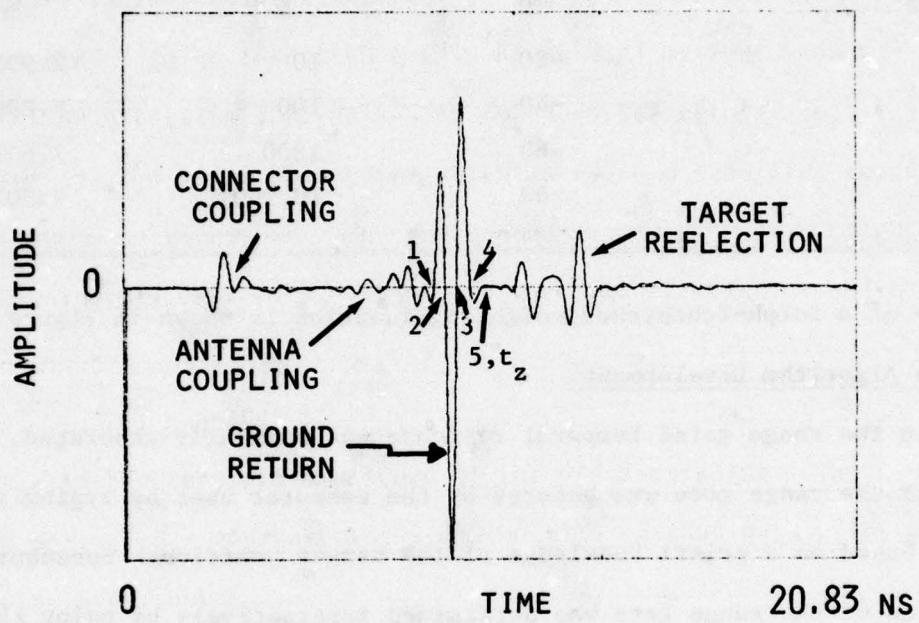


Figure 27. Typical temporal return from a buried land mine.

UNCLASSIFIED

UNCLASSIFIED

data is approximately 0.04 nanoseconds, resulting in a time delay to the n^{th} data point of $n \cdot 0.04$ n in nanoseconds. The first data of interest occur at about 3 nanoseconds, resulting from coupling of the transmitted signal from the transmit antenna coaxial connector to that on the receive antenna. This signal component does not affect the target return and can therefore be disregarded. The next significant component occurs at approximately 9 nanoseconds and is actually a combination of the coupling from the transmit antenna to the receive antenna and the reflection from the surface of the ground. This region exhibits the characteristic positive-negative-positive sequence which is located by the analysis program and identified as the ground return.

Since the ground return necessarily precedes the return from a target buried below ground level, the time associated with the ground return provides a lower limit on the position of target information. In particular the ground return can, with some confidence, be associated with four amplitude peaks, alternating in sign, or equivalently, five zero-crossing points. The end of the ground return can thus be defined to be the time $t_z = 0.04 n_z$, of the first data point occurring after the fifth zero-crossing of the ground return. The time t_z can then be used as a lower bound when determining the target near-range gate.

The last significant, and most important, feature of the temporal data shown in Figure 27 is that resulting from reflections from a buried object. For the data used in these analyses, no target was buried deeper than 6 inches below the surface of the ground, and primary target reflections could not be

UNCLASSIFIED

UNCLASSIFIED

seen in the data past delays of approximately 16 nsec, the 400th data point. Therefore, the search for near and far time gates could be confined to the interval (t_z , 16 nsec).

The development of an automatic range gate technique was based on the supposition that, if a target is present in this data, it should manifest itself as a recognizable deviation from a background level. At least in the drier soils, the presence of a target should cause the amplitude of the reflected signal to be larger than this background by some amount. The first attempt at an algorithm for the search for a target return limit was effected by determining the first data point which exceeded a specified threshold value as shown in Figure 28. The background level, y_{bkgd} was calculated to be the mean value of forty data points past the time of any known target return:

$$y_{bkgd} = \frac{1}{40} \sum_{n=400}^{439} |y_n| \quad (6)$$

where $|y_n|$ is the absolute amplitude of the n^{th} data point. The time of the far time gate, t_{far} , was calculated as the time of that data point y_n first encountered such that

$$(y_n) \geq 4y_{bkgd}, \quad n = 400, 399, 398, \dots, n_z. \quad (7)$$

Likewise the time of the near time gate, t_{near} , was calculated as the time of that data point y_n first encountered such that

$$(y_n) \geq 4y_{bkgd} \quad n = n_z, n_{z+1}, n_{z+2}, \dots, 400 \quad (8)$$

UNCLASSIFIED

UNCLASSIFIED

If no such points could be located which satisfied either criterion, default time gate limits became either t_z or 16 nsec, as appropriate.

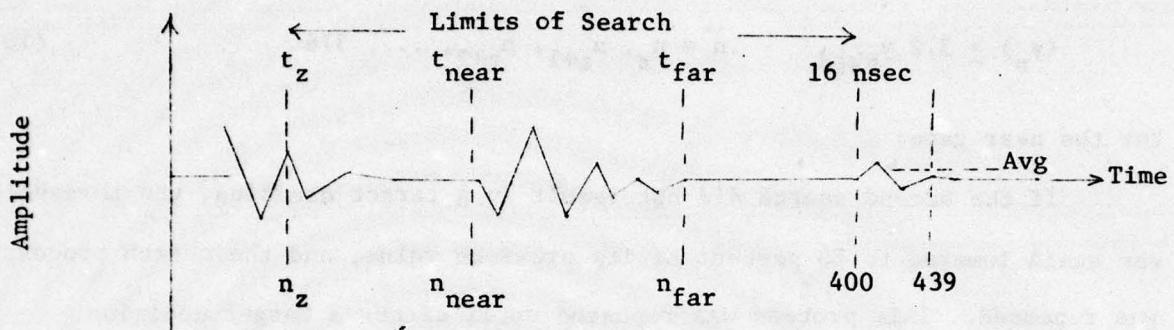


Figure 28. Non-adaptive Threshold Algorithm.

When this automatic gating algorithm was implemented, several shortcomings became apparent. Although a multiplicative factor of 4 was a viable parameter in dry soil conditions most of the time, targets did not always faithfully exceed the background level by the required amount, particularly in moist soil. If this margin between background level and threshold were lowered to accommodate the moist soil conditions, false alarms occur, causing the placement of the gate to stray.

To alleviate this problem, the basic decision mechanism was modified to include provision for an adaptive threshold level. During the initial attempt to locate the time gates, a threshold level equal to 4 times y_{bkgd} would be used, where the background level y_{bkgd} was calculated as previously. Rather than define default gate values if no target decision was made, as

UNCLASSIFIED

UNCLASSIFIED

had been done before, the threshold value was lowered to 80 percent of its previous value and the process renewed. The second search criteria became

$$(y_n) \geq 3.2 y_{\text{bkgd}} \quad n = 400, 399, 398, \dots, n_z + 24 \quad (9)$$

for the far time gate and

$$(y_n) \geq 3.2 y_{\text{bkgd}} \quad n = n_z, n_{z+1}, n_{z+2}, \dots, 376 \quad (10)$$

for the near gate.

If the second search did not result in a target decision, the threshold was again lowered to 80 percent of its previous value, and the search process was repeated. This process was repeated until either a target decision was made or the threshold finally became less than the average background level y_{bkgd} . In the latter case, the appropriate default time gate would be used. To prevent the gates from becoming too close to one another, the far gate would be defined first and the near gate would have to meet the decision criterion and occur at least 24 data points prior to the far gate. (Restricting the far gate to the interval $[n_z + 24, 400]$ prevents the obvious contradiction in location requirements.)

The implementation of such an adaptive threshold resulted in a much improved target detection rate; however, it was noted that this technique was overly sensitive to randomly occurring spikes in the data above the threshold level. In an effort to alleviate this sensitivity, the adaptive threshold scheme was modified so that multiple detections above the threshold would be required to set a time gate.

UNCLASSIFIED

UNCLASSIFIED

Two ways of accomplishing this requirement were investigated: (1) two successive data point detections for gate placement (n and $n-1$), and (2) two detections out of three successive data points (n and $n-1$, n and $n-2$, or $n-1$ and $n-2$) would be required. The performance resulting from the use of two successive target decisions was somewhat superior to that of single detection, while using two out of three resulted in excessive time differences between near and far time gates.

Of all of these techniques which employed straight amplitude thresholds for decisions in setting gates, that which employed two successive decisions against an adaptive threshold was the most effective. However, the level of performance was considered to be far from that which could be obtained by manually setting both gates upon inspection of the temporal data.

In the hope that a more effective automatic technique could be found, a different attack on the problem was sought.

To desensitize the detection algorithm to random spikes in the background data, sliding window averaging was utilized on the absolute value of the amplitude versus time data. This type of averaging accomplishes two things: (1) it suppresses those "spikes" in the data which have short extent (in time) and (2) it enhances the desired signal with respect to an average background level.

The absolute values of the amplitude data (y_n) were averaged using sliding window widths of 13 and 21 points wide in separate tests. A new array was thus created via the relationship

$$y_n = \sum_{m=n-10}^{m=n+10} (y_m), \quad n = n_z + 2, n_z + 3, \dots, 400 \quad (11)$$

UNCLASSIFIED

UNCLASSIFIED

for the 21-wide case or the relationship

$$y_n = \sum_{m=n-6}^{m=n+6} (y_m), \quad n = n_z + 2, n_z + 3, \dots, 400 \quad (12)$$

for the 13-wide case. Note that the averaging was undertaken only between the appropriate end of the ground return and the maximum range of interest, 16 nanoseconds.

A typical plot of the smoothed data y_m is shown in Figure 29. Averaging over 21 data points proved to be superior to that over 13 in terms of amplitude trends for target location identification. The "center" of the target is defined to be that data point at time t_{center} corresponding to the largest member y_{max} of the smoothed array. Thus the largest reflected average signal is construed to be the target.

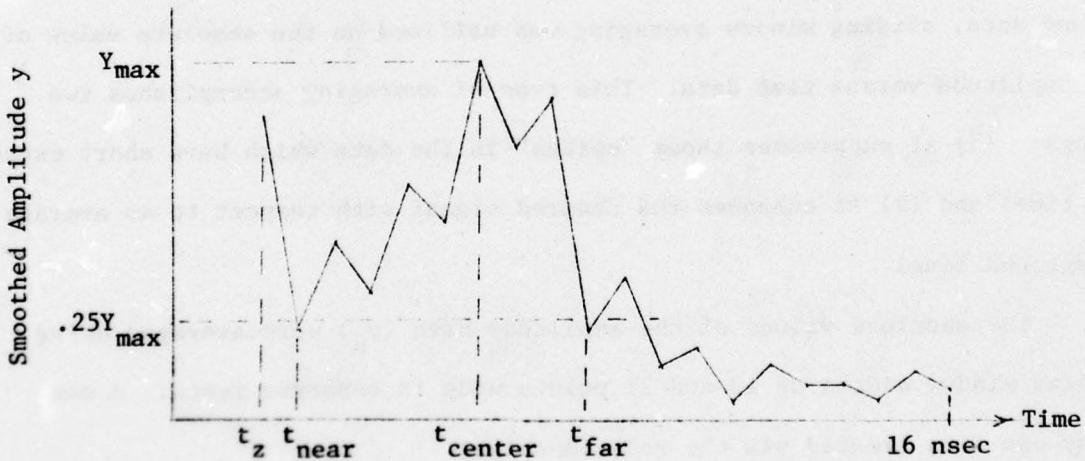


Figure 29. Smoothed Data Array y.

UNCLASSIFIED

UNCLASSIFIED

The temporal extent of the target return is determined by locating the closest local nulls in the smoothed array y_n on either side of the center point at time t_{center} . By observation, these nulls indicate the actually observed target signal boundaries under the following restrictions:

- (1) The values of the nulls of the smoothed data $y(t_{near})$ and $y(t_{far})$ must be less than .25y(max).
- (2) Each null must be located at least 12 time divisions (.48 nanoseconds) from the center of the target return, so that the entire target extent must be at least 24 time units (.96 nanoseconds) long.
- (3) If a null value of the smoothed array cannot be determined, the time gates are placed at the end of the ground return t_z or at 16 nanoseconds, as appropriate.

The operation of this computerized algorithm appears to be similar to manually selected range gates, with few exceptions. It is adequate to produce the range gates for analyzing large quantities of data, but there are some times when the algorithm places the range gate at a less than optimal position.

Removal of Ground Return from Processed Data

The range gate algorithm just described sometimes fails to work properly because of the size of the ground return. When the soil is wet, the return of a buried target is greatly attenuated as compared to the ground return. If a portion of the ground return falls within the time window being searched for the buried target signature, the range gate algorithm is adversely affected.

UNCLASSIFIED

UNCLASSIFIED

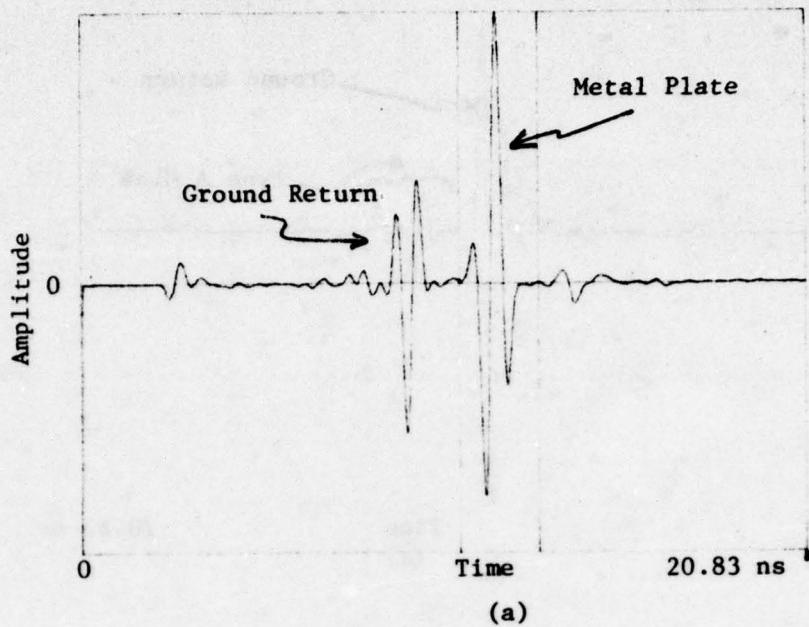
This problem is particularly severe with shallow targets buried at three-inch depths in wet or moist soil. Therefore, a technique to remove the ground return before searching for the target signature was considered and is discussed in the following paragraphs.

When targets of interest are only a few inches below the soil surface, the target return and the ground return overlap in time. To facilitate detection and classification of target returns, it is desirable to remove the overlapping ground return. One way to accomplish this is to record the return from a location where a target is not present and subtract it from the returns obtained in locations where a target of interest may be present. Since measured data exists for areas with and without targets, this scheme was implemented in the data processing program which has been previously described. Since the radar antenna height may change a little with position, the computer program locates the negative peaks of the two ground returns to be subtracted and aligns them by the proper indexing. In addition, the amplitude of the time data is scaled so the amplitude of the two negative peaks are equal. Thus, the subtraction of the two time responses guarantees a zero value where the largest negative peak of the ground return existed.

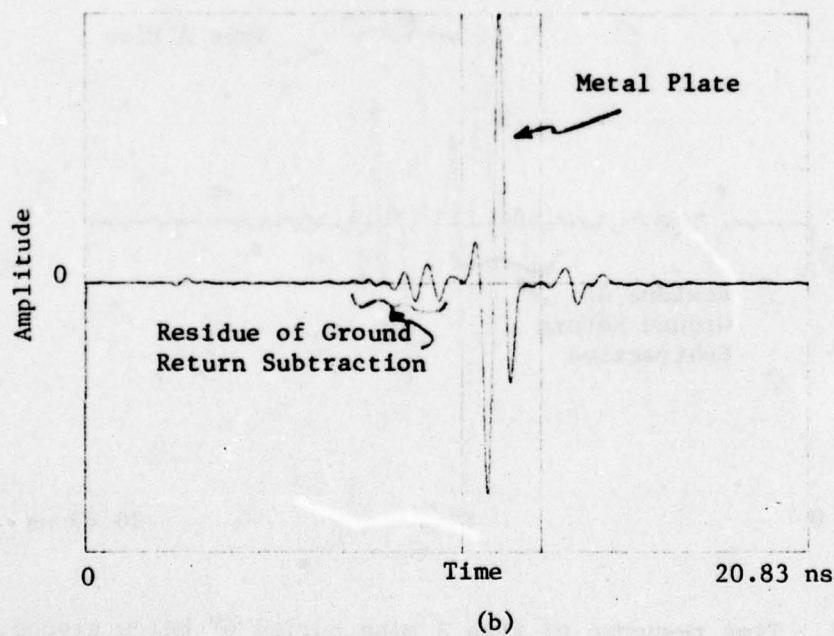
The results are shown in Figures 30 and 31 for two selected cases. In Figure 30, the time response of a metal plate buried 6 inches below the soil surface with and without the ground return present is shown. In Figure 30(b) measured data GT5-65 is subtracted from GT5-68. Note that the subtraction is not perfect. The residue remaining is about 12% of the original peak amplitude shown in Figure 30(a).

UNCLASSIFIED

UNCLASSIFIED



(a)



(b)

Figure 30. Time response of metal plate buried 6" below ground, 7% moisture a.) with ground return present; b.) with ground return subtracted (GT5-65 subtracted from GT5-68).

UNCLASSIFIED

UNCLASSIFIED

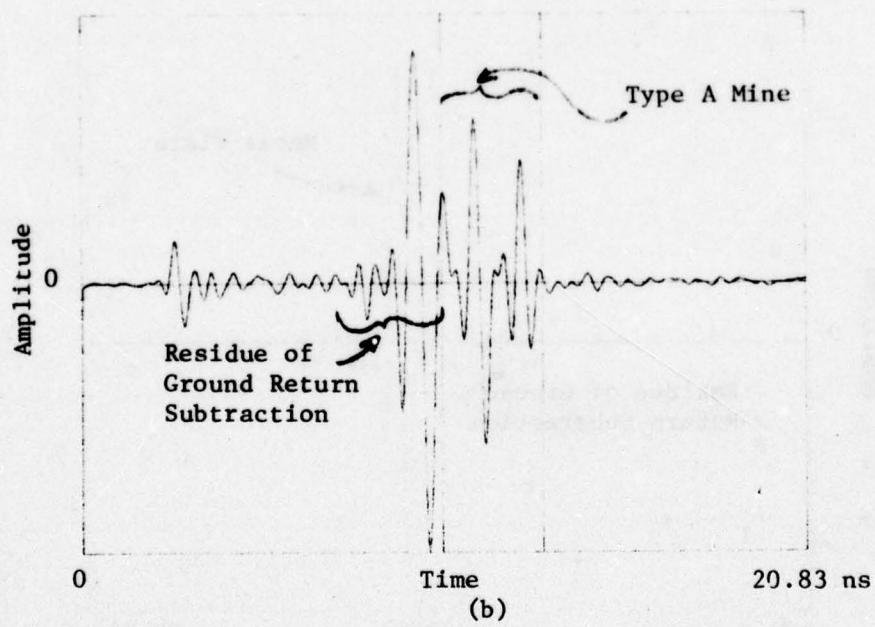
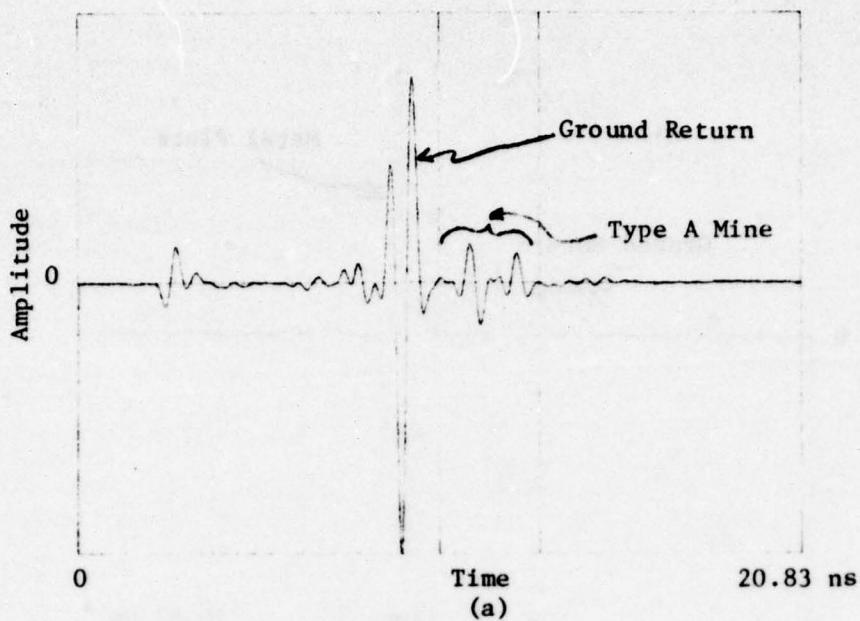


Figure 31. Time response of type A mine buried 6" below ground, 7% moisture (a) with ground return present; (b) with ground return subtracted (GT5-53 subtracted from GT5-56).

UNCLASSIFIED

UNCLASSIFIED

In Figure 31, the time response of the type A mine buried 6" below the ground surface with and without the ground return present is shown. The type A target return is somewhat smaller than the ground return in Figure 31(a). When the ground return is subtracted in Figure 31(b), the remaining time response is scaled by the computer program to fill the figure window. Thus, the type A target return appears larger in Figure 31(b) than in 31(a). If the amplitudes were on the same scale, one would discover that the peak amplitude of the ground subtraction residue in 31(b) is about 20% of the ground return peak amplitude in Figure 31(a).

The results obtained in these two cases are not desirable because the residue is larger than most target returns of interest, especially in wet soil. Hence, the effect of the ground return on shallow targets may still be appreciable. Ways in which to improve the subtraction were sought. It was discovered that one reason the ground returns were subtracting so poorly was the position of the time samples relative to the ground return envelope. The problem is illustrated in Figure 32 where a typical ground return envelope is shown. The ground return is an analog signal sampled in the computer program processing procedure. In the present processing configuration, the sampling period is approximately .041 nanoseconds (41×10^{-12}) seconds) which corresponds to a one way range of 0.5 inch in free space. Since the time position of the samples are fixed, if the antenna height above ground changes by 0.25 inches, the position of the samples relative to the analog envelope changes by one-half sample period as shown in Figure 32(b). If, for example, the two ground returns which are subtracted are each sampled as illustrated in Figure 32(a) and (b), the residue will be sizeable. The computer program

UNCLASSIFIED

UNCLASSIFIED

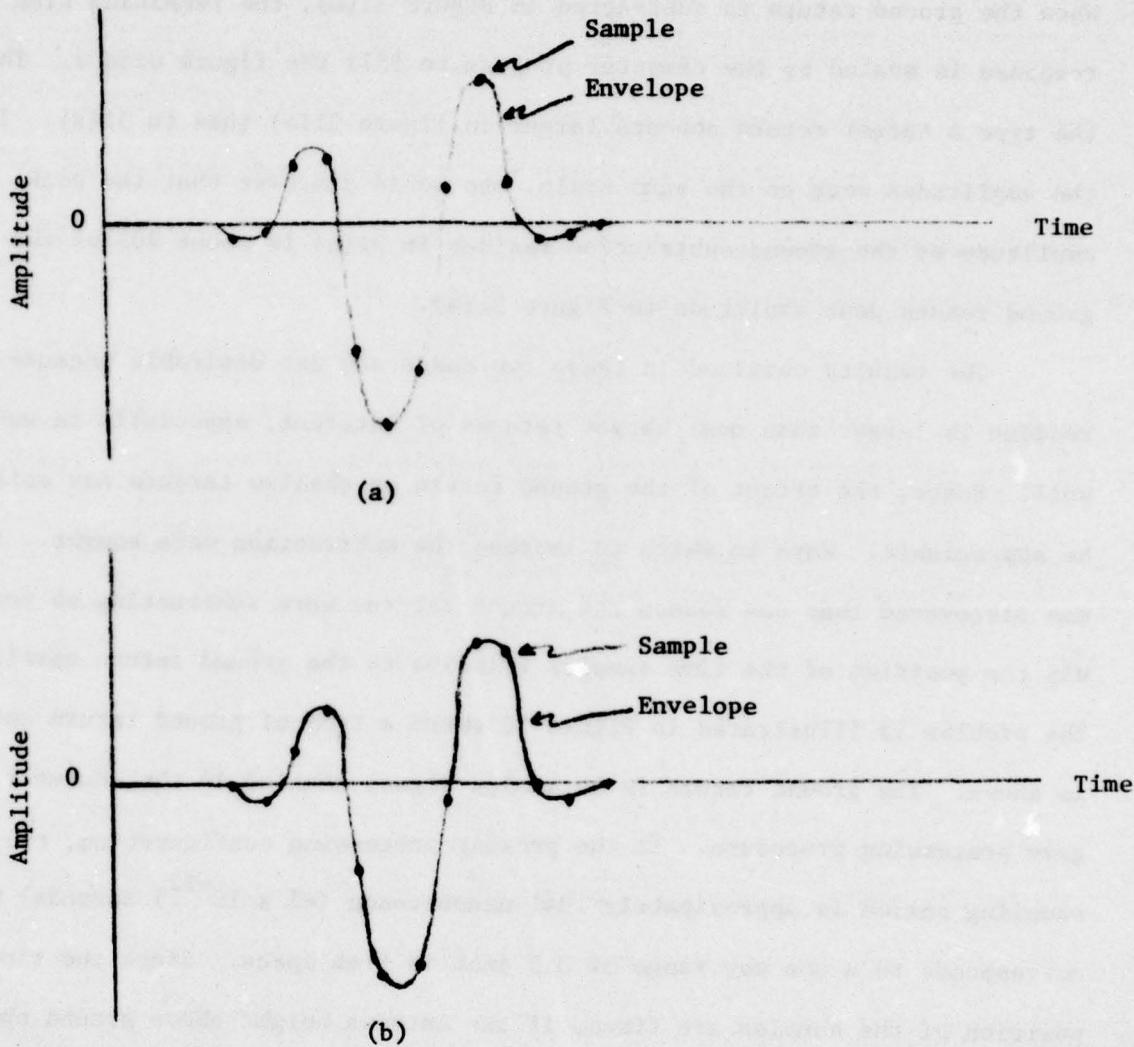


Figure 32. Sampling Position Relative to the Ground Return Analog Envelope. (a) Sampling on Peak Value, (b) Sampling off Peak Value.

UNCLASSIFIED

UNCLASSIFIED

locates the largest sample value in each case, normalizes the two sampled waveforms to have the same maximum value, and then indexes one sampled return relative to the other to align the two maximum samples. Although the maximum values will be aligned, the envelopes will not be. The difference in sampled values near the zero crossing points can be as large as 25% of the peak value.

To alleviate this problem in subtracting the ground return, the measured data with the ground return only (no target present) is modified to reposition the analog envelope relative to the sampling points. This is accomplished by introducing the appropriate linear phase slope in the measured frequency data. The results of this modification to the subtracting procedure is shown in Figure 33 where measured data GT5-71 is subtracted from GT5-74 (type B mine buried 6", 7% moisture). The time responses of these two records are shown in Figure 34 where they have been aligned in time and overlayed on the same plot. Note that the amplitude scale is the same for both Figures 33 and 34.

The subtraction residue is still quite large, about 12% of the ground return peak amplitude. A close observation of the two overlayed waveforms in Figure 34 indicates why. Note that the trailing edges of the two ground returns are significantly different and are the source of the largest part of the residue in Figure 33. Since the type A mine is 6" below the ground surface and is well separated in time from the ground return, this difference cannot be attributed to the type A target time response. It was thought that perhaps the difference was due to the presence of a small rock near the surface of measurement GT5-71. To explore this possibility, another nearby

UNCLASSIFIED

UNCLASSIFIED

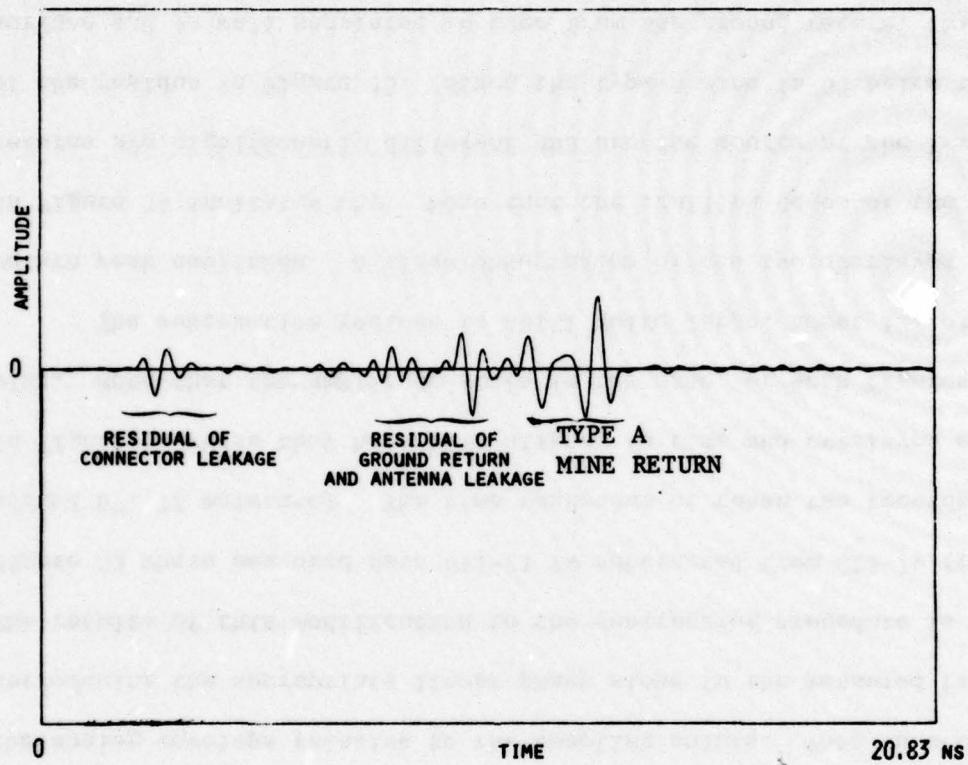


Figure 33. Measured Data. Time response of type A mine buried 6" below ground, 7% moisture--with ground return subtracted--GT5-71 subtracted from GT5-74.

UNCLASSIFIED

UNCLASSIFIED

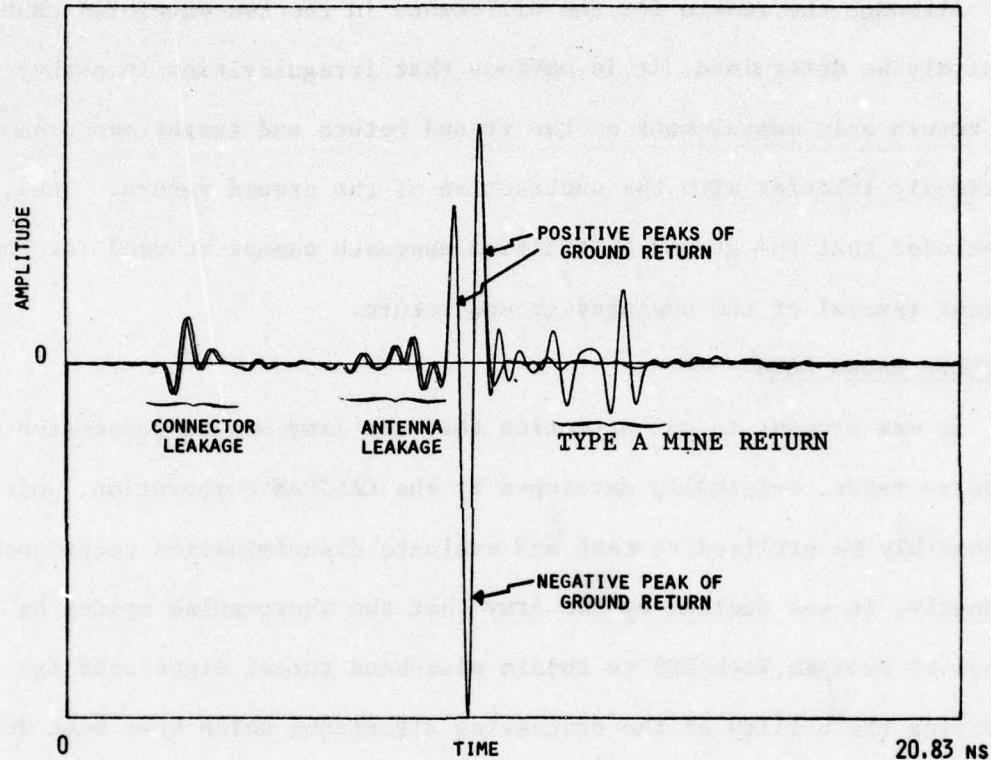


Figure 34. Measured Data. Time response of type A mine buried 6" below ground, 7% moisture--GT5-74. Also time response of adjacent ground without target--GT5-71.

UNCLASSIFIED

UNCLASSIFIED

ground return only measurement, GT5-77, was compared to GT5-71 by plotting both curves on the same plot as given in Figure 35. As will be noted, these two time responses track each other very closely. The only remaining explanation is that there was some irregularity near the soil surface in measurement GT5-74.

Although the reason for the difference in the two waveforms cannot conclusively be determined, it is obvious that irregularities in either the ground return only measurement or the ground return and target measurement can seriously interfere with the subtraction of the ground return. Thus, it was concluded that the ground subtraction approach cannot be used for the consistent removal of the unwanted ground return.

SHORT-PULSE RADAR DATA

It was brought to our attention that the Army was in possession of a short-pulse radar, originally developed by the CALSPAN Corporation, which could possibly be utilized to test and evaluate discrimination techniques. Subsequently, it was decided by the Army that the short-pulse system be used as a tool by Georgia Tech/EES to obtain wide-band target signatures for use in verifying the utility of the processing algorithms which have been developed by Georgia Tech with the Hewlett-Packard network analyzer. The availability of this system, which develops a wide-band transmitted pulse (approximately 1.1 ns) was valuable in the natural follow-on efforts involved with developing actual signal processing algorithms for target discrimination. By virtue of the wide spectrum of the transmitted pulse, this system represented the analog hardware implementation of the FFT technique used to synthesize time domain data in the previous work. With this system, the hardware exists which allowed

UNCLASSIFIED

UNCLASSIFIED

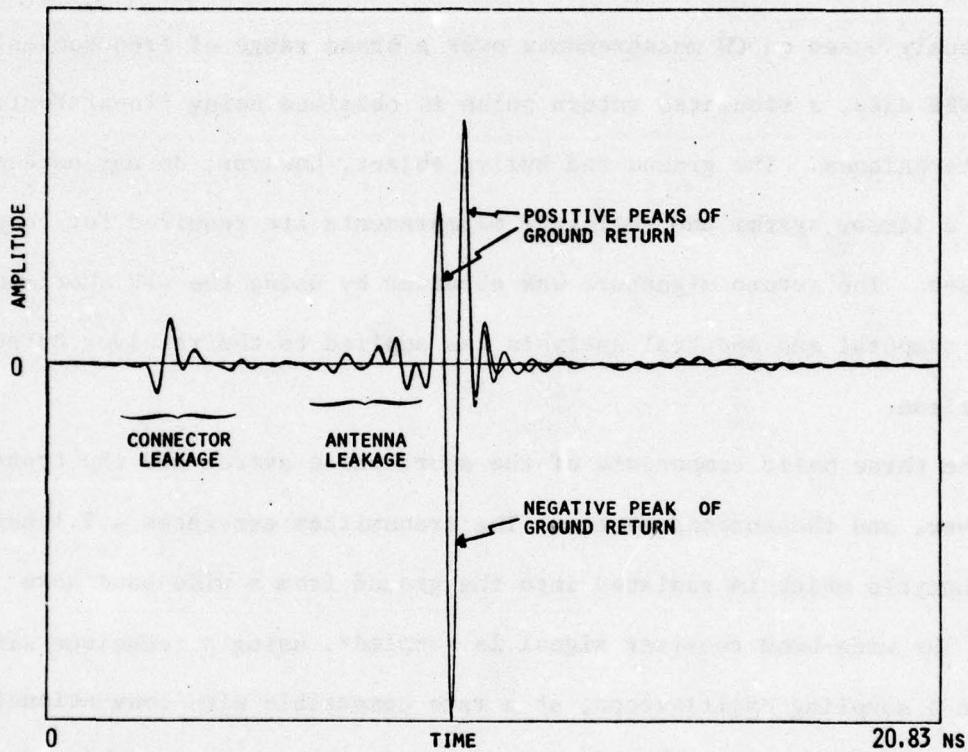


Figure 35. Measured Data. Time responses of ground without target--GT5-71 and GT5-77 (ground areas adjacent to type C mine).

UNCLASSIFIED

UNCLASSIFIED

us to obtain time domain data directly. The radar was used to derive the signatures which were recorded on magnetic tape and read into the CYBER 74 computing system at Georgia Tech for synthetic processing as illustrated in Figure 26. The outputs from the radar were made compatible with the Georgia Tech analysis tools and computer programs. The primary objective and emphasis of these radar measurements were to verify the computerized analysis which was previously based on CW measurements over a broad range of frequencies. With the NBS data, a simulated return pulse is obtained using linear Fourier analysis techniques. The ground and buried object, however, do not necessarily represent a linear system and realistic measurements are required for comparison purposes. The return signature was obtained by using the GFE short-pulse radar and temporal and spectral analysis was applied to the receiver output for comparison.

The three basic components of the short-pulse system are the transmitter, the receiver, and the antenna system. The transmitter generates a 1.1 nanosecond monocyte which is radiated into the ground from a wide-band horn antenna. The wide-band receiver signal is sampled*, using a technique similar to that in a sampling oscilloscope, at a rate compatible with conventional oscilloscope displays, conventional laboratory analyzers, or magnetic tape recording systems.

In order to collect the data for use on the CYBER 74 computer, the low frequency analog signals had to be sampled, stored in a random access

*The effect of this sampling is to expand the time response by $10^6:1$. Thus, the 1.1 nanosecond pulse appears on the radar output as a 1.1 millisecond analog pulse.

UNCLASSIFIED

memory (RAM) and transported from out-of-doors where the measurements were taken to a magnetic tape recorder inside an adjacent building. The digital data was then placed on magnetic tape in a format so as to be compatible with the CYBER 74. The following paragraphs describe some of the hardware and software that was developed to provide data compatible with the computer programs previously developed for the NBS data.

Design and Construction of the Event Recorder

The design and purpose of the portable event recorder is to allow the sampling, digitizing, and storing of an electrical event or return, usually measured from some reference time or marker. In our application, the reference mark was the range gate signal, available from the radar control console. The event recorder sampled the gated video beginning at the range gate mark at a 75 KHz rate, converted the analog video signal to eight bits to form a sign plus magnitude binary word. This sampling/digitizing process continued for approximately 7.0 msec. or until 512 words had been recorded in the RAM. This comprises the "WRITE" mode of operation. The event recorder may then be switched to battery power, unplugged and transported for up to 30 minutes without jeopardizing the recorded data.

This capability greatly simplifies the data-taking process. The "READ" mode is used to transfer the data from memory to a digital tape recorder. Either internal or external clock and TTL or CMOS levels up to 15 VDC may be used to read the data.

The block diagram of the event recorder is shown in Figure 36. As indicated earlier, it is a digital data recorder with associated clocking circuitry.

UNCLASSIFIED

AD-A054 427

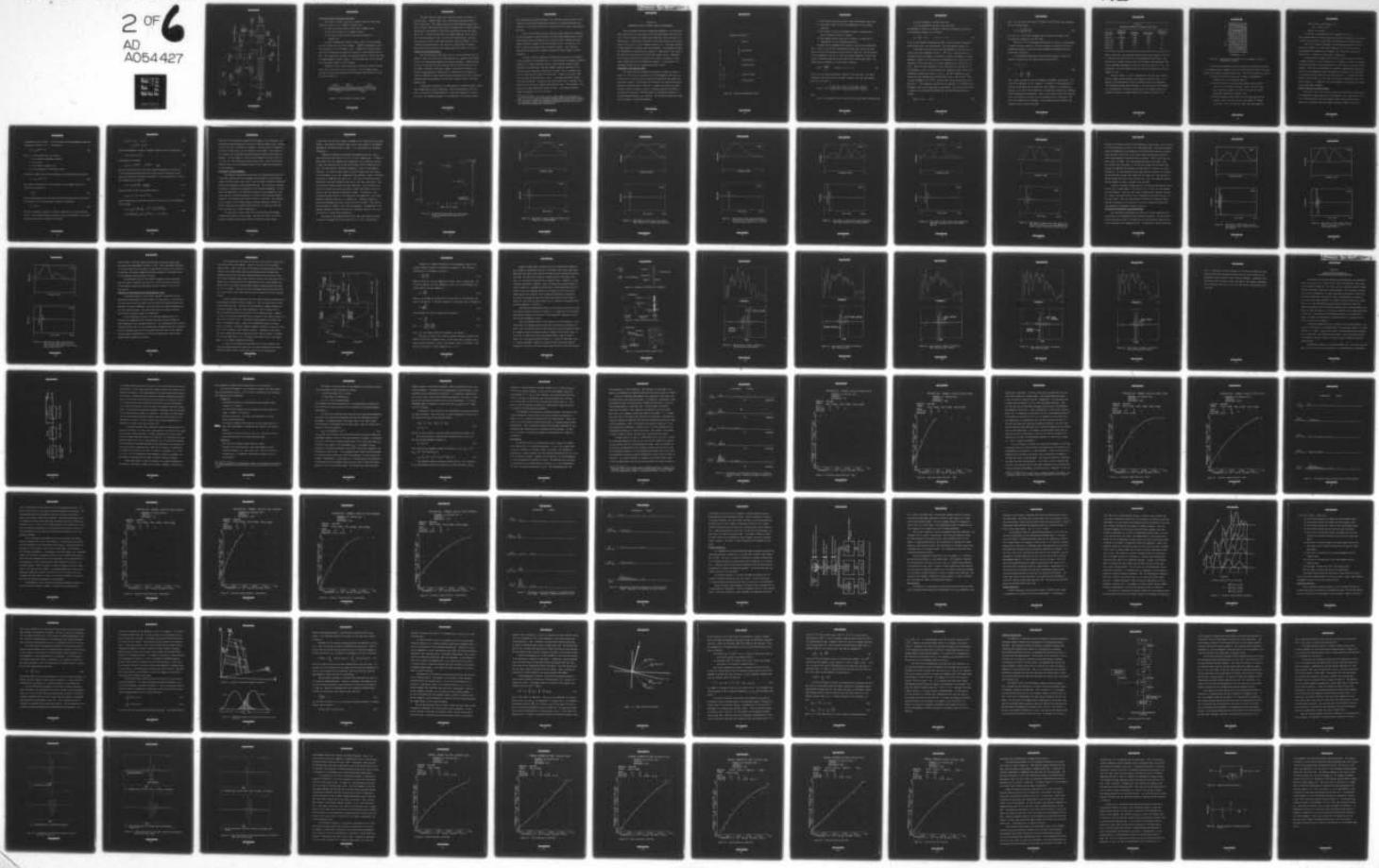
GEORGIA INST OF TECH ATLANTA ENGINEERING EXPERIMENT --ETC F/G 17/9
RADAR DETECTION, DISCRIMINATION, AND CLASSIFICATION OF BURIED N--ETC(U)
FEB 78 J D ECHARD, J A SCHEER, E O RAUSCH DAAG53-76-C-0112

UNCLASSIFIED

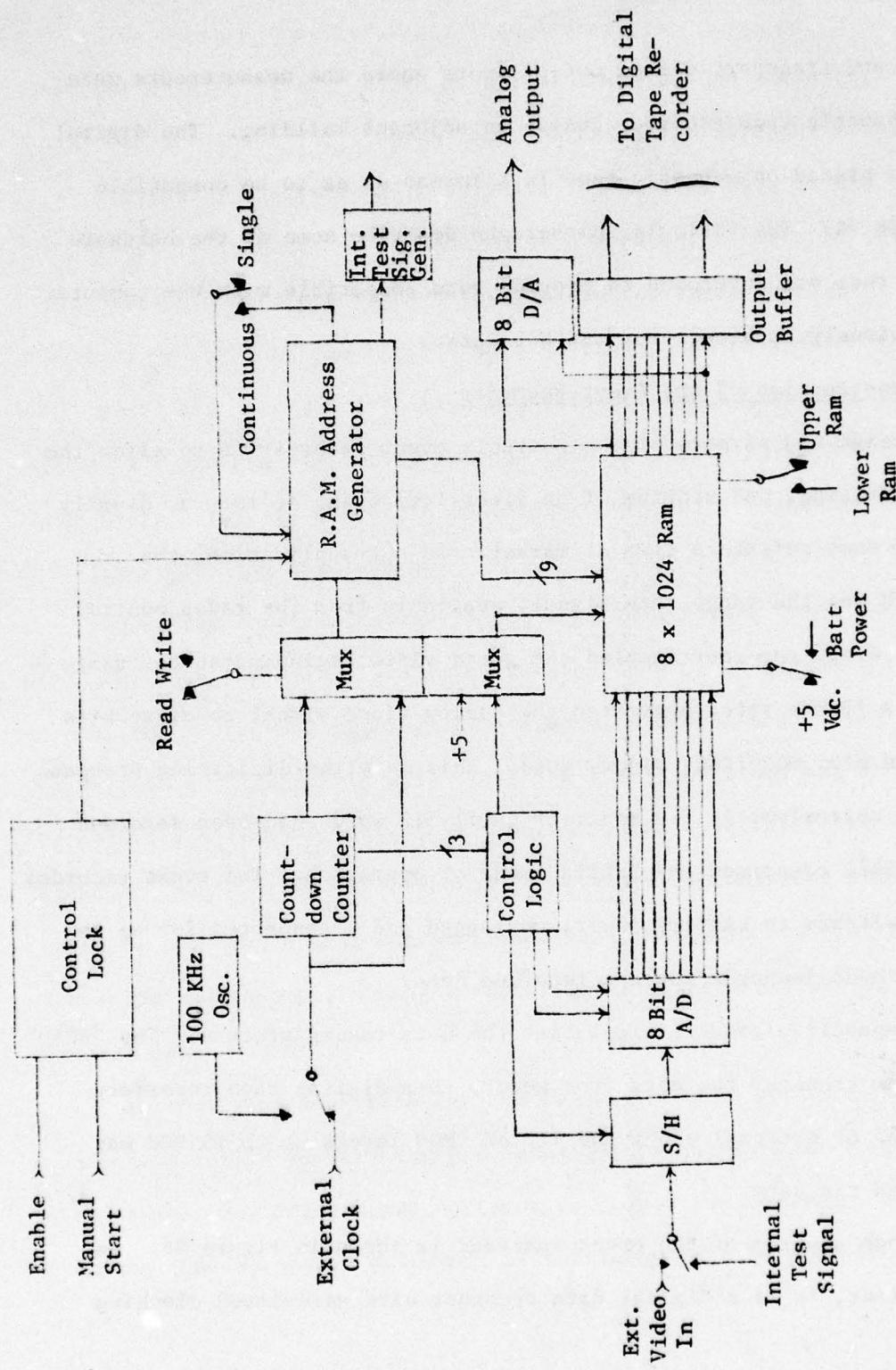
2 of 6
AD
A054427

EES/GIT-A-1828-F-VOL-1

NL



UNCLASSIFIED



UNCLASSIFIED

Figure 36. Block diagram of event recorder.

UNCLASSIFIED

Generating Computer Compatible Data Tapes

After data is stored in the event recorder, there are three steps required to convert it to a CYBER 74 computer file:

- (1) Data is read from event recorder onto a magnetic tape.
- (2) The tape is taken to the computer center.
- (3) The tape is mounted and read and then converted to a useable form.

A special program named "INTAPE" reads a binary file and separates the data in that file into 8-bit integers. "INTAPE" is designed to read a file assigned to a 9-track magnetic tape. "INTAPE" will read the entire input file and determine how many 8-bit integers could be packed into that file. The program then calculates the greatest power of 2 that is less than the maximum number of 8-bit integers. The resulting power of 2 is assumed to be the desired number of 8-bit integers.

"INTAPE" is used to read a tape which contains 8-bit bytes recorded across the 9 tracks (one track is for parity). As the computer reads the tape, the bytes are packed into central memory (CM) with 60 bit words as shown in Figure 37.

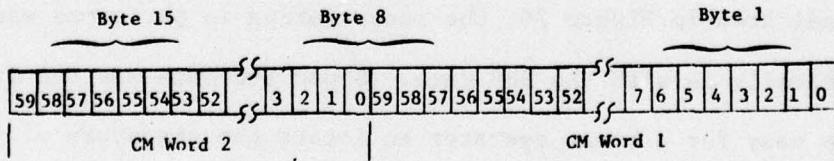


Figure 37. Byte packing on computer tape.

UNCLASSIFIED

UNCLASSIFIED

The 8-bit bytes fit evenly into consecutive pairs of CM words, 15 bytes per word. "INTAPE" takes a pair of CM words and converts them to the 15 8-bit bytes. The program looks at the first word and extracts the first 7 bytes by shifting the word until the desired byte is right-justified. The CM word is then masked or "And" with a word which has only the right 8-bits set. To obtain the 8th byte, the program takes the last 4 bits of the first CM word and the first 4 bits of the second CM word. These two 4-bit words are "Or'ed", then right-justified. Bytes 9 through 15 are obtained by a process similar to the one used to obtain bytes 1 through 7. These 8-bit bytes are stored in an integer array with values of 0 to 255.

Computer Processing Development

Once the short-pulse radar data were in a format compatible with the CYBER 74, then the data files were operated upon by a program called "FREQ" to plot the corresponding temporal and spectral responses. Simply plotting the data in each data file will yield the time plot since the data out of the radar is already in this form. However, the spectral response is obtained by range gating the temporal data to include only the signature of interest, removing a constant amplitude bias introduced by the A/D conversion processing and then performing a Fast Fourier Transform (FFT) on the gated temporal data.

As indicated in Figure 26, the range gating is performed manually rather than automatically as with the NBS data. Since the data was for dry soil only, it was easy for a human operator to locate the signature of interest. Of course, the automated placement of the range gate is preferred; however,

UNCLASSIFIED

UNCLASSIFIED

the range gating algorithm developed for the NBS data would not work for the short-pulse data without modification because the transmitted waveform was different. Time did not allow such a modification; thus, manual range gating was used.

In the A/D conversion process, the input analog signal was represented on the A/D converter output by 8-bits--an output scale ranging from 0 to 255. Thus, negative input voltages as well as positive input voltages are represented by positive numbers on the A/D converter output. Effectively, a DC bias of 128 has been added by this conversion process. This offset was removed before plotting the temporal response and before taking the Fourier Transform.

The gated spectral responses so obtained are utilized by the classification programs to be described later. It was important to generate a spectral response in a format compatible with the classification programs already developed for the NBS data. The NBS frequency response consisted of 128 lines which were separated by multiples of 24 MHz. Thus, a frequency span of 0 to 3.048 GHz was covered by the 128 lines. However, only every forth line was used for classification. Thus, the frequency separation between lines used was 96 MHz. To make the short-pulse data yield a comparable line spectra, only every third temporal data point was used. This provided a line spectra with line separations of about 104 MHz. The resulting spectrum spanned frequencies from 0 to 3.33 GHz.*

* As explained earlier, the radar receiver output signals are expanded by a ratio of $10^6:1$ by a special sampling technique within the short-pulse radar. Thus, the output signals are actually at millisecond and KHz rates. However, for comparison purposes, the unexpanded frequencies and times are used in this discussion (nanoseconds and gigahertz).

UNCLASSIFIED

UNCLASSIFIED

SECTION IV

MATHEMATICAL MODEL OF BURIED TARGET AND ENVIRONMENT

When the measured data was processed and examined, it was noted that radar returns from the same target at the same depth varied with soil moisture. Since consistency in target return signatures seemed lacking in the measured data, a generalized mathematical model was developed for the metal plate and the type A, B, and C targets buried in soil. This model provided an understanding of the target and the environment. The mathematical model was programmed on a general purpose computer to yield plots of the temporal and spectral characteristics of various type target returns. Parameters such as target depth and soil moisture were varied, and changes in target return characteristics were observed and compared. A discussion of the mathematical model and its describing equations follows.

DEVELOPMENT OF MATHEMATICAL MODEL

The target and its surrounding environment is modeled as shown in Figure 38. The source and receiver of the electromagnetic (EM) waves are located above the ground, and the waves are directed into the ground by an appropriate antenna. The EM waves are reflected by the ground surface and dielectric discontinuities in the soil. A target may consist of several different layers of material, each of a different dielectric constant, as illustrated in Figure 38. The model shown is deliberately simplistic so the describing mathematics are tractable. The following simplifying assumptions are made in the model development:

UNCLASSIFIED

UNCLASSIFIED

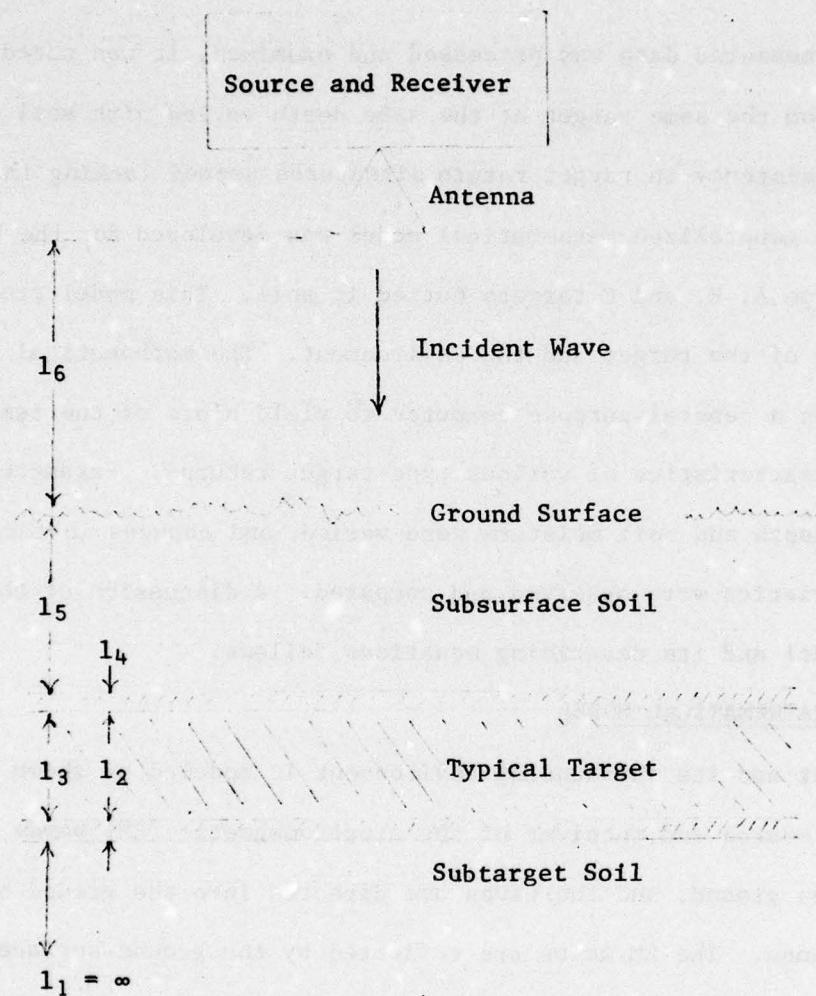


Figure 38. Target and Environment Model.

UNCLASSIFIED

UNCLASSIFIED

- (1) The incident waveform consists of many monochromatic plane waves.
- (2) The ground surface is flat and perpendicular to the incident wavefront.
- (3) The target is totally represented by layers of material each with a different dielectric constant.
- (4) The boundary between each layer is infinite in extent and is perpendicular to the incident EM wavefront.

The model can be mathematically equated to an N-section transmission line. There is a one-to-one correspondence between each section of transmission line and each dielectric region layer in Figure 38. As each section of the transmission line has its own characteristic impedance, so does each region or medium through which the EM wave passes in the target model. The characteristic impedance of the ith layer is given by

$$Z_o(i) = \frac{376.82}{\sqrt{\epsilon_i}} \quad \text{ohms; } i = 1, 2, \dots, N \quad (13)$$

where ϵ_i is the relative dielectric constant of the ith layer. The input impedance of the ith layer (at the upper surface of the layer and looking down into the layer) is

$$Z_{in}(i) = Z_o(i) \left[\frac{Z_L(i) \cosh (\gamma_i \ell_i) + Z_o(i) \sinh (\gamma_i \ell_i)}{Z_o(i) \cosh (\gamma_i \ell_i) + Z_L(i) \sinh (\gamma_i \ell_i)} \right] \quad (14)$$

where

$Z_L(i)$ is the impedance seen at the bottom of the ith layer (looking down),

UNCLASSIFIED

UNCLASSIFIED

ℓ_i is the thickness of the i^{th} layer, and

γ_i is the propagation constant of the i^{th} layer.

The propagation constant is related to free space wavelength (λ_0) and relative dielectric constant (ϵ) as follows:

$$\gamma_i = j \frac{2\pi}{\lambda_0} \cdot \sqrt{\epsilon_i} ; \quad i = 1, 2, \dots, N \quad (15)$$

In all of the equations describing the model, the first layer is assumed to be the bottom layer. The second layer is the next highest region, etc.

In Equation (14) given above, the load impedance of the i^{th} layer is equal to the input impedance of the $(i - 1)^{\text{th}}$ layer. Since the first or bottom-most layer is assumed to be infinite in depth or thickness, its input impedance is equal to its characteristic impedance, $Z_0(1)$. Thus, the load impedance of the second layer is the input impedance of the first layer, or $Z_0(1)$. Also, the input impedance of the second layer is a function of its load impedance, $Z_0(1)$, its own characteristic impedance, $Z_0(2)$, and its own propagation constant and length, γ_2 and ℓ_2 . The input impedance, $Z_{in}(2)$, becomes the load impedance for the third layer, $Z_L(3)$, and so forth. Thus, the input impedance to the N^{th} or top-most layer can be determined by use of Equation 14. This impedance characterizes the response of the incident electromagnetic wave to the target and its environment. The reflected EM spectrum is related to the transmitted spectrum and the reflection coefficient as follows:

$$S_R(f) = \rho(f) \cdot S_T(f) \quad (16)$$

UNCLASSIFIED

UNCLASSIFIED

where the reflection coefficient is related to the N^{th} layer input impedance in the following manner:

$$\rho(f) = \frac{Z_{in}(N) - Z_S}{Z_{in}(N) + Z_S} \quad (17)$$

The term, Z_S , is the source impedance and is assumed to be equal to the characteristic impedance of the N^{th} layer.

Note that all of the equations derived thus far are for a monochromatic or single frequency wavefront. For each frequency or spectral line of the transmitted spectrum, a particular input impedance and complex reflection coefficient is obtained.

If the medium through which the EM wavefront passes is lossy, the dielectric constant will be complex valued as given below:

$$\epsilon = \epsilon_R - j \epsilon_I$$

or

(18)

$$\epsilon = \epsilon_R \left[1 - j \frac{\epsilon_I}{\epsilon_R} \right]$$

where ϵ_R and ϵ_I denote the real and imaginary components, respectively. The ratio of the imaginary to real component is a measure of the attenuation of EM waves in the medium and is called the "loss tangent" of the dielectric material. The value of both components of a dielectric constant is a function of both frequency and temperature. After a brief search, very little information on the dielectric constant of dry and moist soil as a function of frequency and temperature was obtained. The information given in Table 5 was obtained from the sources indicated.

UNCLASSIFIED

UNCLASSIFIED

Table 5
DIELECTRIC CONSTANT OF VARIOUS TYPES OF SOIL

| <u>Soil Type</u> | <u>Degree of Moisture</u> | <u>Frequency</u> | <u>Temperature</u> | <u>Dielectric Constant</u> |
|------------------|---------------------------|------------------|--------------------|----------------------------|
| Sand [3] | Dry | 1 MHz | 20°C | 2.5 |
| Sand [3] | 15% Water | 1 MHz | 20°C | 9 |
| "Soil" [3] | Dry | 1 MHz | 20°C | 3 |
| "Soil" [3] | Moist | 1 MHz | 20°C | 10 |
| Earth [4] | Dry | --- | -- | 5 |
| Earth [4] | Wet | --- | -- | 10 |

Table 5 leads one to the conclusion that the dielectric constant of dry soil at 1 MHz and 20°C varies from 2.5 to 5 depending on the soil type. Also, the dielectric constant for wet soil at the frequency and temperature indicated is somewhat independent of soil type and has a value of 9 or 10. Unfortunately, the cited references did not give any information on the loss tangent for soil.

There is, however, a lot of information on the dielectric constant and loss tangent versus frequency and temperature for pure water. [5] A summary of this information is given in Figure 39 and by the statement, "For frequencies between 300 and 3,000 mc, the power factor (loss tangent) at any temperature is linearly proportional to the frequency, while the dielectric constant is slightly higher at the lower frequencies." [6]

UNCLASSIFIED

UNCLASSIFIED

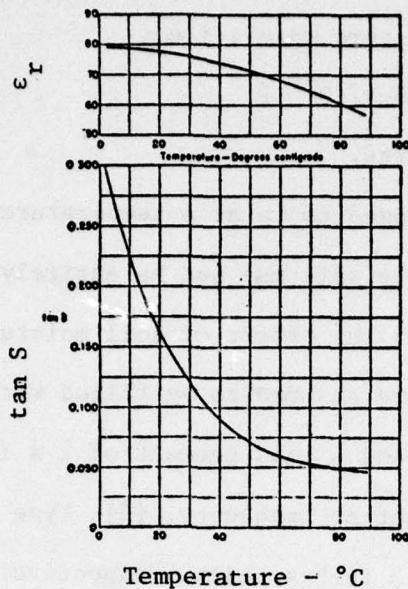


Figure 39. The dielectric constant and loss tangent of water at a frequency of 3,000 mc.

To exercise the mathematical model, assumptions concerning the dielectric constant and loss tangent of soil of various moisture contents were made based on the meager information given above. The soil was modeled as follows:

- (1) The real part of the dielectric constant is independent of frequency for all soil moisture levels.
- (2) The real portion of the dielectric constant varies linearly from 3 to 10 with moisture content. Thus, a dry soil would have a dielectric content of 3 while a very wet soil (30%) would have a dielectric constant of 10.
- (3) The loss tangent varies linearly with frequency and moisture content. For a very dry soil, the loss tangent is assumed to be zero. For a very wet soil (30%), the loss tangent is

UNCLASSIFIED

UNCLASSIFIED

taken as that of pure water; i.e.,

$$\tan \delta = 0.06 \times 10^{-9} f$$

where f is in hertz.

(4) The soil was assumed to be at a temperature of 20°C.

These characteristics for the soil may not be entirely accurate but will serve to provide some insight into the effect of soil moisture on target returns.

Type A and C mines are assumed to be filled with paraffin wax with a dielectric constant of 2.2 and a loss tangent of 2×10^{-4} , both of which are approximately independent of frequency. [5] Type A and C targets are assumed to be 5 inches and 3 inches thick, respectively.

The model shown in Figure 38 will yield a ground reflection as well as a target reflection. In some instances it is desirable to remove or eliminate the ground reflection so the characteristics of the target can be more clearly examined. This can be accomplished with the model by assuming the source and receiver of electromagentic waves are immersed in a medium of the same dielectric constant and loss tangent as the subsurface soil. Of course, the appropriate electric length, ℓ'_6 , will have to be used to simulate the actual electrical length, ℓ_6 . In addition, the source impedance is assumed to be matched to the environment impedance.

EFFECT OF WET SOIL ON TARGET RETURNS

The effect of wet soil on target returns can be determined qualitatively by considering a simple target and its environment; e.g., a metal plate in wet soil. Also assume that the electromagnetic source and receiver are also immersed in a medium of the same complex dielectric constant as the soil

UNCLASSIFIED

UNCLASSIFIED

surrounding the metal plate. In this situation, the monochromatic plane wave impinging on the metal plate is described by

$$E^+ = E_1 e^{j(wt - \gamma x)} \quad (19)$$

where x is the distance the wave travels,

γ is the complex propagation constant,

t is the time,

w is the radian frequency, and

E_1 is the magnitude of the electric field.

Assuming the metal plate has zero impedance, the reflected wave is given by

$$E^- = -E_1 e^{j(wt + \gamma x)} \quad (20)$$

The reflection coefficient, or the position of the incident wave that is reflected, is defined as

$$\rho = \frac{E^-}{E^+} \quad (21)$$

Substituting Equations (19) and (20) into the above equation gives the following expression for the monochromatic reflection coefficient:

$$\rho = -e^{-2\gamma x} \quad (22)$$

where the propagation constant is defined by Equation (15) as was discussed earlier. The reflected voltage spectrum is equal to the product of the transmitted spectrum and the reflection coefficient

UNCLASSIFIED

UNCLASSIFIED

$$\begin{aligned} S_R(f) &= \rho(f) \cdot S_T(f) \\ &= -e^{-2\gamma(f)} \cdot S_T(f) \end{aligned} \quad (23)$$

Since the propagation constant is complex valued, it can be represented by

$$\gamma(f) = \alpha(f) + j\beta(f) \quad (24)$$

and Equation (23) becomes

$$S_R(f) = -e^{-2\alpha(f)x} \cdot e^{-j2\beta(f)x} \cdot S_T(f) \quad (25)$$

Note that the first term in the above equation represents the attenuation of the reflected spectrum whereas the second term only represents a phase shift that varies with distance and frequency. The attenuation factor varies with frequency and is given by

$$\alpha(f) = R_e \left\{ j \frac{2\pi f}{c} \sqrt{\epsilon_{soil}} \right\} \quad (26)$$

Using the model for wet soil described earlier,

$$\epsilon_{soil} = \epsilon_R [1 - j .06 \times 10^{-9} Kf] \quad (27)$$

where K equals zero for dry soil and unity for very wet soil, the attenuation factor becomes

$$\alpha(f) = R_e \left\{ j \frac{2\pi f}{c} \sqrt{\epsilon_R} \sqrt{1 - j .06 \times 10^{-9} Kf} \right\} \quad (28)$$

$$\alpha(f) \approx \frac{2\pi f}{c} \sqrt{\epsilon_R} (.03 \times 10^{-9} Kf); \quad f \leq 3 \times 10^9 \text{ Hz}$$

UNCLASSIFIED

UNCLASSIFIED

Note that $\alpha(f)$ varies as the square of the frequency in this equation. The attenuation versus distance into the soil is shown in Figure 40 for a medium wet soil ($K = \frac{1}{2}$) as a function of frequency. The metal plate is assumed to be buried 6 inches below the soil surface in this example. The effect of soil moisture is to attenuate the high frequencies more than the lower frequencies. In this example, if the soil were assumed to be very wet ($K = 1$, $\epsilon_R = 10$), the 3 GHz attenuation would be about 50 dB. Thus, the reflected spectrum is not only an attenuated version of the transmitted spectrum but is also distorted.

APPLICATION TO NBS MEASUREMENTS

The computer program which calculates the reflected spectrum from the transmitted spectrum and other parameters was exercised for three specific targets--the metal plate, type A mine, and type B mine--assuming a transmitted spectrum corresponding to the processed NBS data. The results are presented in Figures 41 through 49 and discussed in the following paragraphs. In each figure the magnitude of the reflected spectrum is given assuming the transmitted spectrum is amplitude weighted to provide 40 dB Tchebychev temporal sidelobes. The frequency scale runs from zero to 3.048 GHz. Also included in each figure is the reflected temporal waveform obtained by taking the Fourier transform of the complex valued spectrum. In each case, the time scale runs from zero to 20-5/6 nanoseconds.

For each type of target, three soil moisture values were assumed, yielding three figures for each target. The soil loss factor, K, and the dielectric constant (real portion) used are indicated in each figure.

UNCLASSIFIED

UNCLASSIFIED

In each case, the top of the target is assumed to be 6 inches below the ground surface. The number in the upper right corner of each figure is the maximum magnitude of the waveform that is shown. It is used primarily to determine attenuation.

Figures 41 through 43 are spectrum and temporal plots for a metal plate return with loss factors, K, of 0, .5, and 1, respectively. In Figure 41 where there is no loss assumed and the magnitude of the reflection constant is unity, the spectrum shown is also the spectrum of the "transmitted" spectrum. The spectrum has a Tchebychev weighting to provide 40 dB temporal sidelobes. The temporal radar return is shown in Figure 41(b) and, except for an inversion, is also the "transmitted" time waveform. Figure 42 indicates the effect of a moderate loss factor, 0.5. Note that the spectrum has been attenuated at the high frequencies more than at the lower frequencies. Thus, the spectrum is skewed towards the lower frequencies. The time waveform in 42(b) also reflects this effect by having a larger time spread. Also, the period of the time response oscillation is larger. The position of the reflected waveform relative to the origin has been changed due to the larger dielectric constant used; e.g., 6.5 instead of 3. Figure 43 consists of spectral and temporal plots for a large loss factor of unity. The characteristics outlined for Figure 42 are now more pronounced. The magnitude of the temporal responses in Figures 42 and 43 are attenuated relative to the lossless case by 5.2 and 10.4 dB, respectively

The spectral and temporal plots for the type A mine model are shown in Figures 44 through 46 for loss factors of 0, .5, and 1, respectively.

UNCLASSIFIED

UNCLASSIFIED

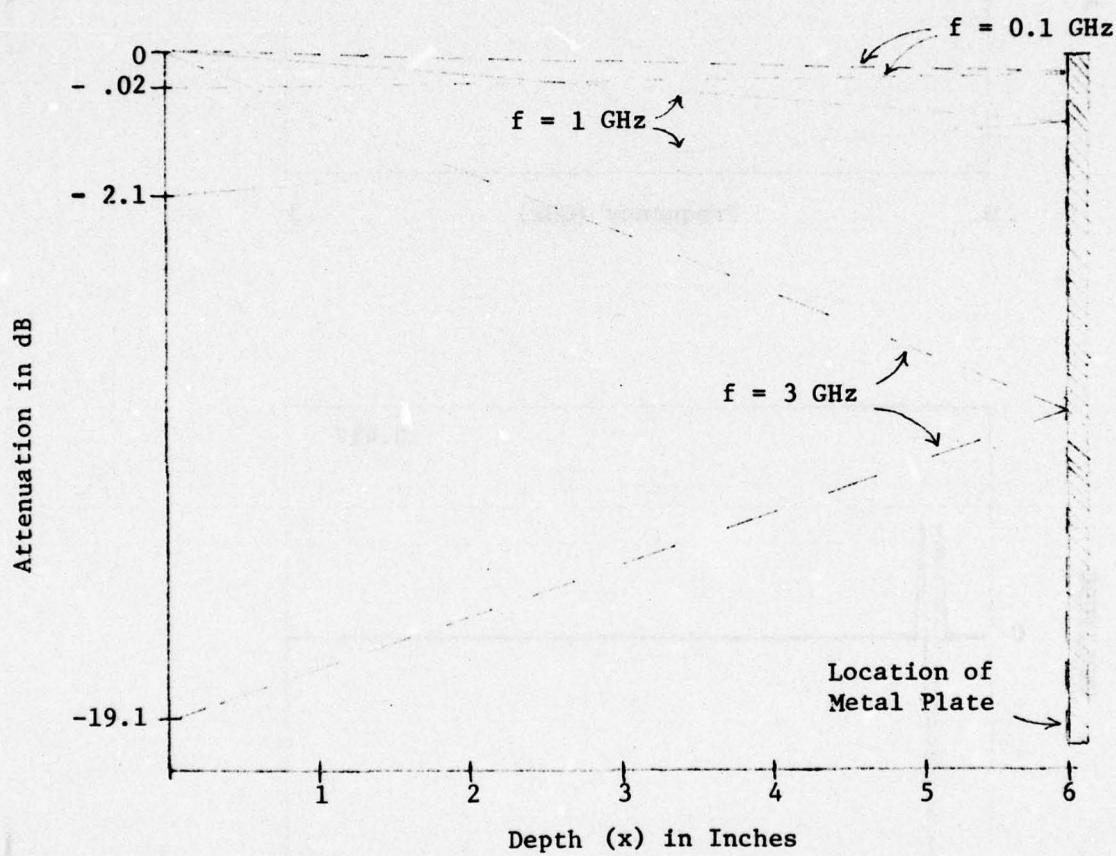


Figure 40. Attenuation Versus Depth for a Metal Plate Target in Moderately Wet Soil ($K = 0.5$, $\epsilon_r = 6.5$).

UNCLASSIFIED

UNCLASSIFIED

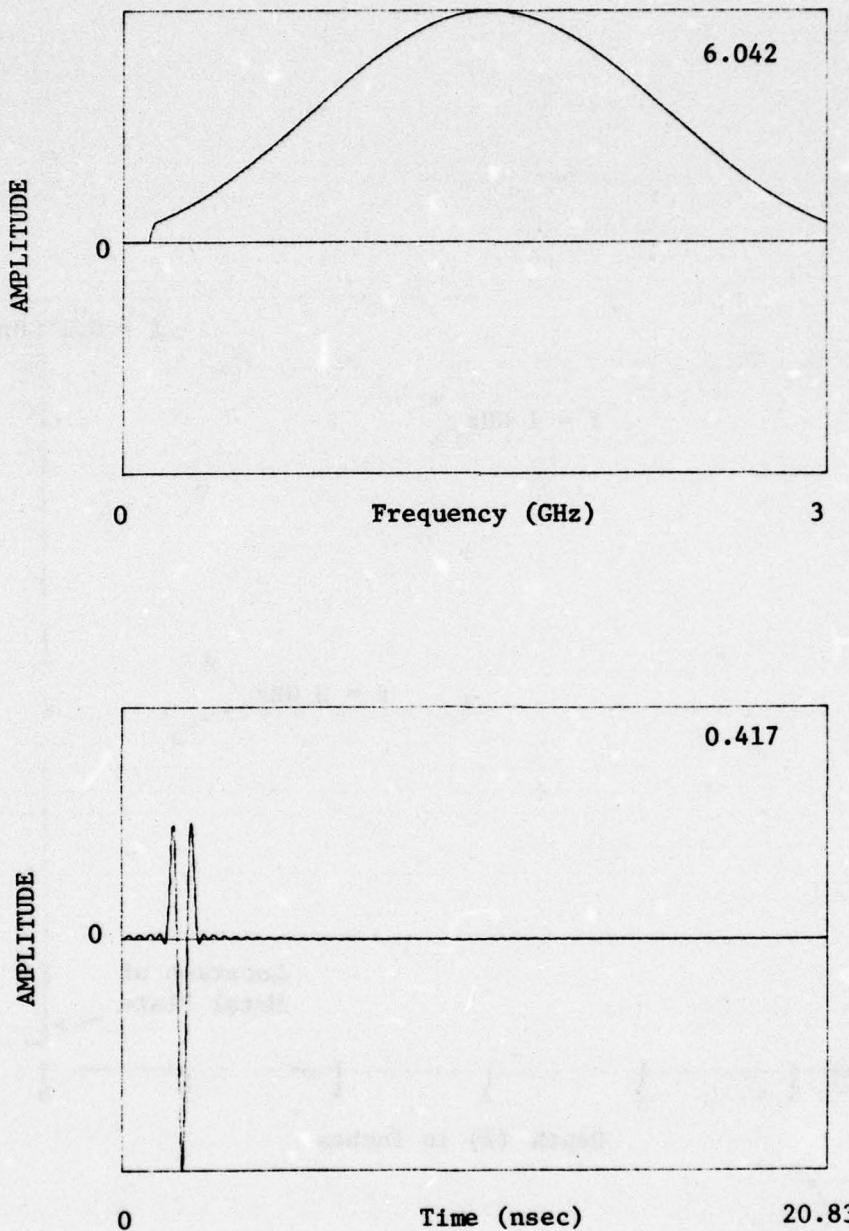


Figure 41. Math model of radar return from metal plate buried in a lossless medium.

UNCLASSIFIED

UNCLASSIFIED

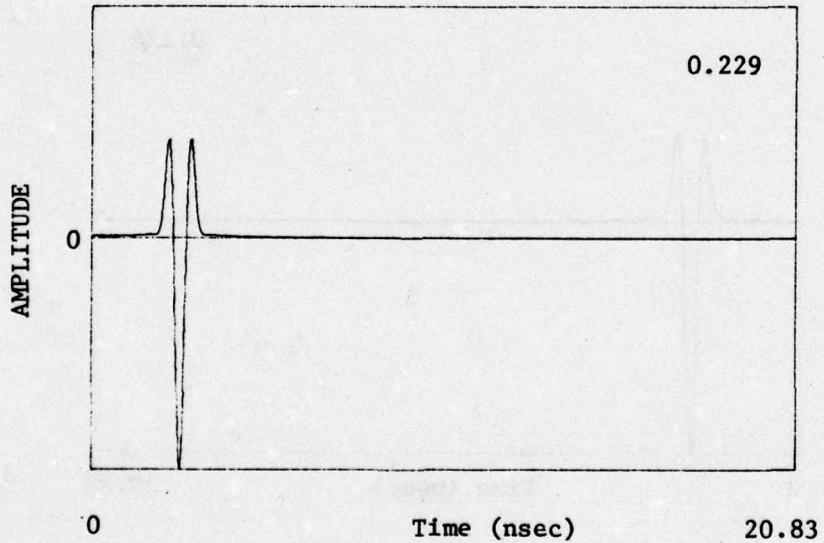
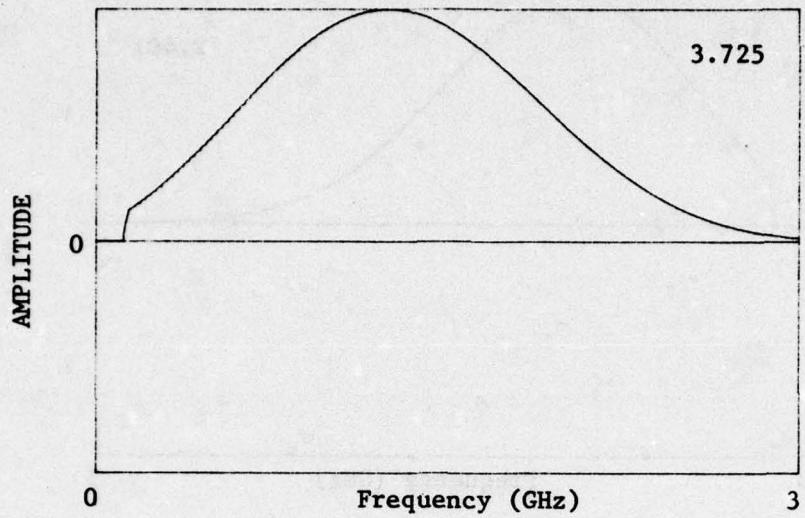


Figure 42. Math model of radar return from a metal plate buried 6" in a lossy medium ($K=0.5$).

UNCLASSIFIED

UNCLASSIFIED

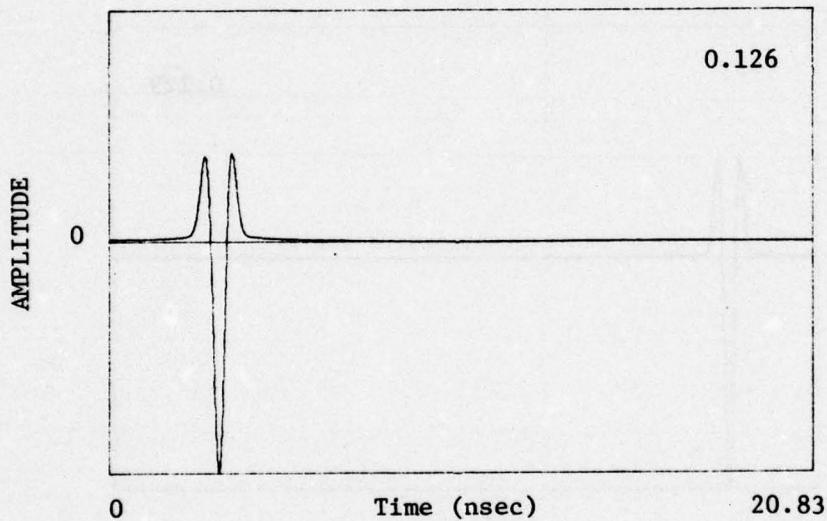
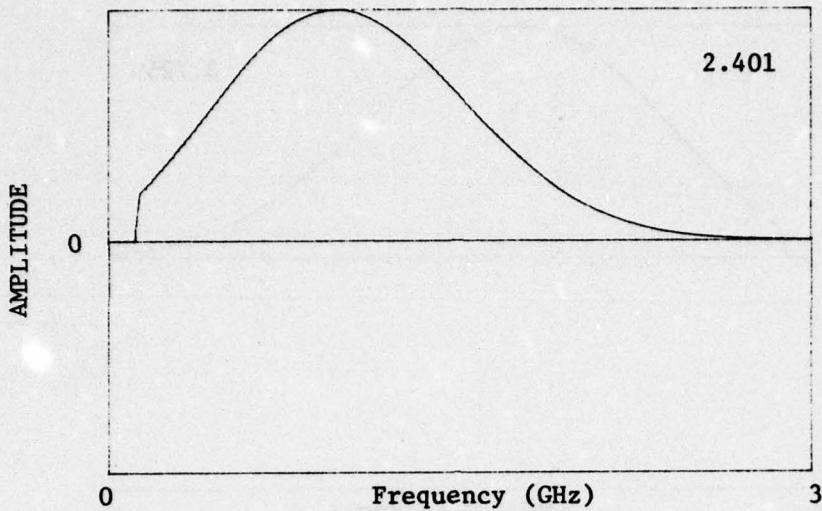


Figure 43. Math model of radar return from metal plate buried 6" in lossy soil (loss equal to that of pure water at 20° C, K=1.0).

UNCLASSIFIED

UNCLASSIFIED

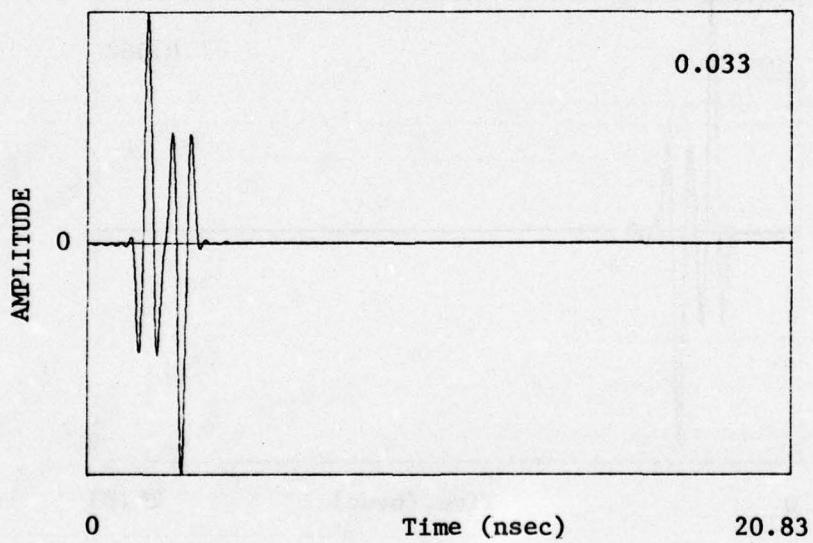
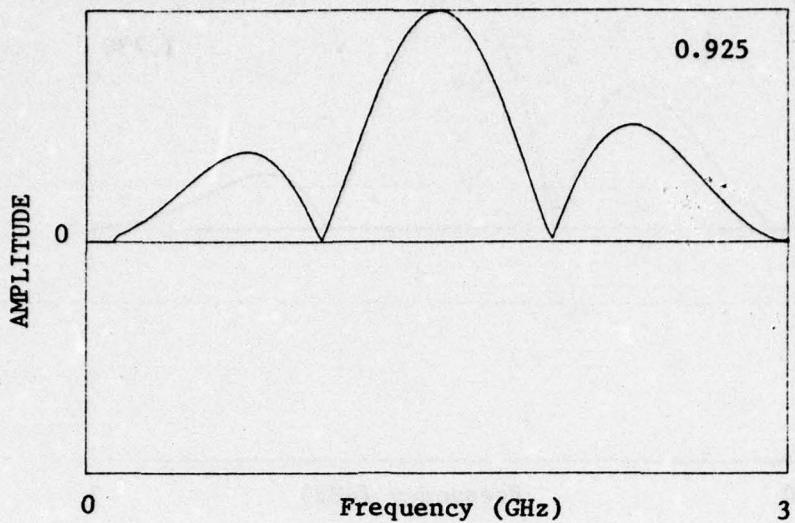


Figure 44. Math model of radar return from non-metallic mine type A buried 6" in lossless medium.

UNCLASSIFIED

UNCLASSIFIED

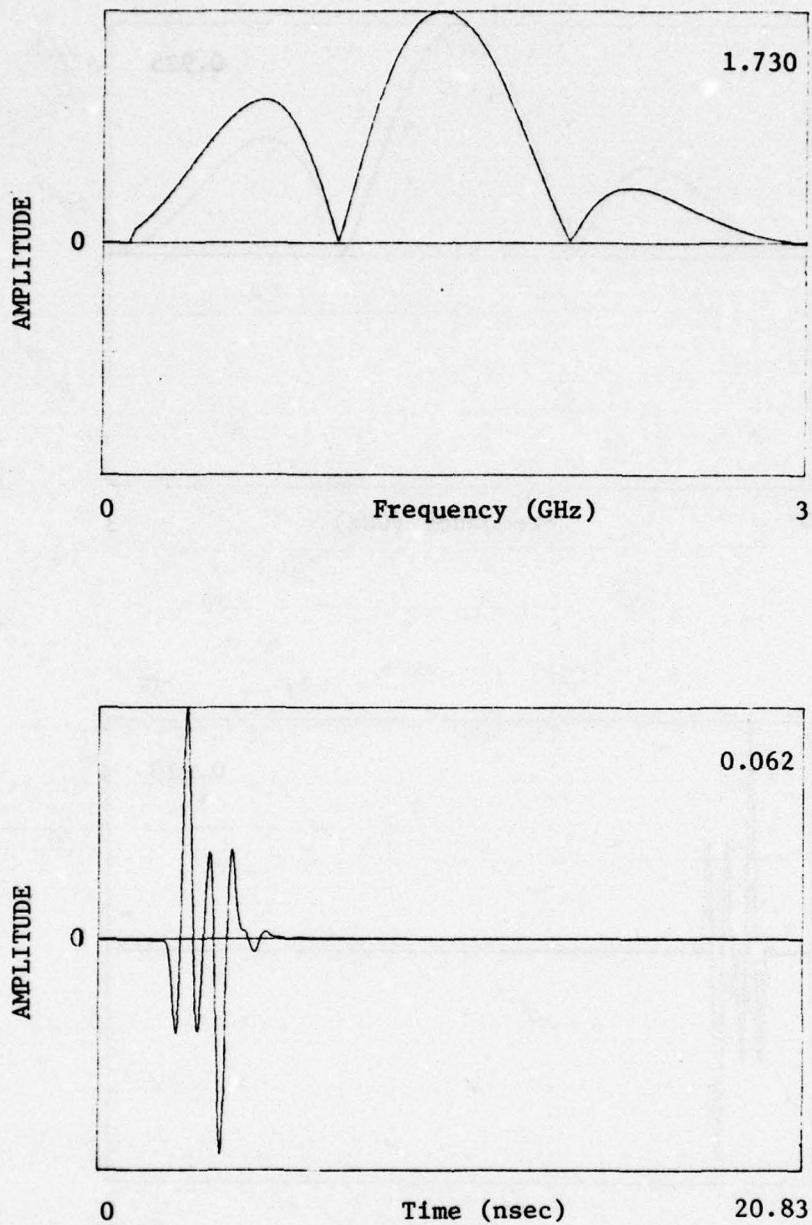


Figure 45. Math model of radar return from non-metallic mine type A buried 6" in a lossy medium ($K=0.5$).

UNCLASSIFIED

UNCLASSIFIED

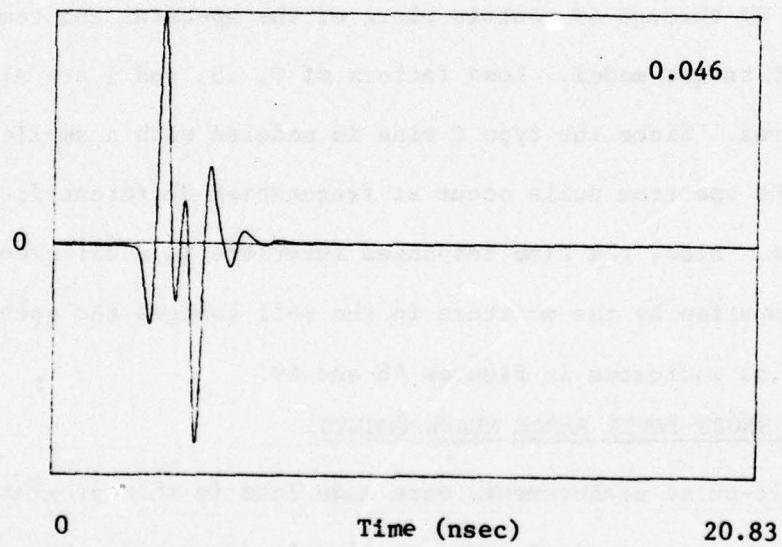
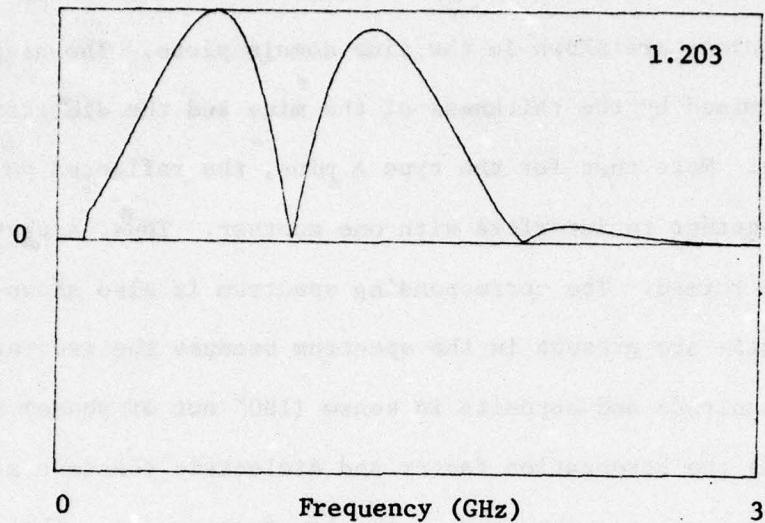


Figure 46. Math model of radar return from non-metallic mine type A buried 6" in a lossy medium (loss equal to that of pure water at 20°C, K=1.0)

UNCLASSIFIED

UNCLASSIFIED

The type A mine model consists of two dielectric discontinuities and, therefore, two reflected pulses are shown in the time domain plots. The distance between pulses is determined by the thickness of the mine and the dielectric material inside the mine. Note that for the type A mine, the reflected pulses are close enough together to interfere with one another. Thus, a particular composite pulse is formed. The corresponding spectrum is also shown. Note that several nulls are present in the spectrum because the two reflections are equal in magnitude and opposite in sense (180° out of phase) at certain frequencies. As the attenuation factor and dielectric constant are increased, the spectrum has a greater skew toward the low frequencies. The spectrum is thereby changed from that of the lossless case. Also, the composite temporal waveform changes as shown in Figures 45(b) and 46(b).

Figures 47 through 49 contain plots of the spectral and temporal returns from the type C target model. Loss factors of 0, .5, and 1 are also assumed for these figures. Since the type C mine is modeled with a smaller thickness of 3 inches, the spectrum nulls occur at frequencies different from those for the type A mine. Also, the time responses interfere in a different manner. Increased attenuation by the moisture in the soil changes the spectrum and time responses as indicated in Figures 48 and 49.

APPLICATION TO SHORT-PULSE RADAR MEASUREMENTS

The short-pulse measurements were made late in this program and were not modeled by the mathematical model previously described. The major difference in applying the model to the NBS data and the short-pulse radar data is in the spectrum of the transmitted pulse. The spectrum of the NBS data spans

UNCLASSIFIED

UNCLASSIFIED

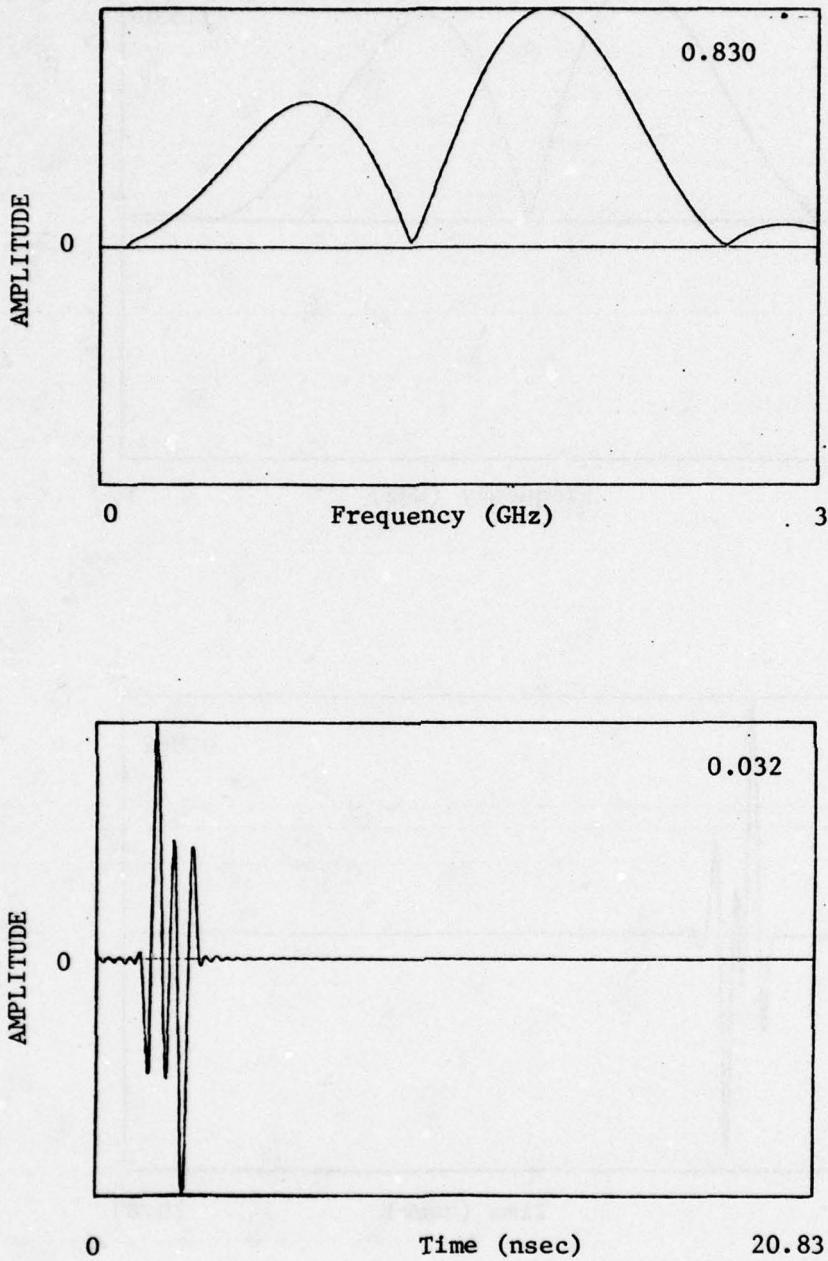


Figure 47. Math model of radar return from non-metallic mine type C buried 6" in lossless medium.

UNCLASSIFIED

UNCLASSIFIED

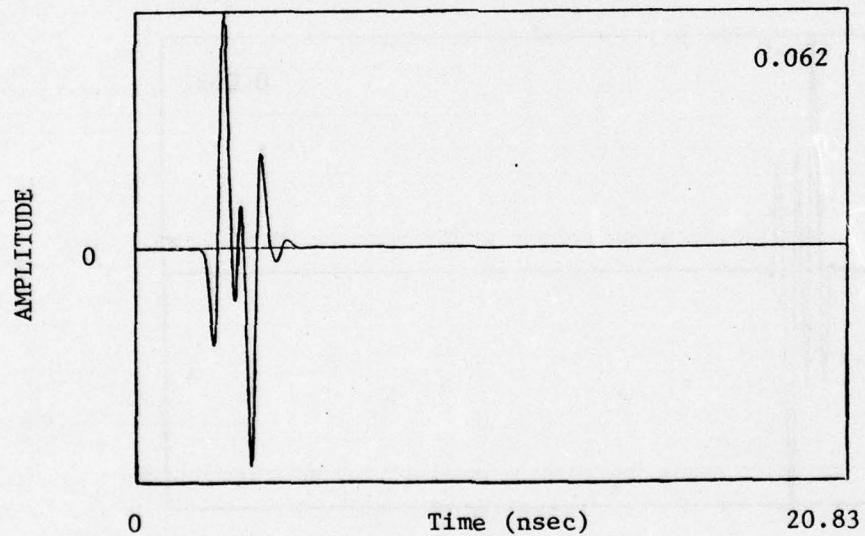
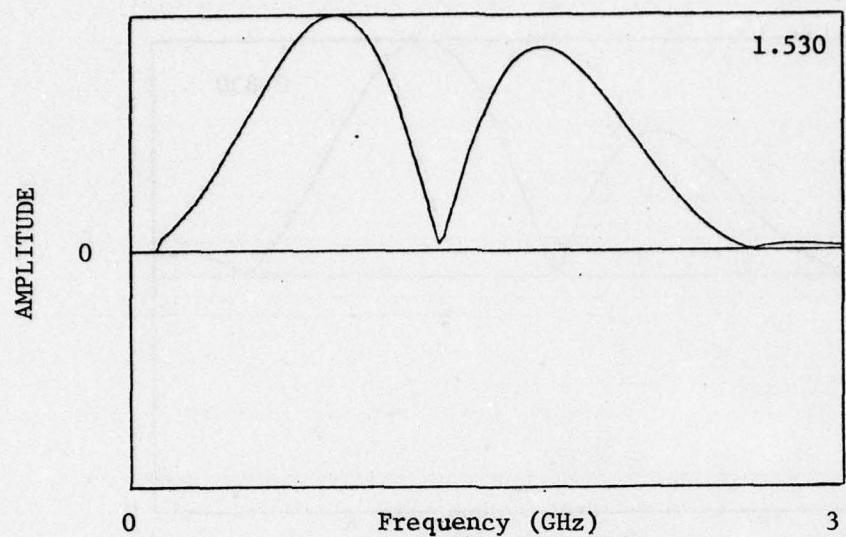


Figure 48. Math model of radar return from non-metallic mine type C buried 6" in a lossy medium ($K=0.5$).

UNCLASSIFIED

UNCLASSIFIED

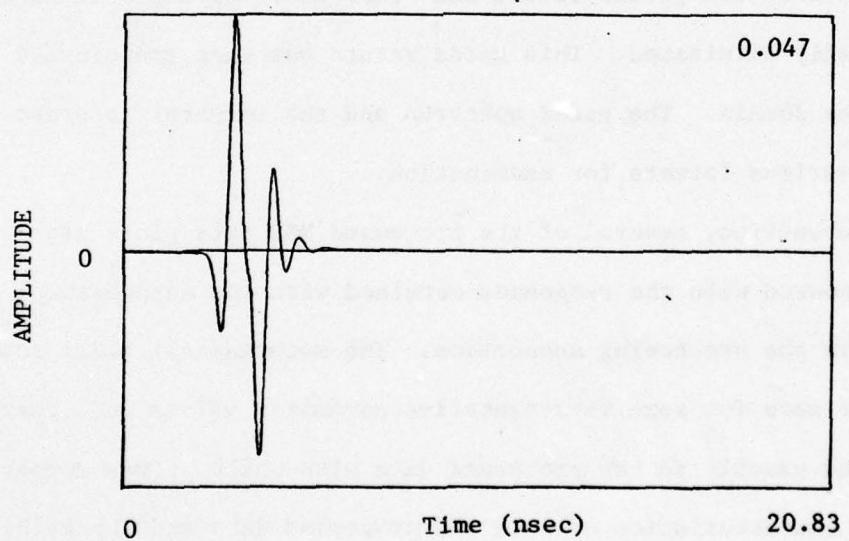
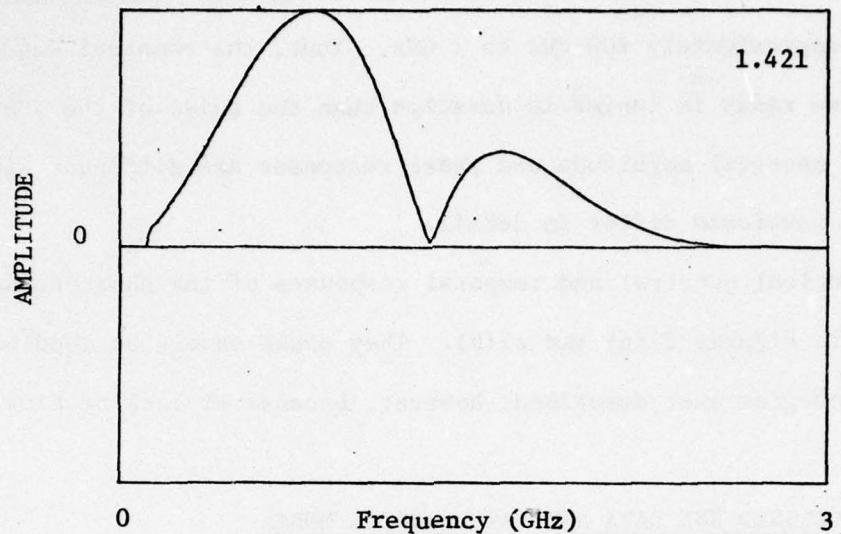


Figure 49. Math model of radar return from non-metallic mine type C buried 6" in a lossy medium (loss equal to that of pure water at 20°C, K=1.0)

UNCLASSIFIED

UNCLASSIFIED

from 120 MHz to 3.048 GHz, whereas the spectrum of the short-pulse radar data spans from approximately 100 MHz to 2 GHz. Thus, the temporal waveform of the short-pulse radar is longer in duration than the pulse of the NBS data. In addition, the spectral magnitude and phase responses are different since the two temporal waveforms differ in detail.

The theoretical spectral and temporal responses of the short-pulse radar are shown in Figures 22(a) and 22(b). They could easily be modeled by the computer program just described; however, because of lack of time they were not.

COMPARISON OF PROCESSED NBS DATA AND MATHEMATICAL MODEL

As explained earlier in this report, the NBS raw measured data was weighted and transformed to the time domain for range gating. The range gate was positioned so that the ground return and other interfering returns were partially or totally eliminated. This gated return was then transformed back into the frequency domain. The gated spectrum and the temporal response were plotted in various formats for examination.

In this subsection, several of the processed NBS data plots are discussed and compared with the responses obtained with the mathematical model presented in the preceding subsection. The mathematical model responses presented earlier were for some representative parameter values and, therefore, did not correspond exactly to the processed data with which it was compared. However, general characteristics of both the processed data and the mathematical model responses were similar.

UNCLASSIFIED

UNCLASSIFIED

The processed data and model for the metal plate buried 6 inches below the ground surface were compared. Figure 50 is a plot of the processed measured data. Figure 50(a) shows the spectrum of the measured data without weighting, and Figure 50(b) shows the corresponding time responses with weighting and with the time gate boundaries marked with two vertical lines. The temporal response between these lines was taken as the metal plate return. Figure 50(c) is the spectrum of the gated portion of the time response, and Figure 50(d) is the gated spectrum phase response ranging between the limits of $-\pi$ to $+\pi$ radians. This data is from the measured data record GT5-68 which is a return from a metal plate buried 6" deep in loam with a 7% soil moisture content.

Compare the gated spectrum of this data with the spectrum obtained with the mathematical model as shown in Figure 41. There is a great deal of similarity between the two. One notes that the spectrum in Figure 50 appears to be skewed slightly toward the lower frequencies. This is because the 7% moist loam does provide some attenuation to the incident EM waves. However, the amount of attenuation presented is not as great as that shown in Figure 42 where the loss factor is 0.5. The spectral phase appears to be linear over most of the frequency range. Based on the mathematical model, one would expect this result. The gated temporal response of Figure 50 is somewhat similar to that of Figure 41, but differs in detail. Comparison of the type A and type B target data with the math model plots found in Figures 44 through 49 yield the same result; i.e., the spectral plots were in very close agreement, but the temporal signatures differed.

At first, it was thought the math model was in error; however, the following simplified analysis shows that the results obtained with the math model were indeed correct and the error was in the data measurements.

UNCLASSIFIED

UNCLASSIFIED

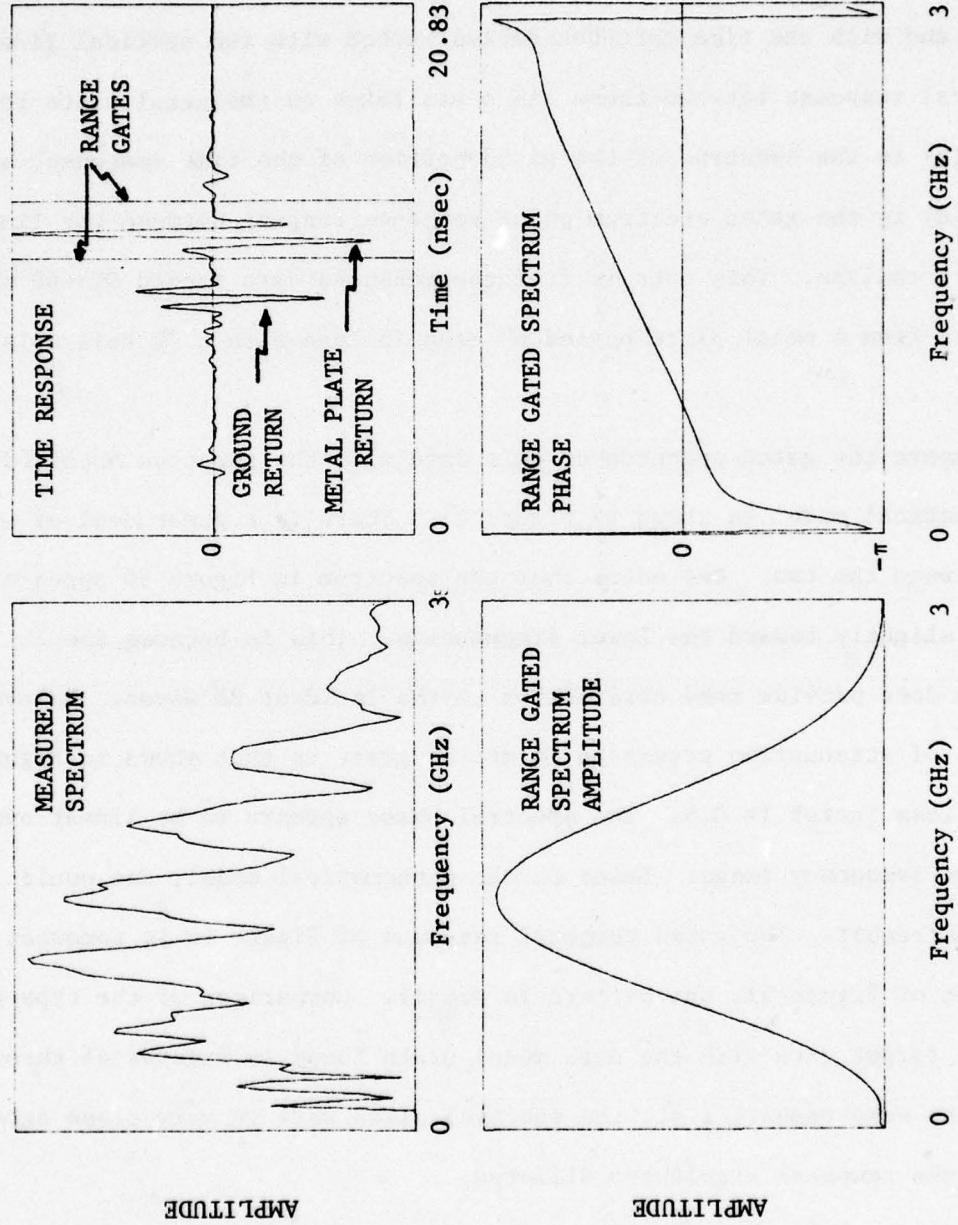


Figure 50. Measured data--metal plate 6" below ground, 7% moisture--
GT5-68.

UNCLASSIFIED

UNCLASSIFIED

Consider for a moment the behavior of electromagnetic waves at the boundary between two media as illustrated in Figure 51. The reflection coefficient at the boundary is given by

$$\rho = \frac{N_2 - N_1}{N_2 + N_1} \quad (29)$$

where N_1 and N_2 are the wave impedances of media 1 and 2, respectively. For a perfect conductor, the wave impedance is zero; for a non-conducting, non-ferrous medium, the wave impedance is

$$N = \sqrt{\frac{\mu_0}{\epsilon}} \quad (30)$$

where μ_0 is the magnetic permittivity of space, and ϵ is the dielectric constant of the medium. If the wave impedance for free space (air) is denoted by

$$N_0 = \sqrt{\frac{\mu_0}{\epsilon_0}} \quad (31)$$

then equations (29) and (30) above may be written as

$$N = \frac{N_0}{\sqrt{\epsilon_r}} \quad (32)$$

$$\text{and } \rho = \frac{\sqrt{\epsilon_{r1}} - \sqrt{\epsilon_{r2}}}{\sqrt{\epsilon_{r1}} + \sqrt{\epsilon_{r2}}} \quad (33)$$

where ϵ_r is the relative dielectric constant of the medium.

Note that if medium 1 has a smaller relative dielectric constant than medium 2, then ρ has a negative value. On the other hand, if medium 1 has a larger relative dielectric constant than medium 2, then ρ is positive. Also, note that for metal, ρ is also negative; i.e., $\rho = -1$.

UNCLASSIFIED

UNCLASSIFIED

Suppose a metal plate is buried in soil as illustrated in Figure 52. Also, assume the transmitted pulse is of the shape shown in the same figure. What should the radar return from the air/soil and the soil/metal interfaces look like? The soil has a dielectric constant greater than that of air; thus, ρ at the air/soil interface has a negative value. Likewise, ρ at the soil/metal interface is negative. Thus, the radar return should appear as shown in Figure 52. Assuming the metal plate is deep enough below the soil surface so the two reflected pulses do not overlap, each of the returns should appear as the inverse of the transmitted waveform as illustrated. Now refer to the measured data for a metal plate buried in soil shown in Figure 50. Note that the plate return is not a replica of the ground return as theory indicates it should be.

Extending this simplified analysis to a mine buried in the soil yields the expected returns illustrated in Figure 53. A comparison of the measured mine temporal signatures with those of this figure also indicates a difference and that something is wrong.

After an extensive search for the reason for this discrepancy, it was found that if the measured spectra lines were shifted down in frequency by about 24 MHz, the measured data and the analytically derived signatures agree. For example, compare the measured temporal signature of the metal plate return after the spectrum has been down-shifted about 24 MHz as shown in Figure 54 to the returns derived in Figure 52. Except for amplitude, there is complete agreement! Figures 55 through 58 show the measured temporal responses of the type A and type C mines before and after the 24 MHz spectral

UNCLASSIFIED

UNCLASSIFIED

$$\rho = \frac{n_2 - n_1}{n_2 + n_1}$$

$$\epsilon = \sqrt{\frac{\mu}{\epsilon}} = \text{Wave Impedance}$$

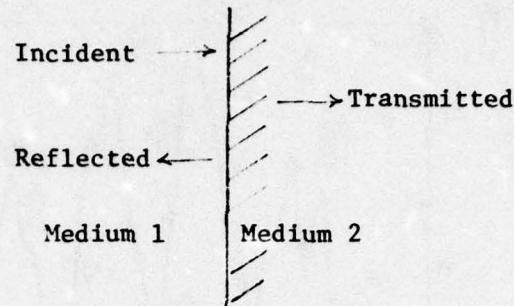


Figure 51. Behavior of EM Waves at a Boundary.

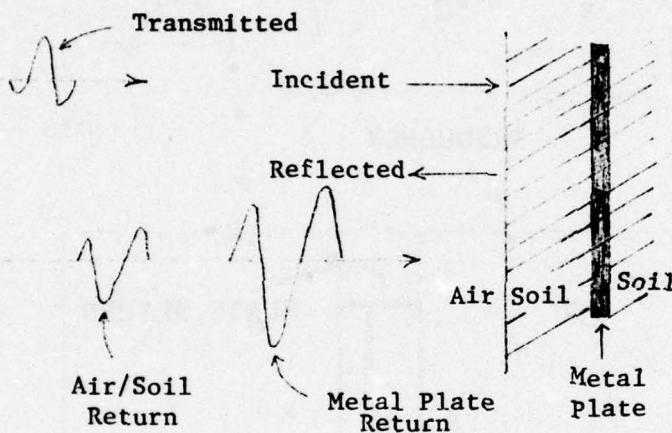


Figure 52. Metal Plate Buried in Soil.

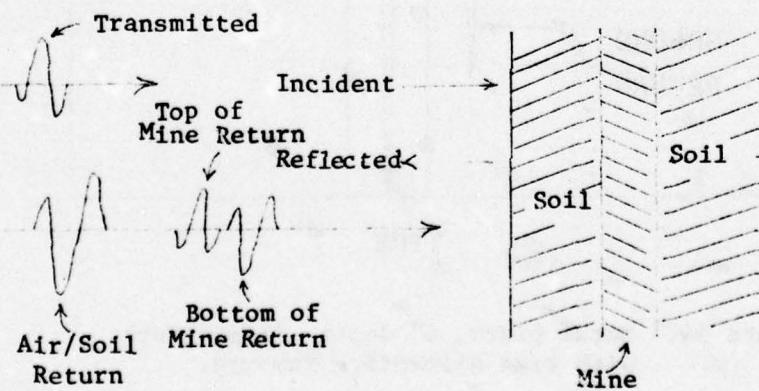


Figure 53. Non-metallic Mine Buried in Soil.

UNCLASSIFIED

UNCLASSIFIED

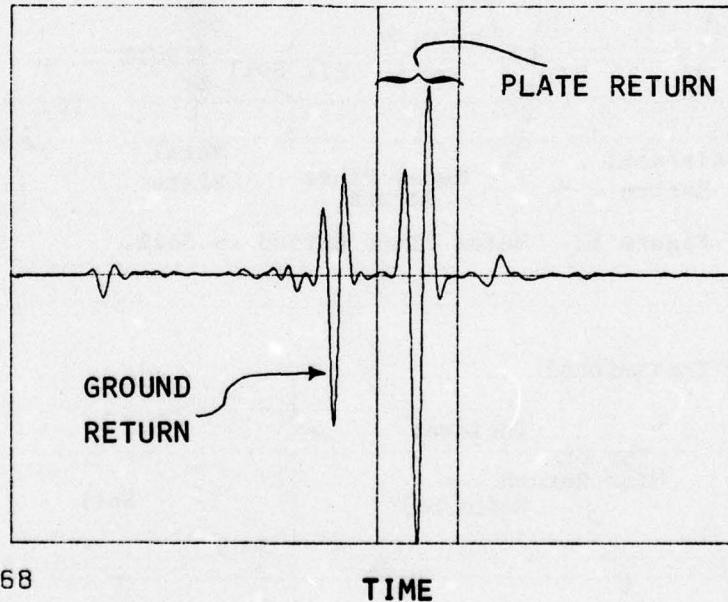
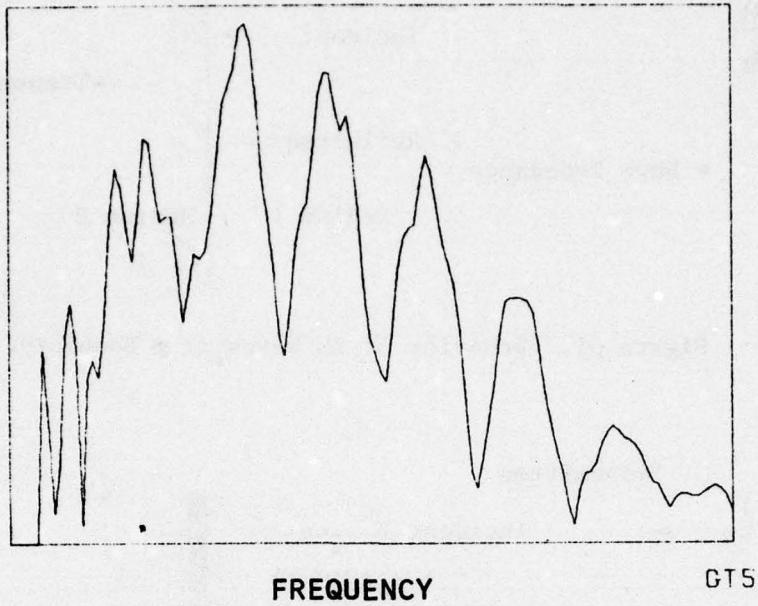
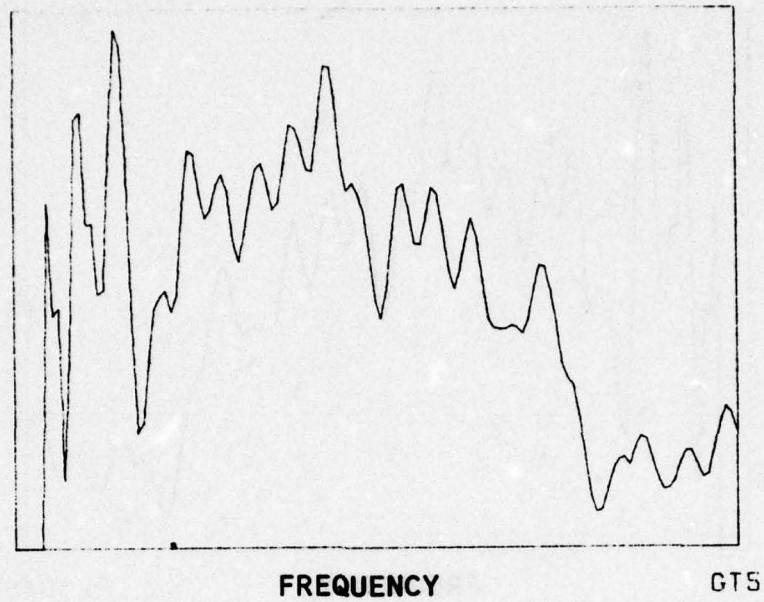


Figure 54. Metal plate, 6" depth, 7% moisture,
with time distortion removed.

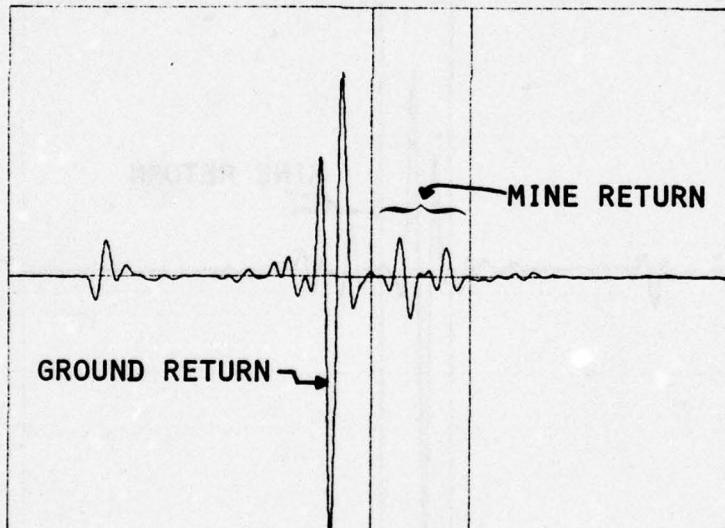
UNCLASSIFIED

UNCLASSIFIED



FREQUENCY

GTS



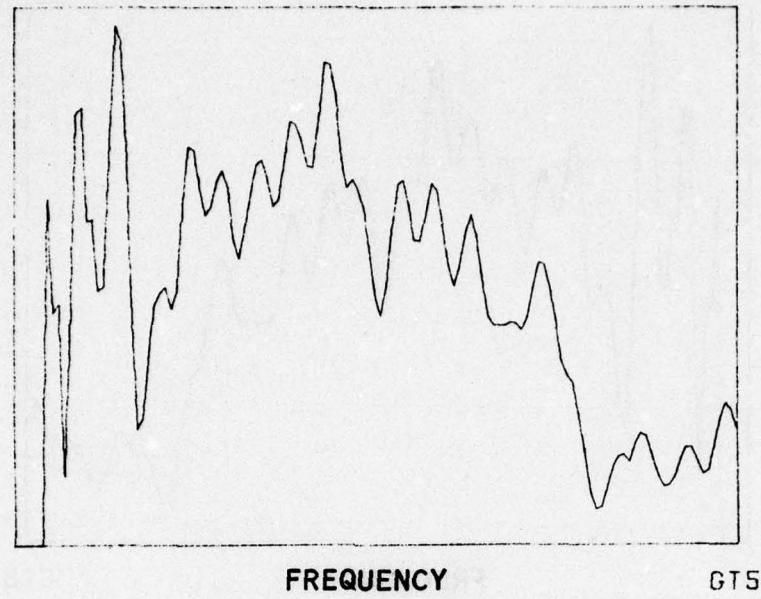
56

TIME

Figure 55. Type A mine, 6" depth, 7% moisture,
with time distortion.

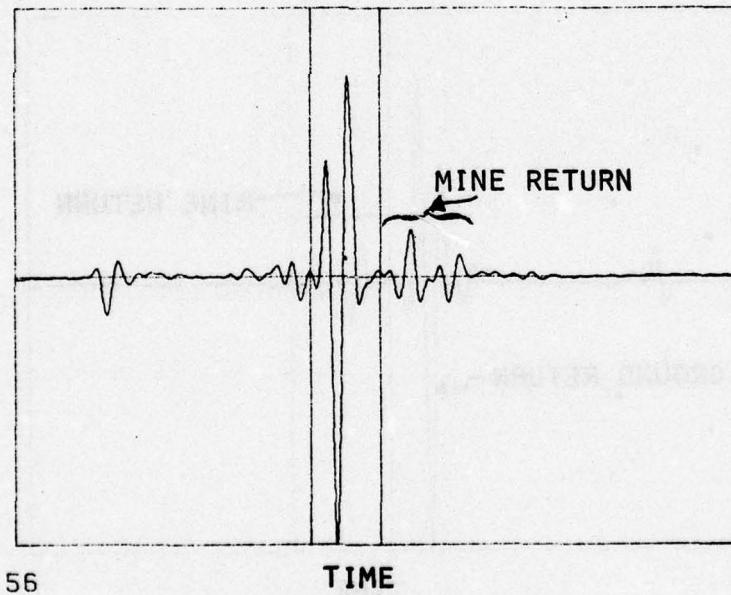
UNCLASSIFIED

UNCLASSIFIED



FREQUENCY

GTS



56

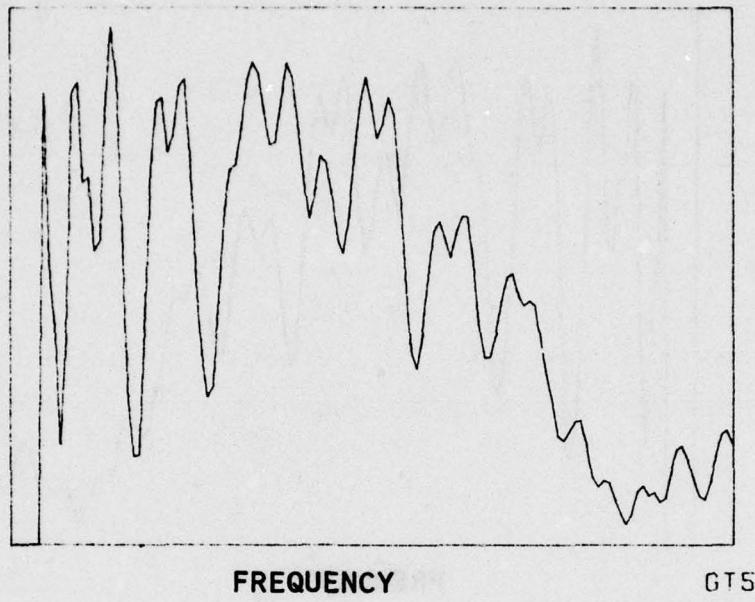
TIME

Figure 56. Type A mine, 6" depth, 7% moisture,
with time distortion removed.

UNCLASSIFIED

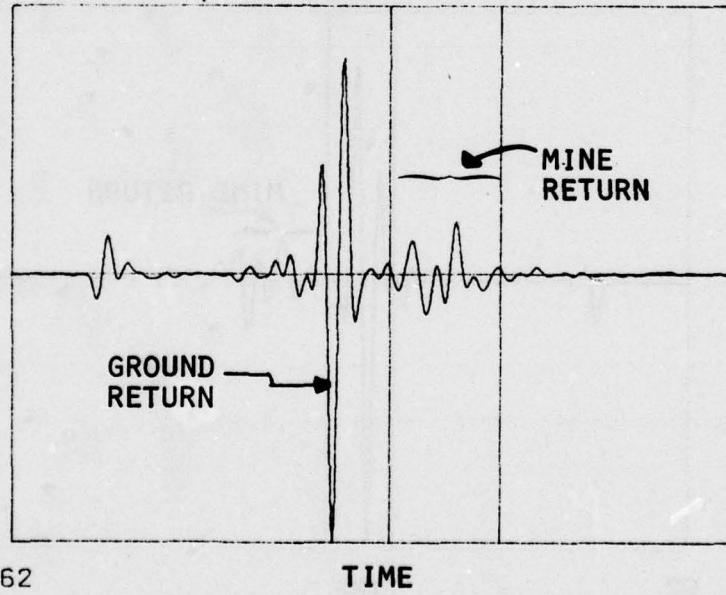
112

UNCLASSIFIED



FREQUENCY

GTS



62

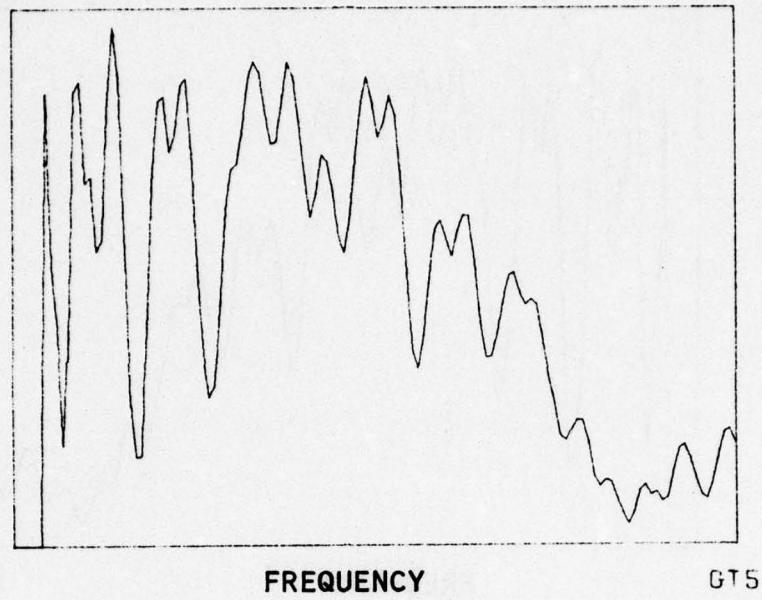
TIME

Figure 57. Type C mine, 6" depth, 7% moisture,
with time distortion.

UNCLASSIFIED

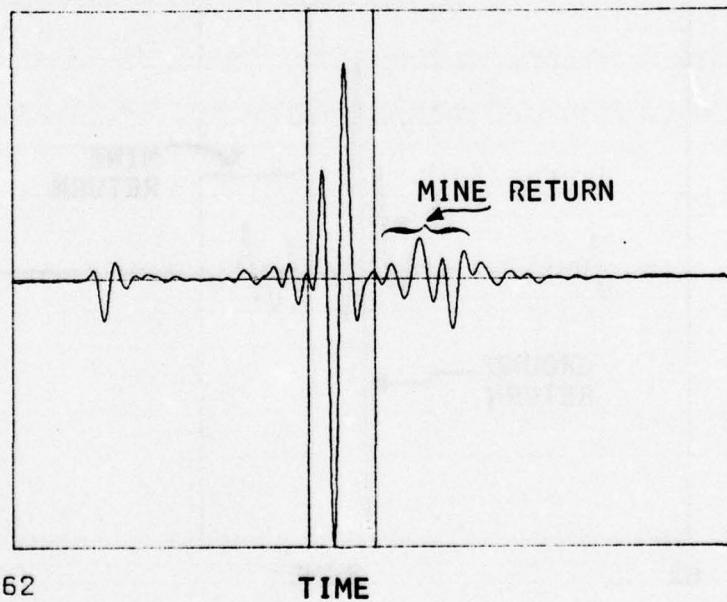
113

UNCLASSIFIED



FREQUENCY

GTS



62

TIME

Figure 58. Type C mine, 6" depth, 7% moisture,
with time distortion removed.

UNCLASSIFIED

114

UNCLASSIFIED

shift. A comparison of these responses of the spectral shifted data with those derived in the simplified analysis and also those derived via the mathematical model indicates almost complete agreement. Apparently, when the NBS data was collected, an error was made in the frequency assignment. After discovering this error, all of the NBS data was corrected by a spectral shift.

UNCLASSIFIED

UNCLASSIFIED

SECTION V

SELECTION AND DEVELOPMENT OF
DISCRIMINATION/CLASSIFICATION ALGORITHMS

The process of initially detecting a potential target and then determining not only if it is a mine, but its type, is divided into three steps as illustrated in Figure 59. The first step is to separate potential target returns from radar returns due to soil anomalies. For this study, a potential target is considered to be any buried object which gives a return significantly larger than from the soil alone. Some examples of buried non-mine objects one might encounter in a typical field are rocks, roots, metal scraps, etc. The discrimination/classification steps which follow the detection process involve a relatively complicated and time-consuming process. Thus, not every location in a field can be subjected to all three steps shown in Figure 59. The purpose of the detection processor is to drastically reduce the number of locations in a field that must be scrutinized by all three sections of the processor.

The second processor section is referred to as the discriminator. The purpose of this step is to determine which of the potential targets are indeed targets; i.e., mines. Later in this report, the algorithm used to accomplish this is described. The third and final section of the three-step processor is designed to indicate to which of several classes of mines the detected target belongs.

The detection process is a relatively simple one. The returns from the upper one foot of the soil are subjected to a threshold which is normalized

UNCLASSIFIED

UNCLASSIFIED

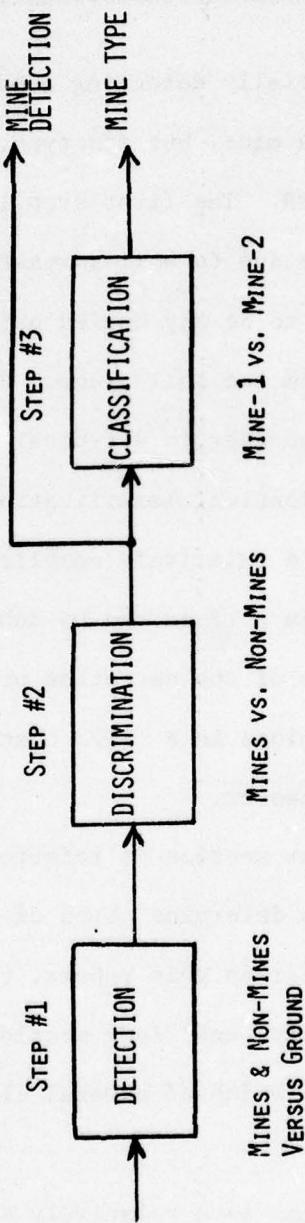


Figure 59. Three-step mine detection/classification processor.

UNCLASSIFIED

UNCLASSIFIED

to the RMS average return from a portion of the soil below one foot from the soil surface. In the region with depth greater than one foot, mines are not likely to be present. This normalization of the radar returns should remove the effects of transmitter power variations and other unexplained variables. Thus, the false alarm rate should be fairly constant for each type of soil. If the radar returns from a particular location do not pass the threshold of the detection processor, they are ignored and another location is interrogated. If the detection processor threshold is exceeded, then the algorithm of the discrimination processor is exercised. Preferably, the false alarm rate for the detection processor should be about one false alarm rate per 1000 meters of travel. As will be shown later, this is equivalent to a probability of false alarm (P_{FA}) of about 10^{-5} .

If the radar returns from a particular location do pass the detection processor threshold, the radar return range profile is searched for the range cell with the largest amplitude. A target signature cell is then defined with the largest amplitude return as its centroid. The spectrum of the time signature within this cell is then obtained by use of the Fourier transform. The discrimination algorithm described in the next section is exercised utilizing the spectral signature data. Based on the output of the algorithm, the signature is declared to be that of a mine or a non-mine, e.g., a rock or a root. If it is decided that the signature is that of a non-mine, the processing is terminated and the radar is moved to the next location.

On the other hand, if a mine is declared, the spectral signature is scrutinized to determine to which class of mine it belongs. At this point,

UNCLASSIFIED

UNCLASSIFIED

the processing is complete and the radar moves to a new location.*

The overall performance of the three-step processor and radar depends upon the operational scenario. For the sake of illustration, the following two scenarios will be considered:

Scenario A

- The width of ground to be covered by the mine detection radar:
4 meters (\sim 13 feet);
- The rate at which ground is to be covered by the mine detection radar: 10 KM/hr (\sim 9 ft/sec);
- The false alarm rate: less than 1 per 1000 meters of linear travel (1 per/3280 feet);
- The ground is sampled by the radar on a 1 foot square grid--i.e., each radar measurement is located one foot from all other measurements;
- The ground is void of any rocks, roots, etc. Only mines or soil exist within the path of the mine detection radar.

Scenario B

- The first four statements under Scenario A apply;
- One-half of the locations where radar measurements are taken contain non-mines--i.e., rocks, roots, etc. The other half contain soil only. In addition, a mine may be present at any of the locations.

*The radar is assumed to be continuously moving. The processing required must be completed before the radar has moved to the next position to be interrogated.

UNCLASSIFIED

UNCLASSIFIED

The number of locations that are interrogated by the radar per second can be determined from the scenarios as follows:

13 locations/linear foot of travel

9 linear feet of travel/second

or $13 \times 9 = 117$ locations/second.

This indicates how much processing has to be accomplished in a given time period and will be used in Section VII to determine the processor hardware requirements.

To convert the specified false alarm rate into false alarm probability, the number of locations interrogated by the radar per 1000 meters must be determined. As indicated above, 3280 linear feet or $13 \times 3280 = 42,640$ locations must be interrogated per one false alarm. Thus, the overall probability of false alarm must be

$$P_{FA} \leq 1/42,640 \approx 2.4 \times 10^{-5} \quad (34)$$

The P_{FA} that each section of the three-step processor must have to meet this requirement depends on which of the above scenarios is assumed. In Scenario A the P_{FA} of $\sim 10^{-5}$ may be divided between steps 1 and 2 since the overall P_{FA} is given by the product of the individual P_{FA} 's. For example, the P_{FA} assigned to the detection processor could be 10^{-4} while that assigned to the discriminator could be 10^{-1} . This assignment would require the discriminator to be exercised only about once in 10^4 interrogations, or once in about 100 seconds. Consequently, a false alarm--i.e., an indication of the presence of a mine when one was not present--would occur only once in about 10^5 interrogations or once in about 1000 seconds. On the other hand, the relatively

UNCLASSIFIED

UNCLASSIFIED

simple processor, the detection processor, would be exercised for every location interrogated. In Scenario B, the P_{FA} assigned to each processor is quite different from that described for Scenario A. To illustrate, suppose there was a rock or root at each location which was searched. The total or overall P_{FA} for the three-step processor is that of the discriminator. If the P_{FA} assignment made for Scenario A is used, the total P_{FA} would be 10^{-1} rather than 10^{-5} as before.

In Scenario B, only one-half of the interrogated locations are assumed to contain non-mines. Thus, the total or overall probability of false alarm is related to the P_{FA} for each step as follows:

$$P_{FA_T} = W_1 \cdot P_{FA_1} \cdot P_{FA_2} + W_2 \cdot P_{FA_2}$$
$$W_1 + W_2 = 1 \quad (35)$$

where W_1 is the fraction of locations without non-mines (soil only), and W_2 is the fraction of locations with non-mines (rock, roots, etc.).

For the situation assumed in Scenario B,

$$W_1 = W_2 = \frac{1}{2} \quad (36)$$

Thus, with the P_{FA} assignment assumed for Scenario A, e.g., $P_{FA_1} = 10^{-4}$, $P_{FA_2} = 10^{-1}$, the overall P_{FA} is

$$P_{FA} = \frac{1}{2} \times 10^{-4} \times 10^{-1} + \frac{1}{2} \times 10^{-1} \approx \frac{1}{2} \times 10^{-1} \quad (37)$$

One concludes from the foregoing analysis that if a fair proportion of the interrogated locations are expected to contain non-mines, the P_{FA}

UNCLASSIFIED

UNCLASSIFIED

assigned to the discriminator processor should be low. To meet the P_{FA} of 10^{-5} for the overall processor, the P_{FA} for the discriminator should be approximately 10^{-5} . Thus, in this situation, the detection processor does little in the way of reducing the data the discriminator has to process. On the other hand, if most of the locations only contain soil, i.e., Scenario A, then the detection processor can significantly reduce the data to be handled by the discriminator/classifier.

The remainder of the section is divided according to the various techniques considered to perform each of the three processes illustrated in Figure 59, e.g., detection, discrimination, and classification. First, the performance of the CFAR type detection processor is evaluated using the NBS measured data. Next, the pattern recognition algorithms considered for discrimination and classification are evaluated with the NBS data. In addition, two types of correlation processing are investigated for target discrimination.

CFAR ANALYSIS

As described earlier, the detection processor subjects the sampled radar range profile to a normalized threshold. If any of the range profile exceeds the threshold, a potential target is declared. The threshold is normalized to the RMS average of the time profile representing the soil 1 foot from the surface or deeper. However, in this analysis, it was advantageous to fix the threshold and normalize the data. The normalization was applied to that portion of the range profile of interest (i.e., that representing the soil 1 foot below the surface or less). The normalized profile was

UNCLASSIFIED

UNCLASSIFIED

then subjected to a fixed threshold. This procedure is equivalent to the process of normalizing the threshold described above and is easier to display.

Each of the NBS data measurements were normalized in this manner and the peak value of each profile was noted. In Figure 60, a histogram of these peak values is given for each moisture category and for either a soil-only (called background) or a mine-only case. In this figure, the profile values which contained a mine signature are denoted by an "X" and those where only a soil signature existed are noted by the symbol "0." In Figure 60(a) the case of 7% moisture with loam soil is illustrated. The magnitude values are spread out along the axis where the mine-only and soil-only values are non-overlapping. Thus, a threshold can be placed at about 1/5 of the axis length and a probability of detection of 1.0 can be obtained with an accompanying probability of false alarm of 0.0. This degree of performance is shown in Figure 61 where P_D versus P_{FA} is plotted for this case.*

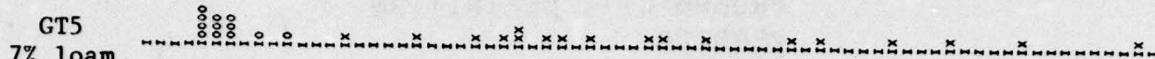
In Figure 60(b), the case of 17-18% moisture with loam soil is shown. The normalized magnitude values for this case are not spread out as much as for the previous case but are overlapping as shown. Thus, the probability of detection performance will not be nearly as good as that of the 7% loam case discussed previously. The corresponding performance curves indicating the probability of detection versus probability of false alarm are shown in Figure 62. In a similar fashion, a histogram of the profile peak values for the 12-20% moisture clay and the 26-30% moisture clay cases is shown in

*Since the number of data points used is somewhat limited, one cannot, with confidence, state that a perfect detection performance will be obtained in a practical application; however, very good performance is highly likely.

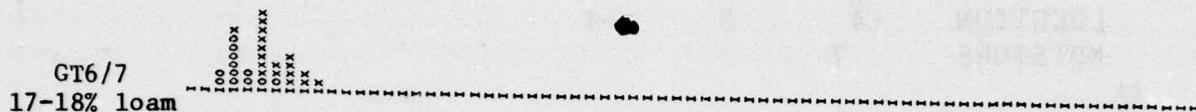
UNCLASSIFIED

UNCLASSIFIED

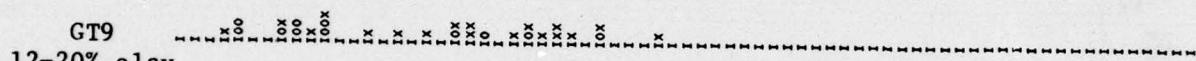
0-background x-mines



(a) magnitude



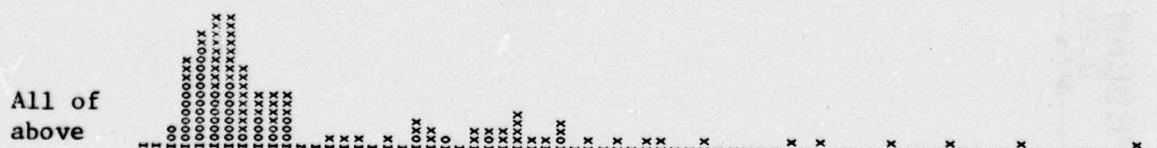
(b) magnitude



(c) magnitude



(d) magnitude



(e) magnitude

Figure 60. Histograms of temporal data subjected to an adaptive threshold (CFAR). Sidelobes of temporal waveform are 40 dB.

UNCLASSIFIED

UNCLASSIFIED

POTENTIAL TARGET DETECTION-CFAR

PROBABILITY DEFINITION 1

VERSION 1

REFERENCE 105

| NONMINE TARGET | BACKGND | TYPE C MINE | TYPE A MINE | TYPE B MINE |
|-------------------|---------|-------------|-------------|-------------|
| DEPTH | | 3 | 6 | |
| LOCATION | | +4 | 0 | -4 |
| MOISTURE | | 7 | | |

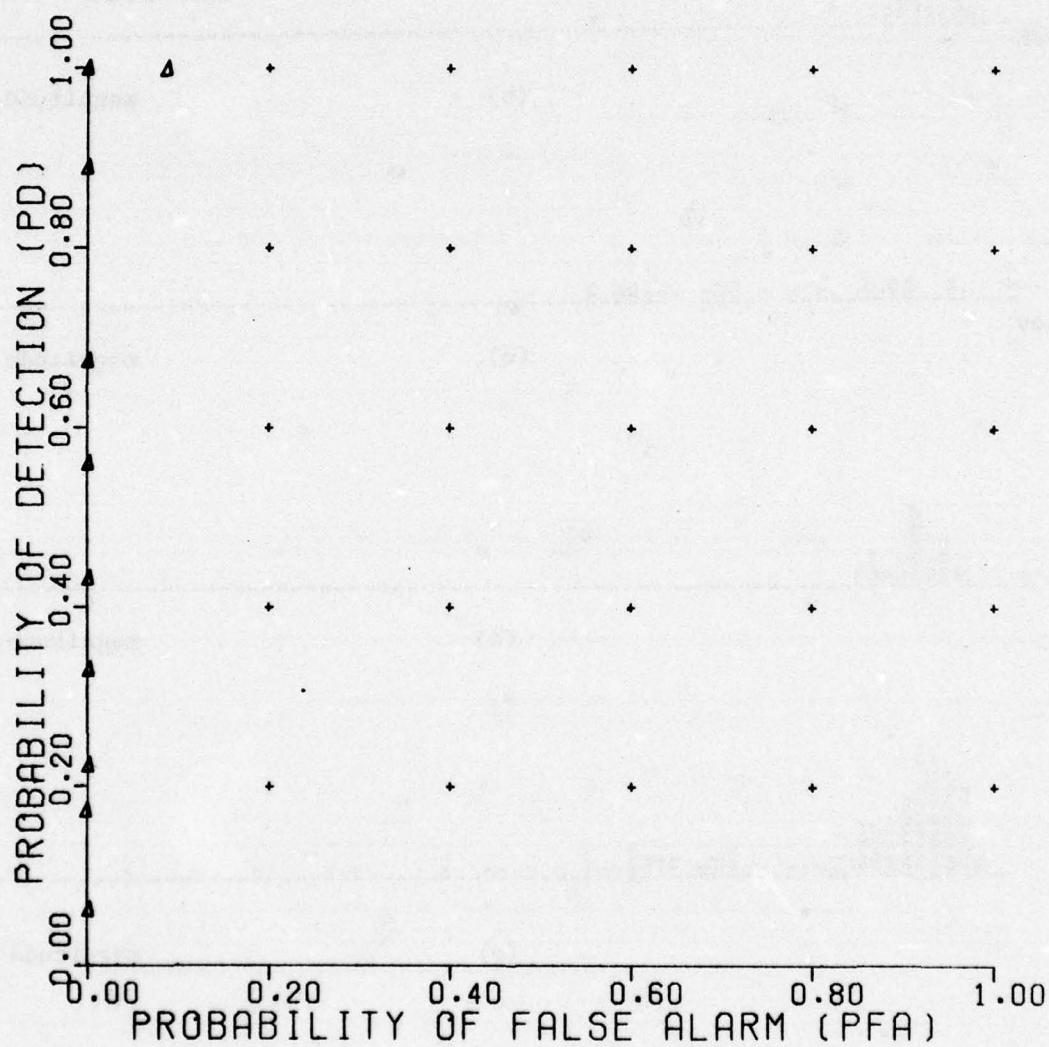


Figure 61. Potential target detection - CFAR.

UNCLASSIFIED

UNCLASSIFIED

POTENTIAL TARGET DETECTION-CFAR

PROBABILITY DEFINITION 1
VERSION 1
REFERENCE 1067

| NONMINE TARGET | BACKGND | TYPE C MINE | TYPE A MINE | TYPE B MINE |
|----------------|---------|-------------|-------------|-------------|
| DEPTH | | 3 | 6 | |
| LOCATION | | +4 | 0 | -4 |
| MOISTURE | | 17 | | |

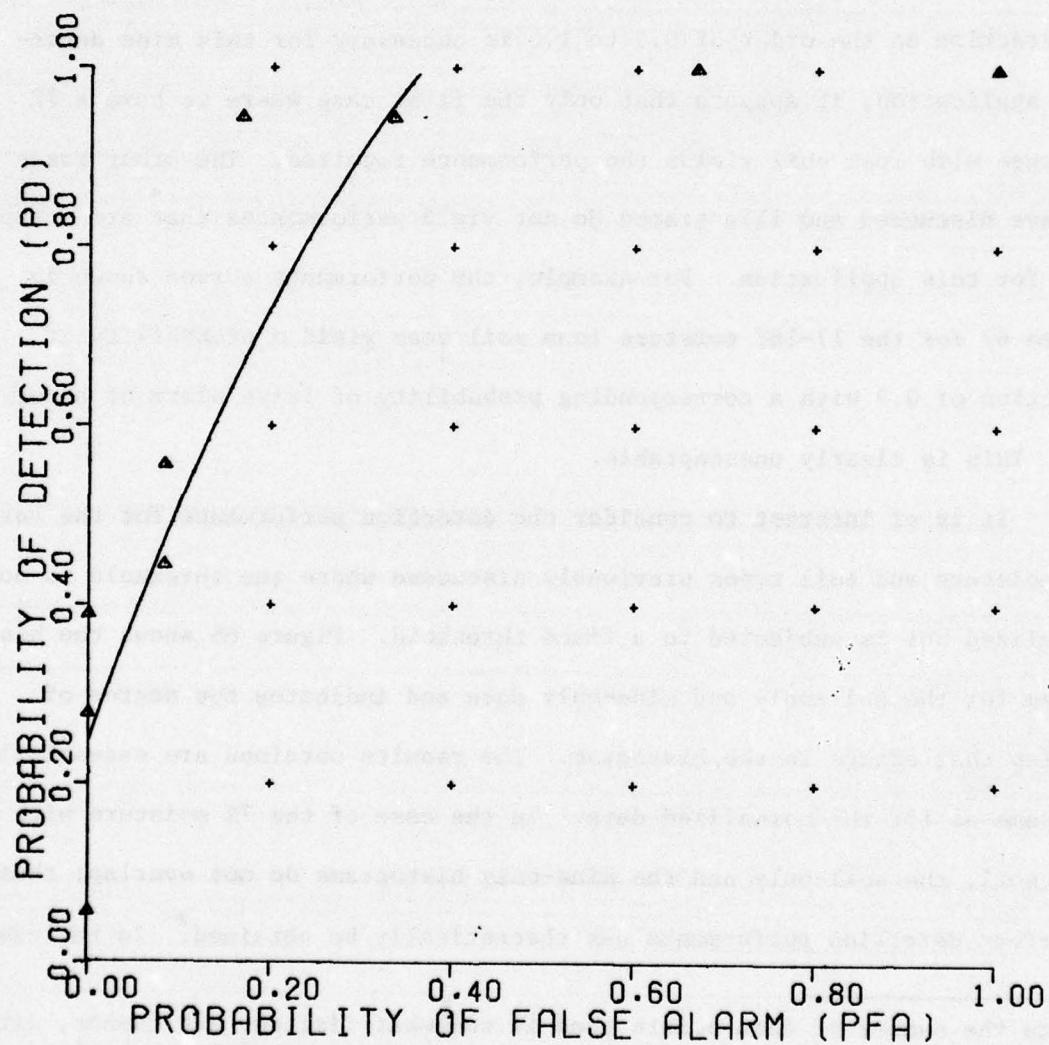


Figure 62. Potential target detection - CFAR.

UNCLASSIFIED

UNCLASSIFIED

Figures 60(c) and 60(d). In each of these cases, the mine-only and soil-only values overlap as in Figure 60(b). The corresponding performance curves are shown in Figures 63 and 64, respectively. The histogram shown in Figure 60(e) includes all of the cases discussed previously. Thus, the soil-only and the mine-only histograms overlap and the corresponding performance is rather poor. Since a probability of false alarm of approximately 10^{-5} , or something of that order, with the corresponding probability of detection on the order of 0.9 to 1.0 is necessary for this mine detection application, it appears that only the first case where we have a 7% moisture with loam soil yields the performance required. The other cases we have discussed and illustrated do not yield performances that are acceptable for this application. For example, the performance curves shown in Figure 62 for the 17-18% moisture loam soil case yield a probability of detection of 0.9 with a corresponding probability of false alarm of about 0.3. This is clearly unacceptable.

It is of interest to consider the detection performance for the various moisture and soil types previously discussed where the threshold is not normalized but is subjected to a fixed threshold. Figure 65 shows the histogram for the soil-only and mine-only data and indicates the degree of overlap that occurs in the histogram. The results obtained are essentially the same as for the normalized data. In the case of the 7% moisture with loam soil, the soil-only and the mine-only histograms do not overlap; thus, a perfect detection performance can theoretically be obtained.* In the case

*Since the number of data points used is somewhat limited, one cannot, with confidence, state that a perfect detection performance will be obtained.

UNCLASSIFIED

POTENTIAL TARGET DETECTION-CFAR

PROBABILITY DEFINITION 1
VERSION 1
REFERENCE 109

| | |
|----------|---|
| NONMINE | BACKGND |
| TARGET | TYPE C MINE TYPE A MINE TYPE B MINE |
| DEPTH | 3 6 |
| LOCATION | +4 0 -4 |
| MOISTURE | 13-16 26-30 |

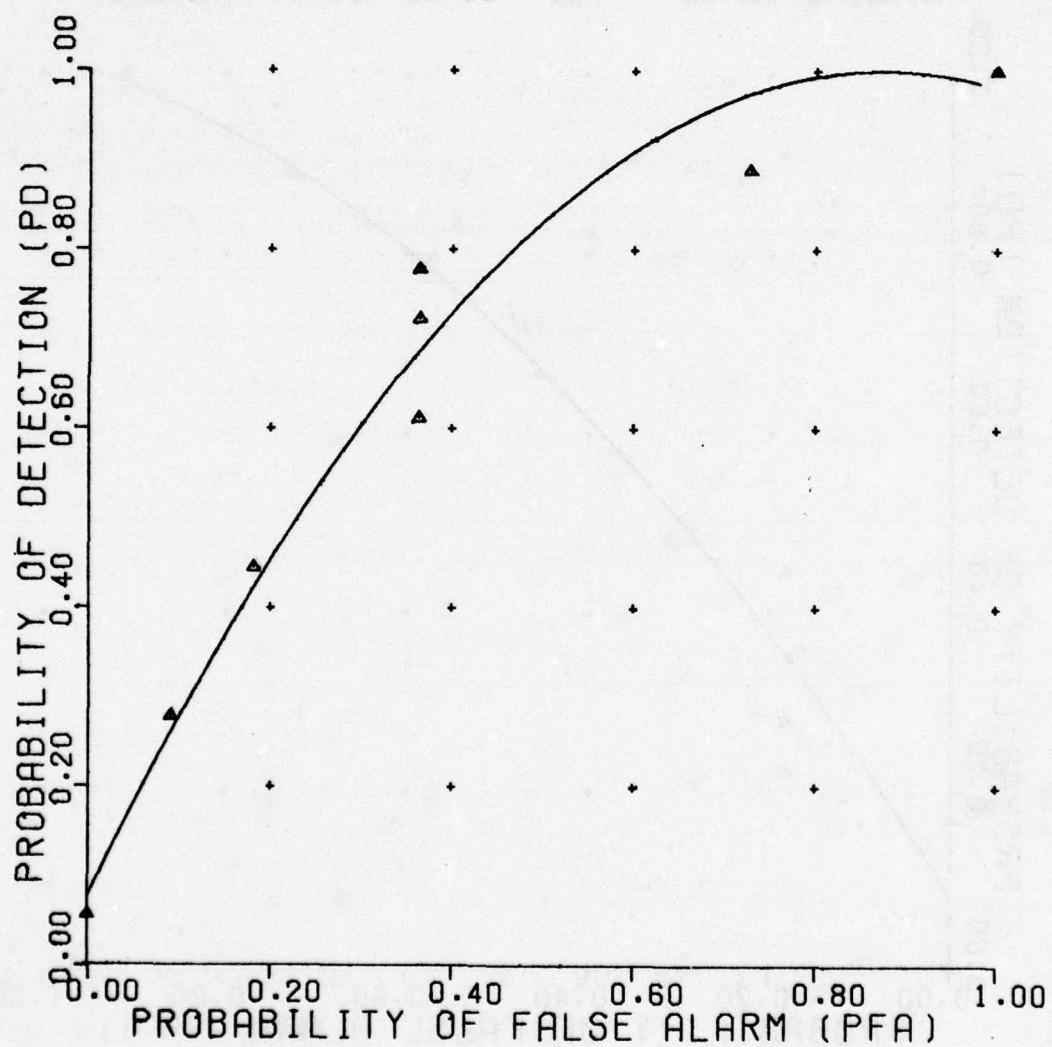


Figure 63. Potential target detection - CFAR.

UNCLASSIFIED

UNCLASSIFIED

POTENTIAL TARGET DETECTION-CFAR

PROBABILITY DEFINITION 1

VERSION 1

REFERENCE 1010

| NONMINE TARGET | BACKGND | TYPE C MINE | TYPE A MINE | TYPE B MINE |
|-------------------|---------|-------------|-------------|-------------|
| DEPTH | | 3 | 6 | |
| LOCATION | | +4 | 0 | -4 |
| MOISTURE | | 26-30 | 30 | |

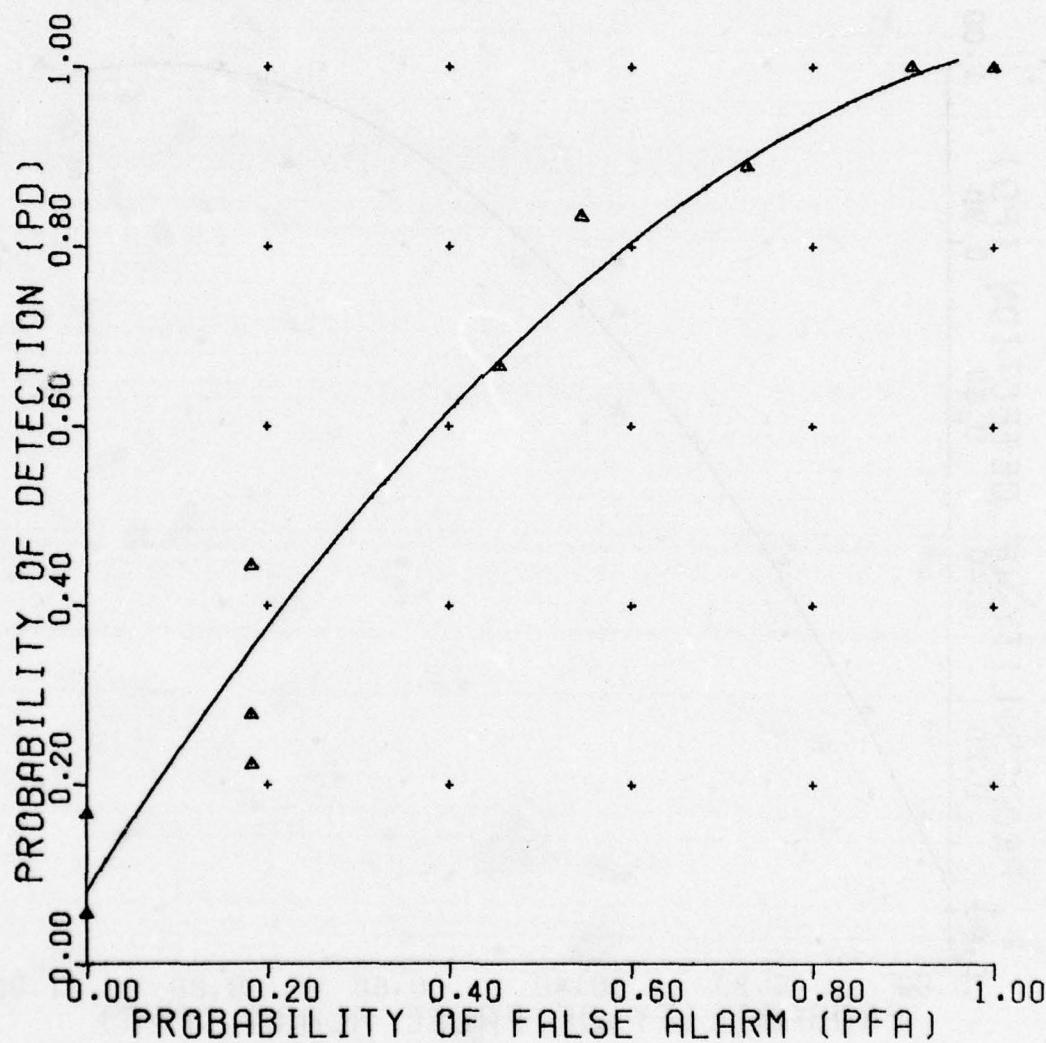


Figure 64. Potential target detection - CFAR.

UNCLASSIFIED

UNCLASSIFIED

0-background x-mines

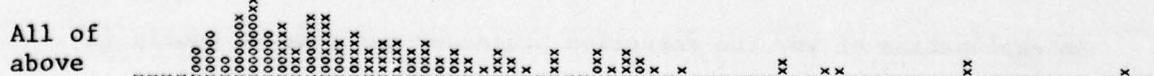
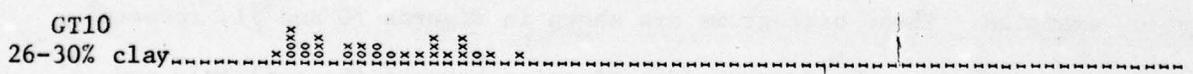
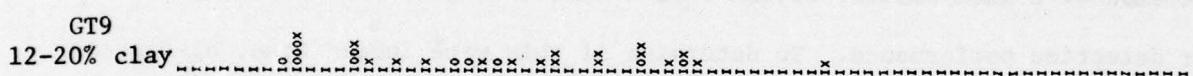
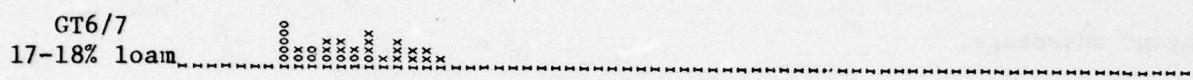
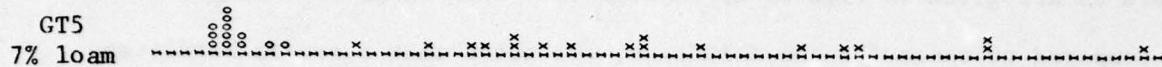


Figure 65. Histograms of time data subjected to fixed threshold.

UNCLASSIFIED

UNCLASSIFIED

of the 17-18% moisture with loam soil, the two histograms do overlap. The same is true of the wet clay cases as shown in Figures 65(c) and 65(d). The corresponding detection performance curves for the cases illustrated in Figure 65 are given in Figures 66 through 69. When these performance curves are compared to those for the CFAR case, one notes that there is hardly any difference at all. Thus, we can conclude, based on this limited set of data, that normalizing the threshold, or normalizing the data which is subject to a fixed threshold, does not improve the detection performance or give any apparent advantage.

All of the previous histograms are for the case where the transmit pulse was designed with a 40 dB time sidelobe. It was thought that perhaps the time sidelobes of the large ground return might be interfering with the detection of a much smaller return from a buried target, thus yielding a poor detection performance. To determine if this were indeed true, histograms similar to those shown in Figures 60 and 65 for the normalized and unnormalized cases were generated where the time sidelobes of the transmitted pulse were designed to be at 60 dB below peak value instead of 40 dB as in the previous examples. These histograms are shown in Figures 70 and 71, respectively. One notes that the degree of overlapping between the soil-only and mine-only histograms are about the same as for the 40 dB data; thus, one concludes that with this set of data, the 40 dB time sidelobes are adequate such that the detection performance is not degraded.

An explanation of why the detection processor performs so poorly in the wetter soils is needed. Perhaps, a reason for the poor detection

UNCLASSIFIED

UNCLASSIFIED

POTENTIAL TARGET DETECTION-UNNORM

PROBABILITY DEFINITION 1

VERSION 1

REFERENCE 115

| NONMINE TARGET | BACKGND | TYPE C MINE | TYPE A MINE | TYPE B MINE |
|-------------------|---------|-------------|-------------|-------------|
| DEPTH | | 3 | 6 | |
| LOCATION | | +4 | 0 | -4 |
| MOISTURE | | 7 | | |

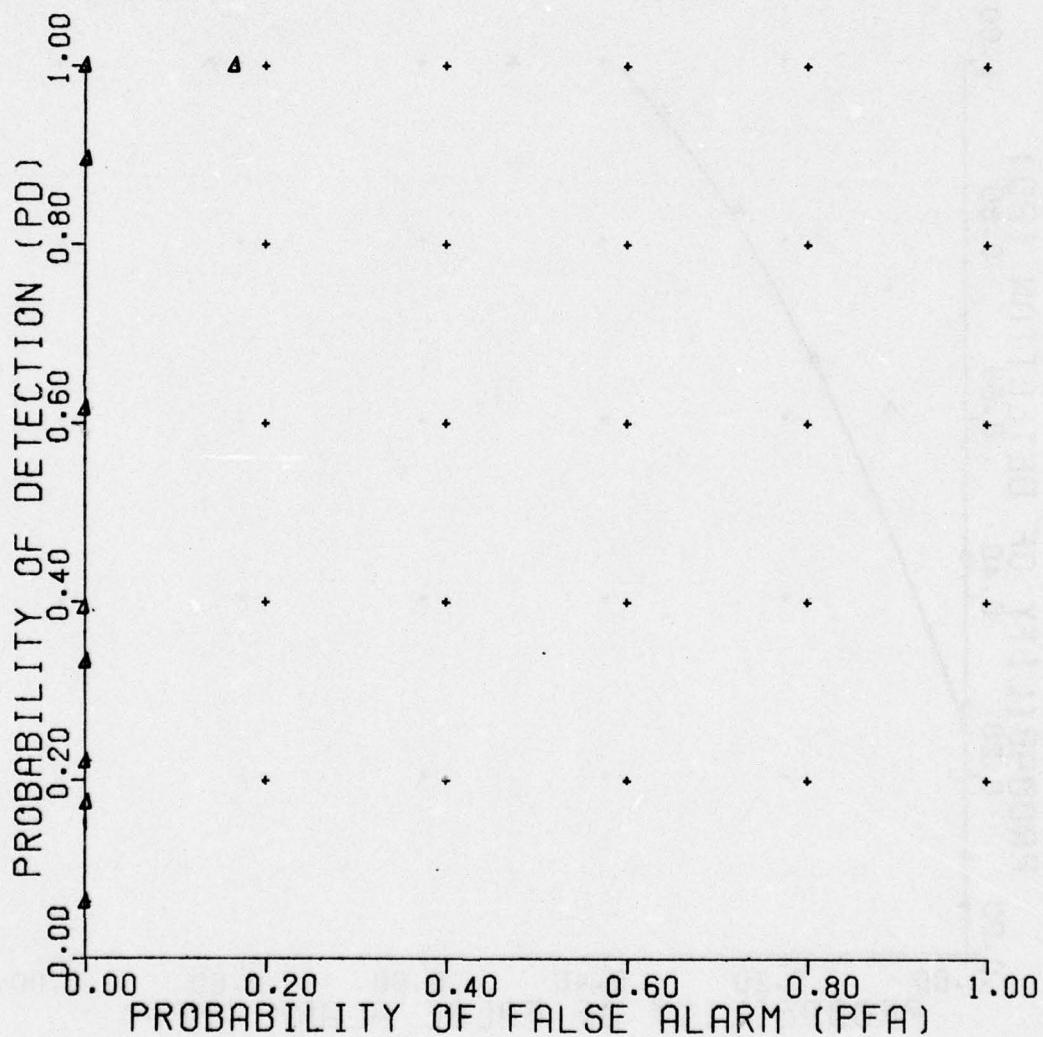


Figure 66. Potential target detection - unnormalized.

UNCLASSIFIED

UNCLASSIFIED

POTENTIAL TARGET DETECTION-UNNORM

PROBABILITY DEFINITION 1
VERSION 1
REFERENCE 1167

| NONMINE TARGET | BACKGND | TYPE C MINE | TYPE A MINE | TYPE B MINE |
|-------------------|---------|-------------|-------------|-------------|
| DEPTH | | 3 | 6 | |
| LOCATION | | +4 | 0 | -4 |
| MOISTURE | | 17 | | |

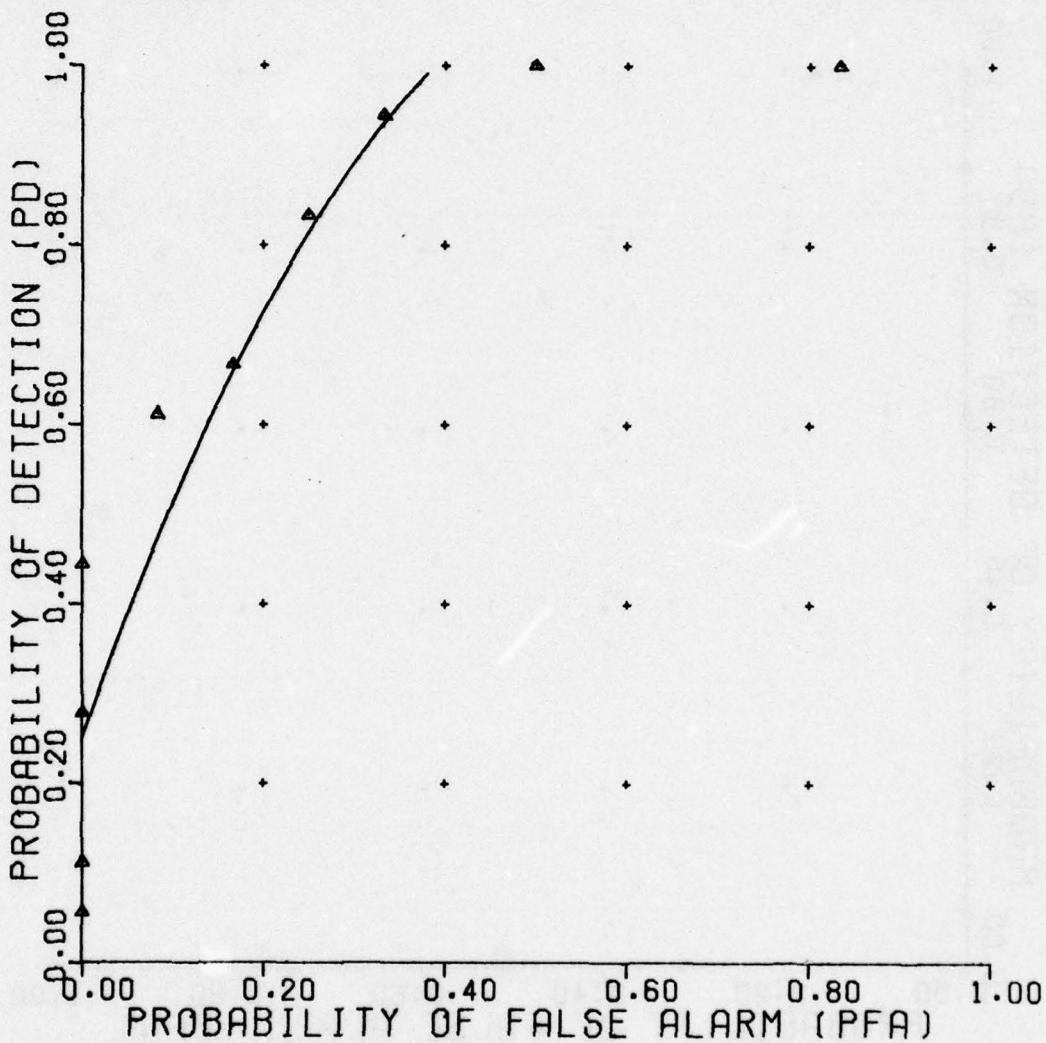


Figure 67. Potential target detection - unnormalized.

UNCLASSIFIED

UNCLASSIFIED

POTENTIAL TARGET DETECTION-UNNORM

**PROBABILITY DEFINITION 1
VERSION 1
REFERENCE 119**

| NONMINE TARGET | BACKGND | TYPE C MINE | TYPE A MINE | TYPE B MINE |
|-------------------|---------|-------------|-------------|-------------|
| DEPTH | | 3 | 6 | |
| LOCATION | | +4 | 0 | -4 |
| MOISTURE | | 12-20 | 13-16 | |

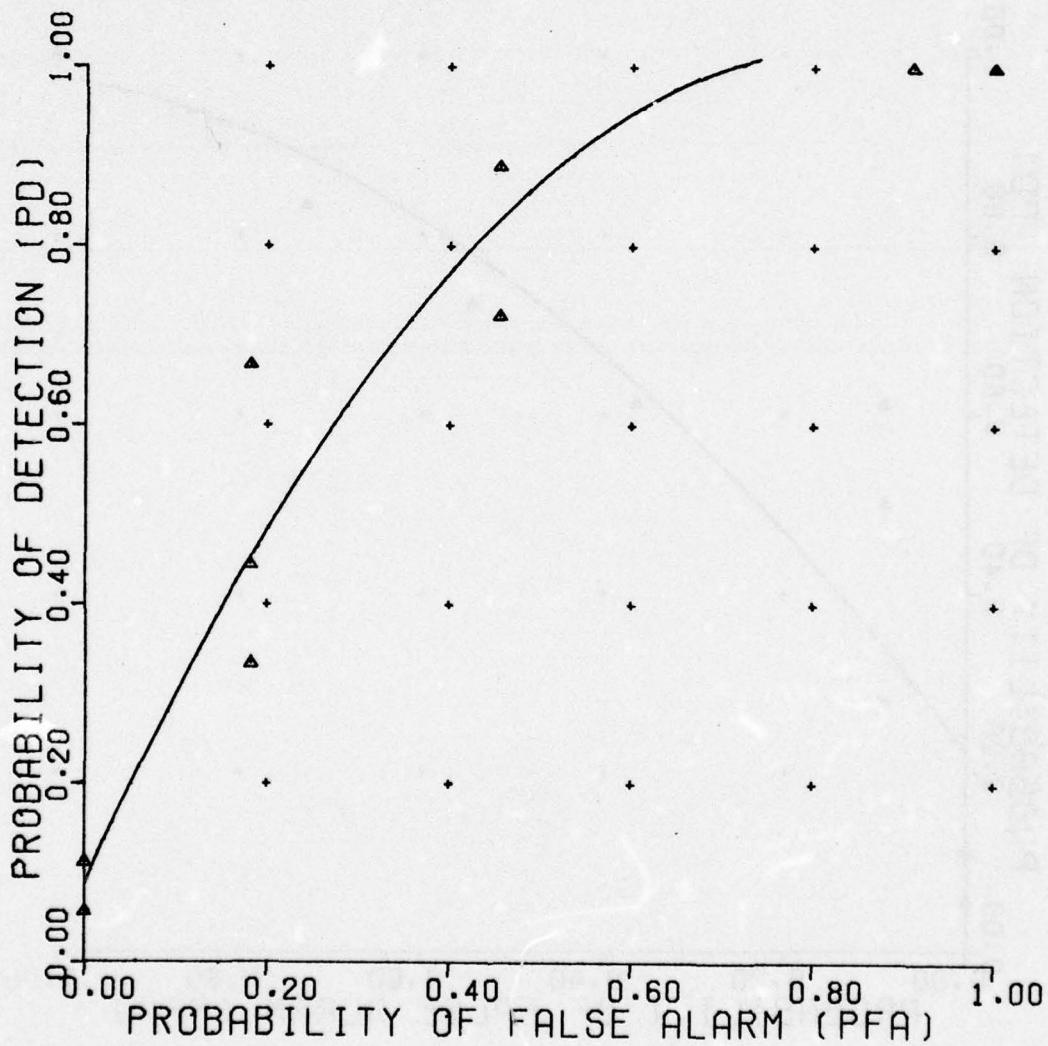


Figure 68. Potential target detection - unnormalized.

UNCLASSIFIED

UNCLASSIFIED

POTENTIAL TARGET DETECTION-UNNORM

PROBABILITY DEFINITION 1
VERSION 1
REFERENCE 1110

| NONMINE TARGET | BACKGND | TYPE C MINE | TYPE A MINE | TYPE B MINE |
|-------------------|---------|-------------|-------------|-------------|
| DEPTH | | 3 | 6 | |
| LOCATION | | +4 | 0 | -4 |
| MOISTURE | | 26-30 | 30 | |

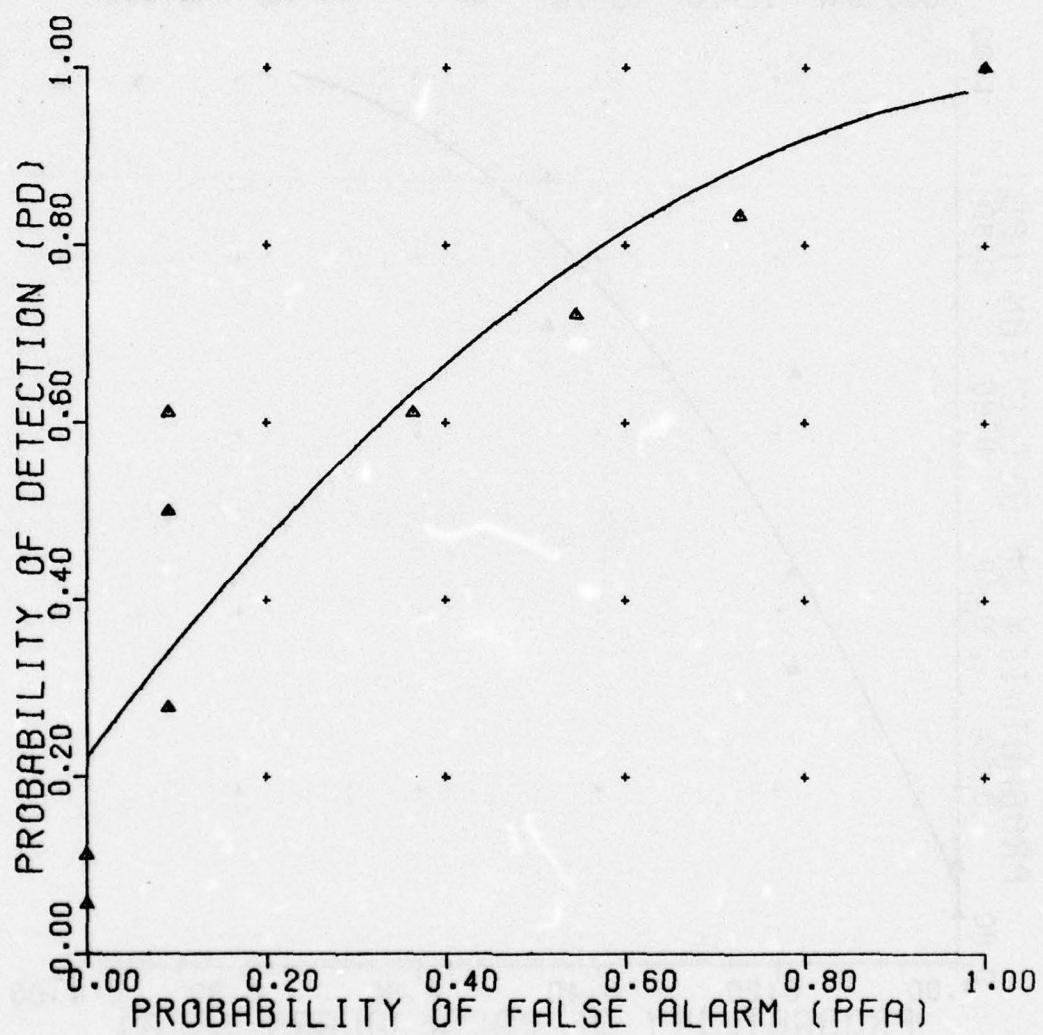


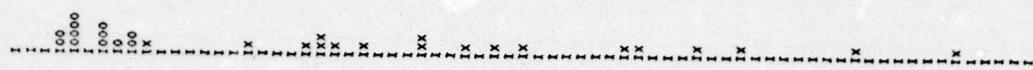
Figure 69. Potential target detection - unnormalized.

UNCLASSIFIED

UNCLASSIFIED

0-background x-mines

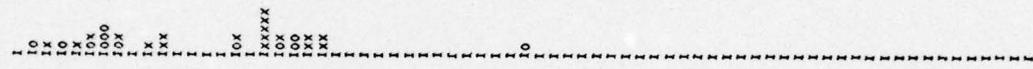
GT5
7% loam



GT6/7
17-18% loam



GT9
12-20% clay



GT10
26-30% clay



All of
above

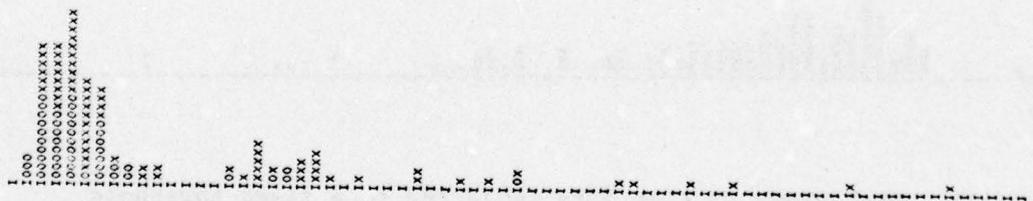


Figure 70. Histograms of time data subjected to an adaptive threshold (CFAR). Sidelobes of temporal waveform is 60 dB.

UNCLASSIFIED

UNCLASSIFIED

0-background x-mines

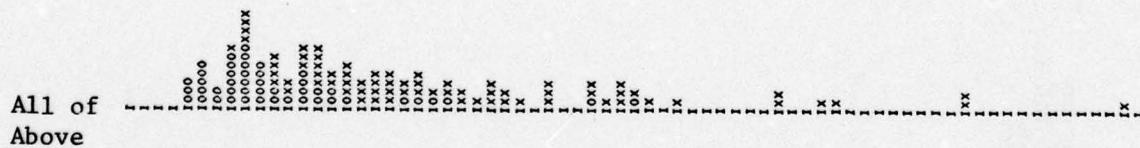
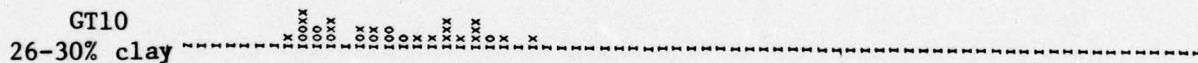
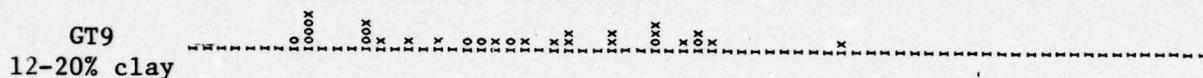
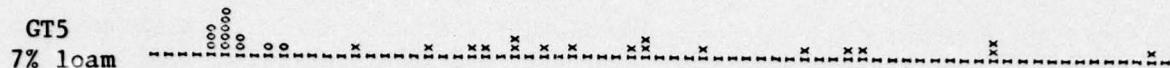


Figure 71. Histograms of time data subjected to a fixed threshold (CFAR). Sidelobes of the temporal waveform is 60 dB.

UNCLASSIFIED

UNCLASSIFIED

performance is that the soil is composed of roughly parallel layers or boundaries which allow deposits of water. Since the dielectric constant of the water deposits is so much larger than that of the surrounding soil, the thin layers of water reflect a substantial portion of the incident microwave energy and thus interfere with the detection of mines buried in soil. Another explanation is that radar returns from close proximity objects above the ground are interfering. For example, perhaps the radar and radar vehicle are reflecting the radar signals to provide a multiple bounce situation. The source of this problem was not determined in this study.

PATTERN RECOGNITION

The information processing discipline known as pattern recognition is implemented whenever a decision is to be made which involves large quantities of data. The object of pattern recognition or pattern classification is to automate the decision process based on the experience of a learning set. A complete classification system encompasses both the design and implementation of computer software and hardware. In this section, only the software system will be described.

The general approach is to divide information processing for the purpose of pattern recognition into three steps: (1) data collection, (2) feature extraction and evaluation, and (3) selection of the classifier.

Figure 72 gives a block diagram of the basic data processing flow for designing various classifiers. The data on magnetic tape is in the frequency domain. From this information, radar signatures are generated and placed

UNCLASSIFIED

UNCLASSIFIED

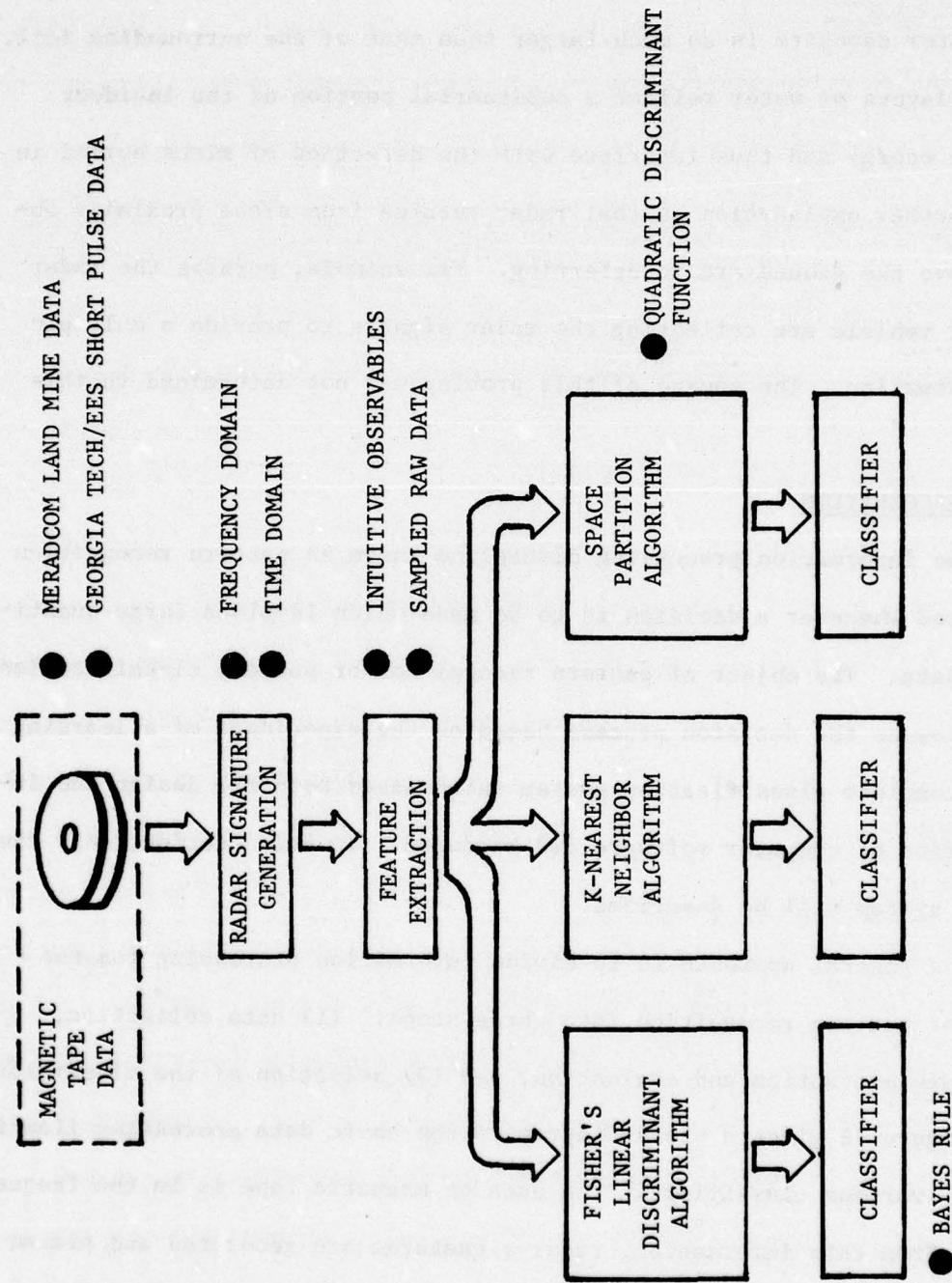


Figure 72. Classification data processing system.

UNCLASSIFIED

UNCLASSIFIED

into a mine or non-mine class. The non-mine category consists of returns from objects which might typically be found in a mine field, e.g., rocks, roots, and flat metal plates. The mine category contains the signatures for the type A, B, and C mines. The preprocessing steps for generating the radar signatures are summarized in the following paragraphs.

The raw data consisted of the S_{12} parameters which were measured at 123 frequencies over a range of several GHz. The data was weighted to reduce the time sidelobes of the ground return, then transformed into the time domain. A range-gated window was set automatically to separate the target signature from the ground return, and that portion of the signature was then transformed into the frequency domain. All classification work used these range-gated frequency profiles.

From each signature a characteristic set of numbers, i.e., features, were extracted according to a prescribed format. The ensemble of features for one particular class such as a rock, root, or a specific mine comprised a learning set for that class. Several of these learning sets were inserted into the pattern recognition programs (e.g., the Fisher's Linear Discriminant or the k-nearest neighbor method) to produce a classification algorithm. The classifier was designed to identify an unknown sample as a mine or non-mine and to minimize the number of misclassified samples.

Data Selection

The majority of classification work discussed in this report was done with the NBS data which consisted of measurements of the S_{12} parameters versus

UNCLASSIFIED

UNCLASSIFIED

frequency for two types of land mines and several non-mine objects such as roots and rocks. The objects were buried under three to six inches of soil, with soil moisture content varying between three and twenty percent. Bistatic measurements were made with the antennas placed at five positions with respect to the target center: -8", -4", 0", 4", and 8".

The selection of data for classification purposes is one of the most critical considerations in the information processing chain. If the data base is too small to include signatures taken for all parameters of interest (e.g., aspect angle, soil moisture, clutter level, etc.), then the resulting design may do a good job in classifying under some conditions but break down when signatures resulting from the neglected conditions are examined. For this work, most of the available data were used for the classifier, with the exception of the data taken with the very wet soil (record GT-10) and the measurements taken at -8" and 8" from the center of the mine. The GT-10 data was discarded because the signal-to-interference ratio was very low and could not be successfully used for classification. Measurements at -8" and 8" were left out because they sometimes yielded small signal levels. At these antenna positions, the mine was only partially illuminated. The former case limits the applicability of the classification performance to soils with moisture content less than about 20%. The latter case would have given over-estimated false alarm rates.

Feature Extraction

Feature extraction is the process whereby a relatively small number of parameters are computed from the input measurements. An advantage of

UNCLASSIFIED

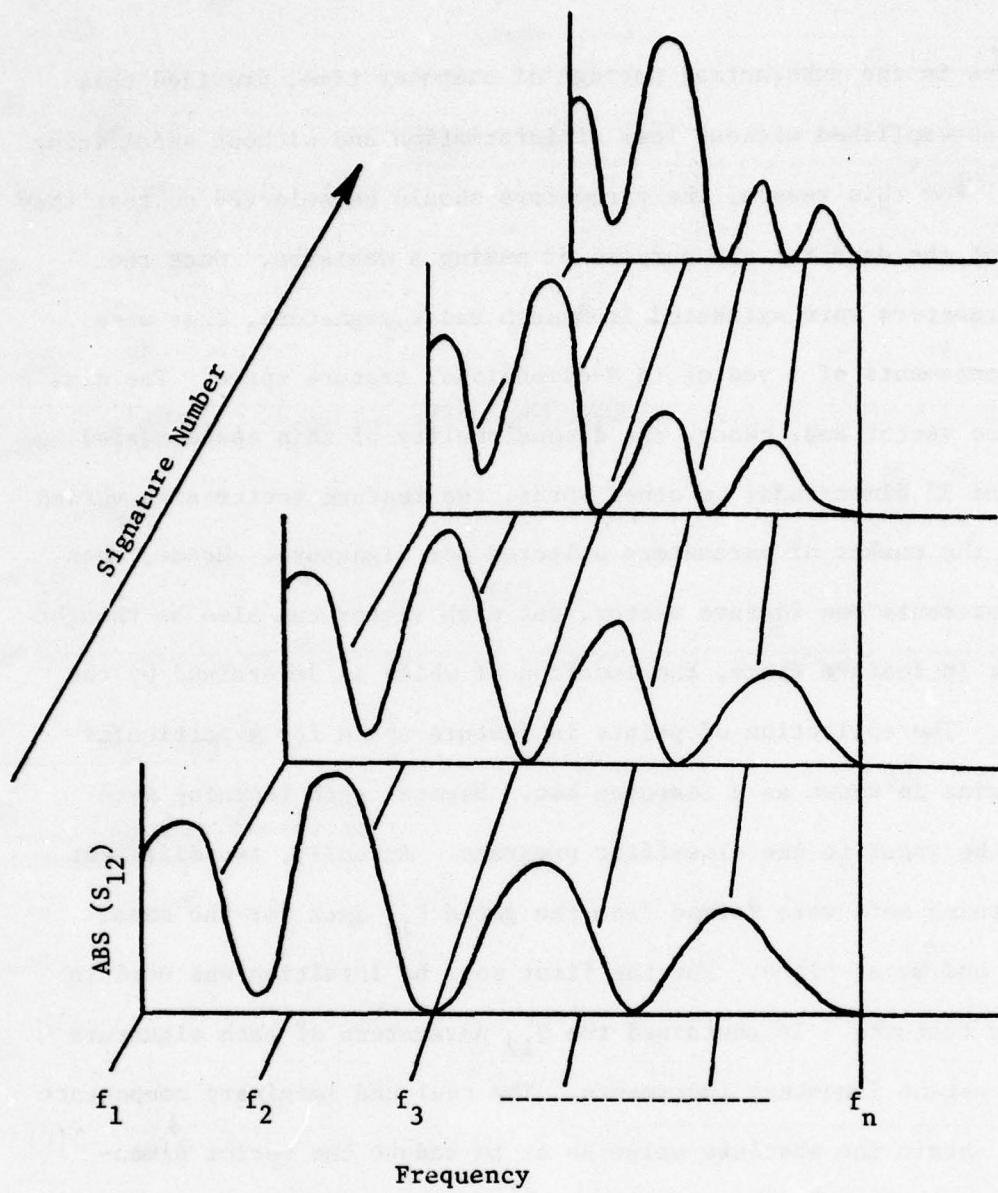
UNCLASSIFIED

this step lies in the substantial savings of computer time, provided this task can be accomplished without loss of information and without sacrificing performance. For this reason, the parameters should be selected so that they best represent the data for the purpose of making a decision. Once the specified parameters were extracted from each radar signature, they were treated as components of a vector in N-dimensional feature space. The size of the feature vector and, hence, the dimensionality of this space varied between 10 and 32 dimensions; in other words, the feature vector size varied according to the number of parameters selected per signature. Hence, each signature represents one feature vector, but each vector can also be thought of as a point in feature space, the location of which is determined by the vector's tip. The collection of points in feature space for a particular mine or non-mine is known as a learning set. Several such learning sets constituted the input to the classifier programs. Actually, two different types of learning sets were formed from the gated S_{12} data for the mine, root, rocks, and metal plate. For the first set, no intuition was used in selecting the features. It contained the S_{12} parameters of each signature sampled at constant frequency increments. The real and imaginary components were used to obtain the absolute value so as to reduce the vector dimensionality. (Another advantage of this step will be discussed in a later paragraph on feature size.) An example of a vector formed from the sampled frequency representation of the S_{12} data profile is shown in Figure 73.

The other set contained ten intuitive features for each signature which were selectively chosen from an original larger set to maximize the separation

UNCLASSIFIED

UNCLASSIFIED



A feature vector will be of the form

$$\bar{x} = \begin{bmatrix} \text{ABS } \{S_{12}(f_1)\} \\ \text{ABS } \{S_{12}(f_2)\} \\ \text{ABS } \{S_{12}(f_n)\} \end{bmatrix}$$

Figure 73. Frequency domain signature ensemble.

UNCLASSIFIED

UNCLASSIFIED

of the data classes. These were:

- (1) The distance between the highest and second highest peaks;
- (2) The distance between the highest and third highest peaks;
- (3) The distance between the second and the third highest peaks;
- (4) The distance between the left most and right most peaks;
- (5) The ratio of the distance between the highest and left most peaks over the distance between the left most and right most peaks;
- (6) The ratio of distance between the second highest and the left most peaks over the distance between the left most and right most peaks;
- (7) The ratio of the amplitude of the second highest over the highest peaks;
- (8) The ratio of the amplitude of the third highest over the highest peaks;
- (9) The number of peaks above 10% of the highest peak;
- (10) The number of peaks above 50% of the highest peak.

The primary motive behind the selection of these intuitive features was to reduce the dimensionality of the feature space. Again, other inherent advantages for this step will be discussed later.

Classifier Selection

Once a data base has been acquired, a set of potential features extracted, and a subset evaluated to be promising as input for decision making, the actual decision rule development process can begin. Usually, the first

UNCLASSIFIED

UNCLASSIFIED

step in that procedure is to divide the input data sets into two equal parts which should be as identical as possible. One part is used as the learning set, the other as the test set. This process is called generalization; however, because of limited amounts of available data, this step was bypassed. Thus, all input data was used not only as a learning but also as a test set.

The second step is to select the classifier. The particular choice depends on such variables as (1) the distribution of vectors in feature space, (2) the amount of time required to process unknown "radar signatures" and, most important, (3) the performance of the classifier. For this reason we investigated three basic types of classifiers. The simplest of these were the linear processors. Here the components of the sample vector X are multiplied by the coefficients W_1 such that

$$S = \sum_i^N W_i X_i \quad (38)$$

The unknown sample X is then characterized as a mine or non-mine depending on whether the sum S exceeds or falls below a threshold S_o . The W_i are determined during the training (i.e., during processing of the learning set).

One of these linear processors is the Fisher's Linear Discriminant (FLD) classifier. The FLD projects the feature vectors in multi-dimensional space onto a vector W such that the scatter between the means of the distributions is maximized and the scatter within each distribution is minimized. Each projected vector defines a point on W . Thus if sufficient data is available, a histogram can be constructed along W . The distributions of the classes can then be approximated by probability density functions. This

UNCLASSIFIED

UNCLASSIFIED

process is illustrated in two dimensions, a and b, in Figure 74. The circles and squares represent the tips of feature vectors for two different classes such as a mine and a non-mine. The dashed lines $\overset{\rightarrow}{W_1}$ and $\overset{\rightarrow}{W_2}$ denote two different choices of the \vec{W} vector. The one marked as $\overset{\rightarrow}{W_1}$ is shown as the solution vector. Along this direction, the projected points form two density distributions which separate into their respective classes; however, the vector marked $\overset{\rightarrow}{W_2}$ clearly cannot be the proper choice because the projected points overlap to a considerable extent. To obtain the classifier, the distributions were separated at the point S_o . Hence, to classify an unknown signature, one must first extract the feature vector X , then multiply it by the vector \vec{W} and evaluate the sum S in Equation (38) to check whether S is greater than or less than S_o . The multiplication projects the vector X onto \vec{W} . Any point which falls below S_o is classified as a mine, for example, whereas points above S_o would be labeled as non-mines.

A classifier using a threshold such as the point S_o is also known as the Bayes classifier. To further illustrate this type of classifier, consider the two-category case shown in Figure 75. The two continuous distributions are similar in appearance to histograms along $\overset{\rightarrow}{W_1}$, but differ from histogram representations by a scale factor such that

$$\int_{-\infty}^{\infty} p(w/x_1) dw = 1 \quad (39)$$

$$\int_{-\infty}^{\infty} p(w/x_2) dw = 1 \quad (40)$$

In other words, they are probability density functions. The function $p(w/x_1)$

UNCLASSIFIED

UNCLASSIFIED

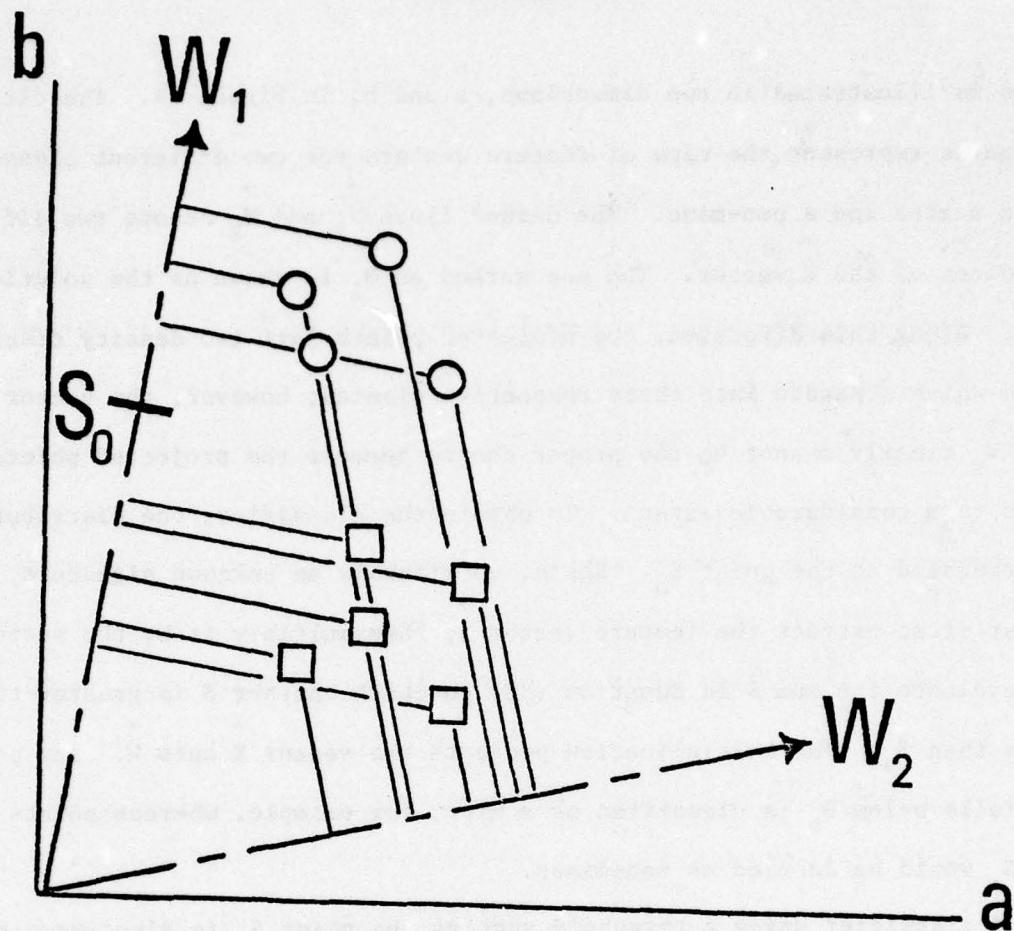


Figure 74. Fisher's Linear Discriminant classifier.

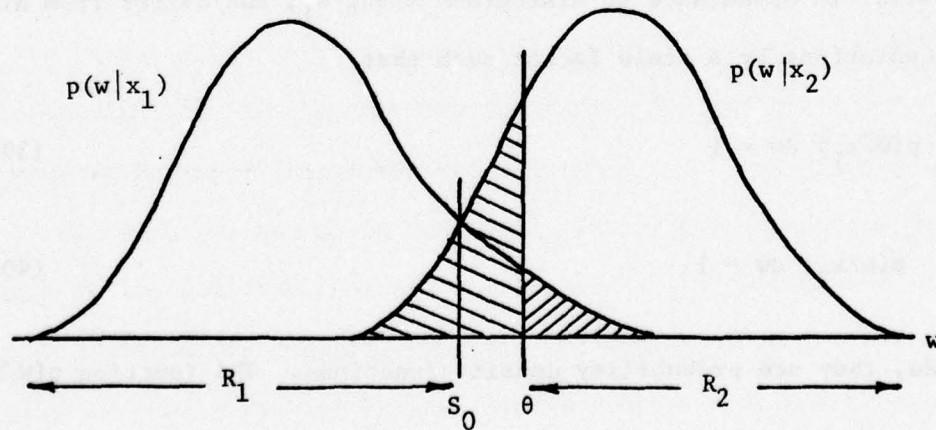


Figure 75. Normalized density distributions projected onto the w vector.

UNCLASSIFIED

UNCLASSIFIED

denotes the normalized density of mine vectors projected onto \vec{w}_1 at any point w . The normalized density for non-mines at the same point is given by $p(w/x_2)$.

Consider the two functions being divided into two regions, R_1 and R_2 at θ . There are two ways in which a classifier error can occur: either a vector falls into R_1 and the true state is x_2 , or it falls into region R_2 and the true state is x_1 . Therefore, the probability of error is given by

$$P(\text{error}) = \int_{R_2} p(w/x_1) P(x_1) dw + \int_{R_1} p(w/x_2) P(x_2) dw \quad (41)$$

where $P(x_1)$ and $P(x_2)$ are the a priori probabilities of the two cases. For instance, if the learning set for the mines would contain 100 signatures and that for the non-mines only 50 signatures, then $P(x_1)$ and $P(x_2)$ would be approximated by values $2/3$ and $1/3$, respectively.

The two terms in Equation 41 are merely the areas under the tails of the functions (shaded portions). Because θ , and hence, the regions R_1 and R_2 , were selected arbitrarily, the probability of error is not as small as it might be. However, the minimum error can be found by differentiating $P(\text{error})$ and setting the result equal to zero such that

$$\frac{\alpha P_{\text{error}}}{\alpha \theta} = 0 \quad (42)$$

The solution to Equation (42) is the necessary condition required to minimize $P(\text{error})$ and is given by

$$p(\theta/x_1) P(x_1) = p(\theta/x_2) P(x_2) \quad (43)$$

UNCLASSIFIED

UNCLASSIFIED

Equation (43) shows that $P(\text{error})$ is a minimum when θ is at S_0 , i.e., the Bayes position.

We used the FLD not only as a classifier but also to select those intuitive features (i.e., feature evaluator) which had the greatest influence on the separation of the projected distributions. Clearly, if one of the W_1 components is zero or much smaller than others, the intuitive feature weighted by that component does not contribute significantly to the separation of the projected classes and, thus, was discarded. In this manner we were able to reduce the dimensionality of our feature vectors yet retain a selected subset of intuitive features which did not alter the classifier performance significantly. That subset was shown previously in the paragraph on feature selection.

Unfortunately, the FLD does not perform well with just any distribution of feature vectors. For example, if the cluster of mine data were contained within the non-mine data, or if the two distributions were to overlap to a significant extent, it is expected that the 1, 3, 5, or 7-nearest neighbor (NN) classifier will give better performances. With the nearest neighbor classifier, all test data was first stored in memory. The vector distances were then measured between a sample of unknown origin and its neighbors, and the unknown was classified into that group containing the largest number of the k-nearest samples.

The NN algorithm works best with data in which the same scale is used to measure the amplitude for all the feature vector dimensions. If the various features are measured on different scales, then the definition of distance becomes a problem because distance between points in one feature

UNCLASSIFIED

UNCLASSIFIED

dimension may be measured on a scale so radically different from the others that the contributions of the other dimensions to the total distance may become negligible. Thus, information from the other features which might be useful in separating data classes is effectively lost. The distance measure is not a problem with feature vectors which were derived from raw data, but may become one when intuitive features are used to form the data vectors.

Another disadvantage with the NN classifier is the fact that storage of the learning set requires a large memory. Furthermore, large processing times are needed since all distances between the unknown point and every other point in the learning set must be calculated. This fact could influence the search speed of the mine detection vehicle. Thus, we turned our attention to a third classifier, the space partition (SP) method.

Points belonging to different classes may be separated directly in feature space by means of a decision or hyper-surface (i.e., surface in n-dimensional space). A quadratic surface is defined by the quadratic discriminant function $G(\vec{X}) = 0$ where

$$\vec{G}(\vec{X}) = \vec{w}_0 + \sum_i^d \vec{w}_i \vec{x}_i + \sum_i^d \sum_j^d \vec{w}_{ij} \vec{x}_i \vec{x}_j \quad (44)$$

and d is the number of dimensions. The \vec{x}_i are the components of a feature vector and w_0 , w_i , and w_{ij} are components of a weight vector. The quadratic discriminant function $\vec{G}(\vec{X})$ is not equal to zero if the vector \vec{X} is either above or below the hyperplane as shown in Figure 76. The figure was simplified to show the hyperplane in a two-dimensional space. In this case, the hyperplane $G(x) = 0$ marks the boundary between two different classes of data.

UNCLASSIFIED

UNCLASSIFIED

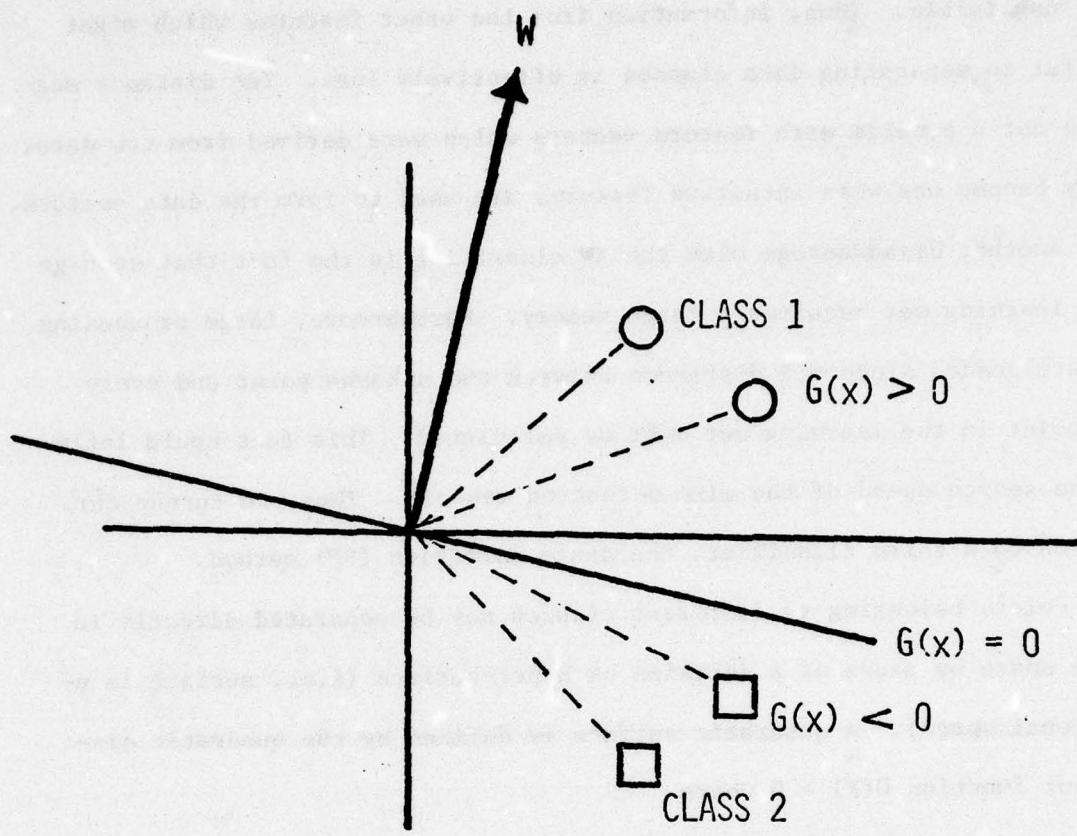


Figure 76. Space partition classifier.

UNCLASSIFIED

UNCLASSIFIED

Vectors (only the tip of each vector is indicated as a circle or square) which fall above the hyperplane will give a value for $G(X)$ which is greater than zero. Below the hyperplane $G(X)$ will always be less than zero. This fact suggests the following decision rule for a two-category case such as mine vs. non-mine:

- +
- (1) Decide class 1 if $G(X) > 0$ (i.e., points on the positive side of the decision surface are labeled class 1);
 - (2) Otherwise [$G(X) < 0$] decide class 2 (i.e., points on the negative side of the surface are labeled class 2).

The actual classification process is similar to the FLD (in fact, the FLD is a special case of the SP classifier) except that the vector X is expanded to include the cross products $x_i x_j$ for a quadratic surface, such that the complete vector X is given by

$$\vec{X} = 1 + x_1 \dots x_n \dots + x_1^2 \dots x_n^2 \dots + x_{12} \dots x_{n-1} x_n \quad (45)$$

The number 1 is needed in case w_o is not equal to zero. All components are then multiplied by their respective weights w_o, w_i, w_{ij} and the product $G(X)$ tested.

To design a classifier of this type, the weights w_i, w_{ij} must be determined to give a minimum number of misclassified samples. Because W is always normal to the decision surface, a reorientation of the vector W is equivalent to reorienting the decision surface. There are several methods of arriving at the correct W . For this report, the perceptron criterion function was used. The first step was to generate a transformation of feature vectors which simplified the treatment of the two-category case, i.e.,

UNCLASSIFIED

UNCLASSIFIED

we set $\vec{Y} = \vec{X}$ if \vec{X} is in data class 1 and $\vec{Y} = -\vec{X}$ if \vec{X} is in data class 2.

This results in $G(\vec{X}) > 0$ for all properly classified data points but $G(\vec{X}) < 0$ for misclassified points. Consider $\vec{Y}'(W)$ to be the set of samples misclassified by weight vector W . The perceptron criterion function $J_p(W)$ which is minimized when W is a solution vector, may then be expressed as

$$J_p(W) = \sum_{y'} (\vec{W} \vec{Y}^m) \quad (46)$$

where the \vec{Y}^m are the feature vectors of misclassified samples. Since $\vec{W} \vec{Y}^m < 0$ for misclassified samples, J_p will always be greater or equal to zero. Moreover, J_p will be zero only if W perfectly separates the data into their respective groups. In order to calculate W which minimizes this function, one must first solve for the gradient of $J_p(W)$ given by

$$\nabla J_p(W) = \sum_{y'} (-\vec{Y}^m) \quad (47)$$

To start the W search sequence, an arbitrary \vec{W}_k is introduced initially. This vector is then moved toward the proper solution by the gradient descent algorithm which states that the next value of W , \vec{W}_{k+1} , is obtained by moving some distance from the initial starting vector \vec{W}_k in the direction of the steepest descent along J_p (i.e., along the negative of the gradient ∇J_p .)

Thus

$$\vec{W}_{k+1} = \vec{W}_k - \rho_k \nabla(J_p) \quad (48)$$

or $\vec{W}_{k+1} = \vec{W}_k + \rho_k \sum_k (\vec{Y}_k^m)$ (49)

where $k \geq 1$. Thus, each vector Y is first tested for misclassification

UNCLASSIFIED

UNCLASSIFIED

[i.e., $\vec{G}(\vec{Y}) < 0$]. If a misclassified vector \vec{Y}^m is found, a fraction of \vec{Y}^m , $\rho_k \vec{Y}^m$, is added to the initial weight vector \vec{W} , to reorient the decision surface. Thereafter, the search for misclassified samples and reorientation of the hyperplane continues until a position is found which results in the minimum number of misclassified samples. The particular \vec{W} corresponding to that position is the solution vector. The variable, ρ_k , was usually set to decrease as $1/k$ for convergence toward a solution.

There are several disadvantages associated with this technique. It was previously pointed out that the quadratic discriminant function uses an expanded vector which includes the cross-terms $X_i X_j$. Thus, if the dimension size of the original vector X is d then the expanded vector \vec{Y} will have dimensions \hat{d} equal to $[(d+1)(d+2)]/2$. For example, for 10 ($d = 10$) intuitive features, \hat{d} will be equal to 66. It is important that each class contain approximately several times more samples than dimensions (for quadratic functions the number of samples should be $\gg 60$ if $d = 10$). Otherwise the vector \vec{W} might converge to a solution which is underdetermined. In other words, with that \vec{W} vector it is likely that "signatures" which were not used for the learning set would be misclassified. Of course, the number of extracted intuitive features can be reduced, for example to two, such that $\hat{d} = 6$. However, the amount of information contained in each feature vector will suffer correspondingly probably resulting in increased overlap of the distribution.

UNCLASSIFIED

UNCLASSIFIED

CORRELATION PROCESSING

In addition to conventional pattern recognition techniques previously discussed, another technique was investigated for discrimination/classification. This technique involved correlating a reference waveform with actual data and submitting the results to a threshold for a decision. The reference waveform is one that is mathematically derived and used to correlate with the measured data. This process is more accurately a cross-correlation of an idealistic waveform with actually measured waveforms. As discussed in Section IV of this report, the mathematically derived temporal responses of mines buried in soil correspond well with the temporal responses of actual measured data. Thus, it is expected that the reference waveforms so generated will look very much like the waveform that is found in the actual measured data and which represents the return from a non-metallic mine buried in soil.

The details of the cross-correlation scheme are shown in Figure 77. This technique was only exercised for the data taken by the National Bureau of Standards, referred to as NBS data. Thus, in Figure 77, it is assumed that the NBS data which exists in the frequency domain is used in this process. This data is transformed by the Fast Fourier transform into the time domain. The portion of the temporal data corresponding to the antenna coupling and the ground return is gated out and only that portion from below the ground surface, including the non-metallic mine, is left. The position of the gate is determined automatically by first locating the most negative peak of the ground return and then setting the gate, or zeroing out the data, a

UNCLASSIFIED

UNCLASSIFIED

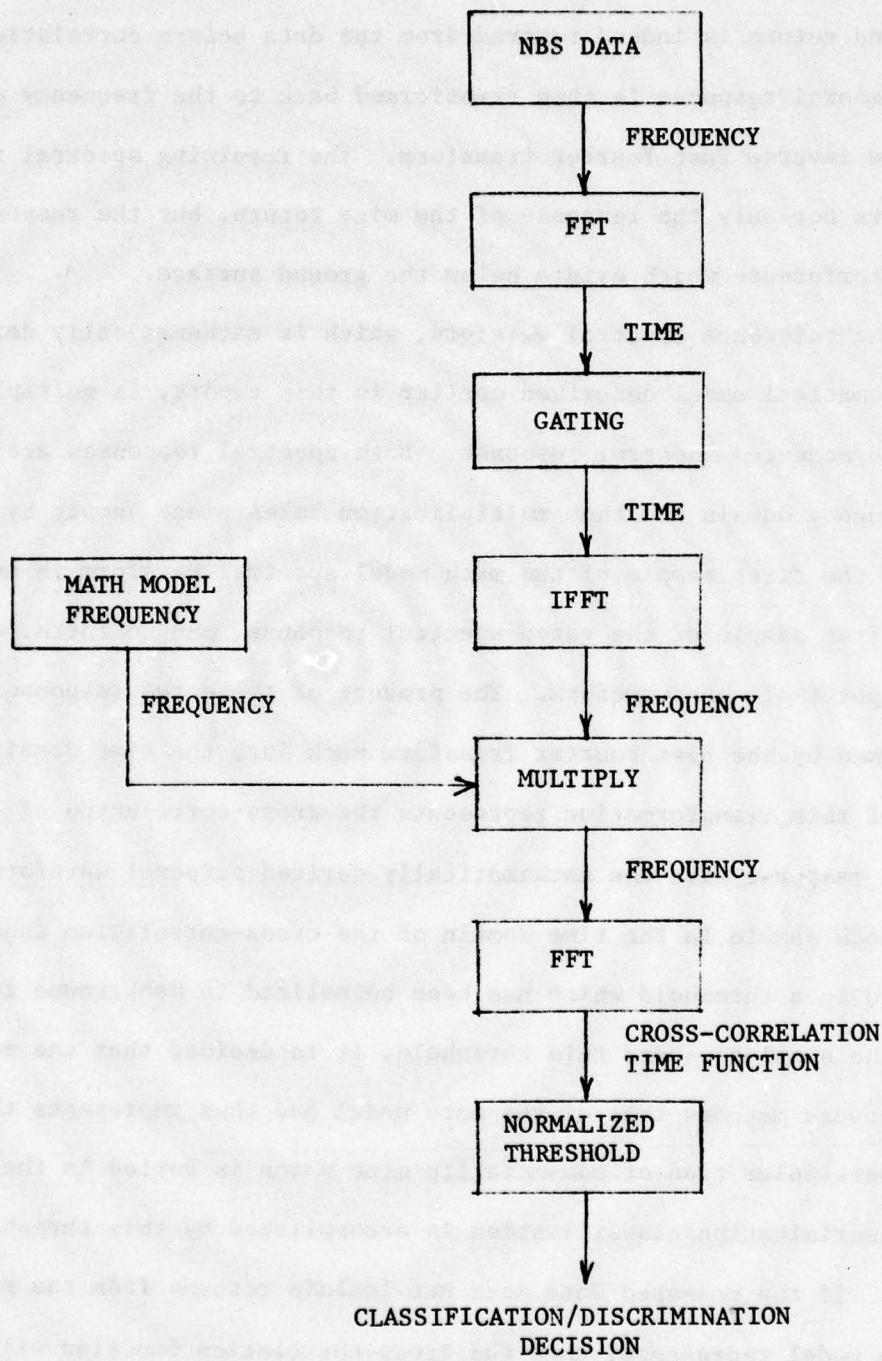


Figure 77. Cross-correlation processor.

UNCLASSIFIED

UNCLASSIFIED

certain number of samples beyond that negative peak, thus guaranteeing that the ground return is indeed removed from the data before correlation. The gated temporal response is then transformed back to the frequency domain by using the inverse Fast Fourier transform. The resulting spectral response represents not only the response of the mine return, but the response of any other interference which exists below the ground surface.

The reference spectral waveform, which is mathematically derived using the mathematical model described earlier in this report, is multiplied with the gated measured spectral response. Both spectral responses are sampled in the frequency domain and thus multiplication takes place sample by sample--that is, the first sample of the math model spectral waveform is multiplied by the first sample of the gated spectral response, and so forth, on through the N^{th} point of each waveform. The product of these two responses is then transformed by the Fast Fourier Transform back into the time domain. The result of this transformation represents the cross-correlation of the gated temporal response with the mathematically derived temporal waveform.

Each sample in the time domain of the cross-correlation function is subjected to a threshold which has been normalized to background level. If any of the samples exceed this threshold, it is decided that the measured data response matches that of the math model and thus represents the return from a particular type of non-metallic mine which is buried in the soil. Thus, discrimination/classification is accomplished by this thresholding process. If the measured data does not include returns from the mine which the math model represents, then the cross-correlation function will not

UNCLASSIFIED

UNCLASSIFIED

exceed normalized threshold and the decision is made that the particular type of mine does not exist in that measured data.

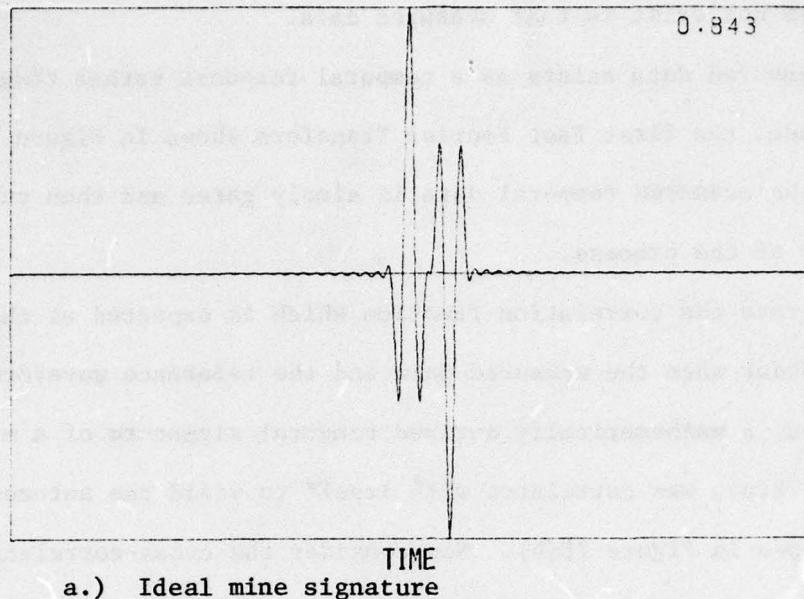
If the measured data exists as a temporal response rather than a frequency response, the first Fast Fourier Transform shown in Figure 77 is not necessary; the measured temporal data is simply gated and then subjected to the remainder of the process.

To illustrate the correlation function which is expected at the output of the processor when the measured data and the reference waveform are perfectly matched, a mathematically derived temporal signature of a mine, shown in Figure 78(a), was correlated with itself to yield the autocorrelation function shown in Figure 78(b). Now consider the cross-correlation of this ideal mine signature, previously referred to as the math model reference, with actual measured data as shown in Figure 79. The measured data is the gated temporal response from a type A mine buried 6 inches deep in soil with 7% moisture. Figure 79(b) shows the result of the cross-correlation. Note that the correlation waveform in Figure 79(b) compares very favorably with the idealistic waveform shown in Figure 78(b). As a comparison, the cross-correlation of the ideal mine signature with the return from a metal plate buried 6 inches deep in 7% moisture soil is shown in Figures 80(a) and 80(b). Not only does the cross-correlation function appear different in structure but the amplitude of the cross-correlation function is significantly smaller than that in Figure 79(b).

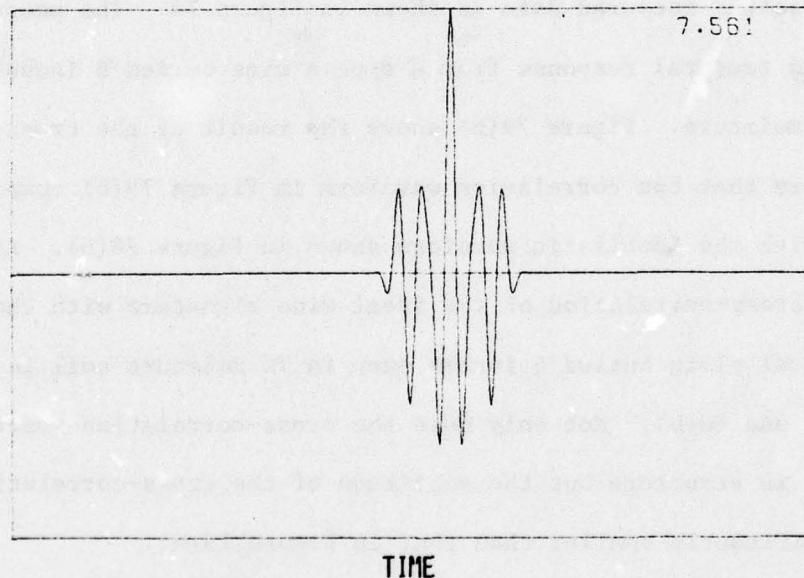
When the cross-correlation function is normalized to the measured temporal response, the amplitude of the metal plate correlation function is

UNCLASSIFIED

UNCLASSIFIED



a.) Ideal mine signature



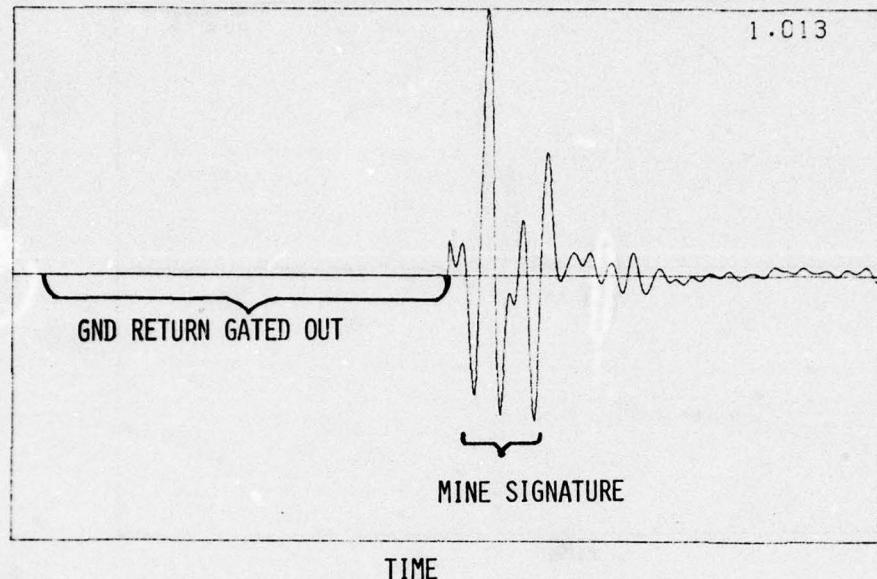
b.) Autocorrelation of ideal mine signature.

Figure 78. Mathematically derived mine signature and auto-correlation function.

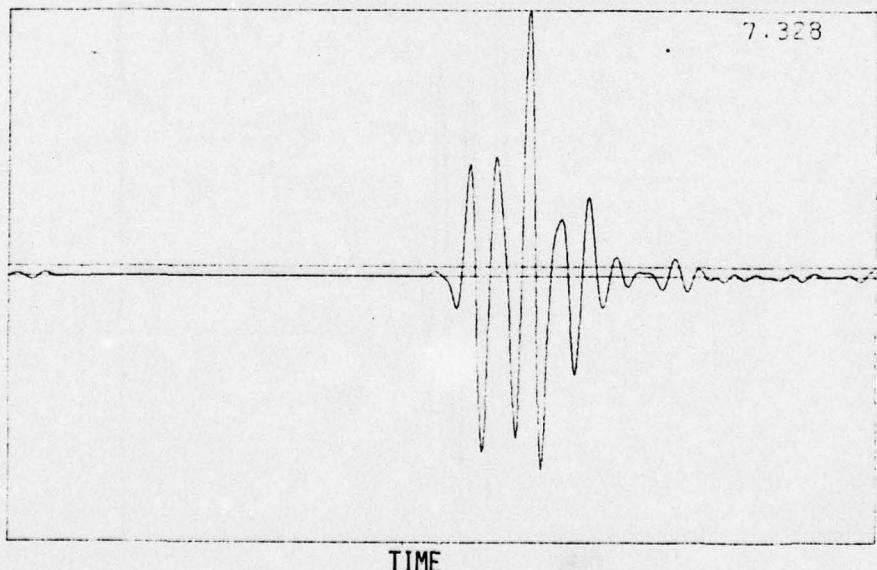
UNCLASSIFIED

160

UNCLASSIFIED



a.) Measured data, GT5-56, type A, 6" depth, 7% moisture.

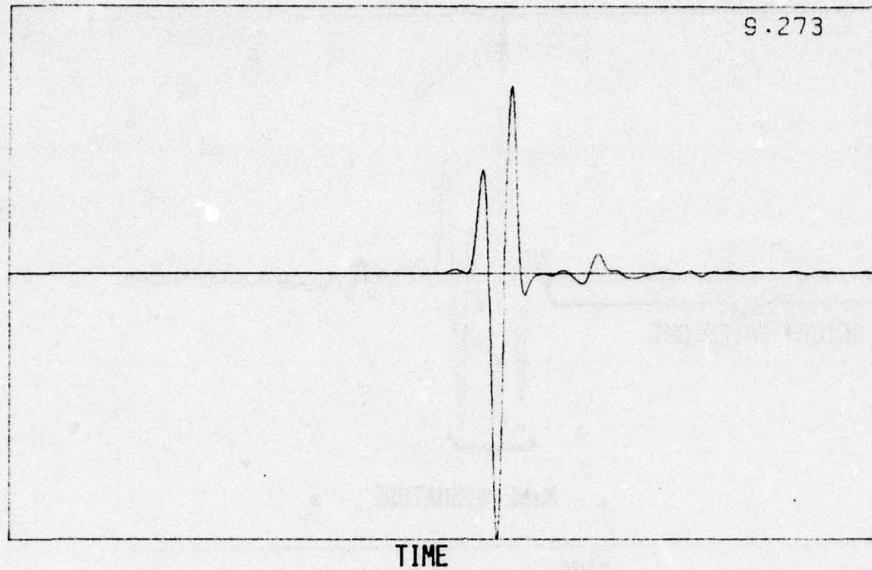


b.) Cross-correlation of reference signal and measured data GT5-56.

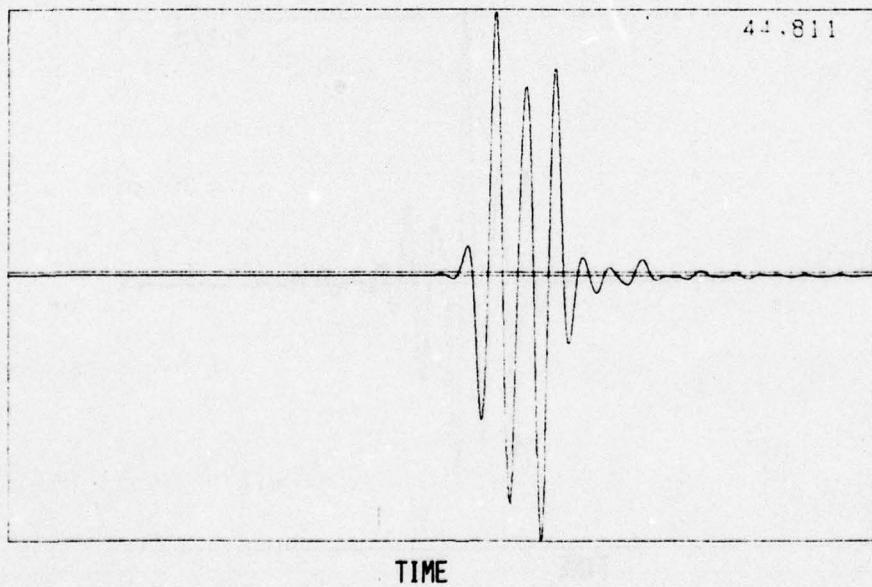
Figure 79. Cross-correlation of ideal mine signature with measured data from a type A mine.

UNCLASSIFIED

UNCLASSIFIED



a.) Measured data, GT-68, metal plate, 6" depth, 7% moisture.



b.) Cross-correlation of reference signal and measured data
GT5-68.

Figure 80. Cross-correlation of ideal mine signature with measured data from a metal plate.

UNCLASSIFIED

UNCLASSIFIED

approximately half that of the mine correlation function. Thus, it is obvious that in these two examples a threshold can be used to differentiate between the metal plate and the type A mine. Non-metallic mines can also be differentiated from other buried objects such as rocks and roots as well. In addition, the potential for differentiating between various types of mines is possible if the thickness of the various mines differ significantly.

The performance of the cross-correlation processor is indicated in Figures 81 through 86 in the form of probability of detection versus probability of false alarm curves. In Figure 81, the performance of the processor is shown for a buried type A mine. The sub-headings at the top of the figure indicate that the data base from which these probabilities were calculated was obtained from type A mines buried at both 3 inches and 6 inches below the soil and is based on measurements made directly over the mine and 4 inches either side of the center of the mine. Also, the data base consists of soils with moisture contents of 7, 17, and 12-20 and 13-16%. False alarm is defined in this figure as the declaration of a target, namely a type A mine, when in fact there is no mine buried in that location. The false alarm is likely generated by anomalies within the soil below the surface of the ground which, as indicated in the figure sub-headings, are called background noise.

As indicated in Figure 81, the detection performance of the cross-correlation processor under these particular circumstances is very poor. For example, a probability of detection of 90% would yield approximately an 80% chance of a false alarm when what is desired is a false alarm probability of something on the order of 1% or less. It should be noted that the solid curve in Figure 81 is a quadratic mean square fit to the data

UNCLASSIFIED

UNCLASSIFIED

CROSS CORRELATION CLASSIFIER

PROBABILITY DEFINITION 1

VERSION 1

REFERENCE 210

| | |
|----------|---------------------------------|
| NONMINE | BACKGND |
| TARGET | TYPE A MINE |
| DEPTH | 3 6 |
| LOCATION | +4 0 -4 |
| MOISTURE | 7 17 12-20 13-16 |

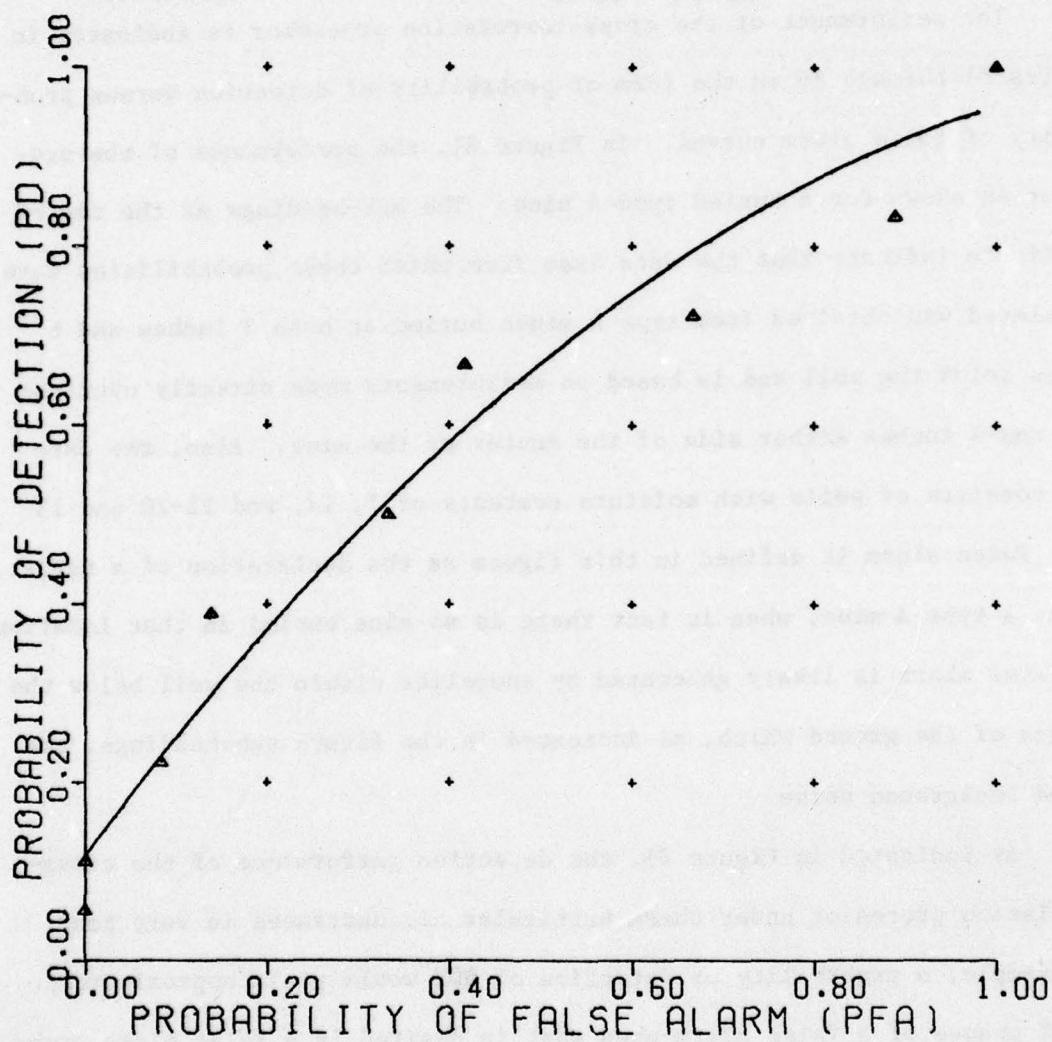


Figure 81. Cross-correlation classifier.

UNCLASSIFIED

UNCLASSIFIED

CROSS CORRELATION CLASSIFIER

PROBABILITY DEFINITION 1

VERSION 1

REFERENCE 211

| | |
|-------------------|---------------------------------|
| NONMINE TARGET | BACKGND |
| | TYPE B MINE |
| DEPTH | 3 6 |
| LOCATION | +4 0 -4 |
| MOISTURE | 7 17 12-20 13-16 |

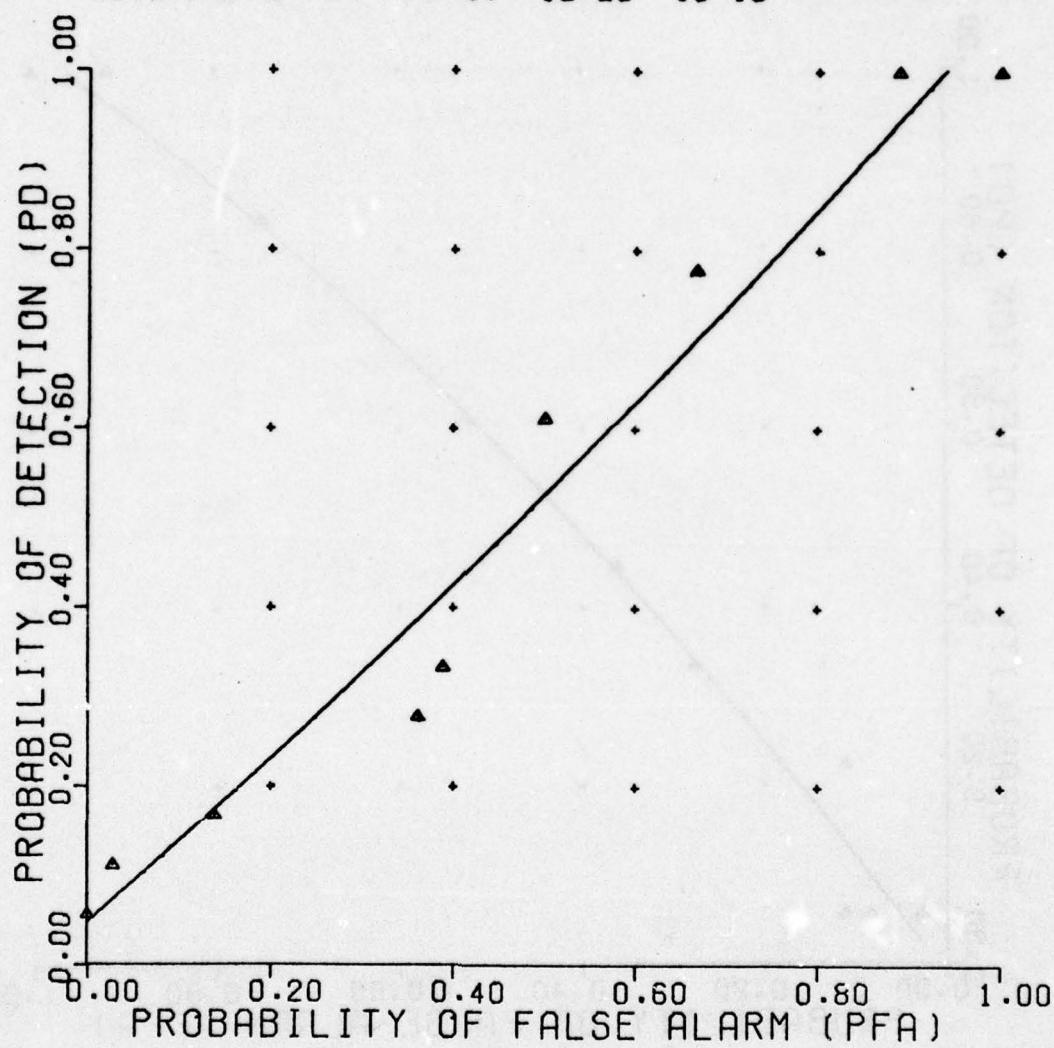


Figure 82. Cross-correlation classifier.

UNCLASSIFIED

UNCLASSIFIED

CROSS CORRELATION CLASSIFIER

PROBABILITY DEFINITION 1

VERSION 1

REFERENCE 212

NONMINE BACKGND
TARGET TYPE C MINE

| | | | | |
|----------|----|----|-------|-------|
| DEPTH | 3 | 6 | | |
| LOCATION | +4 | 0 | -4 | |
| MOISTURE | 7 | 17 | 12-20 | 13-16 |

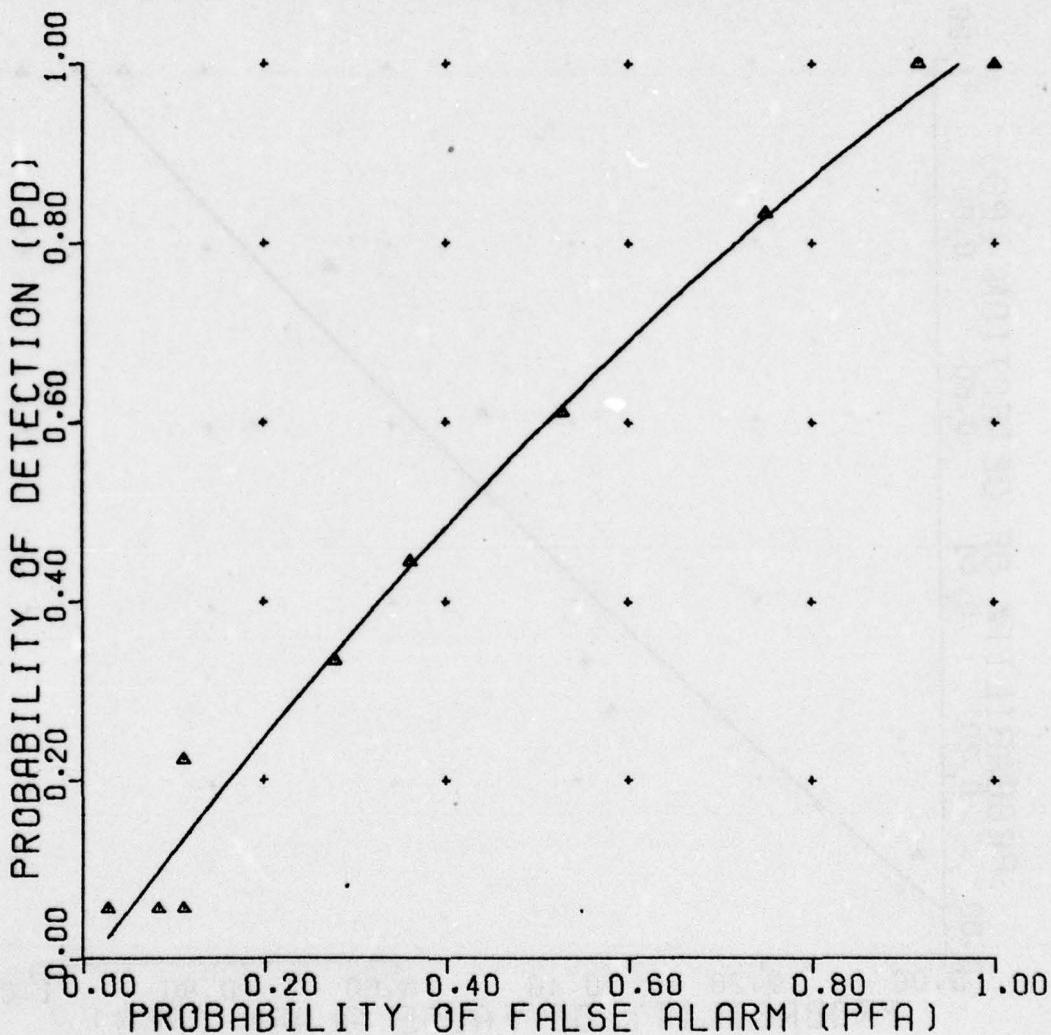


Figure 83. Cross-correlation classifier.

UNCLASSIFIED

UNCLASSIFIED

CROSS CORRELATION CLASSIFIER

PROBABILITY DEFINITION 1
VERSION 1
REFERENCE 207

| NONMINE TARGET | PLATE | ROCK(1) | ROCK(2) | ROOT |
|----------------|-------|---------|---------|-------|
| TYPE A MINE | | | | |
| DEPTH | 3 | 6 | | |
| LOCATION | +4 | 0 | -4 | |
| MOISTURE | 7 | 17 | 12-20 | 13-16 |

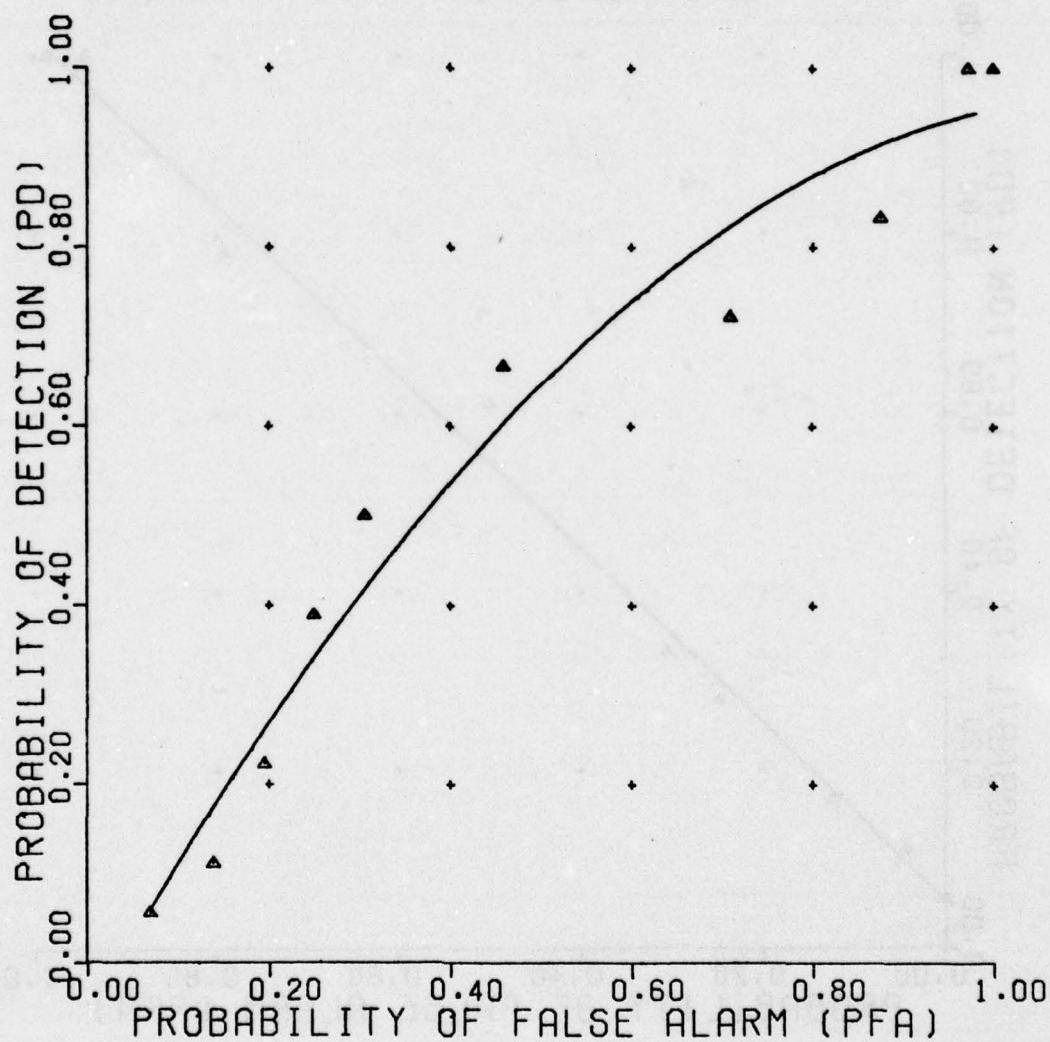


Figure 84. Cross-correlation classifier.

UNCLASSIFIED

UNCLASSIFIED

CROSS CORRELATION CLASSIFIER

PROBABILITY DEFINITION 1

VERSION 1

REFERENCE 208

| NONMINE TARGET | PLATE TYPE B MINE | ROCK(1) | ROCK(2) | ROOT |
|-------------------|----------------------|---------|---------|-------|
| DEPTH | | 3 | 6 | |
| LOCATION | | +4 | 0 | -4 |
| MOISTURE | | 7 | 17 | 12-20 |
| | | | | 13-16 |

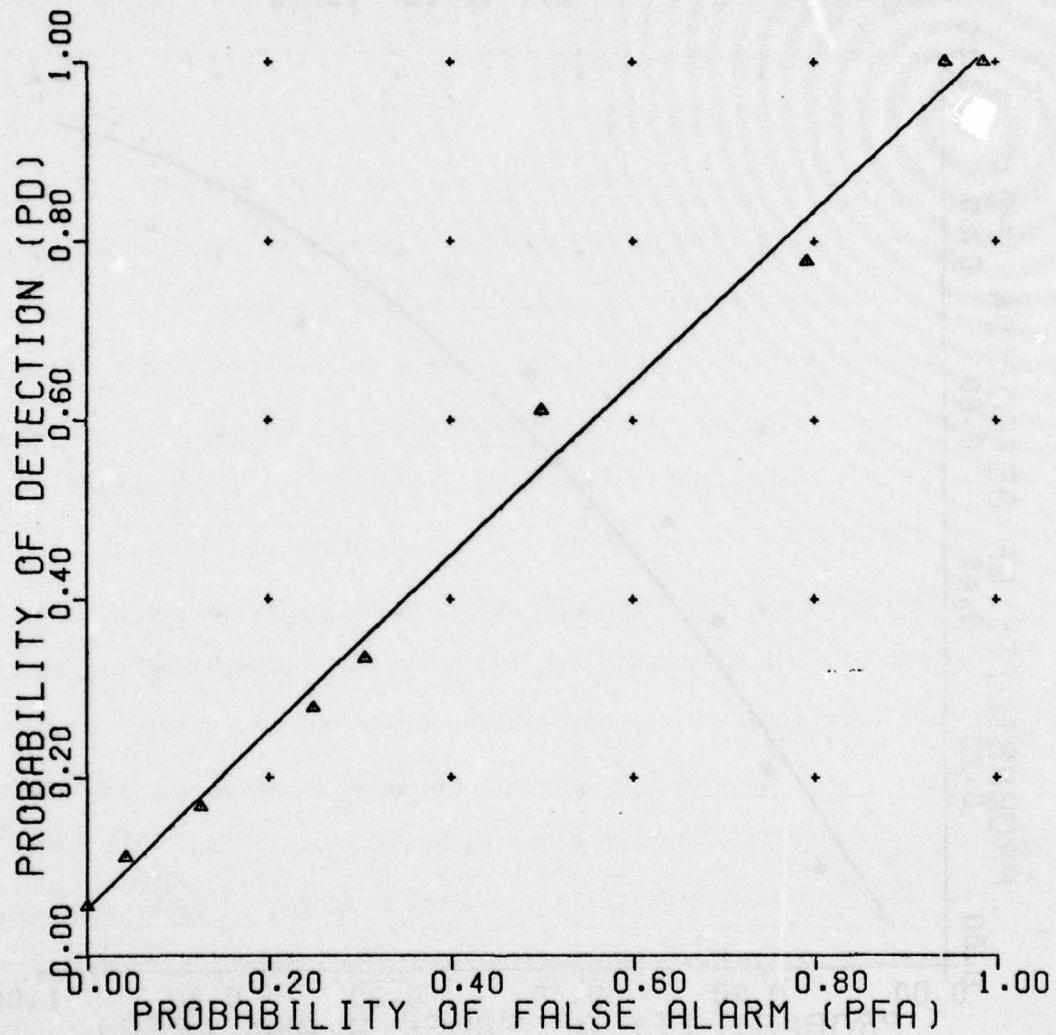


Figure 85. Cross-correlation classifier.

UNCLASSIFIED

UNCLASSIFIED

CROSS CORRELATION CLASSIFIER

PROBABILITY DEFINITION 1
VERSION 1
REFERENCE 209

| | | | | |
|-------------------|-------------|---------|---------|-------|
| NONMINE TARGET | PLATE | ROCK(1) | ROCK(2) | ROOT |
| | TYPE C MINE | | | |
| DEPTH | 3 | 6 | | |
| LOCATION | +4 | 0 | -4 | |
| MOISTURE | 7 | 17 | 12-20 | 13-16 |

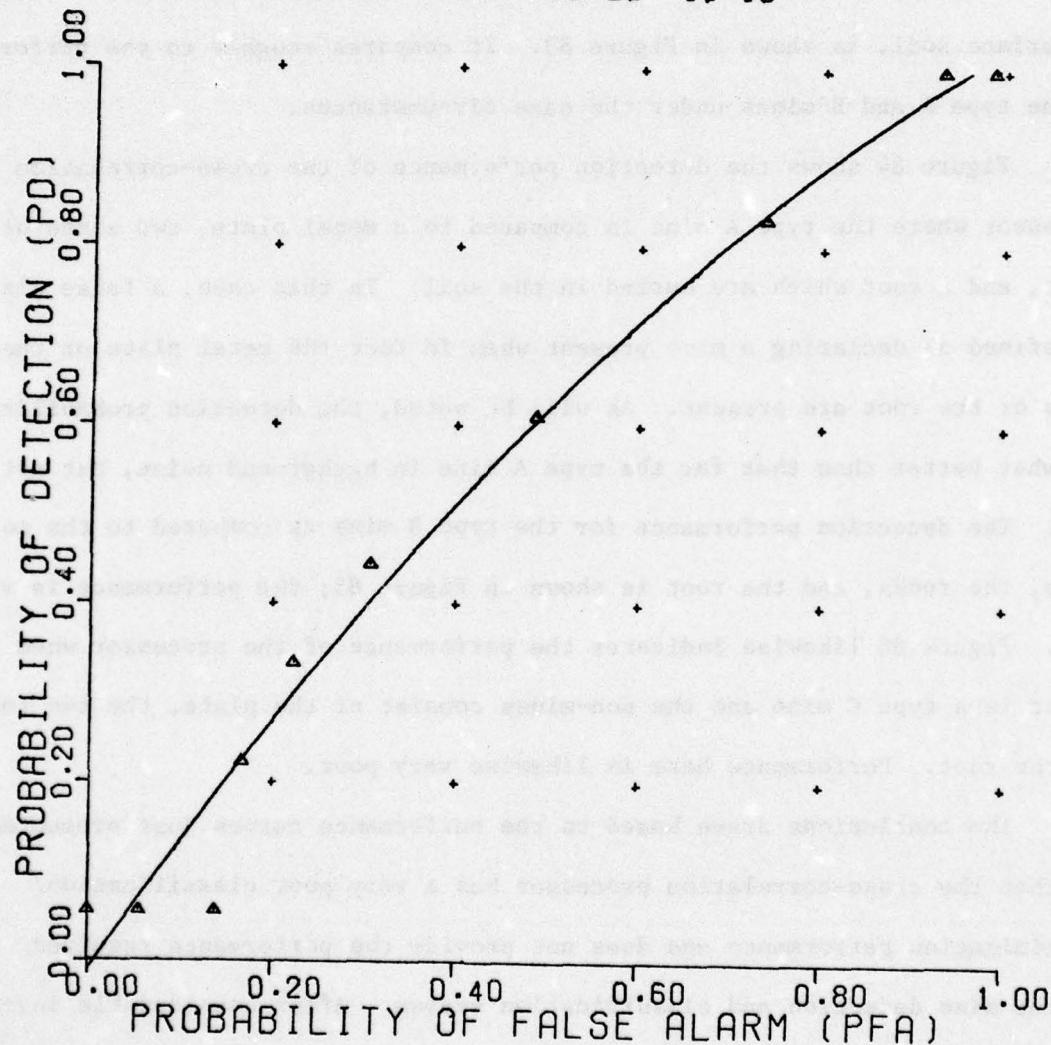


Figure 86. Cross-correlation classifier.

UNCLASSIFIED

UNCLASSIFIED

points which are represented by triangles within the plot.

The detection performance of the correlation processor with a buried type B mine is shown in Figure 82. This mine was somehow different from the type A and the detection performance is likewise different. In general, the detection performance is somewhat poorer than that for the type A mine. The detection performance of the cross-correlation processor for another type of non-metallic mine, the type C mine, as compared to background noise from the subsurface soil, is shown in Figure 83. It compares roughly to the performance of the type A and B mines under the same circumstances.

Figure 84 shows the detection performance of the cross-correlation processor where the type A mine is compared to a metal plate, two sizes of rocks, and a root which are buried in the soil. In this case, a false alarm is defined as declaring a mine present when in fact the metal plate or the rocks or the root are present. As will be noted, the detection probability is somewhat better than that for the type A mine in background noise, but not much. The detection performance for the type B mine as compared to the metal plate, the rocks, and the root is shown in Figure 85; the performance is very poor. Figure 86 likewise indicates the performance of the processor when the target is a type C mine and the non-mines consist of the plate, the two rocks, and the root. Performance here is likewise very poor.

The conclusions drawn based on the performance curves just presented are that the cross-correlation processor has a very poor classification/discrimination performance and does not provide the performance required for the mine detection and classification system. After considerable investigation into the reasons for the poor performance, it has been determined that the mathematical model reference waveform does not sufficiently represent the

UNCLASSIFIED

UNCLASSIFIED

waveform that is to be expected from the mine return. This is because the waveform signature involves variables which are dependent upon soil moisture and dielectric constants of the soil. As indicated previously, if the soil moisture at the top of the mine is different from that at the bottom of the mine, the radar return from the bottom of the mine will be of a different amplitude than that of the top. However, the mathematical reference waveform assumes that same amplitude return from both the bottom and top of the mine. Thus, in general, a mismatch will occur between the reference waveform and the actual returning waveform. Thus, the correlation between the two will not have as large an amplitude as it would if the reference waveform were exactly matched to the returning waveform. The actual returns are significantly different from the reference waveform as indicated in the discussion of Figure 80.

Another type of correlation was considered during this study and is illustrated in Figures 87 and 88. This correlation scheme is called the impulse correlation and is illustrated in Figure 87 with an impulse correlation circuit diagram. The concept is based on the fact that ideally what is desired is that the reference temporal waveform illustrated in Figure 78(a) be correlated with measured data. A close look at the reference waveform indicated in Figure 78(a) indicates that it consists of two major peaks: first, a positive going peak and then a negative going peak separated in time by approximately the thickness of the mine. An approximation to this waveform would be a waveform which consists of two impulses as shown in Figure 88. One of the impulses is negative and one is positive and they are separated by a time, τ_0 , which is approximately the time duration of an

UNCLASSIFIED

UNCLASSIFIED

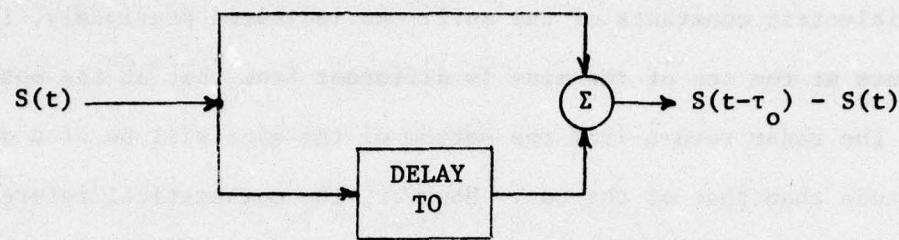


Figure 87. Impulse-correlation circuit.

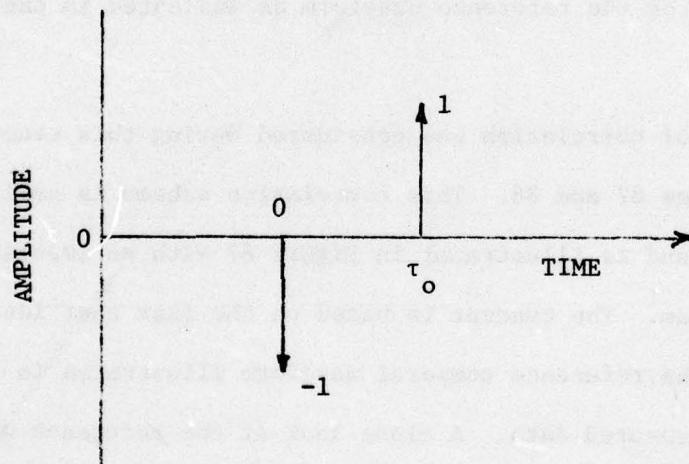


Figure 88. Impulse response of impulse-correlation circuit.

UNCLASSIFIED

UNCLASSIFIED

electromagnetic wave traveling through a non-metallic mine. The impulse correlation circuit shown in Figure 87 takes the measured data and a delayed version of the measured data and subtracts the two. The output of this circuit is equivalent to the correlation of the reference waveform approximation with the actual data. The impulse response of the circuit is what is shown in Figure 88. The output response of the impulse correlation circuit is given by the convolution of the impulse response shown in Figure 88 and the input signal, $s(t)$. The output then is equivalent to a signal which is derived by convolving the reference waveform approximation with the input signal, $s(t)$. Thus, the output is a close approximation to the correlation of the reference waveform and the input data. The advantage of this approach is that less complex processing is required as compared to the cross-correlation processor shown in Figure 77. The detection performance is found to be comparable to that of the cross-correlation processor. Detection performance curves are given in Figures 89 through 94. A comparison of this set of curves with those performance curves given in Figures 81 through 86 for the cross-correlation processor will indicate a very close agreement. Thus, one concludes that the impulse-correlation processor yields roughly comparable performance to that of the cross-correlation processor and is, therefore, unacceptable for the intended application.

UNCLASSIFIED

AD-A054 427

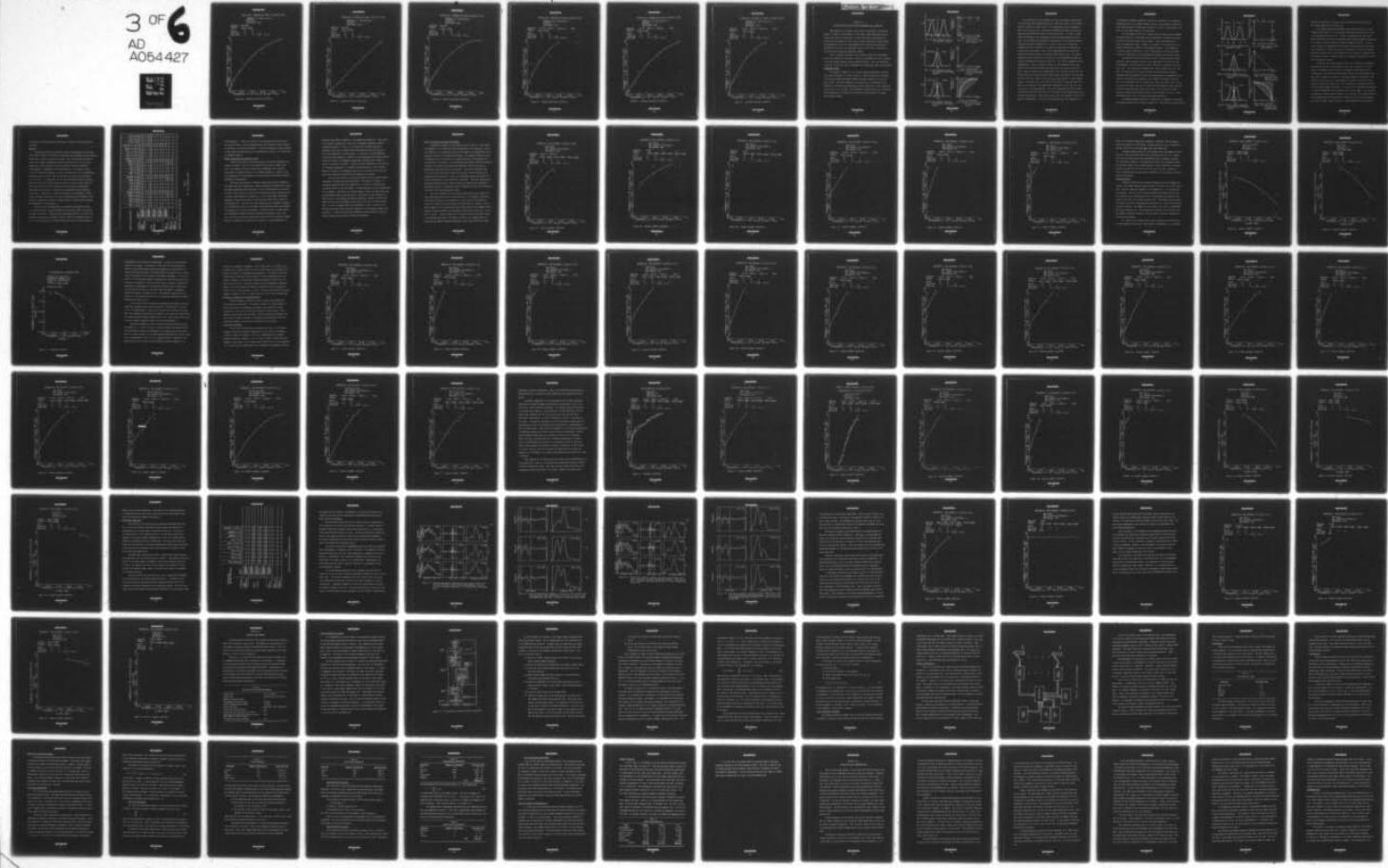
GEORGIA INST OF TECH ATLANTA ENGINEERING EXPERIMENT --ETC F/G 17/9
RADAR DETECTION, DISCRIMINATION, AND CLASSIFICATION OF BURIED N--ETC(U)
FEB 78 J D ECHARD, J A SCHEER, E O RAUSCH DAAG53-76-C-0112

UNCLASSIFIED

3 OF 6
AD
A054427

EES/GIT-A-1828-F-VOL-1

NL



UNCLASSIFIED

IMPULSE CORRELATION CLASSIFIER

PROBABILITY DEFINITION 1
VERSION 1
REFERENCE 204

NONMINE BACKGND
TARGET TYPE A MINE
DEPTH 3 6
LOCATION +4 0 -4
MOISTURE 7 17 12-20 13-16

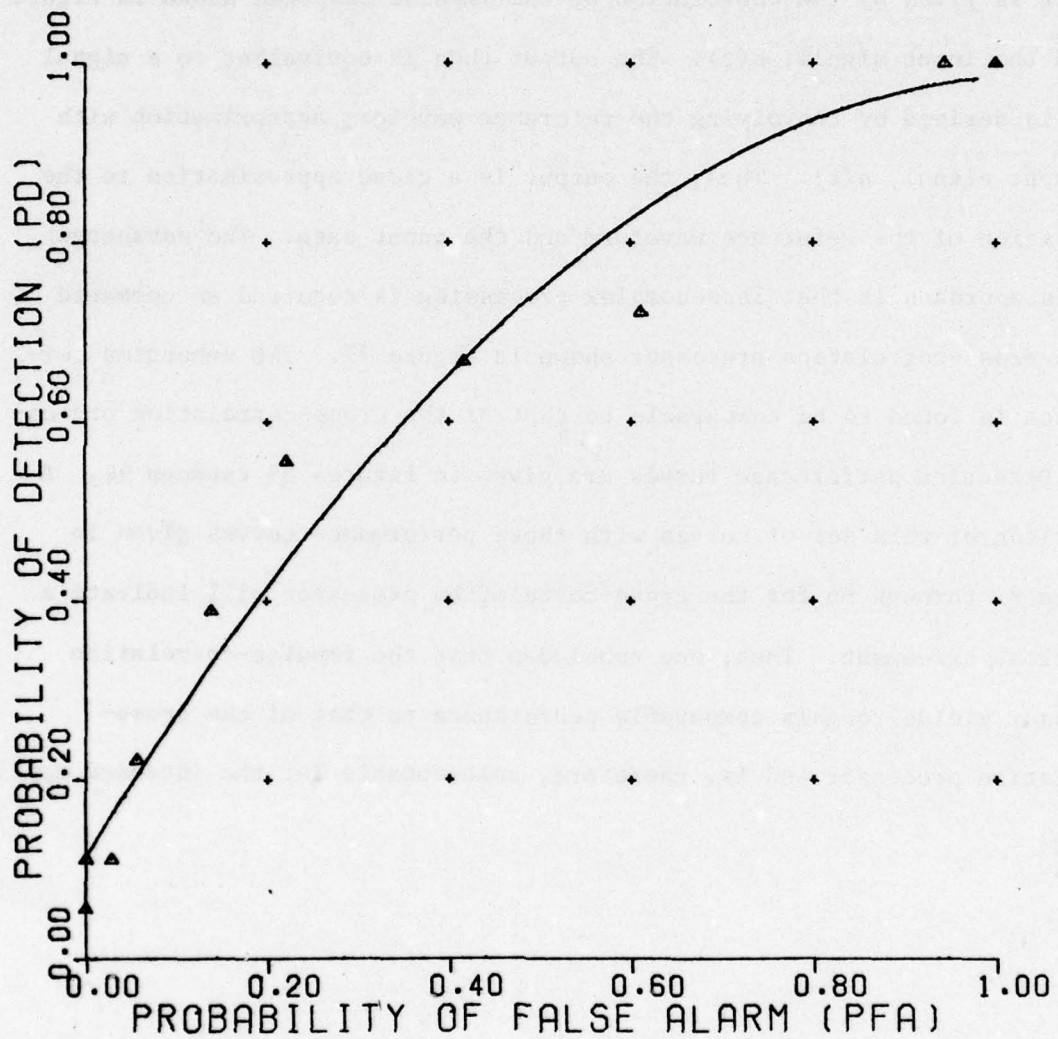


Figure 89. Impulse-correlation classifier.

UNCLASSIFIED

UNCLASSIFIED

IMPULSE CORRELATION CLASSIFIER

PROBABILITY DEFINITION 1

VERSION 1

REFERENCE 205

| | |
|-------------------|---------------------------------|
| NONMINE TARGET | BACKGND TYPE B MINE |
| DEPTH | 3 6 |
| LOCATION | +4 0 -4 |
| MOISTURE | 7 17 12-20 13-16 |

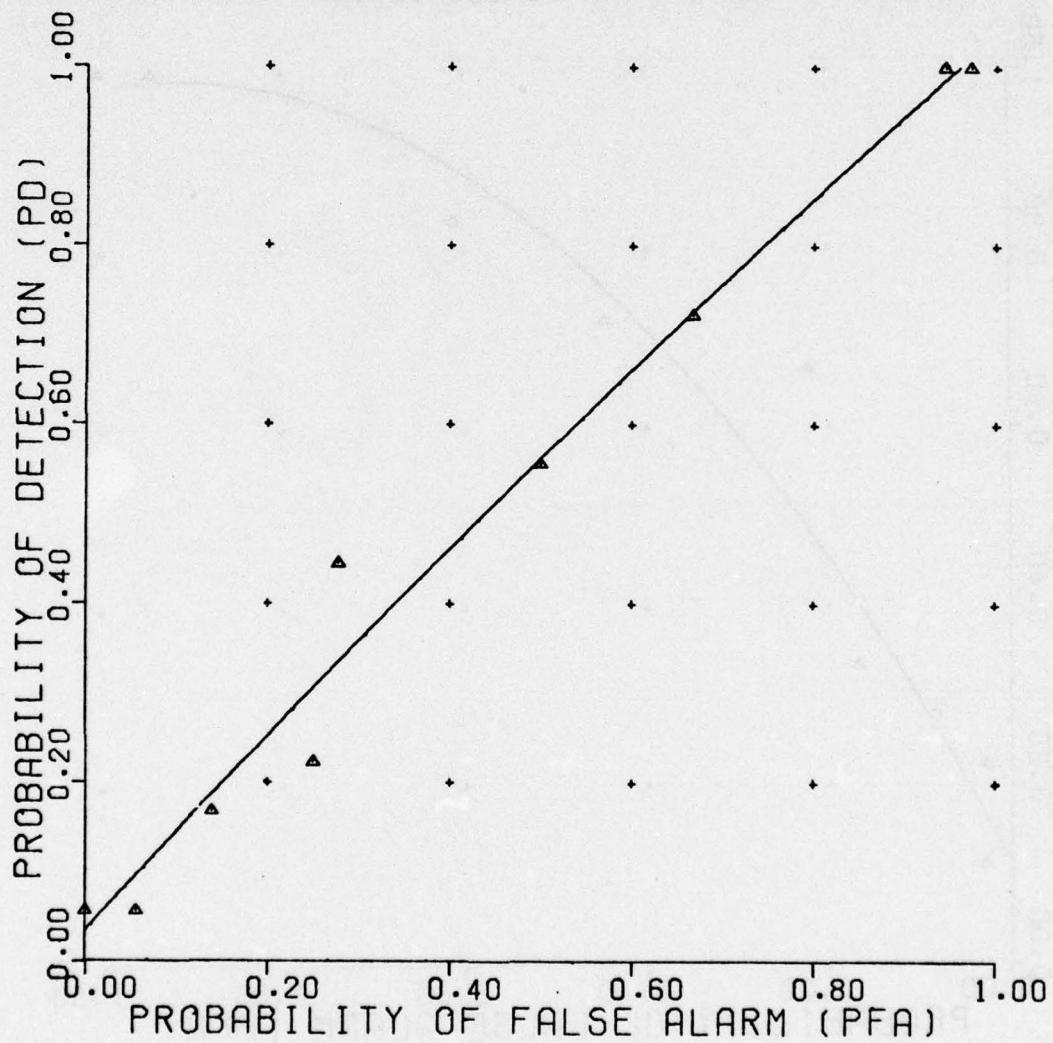


Figure 90. Impulse-correlation classifier.

UNCLASSIFIED

UNCLASSIFIED

IMPULSE CORRELATION CLASSIFIER

PROBABILITY DEFINITION 1

VERSION 1

REFERENCE 206

| | |
|-------------------|---------------------------------|
| NONMINE TARGET | BACKGND |
| DEPTH | 3 6 |
| LOCATION | +4 0 |
| MOISTURE | 7 17 12-20 13-16 |

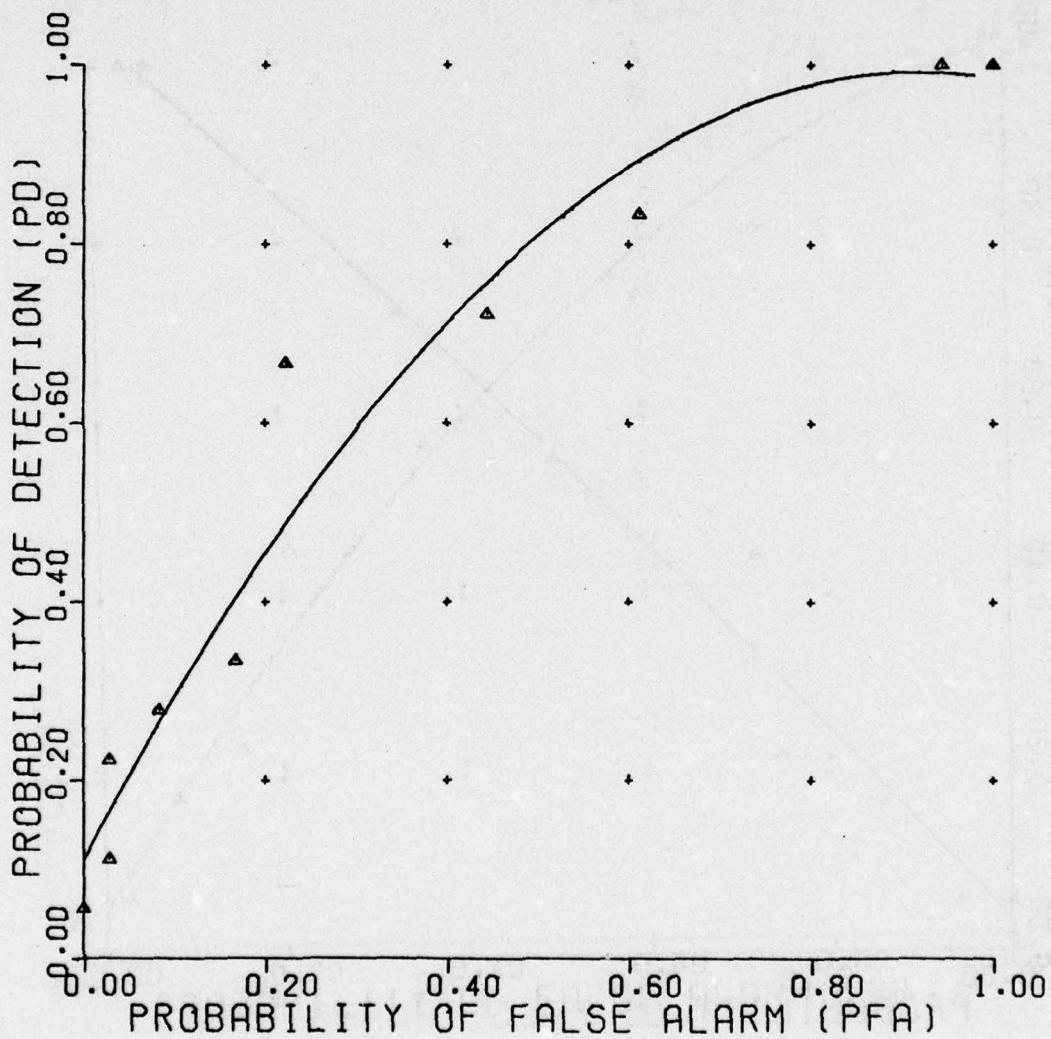


Figure 91. Impulse-correlation classifier.

UNCLASSIFIED

UNCLASSIFIED

IMPULSE CORRELATION CLASSIFIER

PROBABILITY DEFINITION 1

VERSION 1

REFERENCE 201

| NONMINE TARGET | PLATE TYPE A MINE | ROCK(1) | ROCK(2) | ROOT |
|-------------------|----------------------|---------|---------|-------|
| DEPTH | | 3 | 6 | |
| LOCATION | | +4 | 0 | -4 |
| MOISTURE | | 7 | 17 | 12-20 |
| | | | | 13-16 |

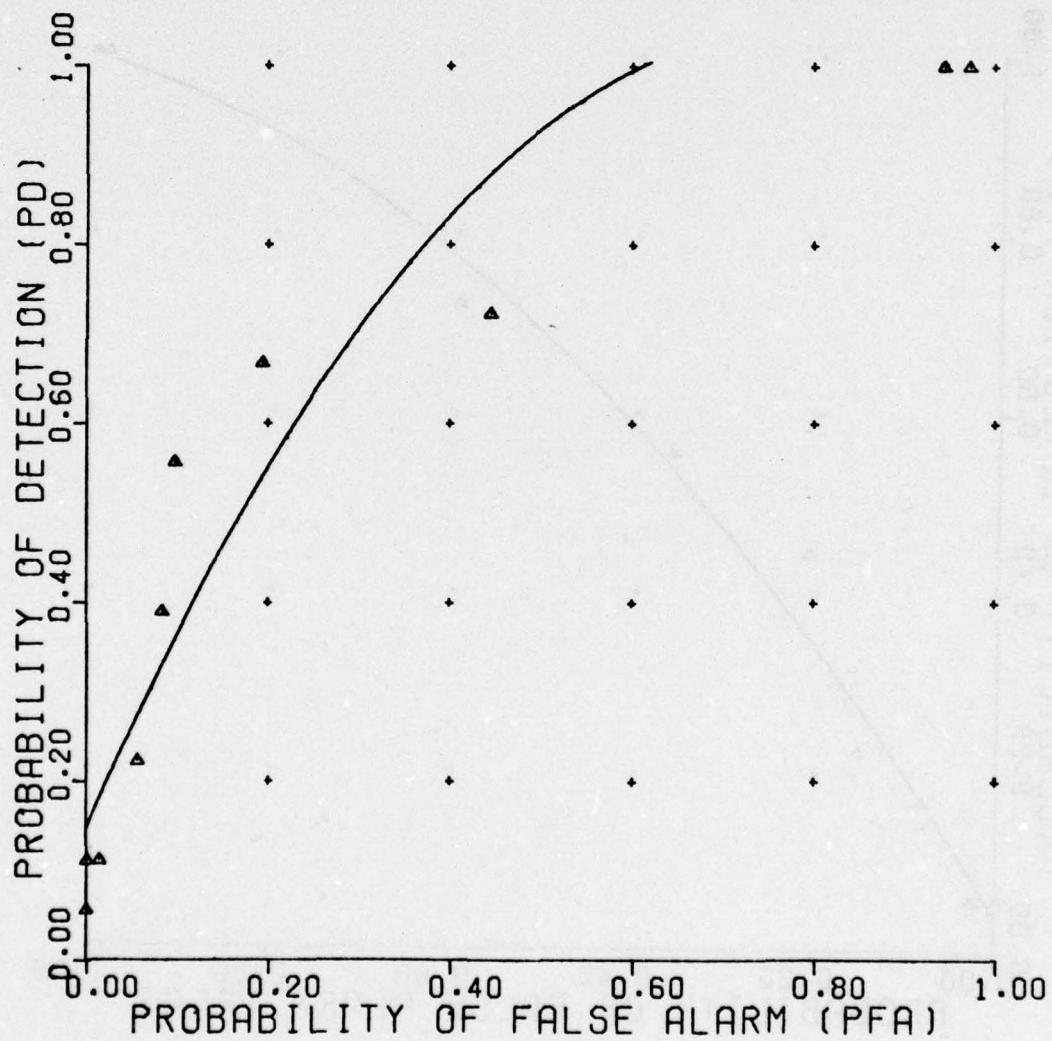


Figure 92. Impulse-correlation classifier.

UNCLASSIFIED

UNCLASSIFIED

IMPULSE CORRELATION CLASSIFIER

PROBABILITY DEFINITION 1

VERSION 1

REFERENCE 202

| NONMINE TARGET | PLATE TYPE B MINE | ROCK(1) | ROCK(2) | ROOT |
|-------------------|----------------------|---------|---------|-------|
| DEPTH | | 3 | 6 | |
| LOCATION | | +4 | 0 | -4 |
| MOISTURE | | 7 | 17 | 12-20 |

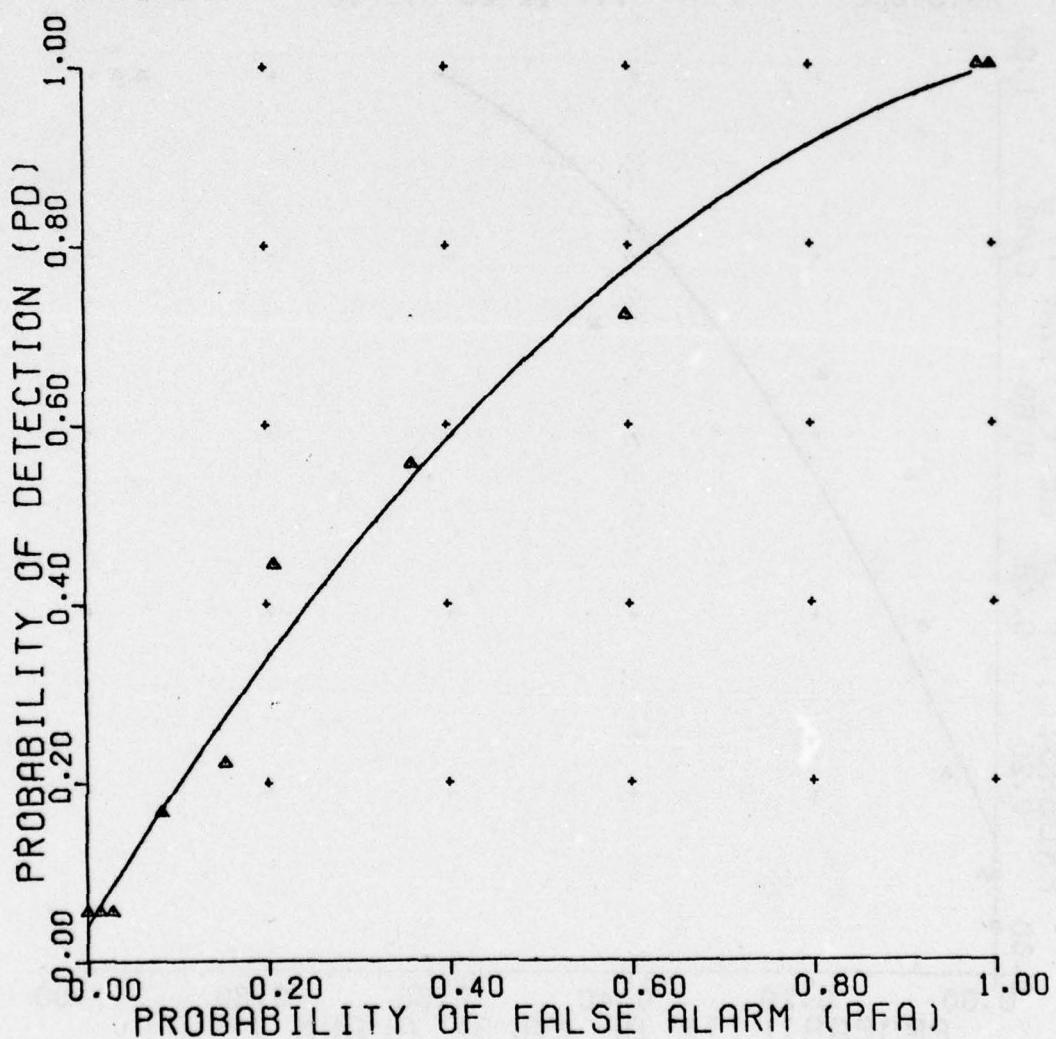


Figure 93. Impulse-correlation classifier.

UNCLASSIFIED

UNCLASSIFIED

IMPULSE CORRELATION CLASSIFIER

PROBABILITY DEFINITION 1

VERSION 1

REFERENCE 203

| | | | | |
|-------------------|-------------|---------|---------|-------|
| NONMINE TARGET | PLATE | ROCK(1) | ROCK(2) | ROOT |
| | TYPE C MINE | | | |
| DEPTH | 3 | 6 | | |
| LOCATION | +4 | 0 | -4 | |
| MOISTURE | 7 | 17 | 12-20 | 13-16 |

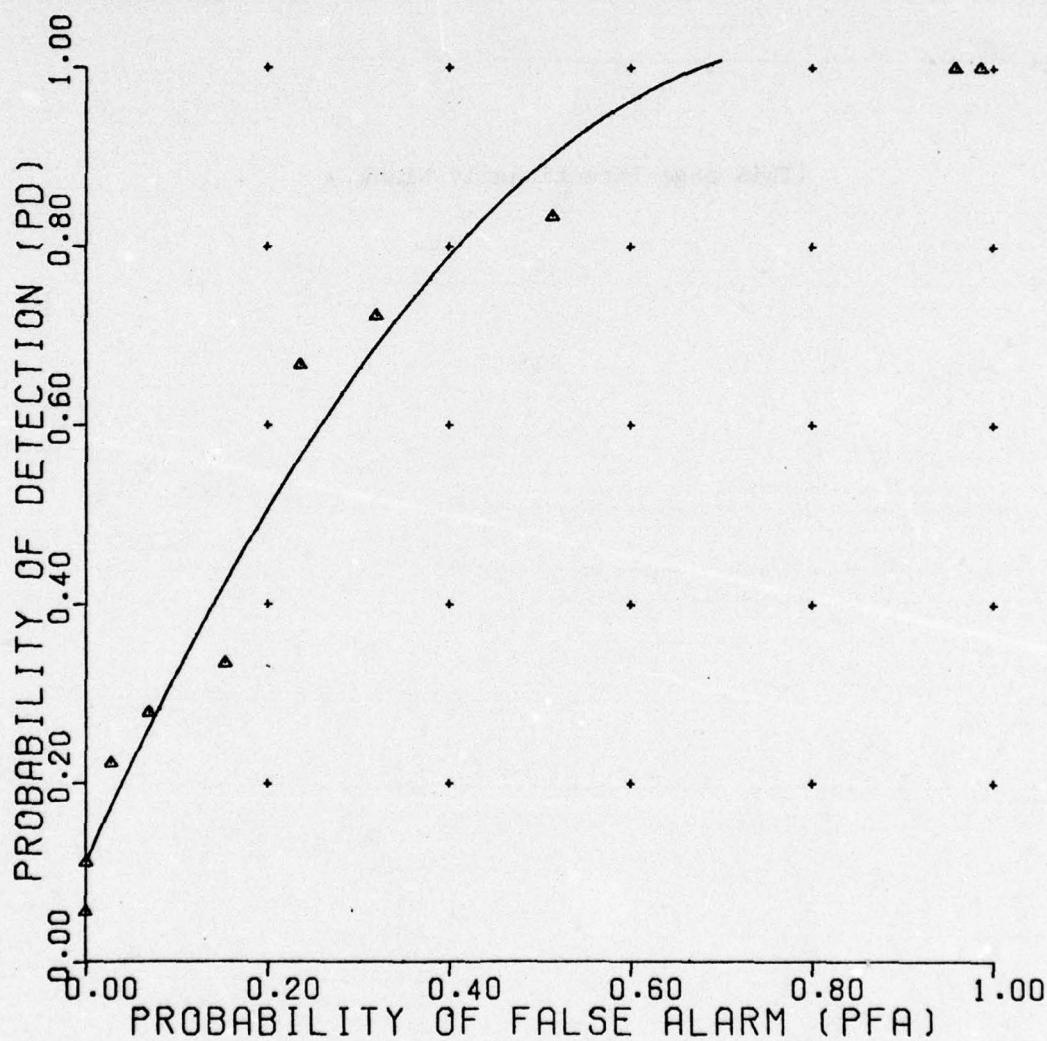


Figure 94. Impulse-correlation classifier.

UNCLASSIFIED

UNCLASSIFIED

SECTION VI

DISCRIMINATION/CLASSIFICATION PERFORMANCE AND COMPARISON

Discrimination is defined as the process of deciding if a potential target is indeed a target (mine) or some other target-like object such as a rock, root, piece of metal, etc. On the other hand, classification is the process of deciding to which class of mines a particular target belongs. The performance of both the discrimination and classification processors considered in Section V are presented in this section with a discussion of how the various processing algorithms compare.

First, a general discussion of the format in which the performance curves are presented is discussed. Limits of performance are also considered to give the reader insight into the measured results. Then the performance curves for the NBS data and the MERADCOM short-pulse radar data are discussed.

PERFORMANCE CURVES

The curves in Figures 96, 98, and 100 show the probability of detection versus probability of false alarm for a range of postulated discriminator processors whose performance ranges from ideal (perfect) to very poor (worst case). Here the probability of detection, P_D , is defined as the probability of having the discriminator decide "mine" for a return resulting from a type A, B, or C mine; the probability of false alarm, P_{FA} , is defined as the probability of having the discriminator decide "mine" for returns from non-mine targets.

UNCLASSIFIED

UNCLASSIFIED

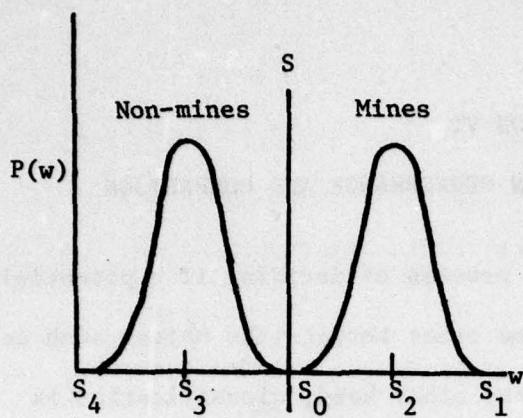


Fig. 95 Prob. density functions for separated classes.

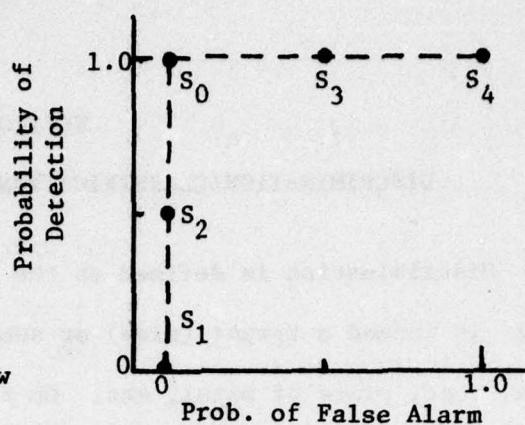


Fig. 96 Prob. plot for separated classes

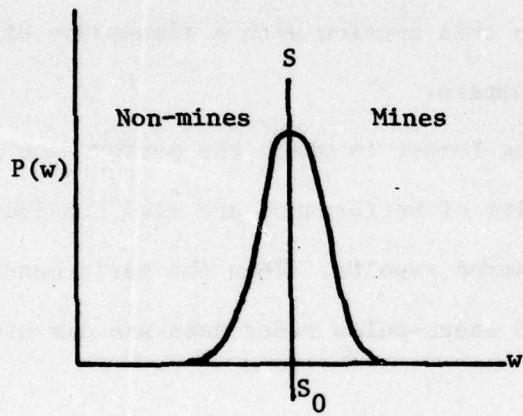


Fig. 97 Prob. density functions for completely overlapping classes.

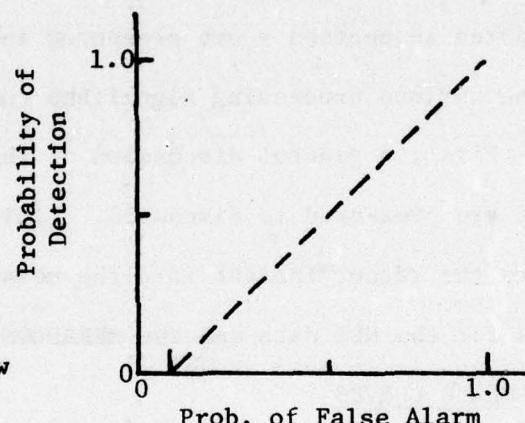


Fig. 98 Prob. plot for completely overlapping classes.

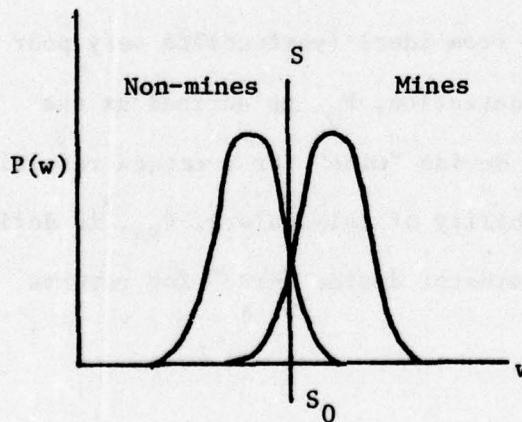


Fig. 99 Prob. density functions for partially overlapping classes.

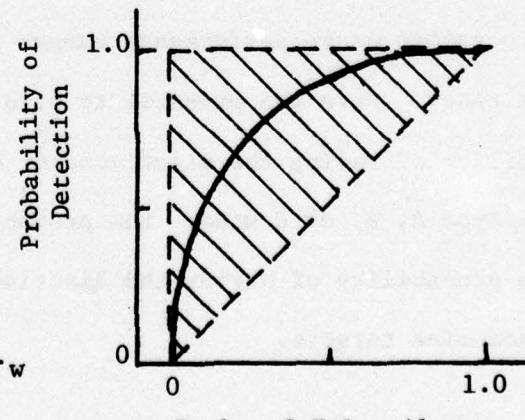


Fig. 100 Prob. plot for partially overlapping classes.

UNCLASSIFIED

UNCLASSIFIED

The performance curves indicate not only the relevant probabilities but also convey some information about the shape and overlap of the distribution of points in feature space. This information can be an important asset since the points are contained in N-dimensional space, and thus the shape of the distribution cannot be observed directly. In order to demonstrate the meaning of the performance curve only two dimensions will be used. Let the mines and non-mines be represented by two continuous density functions as shown in Figures 95, 97, and 99. Then, the corresponding probability curves, Figures 96, 98, and 100 are generated by sweeping the decision line from right to left and by integrating the area under each probability density function on the right hand side up to S_0 . For widely separated density functions as in Figure 95, the corresponding probability curve is the dashed line shown in Figure 96. This line is generated in the following way: when S is placed at point S_1 , the integrated area on the right is zero for both non-mines and mines so P_D and P_{FA} at S_1 are both zero. When S is moved to S_2 , approximately 1/2 of the total area under the density function for mines will be summed whereas the area for the non-mines will still be zero. Hence, at S_2 , the P_D and P_{FA} , become 0.5 and 0 respectively. At the point S_0 the P_D will now be 1.0 but the P_{FA} will still be 0. Hence up to this point, the dashed line extending from $(P_D, P_{FA} = 0, 0)$ to $(P_D, P_{FA} = 1.0, 0)$ was generated. At S_3 the integrated area for the mines is still the total area, but now 1/2 of the area for the non-mines must also be taken into account. Thus, the P_D and P_{FA} will have reached a value of 1.0 and 0.5, respectively. Finally at S_4 both P_D and P_{FA} will be equal to 1.0.

UNCLASSIFIED

UNCLASSIFIED

If the density functions completely overlap as in Figure 97, the resulting probability plot is the dashed straight line $P_D = P_{FA}$ as shown in Figure 98. Other distributions as illustrated in Figure 99 results in performance which fall into the shaded region as in Figure 100.

The performance curves for a classification processor appear somewhat different since one is interested in the probability of properly detecting one class of targets (mines) versus another. Again, decisions must be made in N-dimensional space. However, for simplicity of illustration, the present discussion is limited to two-dimensional space. The probability of class 1 versus probability of class 2 performance curves are generated in much the same manner as the discriminator processor performance curves.

The decision line is now swept from left to right and only the area under the class 1 density function on the right side of the decision line is integrated. The area under the class 2 function is computed on the left side of S_0 . The resulting performances are shown in Figures 102, 104, and 106. To indicate the correlation between the distributions of density functions and the probability curves, the probabilities corresponding to the decision line positions S_1 through S_4 were marked in Figures 101 and 102. Thus, if the decision line S is moved to S_1 , the P_D for class 1 will be 1.0, but the P_D for class 2 will be 0, because the area under the class 2 density function on the left hand side of S_1 is zero. At S_2 , the P_D for class 1 will be 1.0 again, but the P_D for class 2 will be equal to 0.5, etc. This performance curve is for a perfectly performing classifier.

The dashed straight line shown in Figure 104 corresponds to completely overlapping distributions as shown in Figure 103. Distributions which partially

UNCLASSIFIED

UNCLASSIFIED

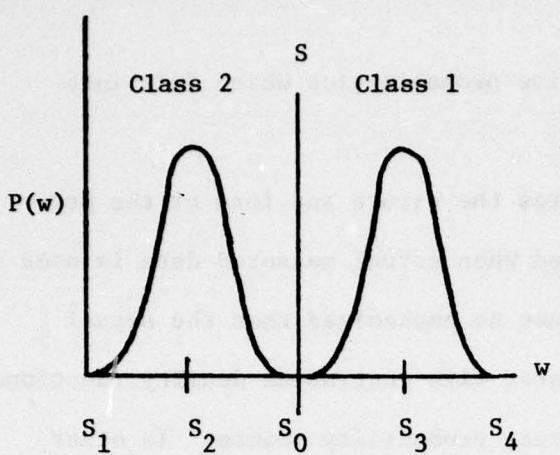


Figure 101 Prob. density functions for separated classes.

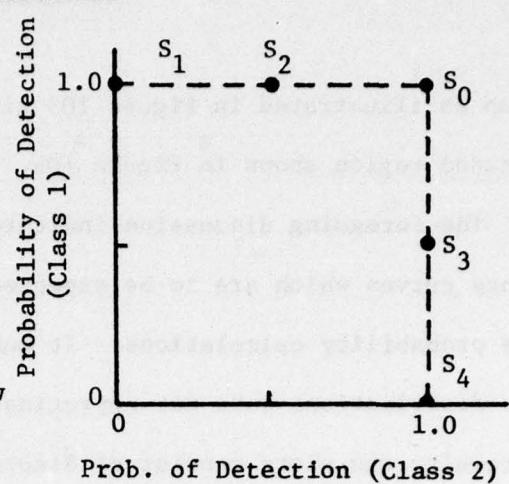


Fig. 102 Prob. plot for separated classes.

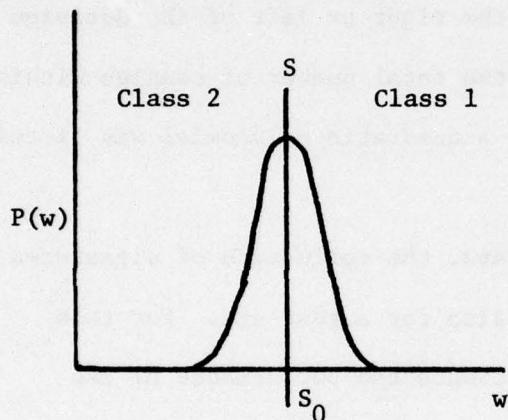


Figure 103 Prob. density functions for completely overlapping classes.

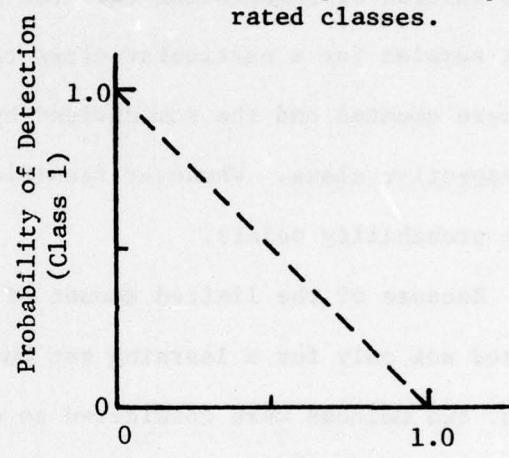


Figure 104 Prob. plot for completely overlapping classes.

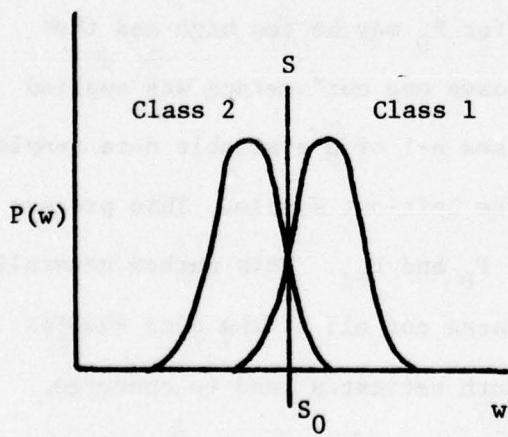


Figure 105 Prob. density functions for partially overlapping classes.

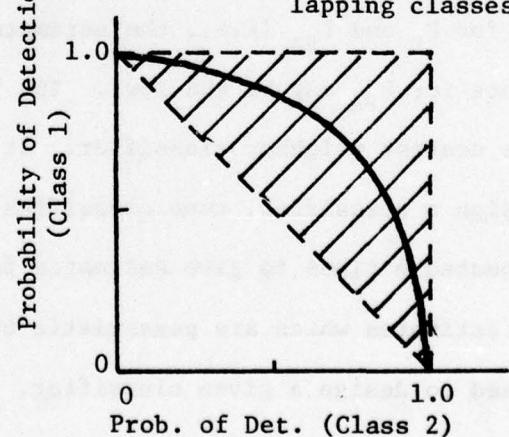


Figure 106 Prob. plot for partially overlapping classes.

UNCLASSIFIED

UNCLASSIFIED

overlap as illustrated in Figure 105 give probabilities which fall into the shaded region shown in Figure 106.

The foregoing discussion indicates the nature and form of the performance curves which are to be expected when actual measured data is used in the probability calculations. It must be emphasized that the actual sample distributions were not approximated with continuous density functions. As a result, the plots consist of discrete probability points. In other words, instead of integrating the area under a density function, the individual samples for a particular class to the right or left of the decision line were counted and the sum divided by the total number of samples within the respective class. Whenever feasible, a quadratic polynomial was fitted to the probability points.

Because of the limited amount of data, the collection of signatures was used not only for a learning set but also for a test set. For this reason, two methods were considered to estimate the performance of the learning set. The FLD and SP classifiers utilized only those samples that were used to design the classifier resulting, perhaps, in optimistic estimates for P_D and P_{FA} (i.e., the estimate for P_D may be too high and the estimate for P_{FA} may be too low). The "leave one out" method was applied to the nearest neighbor classifier. It uses $n-1$ of n available data samples to design a classifier, then classifies the left-out sample. This process is repeated n times to give estimates for P_D and P_{FA} . This method generally gives estimates which are pessimistic because not all of the data samples are used to design a given classifier. Both estimates tend to converge

UNCLASSIFIED

UNCLASSIFIED

toward the true probabilities as the number of samples in the learning set increases.

NBS DATA

The NBS data was used to evaluate algorithm performance for the conditions shown in Table 6 to facilitate comparison of performances between different classifiers, features, mines and non-mines. The numbers within the matrix refer to the figure in Appendix C where the particular plot can be found. References to these figures in this section will include the Appendix figure numbers in parenthesis for cross-reference. The vertical column on the left hand side indicates the type of classifier and the corresponding algorithms that were used. The top row shows the classes that were used for each curve. It is important to note that performance curves were generated not only for all mines versus non-mines but also for their constituents to point out the type of mine which gives the best classification performance and the type of non-mine which consistently gives high false alarm rates. Furthermore, a detailed analysis of the performance of individual non-mines versus mines can lead to identification of parameters which influence signatures and hence to identification of classification problems and suggestions for improvements.

There are many variables that can influence the signatures during the collection phase. These are attenuation of signal, shape of scatterer, and radar pulse shape. Others, such as the gating routine, can distort the signatures during data processing. Finally, there are parameters which do not act on the signatures but become important during the training phase of

UNCLASSIFIED

UNCLASSIFIED

| NBS DATA PROCESSING MATRIX | | UNCLASSIFIED | | | | | | | | | | | | | | | | | | | | | | | |
|------------------------------|--------------------------------|-------------------------|-------------------|----------------------|-----------------|------------------|-------------------|-------------------|------------------|------------------|------------------|------------------|------------------|------------------|-------------------|------------------|------------------|------------------|------------------|------------------|-------------------|------------------|------------------|------------------|--|
| CLASSIFIER | TYPE OF DATA | INTUITIVE OBSERVABLES | | | C-13 C-14 C-15 | | | C-16 C-17 C-18 | | | C-19 C-20 C-21 | | | C-22 C-23 C-24 | | | C-25 C-26 C-27 | | | C-28 C-29 C-30 | | | C-31 C-32 C-33 | | |
| FISHER'S LINEAR DISCRIMINANT | INTUITIVE OBSERVABLES RAW DATA | ALL MINES VS. NON-MINE* | TYPE A VS. TYPE B | TYPE C VS. NON-MINE | TYPE B VS. ROOT | TYPE C VS. PLATE | TYPE B VS. GROUND | TYPE C VS. GROUND | TYPE B VS. ROCKS | TYPE C VS. ROCKS | TYPE B VS. ROCKS | TYPE A VS. ROCKS | TYPE A VS. PLATE | TYPE B VS. PLATE | TYPE B VS. GROUND | TYPE C VS. PLATE | TYPE C VS. ROCKS | TYPE C VS. ROCKS | TYPE C VS. ROCKS | TYPE C VS. PLATE | TYPE C VS. GROUND | TYPE C VS. ROCKS | TYPE C VS. ROCKS | TYPE C VS. ROCKS | |
| NEAREST NEIGHBOR | INTUITIVE OBSERVABLES RAW DATA | ALL MINES VS. NON-MINE* | TYPE A VS. TYPE B | TYPE C VS. NON-MINE* | TYPE B VS. ROOT | TYPE C VS. PLATE | TYPE B VS. GROUND | TYPE C VS. GROUND | TYPE B VS. ROCKS | TYPE C VS. ROCKS | TYPE B VS. ROCKS | TYPE A VS. ROCKS | TYPE A VS. PLATE | TYPE B VS. PLATE | TYPE B VS. GROUND | TYPE C VS. PLATE | TYPE C VS. ROCKS | TYPE C VS. ROCKS | TYPE C VS. ROCKS | TYPE C VS. PLATE | TYPE C VS. GROUND | TYPE C VS. ROCKS | TYPE C VS. ROCKS | TYPE C VS. ROCKS | |
| 3 | INTUITIVE OBSERVABLES RAW DATA | ALL MINES VS. NON-MINE* | TYPE A VS. TYPE B | TYPE C VS. NON-MINE* | TYPE B VS. ROOT | TYPE C VS. PLATE | TYPE B VS. GROUND | TYPE C VS. GROUND | TYPE B VS. ROCKS | TYPE C VS. ROCKS | TYPE B VS. ROCKS | TYPE A VS. ROCKS | TYPE A VS. PLATE | TYPE B VS. PLATE | TYPE B VS. GROUND | TYPE C VS. PLATE | TYPE C VS. ROCKS | TYPE C VS. ROCKS | TYPE C VS. ROCKS | TYPE C VS. PLATE | TYPE C VS. GROUND | TYPE C VS. ROCKS | TYPE C VS. ROCKS | TYPE C VS. ROCKS | |
| 5 | INTUITIVE OBSERVABLES RAW DATA | ALL MINES VS. NON-MINE* | TYPE A VS. TYPE B | TYPE C VS. NON-MINE* | TYPE B VS. ROOT | TYPE C VS. PLATE | TYPE B VS. GROUND | TYPE C VS. GROUND | TYPE B VS. ROCKS | TYPE C VS. ROCKS | TYPE B VS. ROCKS | TYPE A VS. ROCKS | TYPE A VS. PLATE | TYPE B VS. PLATE | TYPE B VS. GROUND | TYPE C VS. PLATE | TYPE C VS. ROCKS | TYPE C VS. ROCKS | TYPE C VS. ROCKS | TYPE C VS. PLATE | TYPE C VS. GROUND | TYPE C VS. ROCKS | TYPE C VS. ROCKS | TYPE C VS. ROCKS | |
| 7 | INTUITIVE OBSERVABLES RAW DATA | ALL MINES VS. NON-MINE* | TYPE A VS. TYPE B | TYPE C VS. NON-MINE* | TYPE B VS. ROOT | TYPE C VS. PLATE | TYPE B VS. GROUND | TYPE C VS. GROUND | TYPE B VS. ROCKS | TYPE C VS. ROCKS | TYPE B VS. ROCKS | TYPE A VS. ROCKS | TYPE A VS. PLATE | TYPE B VS. PLATE | TYPE B VS. GROUND | TYPE C VS. PLATE | TYPE C VS. ROCKS | TYPE C VS. ROCKS | TYPE C VS. ROCKS | TYPE C VS. PLATE | TYPE C VS. GROUND | TYPE C VS. ROCKS | TYPE C VS. ROCKS | TYPE C VS. ROCKS | |
| SPACE PARTITION | INTUITIVE OBSERVABLES RAW DATA | ALL MINES VS. NON-MINE* | TYPE A VS. TYPE B | TYPE C VS. NON-MINE* | TYPE B VS. ROOT | TYPE C VS. PLATE | TYPE B VS. GROUND | TYPE C VS. GROUND | TYPE B VS. ROCKS | TYPE C VS. ROCKS | TYPE B VS. ROCKS | TYPE A VS. ROCKS | TYPE A VS. PLATE | TYPE B VS. PLATE | TYPE B VS. GROUND | TYPE C VS. PLATE | TYPE C VS. ROCKS | TYPE C VS. ROCKS | TYPE C VS. ROCKS | TYPE C VS. PLATE | TYPE C VS. GROUND | TYPE C VS. ROCKS | TYPE C VS. ROCKS | TYPE C VS. ROCKS | |
| CROSS CORRELATION | | | | | | | | | | | | | | | | | | | | | | | | | |
| IMPULSE CORRELATION | | | | | | | | | | | | | | | | | | | | | | | | | |

*Non-MINE INCLUDES ROCKS, ROOT AND PLATE

Table 6

NBS DATA PERFORMANCE MATRIX

UNCLASSIFIED

the learning set. These are the size of the learning set and the size of the feature vectors. All the variables above can influence, either directly or indirectly, classifier performance. Some were discussed in other sections of this report and therefore will be mentioned only briefly. All others will be examined in depth.

Signal Attenuation and Signature Gating

There are two ways an attenuated signal can affect the signature of a mine or non-mine. First, if the signal-to-noise ratio is small, but a part of the signal is clearly visible above background, this situation could result in improper gating of the complete signature. Second, if the attenuation is strong enough, the whole signature could become indistinguishable from background.

The latter case applies to NBS data taken under wet soil conditions. This means that many learning sets contain signatures of buried objects which are indistinguishable from background as far as classification is concerned. The worst cases occurred for soils with 30% moisture content; these were not utilized in generating the learning sets. Still, some highly attenuated signatures collected from soils of lower moisture content were present in the learning sets. The fact that these signatures were retained contributed to a significant increase in the number of misclassified mines and non-mines. Of importance here is the distribution of feature vectors in feature space. The "background" signatures (highly attenuated signatures) in this case will form their own separate distribution from that of the other two classes because the numbers that constitute the features of these signatures are

UNCLASSIFIED

UNCLASSIFIED

generally much smaller compared to "non-background signatures." Thus, there is no reason to assume that a particular "background signature" would be classified properly. In fact, it is likely that the whole cluster is assigned to one class or another affecting thereby not only the P_{FA} but also the probability of classification. In the case of the NN classifier misclassification depends, in general, on the distribution of feature vectors within the cluster of "background signatures" and whether the cluster is closer to one class or another. Clearly, detailed information on the effects of "background signatures" on classification performance is not available. However, the point to be emphasized here is that both mine versus mine and mine versus non-mine classification performances are affected.

The other way in which an attenuated signal can affect classification performance is through the gating procedure. The gating of signals is a convenient method by which the "signature" of an object is separated from its ground return in the time domain. The gate positions are set automatically by the computer. Basically, the search sequence "looks" for peaks above average background beyond the ground return. Therefore, for weak signals, the gates lock on to the highest peak above background. However, this does not mean that the gated time domain contains the actual mine or non-mine signature. In fact, it might contain only background or only a portion of the desired return which would cause the signature in the frequency domain to be distorted. If these distorted mine signatures are misclassified, then improper gating will also affect classifier performance.

UNCLASSIFIED

UNCLASSIFIED

Shape of Scatterer and Radar Pulse Width

Although the diameter of a scatterer such as a mine or a rock affects the magnitude of the return and thus the magnitude of the signature, it does not influence, to a significant extent, the character of the signature (e.g., shape and location of the maxima and minima). The parameter which does play a dominant role in the selection of maxima and minima of the signatures is the thickness of the object. For pulsedwidths much smaller than the scatterer's thickness, two returns were observed provided the second return was not appreciably attenuated within the scatterer. One return originated from the top, the first dielectric interface; the other from the bottom or the second dielectric interface. Hence, the time delay between the returns was directly proportional to the scatterer's thickness. Therefore, those objects which give approximately the same time delays as mines will be improperly classified as mines. Non-mines are easily identified if they have time delays that differ from those produced by mines.

The worst offenders in the non-mine category which gave consistently high false-alarm rates were the rocks and roots. For example, the performance shown in Figures 107 (C-59 mines vs. rocks) and 108 (C-60 mines vs. roots) are inferior to that of Figure 109 (C-61 mines vs. plates). In the mine category, it is the type A and type B which could not be readily distinguished from the non-mines as illustrated in Figures 110 (C-48), 111 (C-53), and 112 (C-58). However, because the rocks and roots were specially chosen to be approximately equal in thickness to mines, it is suggested that the classifier may exhibit improved performance under actual field tests where

UNCLASSIFIED

UNCLASSIFIED

NEAREST NEIGHBOR CLASSIFIER

RAW DATA
NO. NEAREST NEIGHBORS 3
REFERENCE 295

| NONMINE TARGET | ROCK(1) | ROCK(2) | TYPE C MINE | TYPE A MINE | TYPE B MINE |
|----------------|---------|---------|-------------|-------------|-------------|
| DEPTH | 3 | 6 | | | |
| LOCATION | +4 | 0 | -4 | | |
| MOISTURE | 7 | 17 | 12-20 | 13-16 | |

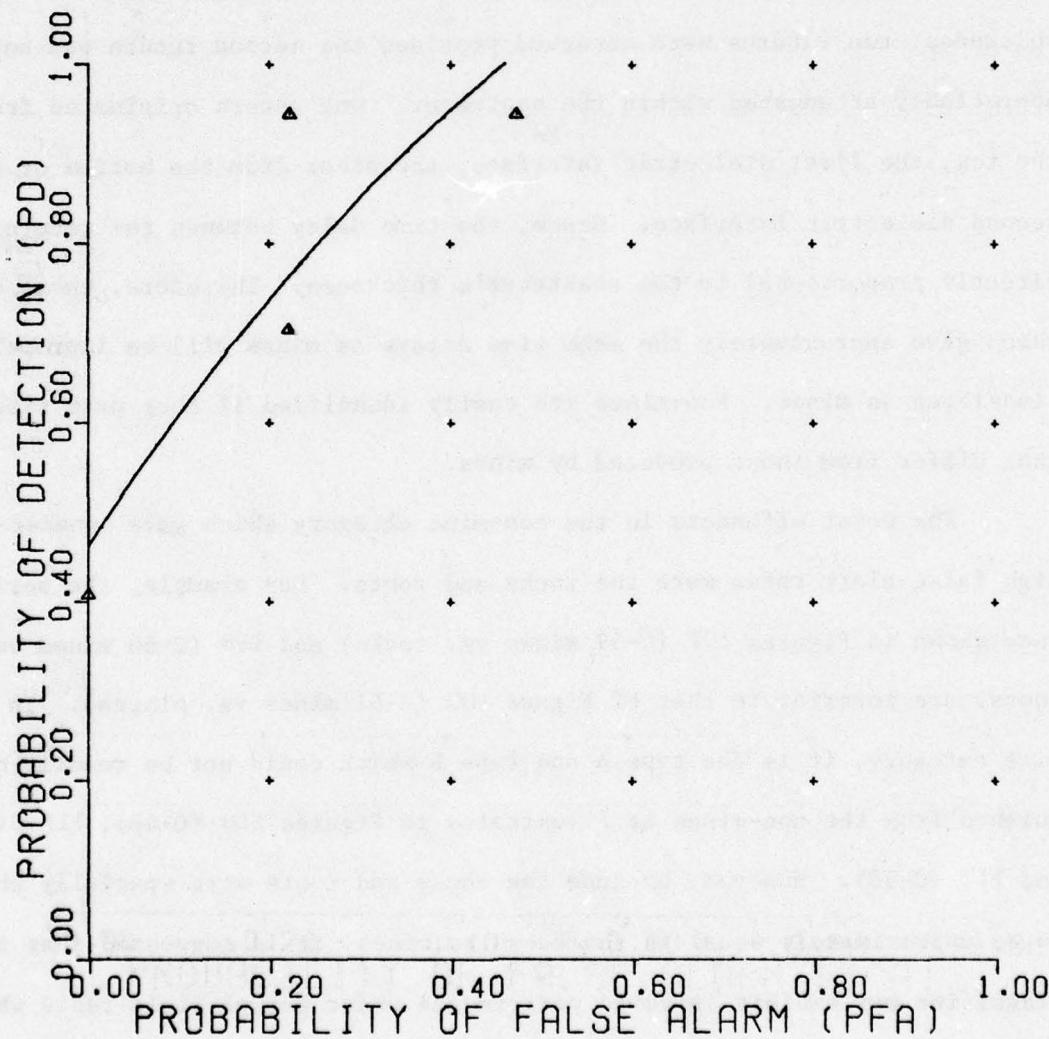


Figure 107. Nearest neighbor classifier.

UNCLASSIFIED

UNCLASSIFIED

NEAREST NEIGHBOR CLASSIFIER

RAW DATA

NO. NEAREST NEIGHBORS 3

REFERENCE 296

| NONMINE | ROOT | TYPE C MINE | TYPE A MINE | TYPE B MINE |
|----------|------|-------------|-------------|-------------|
| TARGET | | | | |
| DEPTH | 3 | 6 | 8 | 8 |
| LOCATION | +4 | -4 | 0 | -4 |
| MOISTURE | 7 | 17 | 12-20 | 13-19 |

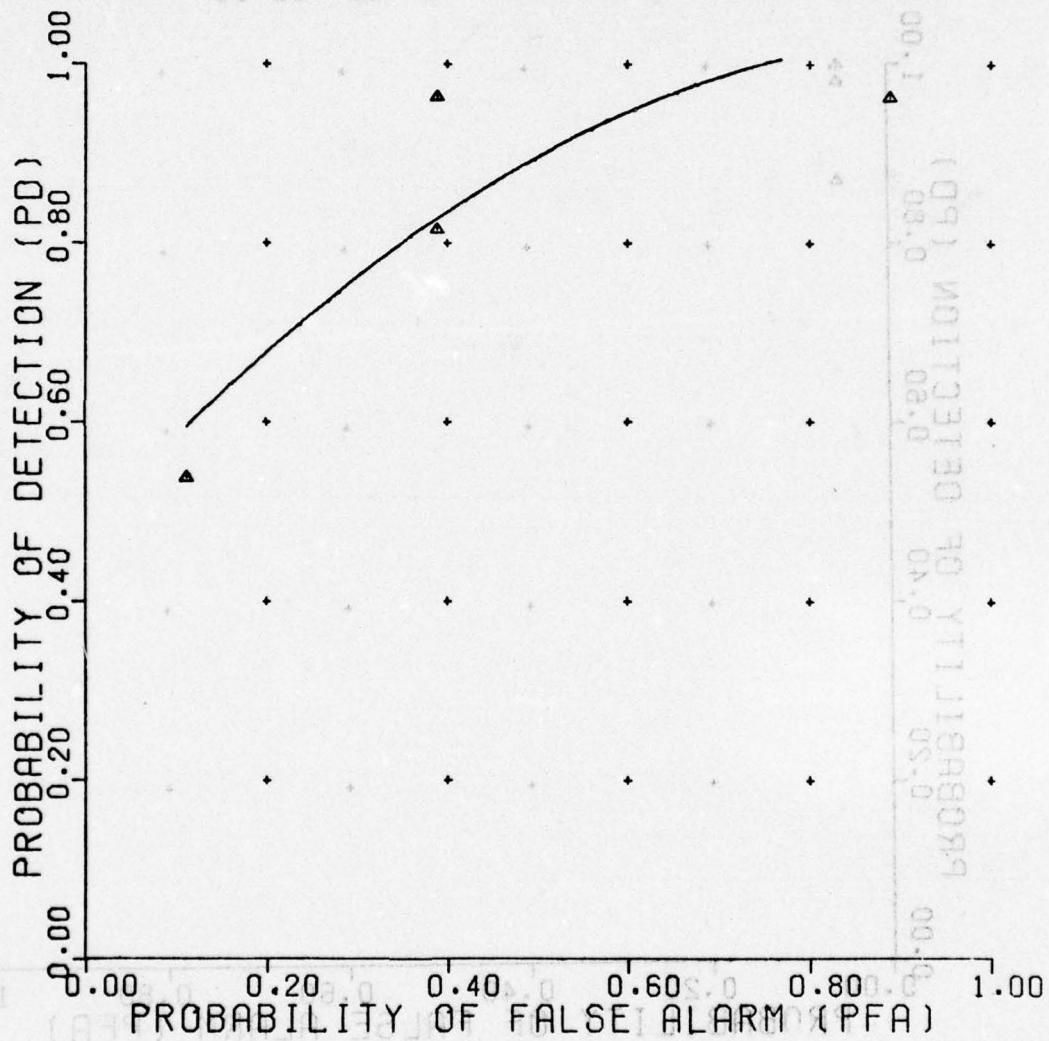


Figure 108. Nearest neighbor classifier.

UNCLASSIFIED

UNCLASSIFIED

NEAREST NEIGHBOR CLASSIFIER

RAW DATA

NO. NEAREST NEIGHBORS 3

REFERENCE 297

| NONMINE TARGET | PLATE | TYPE C MINE | TYPE A MINE | TYPE B MINE |
|-------------------|-------|-------------|-------------|-------------|
| DEPTH | | 3 | 6 | |
| LOCATION | | +4 | 0 | -4 |
| MOISTURE | | 7 | 17 | 12-20 13-16 |

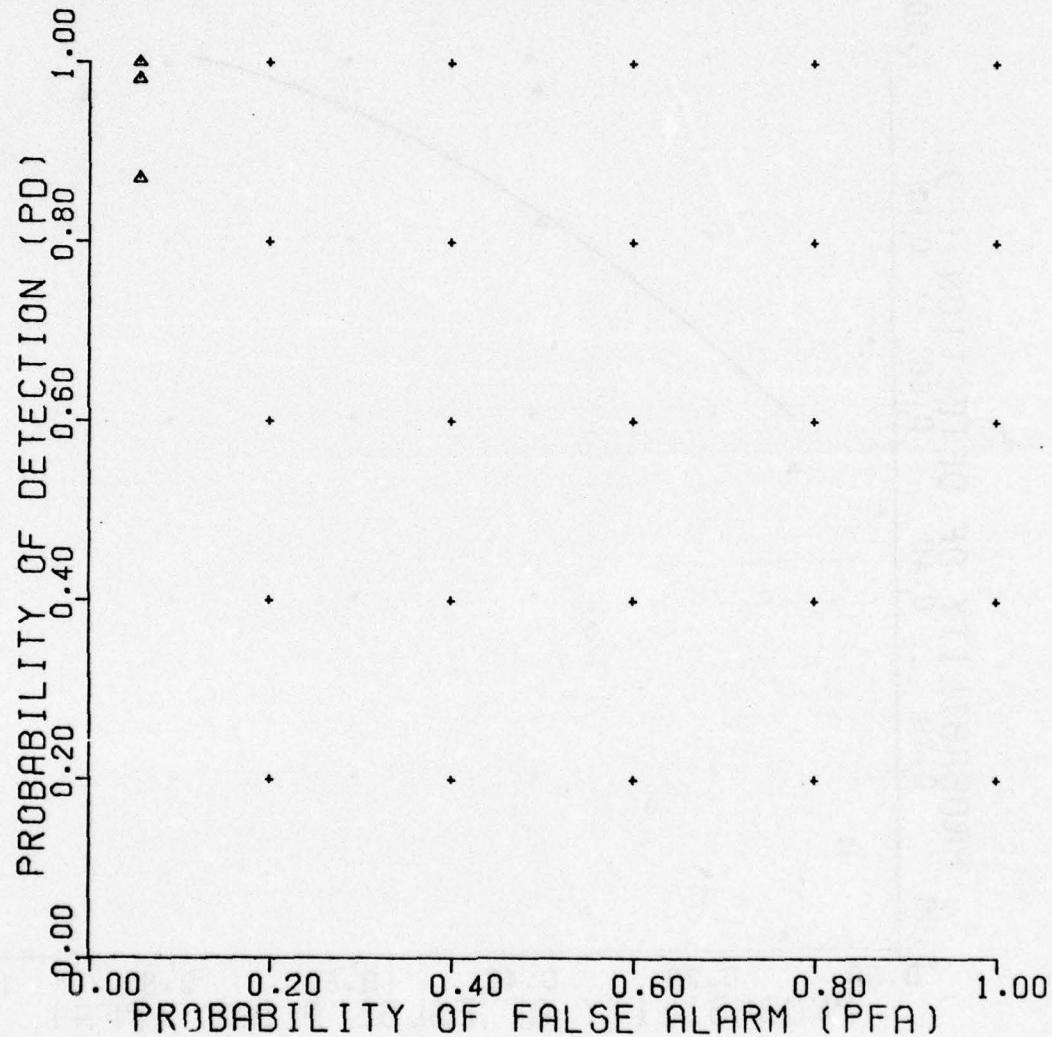


Figure 109. Nearest neighbor classifier.

UNCLASSIFIED

UNCLASSIFIED

NEAREST NEIGHBOR CLASSIFIER

RAW DATA

NO. NEAREST NEIGHBORS 3

REFERENCE 313

| NONMINE TARGET | PLATE | ROCK(1) | ROCK(2) | ROOT |
|-------------------|-------------|---------|---------|-------|
| | TYPE A MINE | | | |
| DEPTH | 3 | 6 | | |
| LOCATION | +4 | 0 | -4 | |
| MOISTURE | 7 | 17 | 12-20 | 13-16 |

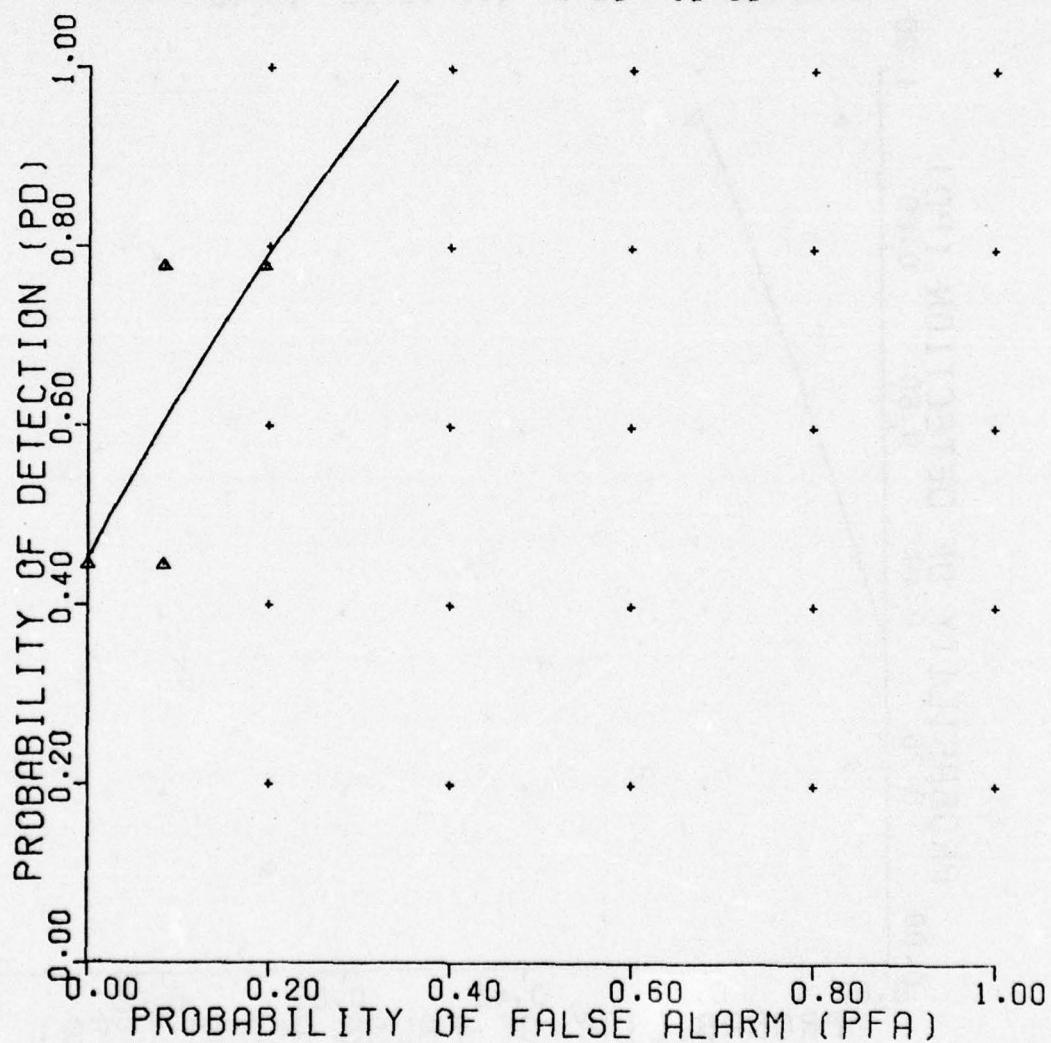


Figure 110. Nearest neighbor classifier.

UNCLASSIFIED

UNCLASSIFIED

NEAREST NEIGHBOR CLASSIFIER

RAW DATA

NO. NEAREST NEIGHBORS 3

REFERENCE 314

| NONMINE TARGET | PLATE TYPE B MINE | ROCK(1) | ROCK(2) | ROOT |
|-------------------|----------------------|---------|---------|-------|
| DEPTH | | 3 | 6 | |
| LOCATION | +4 | 0 | -4 | |
| MOISTURE | 7 | 17 | 12-20 | 13-16 |

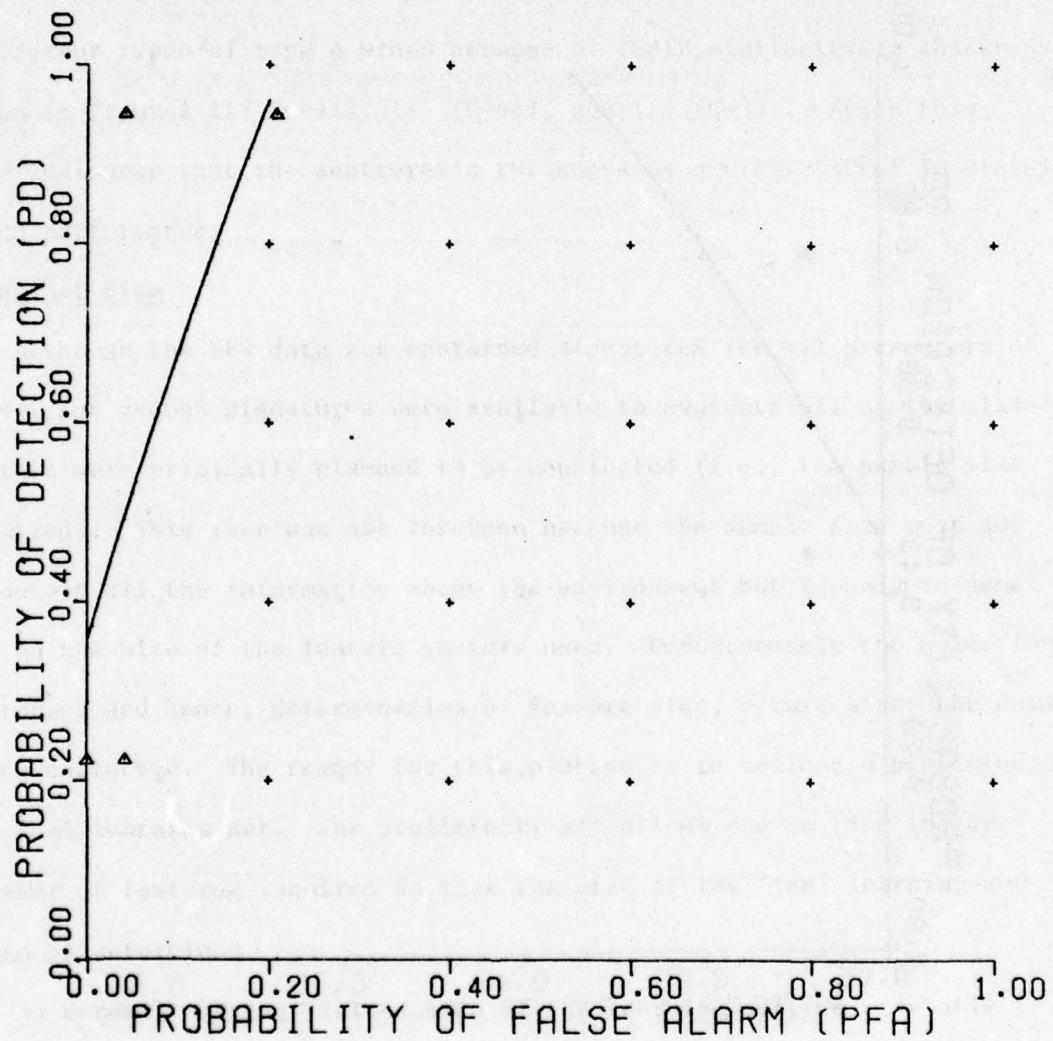


Figure 111. Nearest neighbor classifier.

UNCLASSIFIED

UNCLASSIFIED

NEAREST NEIGHBOR CLASSIFIER

RAW DATA

NO. NEAREST NEIGHBORS 3

REFERENCE 315

| NONMINE TARGET | PLATE | ROCK(1) | ROCK(2) | ROOT |
|-------------------|-------------|---------|---------|-------|
| | TYPE C MINE | | | |
| DEPTH | 3 | 6 | | |
| LOCATION | +4 | 0 | -4 | |
| MOISTURE | 7 | 17 | 12-20 | 13-16 |

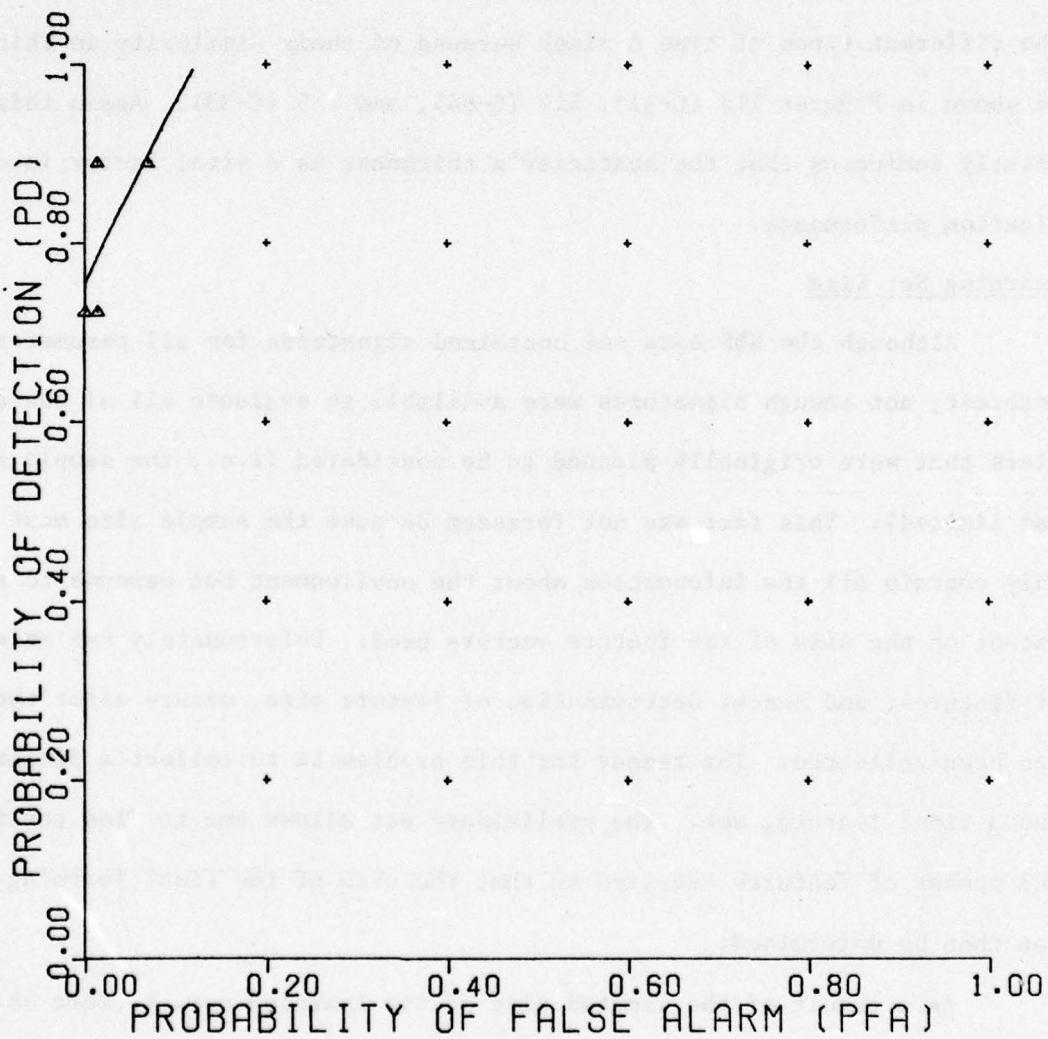


Figure 112. Nearest neighbor classifier.

UNCLASSIFIED

UNCLASSIFIED

rocks of all sizes and shapes are available. Therefore, the performances given here represent a lower bound. In other words, the P_{FA} is expected to decrease and the P_D to increase under field test conditions.

A similar argument applies to the classification performances between the type C and type A mines which have a thickness ratio of 1.47. Regardless of the classifier used, good performances were consistently observed for these mines; however, it was generally difficult to distinguish between the different types of type A mines because of their similarity in thickness as shown in Figures 113 (C-41), 114 (C-64), and 115 (C-33). Again this clearly indicates that the scatterer's thickness is a vital factor in classification performance.

Learning Set Size

Although the NBS data set contained signatures for all parameters of interest, not enough signatures were available to evaluate all of the classifiers that were originally planned to be considered (i.e., the sample size was limited). This fact was not foreseen because the sample size must not only contain all the information about the environment but depends to some extent on the size of the feature vectors used. Unfortunately the selection of features, and hence, determination of feature size, occurs after the data has been collected. The remedy for this problem is to collect a preliminary and a final learning set. The preliminary set allows one to find the type and number of features required so that the size of the final learning set can then be determined.

As a result of the limited size of the learning set, we were able to use only feature vectors with a small number of components (i.e., intuitive

UNCLASSIFIED

UNCLASSIFIED

NEAREST NEIGHBOR CLASSIFIER

INTUITIVE DATA

VERSION 3

REFERENCE 277

TARGET2 TYPE B MINE
TARGET1 TYPE A MINE

| DEPTH | 3 | 6 |
|----------|----|----|
| LOCATION | +4 | 0 |
| MOISTURE | 7 | 17 |

12-20 13-16

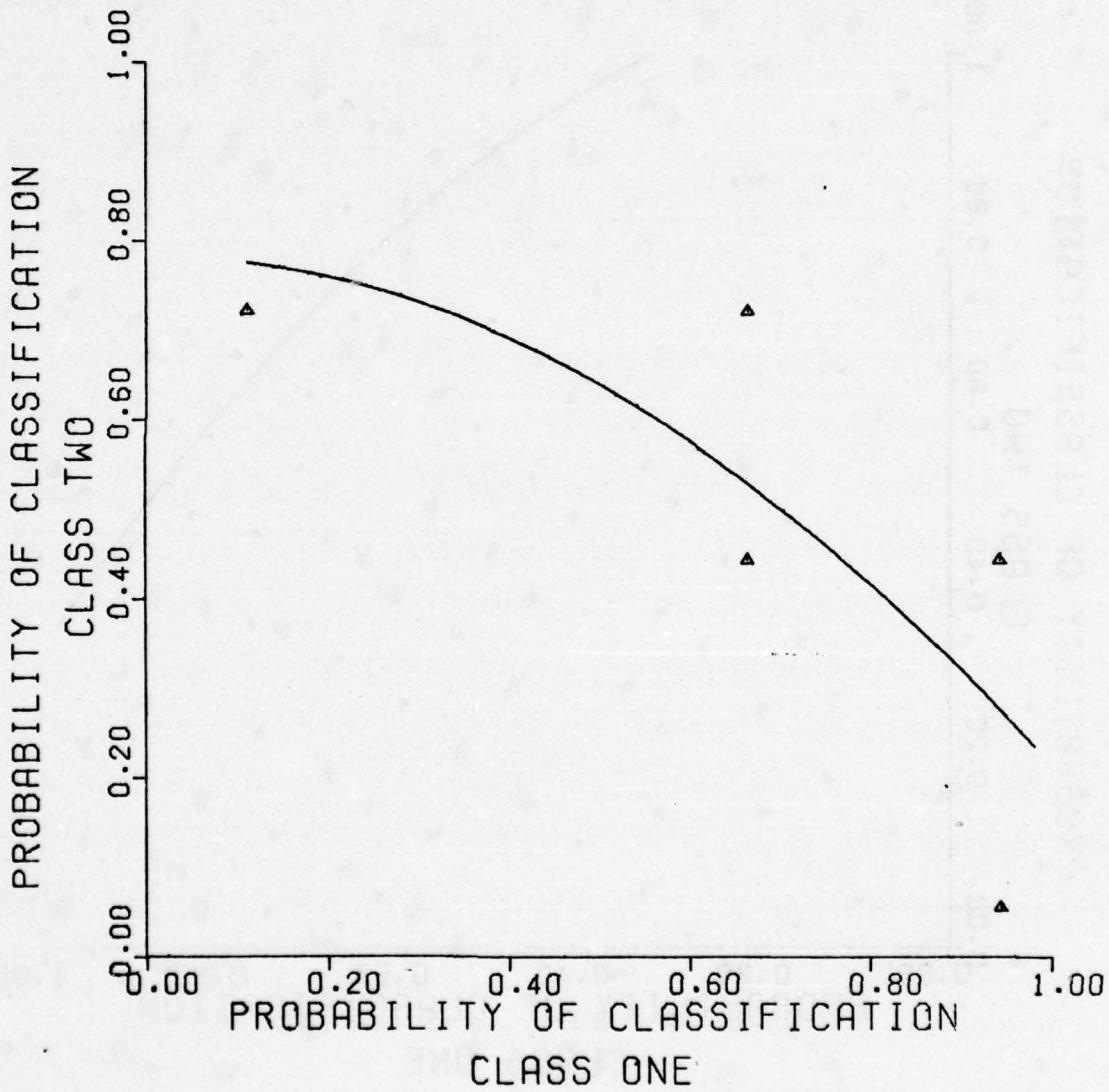


Figure 113. Nearest neighbor classifier.

UNCLASSIFIED

UNCLASSIFIED

NEAREST NEIGHBOR CLASSIFIER

RAW DATA
VERSION 3
REFERENCE 280

TARGET2 TYPE B MINE
TARGET1 TYPE A MINE

| | | | | |
|----------|----|----|-------|-------|
| DEPTH | 3 | 6 | | |
| LOCATION | +4 | 0 | -4 | |
| MOISTURE | 7 | 17 | 12-20 | 13-16 |

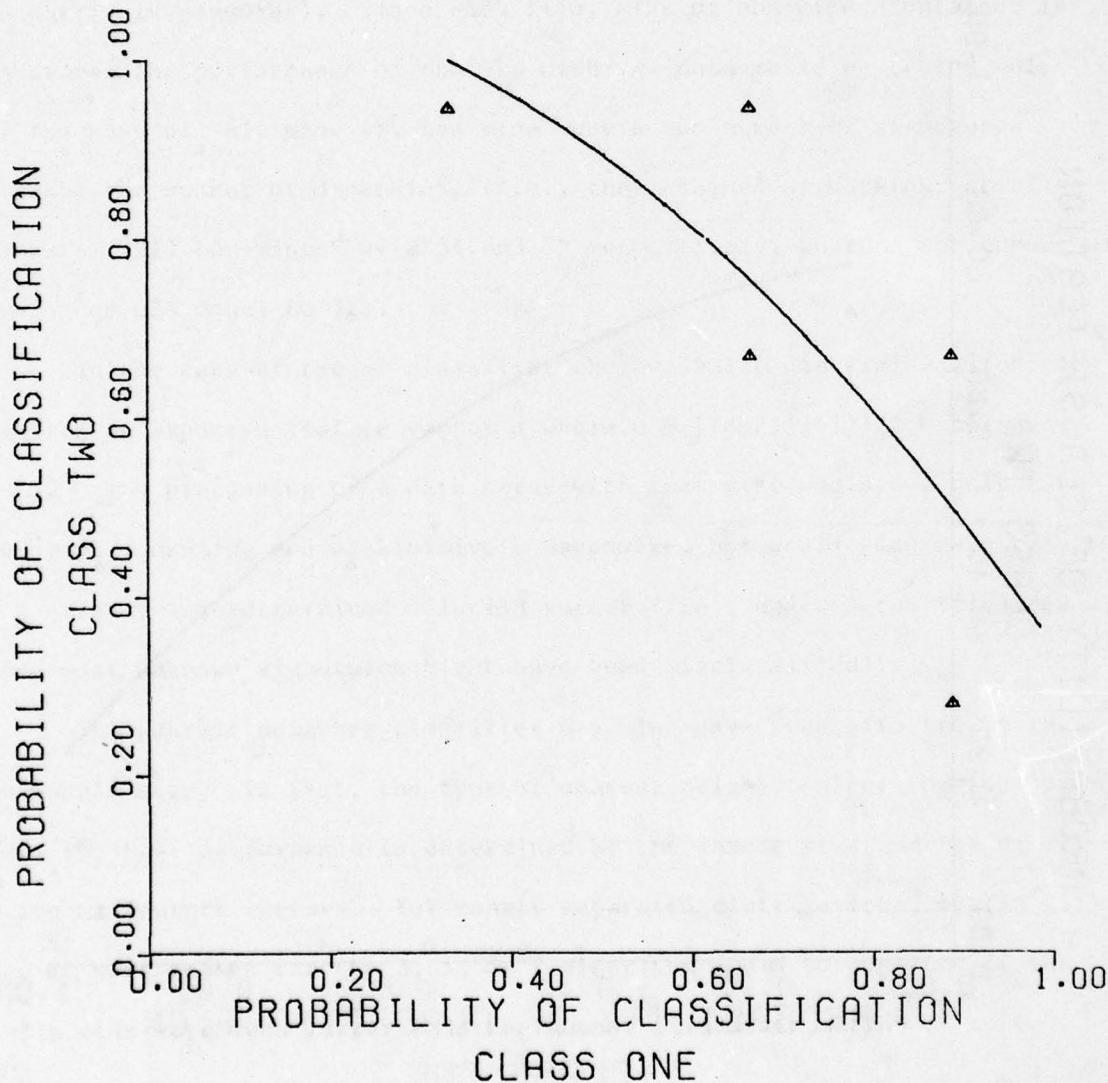


Figure 114. Nearest neighbor classifier.

UNCLASSIFIED

UNCLASSIFIED

FLD/BAYES CLASSIFIER

CLASSIFIER VERSION= 2
REFERENCE NUMBER= 360
CLASS 1= TYPE A MINE
CLASS 2= TYPE B MINE

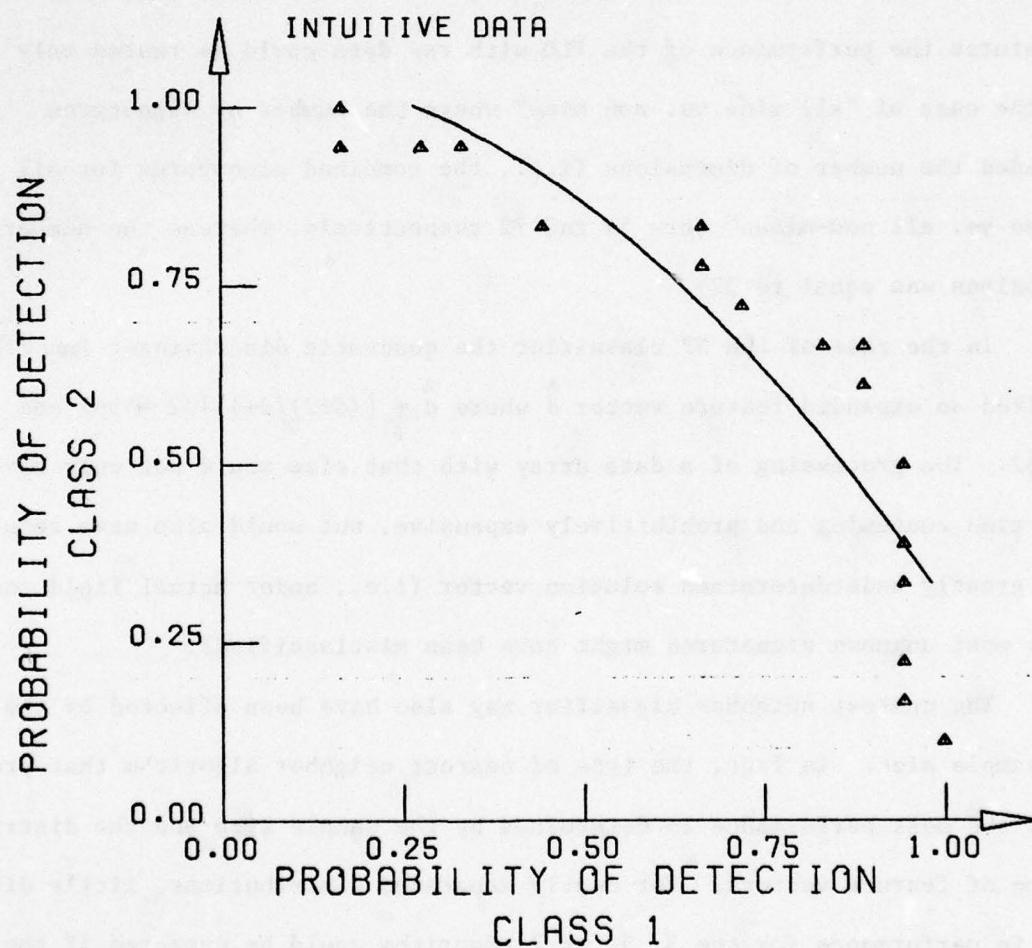


Figure 115. FLD/Bayes classifier.

UNCLASSIFIED

UNCLASSIFIED

observables) for the FLD and SP classifiers. In the case of the FLD the reason is as follows: the solution for the best \vec{W} vector requires the inverse of the within-scatter matrix which measures the distribution of feature vectors with respect to the mean within a particular class. Quite often, this inverse does not exist if the number of samples, n , is of the order of or less than the number of dimensions of the feature vectors (i.e., the matrix is singular). Since each file, mine or non-mine, contained 18 signatures the performance of the FLD with raw data could be tested only for the case of "all mine vs. non mine" where the number of signatures exceeded the number of dimensions (i.e., the combined signatures for all "mines vs. all non-mines" were 54 and 72 respectively, whereas the number of dimensions was equal to 32).

In the case of the SP classifier the quadratic discriminant function required an expanded feature vector $\hat{\vec{d}}$ where $\hat{\vec{d}} = [(d+2)(d+1)]/2 = 561$ and $d = 32$. The processing of a data array with that size would not only have been time consuming and prohibitively expensive, but would also have resulted in a greatly underdetermined solution vector (i.e., under actual field conditions most unknown signatures might have been misclassified).

The nearest neighbor classifier may also have been affected by the low sample size. In fact, the type of nearest neighbor algorithm that provides the best performance is determined by the sample size and the distribution of feature vectors. For nearly separated distributions, little difference in performance for the 3, 5, or 7 algorithm would be expected if the sample size were much larger than the number of nearest neighbors to be

UNCLASSIFIED

UNCLASSIFIED

tested (e.g., hundreds of samples). On the other hand, if the sample size is small (i.e., between 18 and 72 as in our case) then the performances are expected to depend to some degree on the number K. The reason is that the classification probability must decrease to 0.5 as K approaches the total number of samples, n, provided the sample populations for each class are equal, as in our case. This type of behavior can be observed by comparing Figures 116 (C-48) through 119 (C-63) with Figures 120 (C-71) through 123 (C-74), and 124 (C-79) through 127 (C-82). The plots show that the 3-nearest neighbor classifier (K = 3) is clearly superior to all other NN algorithms.

Influence of Feature Size on Classification

In many instances, classifiers using raw data outperformed those using intuitive observables. For example, Figures 116 (C-48) through 119 (C-63) show better discrimination performance than Figures 128 (C-67) through 131 (C-70) where raw data was replaced by intuitive data. This suggests that although only the "best" intuitive features were picked from the original package the amount of information each intuitive vector contained was evidently less than that contained in the raw data.

Classifier Performance

To save time and money some performances with the 5- and 7-nearest neighbor algorithm performances indicated in Table 6 were not evaluated. In order to reduce the number of plots to be analyzed with the nearest neighbor classifier, Columns 5, 10, 15, and 20 in Table 6 (where mines are compared to the class of all non-mines) were tested first, on the assumption that classification of mines versus the constituents of non-mines would give

UNCLASSIFIED

UNCLASSIFIED

NEAREST NEIGHBOR CLASSIFIER

RAW DATA

NO. NEAREST NEIGHBORS 3

REFERENCE 313

| NONMINE TARGET | PLATE TYPE A MINE | ROCK(1) | ROCK(2) | ROOT |
|-------------------|----------------------|---------|---------|-------|
| DEPTH | | 3 | 6 | |
| LOCATION | | +4 | 0 | -4 |
| MOISTURE | | 7 | 17 | 12-20 |
| | | | | 13-16 |

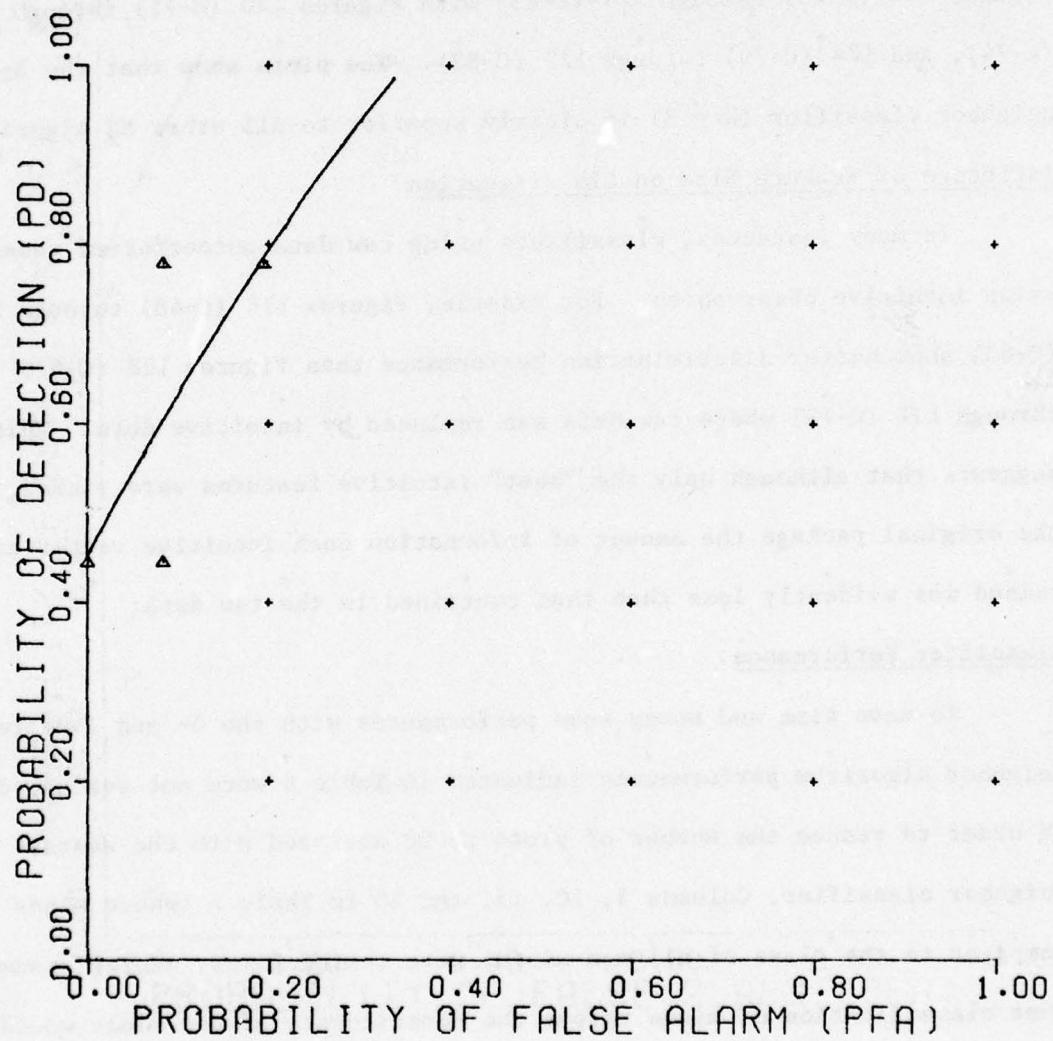


Figure 116. Nearest neighbor classifier.

UNCLASSIFIED

UNCLASSIFIED

NEAREST NEIGHBOR CLASSIFIER

RAW DATA
NO. NEAREST NEIGHBORS 3
REFERENCE 314

| NONMINE TARGET | PLATE TYPE B MINE | ROCK(1) | ROCK(2) | ROOT |
|----------------|-------------------|---------|---------|-------|
| DEPTH | | 3 | 6 | |
| LOCATION | +4 | | 0 | -4 |
| MOISTURE | | 7 | 17 | 12-20 |
| | | | | 13-16 |

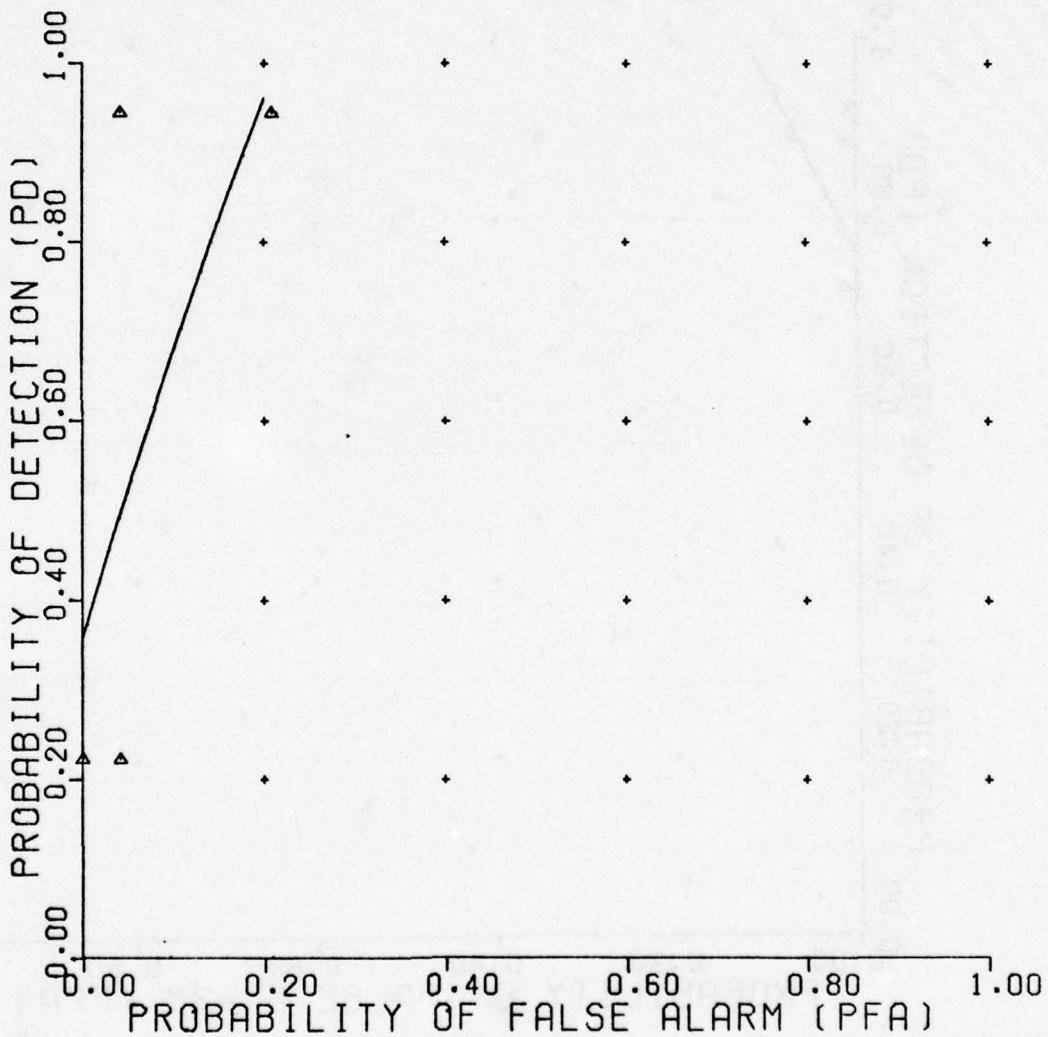


Figure 117. Nearest neighbor classifier.

UNCLASSIFIED

UNCLASSIFIED

NEAREST NEIGHBOR CLASSIFIER

RAW DATA

NO. NEAREST NEIGHBORS 3

REFERENCE 315

| NONMINE TARGET | PLATE TYPE C | ROCK(1) | ROCK(2) | ROOT |
|-------------------|-----------------|---------|---------|-------|
| DEPTH | | 3 | 6 | |
| LOCATION | +4 | | 0 | -4 |
| MOISTURE | | 7 | 17 | 12-20 |
| | | | | 13-16 |

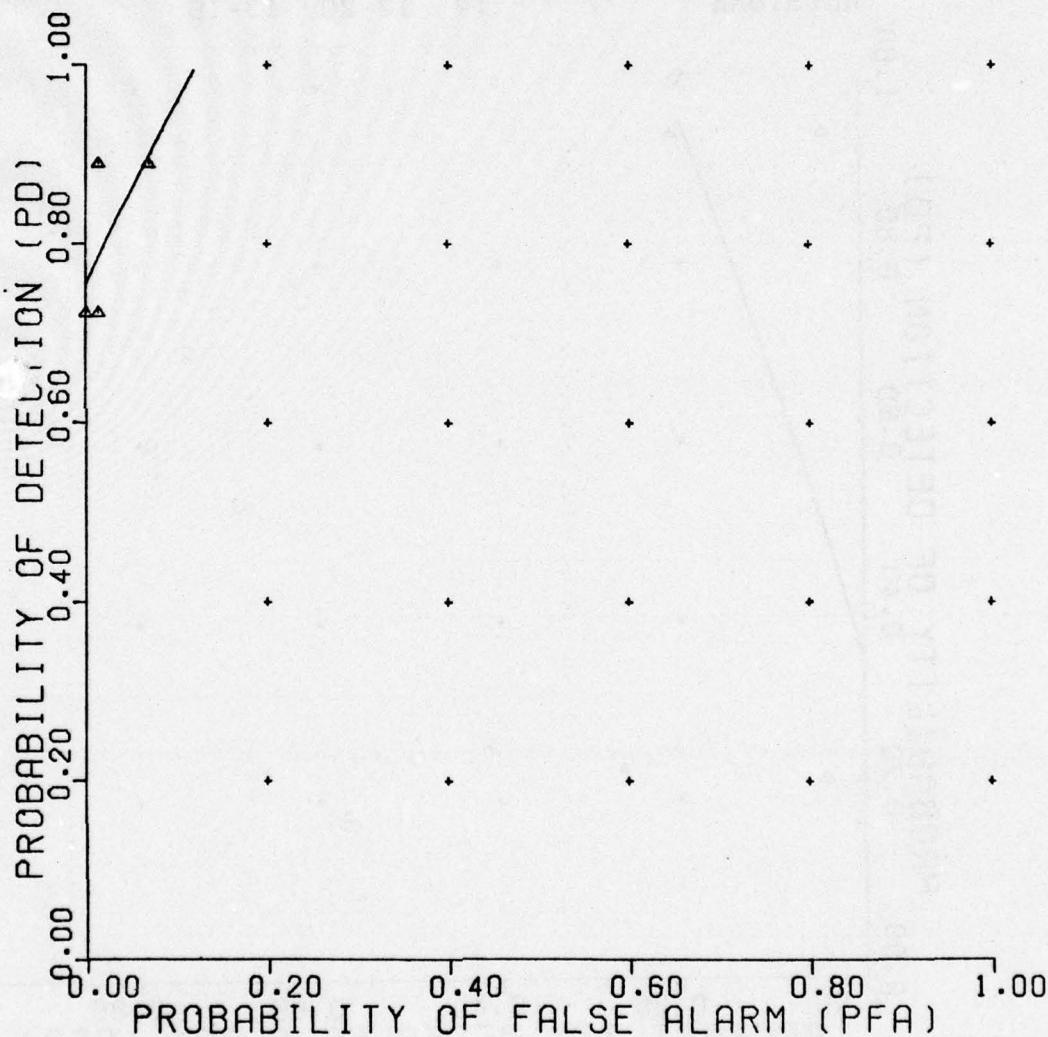


Figure 118. Nearest neighbor classifier.

UNCLASSIFIED

UNCLASSIFIED

NEAREST NEIGHBOR CLASSIFIER

RAW DATA

NO. NEAREST NEIGHBORS 3

REFERENCE 316

| NONMINE TARGET | PLATE TYPE C MINE | ROCK(1) TYPE A MINE | ROCK(2) TYPE B MINE | ROOT MINE |
|-------------------|----------------------|------------------------|------------------------|--------------|
| DEPTH | 3 | 6 | | |
| LOCATION | +4 | 0 | -4 | |
| MOISTURE | 7 | 17 | 12-20 | 13-16 |

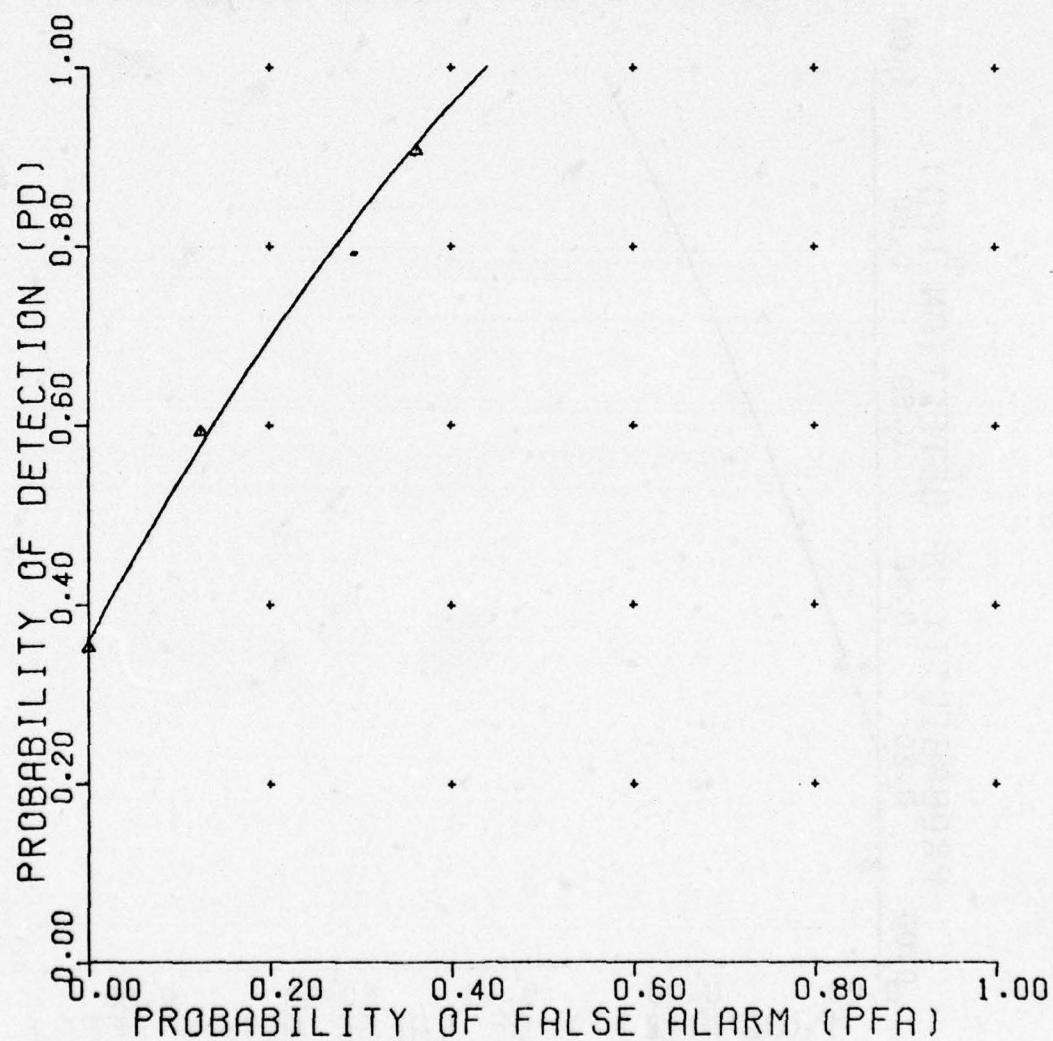


Figure 119. Nearest neighbor classifier.

UNCLASSIFIED

UNCLASSIFIED

NEAREST NEIGHBOR CLASSIFIER

RAW DATA

NO. NEAREST NEIGHBORS 5

REFERENCE 321

| NONMINE TARGET | PLATE TYPE A MINE | ROCK(1) | ROCK(2) | ROOT |
|-------------------|----------------------|---------|---------|-------|
| DEPTH | | 3 | 6 | |
| LOCATION | | +4 | 0 | -4 |
| MOISTURE | | 7 | 17 | 12-20 |
| | | | | 13-16 |

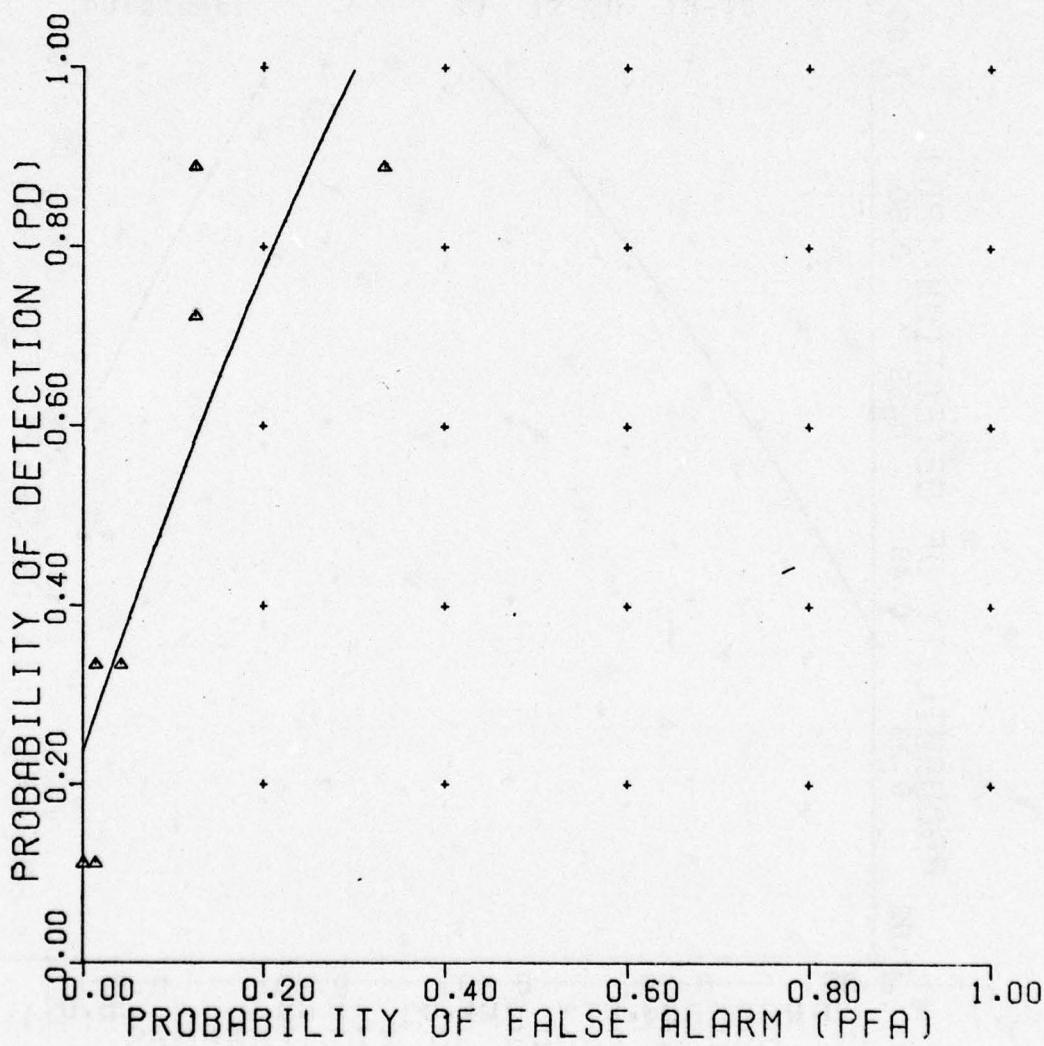


Figure 120. Nearest neighbor classifier.

UNCLASSIFIED

UNCLASSIFIED

NEAREST NEIGHBOR CLASSIFIER

RAW DATA

NO. NEAREST NEIGHBORS 5

REFERENCE 322

| NONMINE TARGET | PLATE TYPE B MINE | ROCK(1) | ROCK(2) | ROOT |
|-------------------|----------------------|---------|---------|-------|
| DEPTH | | 3 | 6 | |
| LOCATION | | +4 | 0 | -4 |
| MOISTURE | | 7 | 17 | 12-20 |
| | | | | 13-16 |

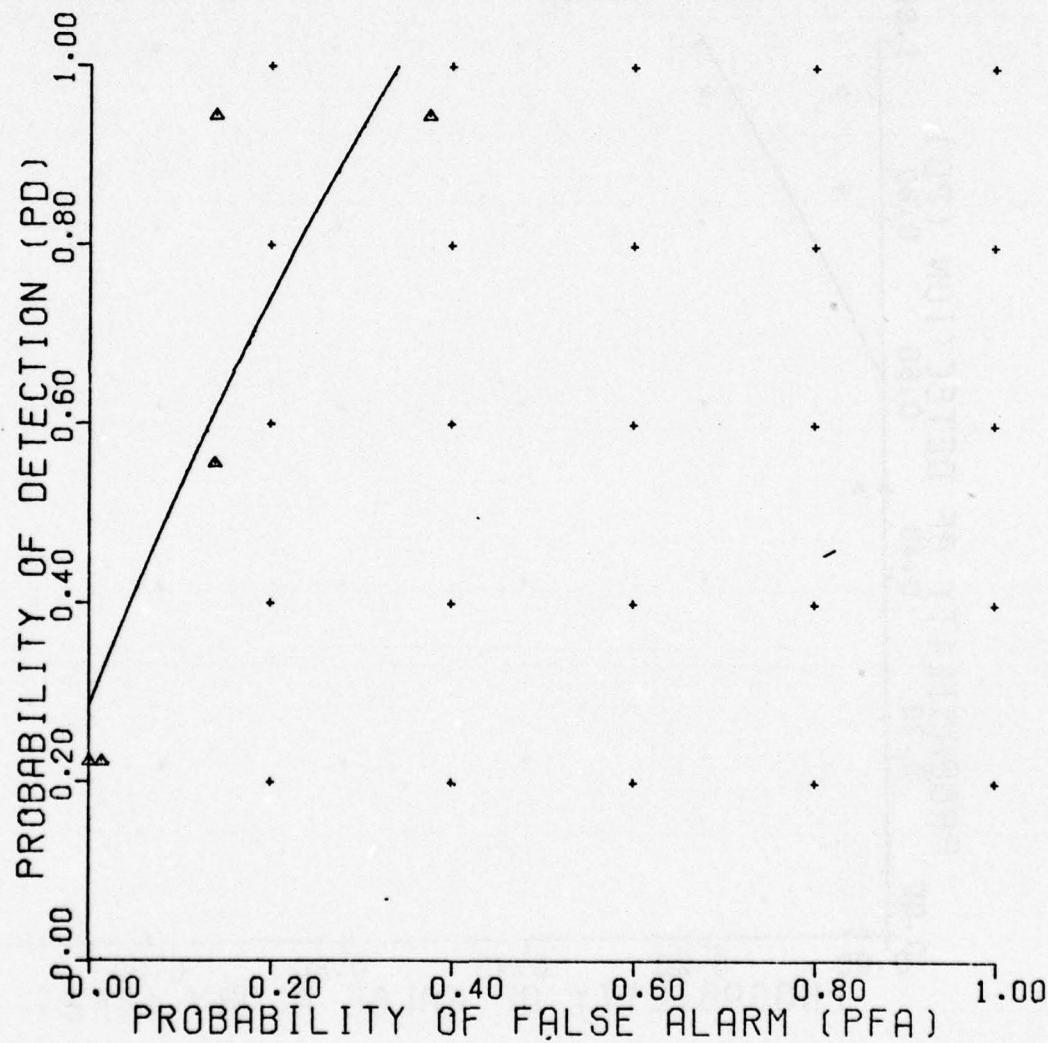


Figure 121. Nearest neighbor classifier.

UNCLASSIFIED

UNCLASSIFIED

NEAREST NEIGHBOR CLASSIFIER

RAW DATA
NO. NEAREST NEIGHBORS 5
REFERENCE 323

| NONMINE TARGET | PLATE TYPE C MINE | ROCK(1) | ROCK(2) | ROOT |
|----------------|-------------------|---------|---------|-------|
| DEPTH | | 3 | 6 | |
| LOCATION | | +4 | 0 | -4 |
| MOISTURE | | 7 | 17 | 12-20 |
| | | | | 13-16 |

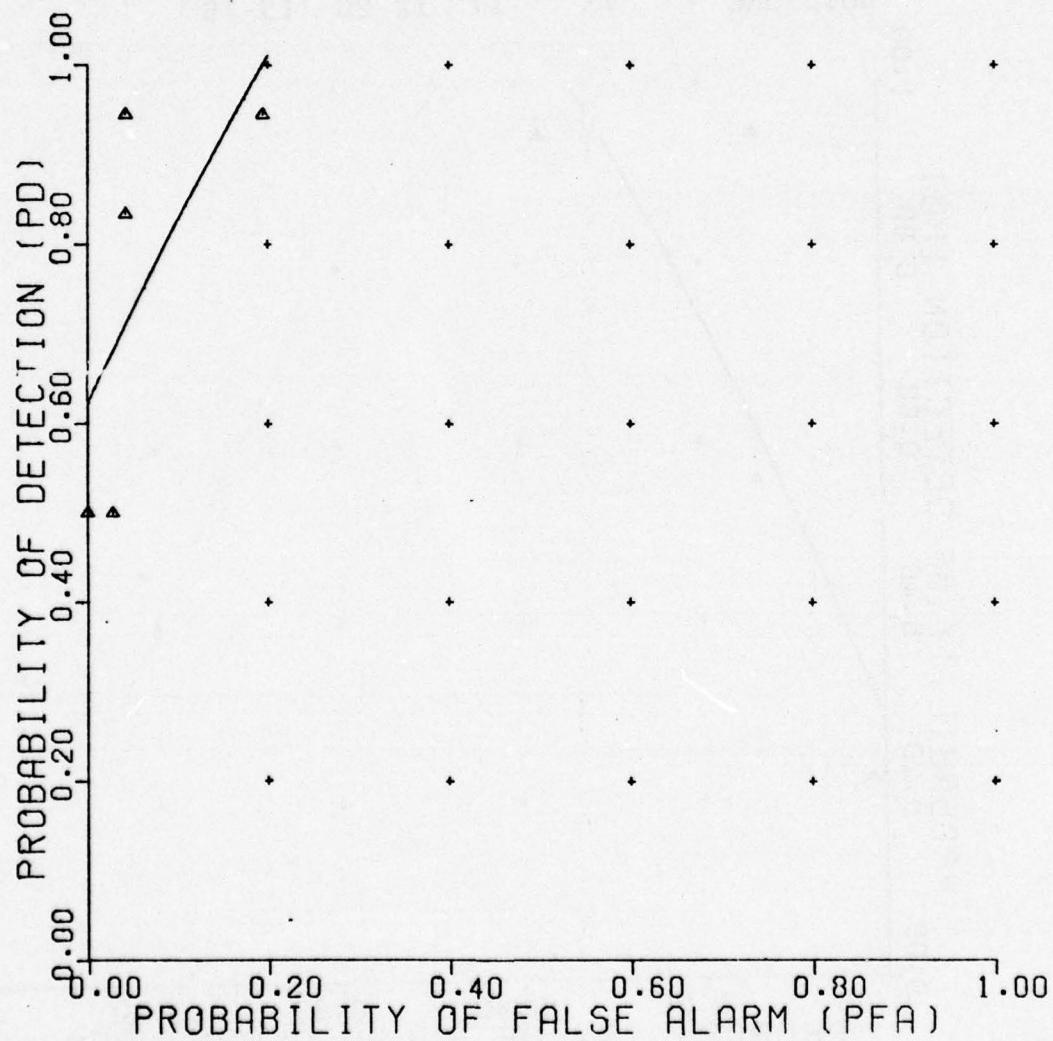


Figure 122. Nearest neighbor classifier.

UNCLASSIFIED

UNCLASSIFIED

NEAREST NEIGHBOR CLASSIFIER

RAW DATA

NO. NEAREST NEIGHBORS 5

REFERENCE 324

| NONMINE TARGET | PLATE TYPE C MINE | ROCK(1) TYPE A MINE | ROCK(2) TYPE B MINE | ROOT |
|-------------------|----------------------|------------------------|------------------------|-------|
| DEPTH | 3 | 6 | | |
| LOCATION | +4 | 0 | -4 | |
| MOISTURE | 7 | 17 | 12-20 | 13-16 |

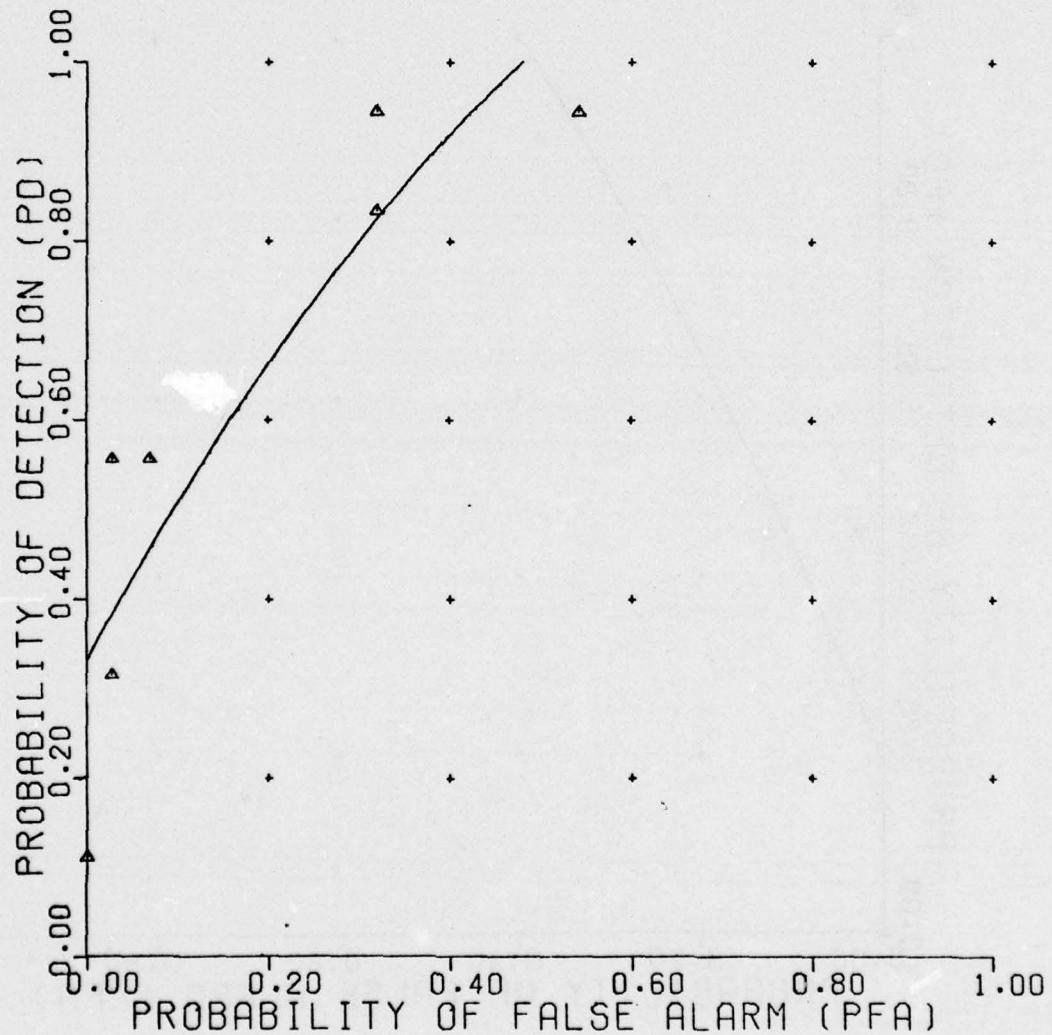


Figure 123. Nearest neighbor classifier.

UNCLASSIFIED

UNCLASSIFIED

NEAREST NEIGHBOR CLASSIFIER

RAW DATA
NO. NEAREST NEIGHBORS 7
REFERENCE 329

| NONMINE TARGET | PLATE TYPE A MINE | ROCK(1) | ROCK(2) | ROOT |
|----------------|-------------------|---------|---------|-------|
| DEPTH | | 3 | 6 | |
| LOCATION | | +4 | 0 | -4 |
| MOISTURE | | 7 | 17 | 12-20 |
| | | | | 13-16 |

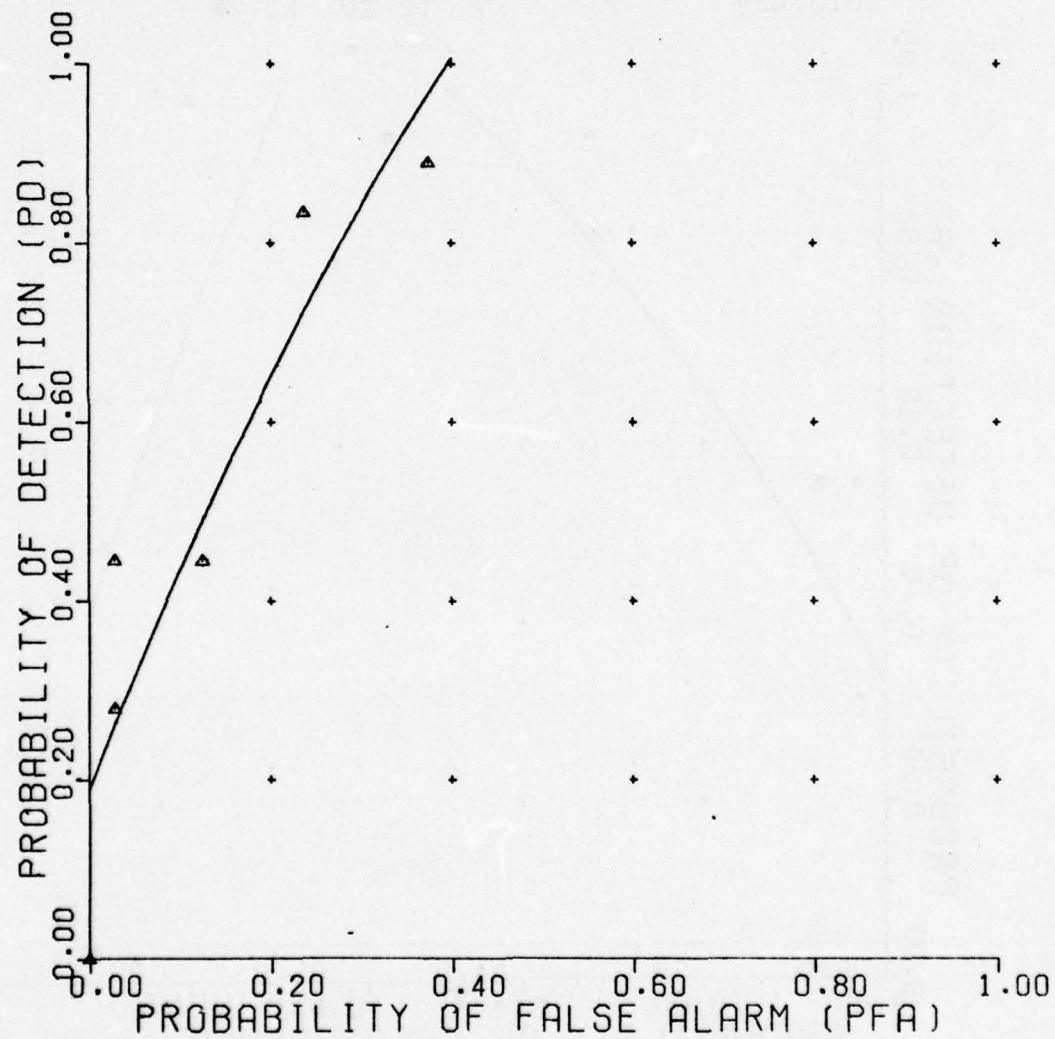


Figure 124. Nearest neighbor classifier.

UNCLASSIFIED

UNCLASSIFIED

NEAREST NEIGHBOR CLASSIFIER

RAW DATA

NO. NEAREST NEIGHBORS 7

REFERENCE 330

| NONMINE TARGET | PLATE TYPE B MINE | ROCK(1) | ROCK(2) | ROOT |
|-------------------|----------------------|---------|---------|-------|
| DEPTH | | 3 | 6 | |
| LOCATION | | +4 | 0 | -4 |
| MOISTURE | | 7 | 17 | 12-20 |
| | | | | 13-16 |

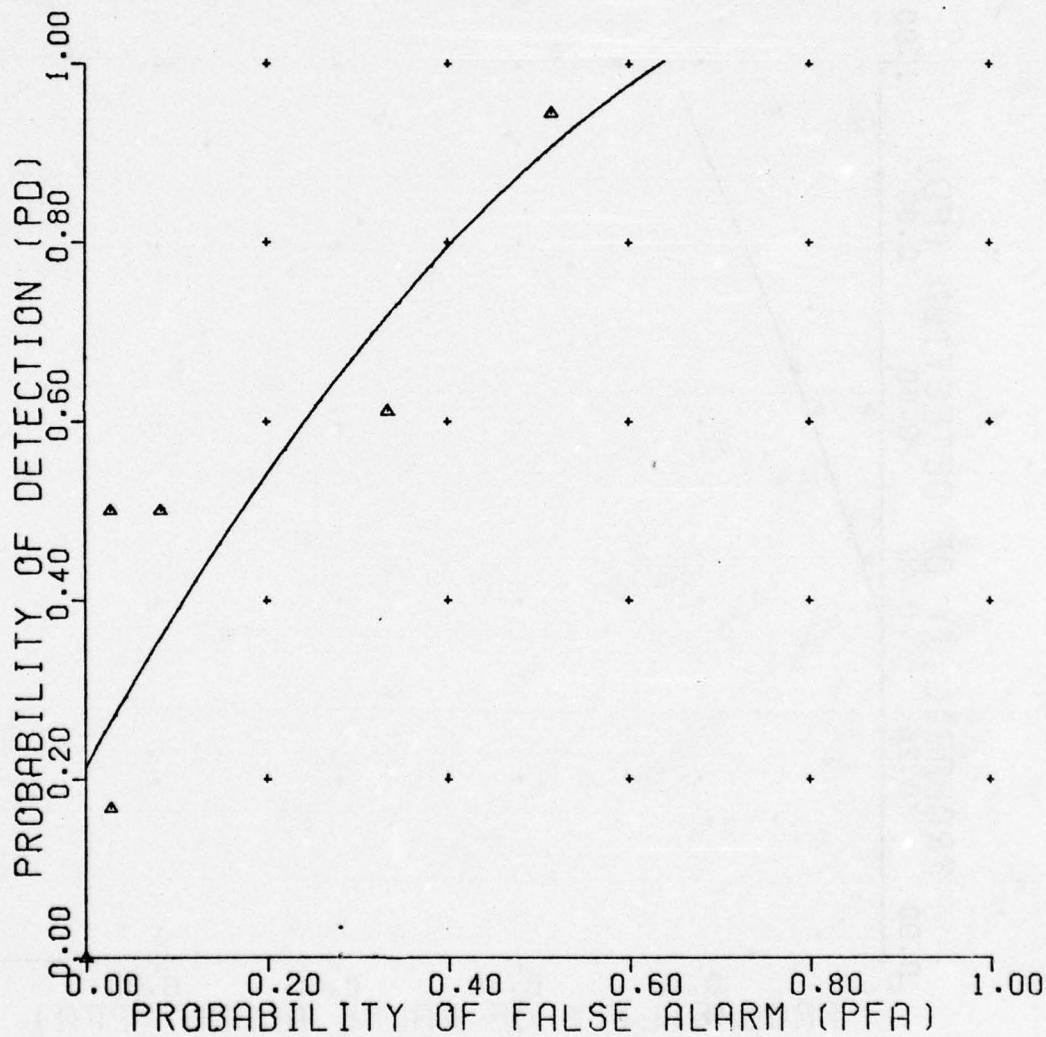


Figure 125. Nearest neighbor classifier.

UNCLASSIFIED

UNCLASSIFIED

NEAREST NEIGHBOR CLASSIFIER

RAW DATA

NO. NEAREST NEIGHBORS 7

REFERENCE 331

| NONMINE TARGET | PLATE TYPE C MINE | ROCK(1) | ROCK(2) | ROOT |
|-------------------|----------------------|---------|---------|-------|
| DEPTH | | 3 | 6 | |
| LOCATION | | +4 | 0 | -4 |
| MOISTURE | | 7 | 17 | 12-20 |
| | | | | 13-16 |

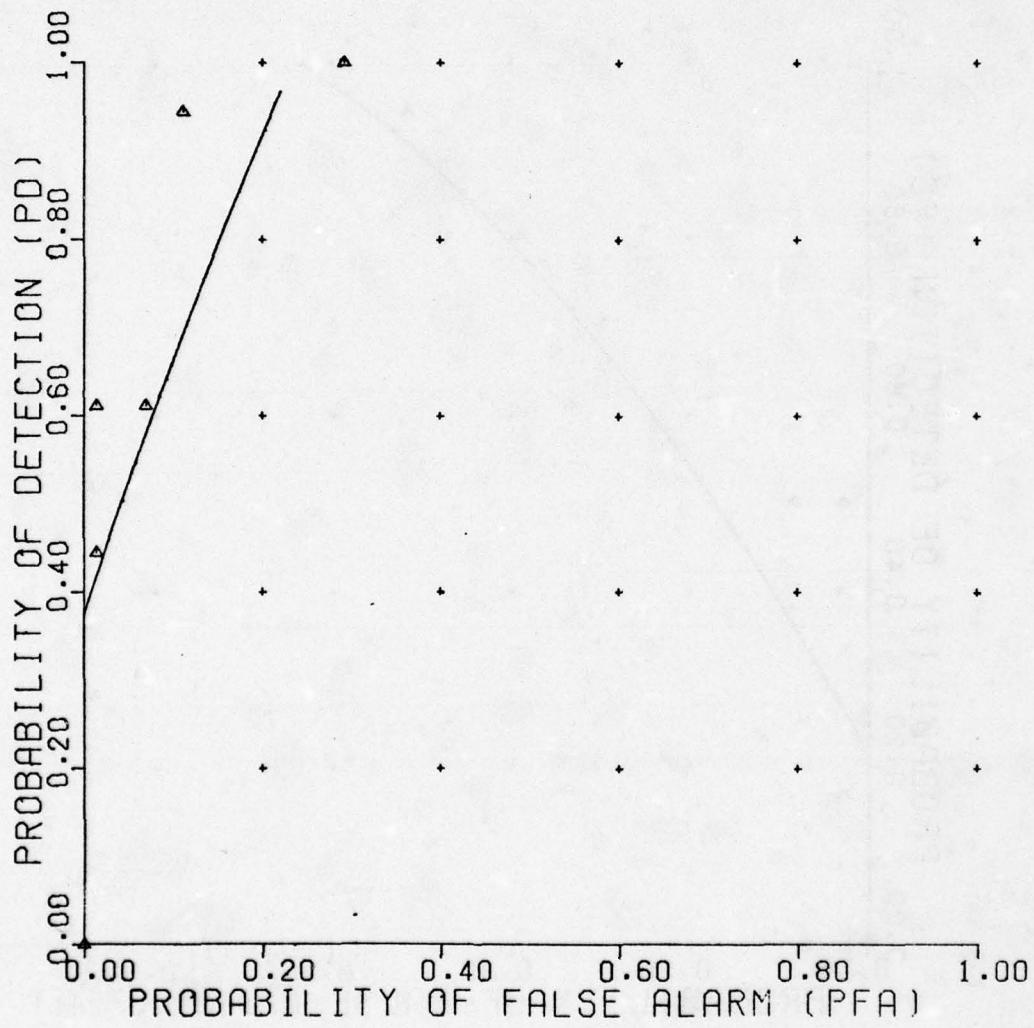


Figure 126. Nearest neighbor classifier.

UNCLASSIFIED

UNCLASSIFIED

NEAREST NEIGHBOR CLASSIFIER

RAW DATA

NO. NEAREST NEIGHBORS 7

REFERENCE 332

| NONMINE TARGET | PLATE | ROCK(1) | ROCK(2) | ROOT |
|-------------------|-------------|-------------|-------------|-------|
| | TYPE C MINE | TYPE B MINE | TYPE A MINE | |
| DEPTH | 3 | 6 | | |
| LOCATION | +4 | 0 | -4 | |
| MOISTURE | 7 | 17 | 12-20 | 13-16 |

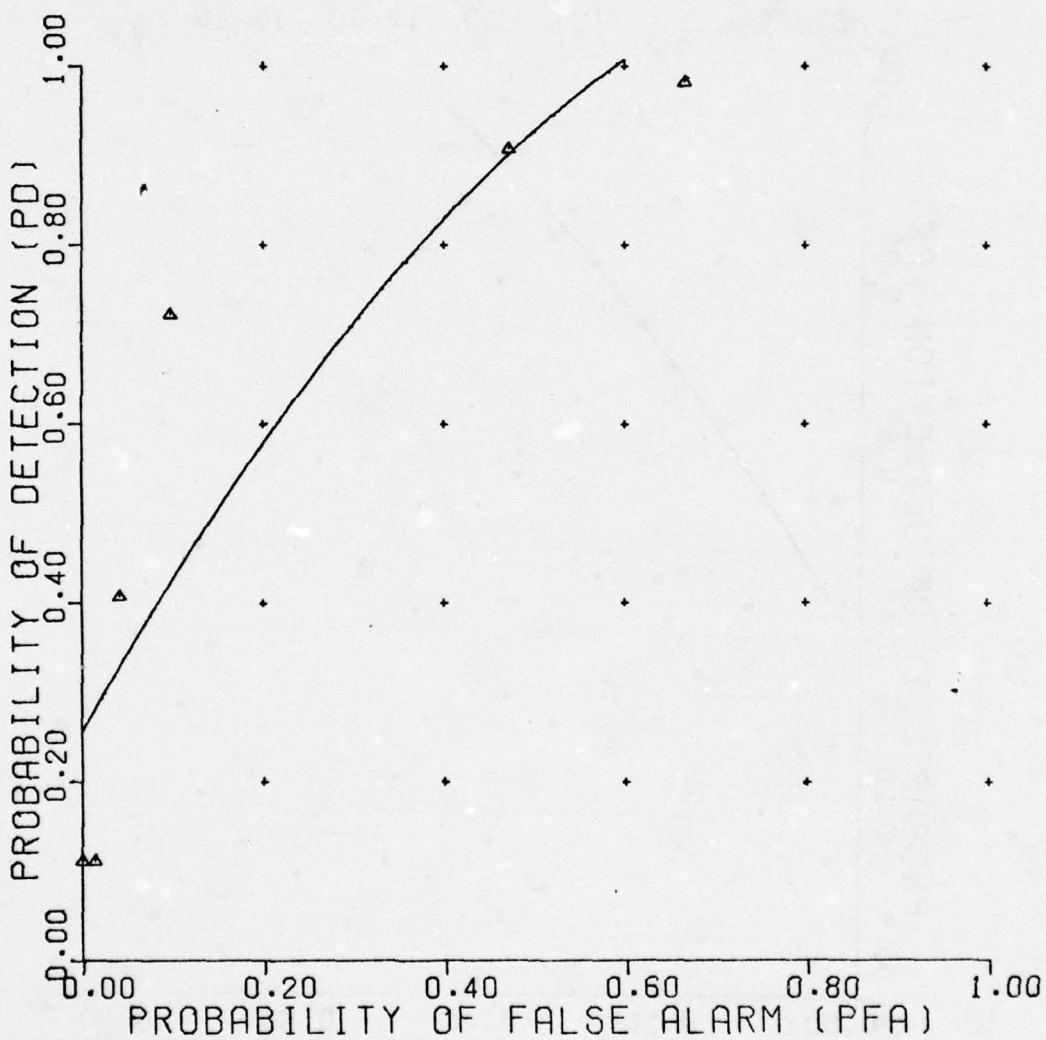


Figure 127. Nearest neighbor classifier.

UNCLASSIFIED

UNCLASSIFIED

NEAREST NEIGHBOR CLASSIFIER

INTUITIVE DATA

NO. NEAREST NEIGHBORS 5

REFERENCE 317

| NONMINE TARGET | PLATE | ROCK(1) | ROCK(2) | ROOT |
|----------------|-------|---------|---------|-------|
| | | | | |
| TYPE A MINE | | | | |
| DEPTH | 3 | 6 | | |
| LOCATION | +4 | 0 | -4 | |
| MOISTURE | 7 | 17 | 12-20 | 13-16 |

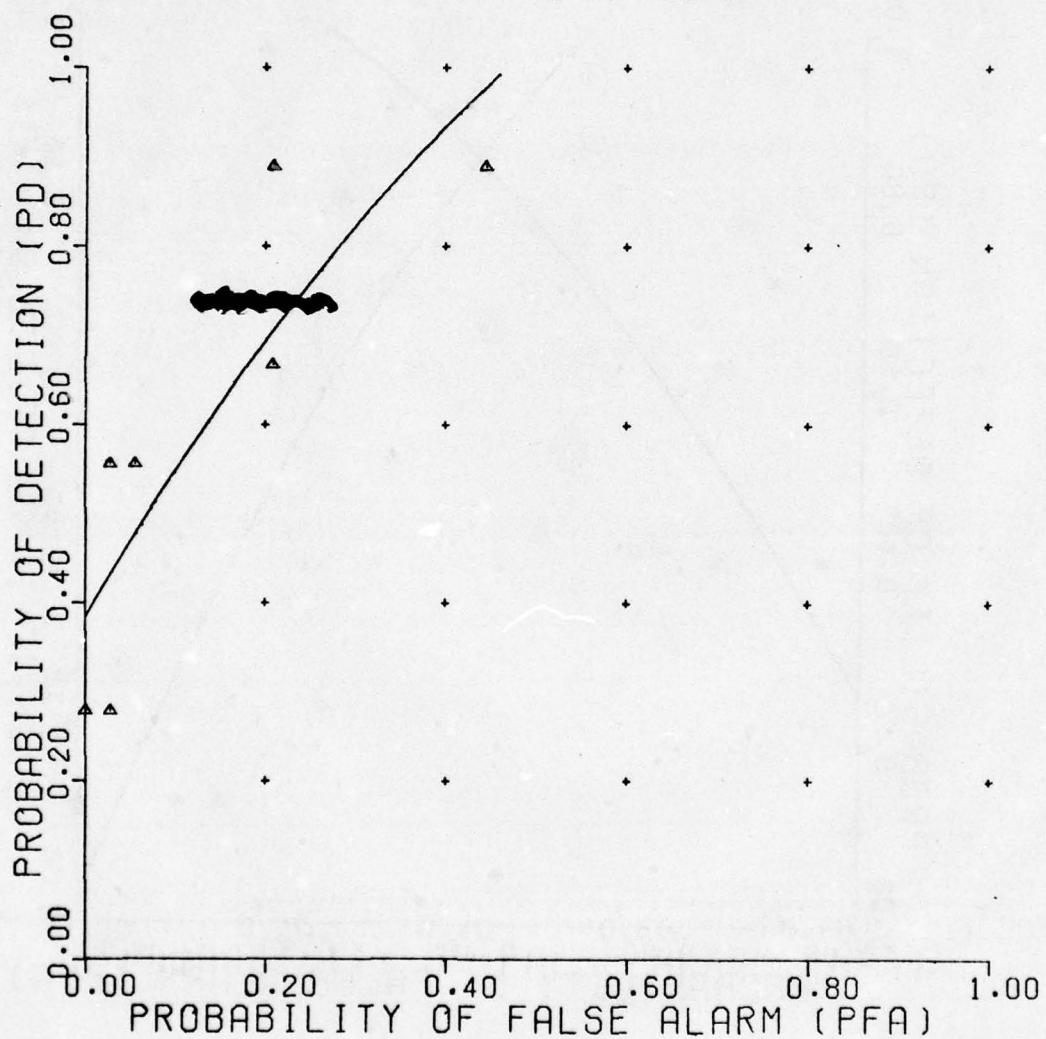


Figure 128. Nearest neighbor classifier.

UNCLASSIFIED

UNCLASSIFIED

NEAREST NEIGHBOR CLASSIFIER

INTUITIVE DATA
NO. NEAREST NEIGHBORS 5
REFERENCE 318

| NONMINE TARGET | PLATE | ROCK(1) | ROCK(2) | ROOT |
|----------------|-------|---------|---------|-------|
| TYPE B MINE | | | | |
| DEPTH | 3 | 6 | | |
| LOCATION | +4 | 0 | -4 | |
| MOISTURE | 7 | 17 | 12-20 | 13-16 |

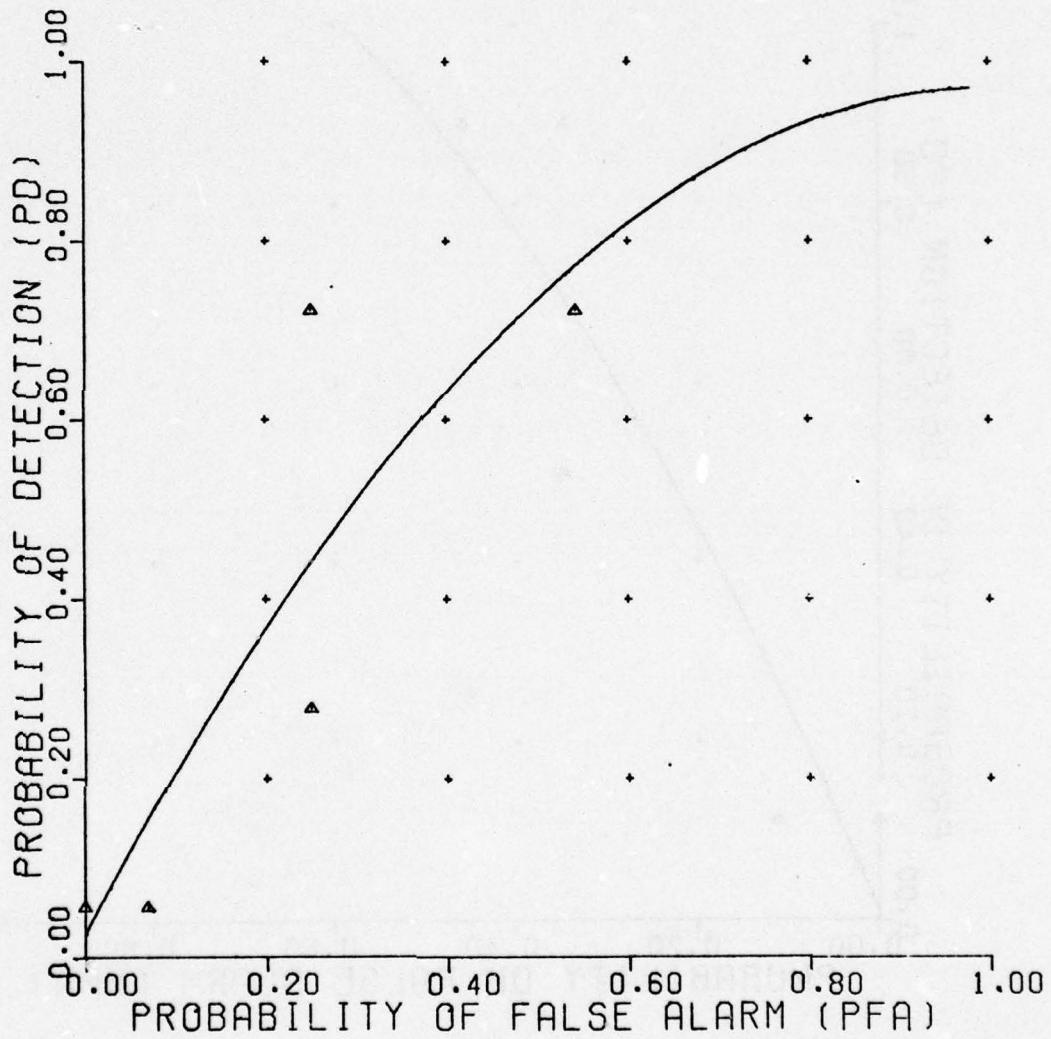


Figure 129. Nearest neighbor classifier.

UNCLASSIFIED

UNCLASSIFIED

NEAREST NEIGHBOR CLASSIFIER

INTUITIVE DATA
NO. NEAREST NEIGHBORS 5
REFERENCE 319

| NONMINE TARGET | PLATE | ROCK(1) | ROCK(2) | ROOT |
|----------------|-------------|---------|---------|-------|
| | TYPE C MINE | | | |
| DEPTH | 3 | 6 | | |
| LOCATION | +4 | 0 | -4 | |
| MOISTURE | 7 | 17 | 12-20 | 13-16 |

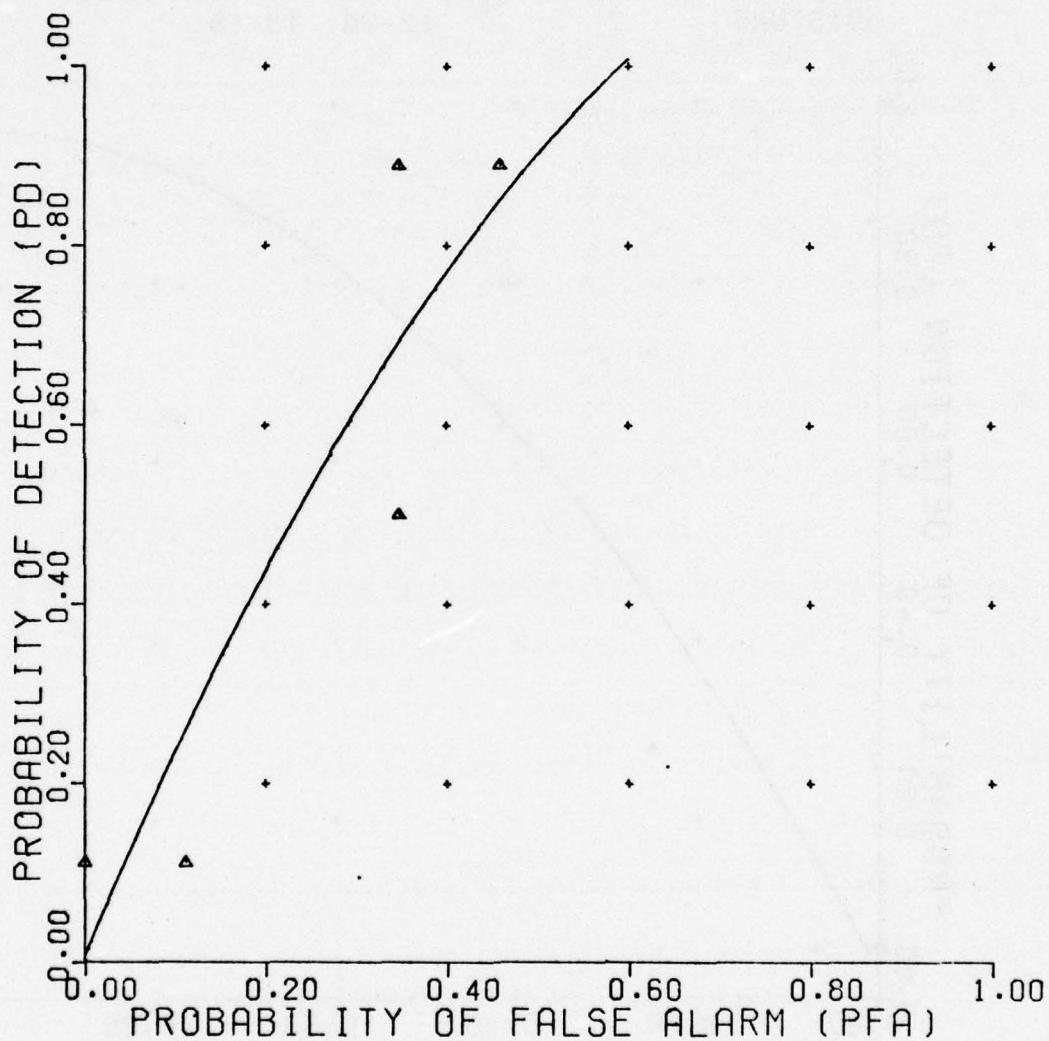


Figure 130. Nearest neighbor classifier.

UNCLASSIFIED

UNCLASSIFIED

NEAREST NEIGHBOR CLASSIFIER

INTUITIVE DATA

NO. NEAREST NEIGHBORS 5

REFERENCE 320

| NONMINE TARGET | PLATE | ROCK(1) | ROCK(2) | ROOT |
|-------------------|-------|-------------|-------------|-------------|
| DEPTH | | TYPE C MINE | TYPE A MINE | TYPE B MINE |
| LOCATION | +4 | 0 | -4 | |
| MOISTURE | 7 | 17 | 12-20 | 13-16 |

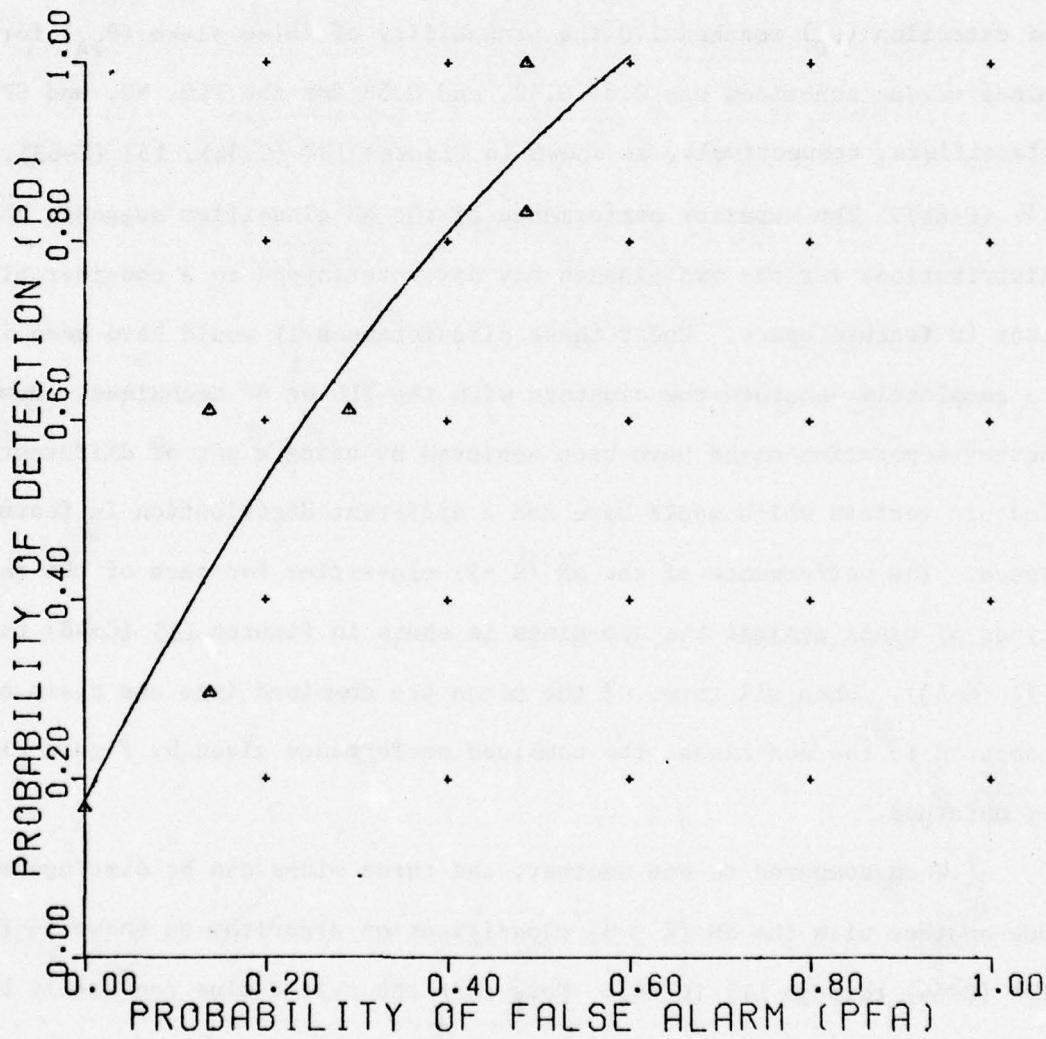


Figure 131. Nearest neighbor classifier.

UNCLASSIFIED

UNCLASSIFIED

comparable or better performances. When it was established which algorithm would perform best, the data in other columns for that algorithm were also tested.

An overall comparison of the performances for all three classifiers indicated the 3-nearest neighbor algorithm to be as good as, or more often better than, other classifier techniques. For example, when the probability of detection (P_D) reached 1.0 the probability of false alarm (P_{FA}) for all mines versus non-mines was 0.6, 0.42, and 0.58 for the FLD, NN, and SP classifiers, respectively, as shown in Figures 132 (C-36), 133 (C-63), and 134 (C-86). The superior performance of the NN classifier suggests that the distributions for the two classes may have overlapped to a considerable extent in feature space. Under these circumstances it would have been impossible to completely separate the clusters with the FLD or SP technique. However, better separation might have been achieved by using a set of different feature vectors which would have had a different distribution in feature space. The performance of the NN ($K = 3$) classifier for each of the three types of mines against the non-mines is shown in Figures 135 (C-48) through 137 (C-58). When all three of the mines are combined into one class and compared to the non-mines, the combined performance given by Figure 133 (C-63) is obtained.

When compared to one another, the three mines can be distinguished from one another with the NN ($K = 3$) classification algorithm as shown in Figures 138 (C-64) through 140 (C-66). Note that the type C mine can easily be distinguished from either the type A or B mines. However, the type A and B

UNCLASSIFIED

UNCLASSIFIED

FLD/BAYES CLASSIFIER

RAW DATA
VERSION 0
REFERENCE 308

| NONMINE TARGET | PLATE TYPE C MINE | ROCK(1) TYPE A MINE | ROCK(2) TYPE B MINE | ROOT |
|-------------------|----------------------|------------------------|------------------------|-------|
| DEPTH | 3 | 6 | | |
| LOCATION | +4 | 0 | -4 | |
| MOISTURE | 7 | 17 | 12-20 | 13-16 |

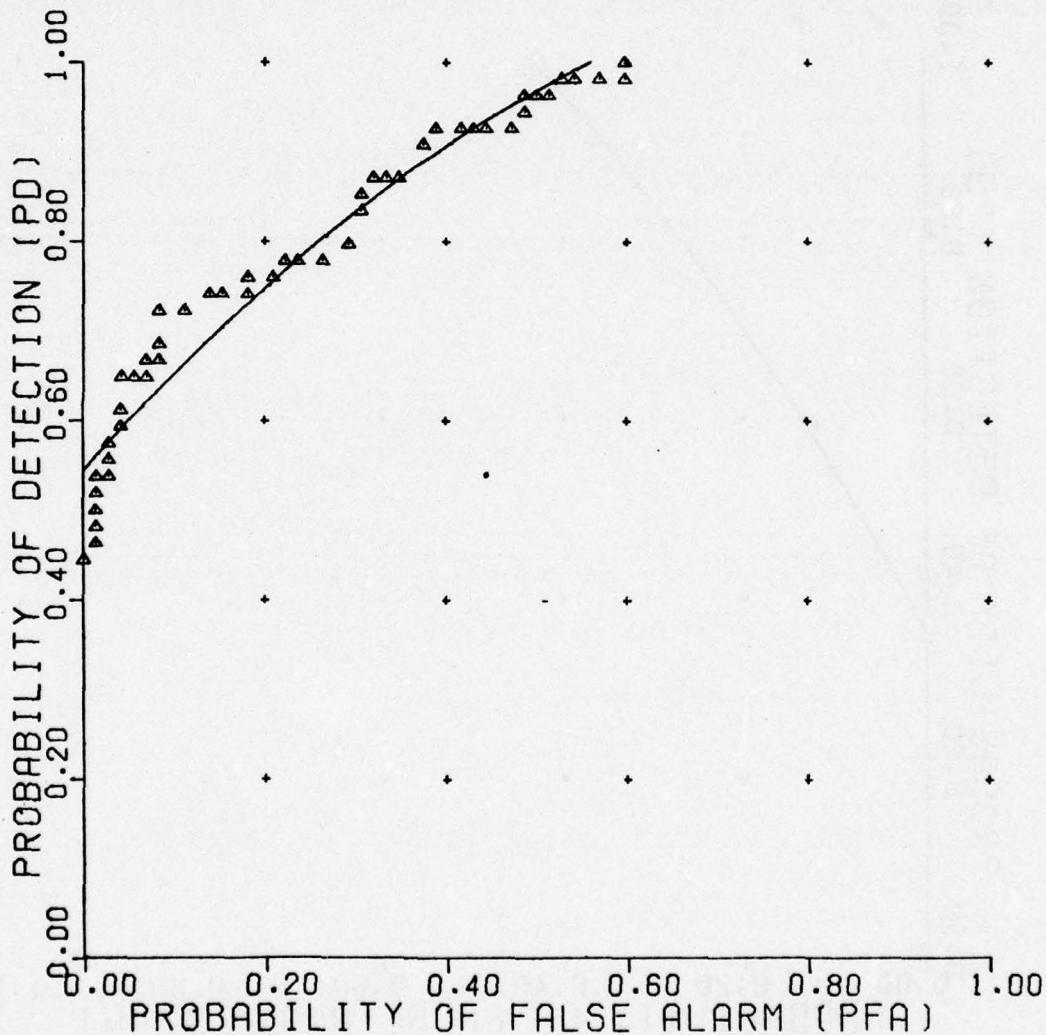


Figure 132. FLD/Bayes classifier.

UNCLASSIFIED

UNCLASSIFIED

NEAREST NEIGHBOR CLASSIFIER

RAW DATA

NO. NEAREST NEIGHBORS 3

REFERENCE 316

| NONMINE TARGET | PLATE | ROCK(1) | ROCK(2) | ROOT |
|-------------------|-------------|-------------|-------------|-------|
| | TYPE C MINE | TYPE A MINE | TYPE B MINE | |
| DEPTH | 3 | 6 | | |
| LOCATION | +4 | 0 | -4 | |
| MOISTURE | 7 | 17 | 12-20 | 13-16 |

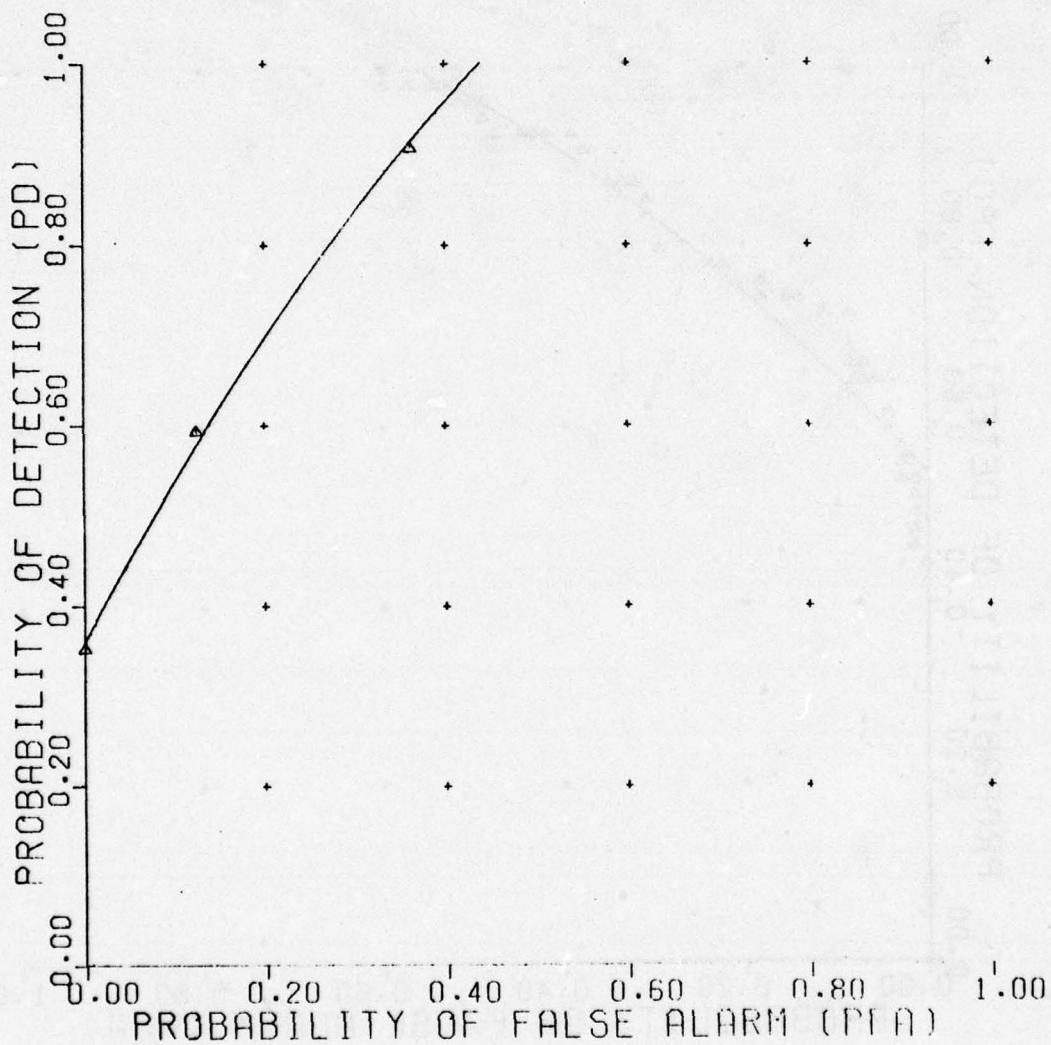


Figure 133. Nearest neighbor classifier.

UNCLASSIFIED

UNCLASSIFIED

SPACE PARTITION CLASSIFIER
(QUADRATIC DISCRIMINANT)

INTUITIVE DATA
VERSION 2
REFERENCE 355

| NONMINE TARGET | PLATE TYPE C MINE | ROCK(1) TYPE A MINE | ROCK(2) TYPE B MINE | ROOT |
|-------------------|----------------------|------------------------|------------------------|-------|
| DEPTH | 3 | 6 | | |
| LOCATION | +4 | 0 | -4 | |
| MOISTURE | 7 | 17 | 12-20 | 13-16 |

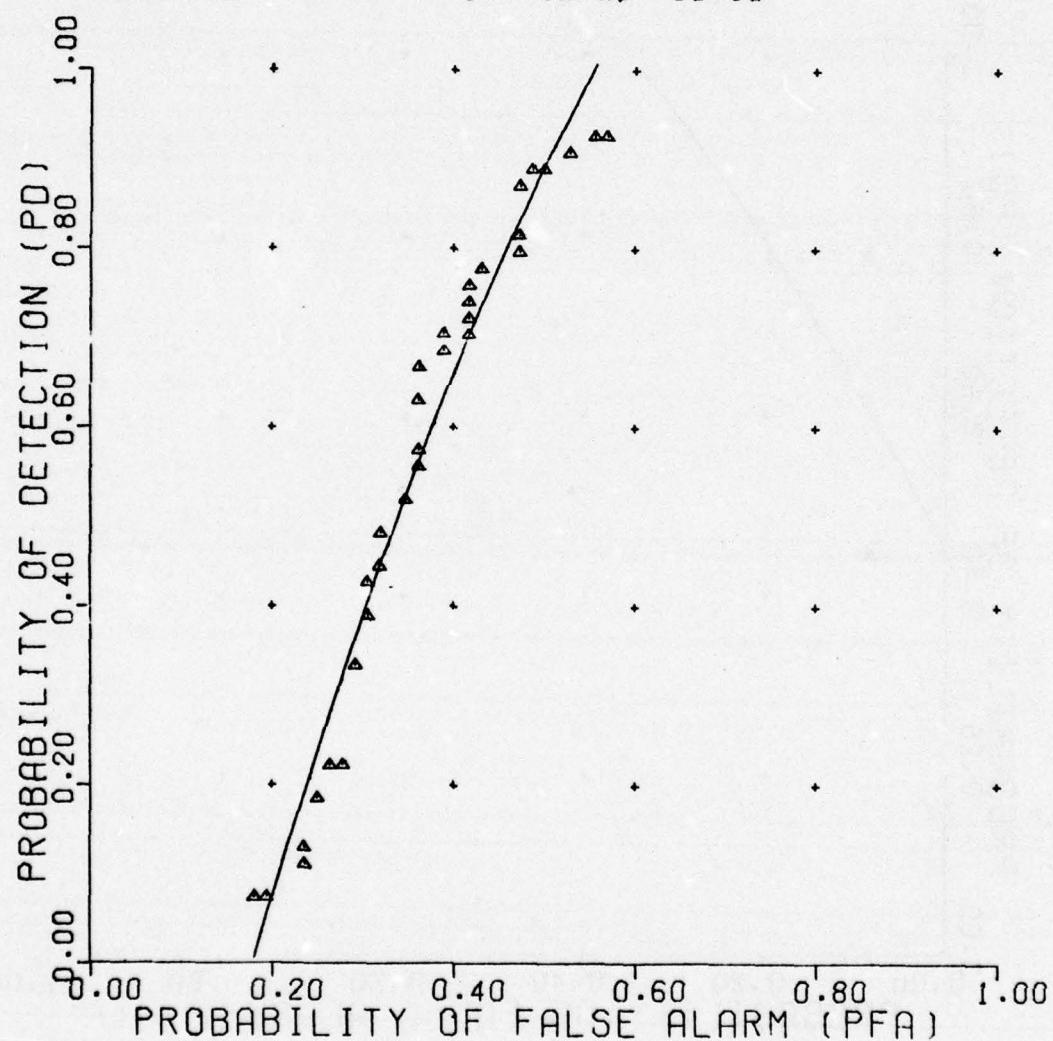


Figure 134. Space partition classifier.

UNCLASSIFIED

UNCLASSIFIED

NEAREST NEIGHBOR CLASSIFIER

RAW DATA

NO. NEAREST NEIGHBORS 3

REFERENCE 313

| NONMINE TARGET | PLATE TYPE A MINE | ROCK(1) | ROCK(2) | ROOT |
|-------------------|----------------------|---------|---------|----------------|
| DEPTH | | 3 | 6 | |
| LOCATION | | +4 | 0 | -4 |
| MOISTURE | | 7 | 17 | 12-20 13-16 |

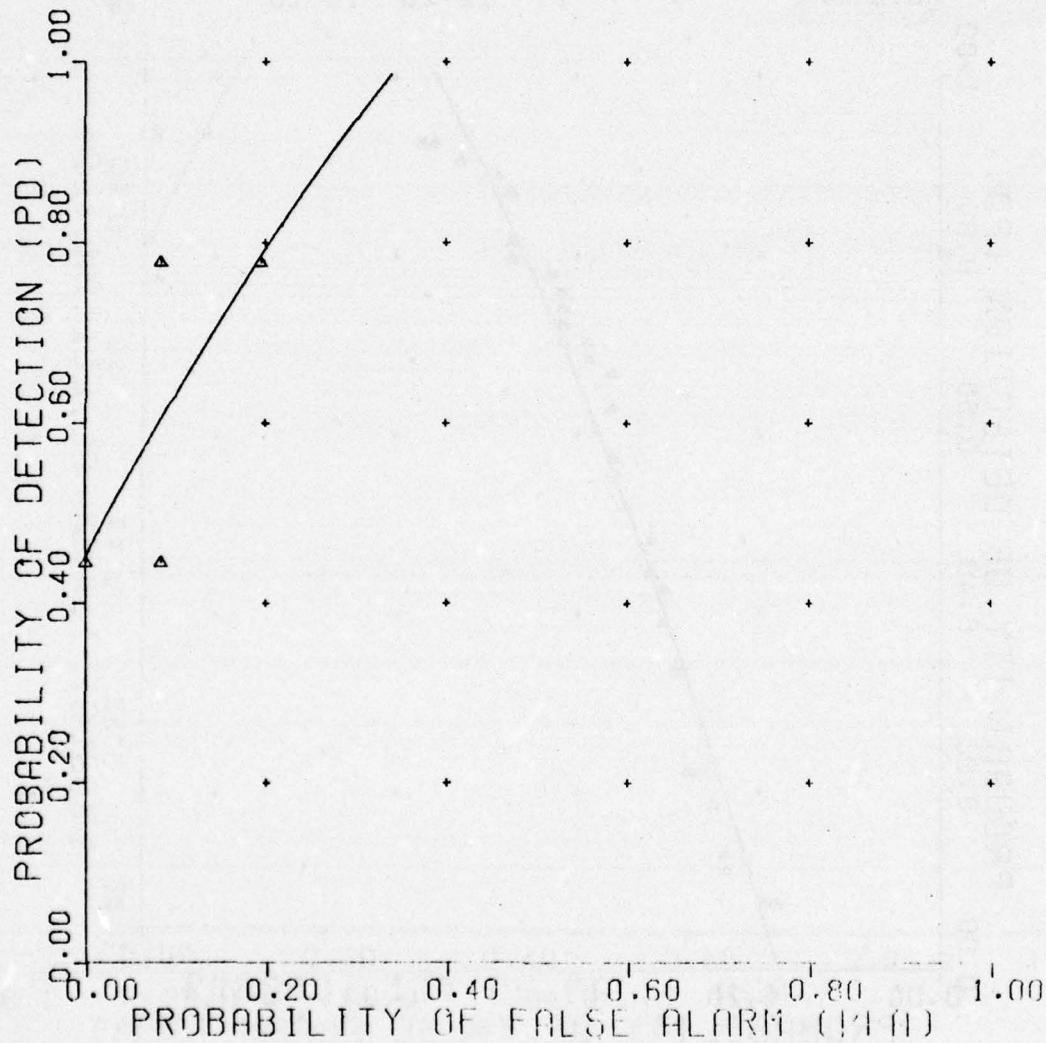


Figure 135. Nearest neighbor classifier.

UNCLASSIFIED

UNCLASSIFIED

NEAREST NEIGHBOR CLASSIFIER

RAW DATA
NO. NEAREST NEIGHBORS 3
REFERENCE 314

| NONMINE TARGET | PLATE TYPE B | ROCK(1) | ROCK(2) | ROOT |
|-------------------|-----------------|---------|---------|-------|
| DEPTH | | 3 | 6 | |
| LOCATION | | +4 | 0 | -4 |
| MOISTURE | | 7 | 17 | 12-20 |
| | | | | 13-16 |

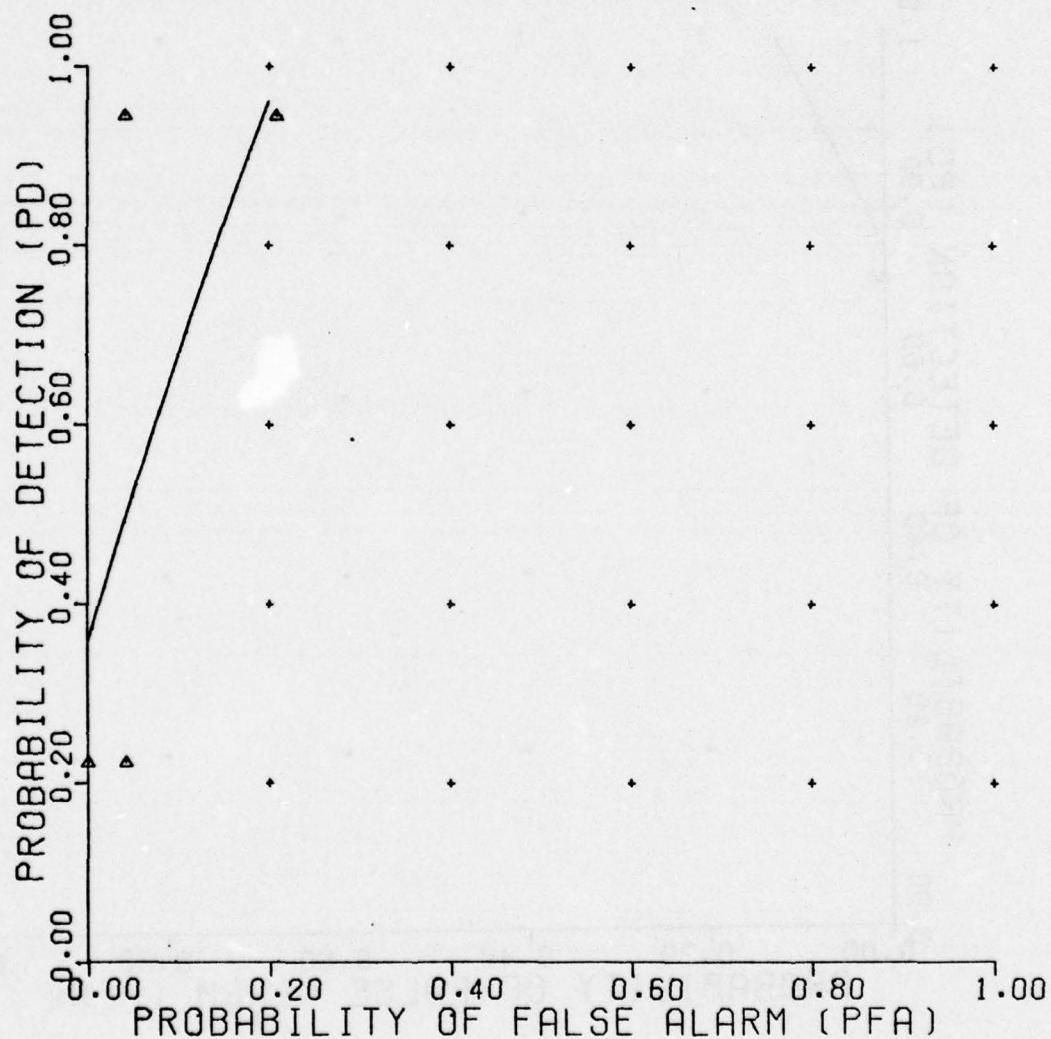


Figure 136. Nearest neighbor classifier.

UNCLASSIFIED

UNCLASSIFIED

NEAREST NEIGHBOR CLASSIFIER

RAW DATA

NO. NEAREST NEIGHBORS 3

REFERENCE 315

| NONMINE TARGET | PLATE TYPE C | ROCK(1) | ROCK(2) | ROOT |
|-------------------|-----------------|---------|---------|-------|
| DEPTH | | 3 | 6 | |
| LOCATION | | +4 | 0 | -4 |
| MOISTURE | | 7 | 17 | 12-20 |
| | | | | 13-16 |

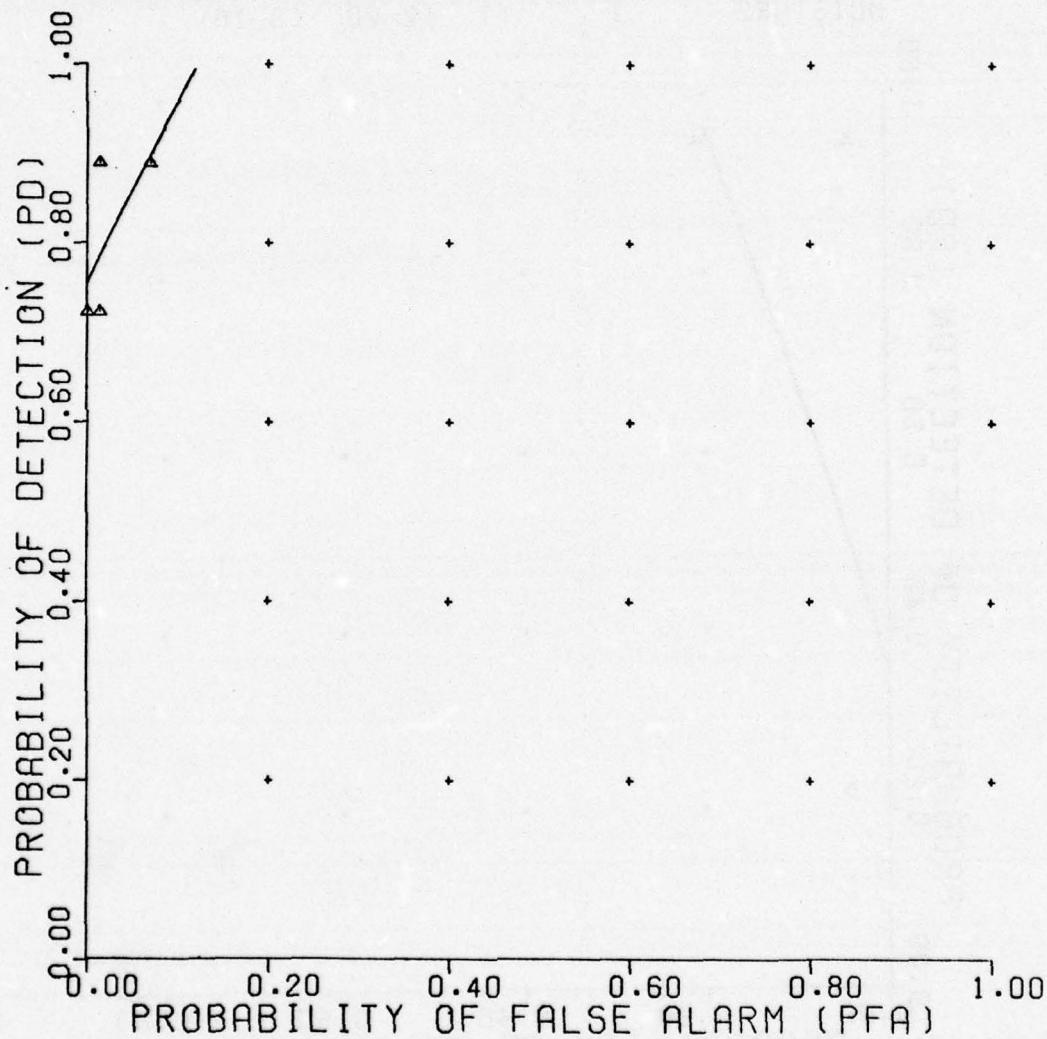


Figure 137. Nearest neighbor classifier.

UNCLASSIFIED

UNCLASSIFIED

NEAREST NEIGHBOR CLASSIFIER

RAW DATA
VERSION 3
REFERENCE 280

TARGET2 TYPE B MINE

TARGET1 TYPE A MINE

| | | | | |
|----------|----|----|-------|-------|
| DEPTH | 3 | 6 | | |
| LOCATION | +4 | 0 | -4 | |
| MOISTURE | 7 | 17 | 12-20 | 13-16 |

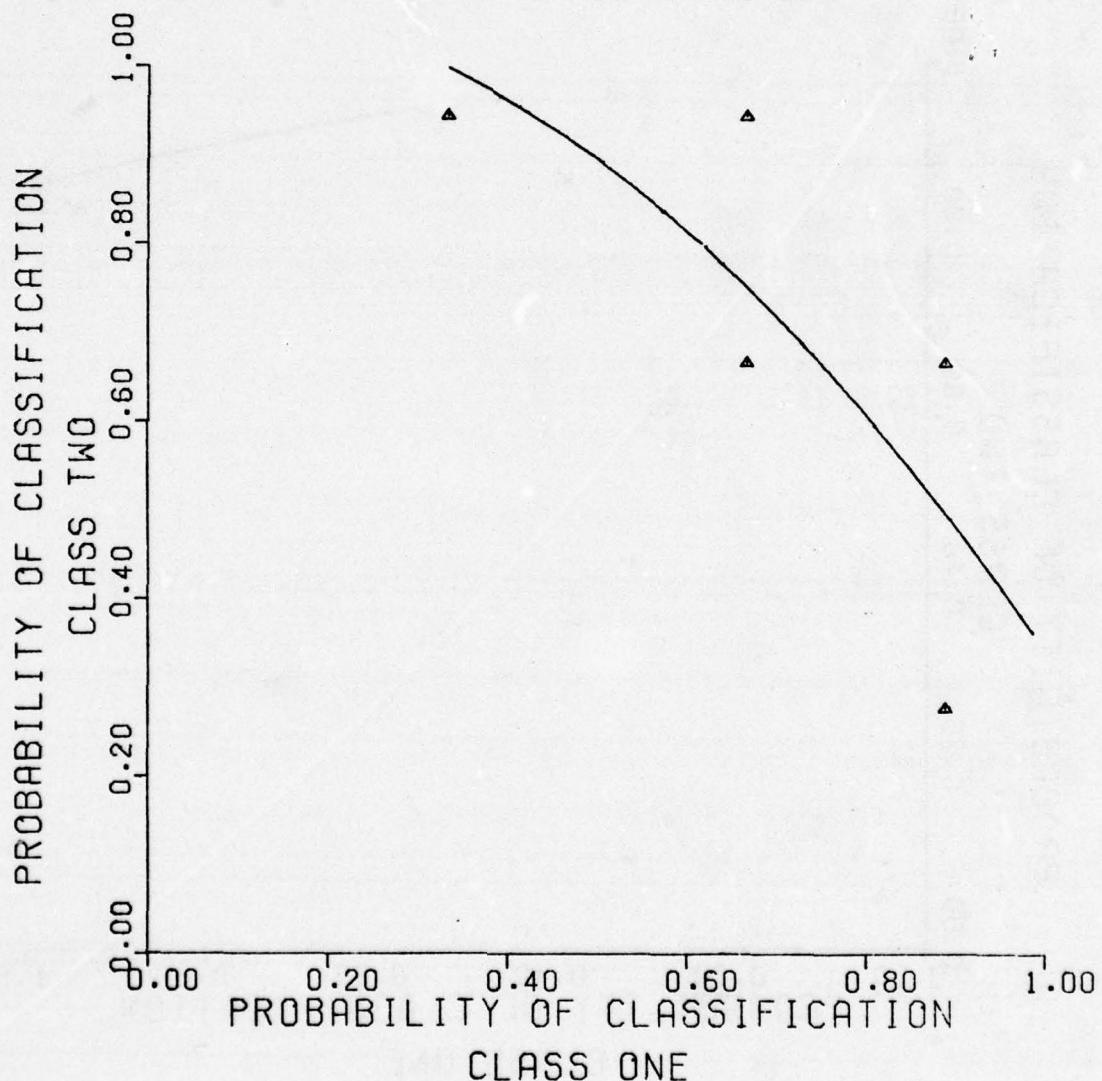


Figure 138. Nearest neighbor classifier.

UNCLASSIFIED

UNCLASSIFIED

NEAREST NEIGHBOR CLASSIFIER

RAW DATA
VERSION 3
REFERENCE 281

TARGET2 TYPE C MINE

TARGET1 TYPE A MINE

| DEPTH | 3 | 6 |
|----------|----|----|
| LOCATION | +4 | 0 |
| MOISTURE | 7 | 17 |

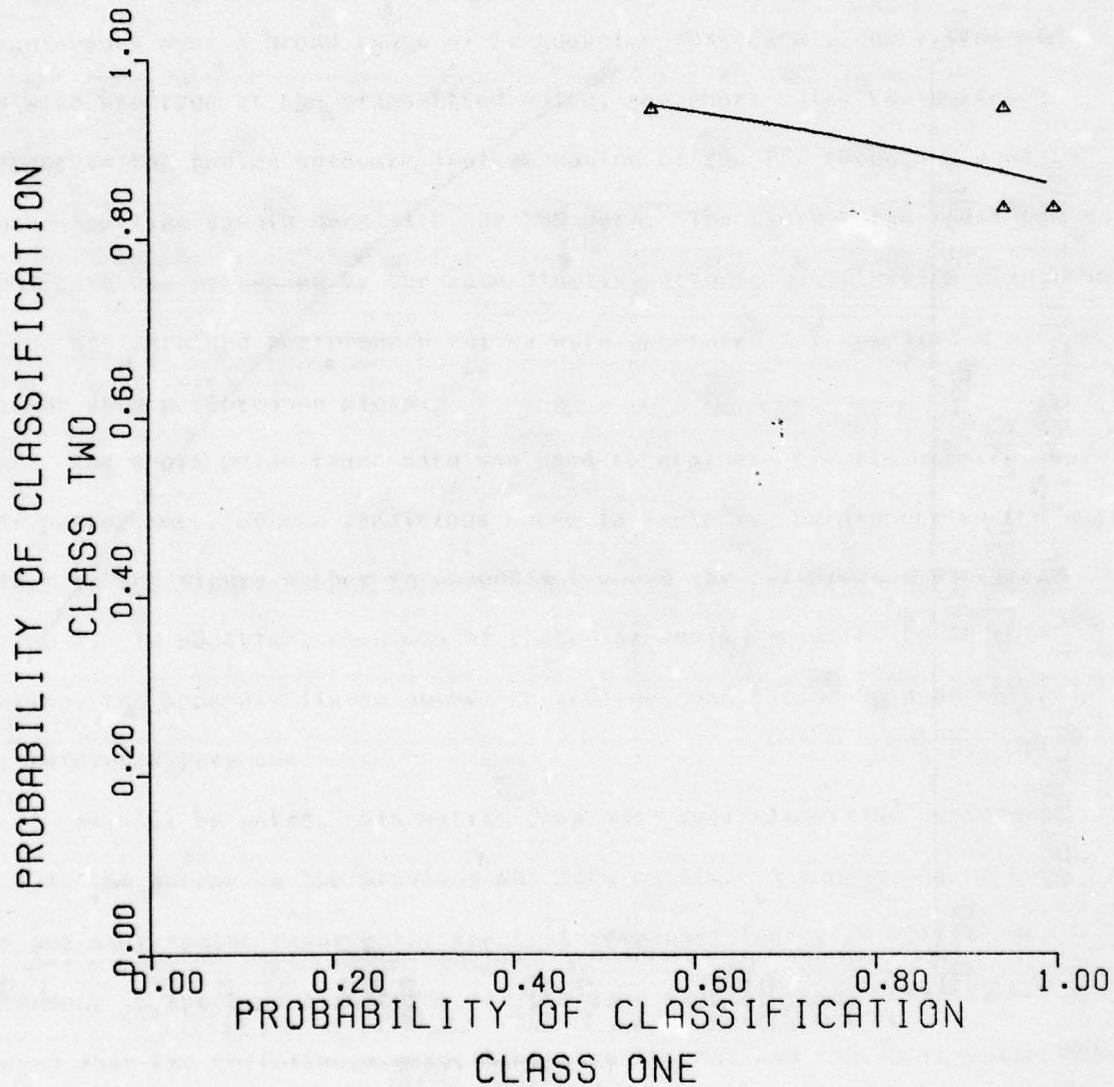


Figure 139. Nearest neighbor classifier.

UNCLASSIFIED

UNCLASSIFIED

NEAREST NEIGHBOR CLASSIFIER

RAW DATA

VERSION 3

REFERENCE 282

TARGET2 TYPE C MINE

TARGET1 TYPE B MINE

| | | | | |
|----------|----|----|-------|-------|
| DEPTH | 3 | 6 | | |
| LOCATION | +4 | 0 | | |
| MOISTURE | 7 | 17 | 12-20 | 13-16 |

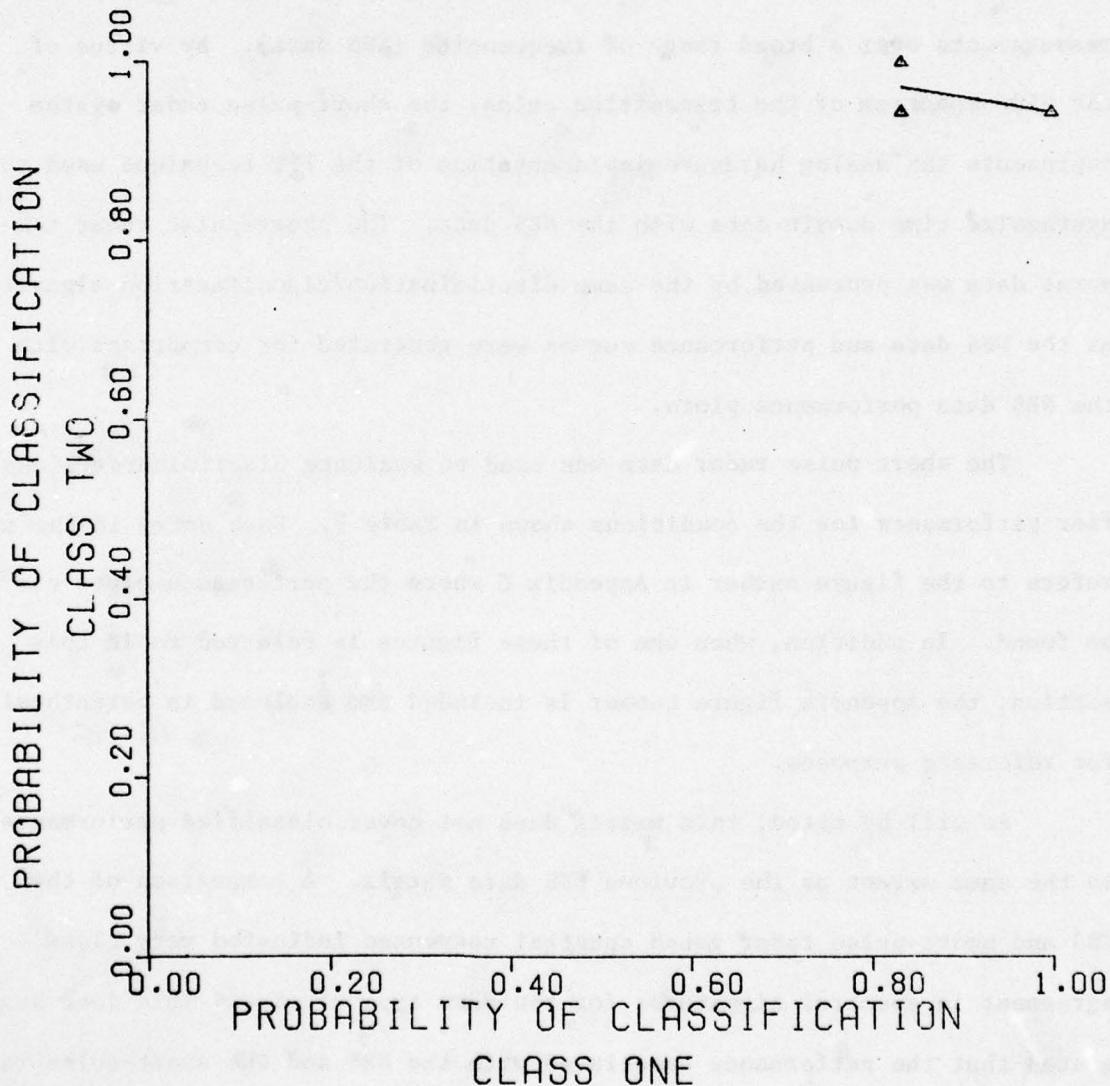


Figure 140. Nearest neighbor classifier.

UNCLASSIFIED

UNCLASSIFIED

mines are not as easily separated. This result is not surprising when it is remembered that the type A and B mines are the same mine design (thickness) with some minor (unknown) differences.

SHORT-PULSE RADAR DATA

The motivation for collecting and processing short-pulse radar data was to verify the previous computerized analysis which was based on CW measurements over a broad range of frequencies (NBS data). By virtue of the wide spectrum of the transmitted pulse, the short-pulse radar system represents the analog hardware implementation of the FFT technique used to synthesize time domain data with the NBS data. The short-pulse radar temporal data was processed by the same discrimination/classification algorithms as the NBS data and performance curves were generated for comparison with the NBS data performance plots.

The short pulse radar data was used to evaluate discriminator/classifier performance for the conditions shown in Table 7. Each entry in the matrix refers to the figure number in Appendix C where the performance plots can be found. In addition, when one of these figures is referred to in this section, the Appendix figure number is included and enclosed in parenthesis for reference purposes.

As will be noted, this matrix does not cover classified performances to the same extent as the previous NBS data matrix. A comparison of the NBS and short-pulse radar gated spectral responses indicated very close agreement in spectral signatures for the same type of mine. This fact suggested that the performance associated with the NBS and the short-pulse radar

UNCLASSIFIED

UNCLASSIFIED

**MERADCOM RADAR
DATA PROCESSING MATRIX**

| CLASSIFIER | TYPE OF DATA | PERFORMANCE MATRIX | | | | | | | | | |
|------------------------------|-----------------------------------|--------------------|-------|-------|-------|-------|-------|-------|-------|-------|-------|
| FISHER'S LINEAR DISCRIMINANT | INTUITIVE OBSERVABLES RAW DATA | | | | | | | | | | |
| NEAREST NEIGHBOR | INTUITIVE OBSERVABLES RAW DATA | C-99 | C-100 | C-101 | C-102 | C-103 | C-104 | C-105 | C-106 | C-107 | C-108 |
| NEAREST NEIGHBOR | INTUITIVE OBSERVABLES RAW DATA | C-109 | C-110 | C-111 | C-112 | C-113 | C-114 | C-115 | C-116 | C-117 | C-118 |
| NEAREST NEIGHBOR | INTUITIVE OBSERVABLES RAW DATA | C-119 | C-120 | C-121 | C-122 | C-123 | C-124 | C-125 | C-126 | C-127 | C-128 |
| SPACE PARTITION | INTUITIVE OBSERVABLES RAW DATA | | | | | | | | | | |
| CROSS CORRELATION | | | | | | | | | | | |
| IMPULSE CORRELATION | | | | | | | | | | | |

UNCLASSIFIED

UNCLASSIFIED

data might be quite similar. Consequently, to conserve our resources, we elected to use only the NN classification algorithm which had previously given the best performance.

The short-pulse radar data was only taken in dry soil comparable to the 7% moisture soil used in the NBS data collection. A limited number of non-mine objects were included in the data collection--e.g., a rock and a metal plate buried 6 inches in dry soil. Soil-only data where no mine-like objects were present was used to exercise the classification algorithm.

The various combinations of mines and non-mines analyzed is shown in Table 7, Short-Pulse Radar Data Performance Matrix.

It should be noted that the MERADCOM short-pulse radar data contained fewer measurements or signatures than the NBS data. For example, the short-pulse data consisted of 12 type C mine signatures as compared to 18 for the NBS data. Consequently, the statistical confidence level for the short-pulse data is not quite as good as for the NBS data. Nevertheless, the short-pulse data does allow a relative comparison of performance for the two measurements systems.

In the performance comparison, first consider the gated spectral signatures of the two basic classes of non-metallic mines--the type A and the type C mine. The spectral response of the type A mine buried in dry soil for the NBS data and the short-pulse data is shown in Figures 141 and 142 respectively. Comparable responses for the type C mine buried in dry soil are shown in Figures 143 and 144. Note that for each set of data, the type A mine is characterized by nulls separated by about 750 MHz or approximately

UNCLASSIFIED

UNCLASSIFIED

GT5

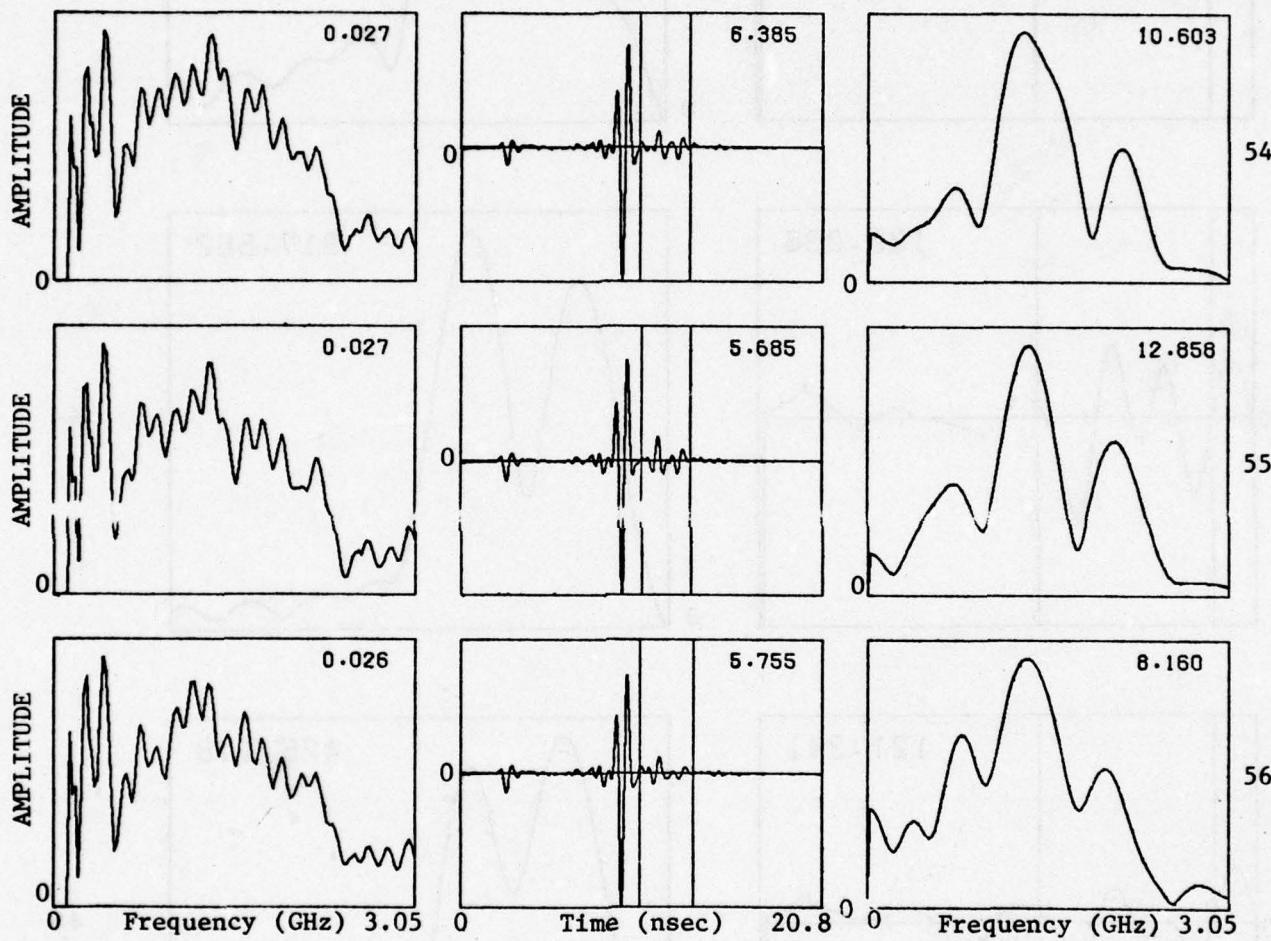


Figure 141. Spectral and temporal responses of type A mines buried in dry soil (7% moisture in loam) from NBS measurements. Files 54, 55, and 56 represent positions -4, 0, and +4 inches over buried mine.

UNCLASSIFIED

UNCLASSIFIED

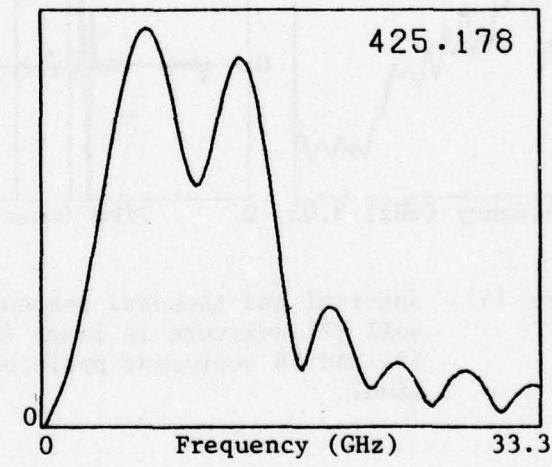
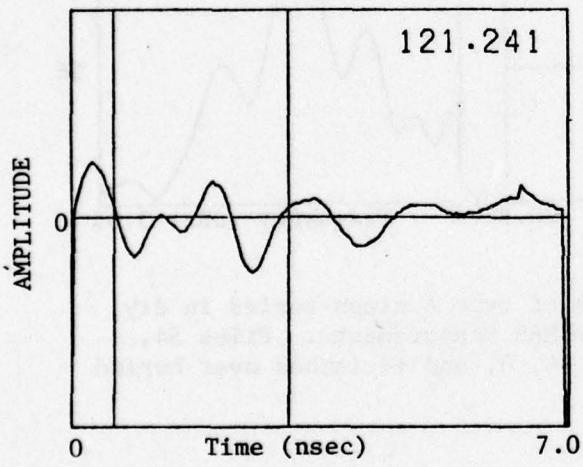
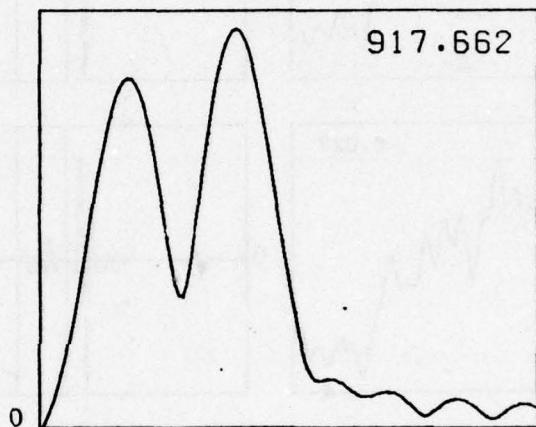
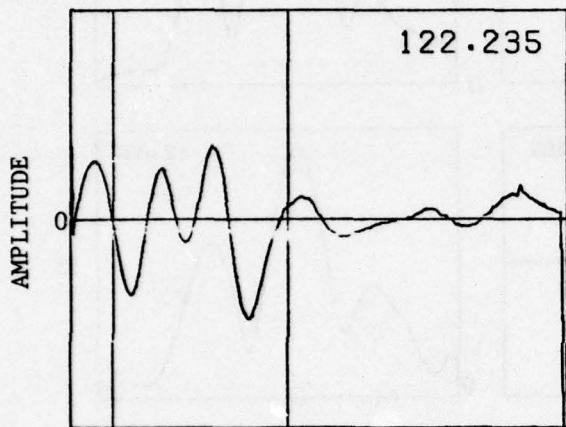
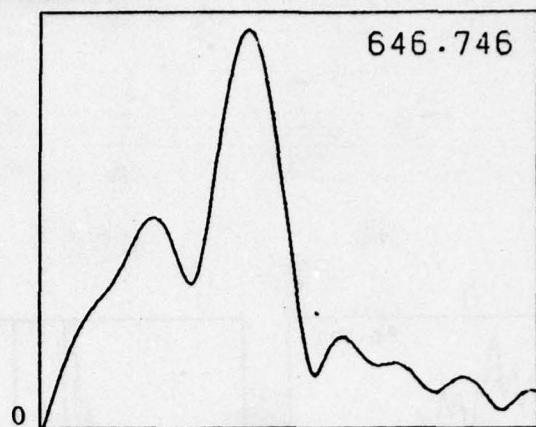
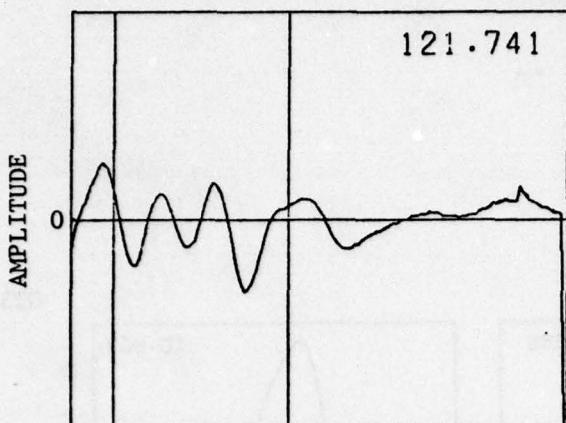


Figure 142. Spectral and temporal responses of type A mines buried in dry soil from short-pulse radar measurements. Files 43, 44, and 45 represent measurement positions -4, 0, and +4 inches over buried mine.

UNCLASSIFIED

UNCLASSIFIED

GT5

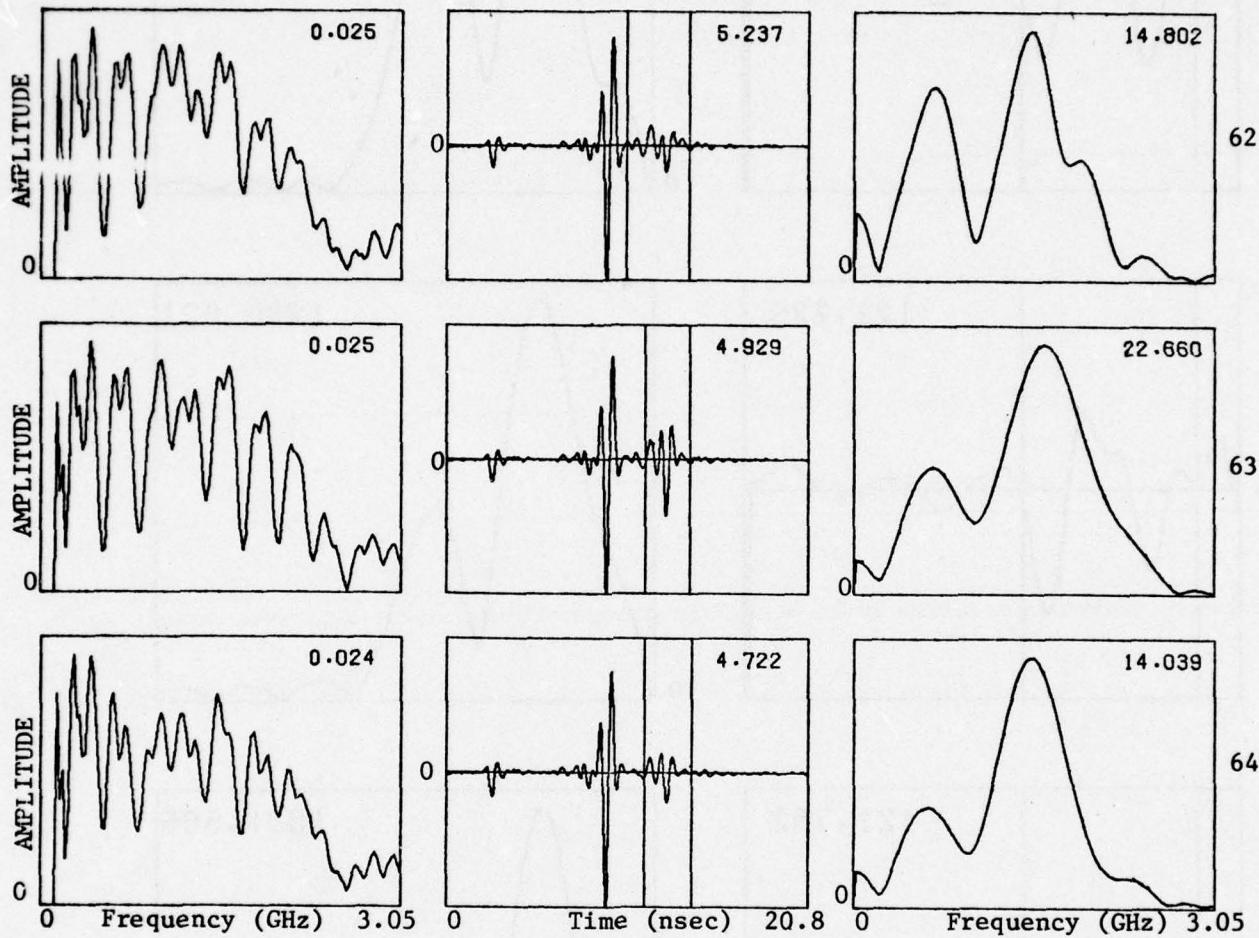


Figure 143. Spectral and temporal responses of type C mines buried in dry soil (7% moisture in loam) from NBS measurements. Files 62, 63, and 64 represent measurement positions -4, 0, and +4 inches over buried mine.

UNCLASSIFIED

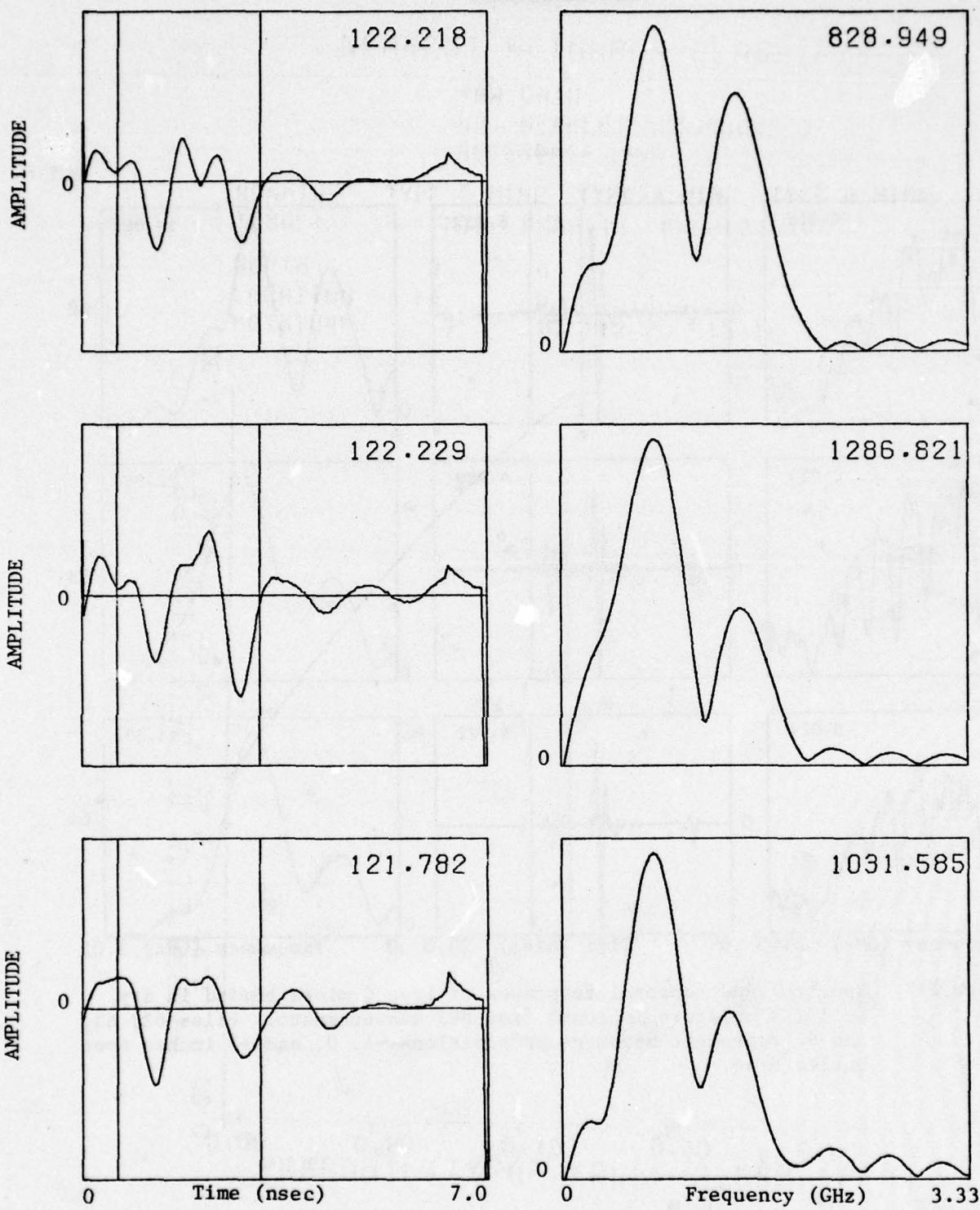
UNCLASSIFIED

Figure 144. Spectral and temporal responses of type C mines buried in dry soil from short-pulse radar measurements. Files 46, 47, and 48 represent measurement positions -4, 0, and +4 inches over buried mine.

UNCLASSIFIED

UNCLASSIFIED

the reciprocal of its thickness time extent. Since the type C mine is not as thick as the type A, the nulls in its spectral response for each set of data is about 900 MHz. The bandwidth of the short pulse data is not as large as that of the NBS data; therefore, the spectral responses of the two data sets do not compare beyond about 1.8 GHz.

The spectral responses just presented are but several examples of many such responses found in Appendix C. Reference to the Appendix will confirm the conclusion that the spectral signatures of the NBS and short-pulse data for the same type of target are in very close agreement when the soil conditions are similar. Thus, one surmises that the classification algorithms designed for the NBS data should perform just as well for the short-pulse data.

Detection probability versus false alarm curves for the short-pulse data processed by the various NN algorithms are given in Appendix C. As indicated previously, each of the mine, non-mine combinations listed in Table 7 has a corresponding detection performance curve in Appendix C. Several of these performance curves are presented here for consideration.

In comparing the detection performance curves of the NBS and short-pulse data, the reader should remember that the NBS data curves are for a variety of soil moistures ranging from 7% (relatively dry soil) to 20% (relatively wet) whereas the short-pulse data curves are for dry soil only (comparable to the 7% moisture soil). Thus, one expects the short-pulse data detection curves to indicate better performance than the NBS data curves. This conclusion is verified by comparing Figures 145 (C-59) and 146 (C-103) which represent the performance of the NN ($K = 3$) algorithm

UNCLASSIFIED

UNCLASSIFIED

NEAREST NEIGHBOR CLASSIFIER

RAW DATA

NO. NEAREST NEIGHBORS 3

REFERENCE 295

| NONMINE TARGET | TYPE C MINE | TYPE A MINE | TYPE B MINE |
|----------------|-------------|-------------|-------------|
| | M19 | PM60(1) | PM60(2) |
| DEPTH | 3 | 6 | |
| LOCATION | +4 | 0 | -4 |
| MOISTURE | 7 | 17 | 12-20 |

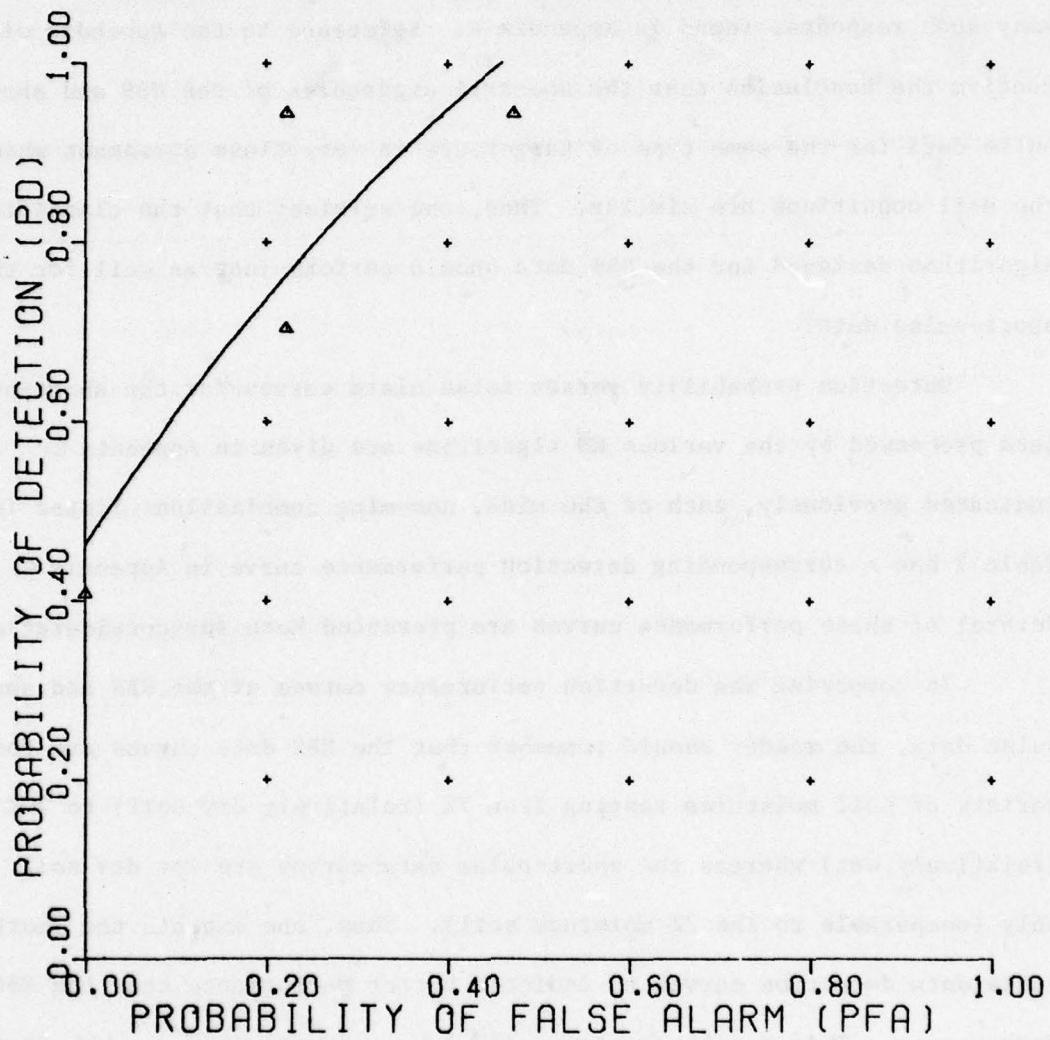


Figure 145. Nearest neighbor classifier.

UNCLASSIFIED

UNCLASSIFIED

NEAREST NEIGHBOR CLASSIFIER

RAW DATA

NO. NEAREST NEIGHBORS 3

REFERENCE 434

| | |
|----------|-------------|
| NONMINE | ROCK |
| TARGET | TYPE C MINE |
| DEPTH | 6 |
| LOCATION | +4 |
| MOISTURE | DRY |

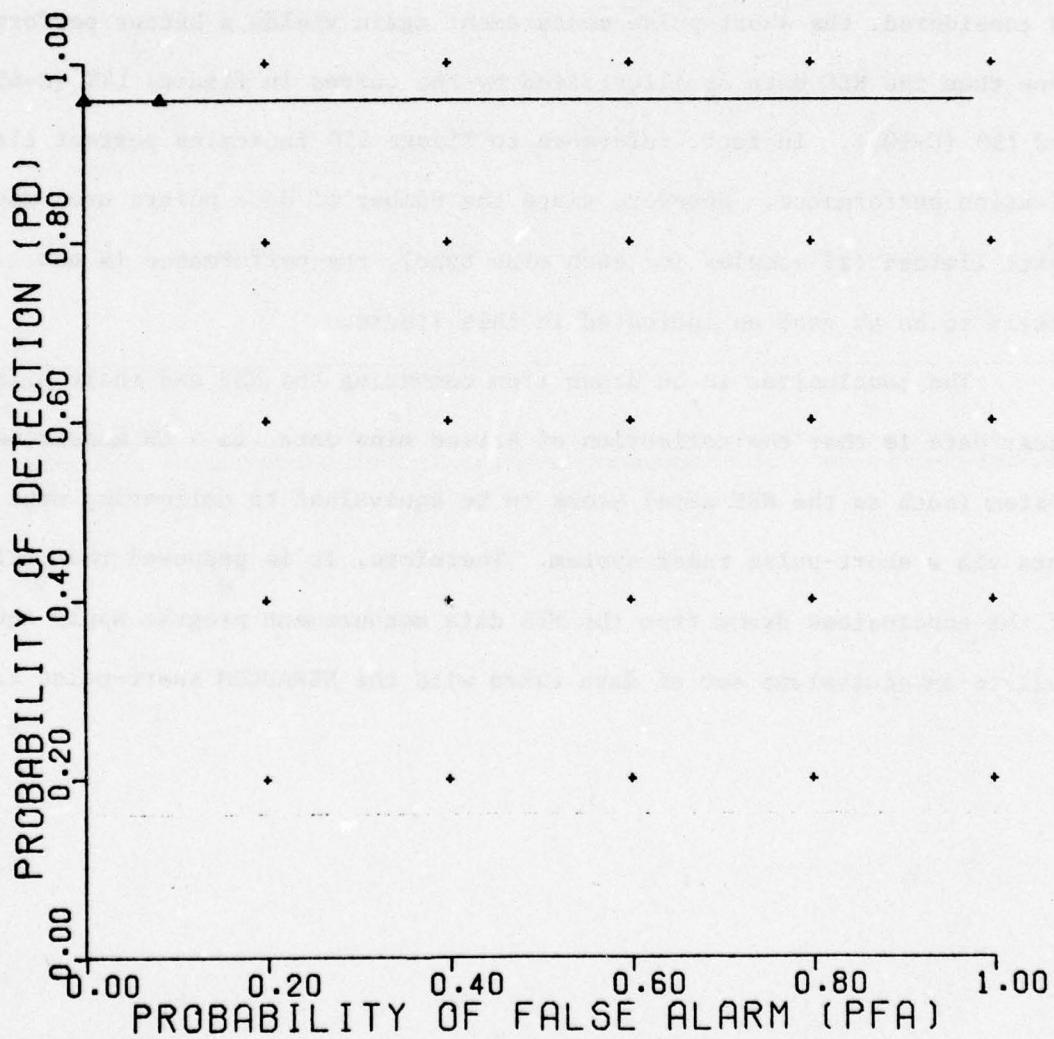


Figure 146. Nearest neighbor classifier.

UNCLASSIFIED

UNCLASSIFIED

with the NBS and short-pulse data of all-mines versus a mine-sized rock. Similar results are obtained when all-mines versus a metal plate are presented to the algorithm as shown in Figures 147 (C-61) and 148 (C-104). The short-pulse measurements yield a better discrimination performance than the all-moisture NBS data.

When the ability of the algorithm to distinguish between mine types is considered, the short-pulse measurement again yields a better performance than the NBS data as illustrated by the curves in Figures 149 (C-65) and 150 (C-105). In fact, reference to Figure 150 indicates perfect classification performance. However, since the number of data points used was quite limited (12 samples for each mine type), the performance is not likely to be as good as indicated in this figure.

The conclusions to be drawn from comparing the NBS and short-pulse radar data is that the collection of buried mine data via a CW measurement system (such as the NBS data) seems to be equivalent to collecting mine data via a short-pulse radar system. Therefore, it is proposed that all of the conclusions drawn from the NBS data measurement program apply equally well to an equivalent set of data taken with the MERADCOM short-pulse radar.

UNCLASSIFIED

UNCLASSIFIED

NEAREST NEIGHBOR CLASSIFIER

RAW DATA

NO. NEAREST NEIGHBORS 3

REFERENCE 297

| NONMINE TARGET | PLATE | | |
|-------------------|-------------|-------------|-------------|
| | TYPE C MINE | TYPE A MINE | TYPE B MINE |
| DEPTH | 3 | 6 | |
| LOCATION | +4 | 0 | -4 |
| MOISTURE | 7 | 17 | 12-20 |
| | | | 13-16 |

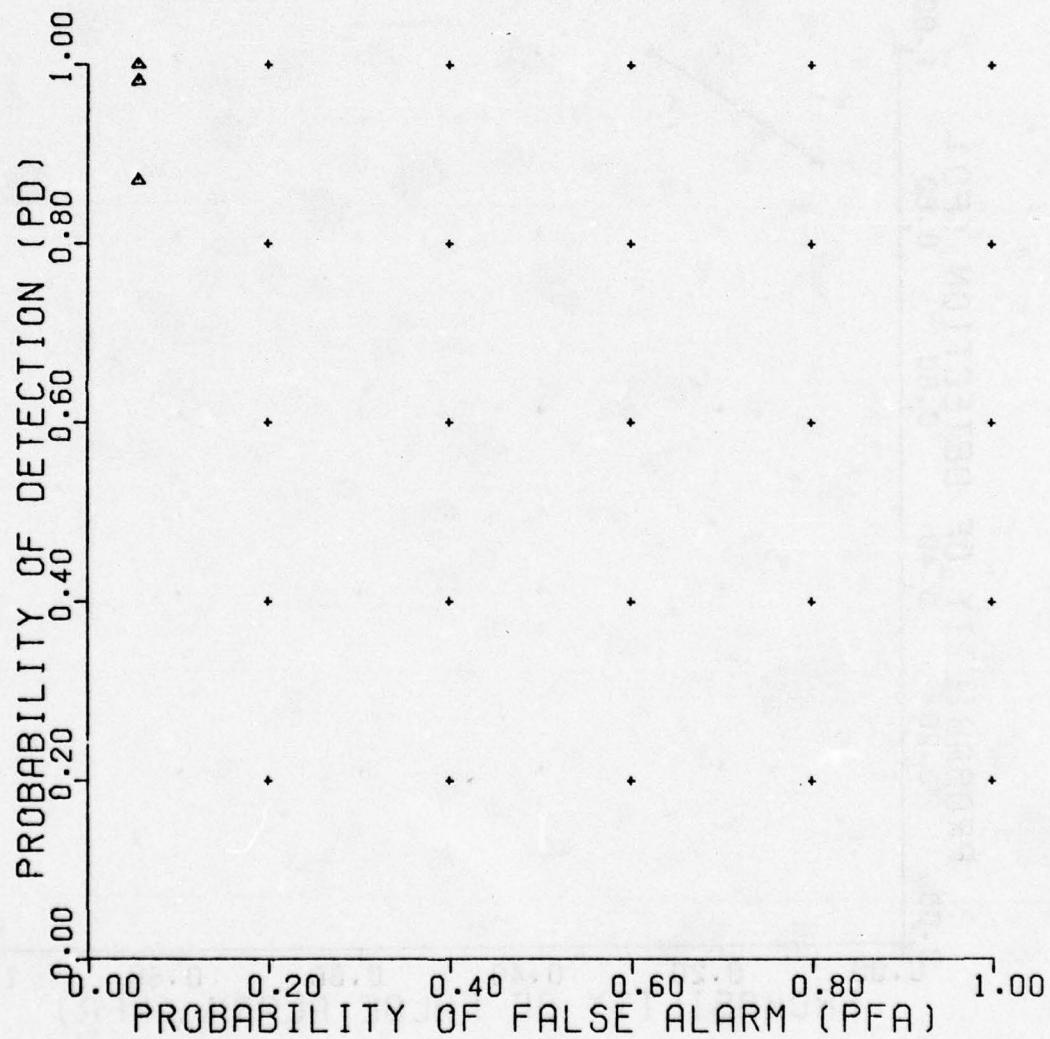


Figure 147. Nearest neighbor classifier.

UNCLASSIFIED

UNCLASSIFIED

NEAREST NEIGHBOR CLASSIFIER

RAW DATA

NO. NEAREST NEIGHBORS 3

REFERENCE 437

| NONMINE TARGET | PLATE | TYPE C MINE | TYPE A MINE | TYPE B MINE |
|-------------------|-------|-------------|-------------|-------------|
| DEPTH | | 6 | | |
| LOCATION | | +4 | 0 | -4 |
| MOISTURE | DRY | | | |

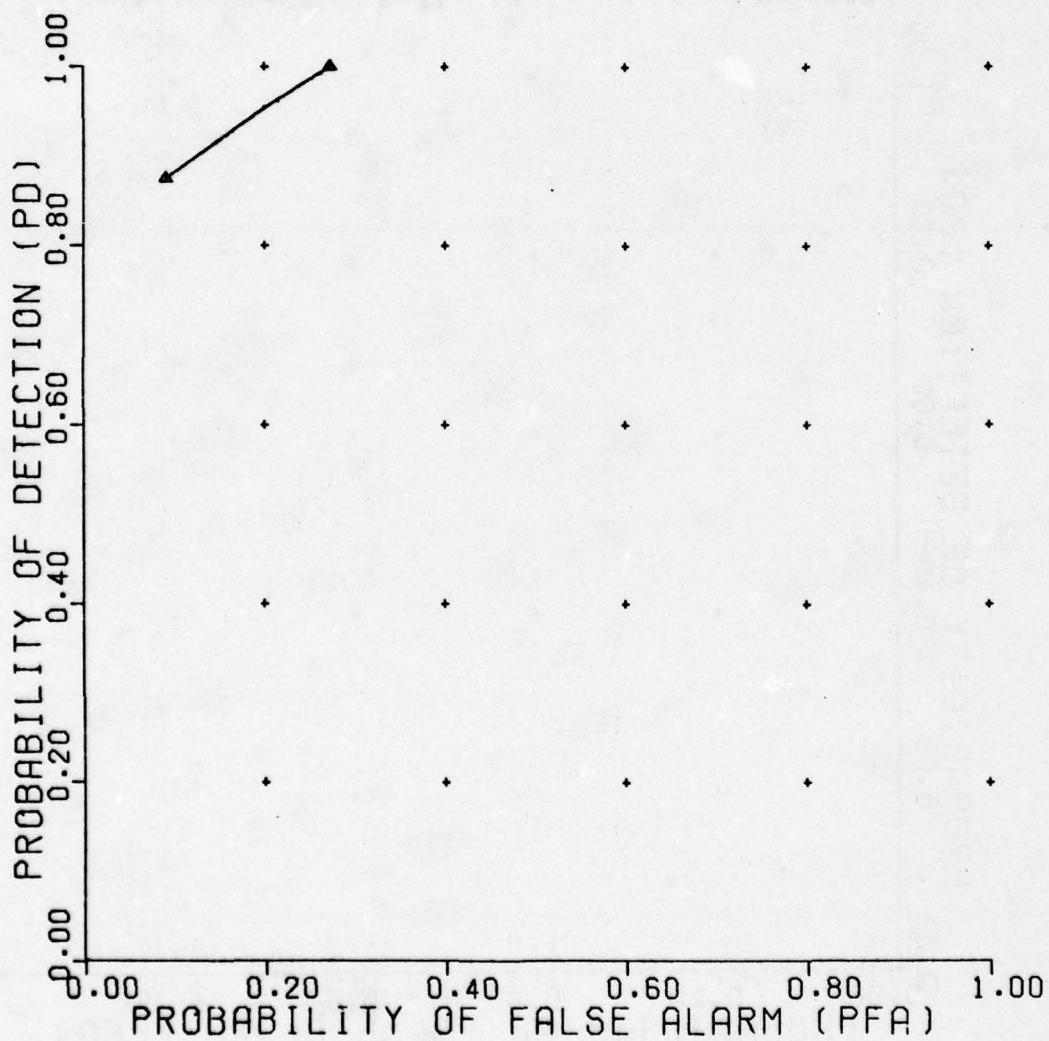


Figure 148. Nearest neighbor classifier.

UNCLASSIFIED

UNCLASSIFIED

NEAREST NEIGHBOR CLASSIFIER

RAW DATA

VERSION 3

REFERENCE 281

TARGET2 TYPE C MINE

TARGET1 TYPE A MINE

DEPTH 3 6

LOCATION +4 0 -4

MOISTURE 7 17 12-20 13-16

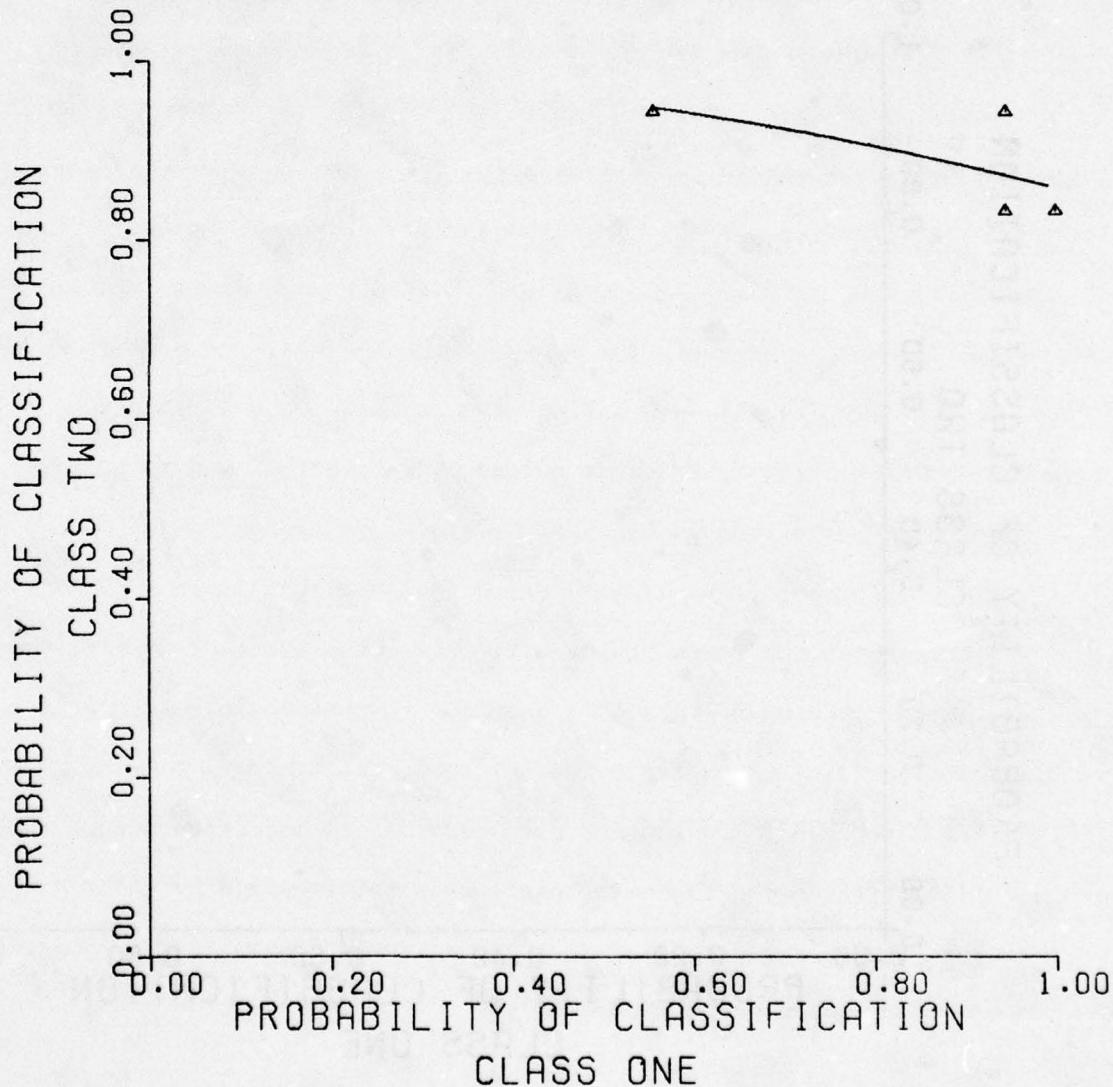


Figure 149. Nearest neighbor classifier.

UNCLASSIFIED

UNCLASSIFIED

NEAREST NEIGHBOR CLASSIFIER

RAW DATA
VERSION 3
REFERENCE 440

| | |
|----------|-------------------------|
| TARGET2 | TYPE C MINE |
| TARGET1 | TYPE A MINE TYPE B MINE |
| DEPTH | 6 |
| LOCATION | +4 0 -4 |
| MOISTURE | DRY |

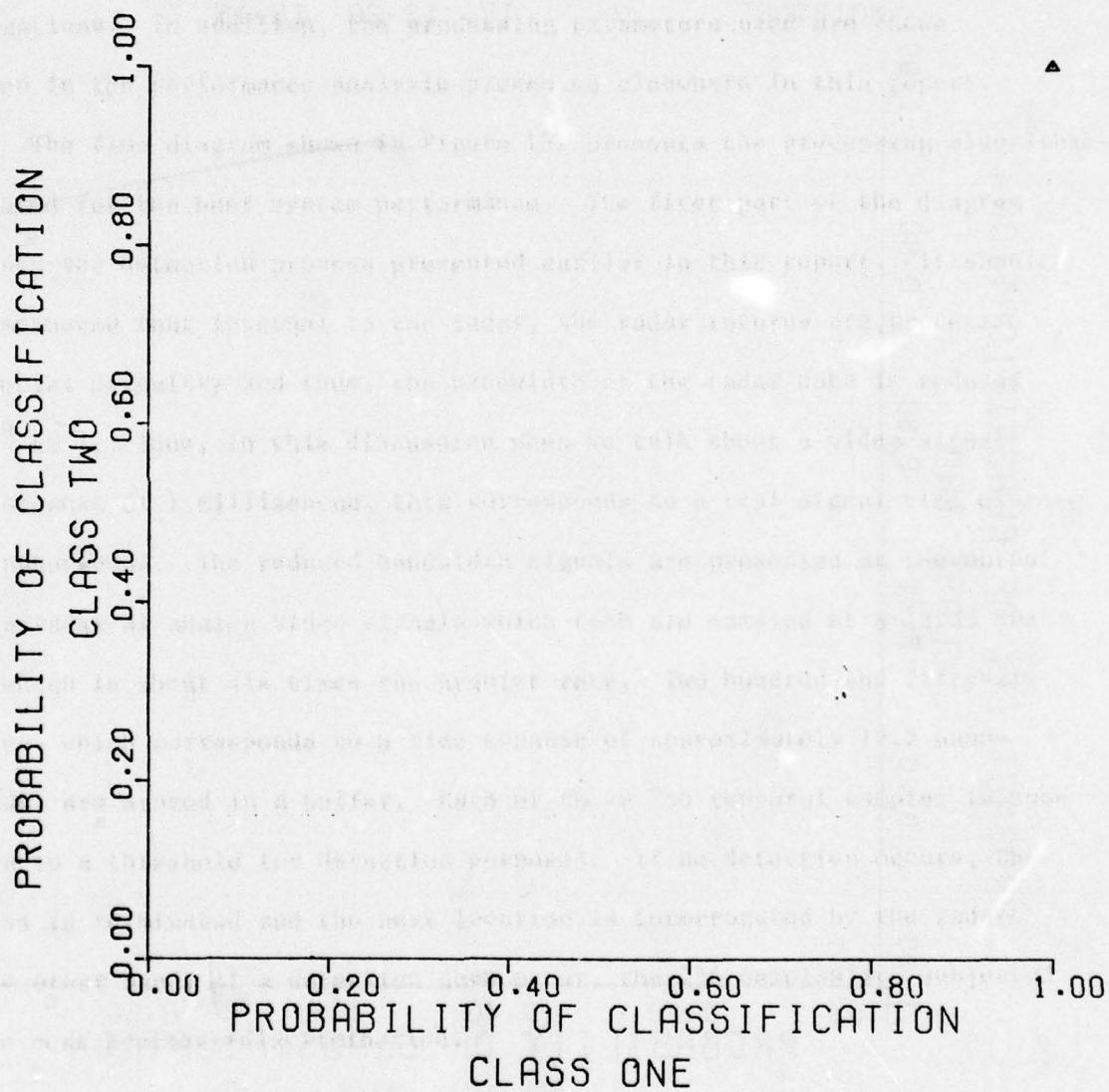


Figure 150. Nearest neighbor classifier.

UNCLASSIFIED

UNCLASSIFIED

SECTION VII

HARDWARE REQUIREMENTS

The mine detection system that will achieve the objectives listed in Table 8 is presented in this section. The emphasis of this study was on the signal processing required with short-pulse radar returns. Thus, the design of the processing required to achieve these objectives is the major subject of concern in this discussion.

The radar to be used in the mine detection system is assumed to be the MERADCOM short-pulse radar furnished by the government. A comparison of the processor performance with the NBS data and the short-pulse radar data indicates approximately equivalent performance. Therefore, it is proposed that the hardware requirements for the short-pulse radar as listed in the CALSPAN report No. MA-5366-E-3 entitled "Vehicular-Mounted Mine Detector Radar Operational Manual," June 1976, are sufficient for the mine detection system under consideration.

Table 8
MINE DETECTION SYSTEM REQUIREMENTS

| | |
|--|-----------------------------|
| Target Depth | 3 to 12 inches |
| Target Type | Non-metallic anti-vehicle |
| Number of Target Classes | 3 |
| Instantaneous Width Coverage | 4 meters |
| Vehicle-Mounted Radar Speed | 10 km/hr |
| False Alarm Rate | Less than 1 per 1000 meters |
| Target Type Identification | Yes |
| Recalibration with Change in Location | No |
| Adjustment in Detection Threshold Setting With Change in Soil Moisture | Yes |
| Standard Parts Used in Design | Yes |

UNCLASSIFIED

UNCLASSIFIED

SIGNAL PROCESSING ALGORITHM

In recommending a processor design, the maximum performance achieved with the processing algorithm considered in this study was deemed necessary to meet the requirements listed in Table 8. This implies that the target search pattern consists of subterranean interrogations on a 1-foot square grid. That is, each interrogation is made within one foot of all other interrogations. In addition, the processing parameters used are those assumed in the performance analysis presented elsewhere in this report.

The flow diagram shown in Figure 151 presents the processing algorithms suggested for the best system performance. The first part of the diagram outlines the detection process presented earlier in this report. It should be remembered that internal to the radar, the radar returns are processed by special circuitry and thus, the bandwidth of the radar data is reduced by 10^6 to 1. Thus, in this discussion when we talk about a video signal time expanse of 1 millisecond, this corresponds to a real signal time expanse of 1 nanosecond. The reduced bandwidth signals are presented at the output of the radar as analog video signals which then are sampled at a 13.33 KHz rate which is about six times the nyquist rate. Two hundred and fifty-six samples, which corresponds to a time expanse of approximately 19.2 nanoseconds, are stored in a buffer. Each of these 256 temporal samples is subjected to a threshold for detection purposes. If no detection occurs, the process is terminated and the next location is interrogated by the radar. On the other hand, if a detection does occur, the 256 samples are subjected to the next process--discrimination.

UNCLASSIFIED

UNCLASSIFIED

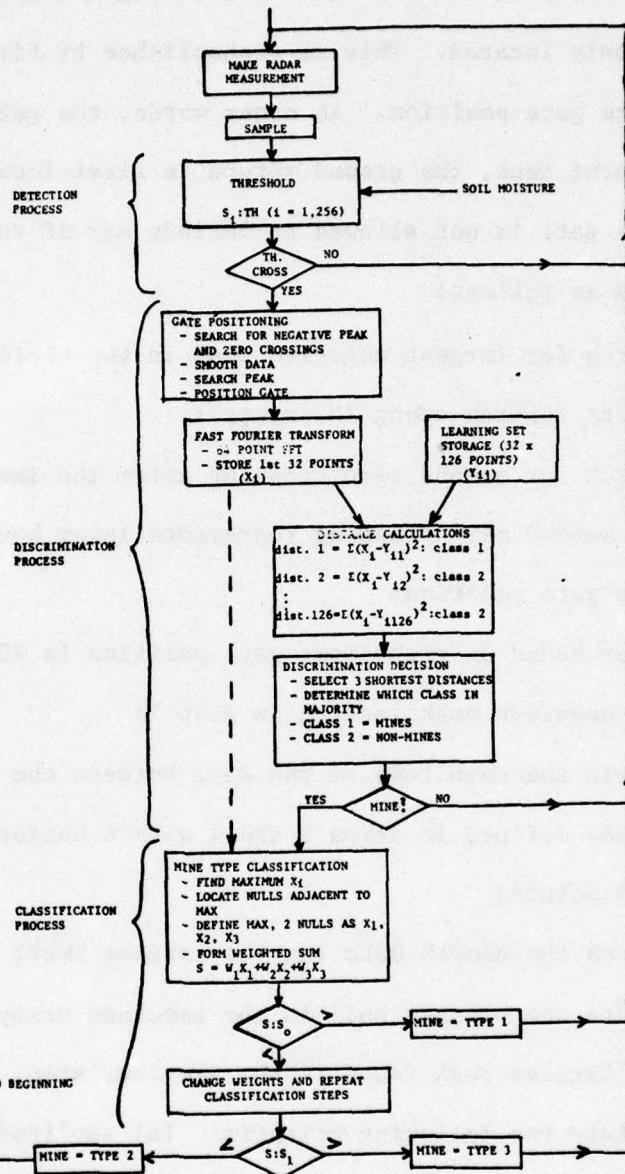


Figure 151. Flow diagram of signal processing algorithm.

UNCLASSIFIED

UNCLASSIFIED

In this process, the location of the target temporal signature must first be precisely located. This is accomplished by first placing limits on the signature gate position. In other words, the gate must not include the ground return; thus, the ground return is first located and the lower boundary of the gate is not allowed to include any of this return. The gate is located as follows:

- (1) Search for largest negative peak in the vicinity of the ground return (search among 30 points);
- (2) Search for second zero crossing after the largest negative peak;
- (3) The second zero crossing represents lower bound on the left most gate position;
- (4) Upper bound on right most gate position is 200 points beyond the negative peak located in step 1;
- (5) Smooth the magnitude of the data between the upper and lower bounds defined in steps 3 and 4 with a uniform amplitude window of 5 points;
- (6) Search the smooth data for the largest peak;
- (7) Locate the closest null in the smoothed array on either side of the largest peak found in the previous step. These nulls must satisfy the following criteria: (a) amplitude of the null must be less than or equal to the maximum divided by 4; (b) the first null location must be less than or equal to the maximum location minus seven points; (c) the second null location must be greater than the maximum location plus seven points. The gate extremities

UNCLASSIFIED

UNCLASSIFIED

are set at the two null locations which satisfy the criteria above.

- (8) If the null values do not satisfy the criteria outlined in step 7, set the gate limits to the upper and lower bounds determined in steps 3 and 4 above.

After locating the temporal target signature and gating out all other parts of the radar return, the remaining samples representing the temporal signature are transformed to the frequency domain by the use of a 64 point Fast Fourier Transform. The number of time samples is assumed to be less than 32 samples, or equivalently, they are assumed to occupy less than 2.4 nanoseconds. Only the magnitude of the first 32 points of the frequency domain is used in the remainder of the processor. As indicated in the flow diagram of Figure 151, these frequency samples are denoted by (X_i ; $i = 1, 2, \dots, 32$). In a later discussion these 32 samples denoted by the vector X will represent one vector in a 32-dimensional space.

The nearest neighbor ($K = 3$) algorithm is used in the discrimination processor since this algorithm yielded the best performance in the data analysis. It is assumed that a learning set of data has been collected and placed in permanent storage. Furthermore, it is assumed that the learning set consists of 126 different spectral measurements, each consisting of 32 frequency samples consistent in the frequency span with the measured spectral data. That is, the 32 samples represent frequencies from 0 to 3.33 GHz. This array size was the one used in the data analysis previously discussed and was assumed here for convenience. A larger array can be used with possibly better performance and also at a higher hardware complexity and cost. The

UNCLASSIFIED

UNCLASSIFIED

learning set consists of a 32×126 point array whose members are denoted by $(Y_{ij}; i = 1, \dots, 32; j = 1, \dots, 126)$. Another way of viewing this learning set is that it represents the location of 126 vectors or points in 32 dimensional space. Some of these 126 points belong to the mine category or class and some of them belong to the non-mine category or class. As indicated by the flow diagram, the next step in the discrimination process is to calculate the distance between the measured vector or point X and each of the 126 points located in the learning set. An example of how the distance is calculated for the k^{th} point in the learning set is as follows:

$$k^{\text{th}} \text{ distance} = \sum_{i=1}^{32} (X_i - Y_{ik})^2 \quad (50)$$

Each distance is associated with one of 132 vectors. Thus, each distance is associated with either the mine class or the non-mine class. The discrimination decision is made by selecting the three shortest distances which have been calculated and determining which of the two classes are in the majority. This is equivalent to determining which three of the learning set vectors are closest to the measured vector. The measured vector is assumed to be of the same class as the majority; thus, the measured vector is designated as a mine or a non-mine. If it is called a non-mine, the processing is terminated and another location is interrogated by the radar. On the other hand, if the measurement is decided to represent a mine, the classification process is initiated.

The classification process determines which type of mine is most likely represented by the radar return under investigation. Since the result of an error in mine type classification was not deemed as disastrous as an error

UNCLASSIFIED

UNCLASSIFIED

in discrimination, a simpler and less complex classification algorithm was used in this processing, namely the Fisher's Linear Discriminant. Its performance with the NBS data was not quite as good as that of the nearest neighbor algorithm but was deemed adequate. A classification algorithm described by the remainder of the flow diagram of Figure 151 provides the classification between the three types of non-metallic anti-vehicular mines. Thus, the Fisher's Linear Discriminant algorithm is applied twice.

The procedure utilizes the 32 dimension vector or point representing the gated spectrum, (X_i , $i = 1, 2 \dots 32$) as follows:

- (1) Find maximum X_i .
- (2) Locate nulls adjacent to the maximum.
- (3) Define the maximum and the two nulls as X_1 , X_2 , X_3 .
- (4) Form weighted sum

$$S = w_1 X_1 + w_2 X_2 + w_3 X_3 \quad (51)$$

The weighted sum, S , is subjected to a fixed threshold, S_o . If the threshold is exceeded by the weighted sum, a type 1 mine is declared and the processing is terminated. If the threshold is not exceeded, the classification weights, w_1 , w_2 , w_3 , used with the Fisher's Linear Discriminant are changed to another pre-selected set and the resulting sum is subjected to another threshold, S_1 . If this threshold is exceeded, a type 3 mine is declared. If this threshold is not exceeded, a type 2 mine is assumed.

SIGNAL PROCESSING EQUIPMENT

The signal processing equipment used in the mine detection system must be capable of handling 13 mine detection radars and must solve the processing

UNCLASSIFIED

UNCLASSIFIED

algorithms in 111.1 milliseconds. These requirements are based on an overall operational requirement that the system cover a single look area 1 foot long by 13.1 feet wide with the vehicle moving at a speed of 10 km/hr. These requirements place a large burden on the signal processing hardware both in terms of data handling requirements and processing time. The signal processing approach that will be discussed emphasizes low technical risk over system cost. Hardware trade-offs will be discussed which lead to a lower system cost if the processing time requirements can be met.

Systems Configuration

Figure 152 illustrates the suggested signal processing hardware configuration. A minicomputer serves as the central processor and handles the majority of the processing load. The data from the 13 radars could be multiplexed into the minicomputer but this would place a considerable burden on the computer. Instead, it is proposed that a preprocessor be used for each radar. This reduces the data flow problem and the processing time requirements. In addition to the minicomputer, the system contains a cassette loader for software loading, the computer control box, special operator displays, and a high speed Fast Fourier Transform module. All the equipment is capable of meeting military specifications.

The mine detection/classification algorithms involve a three step process: detection, discrimination, and classification. The microprocessors would handle the detection processing. In addition, the microprocessors handle the A/D conversion processing and putting the post-detection data into a format compatible with the minicomputer input requirements. Data would be inputted into the minicomputer in a Direct Memory Access (DMA) mode.

UNCLASSIFIED

UNCLASSIFIED

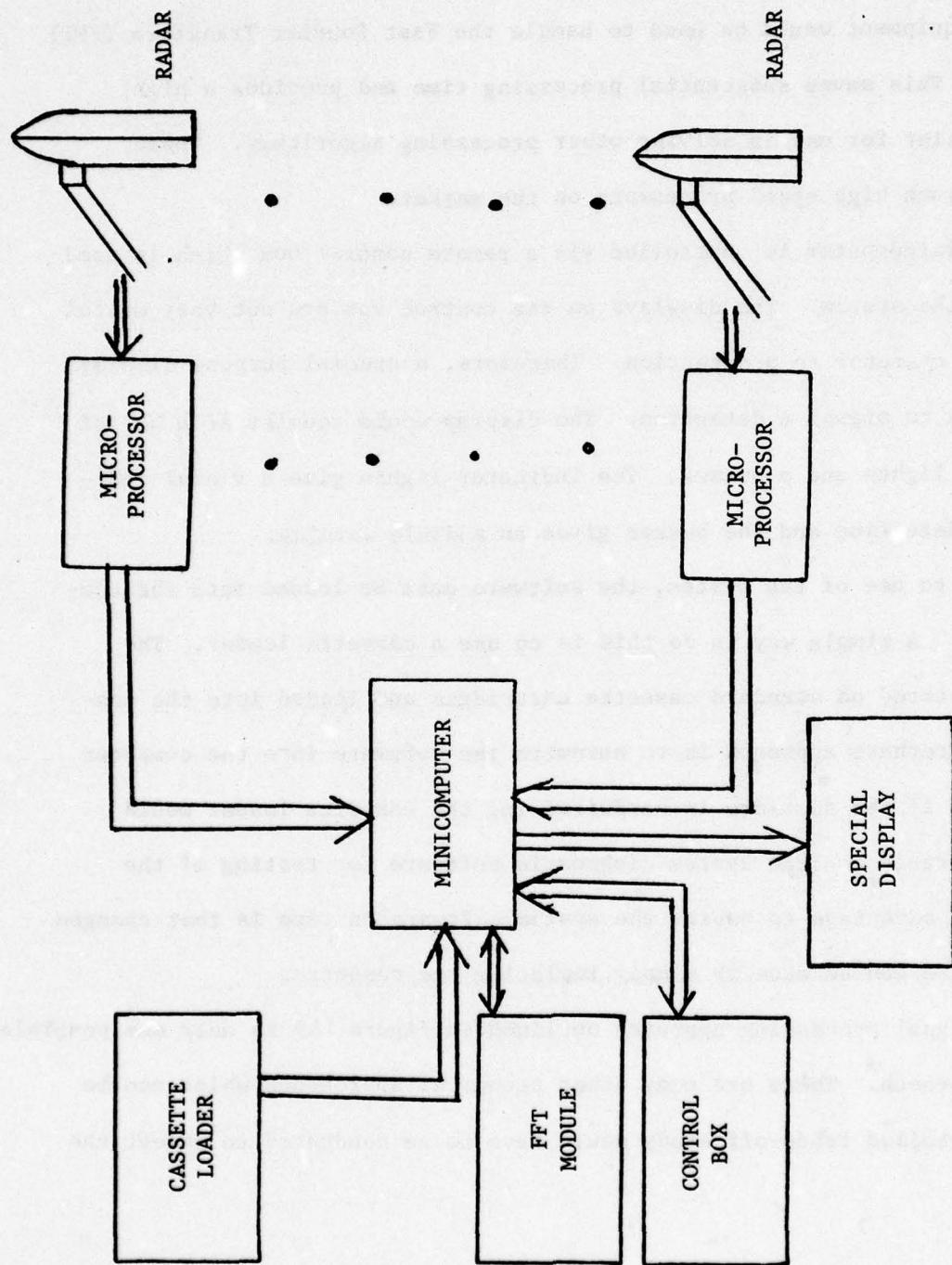


Figure 152. Signal processing hardware.

UNCLASSIFIED

UNCLASSIFIED

As will be discussed later, the processing time of the minicomputer is too slow to satisfy the processing requirements associated with the discrimination and classification algorithms. Therefore, separate high speed processing equipment would be used to handle the Fast Fourier Transform (FFT) algorithms. This saves substantial processing time and provides a high speed multiplier for use in solving other processing algorithms. There are several such high speed processors on the market.

The minicomputer is controlled via a remote control box which is used to start up the system. The displays on the control box are not very useful to alert the operator to a detection. Therefore, a special purpose display would be used to signal a detection. The display would consist of a set of 13 indicator lights and a buzzer. The indicator lights give a visual indication of a detection and the buzzer gives an audible warning.

Prior to use of the system, the software must be loaded into the computer memory. A simple way to do this is to use a cassette loader. The software is stored on standard cassette cartridges and loaded into the computer. An alternate approach is to hardwire the software into the computer memory. Even if the software is hardwired in, the cassette loader would still be desirable to load system diagnostic software for testing of the computer. An advantage to having the system software on tape is that changes to the software can be made by simply replacing the cassette.

The signal processing approach outlined in Figure 152 is only one possible technical approach. There are many other technical approaches which can be used and a detailed trade-off study would have to be conducted to select the

UNCLASSIFIED

UNCLASSIFIED

best technical approach. Acceptable system cost would have to be an input to such a trade-off study.

Minicomputer

There are many minicomputers which could be used in the signal processing hardware. One that Georgia Tech has considerable experience with is the Rolm 1602 processor which is militarized. The Rolm computer has a 1 μ s cycle time and permits up to 64K of memory. In addition, a DMA option is available at a maximum input rate of 666K words/second. Some of the important execution times are listed in Table 9; these will be important in the following discussions.

Table 9
1602 EXECUTION TIMES

| <u>Operation</u> | <u>Execution Time</u> |
|------------------|-----------------------|
| Core Cycle Time | 1 μ s |
| Add | 1 μ s |
| Subtract | 1 μ s |
| Multiply | 5.4 μ s |
| Divide | 12.6 μ s |

The 1602 processor is physically 7.62" x 10.12" x 19.56" and weighs 47 pounds (with 64K memory). This does not include the control box which is 7.75" x 10.25" x 5.35" and weighs 9 pounds. The computer can be mounted to the bulkhead of a military vehicle. The power requirements of the unit are 47-400 Hz, 115 vac power. The total power requirement is up to 250 watts (64K memory).

UNCLASSIFIED

UNCLASSIFIED

The software for the Rolm computer operates under a Real Time Operating System (RTOS) executive. The executive is task-oriented with a priority assigned to each task. This permits multiple tasks to be run at the same time. The Rolm computer has extensive software support which eases the software development problem.

Preprocessors

There are many microprocessors which can be used for this application. The new Bit Slice microprocessors are quite fast and provide a great deal of flexibility in their architecture. Georgia Tech has considerable experience with these devices and has developed a standard microprocessor for radar applications around the devices. There are other devices such as the INTEL 8080 or 8085 which can be used and a trade-off study would have to be conducted to select the best microprocessor for this application. The Bit Slice microprocessors are a good first start.

The execution times for the Bit Slice microprocessor are comparable with the Rolm computer and can be faster. An add takes approximately .8 μ s and a multiply takes 3.2 μ s for a 5 MHz clock. In the following analysis, the execution times of the Rolm computer were used for all the execution time estimates.

One of the advantages of the Bit Slice microprocessors is that they use a 16-bit word which is compatible with the Rolm computer. Many of the microprocessors use an 8-bit word which requires reformatting of the data words and may force the use of double precision calculations. There are 16-bit microprocessors which can be used in this application as alternatives to the Bit Slice microprocessors.

UNCLASSIFIED

UNCLASSIFIED

High Speed Processing Equipment

The signal processing algorithms involve solving an FFT which places a substantial burden on the processing equipment. Since FFT's are commonly encountered in signal processing applications, a number of special purpose, high speed signal processors have become available on the market. One unit is capable of solving a 64 point real FFT in .14 milliseconds. This is a considerable reduction over the time that it would take with the Rolm computer. Since the Rolm computer operates on a task basis with a priority assignment, the computer can send data to the FFT module and process other data while it is waiting for a solution.

Processing Requirements

Two of the primary data processing constraints are memory requirements and processing time. The signal processor memory requirements are not that substantial. The computer does have to store a learning set which consists of an array of dimensions 32 x 6 x 126 which corresponds to 4032 words of memory. The same learning set is used for each antenna return. A total of 32K memory should be sufficient to handle the operating system, task software, and data storage requirements.

The more difficult problem is processing time. This problem will be addressed by looking at each step of the signal processing procedure. First, it is helpful to estimate all the basic processing times. This has already been done for the basic arithmetic operations. The two missing operations are square root and FFT. The FFT operation can be handled using special purpose processing equipment as has already been noted. If the FFT is solved in the Rolm, it would take 10-12 milliseconds which becomes a significant

UNCLASSIFIED

UNCLASSIFIED

part of the processing. This, coupled with the fact that an FFT only has to be solved when a detection is obtained, provides a strong case for the processing configuration shown in Figure 152.

The square root operation can be handled in a number of ways. One approach is to use the approximation:

$$(x^2 + y^2)^{1/2} = \max(x, y) + 1/2 \min(x, y) \quad (52)$$

This involves a compare, an add and a shift operation which can be completed in 3 μ s or less. A second approach is to use the Newton-Raphson approach which is an iterative technique. Each iteration would require 1 multiply, 1 divide, 2 adds and one shift for a total of 21 μ seconds. If five iterations are performed, .105 milliseconds are required to perform a square root operation. It is, therefore, advantageous to use the previous approximation technique which requires only 3 μ s.

Detection Processing

The detection processing consists of a CFAR calculation and a gating procedure. The CFAR calculation involves forming a sum of the form

$$S = \sum_{i=1}^{256} s_i \quad (53)$$

This sum is multiplied by a constant to form a threshold which is compared with all 256 range bins. Table 10 summarizes the computational requirements. The total execution time of the CFAR process takes approximately 2 milliseconds.

In addition to the CFAR computations, a time gate must be put around the target return. The lower position of the gate is the second zero crossing after the largest negative peak in the vicinity of the ground return.

UNCLASSIFIED

UNCLASSIFIED

Table 10
CFAR PROCESSING

| <u>Operation</u> | <u>Number of Operations</u> | <u>Execution Time</u> |
|------------------|-----------------------------|-----------------------|
| Multiply | 257 | 1387.8 μ s |
| Add | 255 | 255.0 μ s |
| Compare | 256 | 256.0 μ s |
| Memory Cycle | 10 | 10.0 μ s |

The upper end of the gate is 200 points from the lower end. The data within the 200 point window is smoothed using a five point uniform amplitude average. The largest peak in the smoothed data is found along with the closest nulls on both sides of the peak. The nulls must satisfy the requirements:

- (1) Their amplitude must be less than one quarter the peak value;
- (2) The location of the first null must be less than or equal to the location of the peak minus 7, and
- (3) The location of the second null must be less than or equal to the location of the peak plus seven.

These two nulls set the gate position. If no such pair of nulls can be found, the previously computed gate positions are used.

The computational requirements of the gate setting search procedure are a function of the data. A worst case estimate is given in Table 11. This gives a worst case computational time of 3.75 milliseconds; the total computational time for the detection processing is 5.66 milliseconds.

UNCLASSIFIED

UNCLASSIFIED

Table 11
GATE SETTING PROCESSING

| <u>Operation</u> | <u>Number of Operations</u> | <u>Execution Time</u> |
|------------------|-----------------------------|-----------------------|
| Divide | 200 | 2520 μ s |
| Add | 398 | 398 μ s |
| Compare | 831 | 831 μ s |

Discrimination Processing

The FFT portion of the discrimination processing has already been discussed. Once the 32 point complex FFT has been performed on the gated data, the following computations are performed between the FFT data and a learning set consisting of 126 sets of 32 points:

- (1) Calculate the distance between the FFT data and each member of the learning set;
- (2) Select 3 largest distances; and
- (3) Determine which class is in the majority.

The class type is associated with the member of the learning set.

Table 12 lists the computational requirements of the discrimination algorithms. The total discrimination process would take 26.54 milliseconds; this assumes a high speed FFT module.

Classification Processing

The classification process classifies the mines as to 1 of 3 types. First, the maximum of the 32 FFT samples is found. Then the minimum on either side of the maximum which is less than 1/2 the maximum is found. The maximum

UNCLASSIFIED

UNCLASSIFIED

Table 12
DISCRIMINATION PROCESSING

| <u>Operation</u> | <u>Number of Operations</u> | <u>Execution Time</u> |
|------------------|-----------------------------|--|
| FFT | 1 | 14 μ s |
| Multiply | 4096 | 22118.4 μ s |
| Add | 3938 | 3938 μ s |
| Square Root | 32 | 96 μ s |
| Compare | 374 | <u>374 μs</u> |
| | | TOTAL <u>26540.4 μs</u> |

and two minima form a set of three numbers, x_i . The weighted sum

$$S = \sum_{i=1}^3 w_i x_i \quad (54)$$

is formed where the w_i 's are weight factors. The sum is compared to a threshold which determines if it is type 1. If the mine is not type 1, the weighted sum is recomputed using a second set of weights and compared to a second threshold. This specifies whether it is type 2 or 3.

The computational requirements associated with the classification process are summarized in Table 13. The total computational time required for the classification processing is 1.33 milliseconds; this is quite small compared to the discrimination processing.

Table 13
CLASSIFICATION PROCESSING

| <u>Operation</u> | <u>Number of Operations</u> | <u>Execution Time</u> |
|------------------|-----------------------------|--------------------------------------|
| Multiply | 7 | 37.8 μ s |
| Add | 4 | 4 μ s |
| Compare | 91 | <u>91 μs</u> |
| | | TOTAL <u>132.8 μs</u> |

UNCLASSIFIED

UNCLASSIFIED

Total Processing Requirements

As can be seen from the preceding analysis, the discrimination processing takes the largest amount of processing time. This would be even more the case if a high speed FFT processor is not used. The total processing time depends on number of detections, number of mines, and number of non-mines encountered during any given pass of the radar. If one mine is detected, discriminated and classified, the total processing time is 32.33 milliseconds. This is about a third of the total time available; in addition, is the execution time of the software executive and other miscellaneous operations. For the target false alarm requirements set of the system, this should provide sufficient time for the worst case processing load. It may be possible to reduce the 32.33 milliseconds by using the high speed multiply in the FFT module if available.

Alternate Hardware Configurations

It is felt that the processing system outlined in Figure 151 is the best processing approach for the mine detection system outlined in this report. The primary trade-off from a cost savings standpoint would be to use a micro-processor in place of the minicomputer. This would save about \$30,000 in hardware cost but would add to software development cost since the minicomputer based system has higher level software which reduces the software development problems. This trade-off would have to be looked at in more detail during the system development. The other hardware trade-offs center around the selection of the specific hardware to be used and the exact specifications that the hardware must meet.

UNCLASSIFIED

UNCLASSIFIED

Signal Processing

At this time, it is difficult to go into much more detail on the hardware interfaces shown in Figure 152. Each microprocessor shown in Figure 152 must have an A/D converter on the input and the A/D conversion process must be synchronized with the radar clock (main bang). The data transfer into the minicomputer is via the DMA mode and a Data Channel Controlled would be included in the minicomputer. The minicomputer would interrogate each microprocessor sequentially to check if the microprocessor has data to transfer (i.e., a detection). The minicomputer interfaces with the operator via a small display box which consists of a set of 13 LED's and a buzzer. All the other interfaces are standard computer peripheral interfaces.

It is difficult at this early stage of design to estimate the system size, weight, and cost. Table 14 is a rough estimate of the system breakdown. The total cost represents only the hardware cost. The cost to prototype a unit is estimated to be \$200,000 plus the hardware cost. The cost of an engineering unit is very difficult to estimate and depends on the production size. No attempt, therefore, was made to estimate the engineering cost.

Table 14
SYSTEM CHARACTERISTICS

| <u>Unit</u> | <u>Weight</u> | <u>Volume</u> | <u>Cost</u> |
|-------------------|-----------------|---------------------------|------------------|
| Minicomputer | 47 lbs. | 1.12 ft ³ | \$ 45,000 |
| 13 microprocessor | 150 lbs. | 1.6 ft ³ | 104,000 |
| Cassette loader | 7 lbs. | .16 ft ³ | 5,000 |
| FFT processor | 20 lbs. | .5 ft ³ | 20,000 |
| Display | 5 lbs. | .12 ft ³ | 2,000 |
| Power Supply | <u>30 lbs.</u> | <u>1 ft³</u> | <u>5,000</u> |
| TOTALS | 229 lbs. | 4.5 ft³ | \$181,000 |

UNCLASSIFIED

UNCLASSIFIED

It is felt that the proposed signal processing system is the best technical approach to the mine detection problem. The cost is high but can be reduced through careful hardware trade-offs and a relaxation of some of the hardware requirements. The two driving factors are the number of radars that must be handled and the limits on the processing time.

UNCLASSIFIED

UNCLASSIFIED

SECTION VIII

CONCLUSIONS AND RECOMMENDATIONS

The collection and analysis of data taken with the NBS automatic network analyzer and the MERADCOM short-pulse radar were completed. Temporal and spectral plots of all collected data are presented in this report. In particular, the signature spectra of mines and non-mines (i.e., rocks, a root, and a metal plate, as well as two types of non-metallic mines) have been included. Visual inspection of these data indicated that both the temporal and spectral responses of these buried objects differ sufficiently to allow discrimination and classification into distinct categories. This was particularly true of those objects buried in relatively dry soil (e.g., 7% moisture). As the soil moisture content was increased, the target radar returns were attenuated by the moisture and the target signature was sometimes obscured. The 30% moisture soils attenuated the radar signals so much that the target signatures could not be visibly distinguished from the background noise.

Visual inspection of the temporal and spectral responses suggested that the target signatures in the frequency domain would likely be more useful than the temporal signatures. Thus, the major thrust of this study was to discriminate and classify targets based on the frequency domain differences.

The physical characteristics which allowed object discrimination/classification were (1) the vertical thickness of the object (the dimension of the object in the direction of electromagnetic wave propagation), and

UNCLASSIFIED

UNCLASSIFIED

(2) the attenuation and dielectric characteristics of the object's interior.

A mathematical model including the effects of these characteristics as well as the soil environment was derived and used to verify this conjecture. The math model yielded temporal and spectral responses almost identical to those measured with the actual objects. Each of the objects included in the data collection program had different internal attenuation and dielectric characteristics and some had different thicknesses. Thus, different temporal and spectral responses were obtained. Based on these different responses, the objects were distinguished from one another. Even for objects of the same thickness, but of a different interior, the objects were distinguished from one another.

Based on the spectral characteristics which were different for each buried object of concern, algorithms were designed to automatically operate on the received radar spectral signatures to indicate if a mine was present and to which mine category it belonged. The process of initially detecting a buried object, determining whether the detected object was a mine, then identifying the type of mine was divided into three steps. The first step was to separate radar returns due to potential targets from radar returns due to soil anomalies. For this study, a potential target was considered to be any buried object which caused a radar return that was significantly different from radar returns caused by the soil alone. Some examples of buried non-mine objects that might be encountered in a typical field are rocks, roots, metal scraps, etc.

The discrimination/classification steps which follow the detection process involve a relatively complicated and time-consuming process; thus,

UNCLASSIFIED

UNCLASSIFIED

not every location in the field can be subjected to all three steps. The detection processor was designed to drastically reduce the number of locations in a field that must be scrutinized by the remaining sections of the processor. The discrimination processor, the second processing section, was designed to determine whether the potential targets are indeed targets (i.e., mines). The classification processor, the third and final processing section, was designed to identify the class of mine to which the target belongs, choosing from several classes of mines.

Several algorithms were designed for each section of the three processor concept. The algorithms were tested using the collected data, and the performance of each algorithm was calculated and presented as a curve. The measure of performance used was the probability of detection versus the probability of false alarm. The performance of the first processor in the three step processor, the detector, was ideal for dry soil (i.e., the detection probability was 1.0, and the false alarm probability was 0). Since the number of data points used was somewhat limited, detection performance that will be obtained in a practical application may be somewhat different. Very good performance, however, is highly likely. As the amount of moisture was increased to 15 or 20% in loam or clay soil, the detection performance deteriorated noticeably.

The discrimination processor separated non-mines (i.e., rocks, roots, etc.) from mines reasonably well in dry soil. For example, with the best algorithm considered, the mine detection probability was about 0.9 and the false alarm probability (declaring the rock, root, etc., as a mine) was about 0.1.

UNCLASSIFIED

UNCLASSIFIED

If the area being searched is relatively free of rocks, roots, or metal scraps, the false alarm probability for the detector and discriminator in cascade is the product of the individual false alarm probabilities, and a discriminator false alarm probability of 0.1 is acceptable. But if there is a large number of non-mines, false alarm probability will be that of the discriminator (e.g., 0.1). If a fair proportion of the interrogated locations are expected to include non-mines, one concludes from the foregoing that the false alarm probability assigned to the discrimination processor should be low. To meet a false alarm probability of 10^{-5} for the overall processor, the false alarm probability for the discriminator should be approximately 10^{-5} . Thus, for a large number of non-mine targets, the detection processor algorithms considered in this study do little in the way of reducing the data the discriminator has to process. If most of the locations only contain soil, however, the detection processor significantly reduces the data to be handled by the discriminator/classifier, and the overall processor performance in dry soil is reasonable.

The last stage of the three step processor also performed reasonably well in dry soil. The probability of correctly classifying a type 1 or type 2 mine was on the order of 0.9 for the best algorithm considered.

The conclusions described above are primarily based on the NBS collected data which was much more abundant than the MERADCOM short-pulse radar data. The few temporal and spectral plots and performance curves made with the limited short-pulse radar data were compared to the NBS data plots. The conclusion drawn in comparing the NBS data with short-pulse radar data was that the collection of mine data by a CW measurement system such as the NBS

UNCLASSIFIED

UNCLASSIFIED

system is equivalent to collecting mine data by a short-pulse radar system. Therefore, all of the conclusions drawn from the NBS data measurement program should apply equally well to an equivalent set of data taken with the MERADCOM short-pulse radar.

The hardware requirements for a mine detection system as considered in this report were determined. The emphasis, however, was on the signal processing required for short-pulse returns. The radar to be used in the postulated mine detection system was assumed to be the MERADCOM short-pulse radar furnished by the government. A comparison of the processor performance using the NBS data and the short-pulse radar data indicated approximately equivalent performance. Therefore, the hardware requirements for the short-pulse radar as listed in the CALSPAN Report No. MA-5366-E-3 entitled "Vehicular Mounted Mine Detection Radar Operational Manual," June 1976, should be sufficient for the mine detection system under consideration.

In recommending a processor design, the maximum performance achieved with the processing algorithms considered in this study was deemed necessary to meet system requirements. This implies a target search pattern with subterranean interrogations on a one-foot square grid (i.e., each interrogation is made within one foot of all other interrogations). In addition, the processing parameters used are those assumed in the performance analysis presented elsewhere in this report.

The hardware requirements analysis indicated that discrimination processing takes the largest amount of processing time. This would be even more the case if the proposed high speed FFT processor were not used. The total processing time depends on the number of detections, number of mines, and

UNCLASSIFIED

UNCLASSIFIED

number of non-mines encountered during any given pass of the radar. If one mine is detected, discriminated, and classified, the total processing time is approximately 32 milliseconds for the processor proposed. This is about a third of the total time available. Some of the total time available, however, must be reserved for execution time of the software executive and other miscellaneous operations which might require another 10 milliseconds. For the target false alarm requirement set for the system, this should provide sufficient time for the worst case processing load. It may be possible to reduce the 40 milliseconds by using a high speed multiply in the FFT module.

RECOMMENDATIONS

A study of the spectral characteristics of the two different sizes of non-metallic mines used in this program suggests that only part of the 0.1 GHz to 3.0 GHz frequency band is required for successful discrimination/classification. For example, if only the band from 0.5 to 1.5 GHz is used, much of the target signature is still visible and the spectrum signatures are sufficiently different to distinguish between the two mines. The two inert mines used are representative of the mine sizes expected. Thus, all other mines of approximately the same size will have signatures in the same spectral band, and the signature characteristics should be sufficiently different to permit classification.

The benefits to be gained by designing a radar system for this narrow frequency band become clear when such a system is compared to the present MERADCOM short-pulse radar which was designed for a much larger bandwidth. In addition to reducing the requirements on the radar transmitter and receiver, the antenna can be significantly reduced in length. The elimination of the

UNCLASSIFIED

AD-A054 427

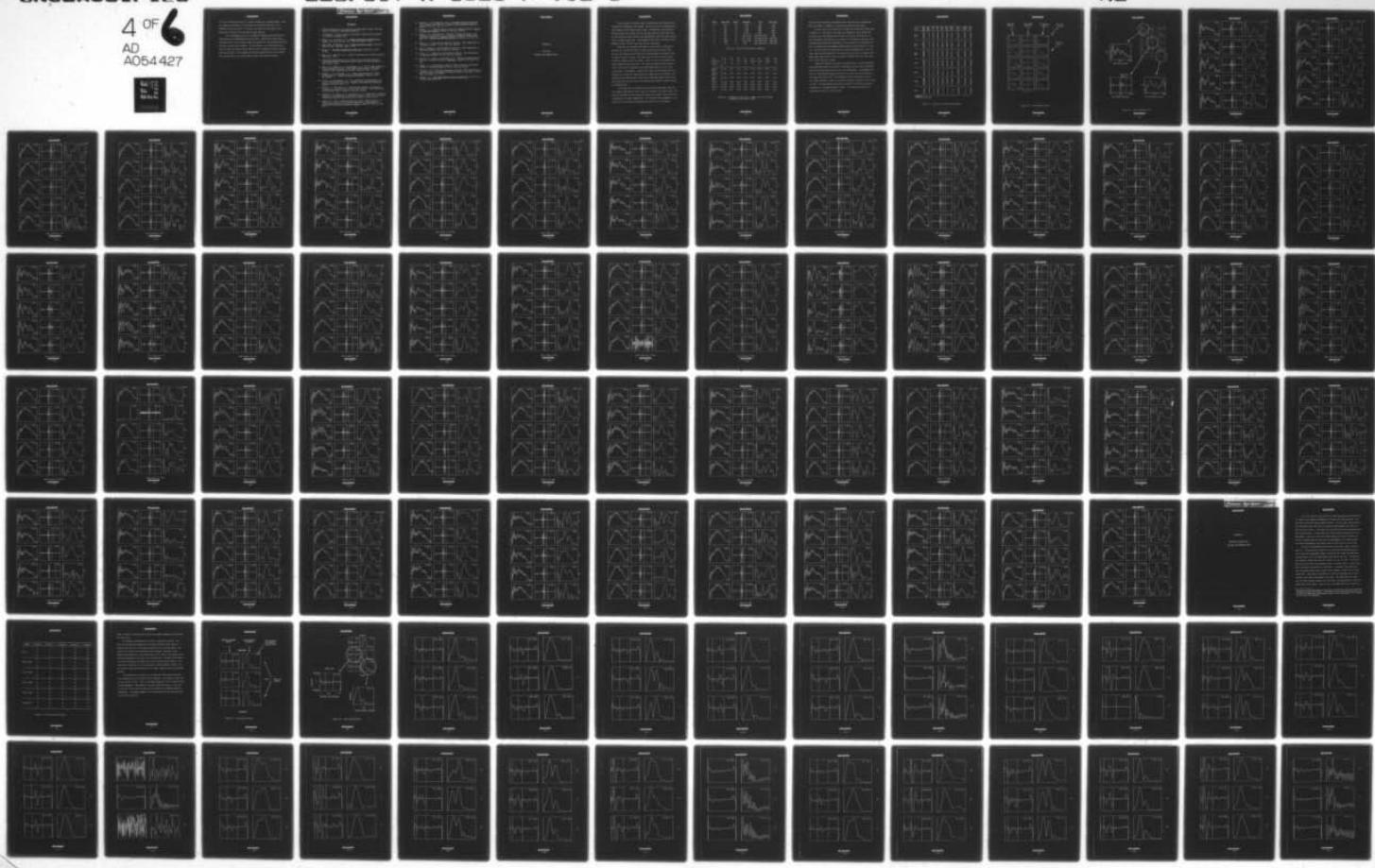
GEORGIA INST OF TECH ATLANTA ENGINEERING EXPERIMENT --ETC F/G 17/9
RADAR DETECTION, DISCRIMINATION, AND CLASSIFICATION OF BURIED N--ETC(U)
FEB 78 J D ECHARD, J A SCHEER, E O RAUSCH DAAG53-76-C-0112

UNCLASSIFIED

EES/GIT-A-1828-F-VOL-1

NL

4 of 6
AD
A054427



UNCLASSIFIED

0.12 to 0.5 GHz band allows for a shorter antenna and a simpler design. Thus, the weight and bulkiness of the antenna can be reduced from that of the MERADCOM short-pulse system. Of course, the final size and weight of the antenna will depend on the particular design selected.

It is recommended that such an antenna be designed and fabricated for installation on the MERADCOM short-pulse radar. Limited data should then be collected with this new antenna design and subjected to the algorithms selected and used in this present program. The performance of the short-pulse radar with the newer and smaller antenna should then be compared to the data already taken and analyzed. This suggested follow-on program will allow for performance verification of the new and smaller radar mine detection system.

UNCLASSIFIED

UNCLASSIFIED

REFERENCES

1. "Mobile Microwave Test Set Operating and Maintenance Manual," National Bureau of Standards, unpublished manuscript.
2. "S-Parameters...Circuit Analysis and Design," Hewlett-Packard Application Note 95, September 1968.
3. Kaye, G. W. C. and Laby, T. H., Tables of Physical and Chemical Constants, John Wiley and Sons, Inc., New York, 1966, p. 101.
4. Ramo, Simon and Whinnery, J. R., Fields and Waves in Radio, John Wiley and Sons, Inc., New York, 1960, p. 312.
5. Moreno, T., Microwave Transmission Design Data, McGraw-Hill, 1948, p. 200.
6. Duda, R. O., and Hart, P. E., "Pattern Classification and Scene Analysis", John Wiley, 1973.
7. "Detection and Estimation of P-PP Delay Time by Cepstrum Analysis," Transactions-American Geophysical Union, Volume 57, Texas Instruments, Inc., 1976, p. 963.
8. Chen, C. S., Roemer, L. E., and Grumback, R. S., "Power Cable Diagnostics Using Cepstrum Processing of Time Domain Reflectometry," IEEE Transactions on Power Apparatus and Systems, Volume 95, 1976, p. 1762.
9. Hammond, J. K. and Peardon, L. G., "Power Cepstrum Applied to Multi-Peaked Wavelets," Journal of Sound and Vibration, Volume 48, 1976, pp. 537-541.
10. Poche, L. B. and Rogers, P. H., "Echo Reduction in Low-Frequency Calibration Using Complex Cepstrum," Journal of the Acoustical Society of America, Volume 60, 1976, p. 25.
11. Hassab, J. C. and Boucher, R., "Probabilistic Analysis of Time-Delay Extraction by Cepstrum in Stationary Gaussian Noise," IEEE Transactions on Information Theory, Volume 22, 1976, pp. 444-454.
12. Zimdars, M. A., Taylor, R. W., and Willis, D. E., "Application of Cepstrum Analysis to Discrimination of Multiple Arrivals at First Zone Distances," Transactions American Geophysical Union, Volume 57, 1976, p. 85.
13. Fjell, P. O., "Use of Cepstrum Method for Arrival Times Extraction of Overlapping Signals Due to Multipath Conditions in Shallow-Water," Journal of the Acoustical Society of America, Volume 59, 1976, pp. 209-211.

UNCLASSIFIED

UNCLASSIFIED

14. Mitchell, S. K. and Bedford, N. R., "Long-Range Sensing of Explosive Source Depths Using Cepstrum," Journal of the Acoustical Society of America, Volume 58, 1975, p. 20.
15. Hassab, J. C., "Network Function Theory and Complex Cepstrum," Journal of Sound and Vibration, Volume 41, 1975, pp. 127-128.
16. Hassab, J. C., and Boucher R., "Analysis of Signal Extraction, Echo Detection and Removal by Complex Cepstrum in Presence of Distortion and Noise," Journal of Sound and Vibration, Volume 40, 1975, pp. 321-335.
17. Smith, R. G., "Cepstrum Discrimination Function," IEEE Transactions on Information Theory, VIT 21, 1975, pp. 332-334
18. Rom, R, "Cepstrum of Two-Dimensional Functions," IEEE Transactions on Information Theory, VIT 21, 1975, pp. 214-127.
19. Bohme, J. F., Cepstrum as a Generalized Function," IEEE Transactions on Information Theory, VIT 20, 1974, pp. 650-653.
20. Stoffa, P. L., Buhl, P., and Bryan, G. M., "Cepstrum Aliasing and Calculation of Hilbert Transform," Geophysics, Volume 39, 1974, pp. 543-544.
21. Hassab, J. C., "Convergence Interval of Power Cepstrum," IEEE Transactions on Information Theory, VIT 20, 1974, pp. 111-112.
22. Tribolet, J. M., "New Phase Unwrapping Algorithm," IEEE Transactions on Acoustics, Speech, and Signal Processing, Volume 25, MIT Dept. of Elect. Engn. and Comp., pp. 170-177.
23. Skinner, D. P., Real-Time Composite Signal Decomposition, University of Florida, Gainesville, FL.

UNCLASSIFIED

UNCLASSIFIED

APPENDIX A

NBS DATA

SPECTRAL AND TEMPORAL PLOTS

UNCLASSIFIED

UNCLASSIFIED

After receipt of the data tapes at Georgia Tech, the contents were transferred to permanent disk storage. The data were later converted from ASCII format to more compact binary codes. Occasionally, the pre-burial background data were recorded on the same tape used for target data, and in those cases the tape contents were appropriately split into two separate files to reduce access time. The background runs are not included in this appendix; hence, the data file names are not contiguous.

Files GT5, GT6, and GT7 were used to store the data collected at the NBS site, and GT9 and GT10 for those collected at Gun Barrel Hill. The moisture content at the second site varied somewhat with depth; hence, a range of values is listed. The range given is felt to be descriptive of the soil directly over the target. Table A-1 lists the pertinent parameters associated with each file. Note that the higher moisture content (17% or 18%) was not included in the measurement matrix for the 3-inch burial depth. Furthermore, a lapse of four days occurred between the measurements of GT6 and GT7 during which the targets were not disturbed. Although the test lane had been covered with tarpaulins against desiccation, heavy rains fell in the interim and increased the moisture content by about a percentage point.

Each target and its environs were therefore probed eight times for the various combinations of soil type, soil moisture, and burial depth. The data are presented in seven groups (one group per target), with each group consisting of the eight combinations. The locations and arrangement of the data sets in this report are summarized in Table A-2 for reference.

UNCLASSIFIED

UNCLASSIFIED

| <u>Group</u> | <u>Data File</u> | <u>Depth</u> | <u>Moisture</u> | <u>Site</u> | <u>Soil Type</u> |
|--------------|------------------|--------------|-----------------|-----------------|------------------|
| 1 | GT5 | 3" | 6.8% | NBS | Loam |
| 2 | GT5 | 6" | 6.8% | NBS | Loam |
| 3 | GT6 | 6" | 17.0% | NBS | Loam |
| 4 | GT7 | 6" | 17.8% | NBS | Loam |
| 5 | GT9 | 3" | 12% to 20% | Gun Barrel Hill | Loam |
| 6 | GT9 | 6" | 13% to 16% | Gun Barrel Hill | Bentonite |
| 7 | GT10 | 6" | 26% to 30% | Gun Barrel Hill | Bentonite |
| 8 | GT10 | 3" | 30% | Gun Barrel Hill | Bentonite |

Table A-1. Data file measurement conditions.

| | | | | | | | | |
|-------------|------|------|------|------|--------|--------|--------|------|
| File | GT5 | GT5 | GT6 | GT7 | GT9 | GT9 | GT10 | GT10 |
| Moisture | 7% | 7% | 17% | 18% | 12-20% | 13-16% | 26-30% | 30% |
| Depth | 3" | 6" | 6" | 6" | 3" | 6" | 6" | 3" |
| Type A Mine | A-8 | A-9 | A-10 | A-11 | A-12 | A-13 | A-14 | A-15 |
| Type B Mine | A-16 | A-17 | A-18 | A-19 | A-20 | A-21 | A-22 | A-23 |
| Type C Mine | A-24 | A-25 | A-26 | A-27 | A-28 | A-29 | A-30 | A-31 |
| Plate | A-32 | A-33 | A-34 | A-35 | A-36 | A-37 | A-38 | A-39 |
| Rock 1 | A-40 | A-41 | A-42 | A-43 | A-44 | A-45 | A-46 | A-47 |
| Rock 2 | A-48 | A-49 | A-50 | A-51 | A-52 | A-53 | A-54 | A-55 |
| Root | A-56 | A-57 | A-58 | A-59 | A-60 | A-61 | A-62 | A-63 |

Table A-2. Arrangement of the data. Number listed is the page on which the data may be found.

UNCLASSIFIED

UNCLASSIFIED

Table A-3 lists additional information about the data sets, including the data run numbers as numbered in Georgia Tech numerical data files.

The data plots are presented on 56 pages, all having the format shown in Figure A-1. The plots on each page are arranged in three columns and five rows, each row being the data for one of the five positions over or near the target. The first plot in each row is the measured spectrum; this spectrum was weighted and transformed to the time domain, as explained earlier, to generate the time domain response shown in the second plot of each row. The data within the range gate were then transformed back to the frequency spectrum and unweighted. The Georgia Tech data file is shown in the upper right corner and the data set number is printed along the right hand side of each sequence of plots.

Figure A-2 explains the scales on the data plots. Both the measured and deconvolved spectra run from DC to 3048 MHz, and note that the measured spectra have been zeroed for the first five frequencies. The maximum ordinates for the measured spectra vary from plot to plot and were typically in the range from 0.02 to 0.03. The ordinates for the deconvolved spectra also varied from plot to plot, but were much smaller, typically of the order of 0.002. The time domain plots span an interval of 20-5/6 nsec and were normalized to a maximum amplitude of unity. The range gate position is indicated by a pair of vertical lines.

UNCLASSIFIED

UNCLASSIFIED

| TARGET | ABS POS (IN) | REL POS (IN) | GT5 7% 3" | GT5 7% 6" | GT6 17% 6" | GT7 18% 6" | GT9 12-20% 3" | GT9 13-16% 6" | GT10 26-30% 6" | GT10 30% 3" |
|----------------|--------------|--------------|-----------|-----------|------------|------------|---------------|---------------|----------------|-------------|
| TYPE A MINE | 142 | -8 | 13 | 54 | 13 | 13 | 13 | 54 | 13 | 54 |
| | 146 | -4 | 14 | 55 | 14 | 14 | 14 | 55 | 14 | 55 |
| | 150 | 0 | 15 | 56 | 15 | 15 | 15 | 56 | 15 | 56 |
| | 154 | 4 | 16 | 57 | 16 | 16 | 16 | 57 | 16 | 57 |
| | 158 | 8 | 17 | 58 | 17 | 17 | 17 | 58 | 17 | 58 |
| TYPE B MINE | 322 | -8 | 31 | 71 | 31 | 31 | 31 | 72 | 31 | 72 |
| | 326 | -4 | 32 | 72 | 32 | 32 | 32 | 73 | 32 | 73 |
| | 330 | 0 | 33 | 73 | 33 | 33 | 33 | 74 | 33 | 74 |
| | 334 | 4 | 34 | 74 | 34 | 34 | 34 | 75 | 34 | 75 |
| | 338 | 8 | 35 | 75 | 35 | 35 | 35 | 76 | 35 | 76 |
| TYPE C MINE | 202 | -8 | 19 | 60 | 19 | 19 | 19 | 60 | 19 | 60 |
| | 206 | -4 | 20 | 61 | 20 | 20 | 20 | 61 | 20 | 61 |
| | 210 | 0 | 21 | 62 | 21 | 21 | 21 | 62 | 21 | 62 |
| | 214 | 4 | 22 | 63 | 22 | 22 | 22 | 63 | 22 | 63 |
| | 218 | 8 | 23 | 64 | 23 | 23 | 23 | 64 | 23* | 64 |
| PLATE | 262 | -8 | 25 | 65 | 25 | 25 | 25 | 66 | 25 | 66 |
| | 266 | -4 | 26 | 66 | 26 | 26 | 26 | 67 | 26 | 67** |
| | 270 | 0 | 27 | 67 | 27 | 27 | 27 | 68 | 27 | 68 |
| | 274 | 4 | 28 | 68 | 28 | 28 | 28 | 69 | 28 | 69 |
| | 278 | 8 | 29 | 69 | 29 | 29 | 29 | 70 | 29 | 70 |
| ROCK 1 | 82 | -8 | 7 | 48 | 7 | 7 | 7 | 48 | 7 | 48 |
| | 86 | -4 | 8 | 49 | 8 | 8 | 8 | 49 | 8 | 49 |
| | 90 | 0 | 9 | 50 | 9 | 9 | 9 | 50 | 9 | 50 |
| | 94 | 4 | 10 | 51 | 10 | 10 | 10 | 51 | 10 | 51 |
| | 98 | 8 | 11 | 52 | 11 | 11 | 11 | 52 | 11 | 52 |
| ROCK 2 | 382 | -8 | 37 | 77 | 37 | 37 | 37 | 78 | 37 | 78 |
| | 386 | -4 | 38 | 78 | 38 | 38 | 38 | 79 | 38 | 79 |
| | 390 | 0 | 39 | 79 | 39 | 39 | 39 | 80 | 39 | 80 |
| | 394 | 4 | 40 | 80 | 40 | 40 | 40 | 81 | 40 | 81 |
| | 398 | 8 | 41 | 81 | 41 | 41 | 41 | 82 | 41 | 82 |
| ROOT | 22 | -8 | 1 | 42 | 1 | 1 | 1 | 42 | 1 | 42 |
| | 26 | -4 | 2 | 43 | 2 | 2 | 2 | 43 | 2 | 43 |
| | 30 | 0 | 3 | 44 | 3 | 3 | 3 | 44 | 3 | 44 |
| | 34 | 4 | 4 | 45 | 4 | 4 | 4 | 45 | 4 | 45 |
| | 38 | 8 | 5 | 46 | 5 | 5 | 5 | 46 | 5 | 46 |

* Noisy data

** Contains a faulty datum

Table A-3. Tape and run identification numbers.

UNCLASSIFIED

UNCLASSIFIED

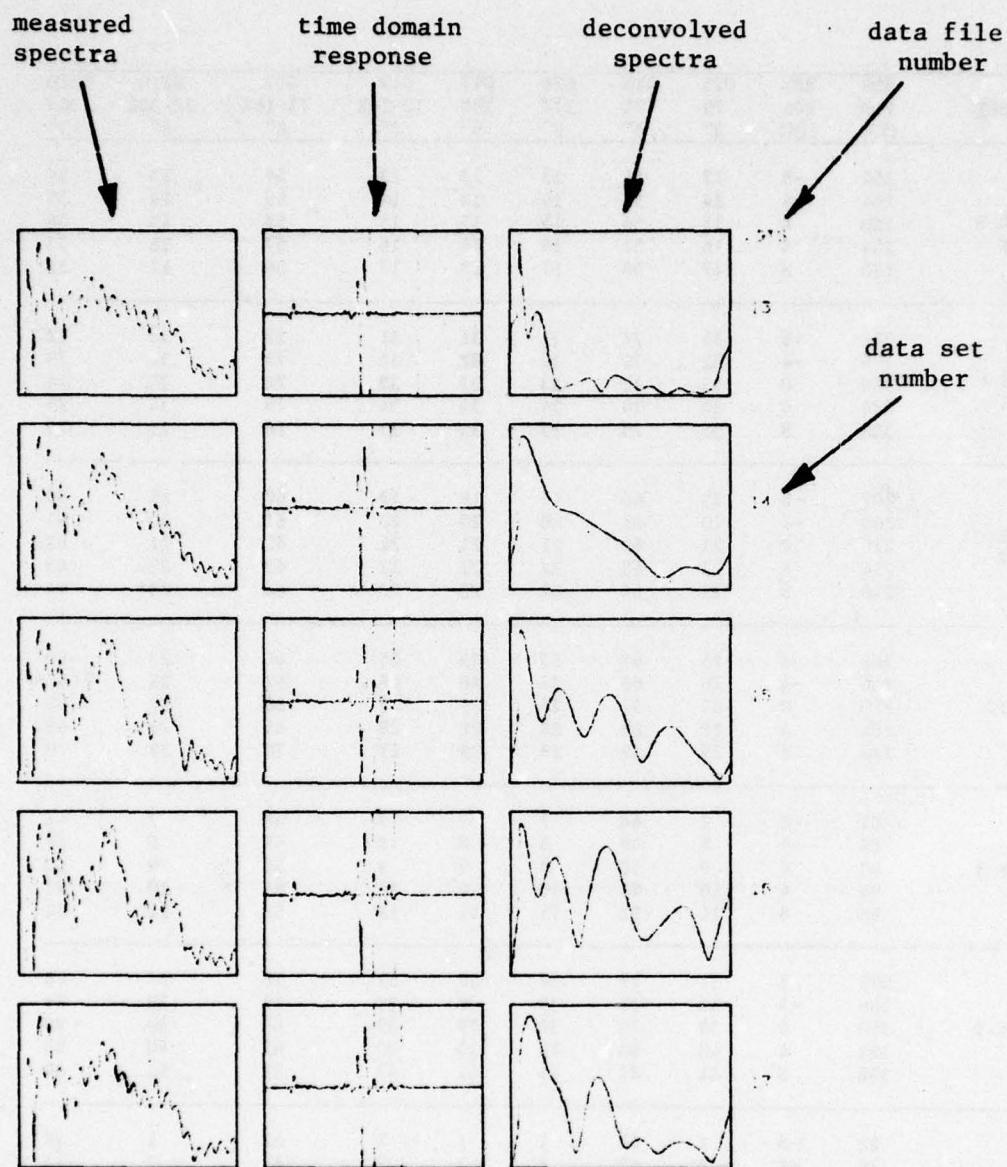


Figure A-1. Data display format.

UNCLASSIFIED

UNCLASSIFIED

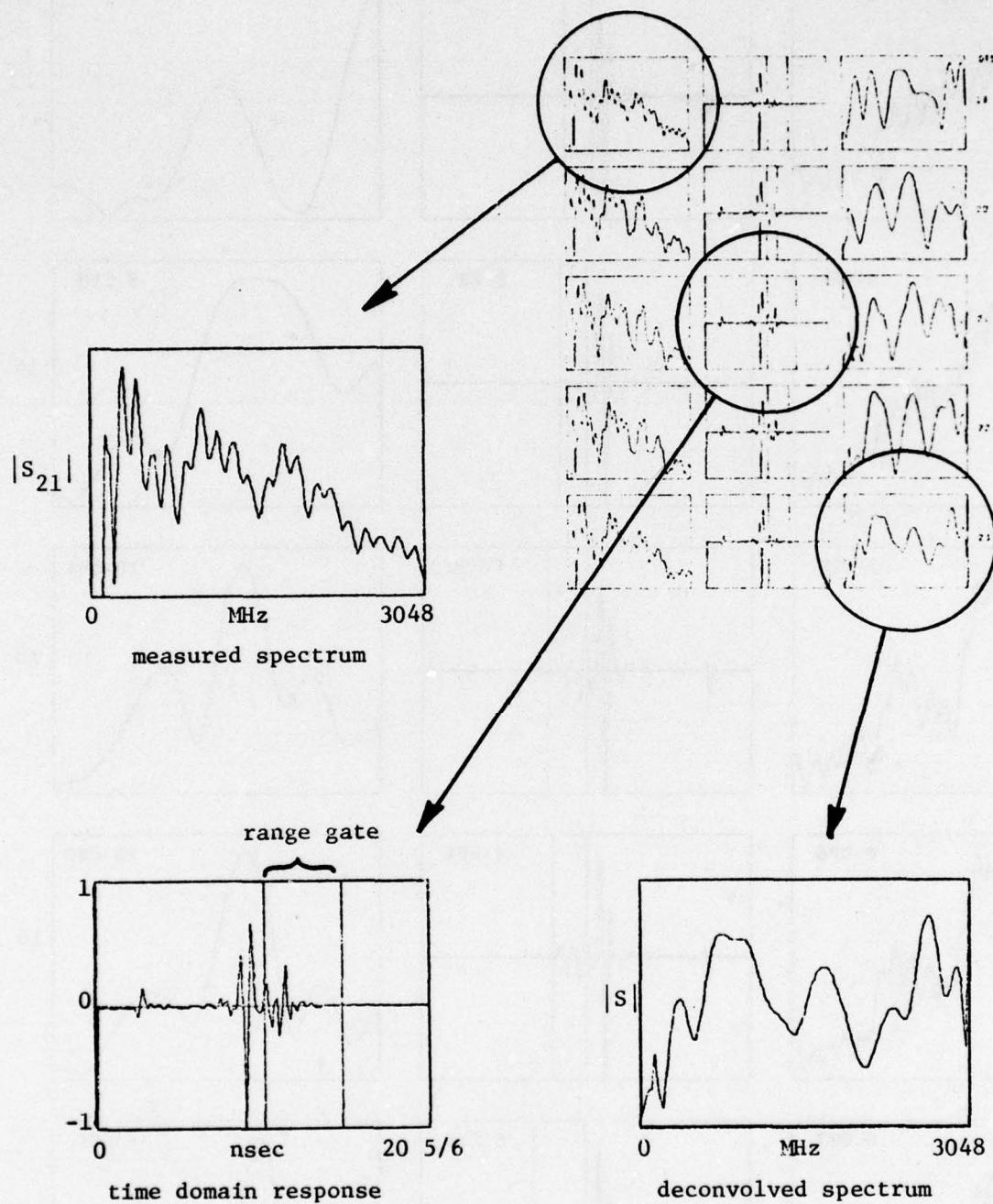
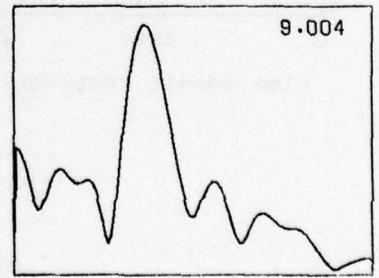
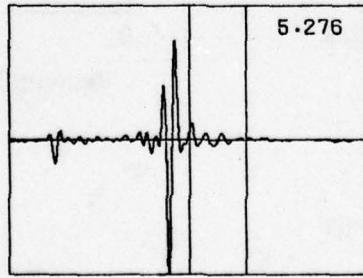
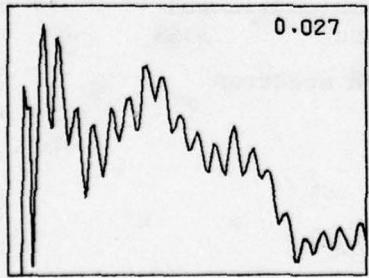
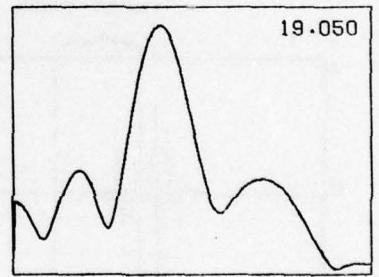
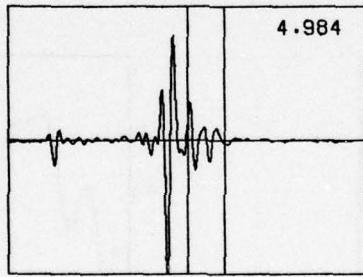
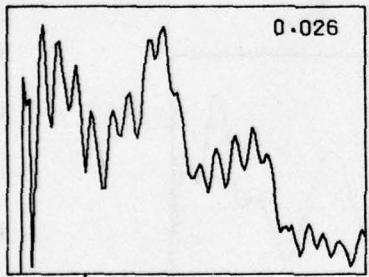
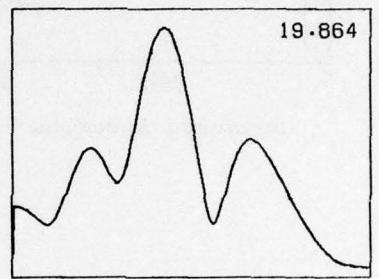
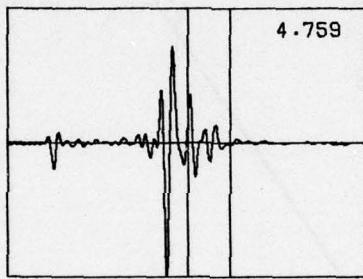
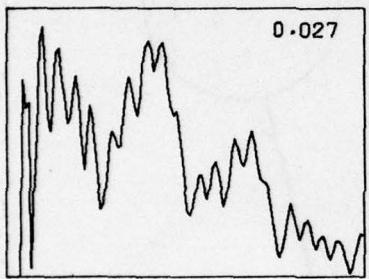
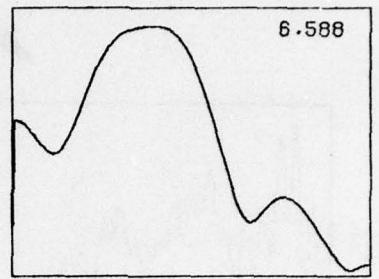
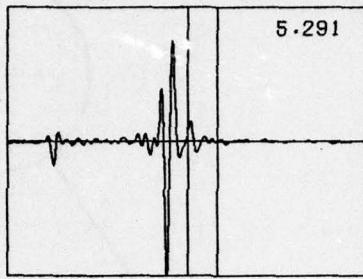
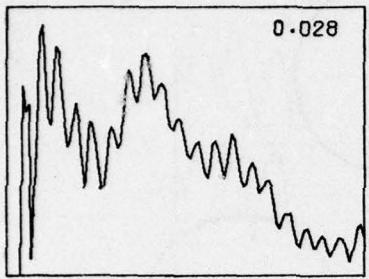
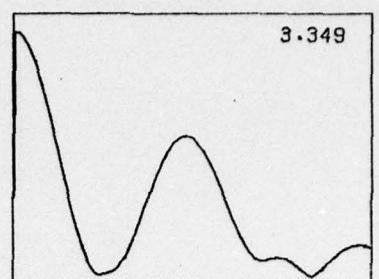
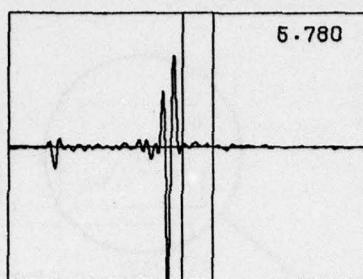
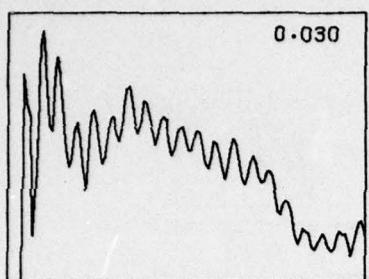


Figure A-2. Data characteristics.

UNCLASSIFIED

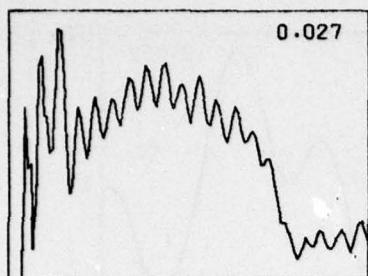
UNCLASSIFIED



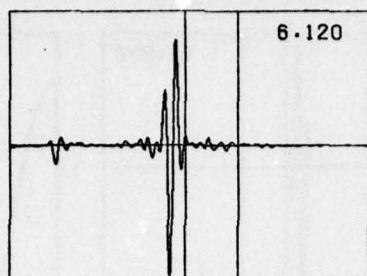
Type A mine, 3", 7%

UNCLASSIFIED

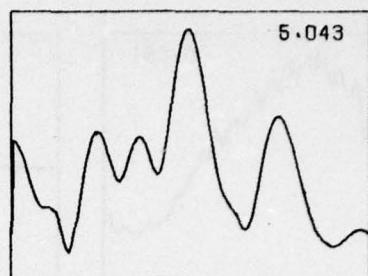
UNCLASSIFIED



0.027

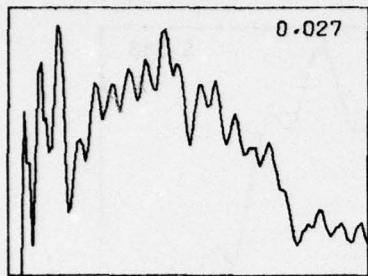


6.120

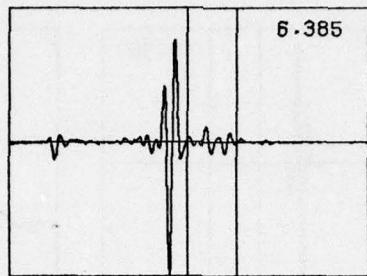


5.043

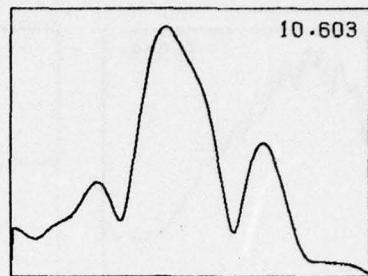
GT5



0.027

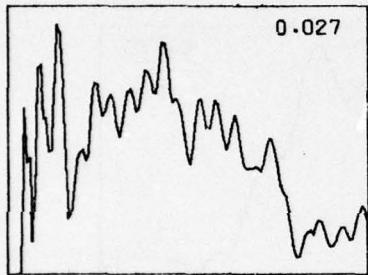


6.385

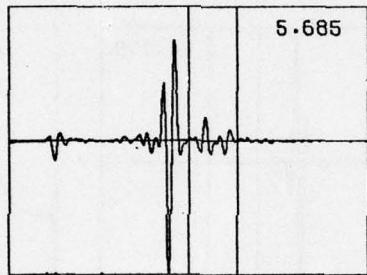


10.603

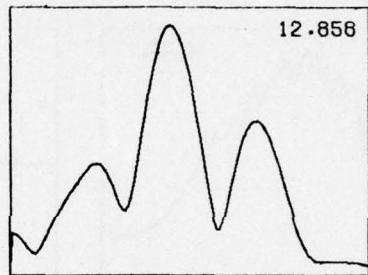
54



0.027

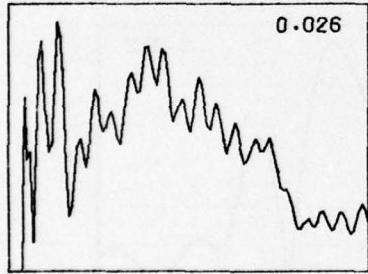


5.685

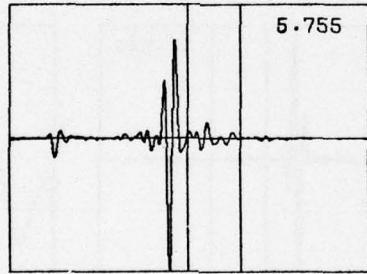


12.858

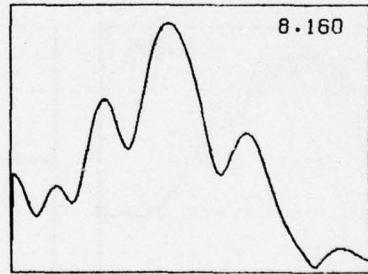
55



0.026

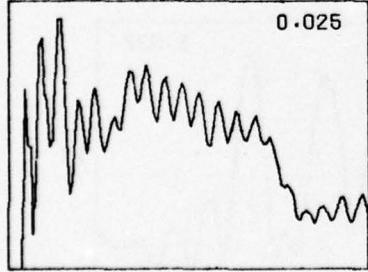


5.755

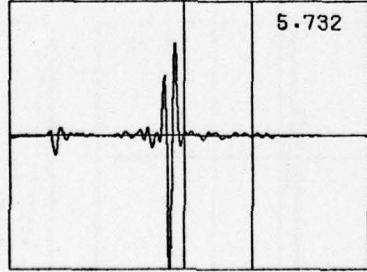


8.160

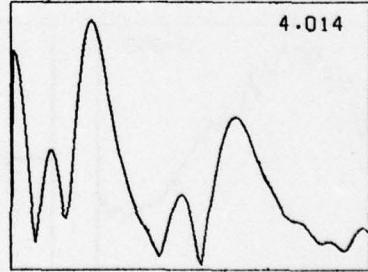
56



0.025



5.732



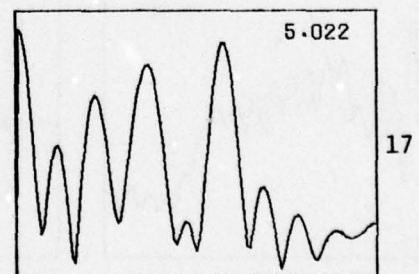
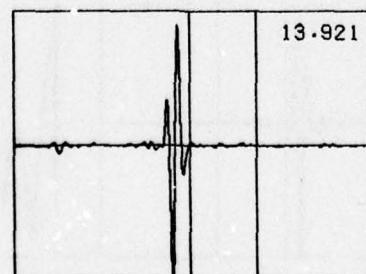
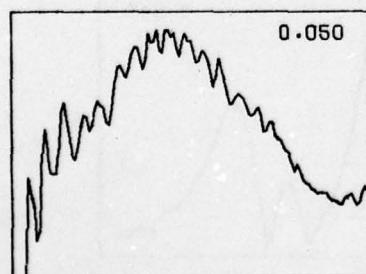
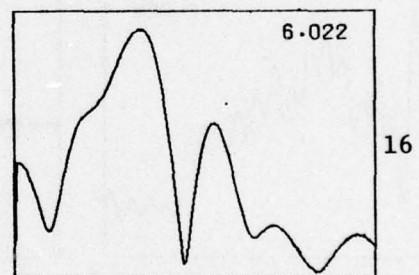
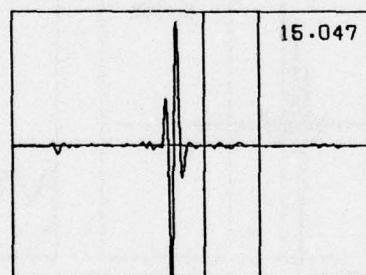
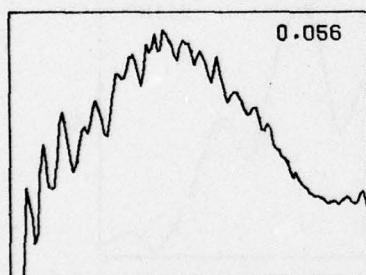
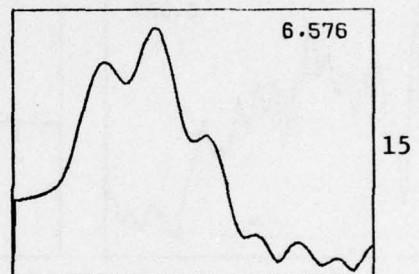
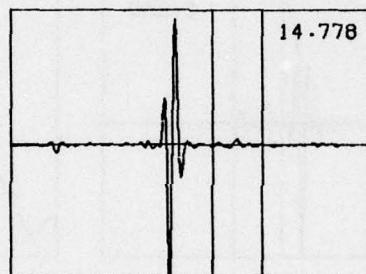
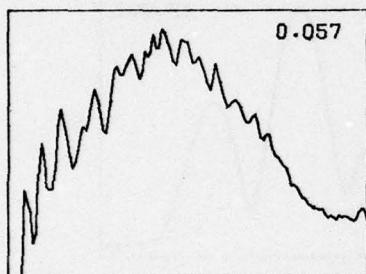
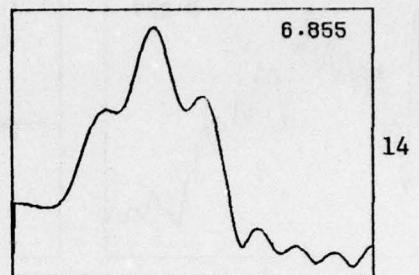
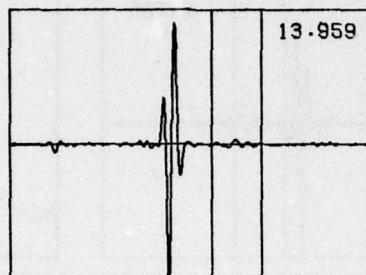
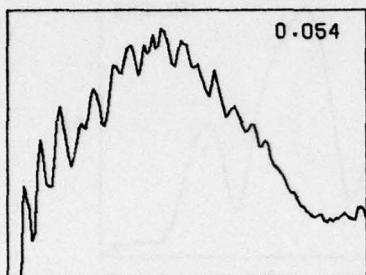
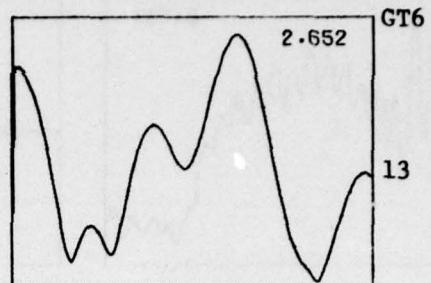
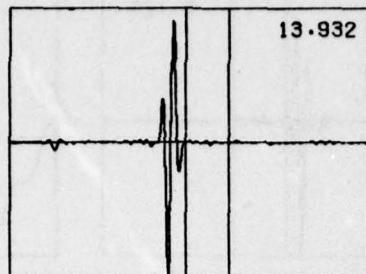
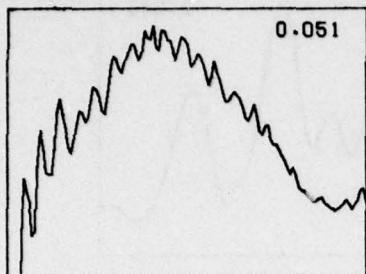
4.014

57

Type A mine, 6", 7%

UNCLASSIFIED

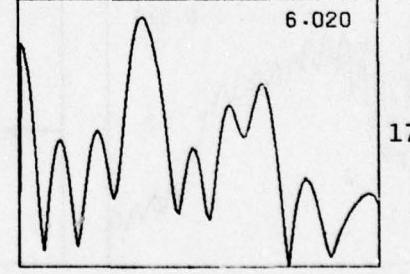
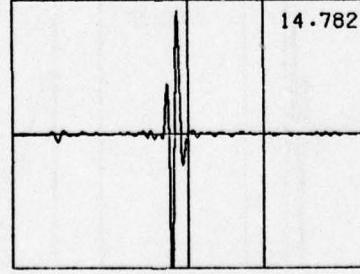
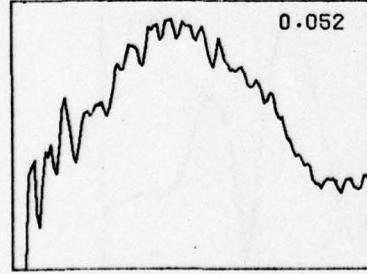
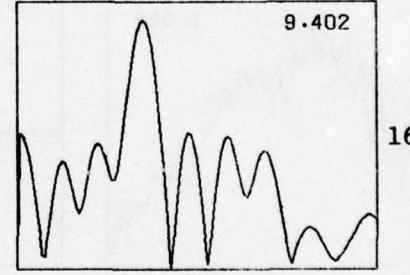
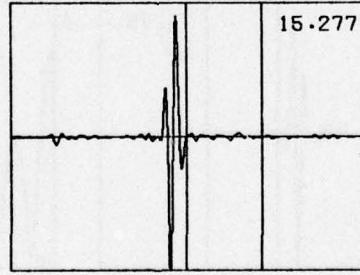
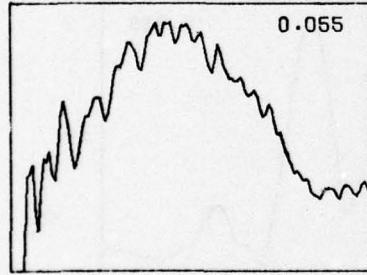
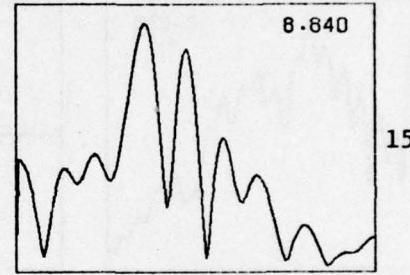
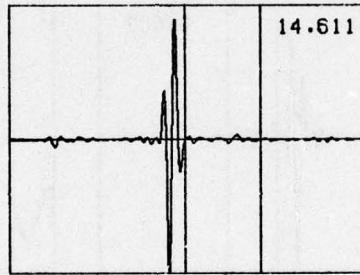
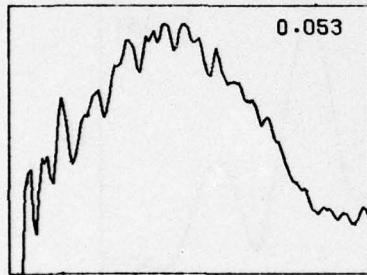
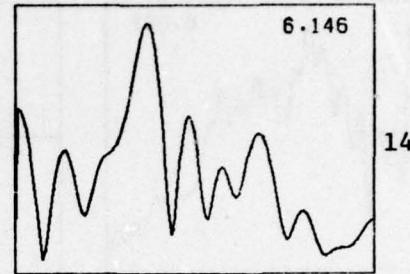
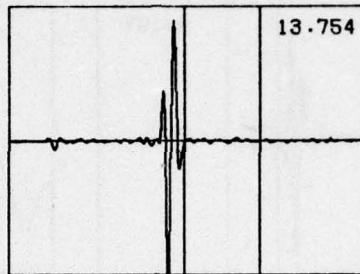
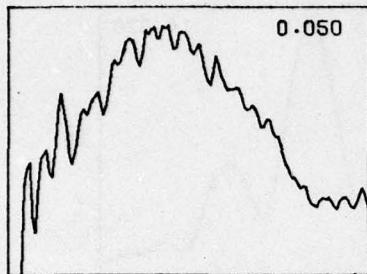
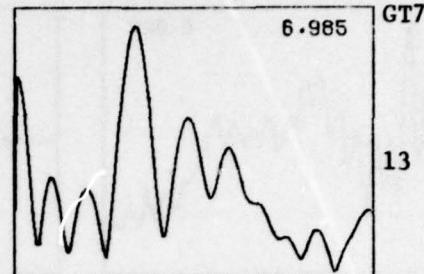
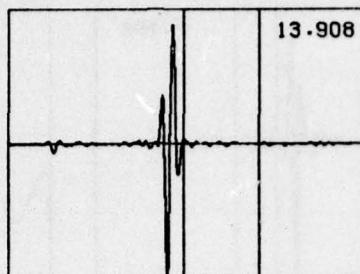
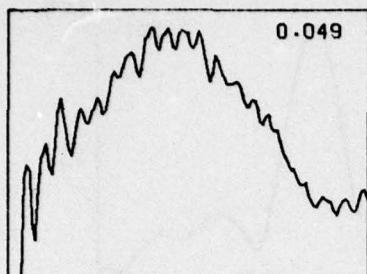
UNCLASSIFIED



Type A mine, 6", 17%

UNCLASSIFIED

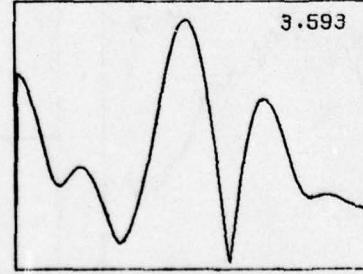
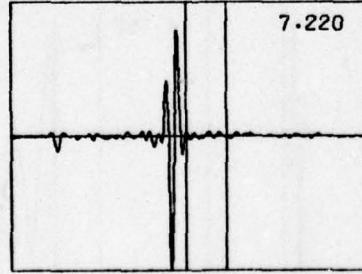
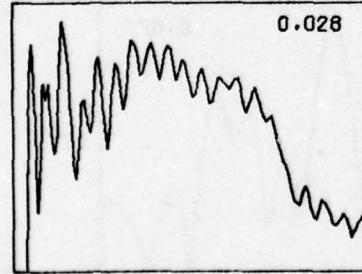
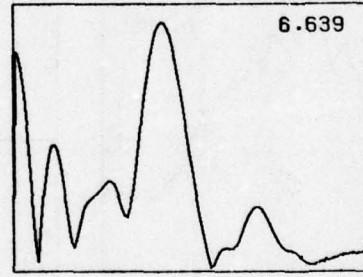
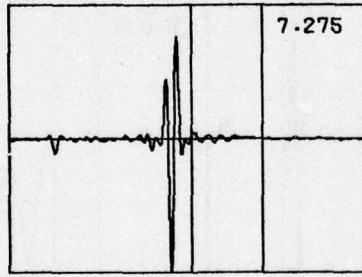
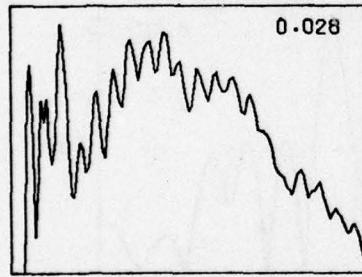
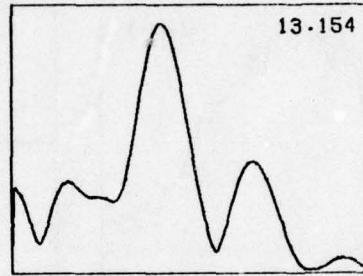
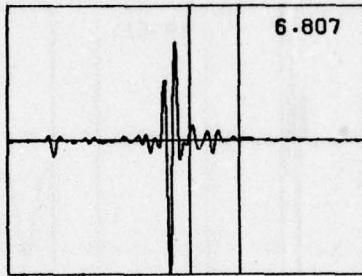
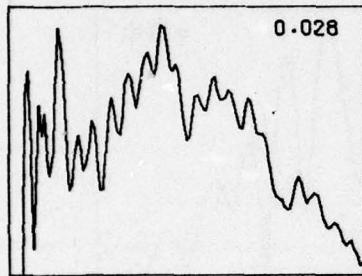
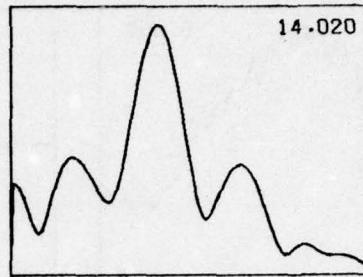
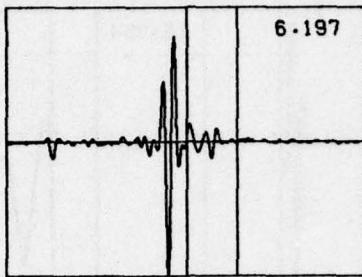
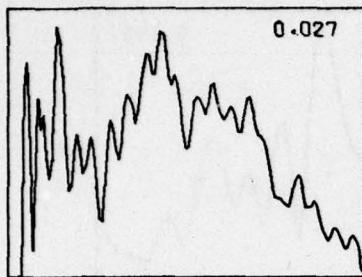
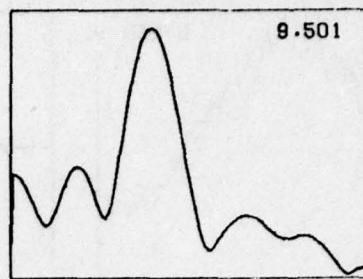
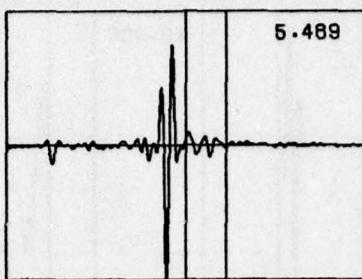
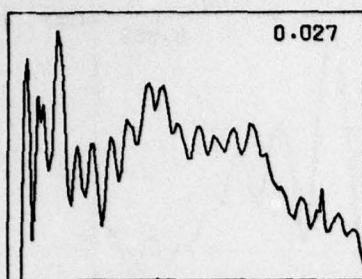
UNCLASSIFIED



Type A mine, 6", 18%

UNCLASSIFIED

UNCLASSIFIED

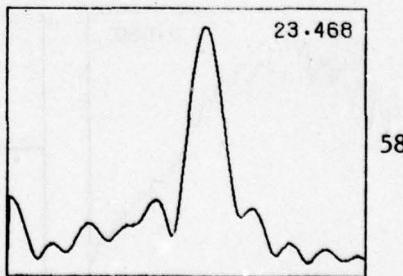
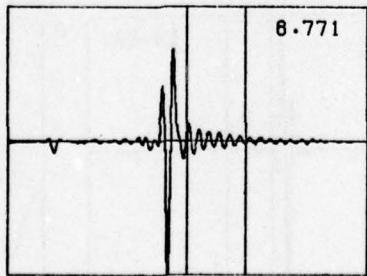
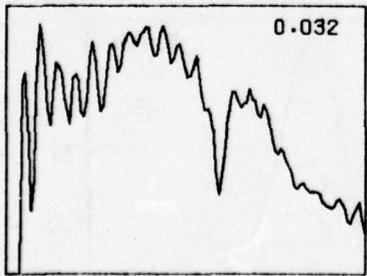
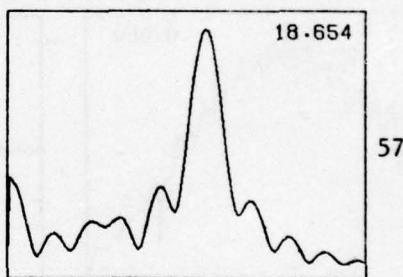
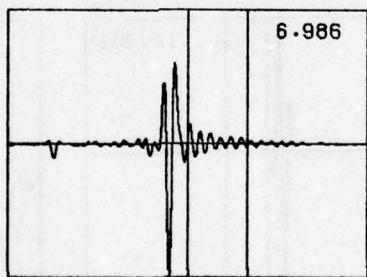
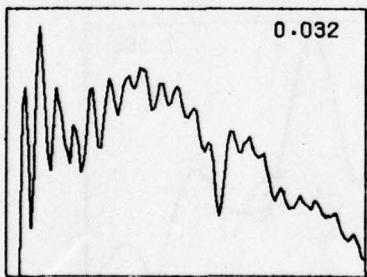
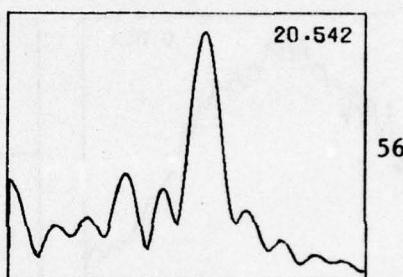
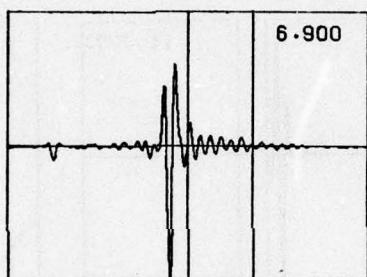
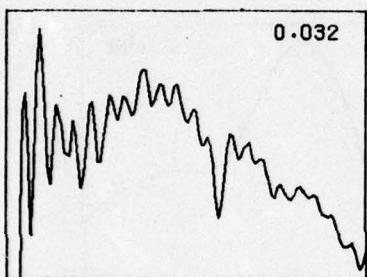
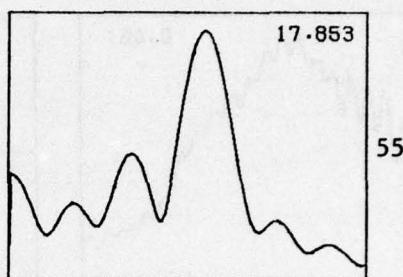
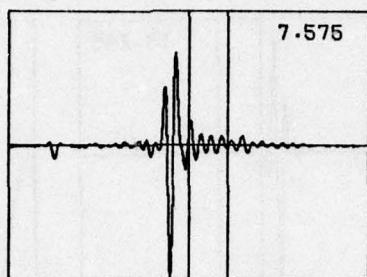
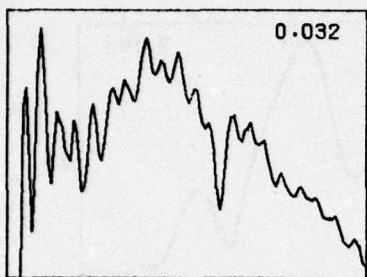
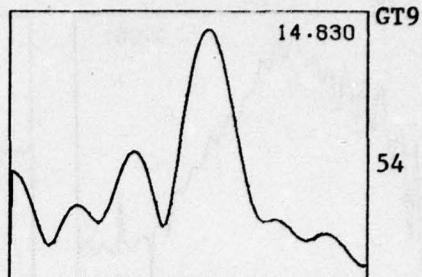
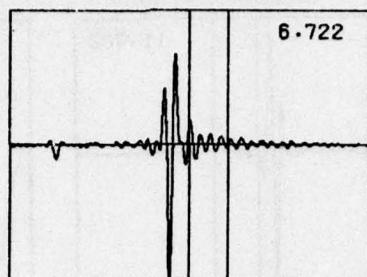
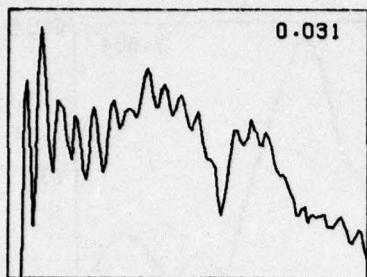


Type A mine, 3", 12-20%

UNCLASSIFIED

A-12

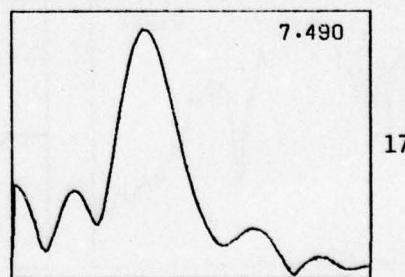
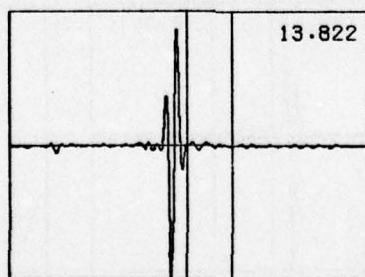
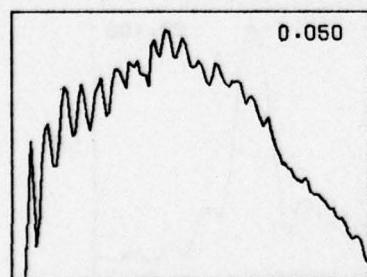
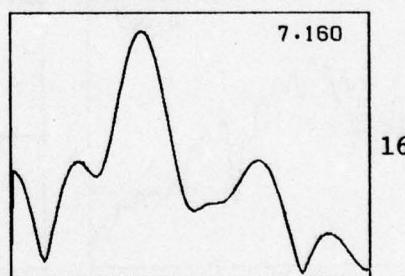
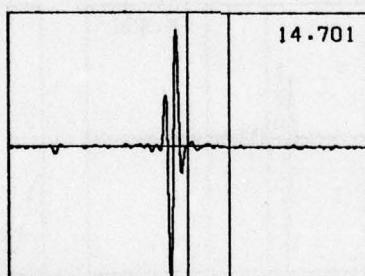
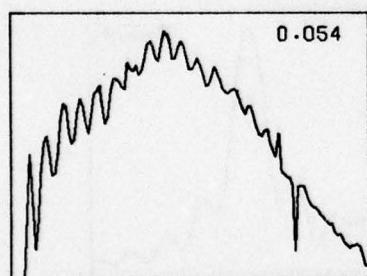
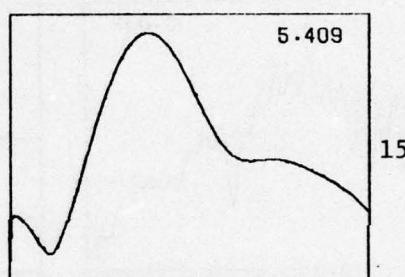
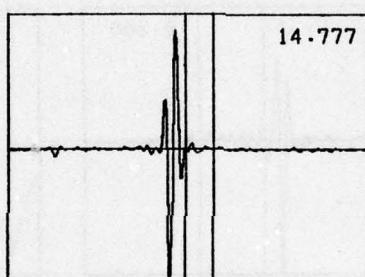
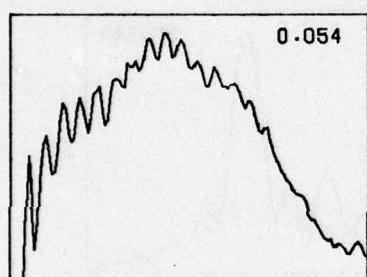
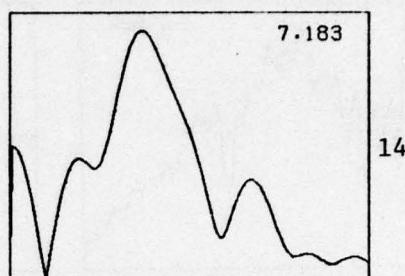
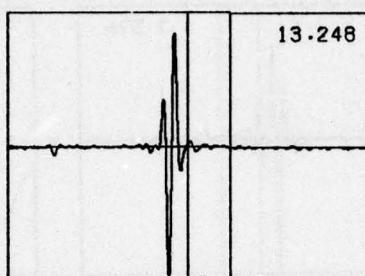
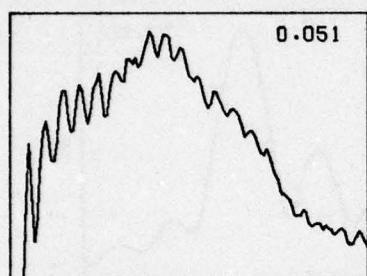
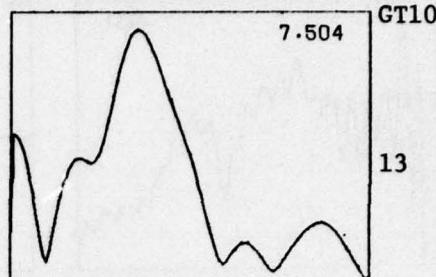
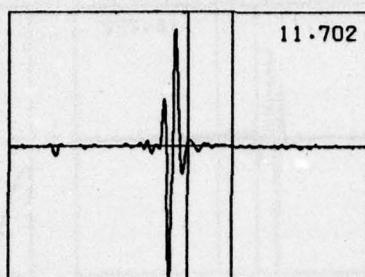
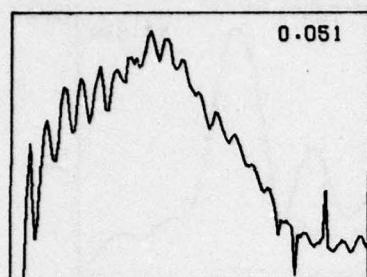
UNCLASSIFIED



Type A mine, 6", 13-16%

UNCLASSIFIED

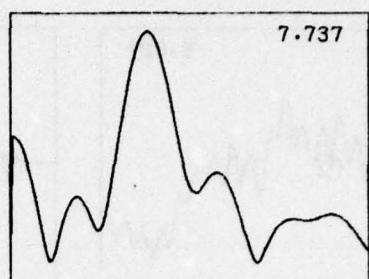
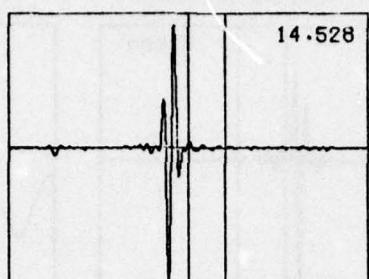
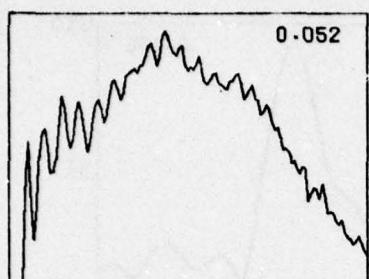
UNCLASSIFIED



Type A mine, 6", 26-30%

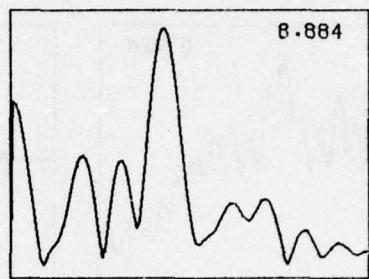
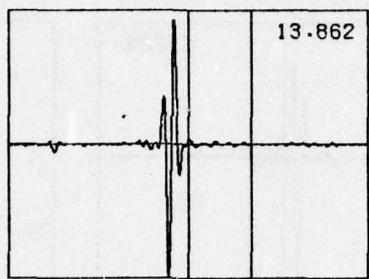
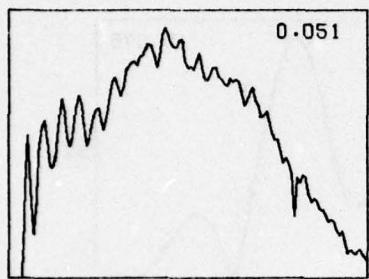
UNCLASSIFIED

UNCLASSIFIED

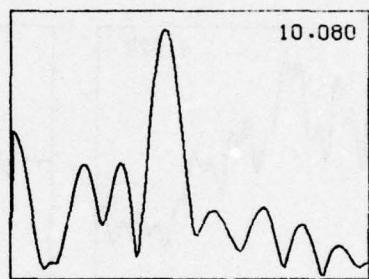
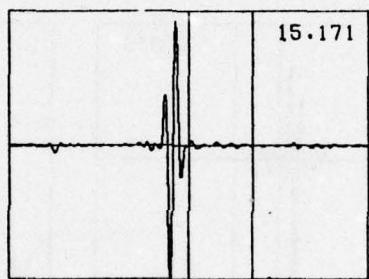
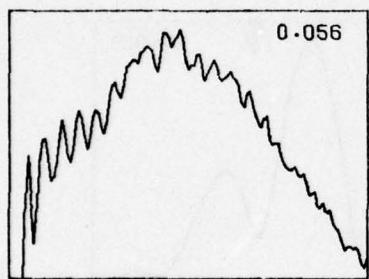


GT10

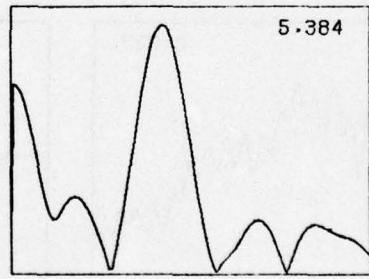
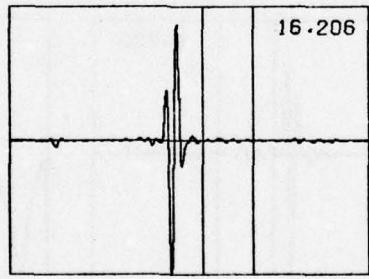
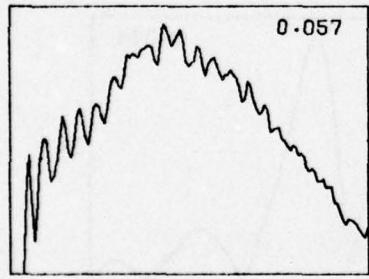
54



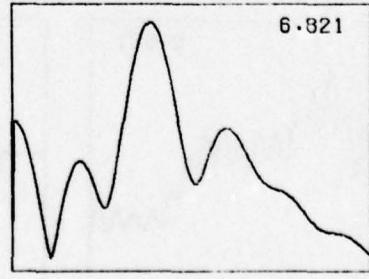
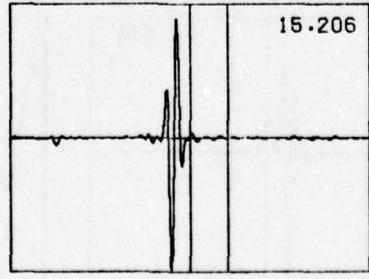
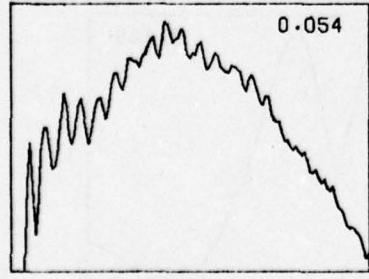
55



56



57

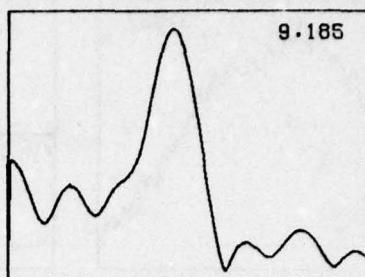
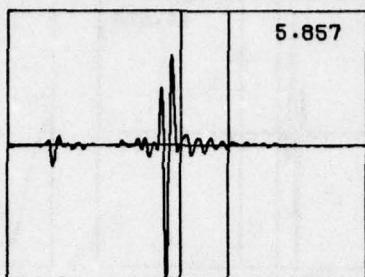
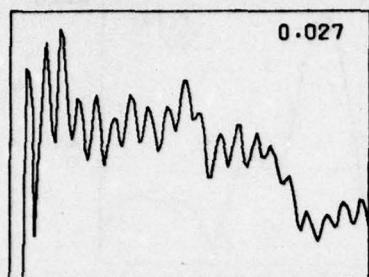


58

Type A mine, 3", 30%

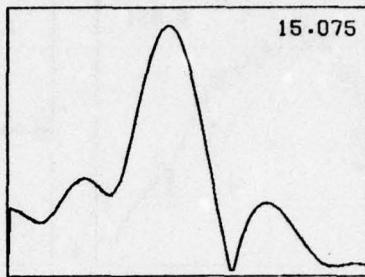
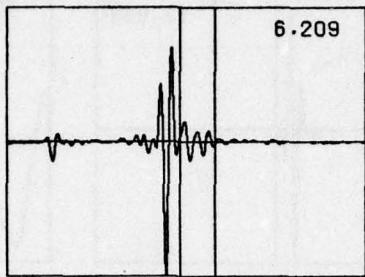
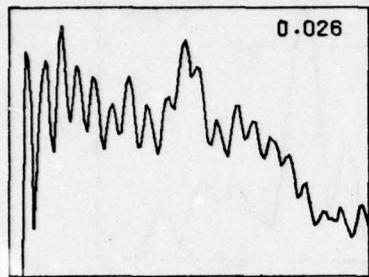
UNCLASSIFIED

UNCLASSIFIED

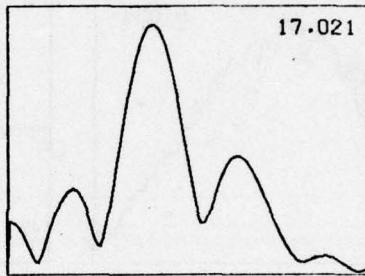
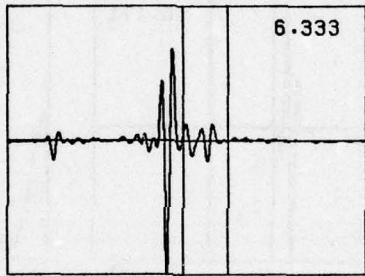
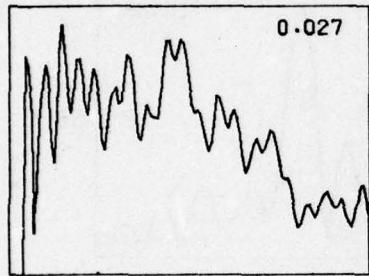


GT5

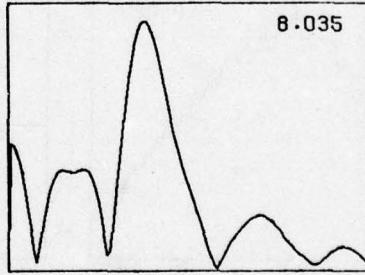
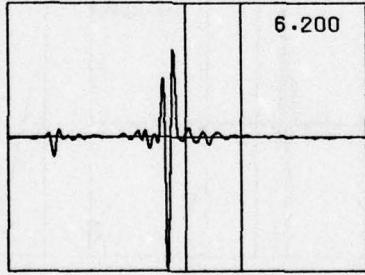
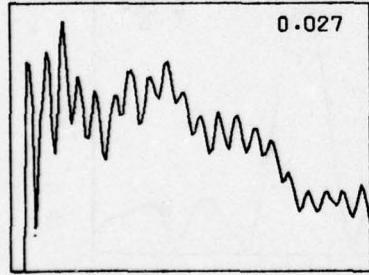
31



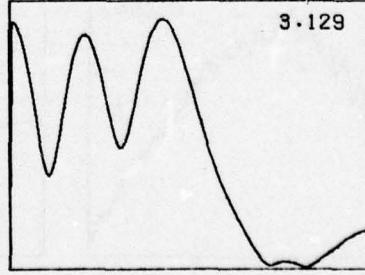
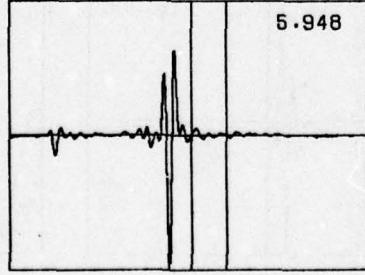
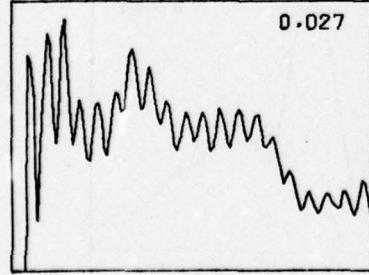
32



33



34

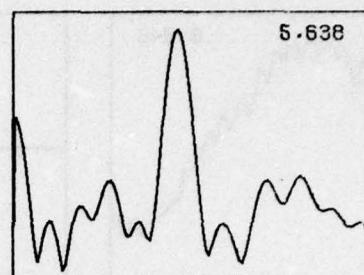
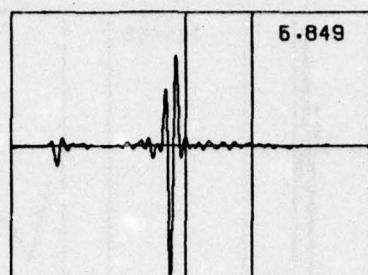
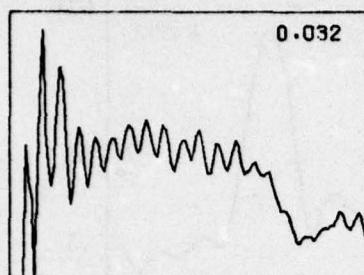


35

Type B mine, 6", 7%

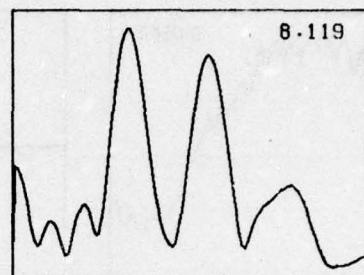
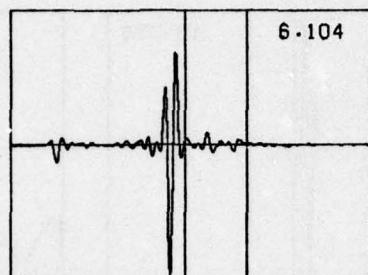
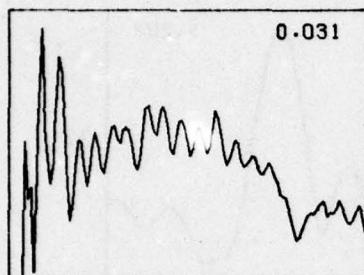
UNCLASSIFIED

UNCLASSIFIED

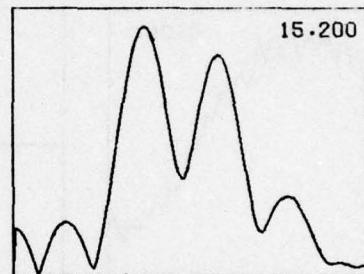
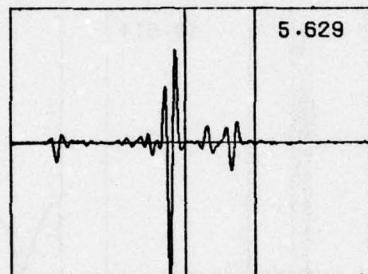
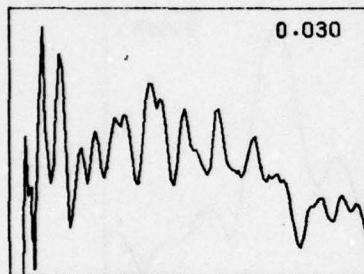


GT5

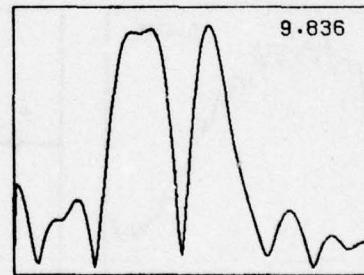
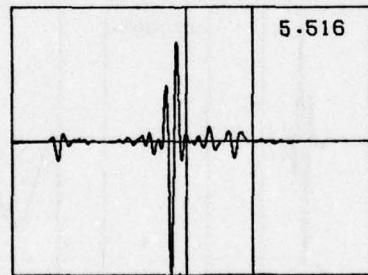
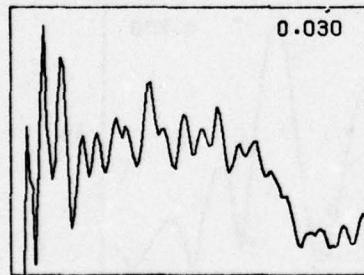
72



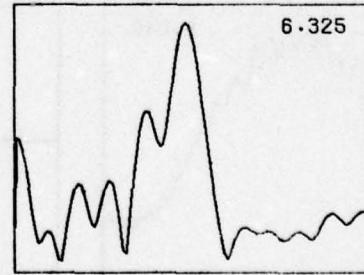
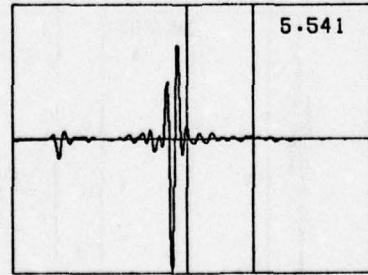
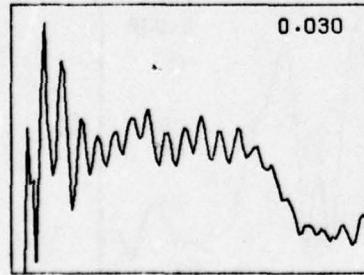
73



74



75



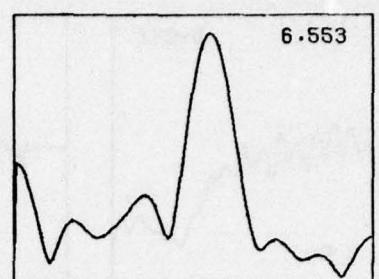
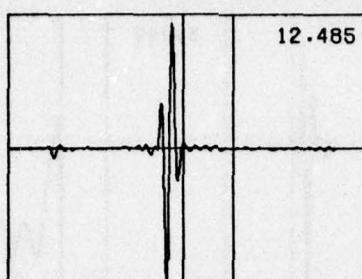
76

Type B mine, 3", 7%

UNCLASSIFIED

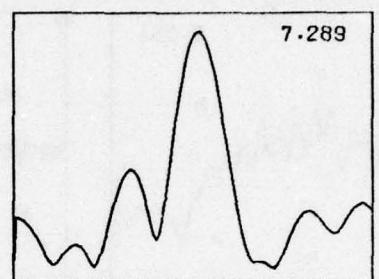
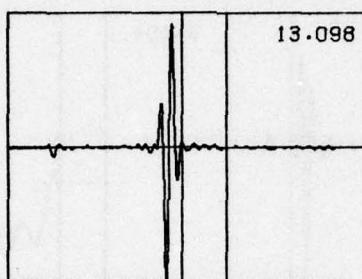
A-17

UNCLASSIFIED

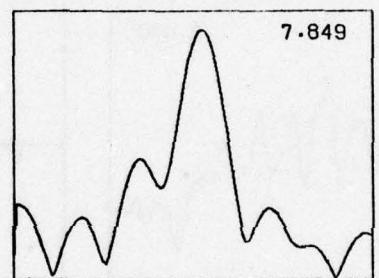
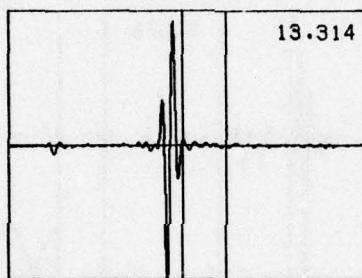
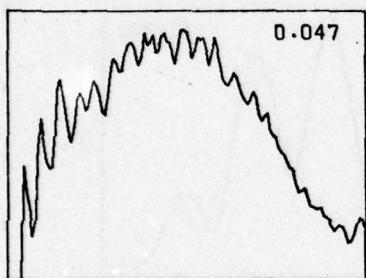


GT6

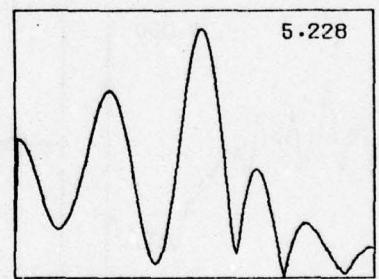
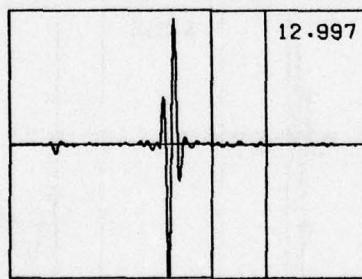
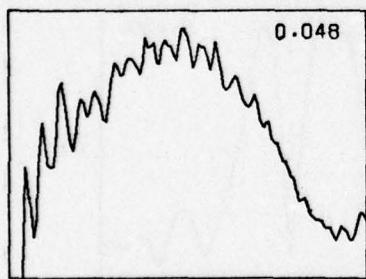
31



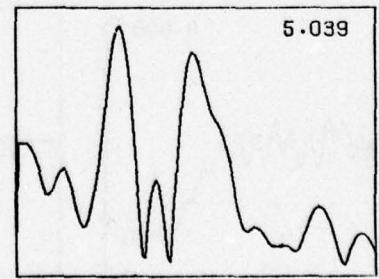
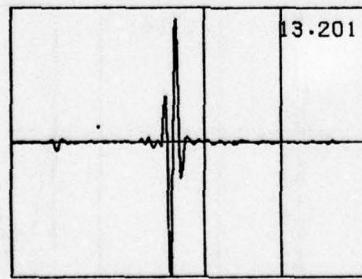
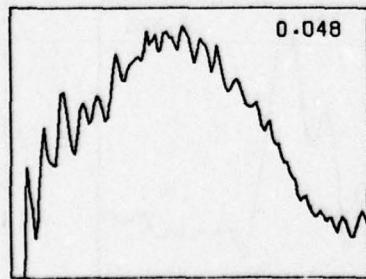
32



33



34



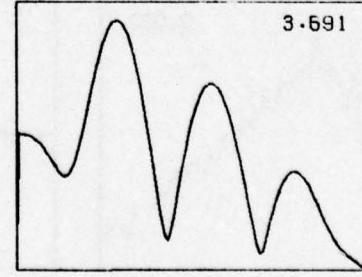
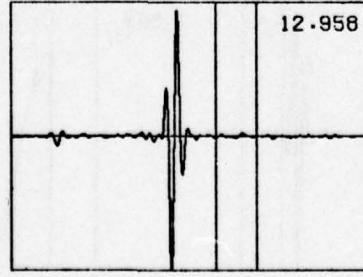
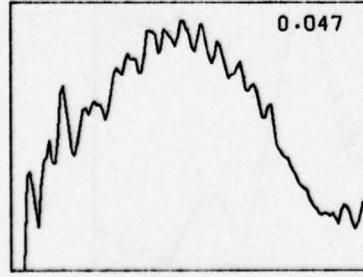
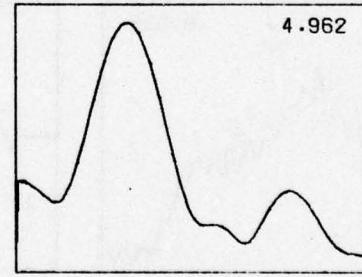
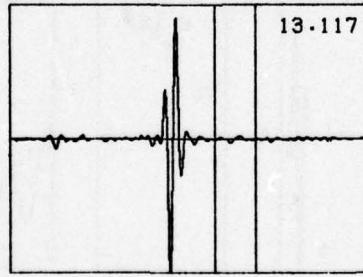
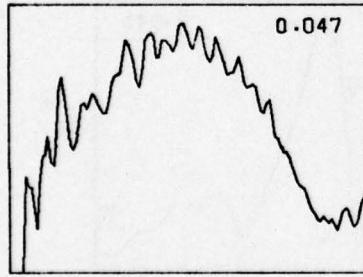
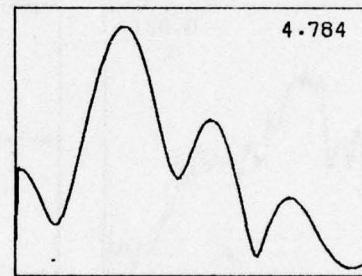
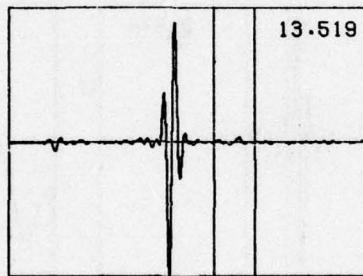
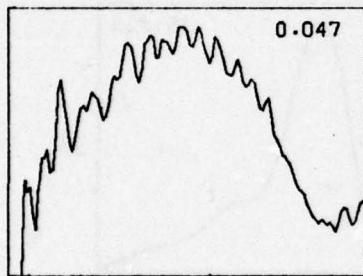
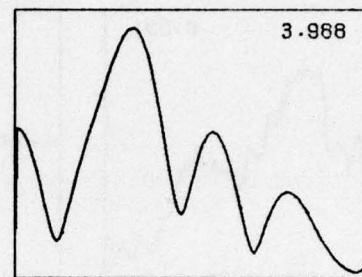
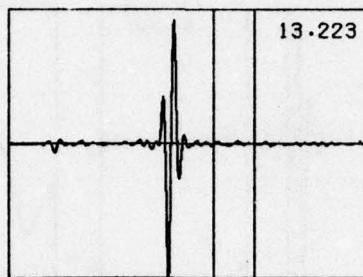
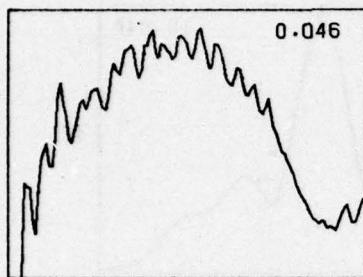
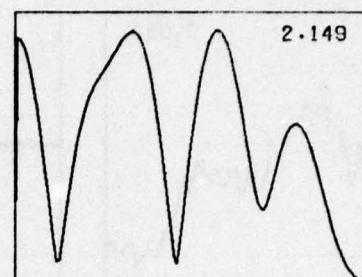
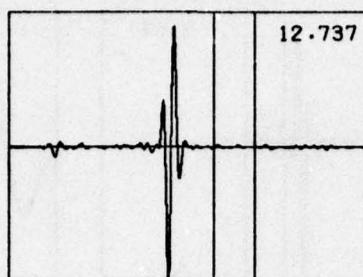
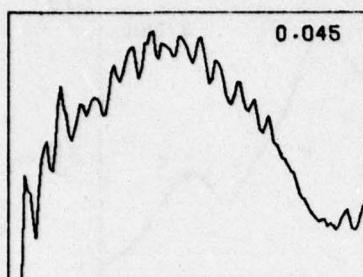
35

Type B mine, 6", 17%

UNCLASSIFIED

A-18

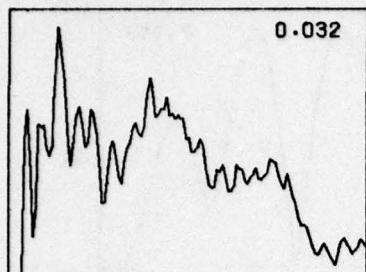
UNCLASSIFIED



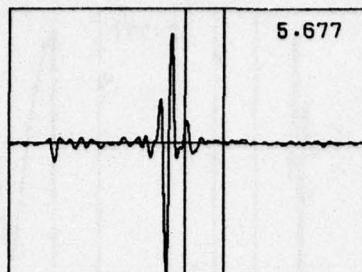
Type B mine, 6", 18%

UNCLASSIFIED

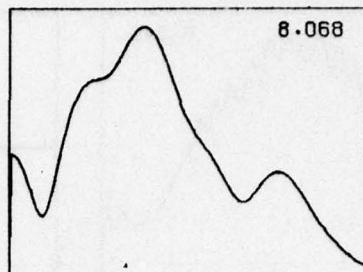
UNCLASSIFIED



0.032



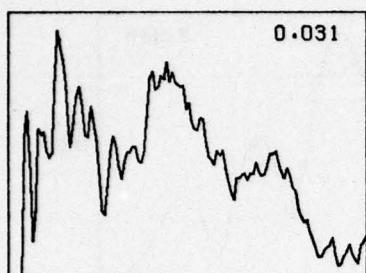
5.677



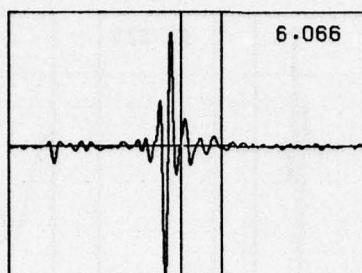
8.068

GT9

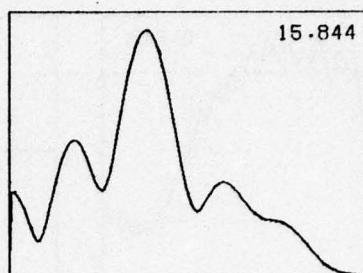
31



0.031

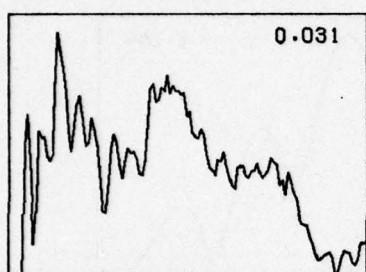


6.066

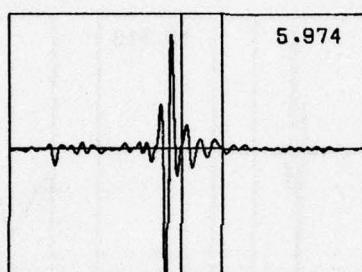


15.844

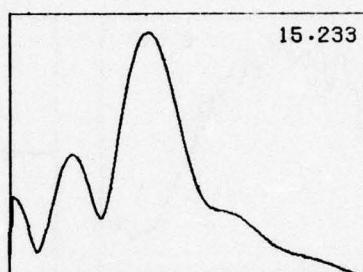
32



0.031

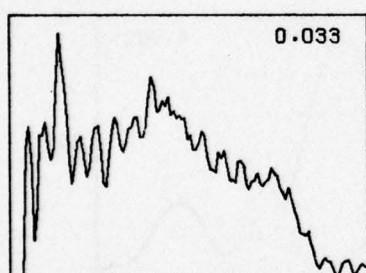


5.974

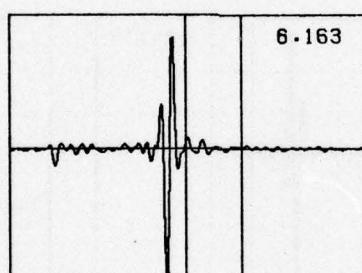


15.233

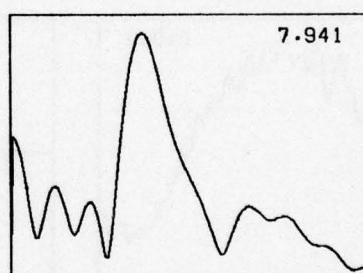
33



0.033

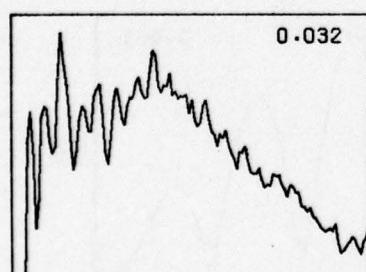


6.163

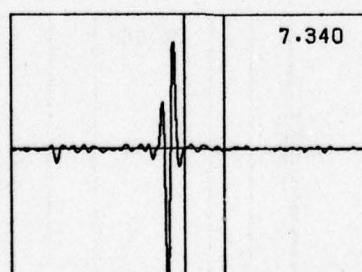


7.941

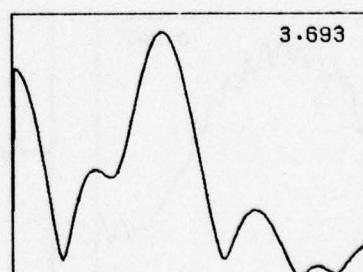
34



0.032



7.340



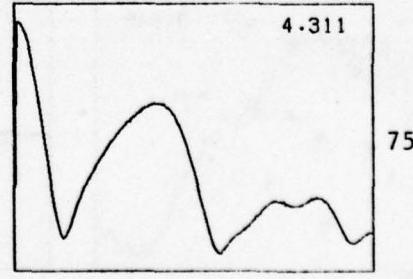
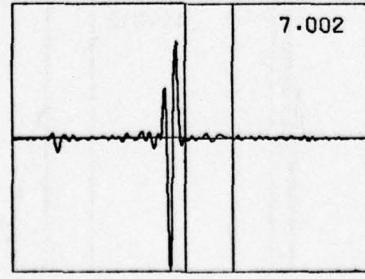
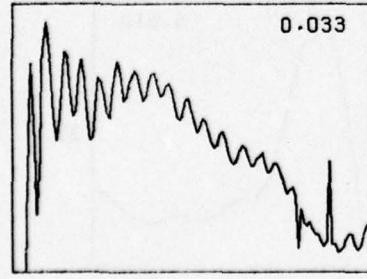
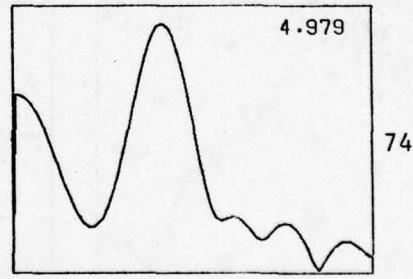
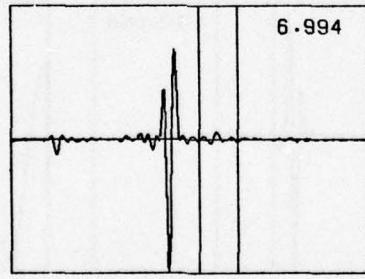
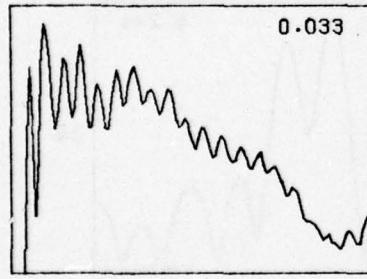
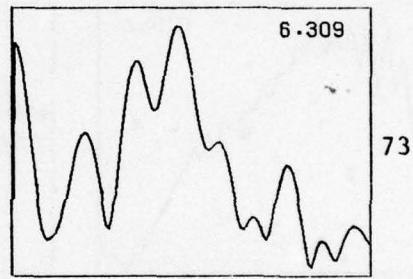
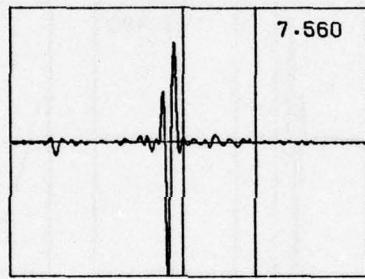
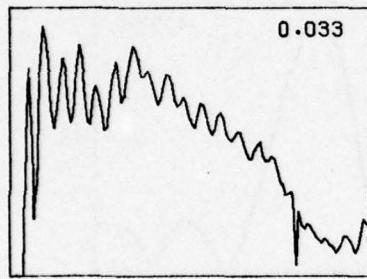
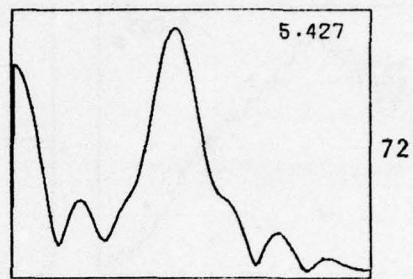
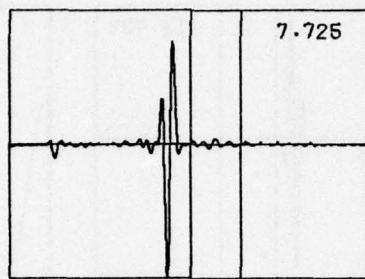
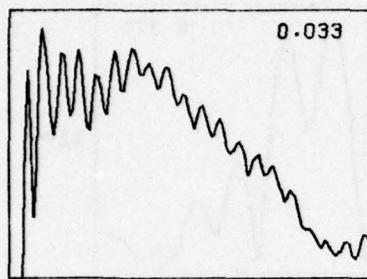
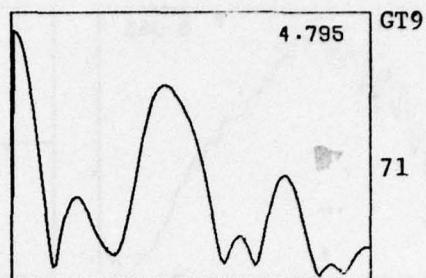
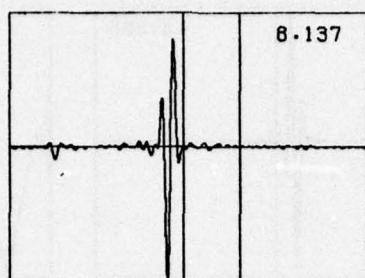
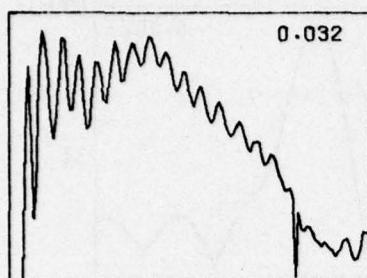
3.693

35

Type B mine, 3", 12-20%

UNCLASSIFIED

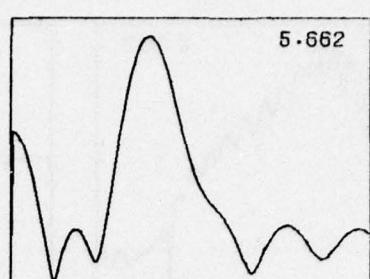
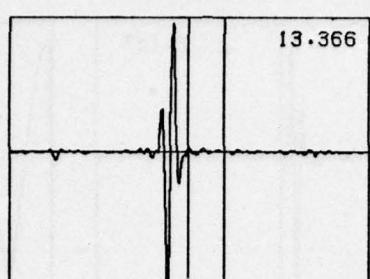
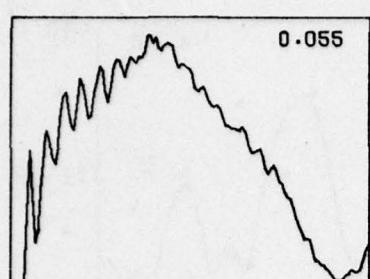
UNCLASSIFIED



Type B mine, 6", 13-16%

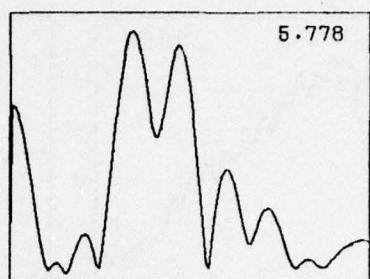
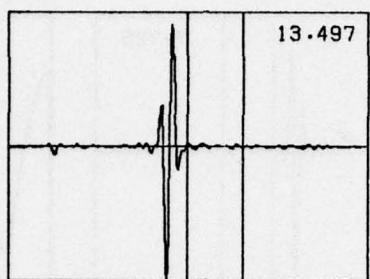
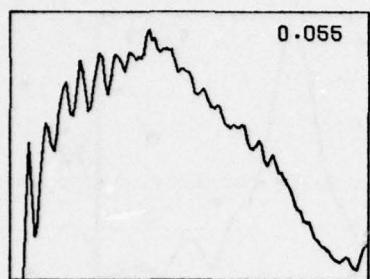
UNCLASSIFIED

UNCLASSIFIED

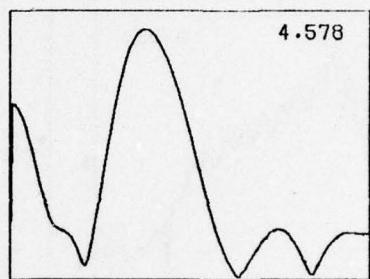
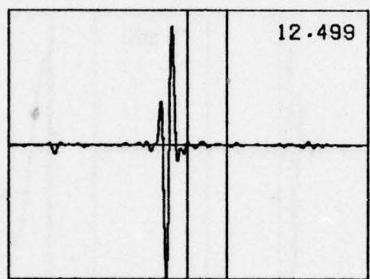
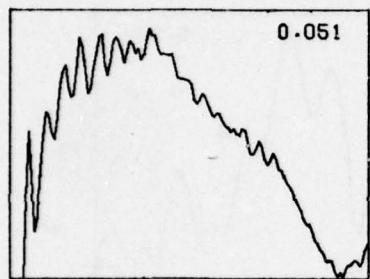


GT10

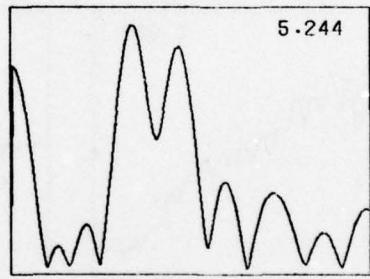
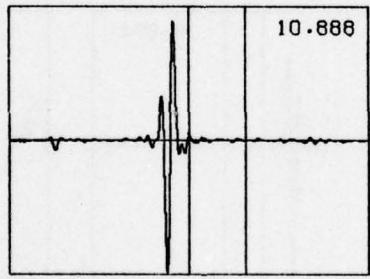
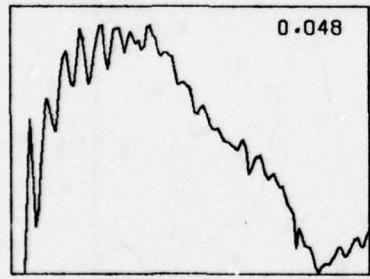
31



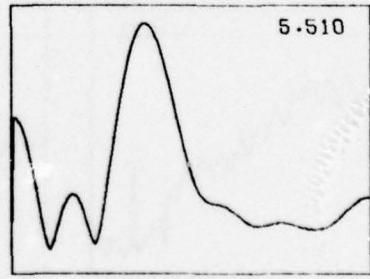
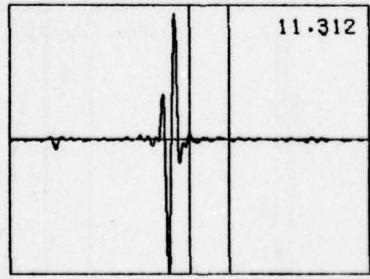
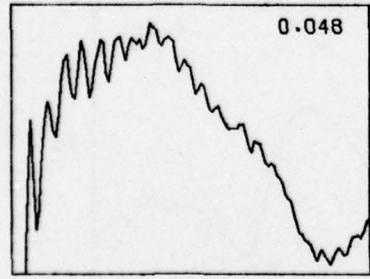
32



33



34



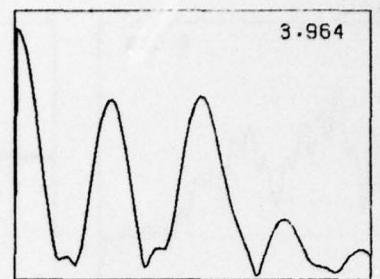
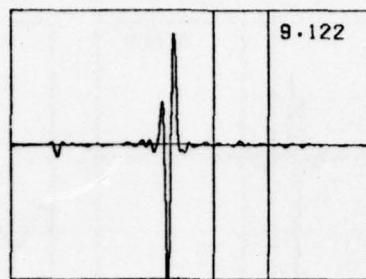
35

Type B mine, 6", 26-30%

UNCLASSIFIED

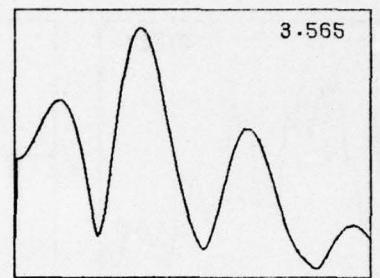
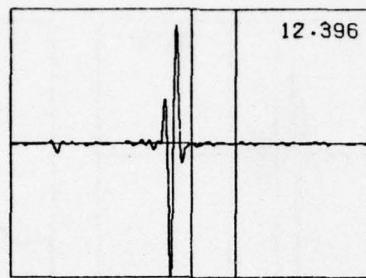
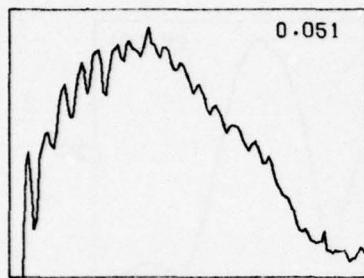
A-22

UNCLASSIFIED

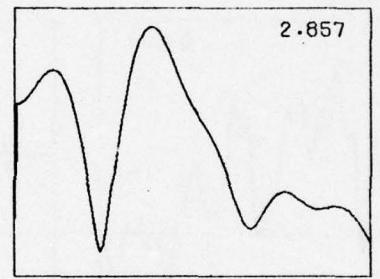
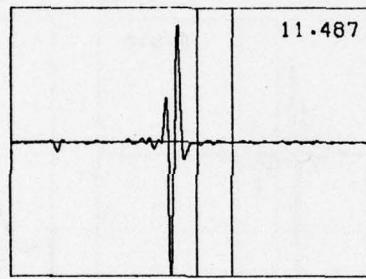
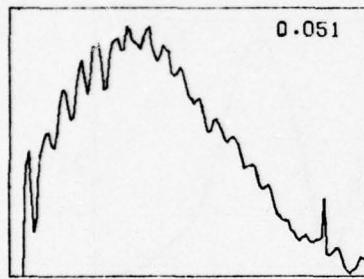


GT10

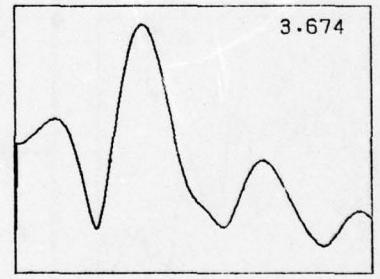
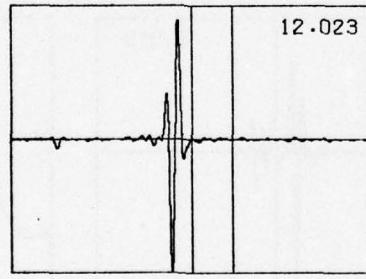
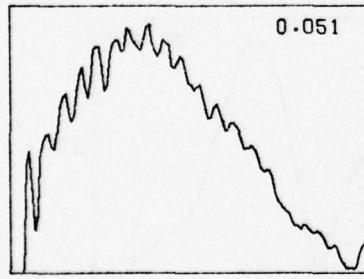
72



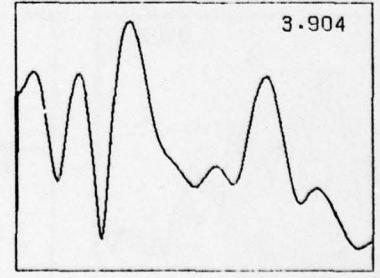
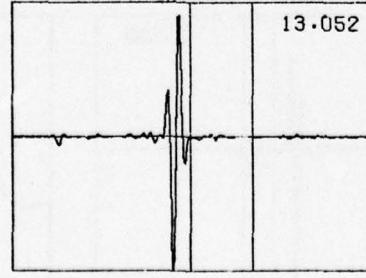
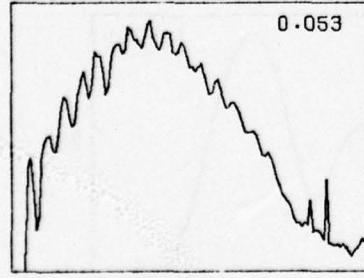
73



74



75

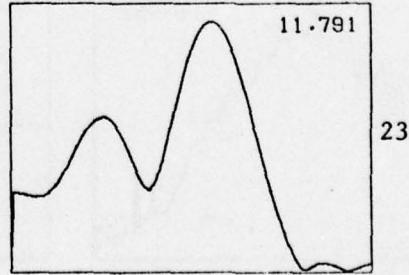
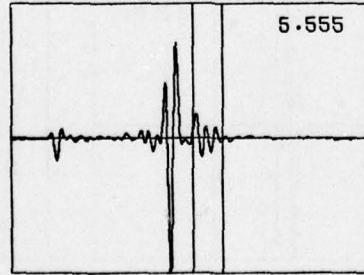
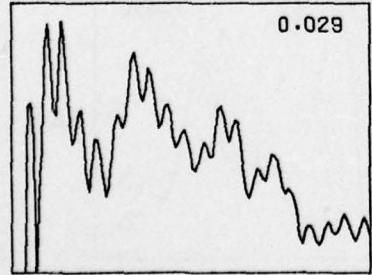
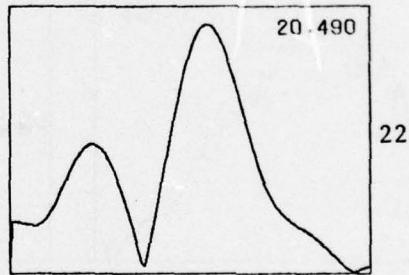
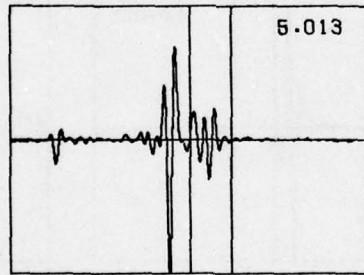
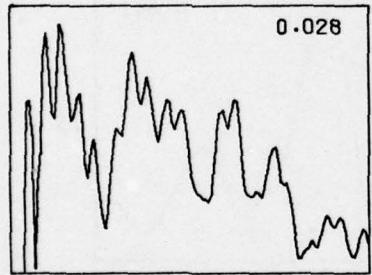
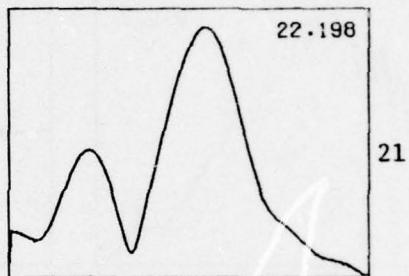
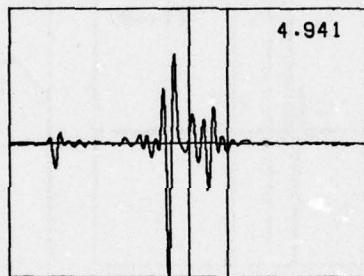
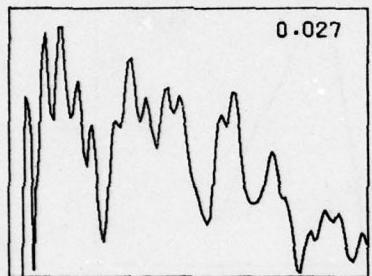
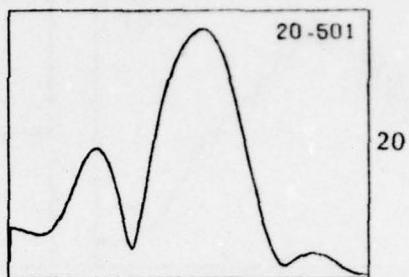
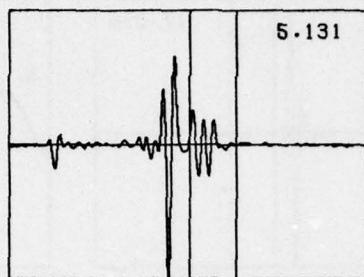
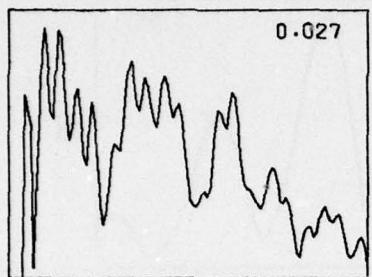
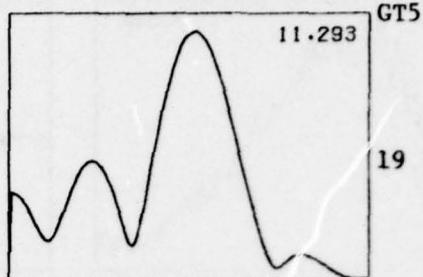
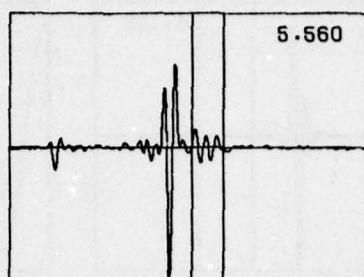
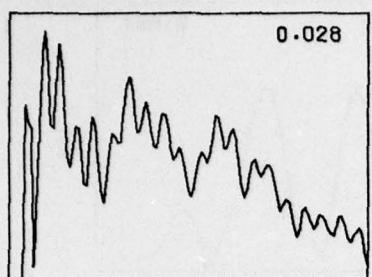


76

Type B mine, 3", 30%

UNCLASSIFIED

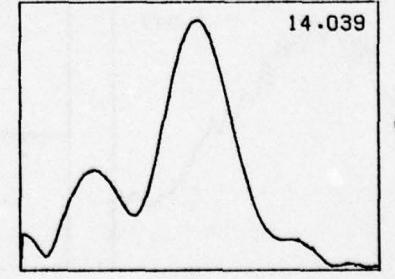
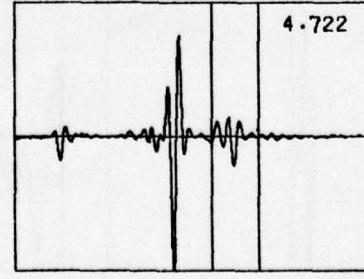
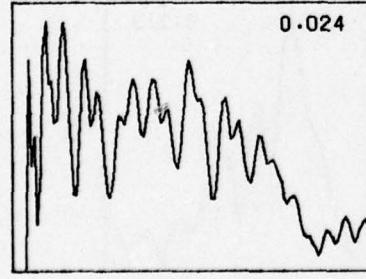
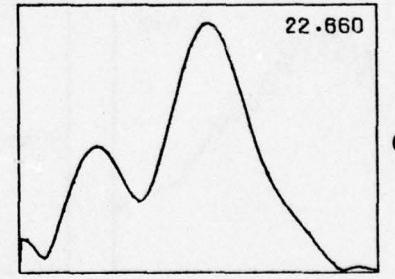
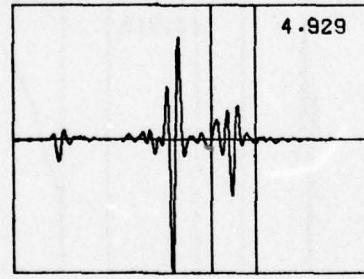
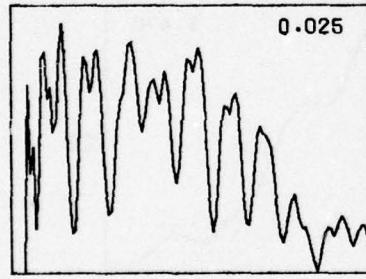
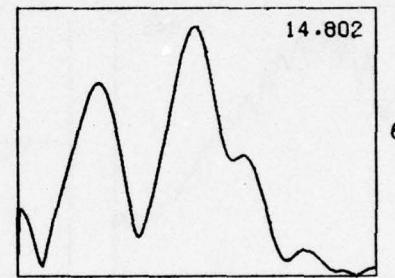
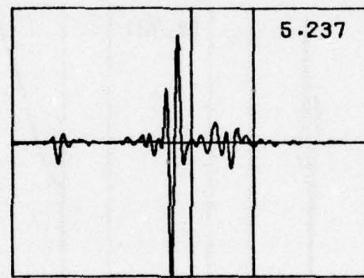
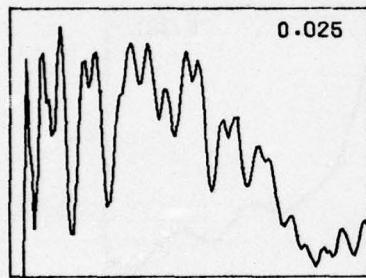
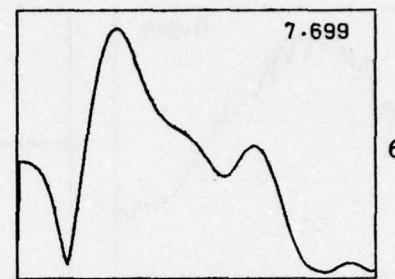
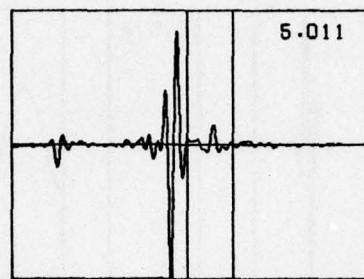
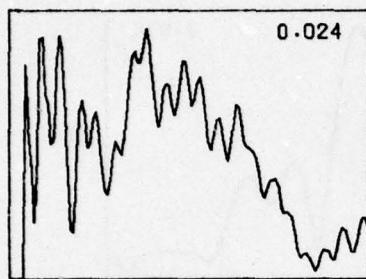
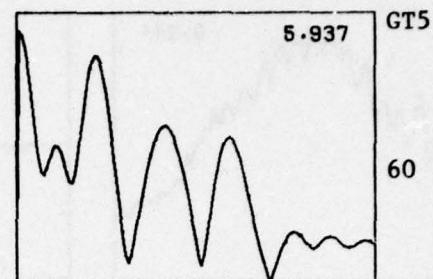
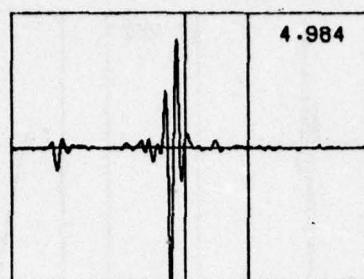
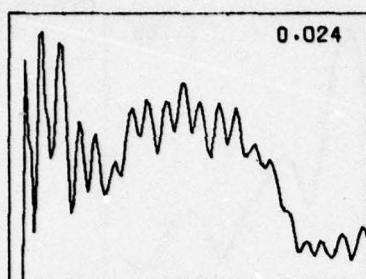
UNCLASSIFIED



Type C mine, 3", 7%

UNCLASSIFIED

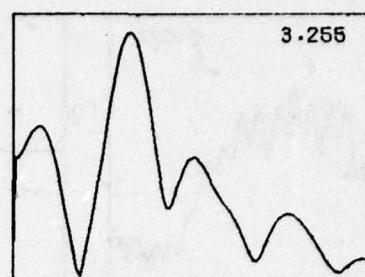
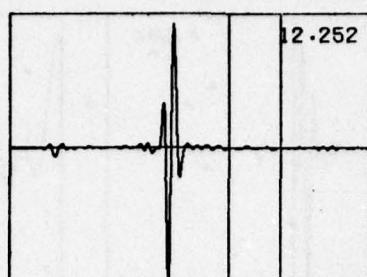
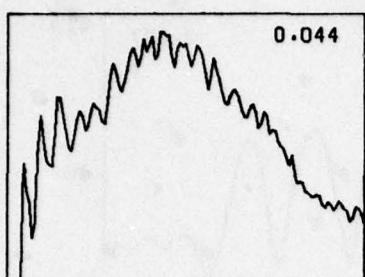
UNCLASSIFIED



Type C mine, 6", 7%

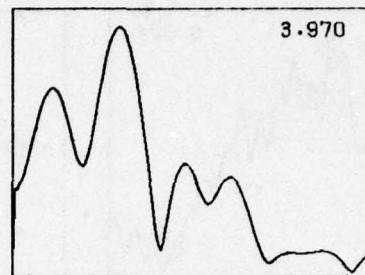
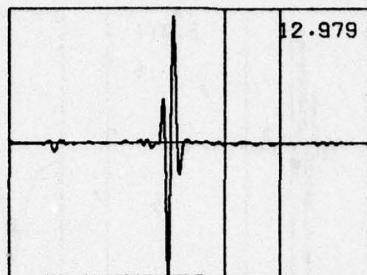
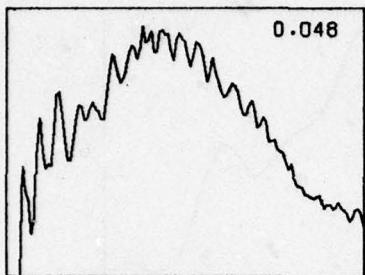
UNCLASSIFIED

UNCLASSIFIED

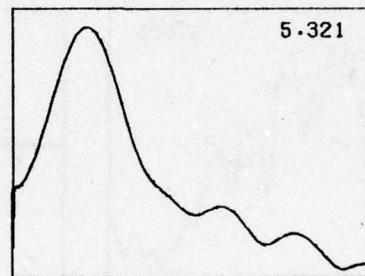
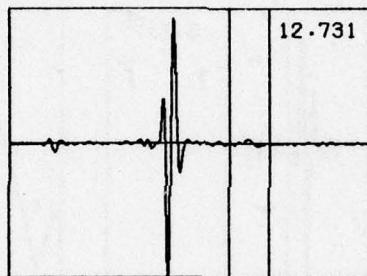
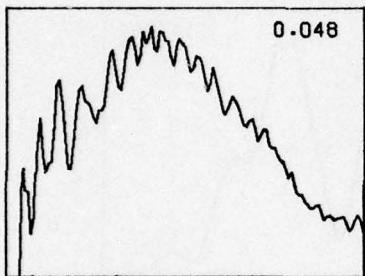


GT6

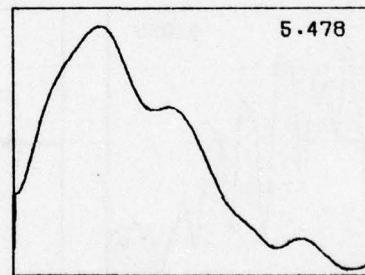
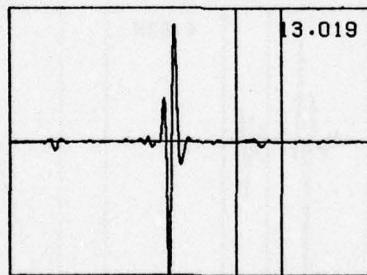
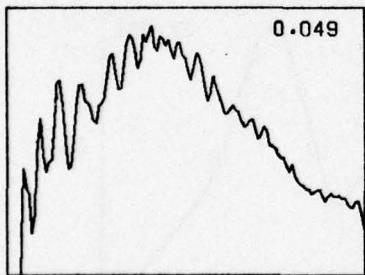
19



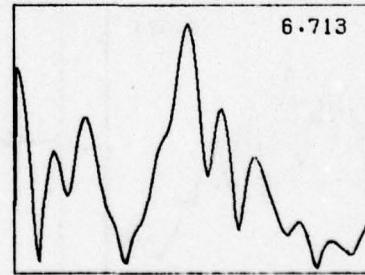
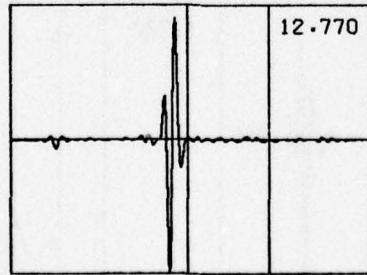
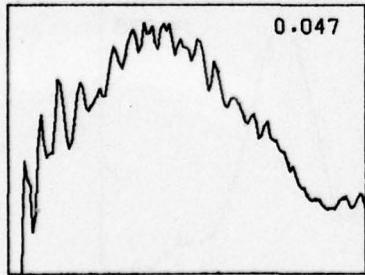
20



21



22

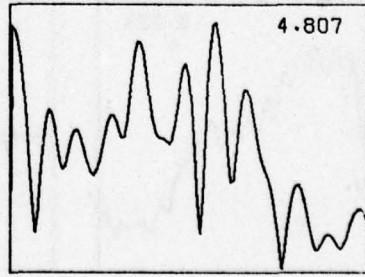
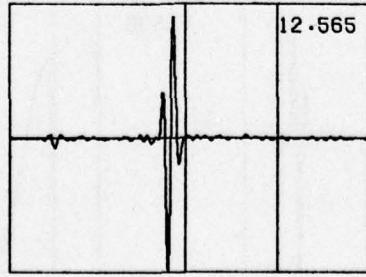
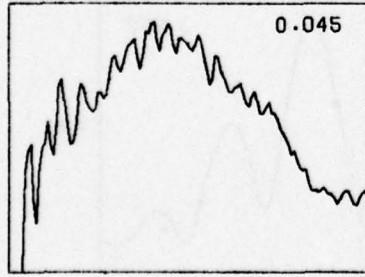
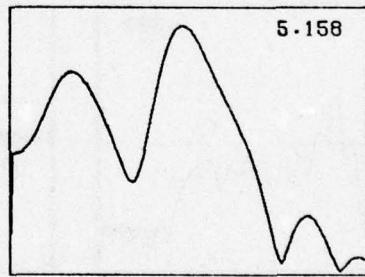
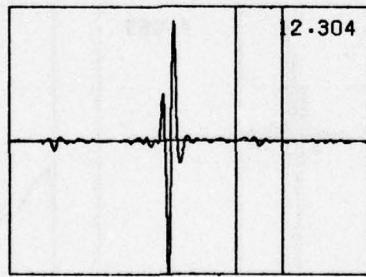
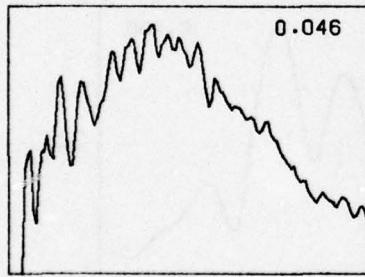
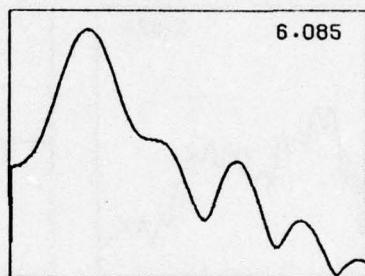
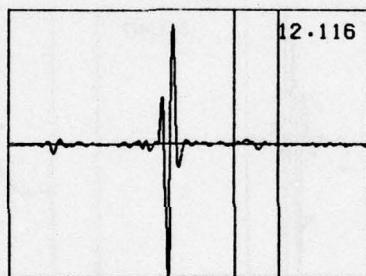
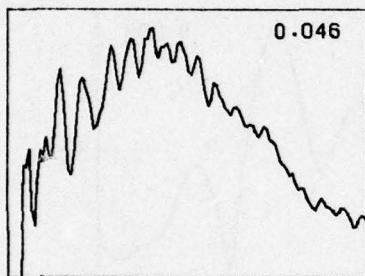
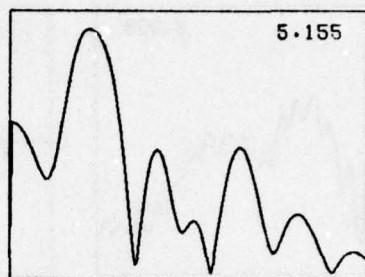
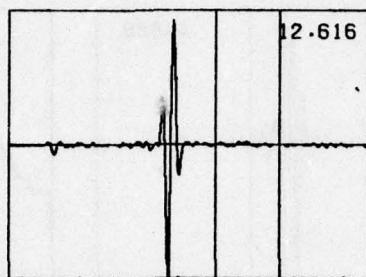
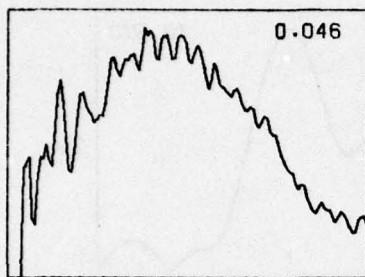
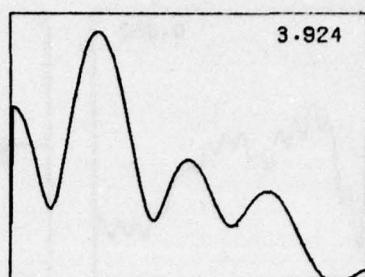
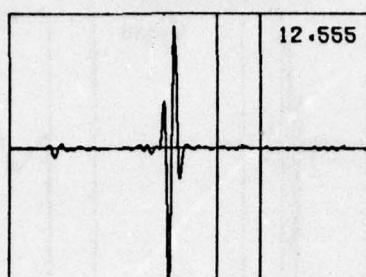
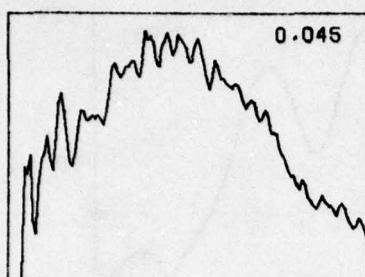


23

Type C mine, 6", 17%

UNCLASSIFIED

UNCLASSIFIED

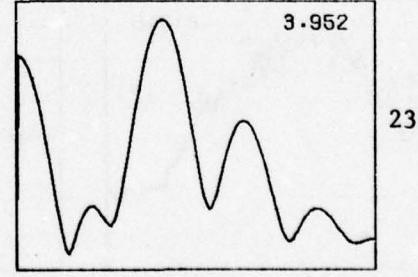
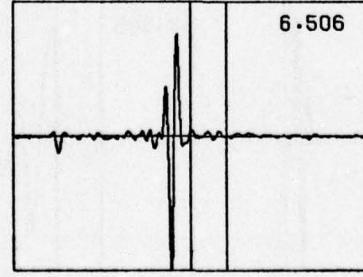
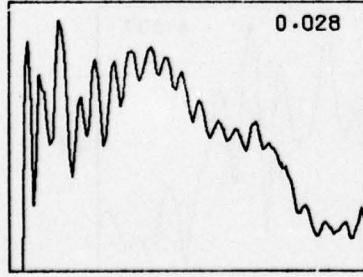
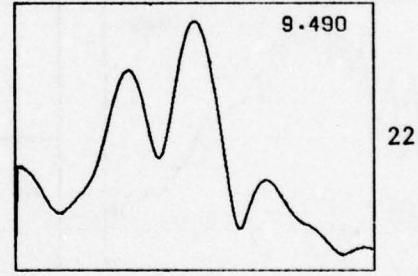
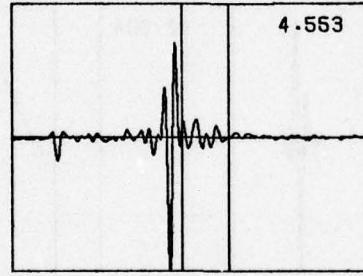
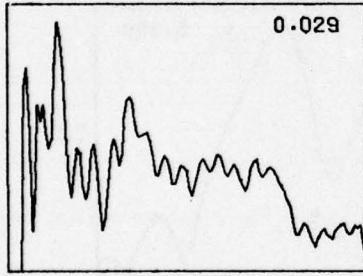
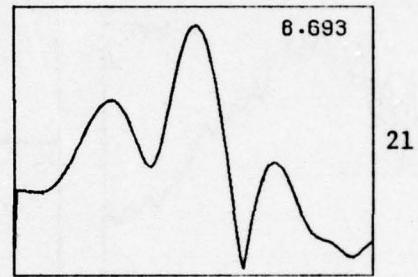
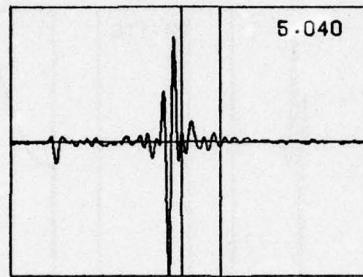
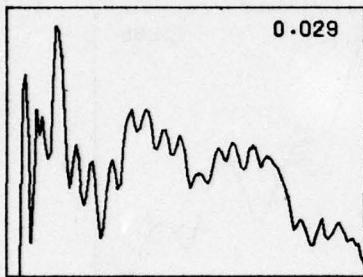
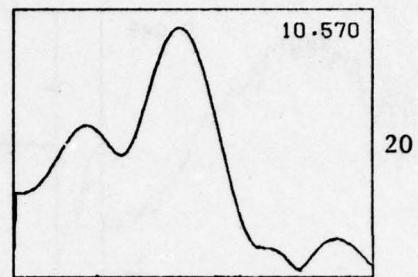
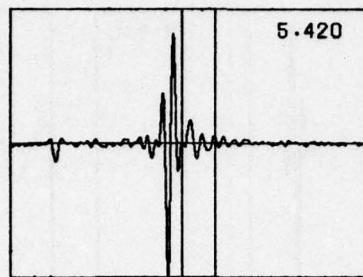
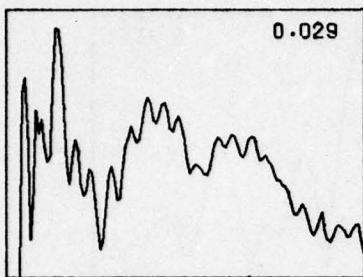
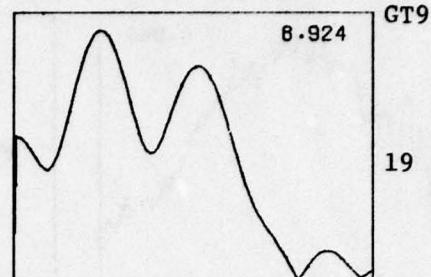
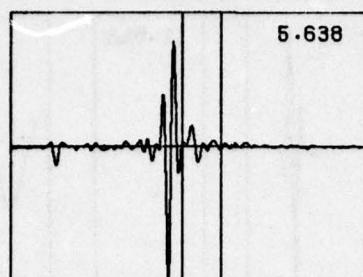
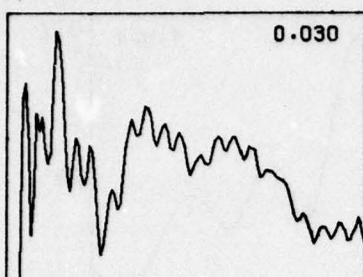


Type C mine, 6", 18%

UNCLASSIFIED

A-27

UNCLASSIFIED

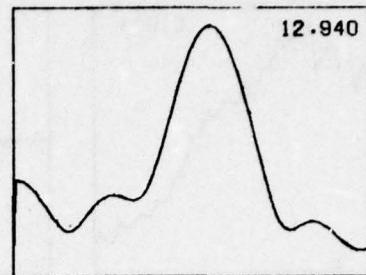
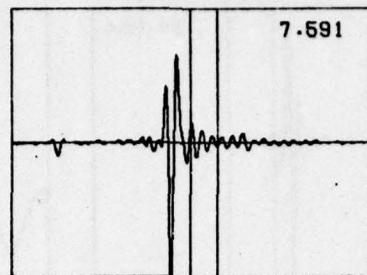
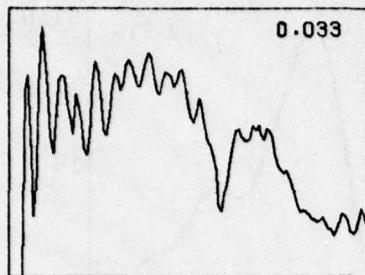


Type C mine, 3", 12-20%

UNCLASSIFIED

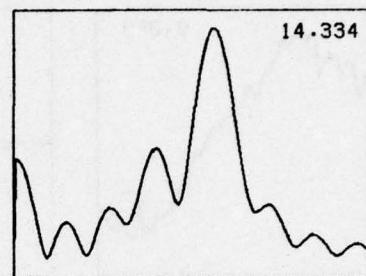
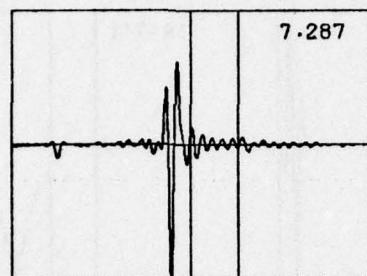
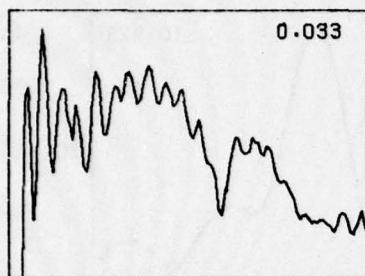
A-28

UNCLASSIFIED

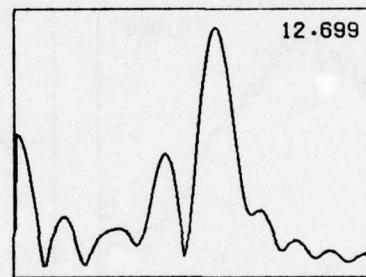
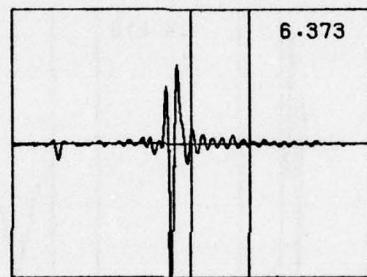
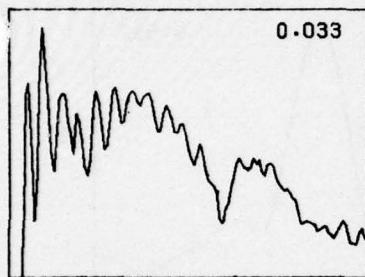


GT9

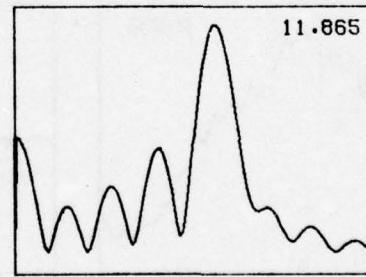
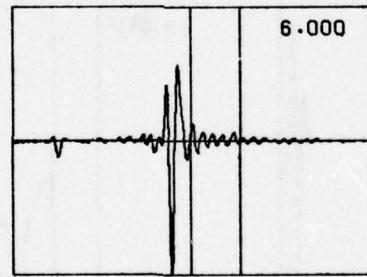
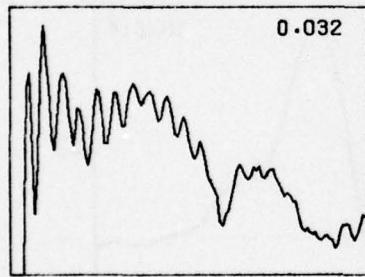
60



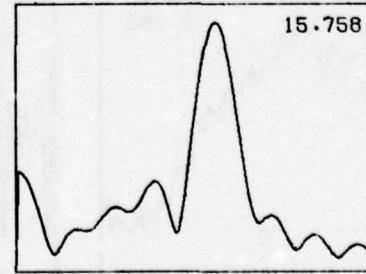
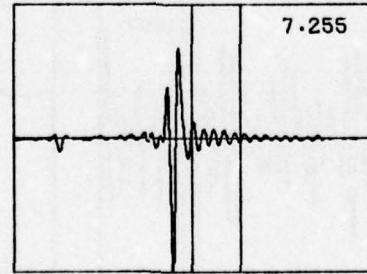
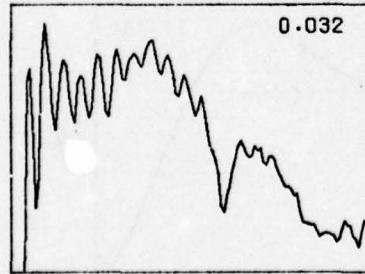
61



62



63

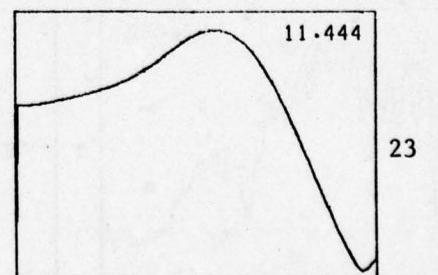
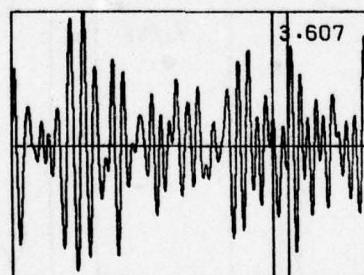
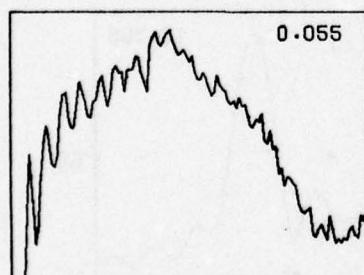
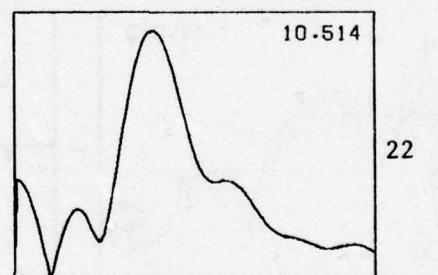
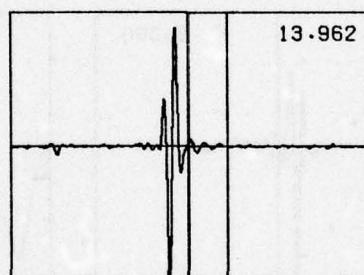
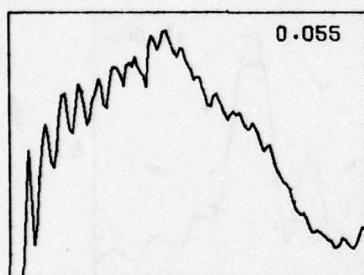
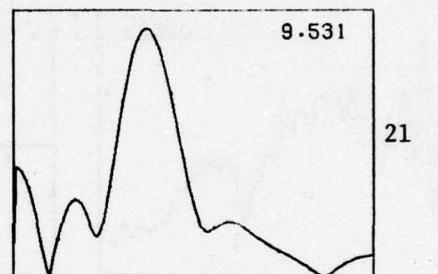
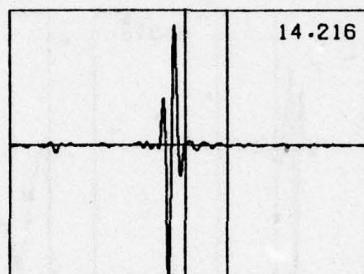
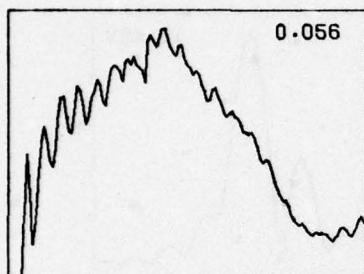
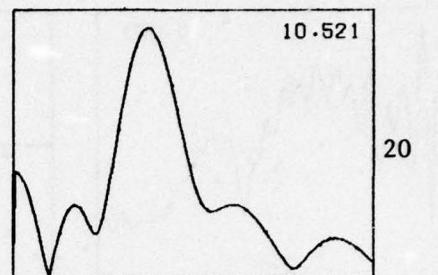
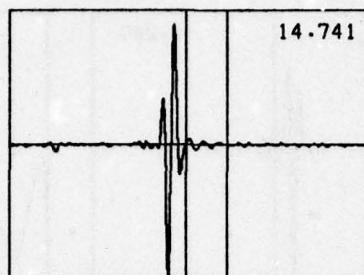
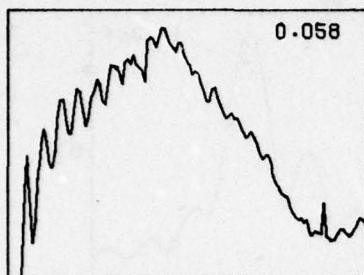
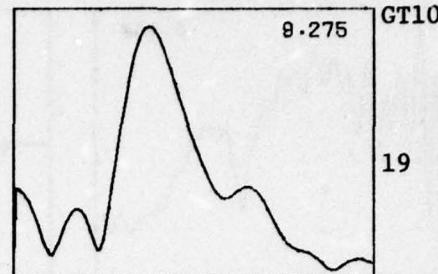
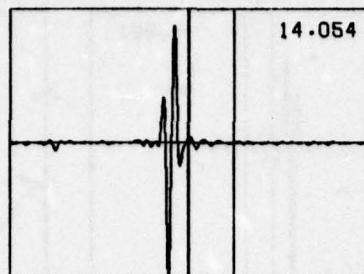
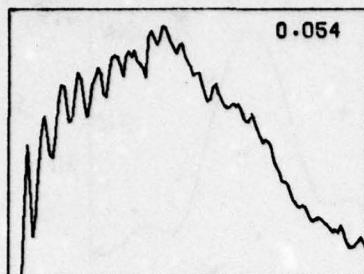


64

Type C mine, 13-16%

UNCLASSIFIED

UNCLASSIFIED

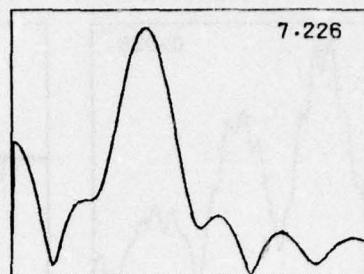
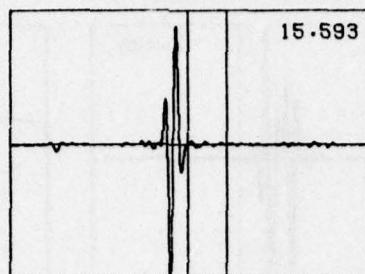
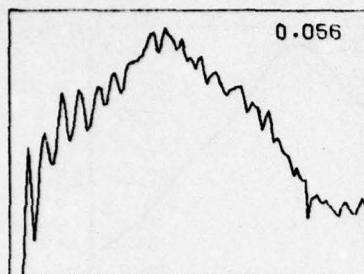


Type C mine, 6", 26-30%

UNCLASSIFIED

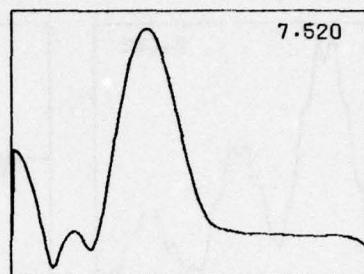
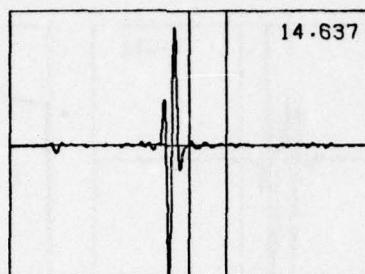
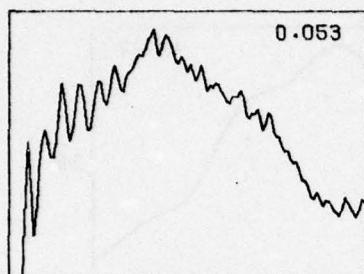
A-30

UNCLASSIFIED

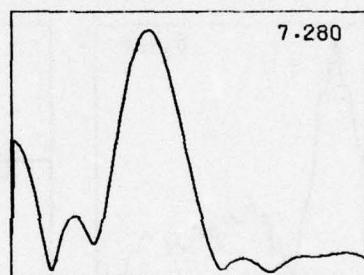
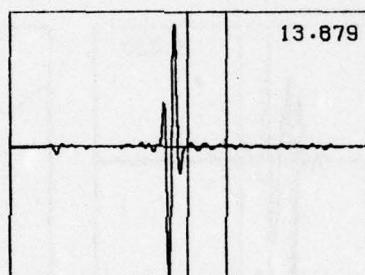
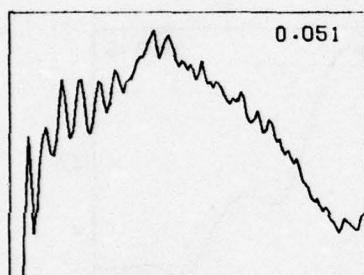


GT10

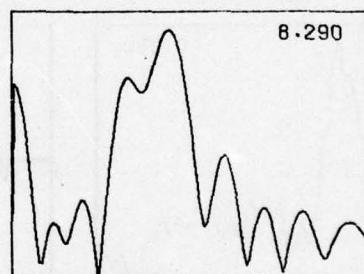
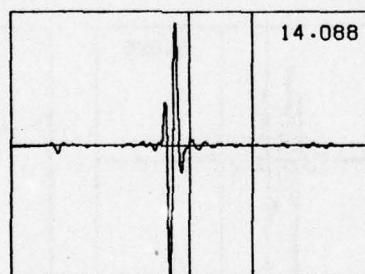
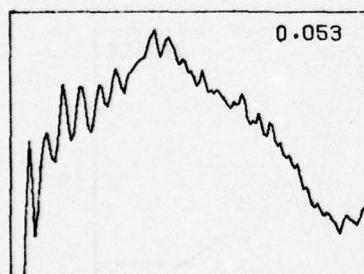
60



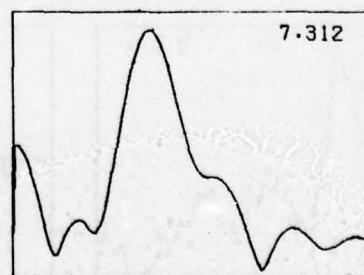
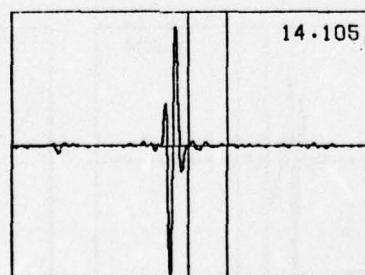
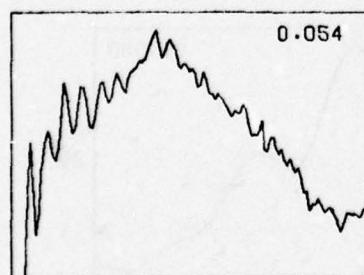
61



62



63

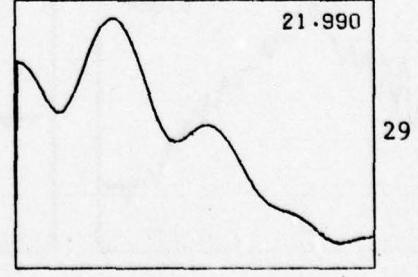
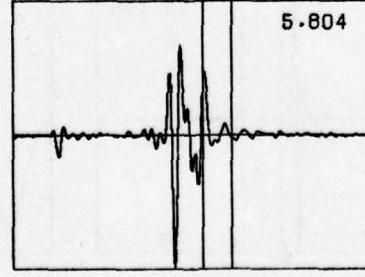
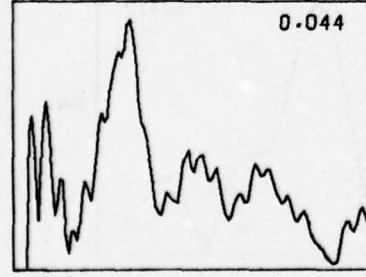
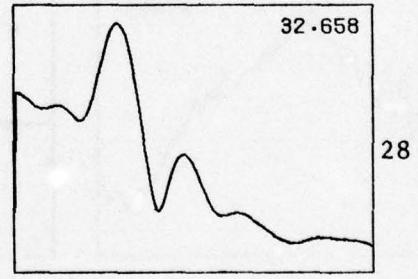
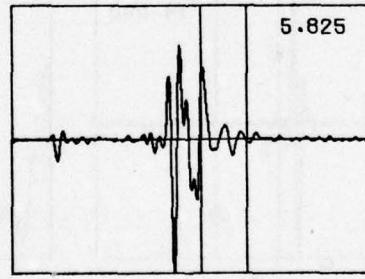
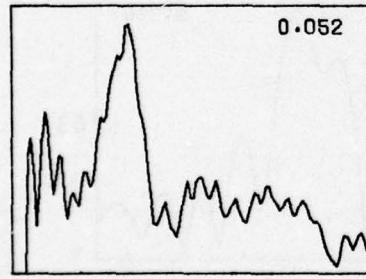
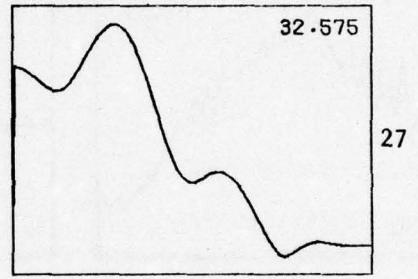
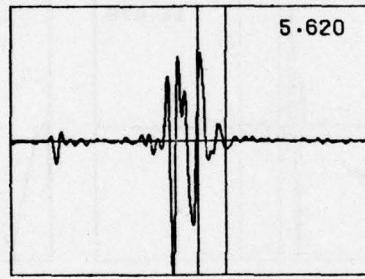
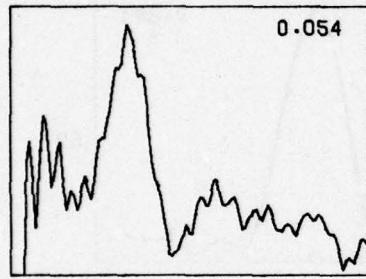
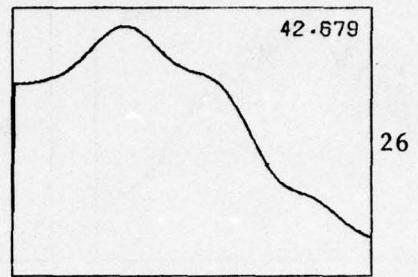
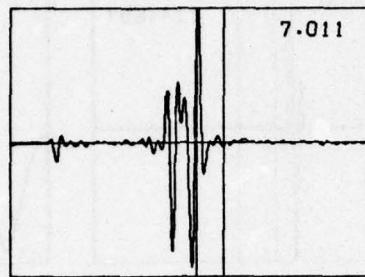
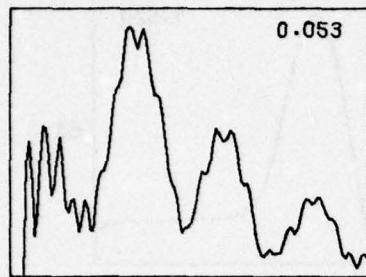
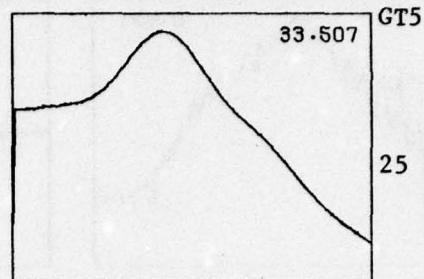
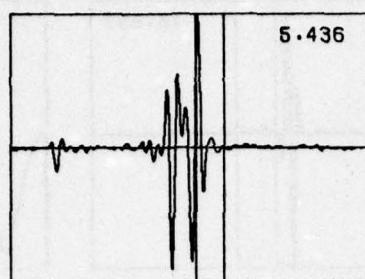
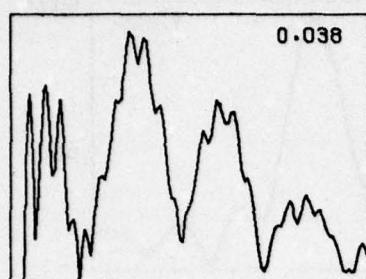


64

Type C mine, 3", 30%

UNCLASSIFIED

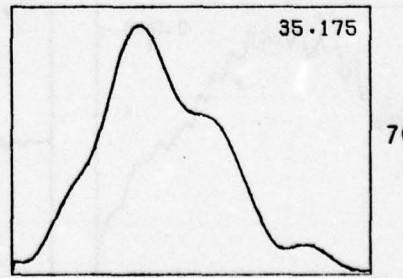
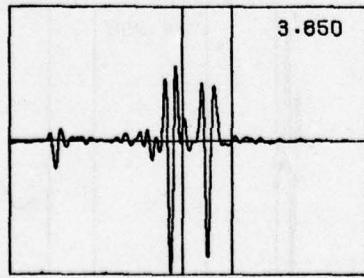
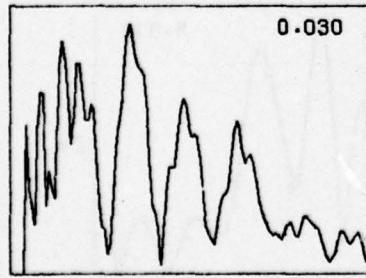
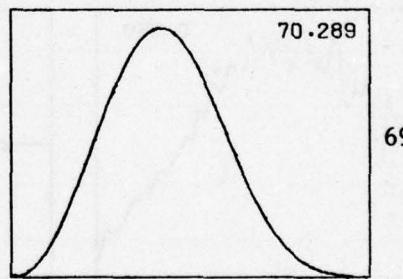
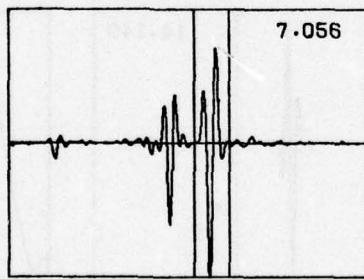
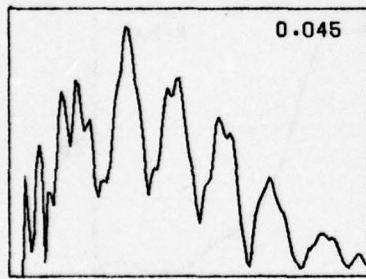
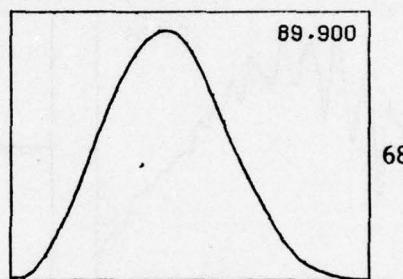
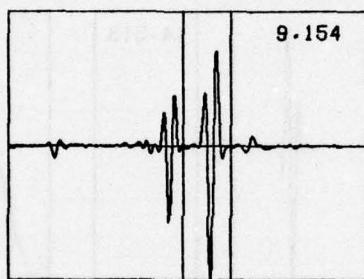
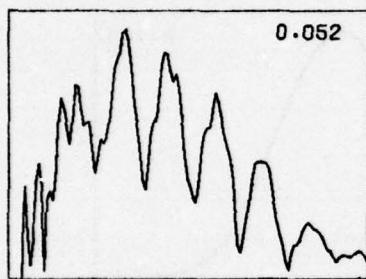
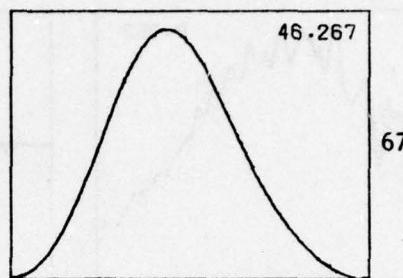
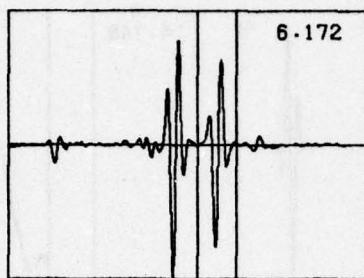
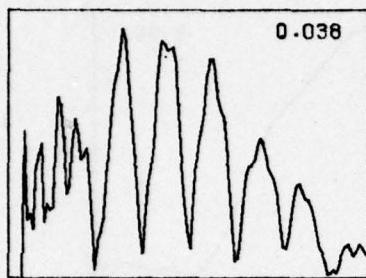
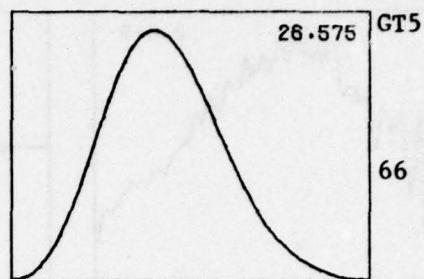
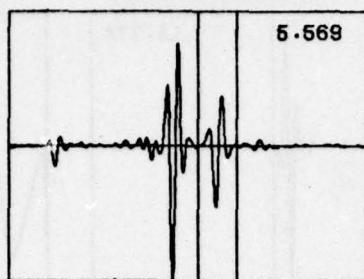
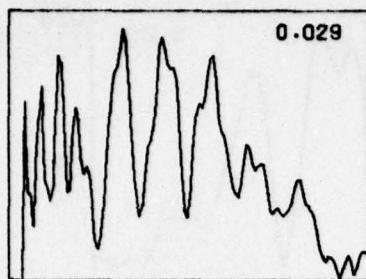
UNCLASSIFIED



Metal Plate 3", 7%

UNCLASSIFIED

UNCLASSIFIED

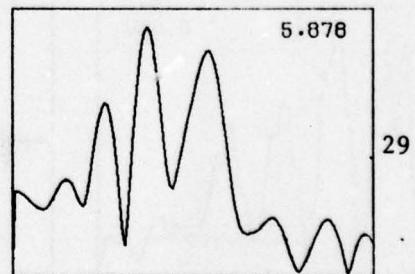
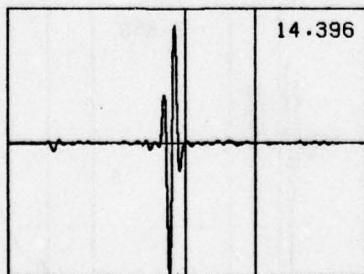
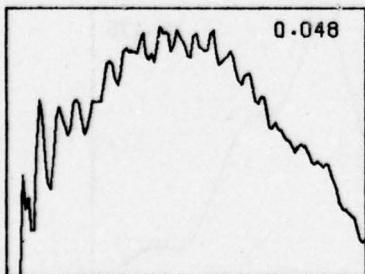
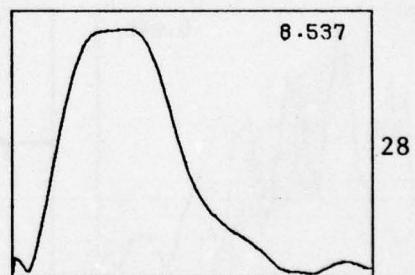
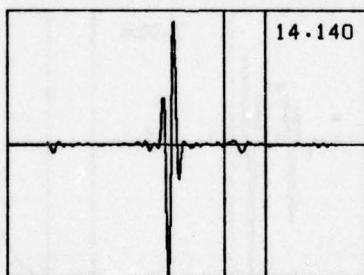
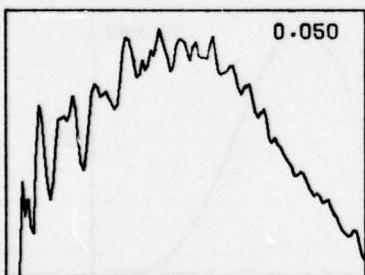
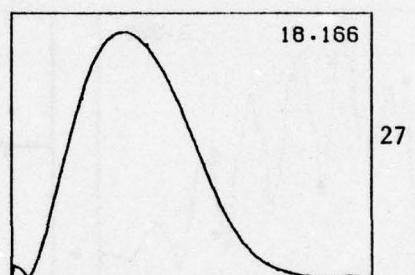
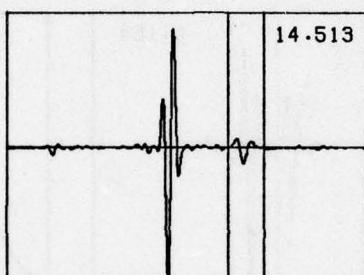
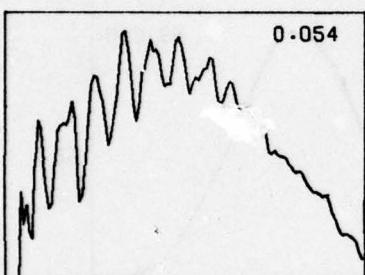
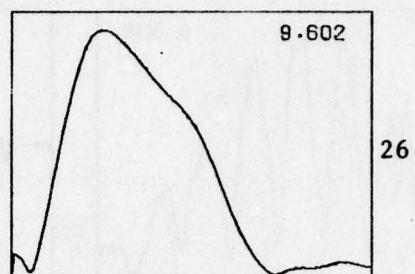
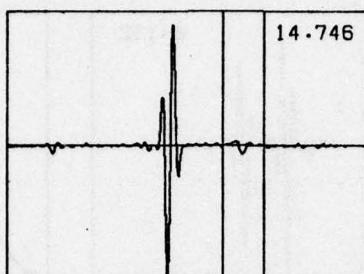
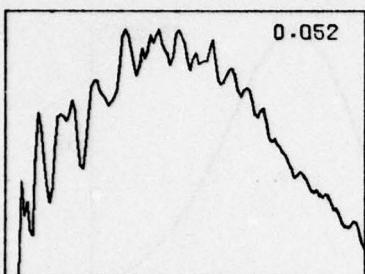
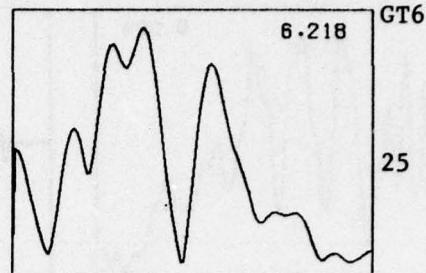
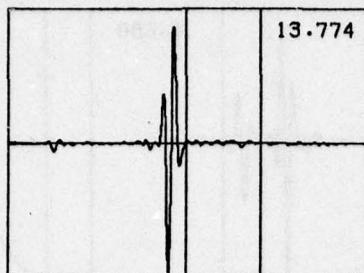
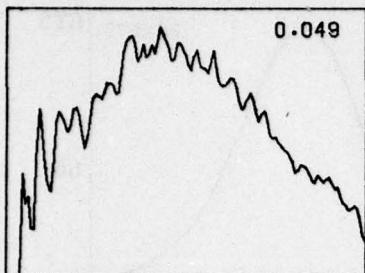


Metal Plate, 6", 7%

UNCLASSIFIED

A-33

UNCLASSIFIED

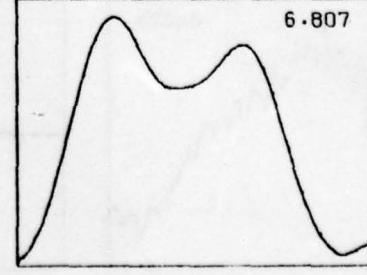
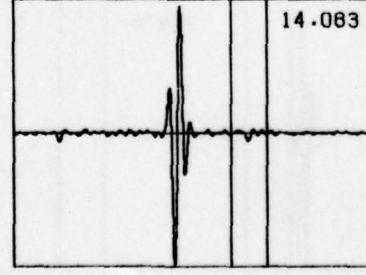
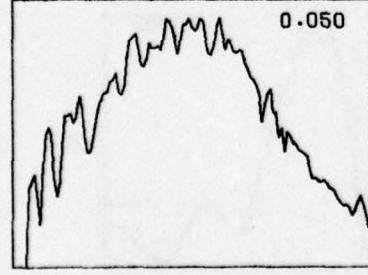
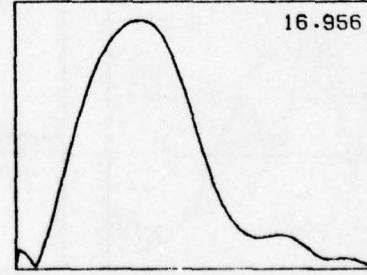
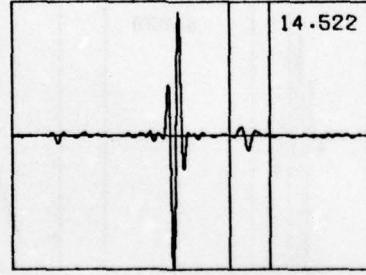
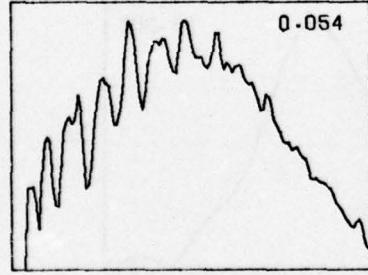
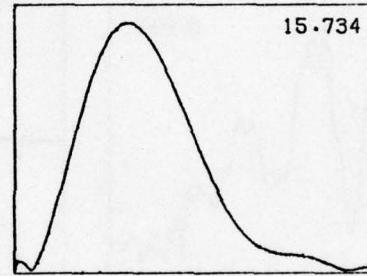
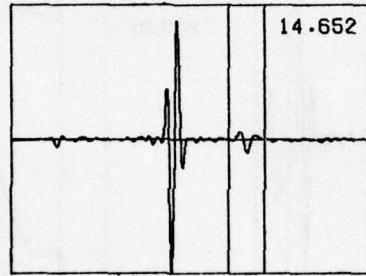
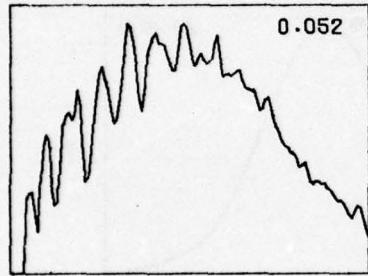
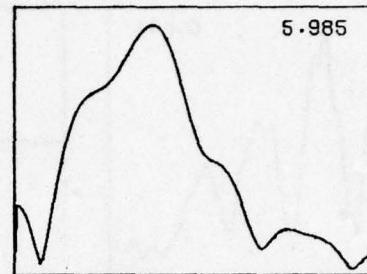
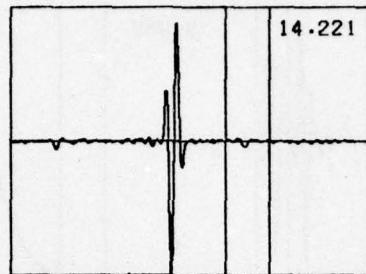
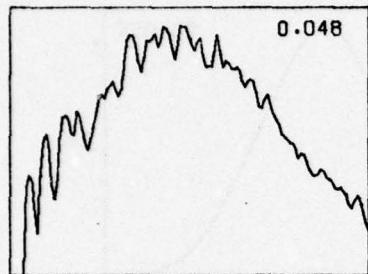
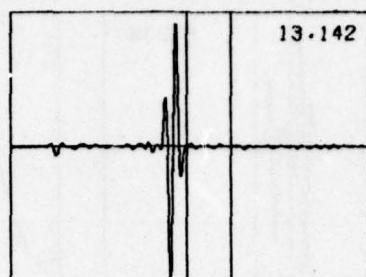
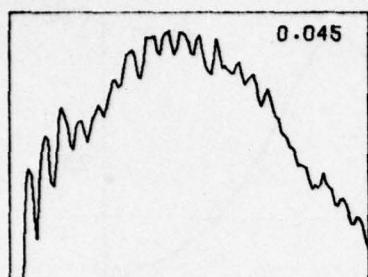


Metal Plate, 6", 17%

UNCLASSIFIED

A-34

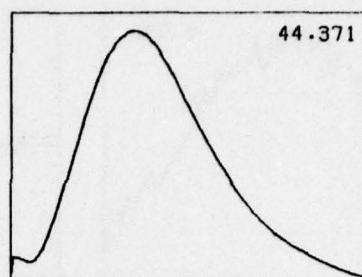
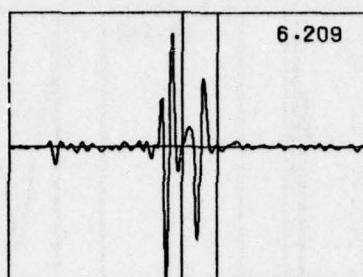
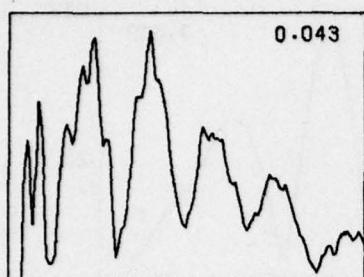
UNCLASSIFIED



Metal Plate, 6", 18%

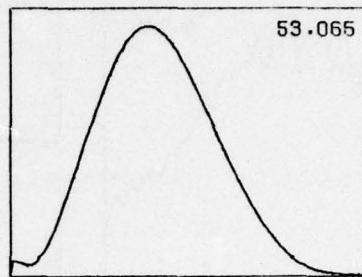
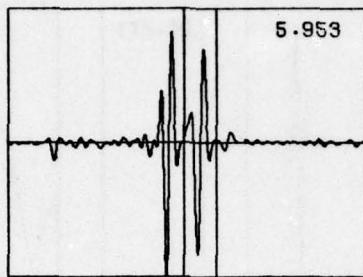
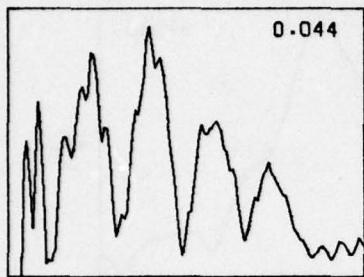
UNCLASSIFIED

UNCLASSIFIED

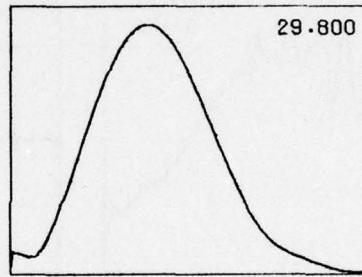
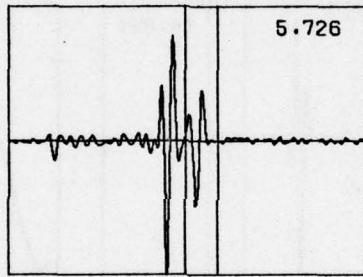
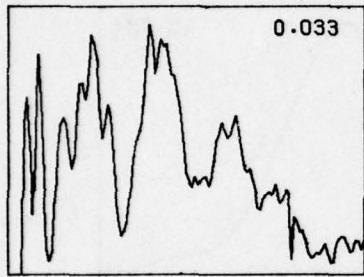


GT9

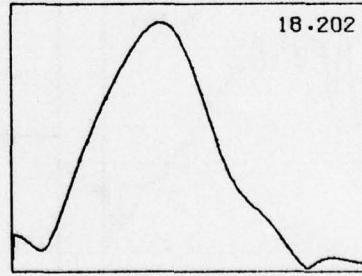
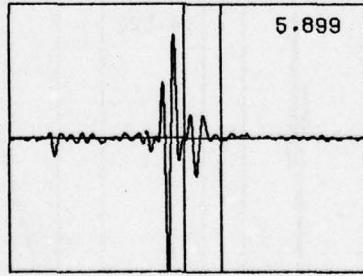
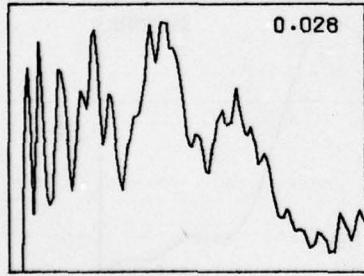
25



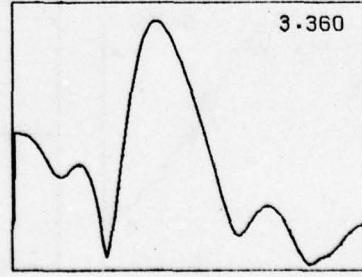
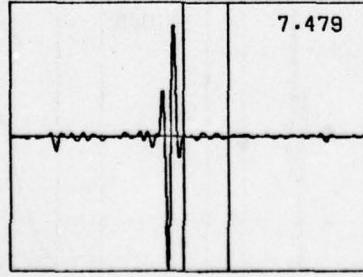
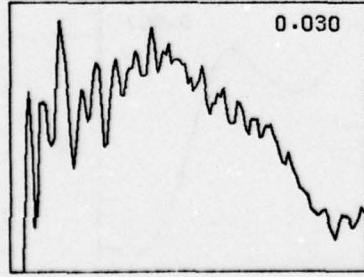
26



27



28



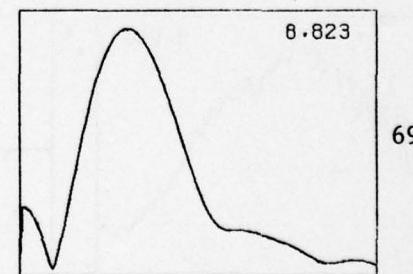
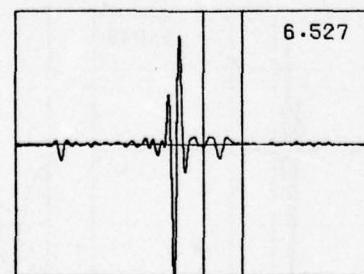
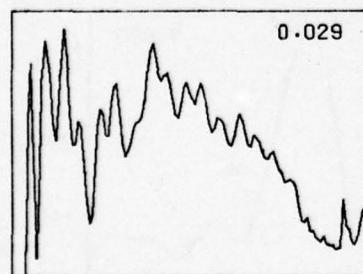
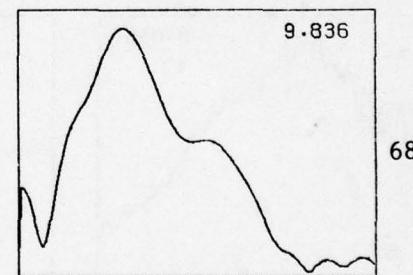
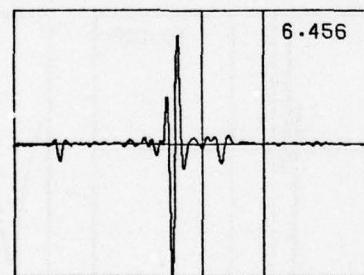
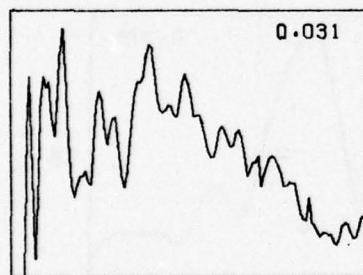
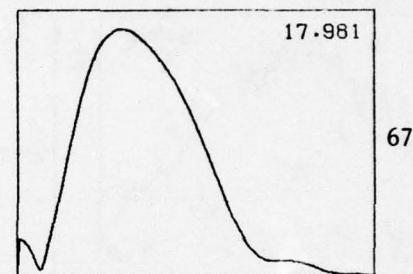
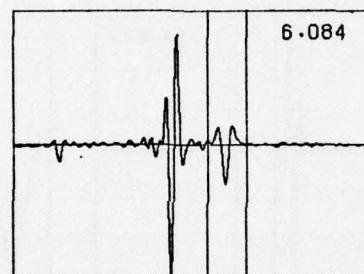
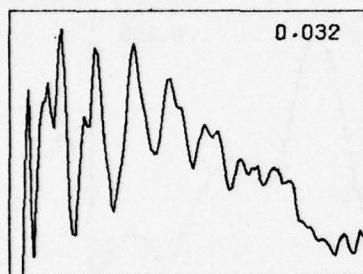
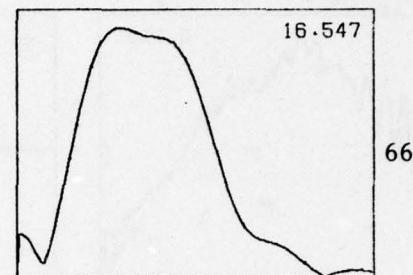
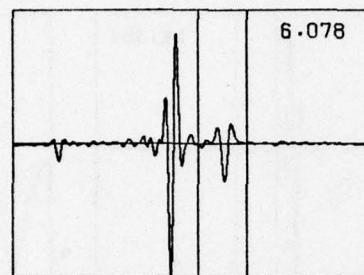
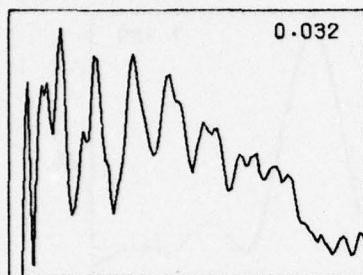
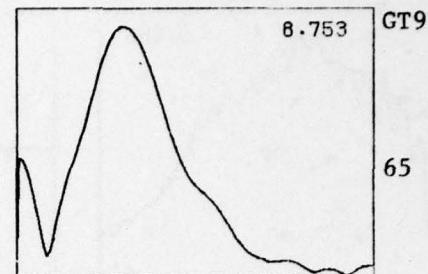
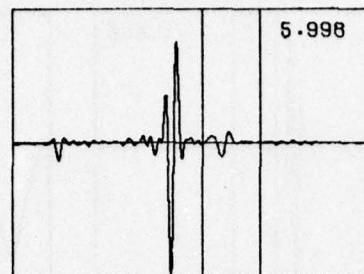
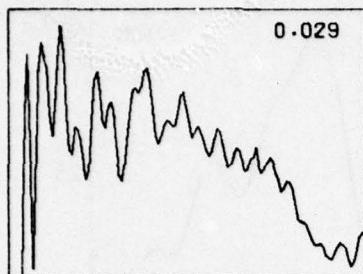
29

Metal Plate, 3", 12-20%

UNCLASSIFIED

A-36

UNCLASSIFIED

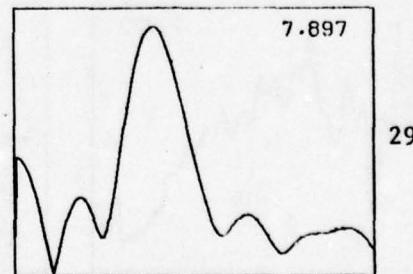
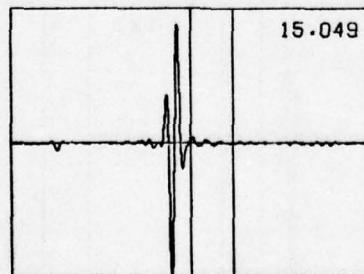
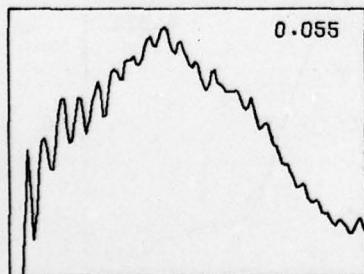
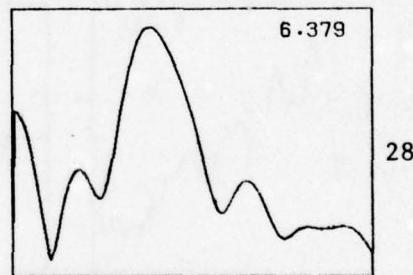
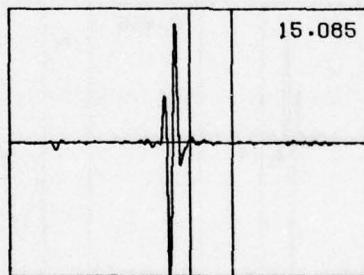
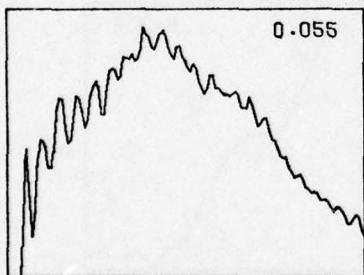
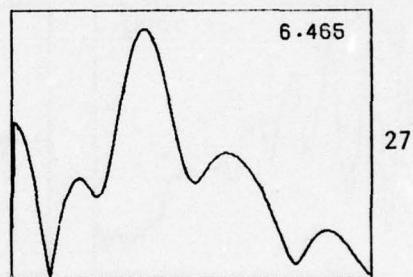
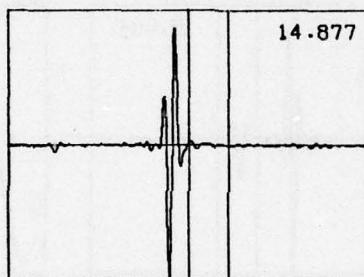
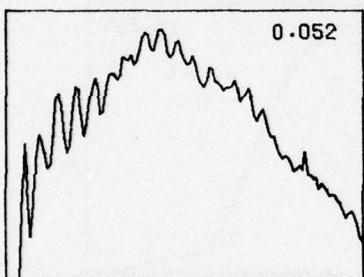
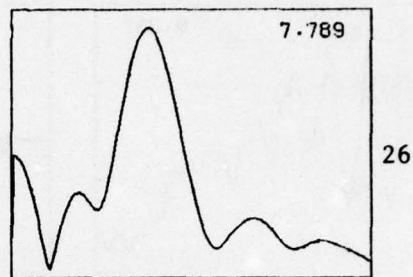
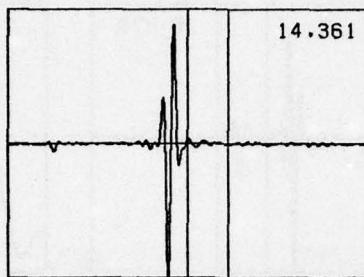
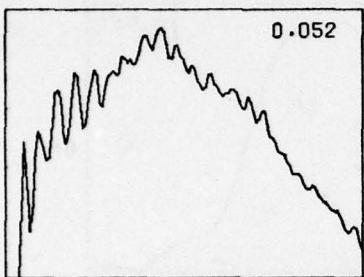
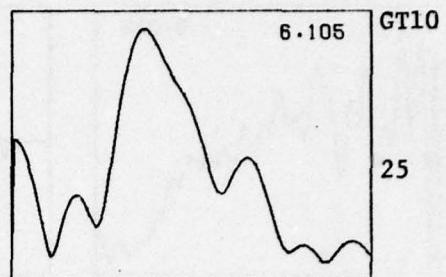
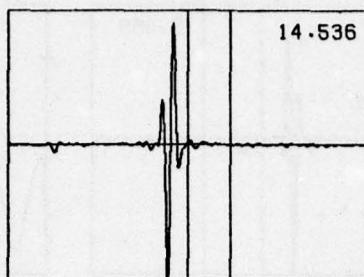
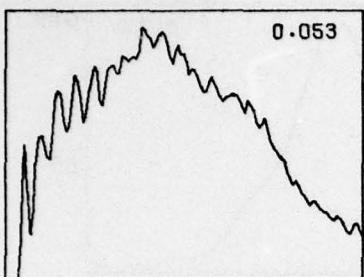


Metal Plate, 6", 13-16%

UNCLASSIFIED

A-37

UNCLASSIFIED

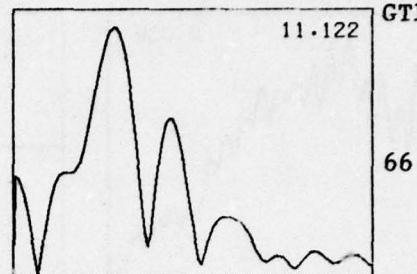
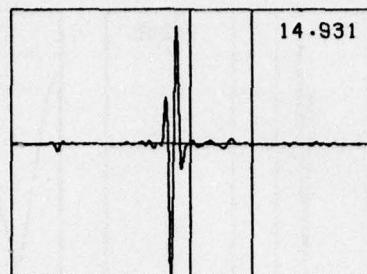
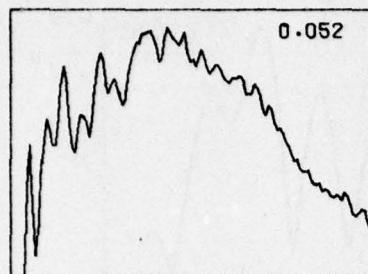


Metal Plate, 6", 26-30%

UNCLASSIFIED

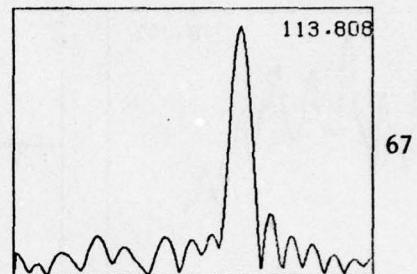
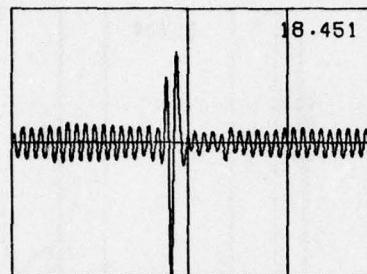
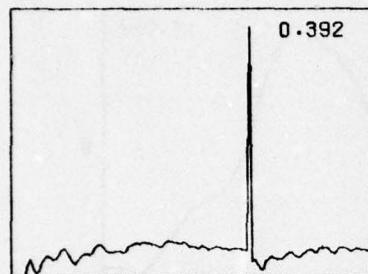
A-38

UNCLASSIFIED

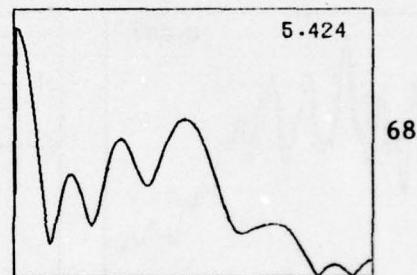
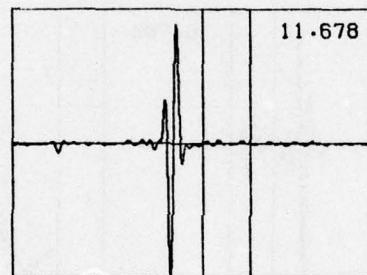
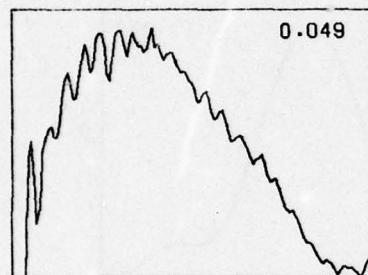


GT10

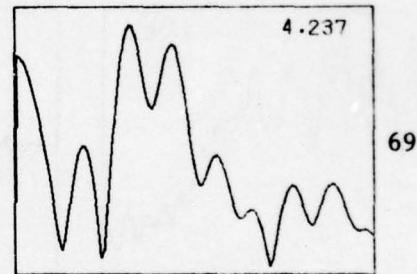
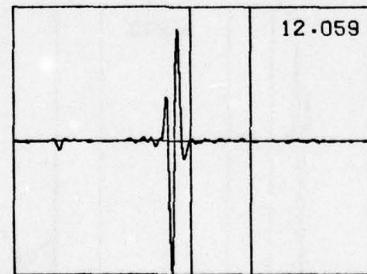
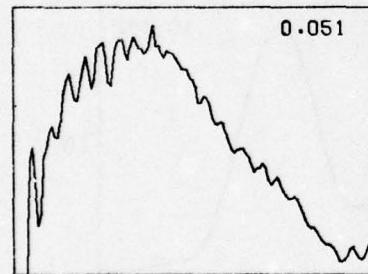
66



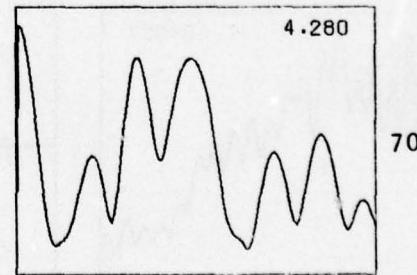
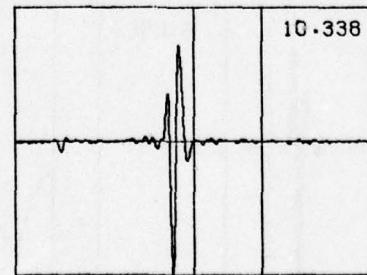
67



68



69

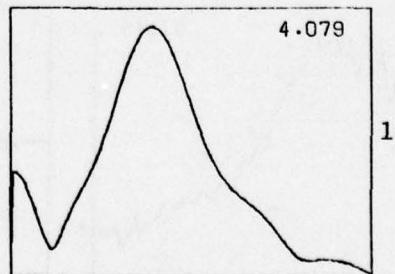
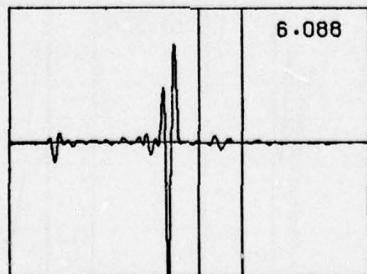
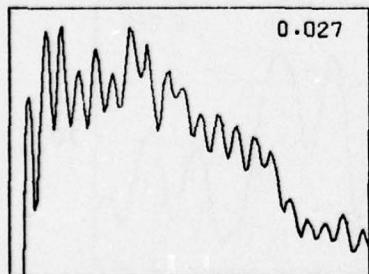
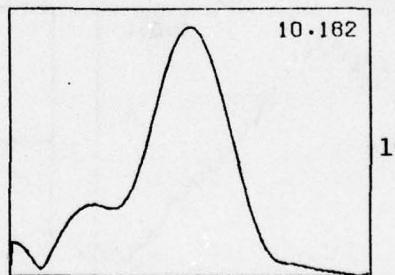
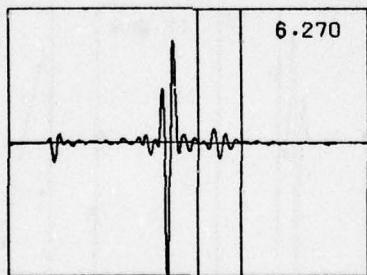
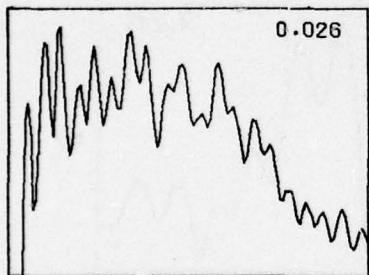
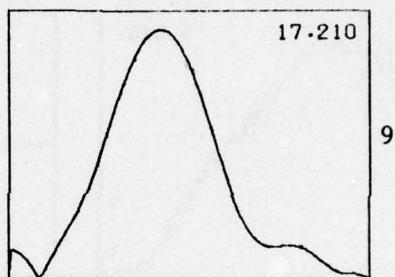
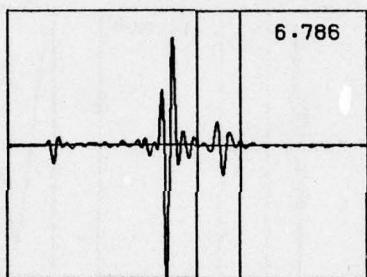
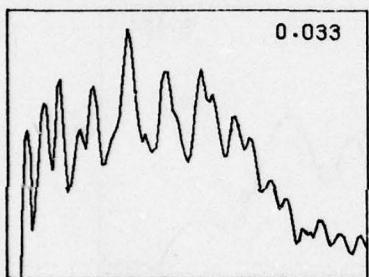
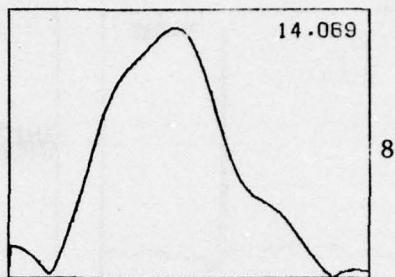
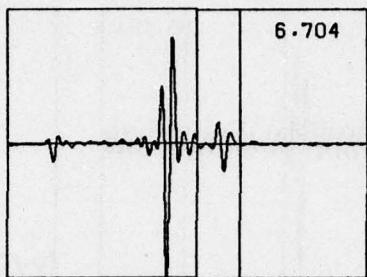
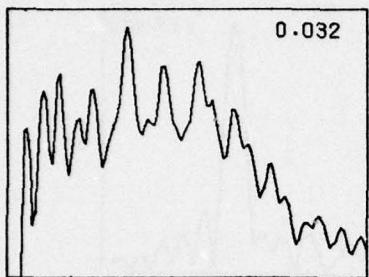
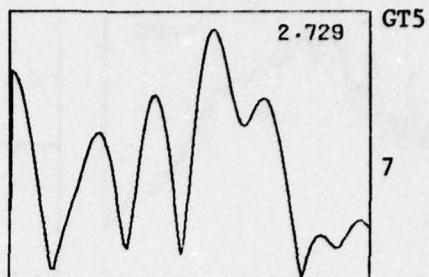
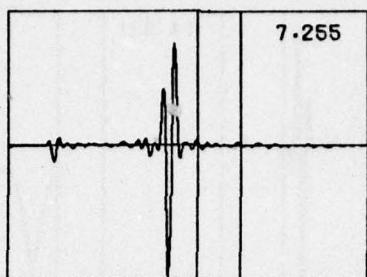
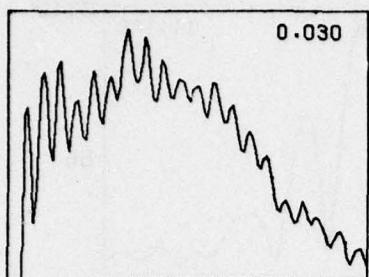


70

Metal Plate, 3", 30%

UNCLASSIFIED

UNCLASSIFIED

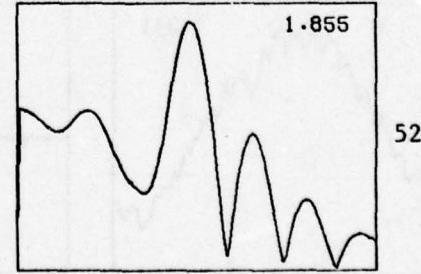
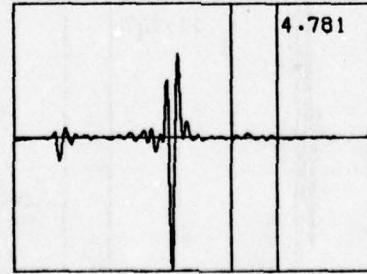
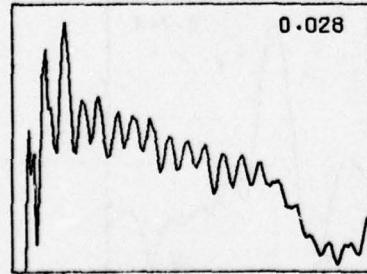
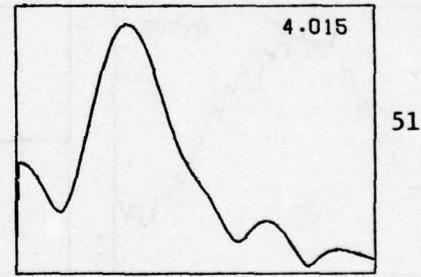
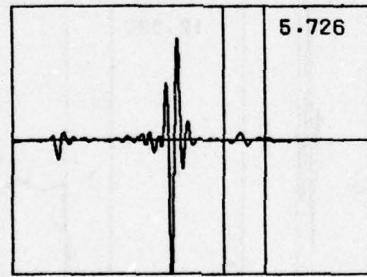
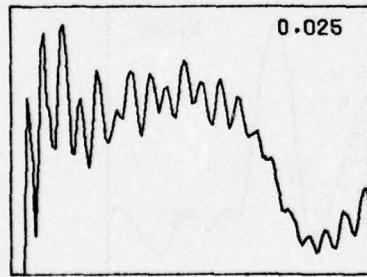
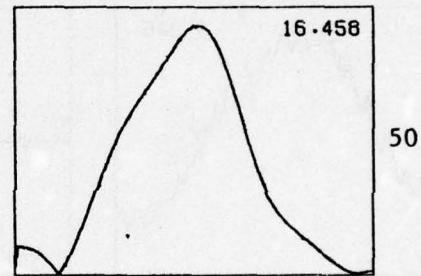
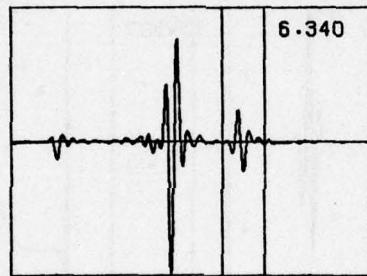
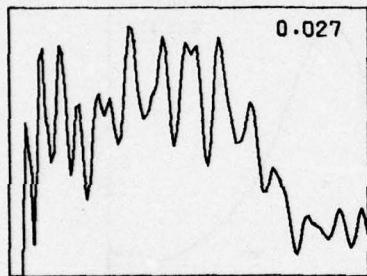
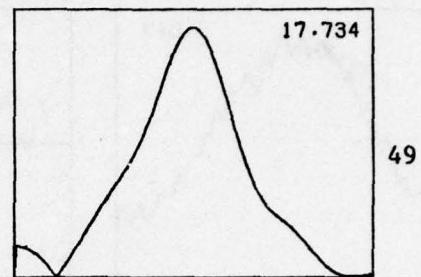
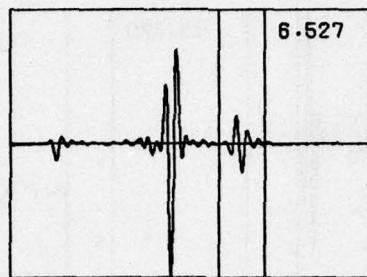
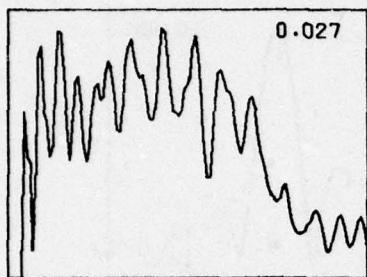
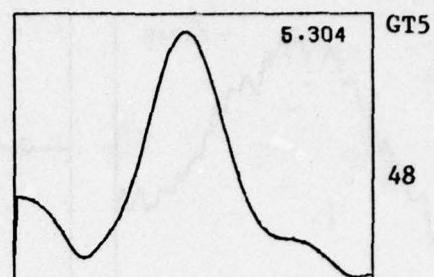
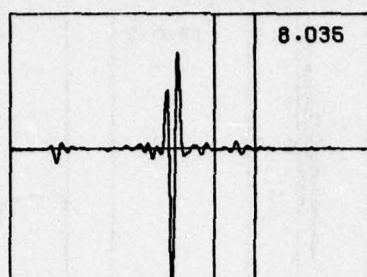
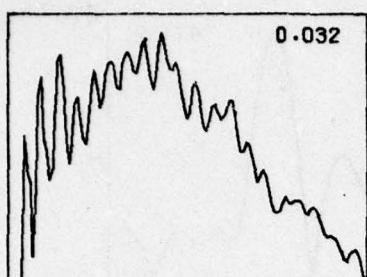


Rock 1, 3", 7%

UNCLASSIFIED

A-40

UNCLASSIFIED

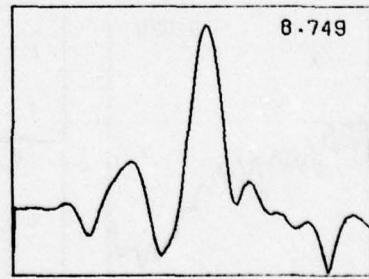
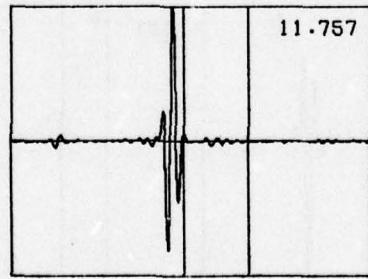
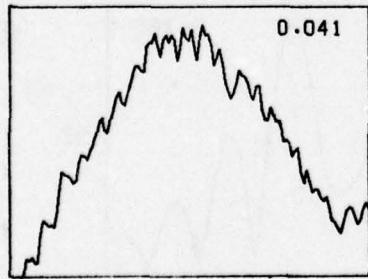
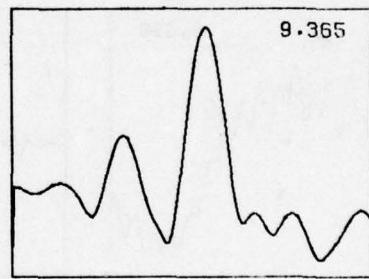
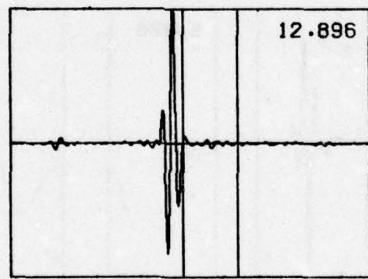
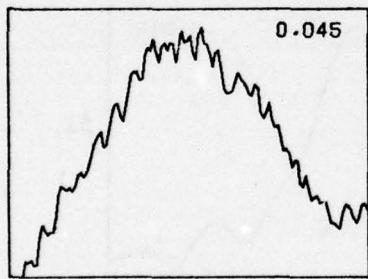
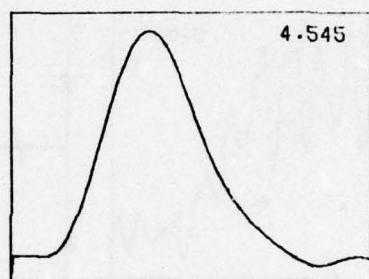
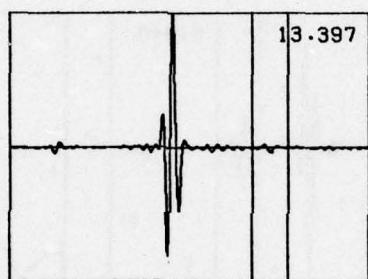
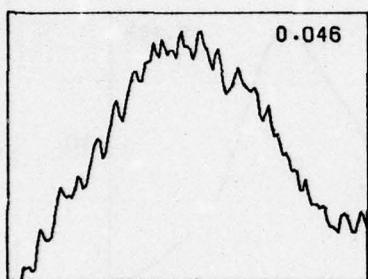
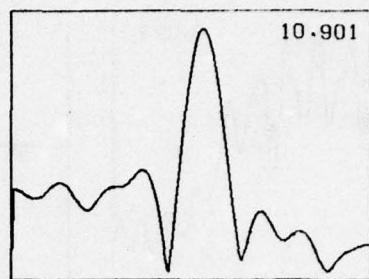
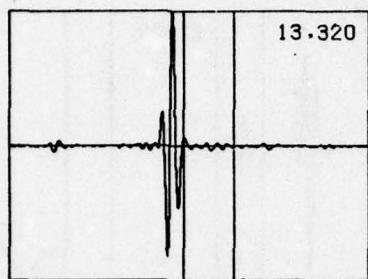
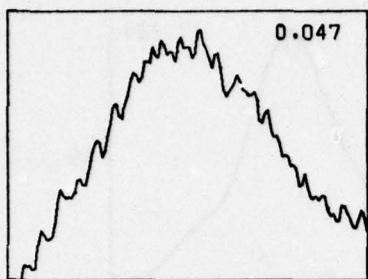
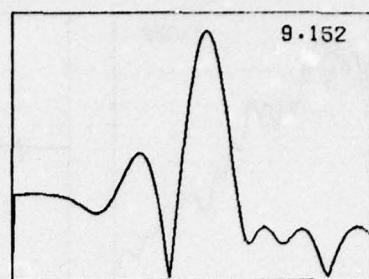
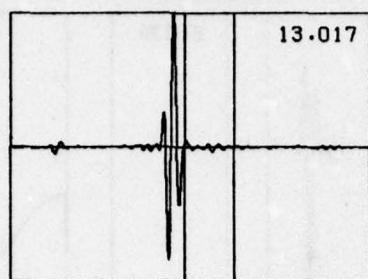
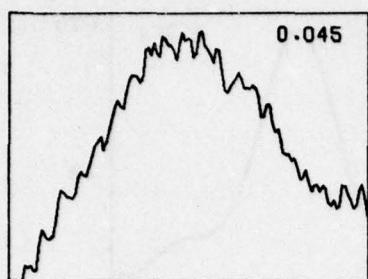


Rock 1, 6", 7%

UNCLASSIFIED

A-41

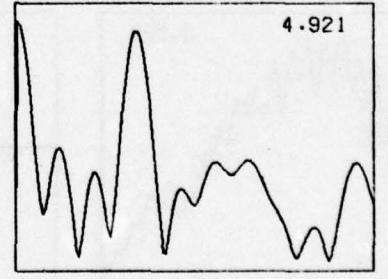
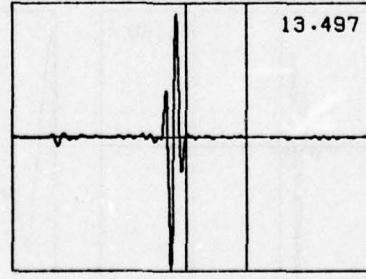
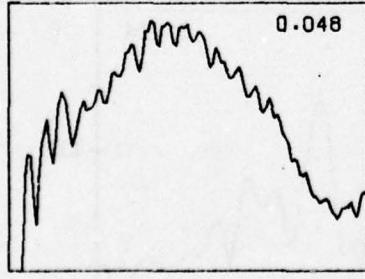
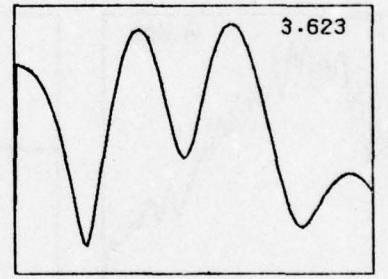
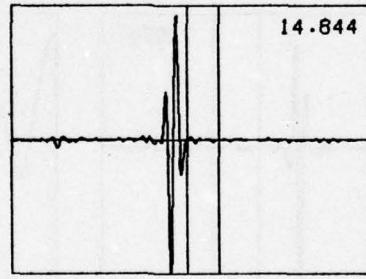
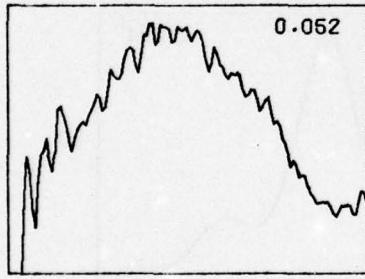
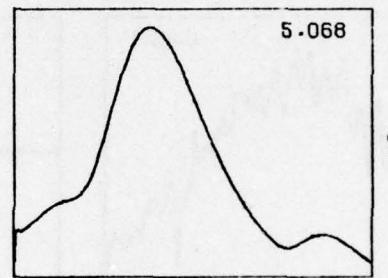
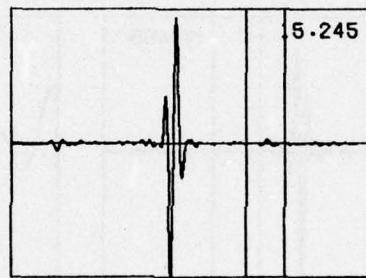
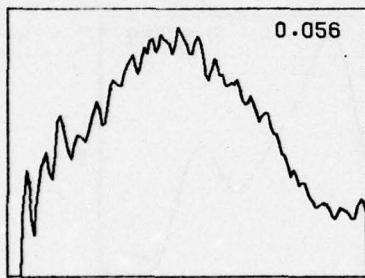
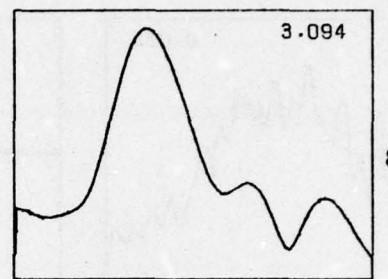
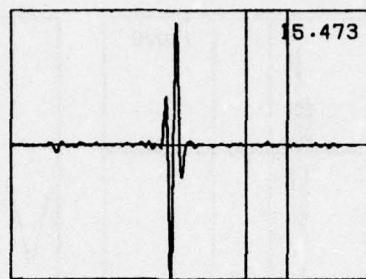
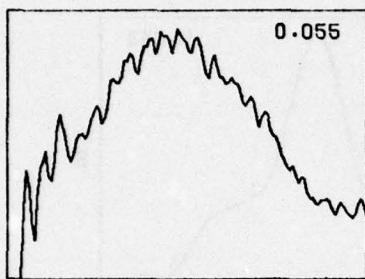
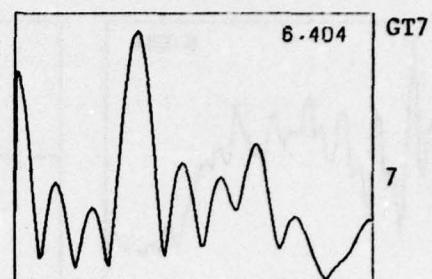
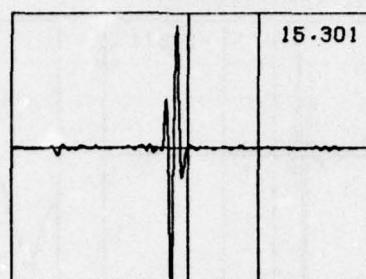
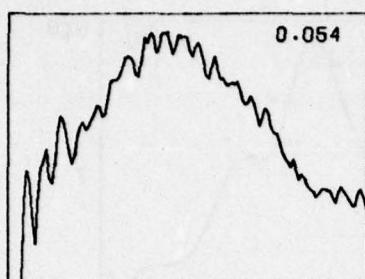
UNCLASSIFIED



Rock 1, 6", 17%

UNCLASSIFIED

UNCLASSIFIED

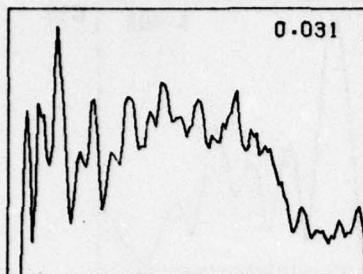


Rock 1, 6", 18%

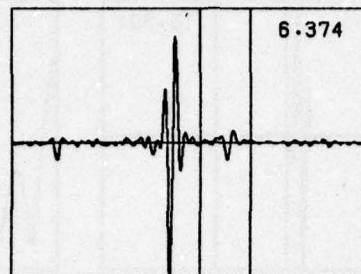
UNCLASSIFIED

A-43

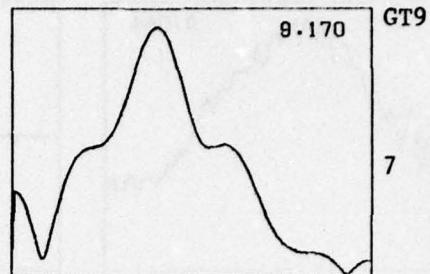
UNCLASSIFIED



0.031



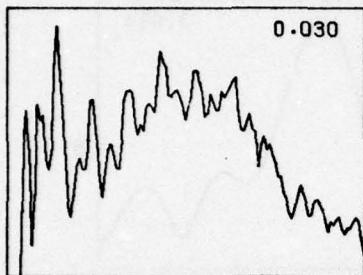
6.374



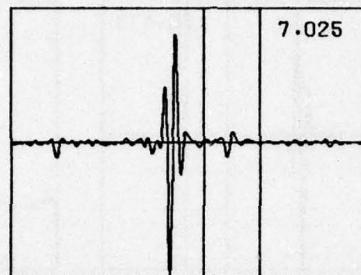
9.170

GT9

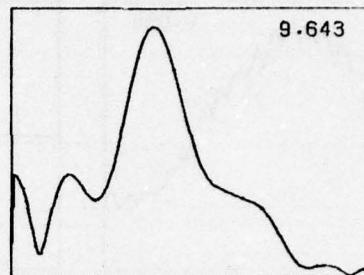
7



0.030

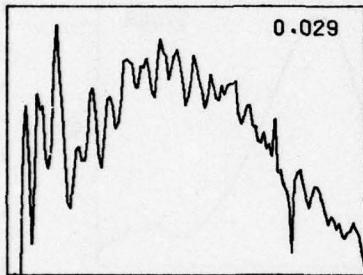


7.025

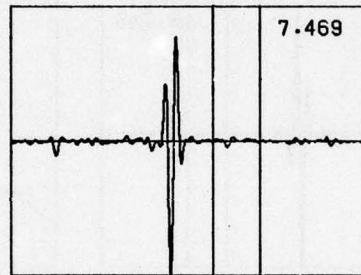


9.643

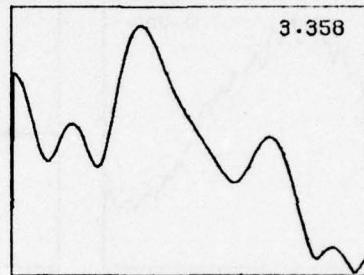
8



0.029

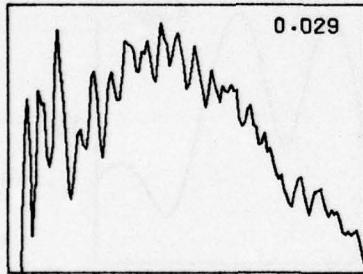


7.469

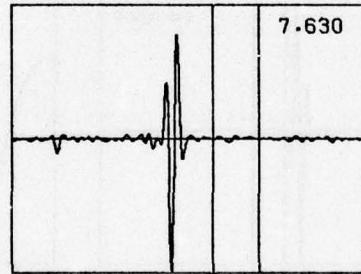


3.358

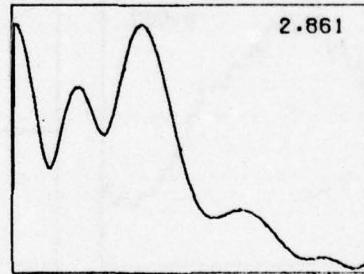
9



0.029

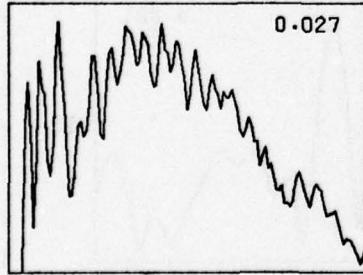


7.630

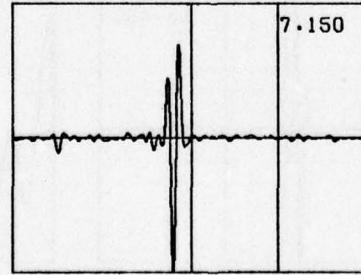


2.861

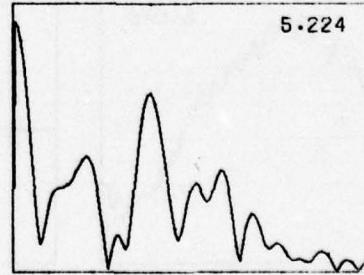
10



0.027



7.150



5.224

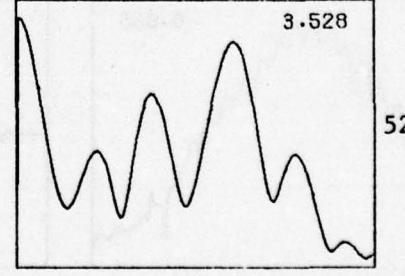
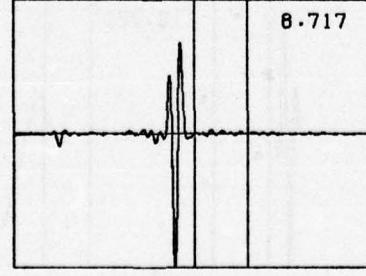
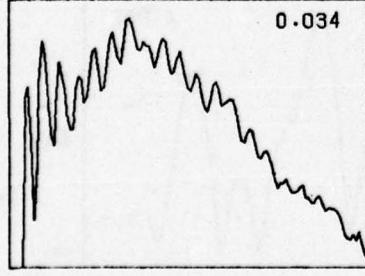
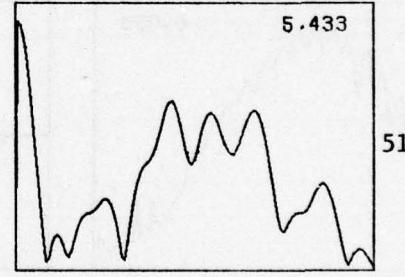
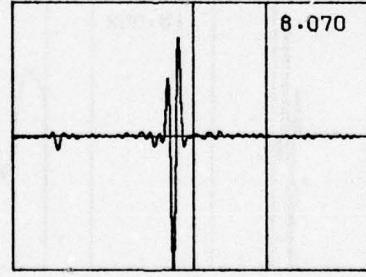
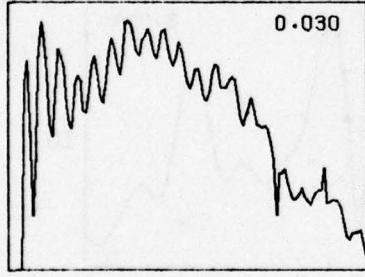
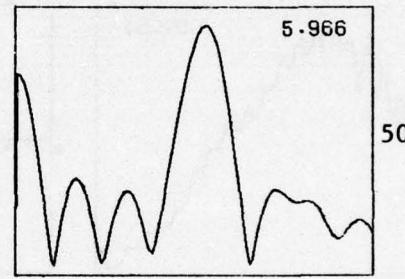
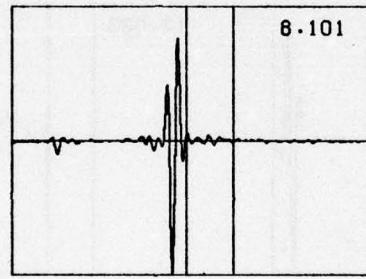
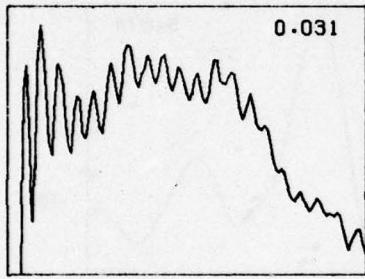
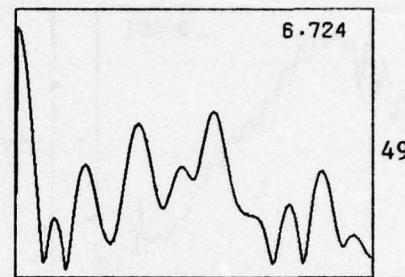
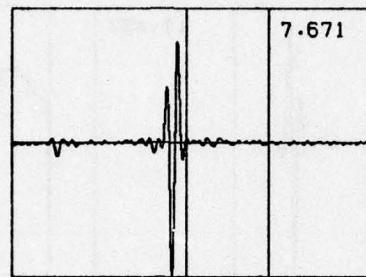
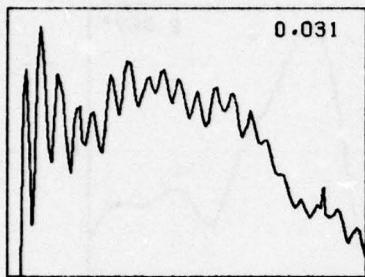
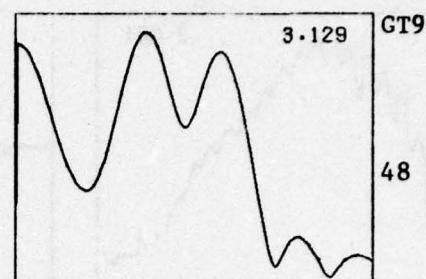
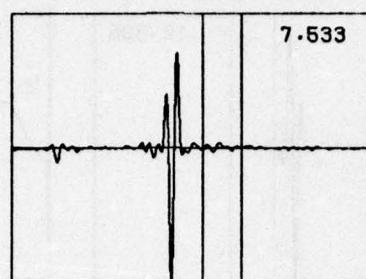
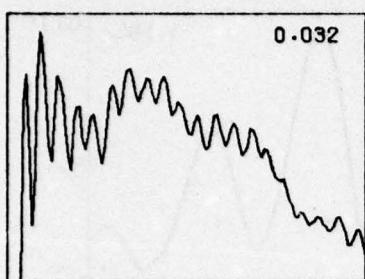
11

Rock 1, 3", 12-20%

UNCLASSIFIED

A-44

UNCLASSIFIED

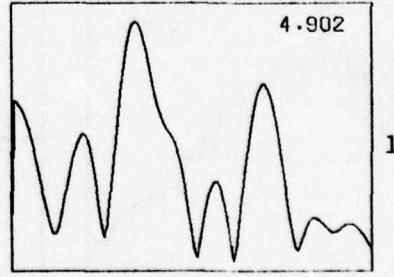
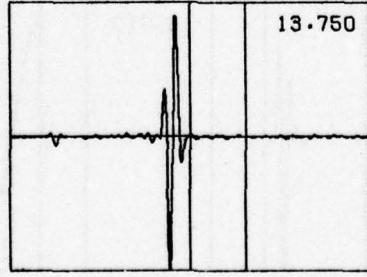
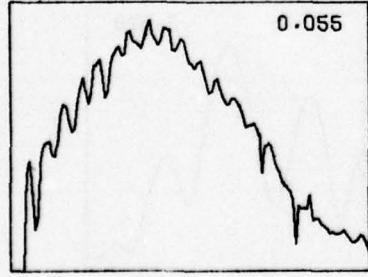
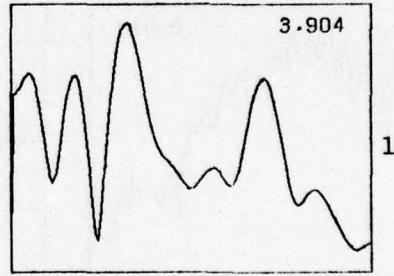
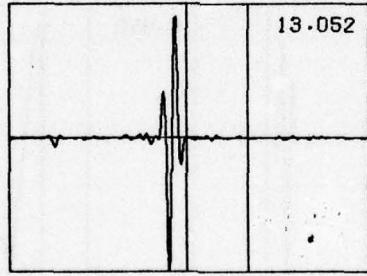
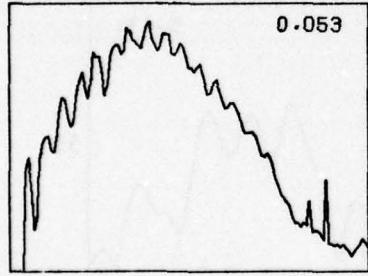
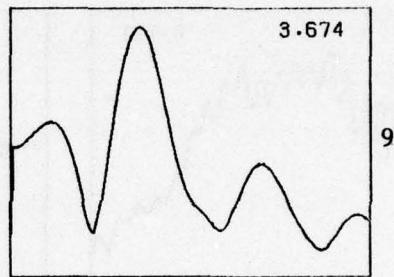
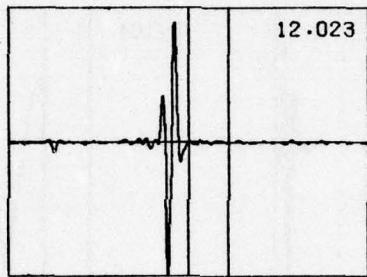
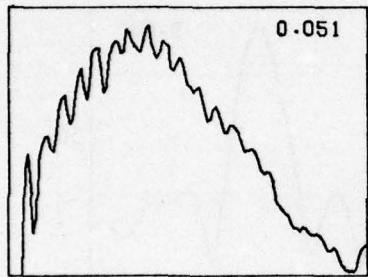
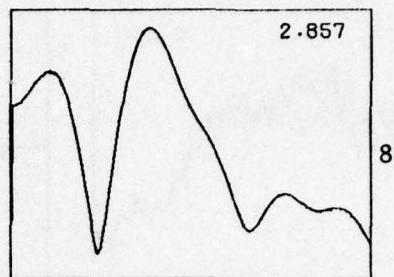
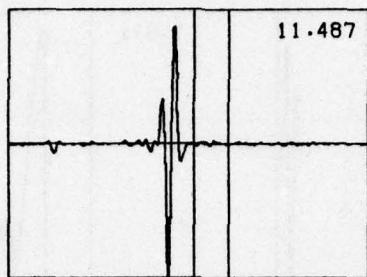
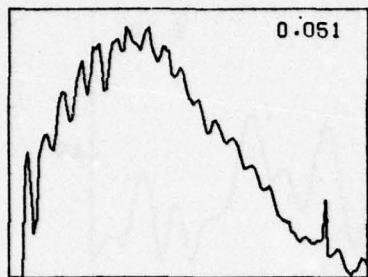
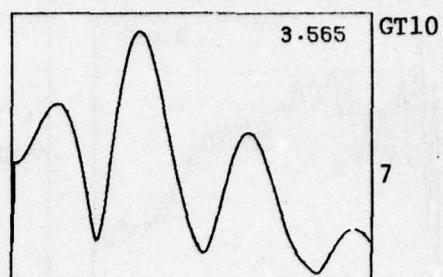
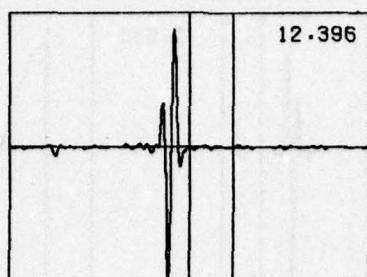
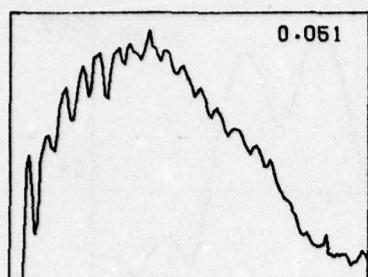


Rock 1, 6", 13-16%

UNCLASSIFIED

A-45

UNCLASSIFIED

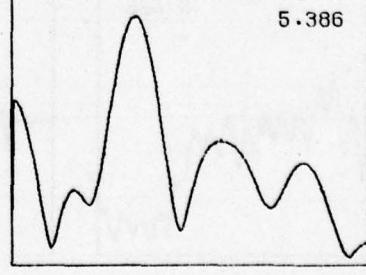
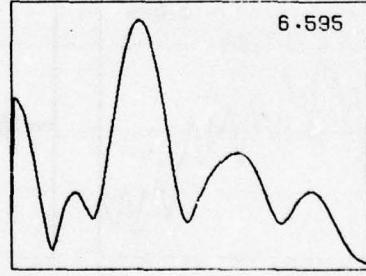
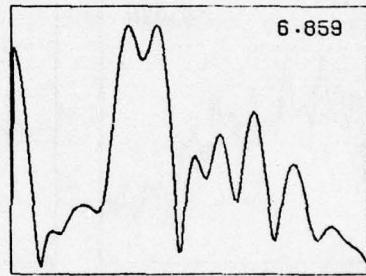
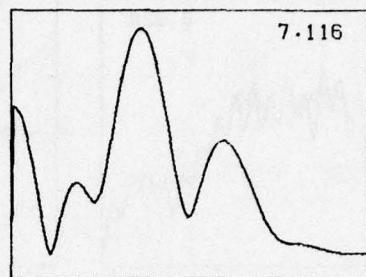
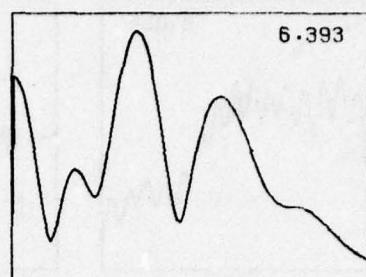
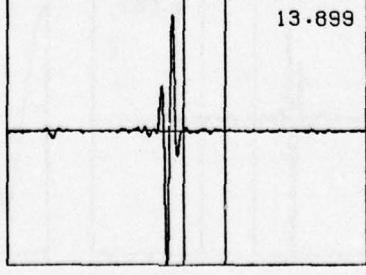
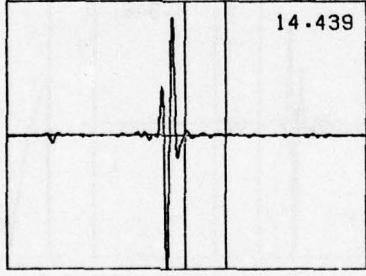
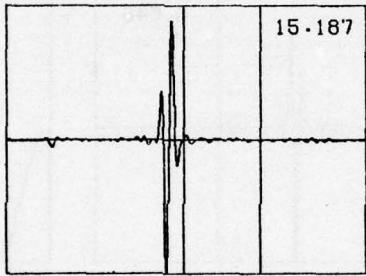
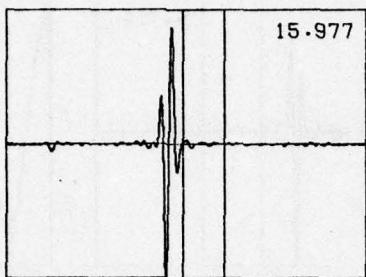
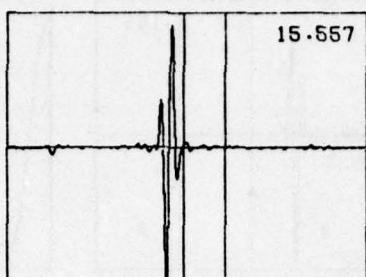
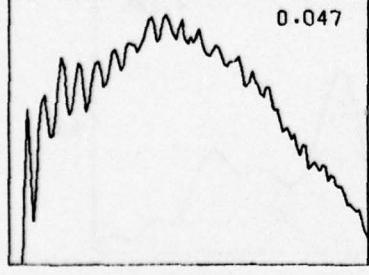
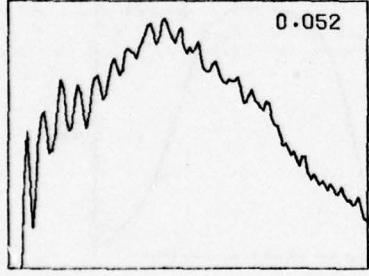
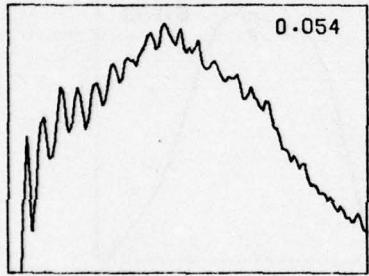
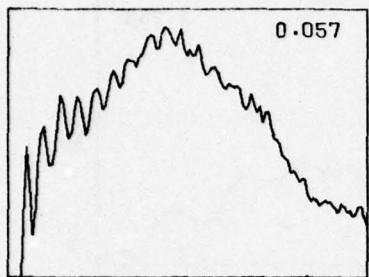
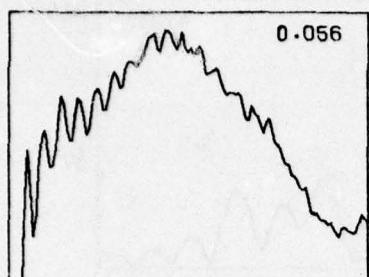


Rock 1, 6", 26-30%

UNCLASSIFIED

A-46

UNCLASSIFIED



GT10

48

7.116

49

6.859

50

6.595

51

5.386

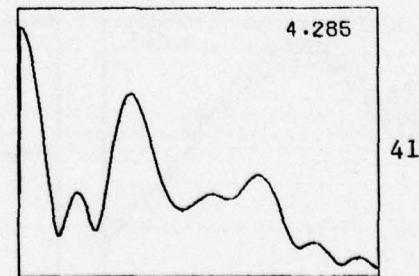
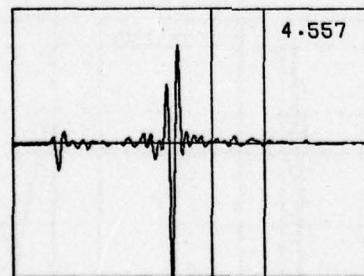
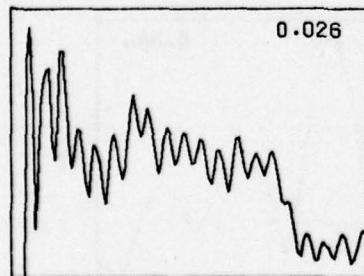
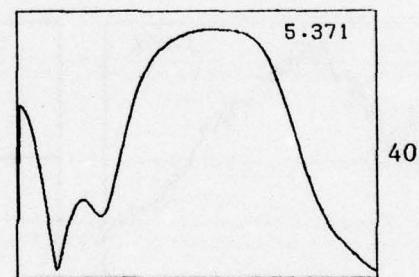
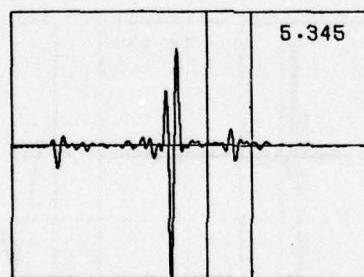
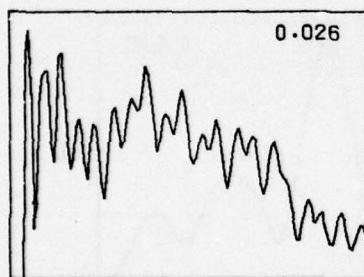
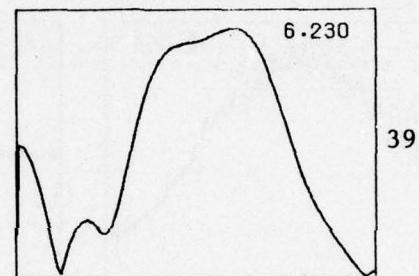
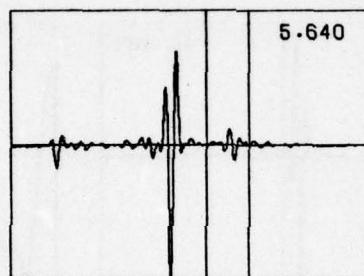
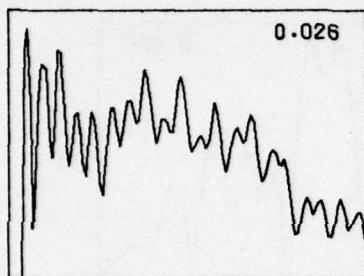
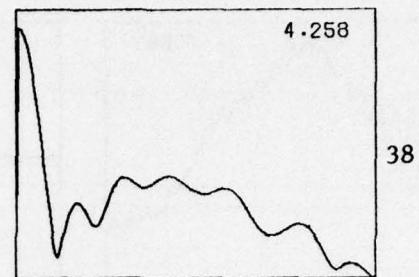
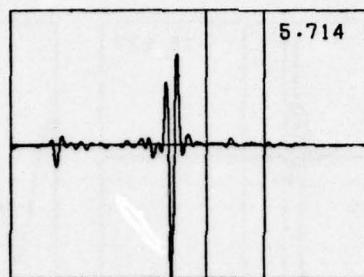
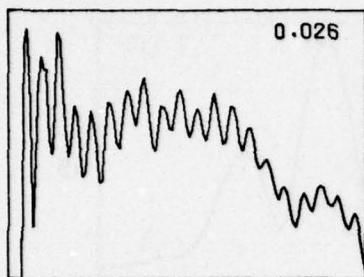
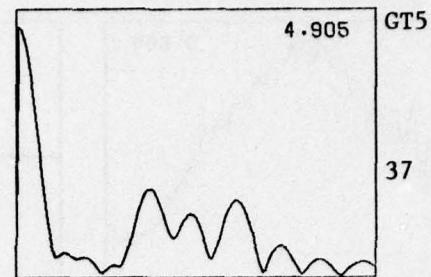
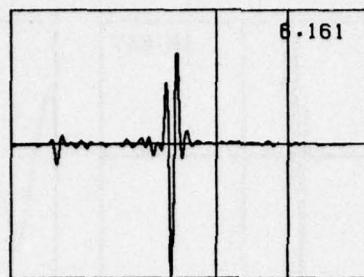
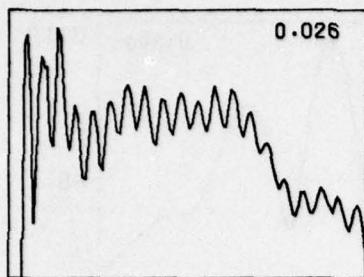
52

Rock 1, 3", 30%

UNCLASSIFIED

A-47

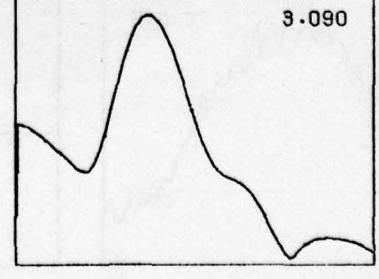
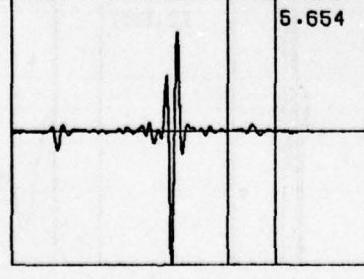
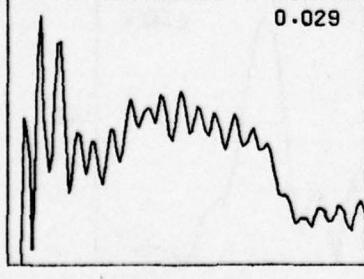
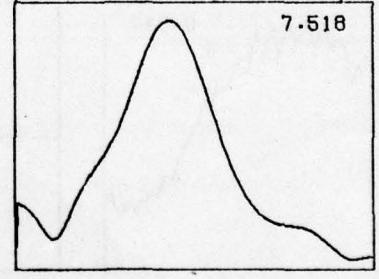
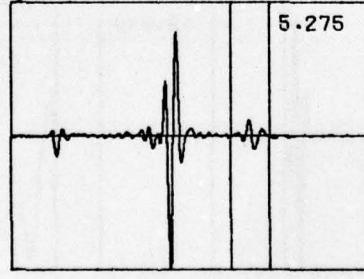
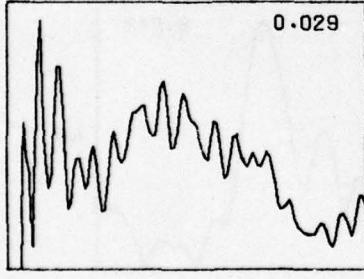
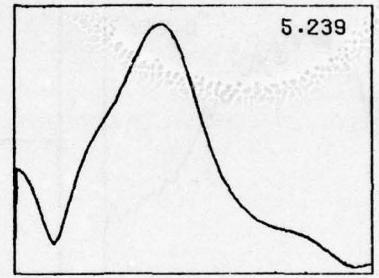
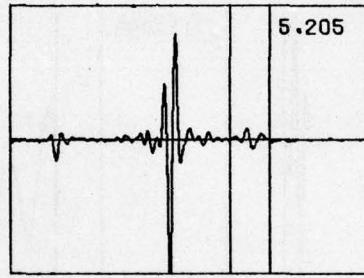
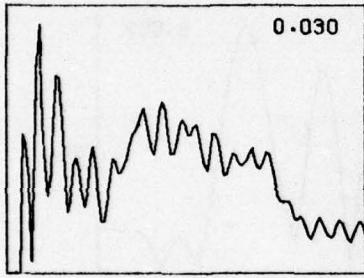
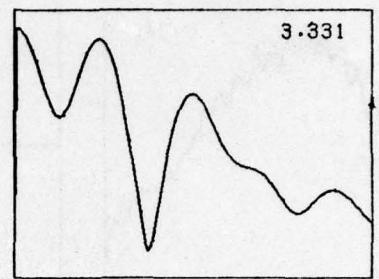
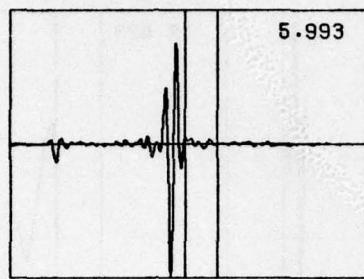
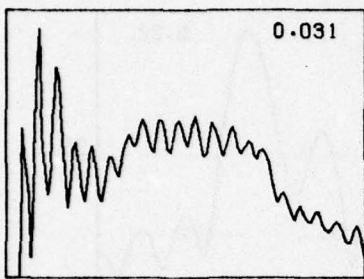
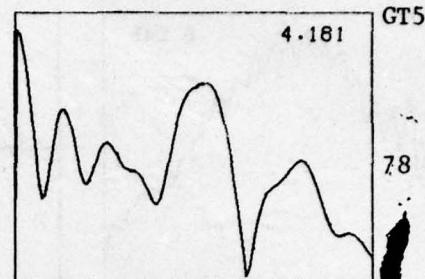
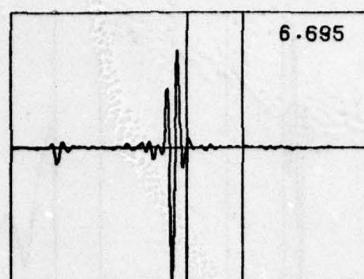
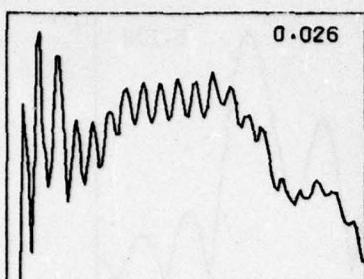
UNCLASSIFIED



Rock 2, 3", 7%

UNCLASSIFIED

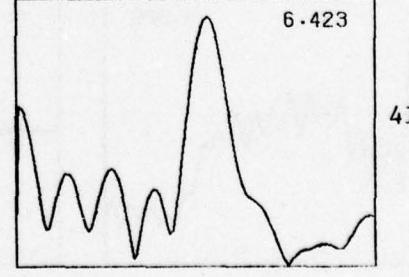
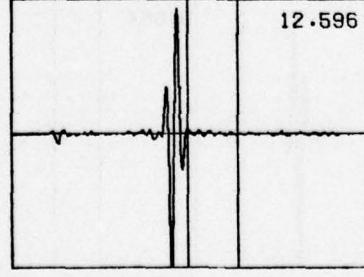
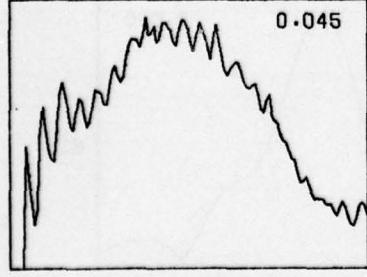
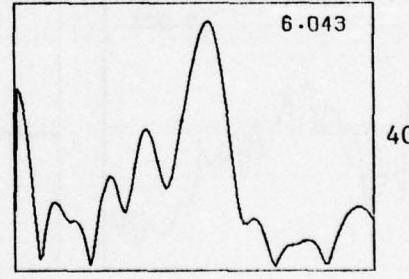
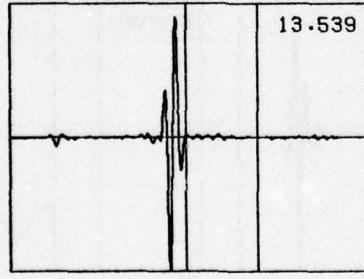
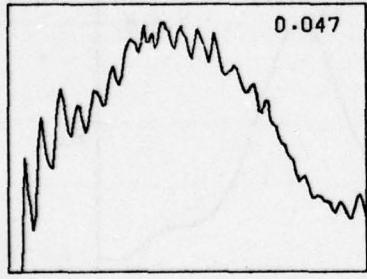
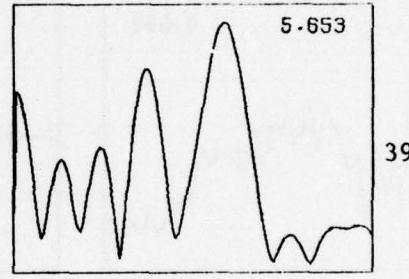
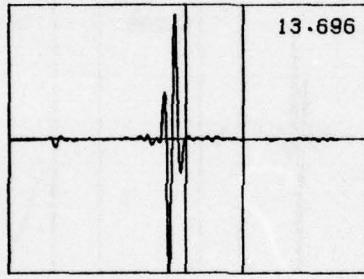
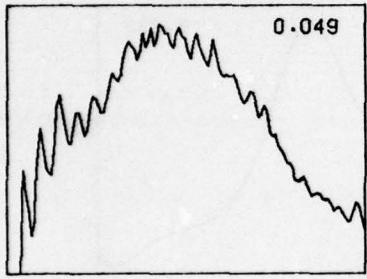
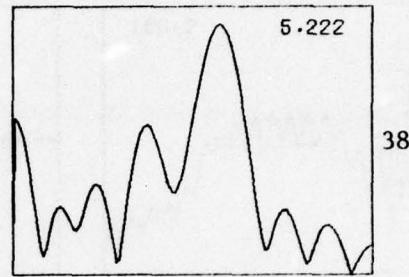
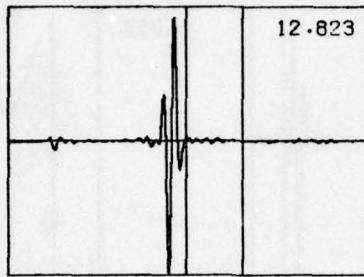
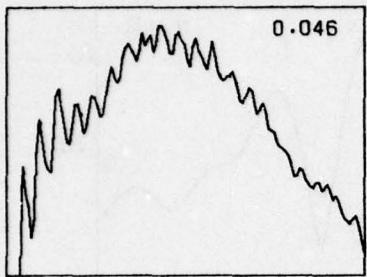
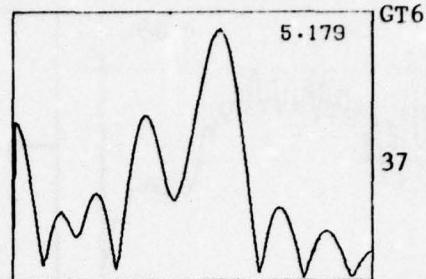
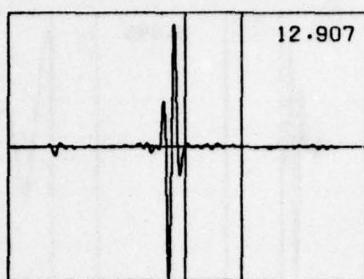
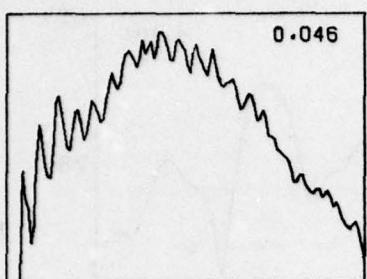
UNCLASSIFIED



Rock 2, 6", 7%

UNCLASSIFIED
A-49

UNCLASSIFIED

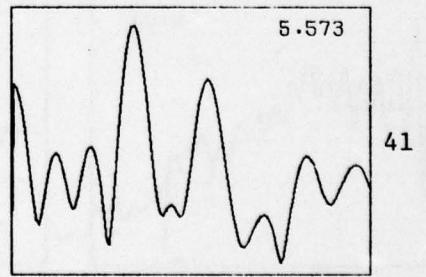
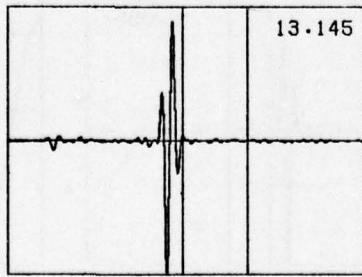
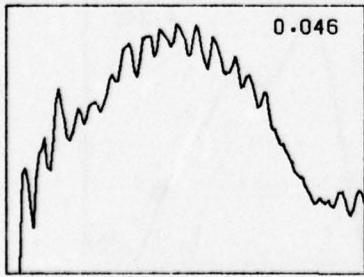
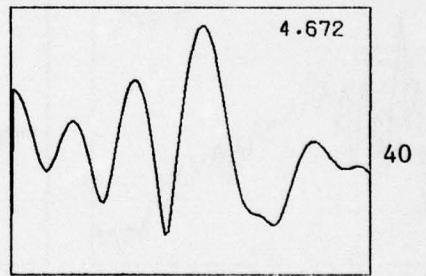
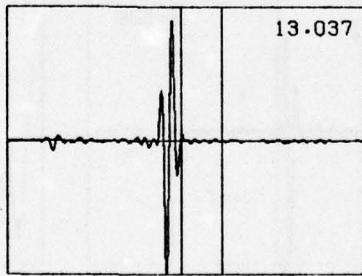
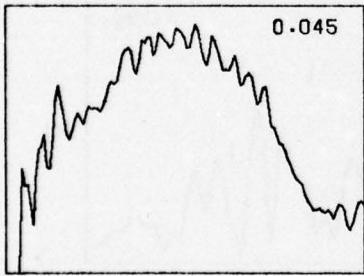
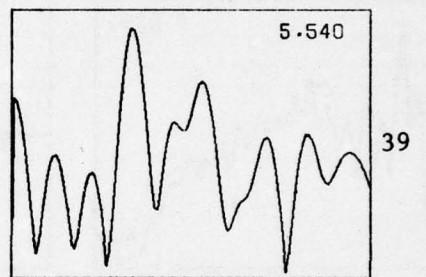
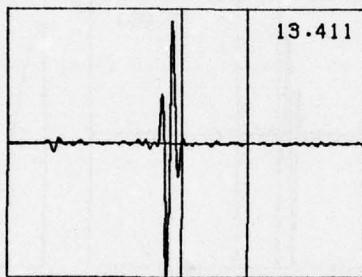
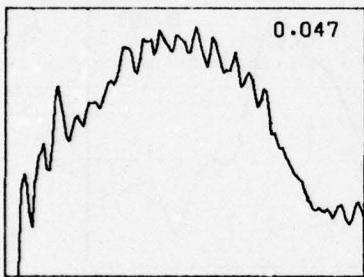
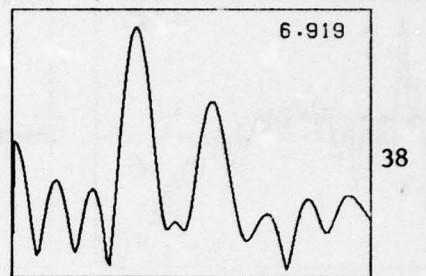
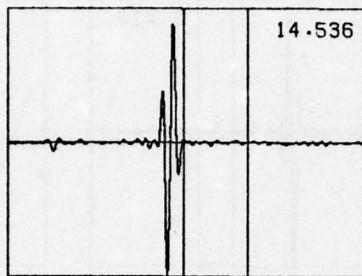
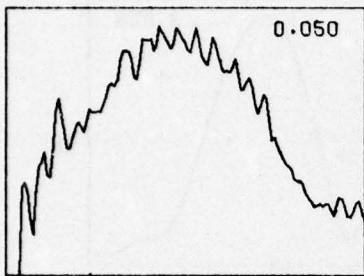
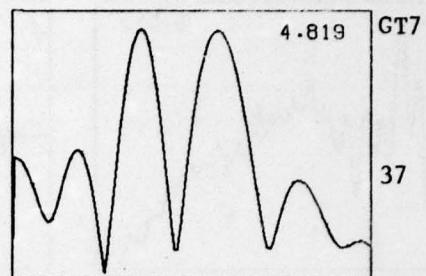
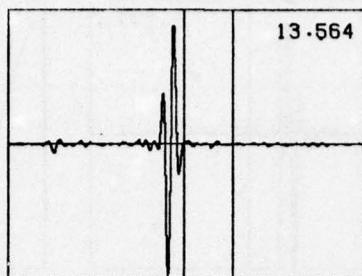
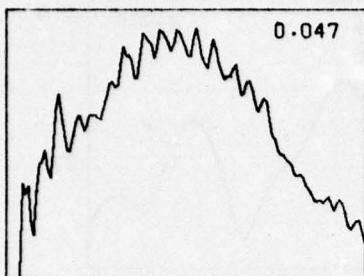


Rock 2, 6", 17%

UNCLASSIFIED

A-50

UNCLASSIFIED

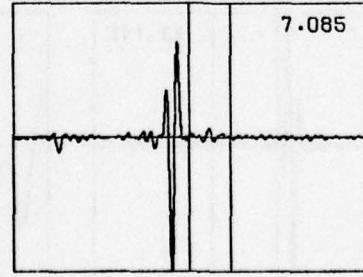
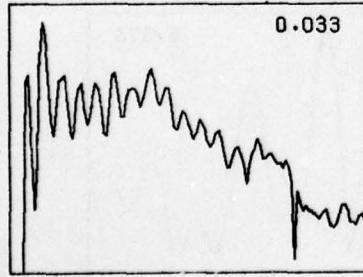
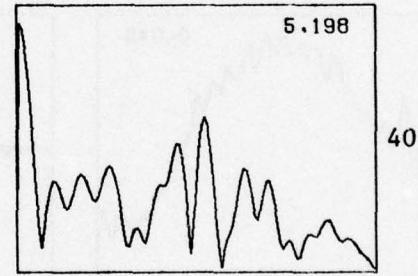
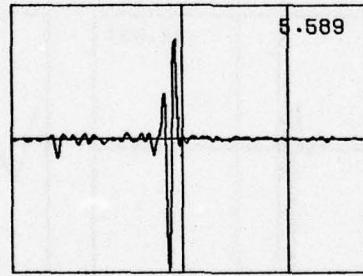
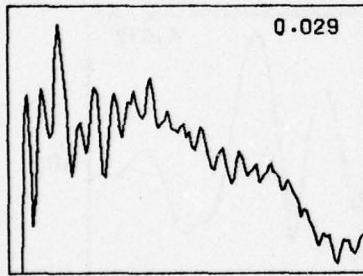
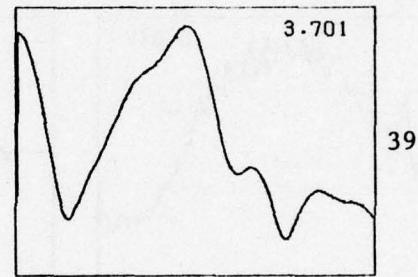
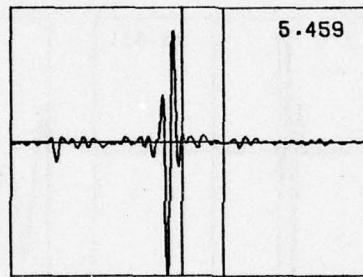
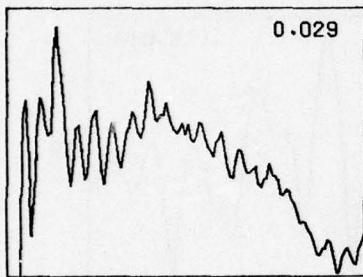
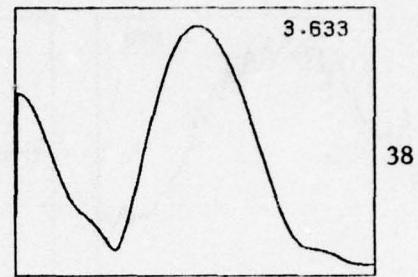
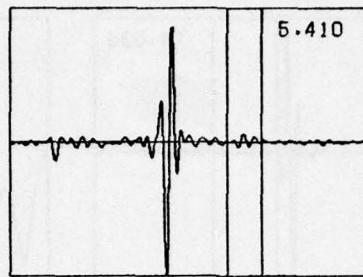
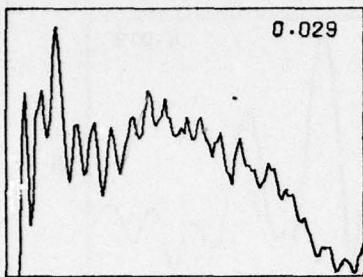
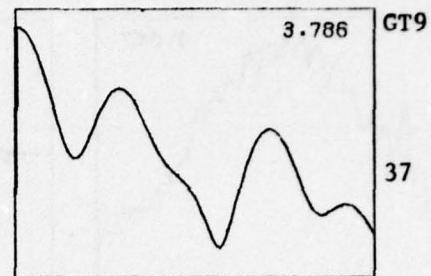
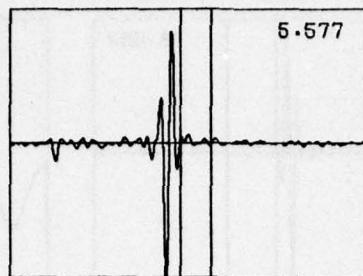
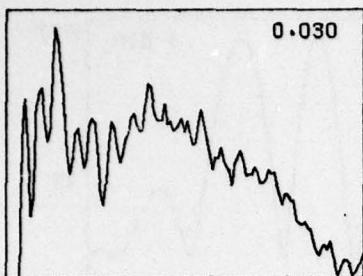


Rock 2, 6", 18%

UNCLASSIFIED

A-51

UNCLASSIFIED

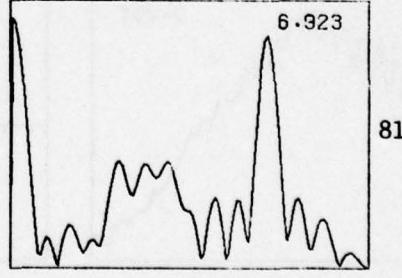
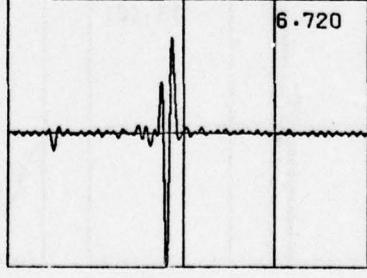
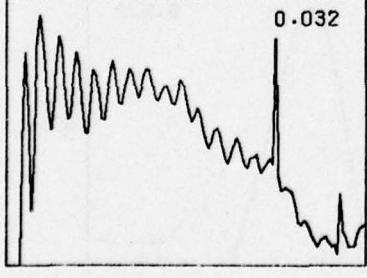
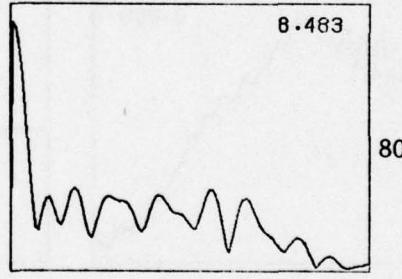
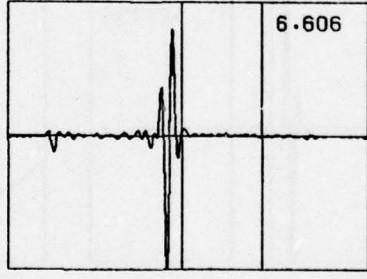
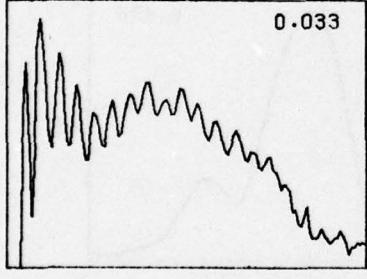
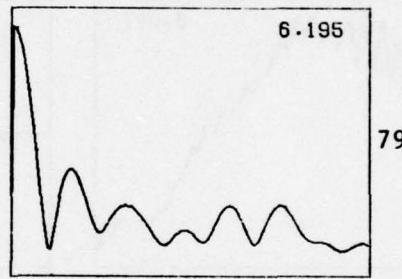
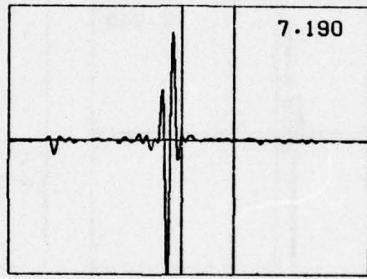
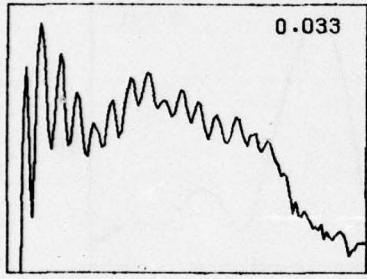
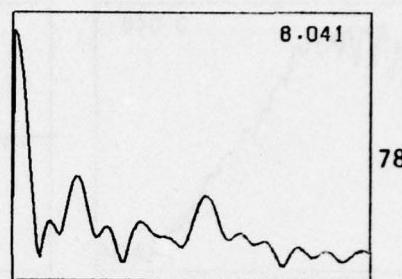
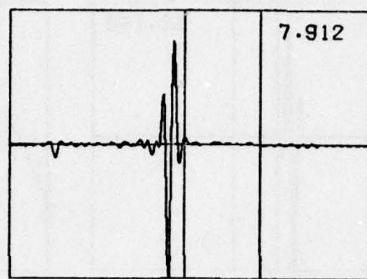
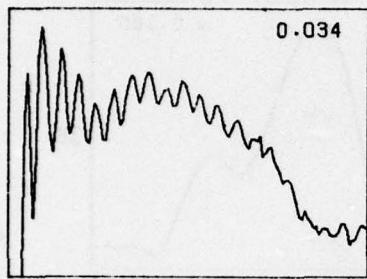
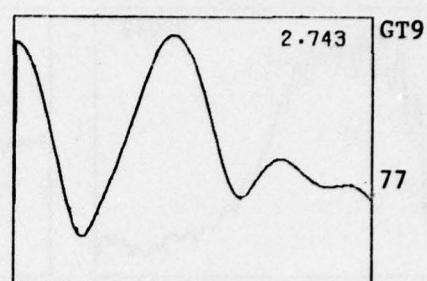
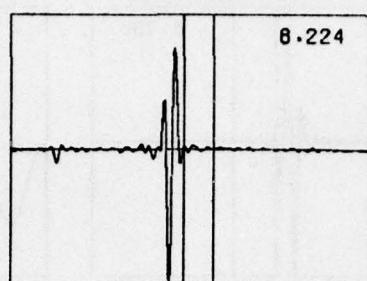
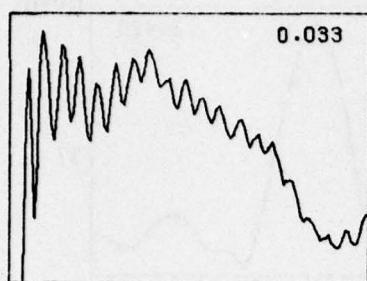


Rock 2, 3", 12-20%

UNCLASSIFIED

A-52

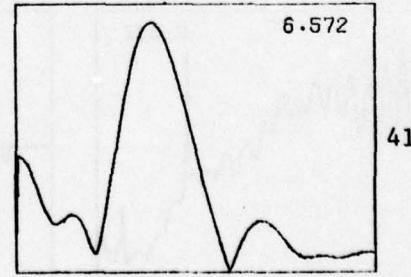
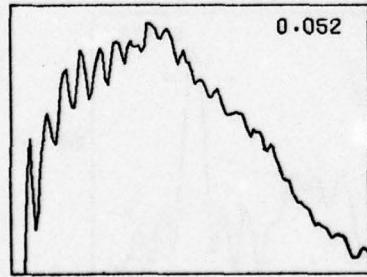
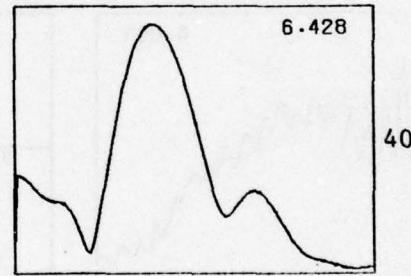
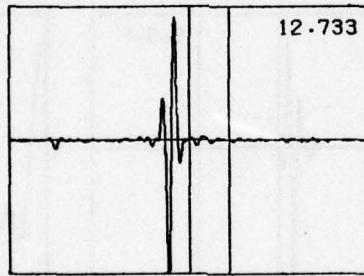
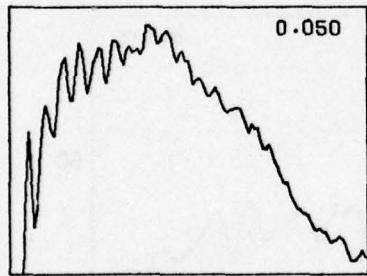
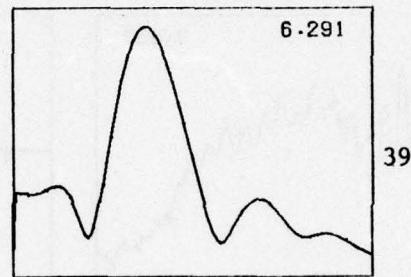
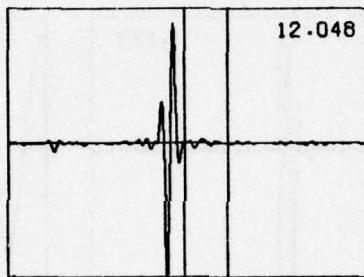
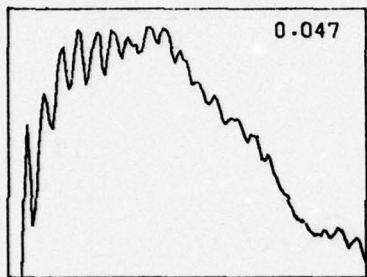
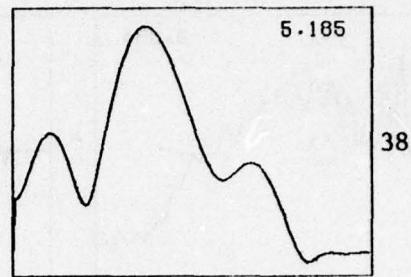
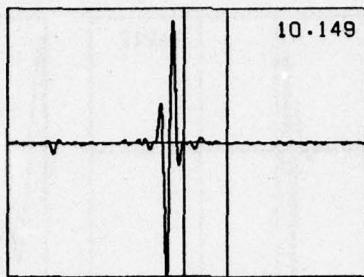
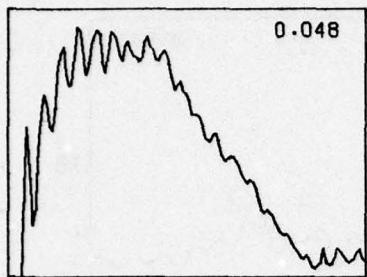
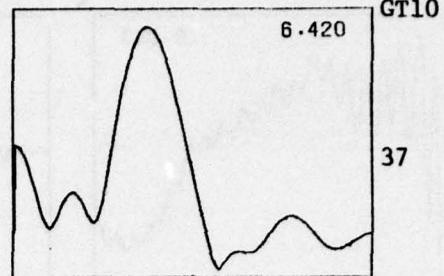
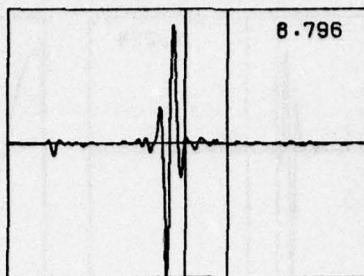
UNCLASSIFIED



Rock 2, 6", 13-16%

UNCLASSIFIED

UNCLASSIFIED

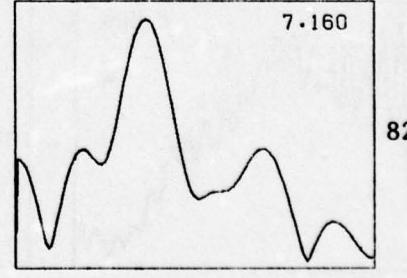
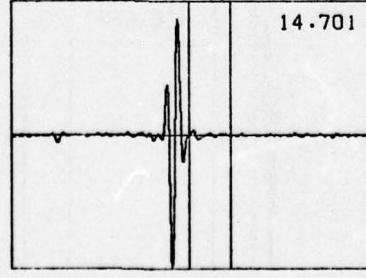
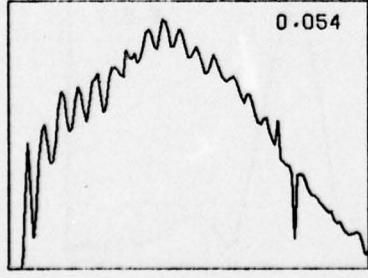
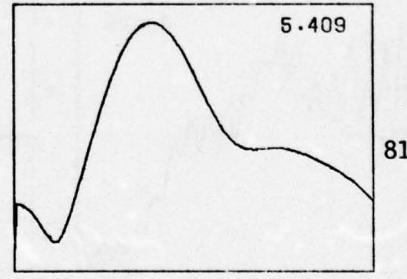
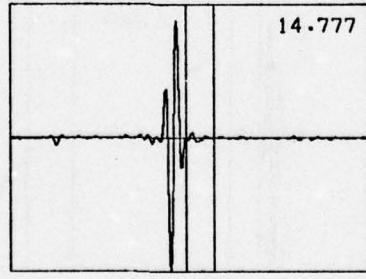
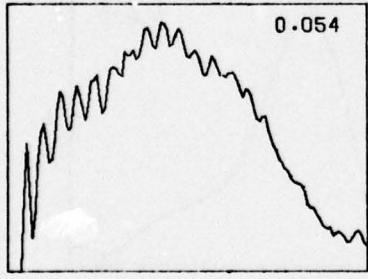
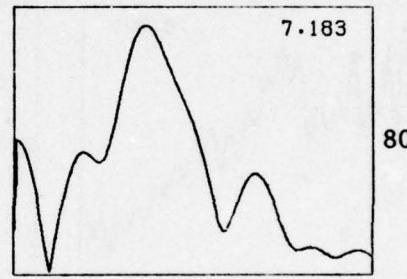
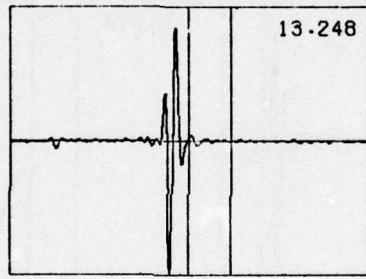
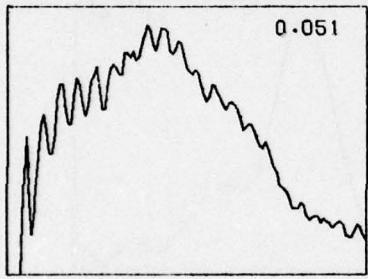
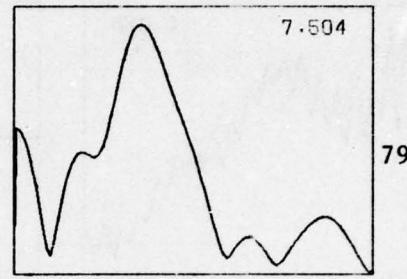
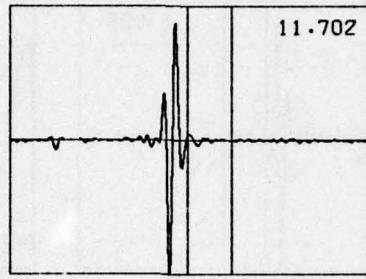
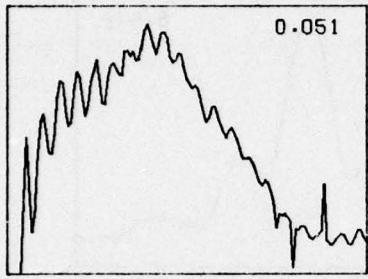
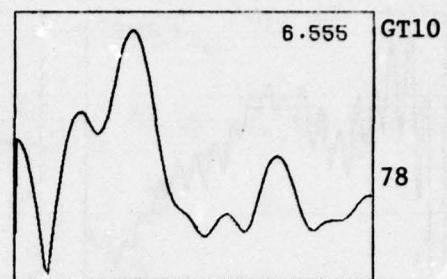
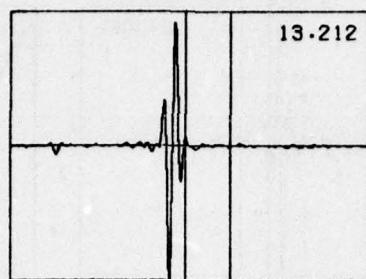
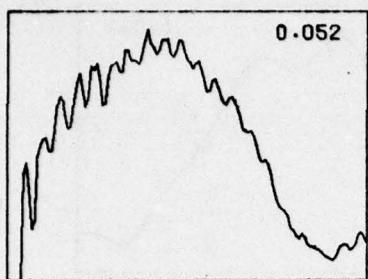


Rock 2, 6", 26-30%

UNCLASSIFIED

A-54

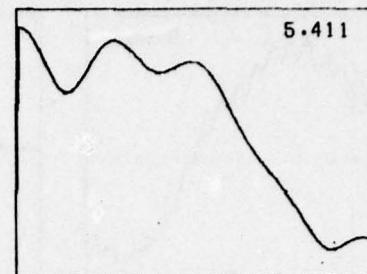
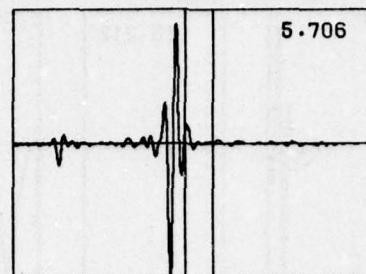
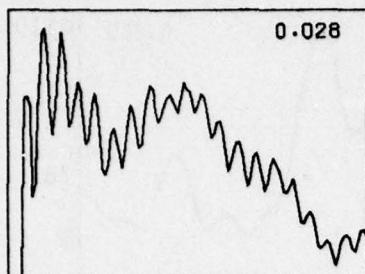
UNCLASSIFIED



Rock 2, 3", 30%

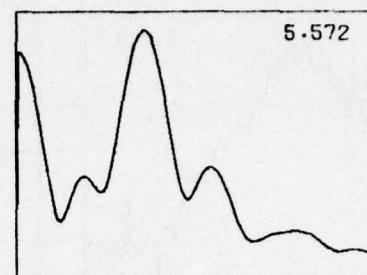
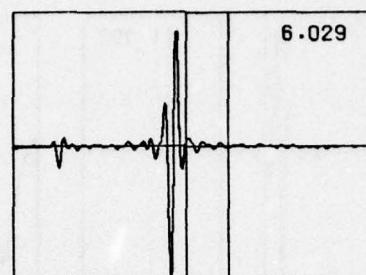
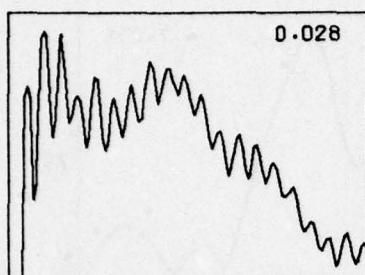
UNCLASSIFIED

UNCLASSIFIED

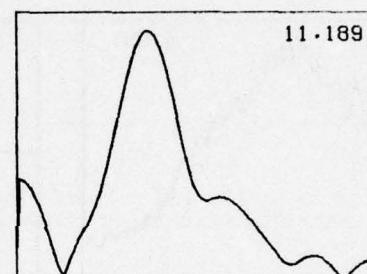
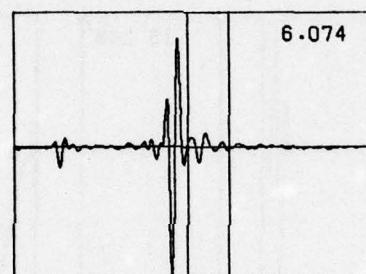
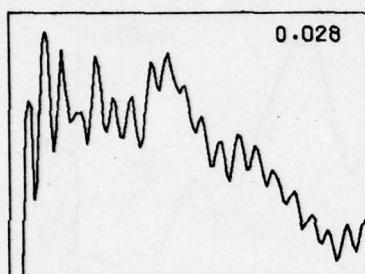


GT5

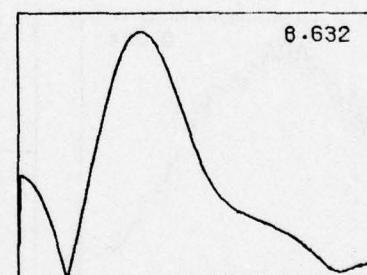
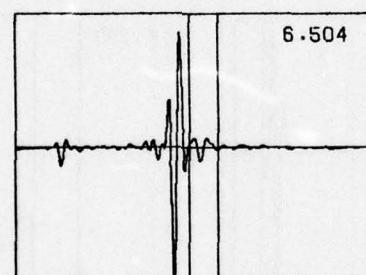
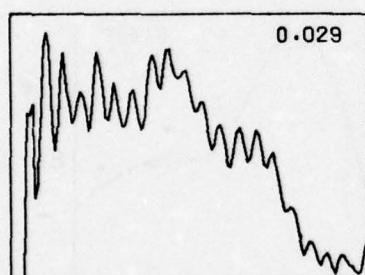
1



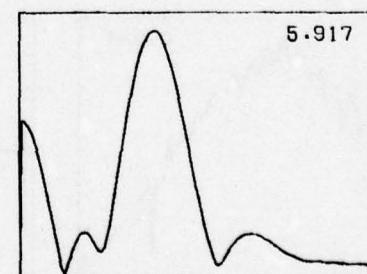
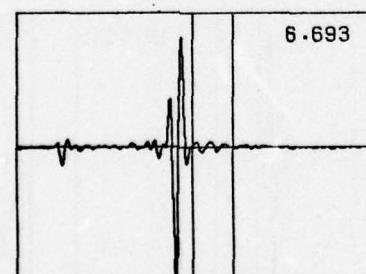
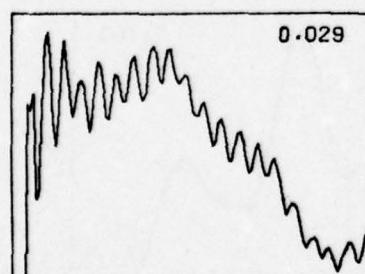
2



3



4



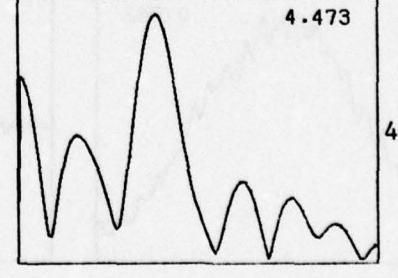
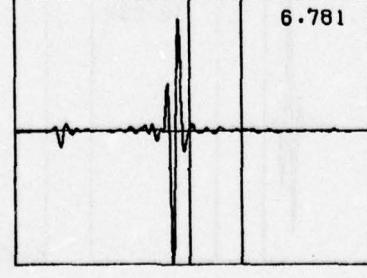
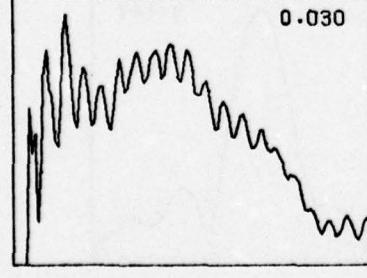
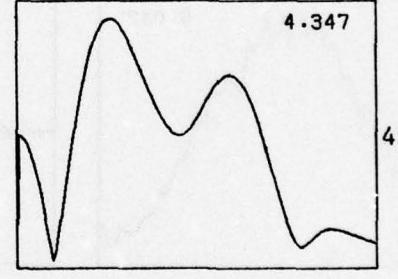
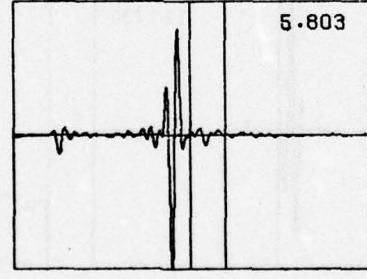
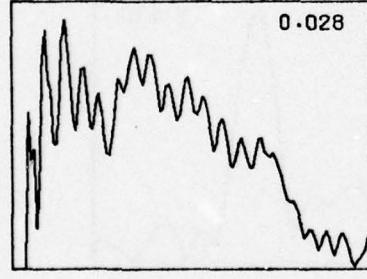
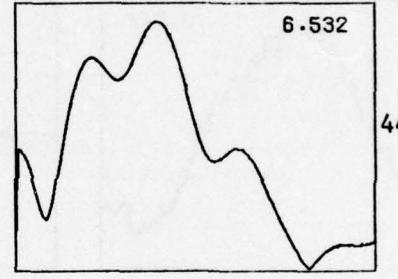
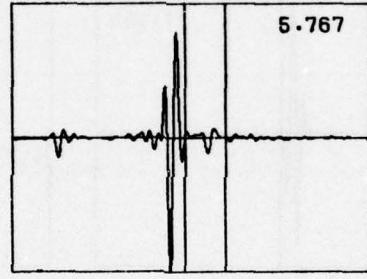
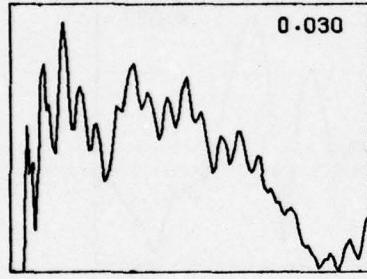
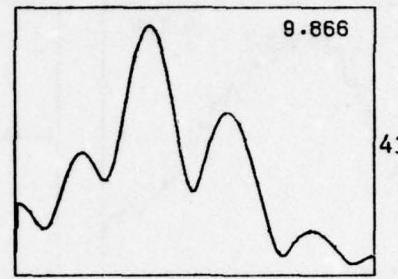
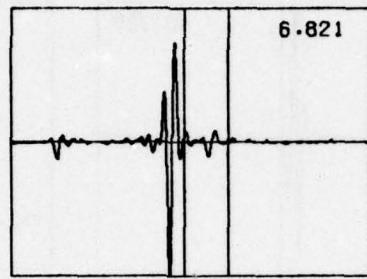
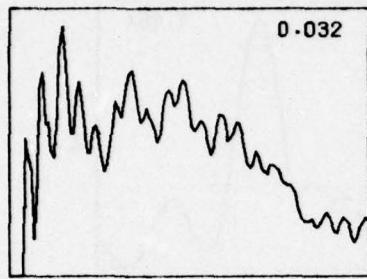
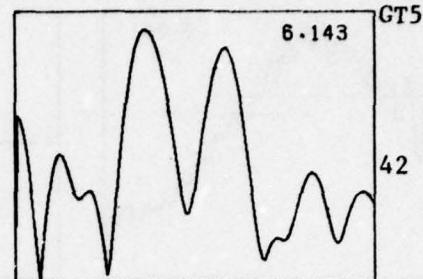
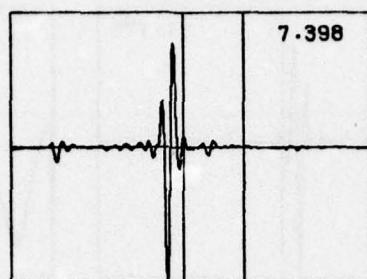
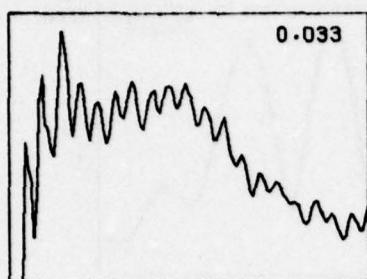
5

Root, 3", 7%

UNCLASSIFIED

A-56

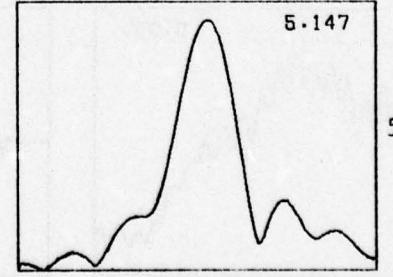
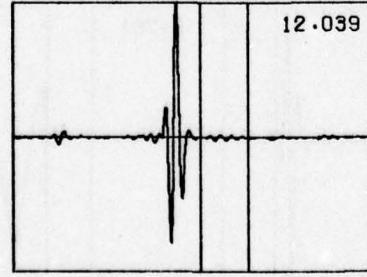
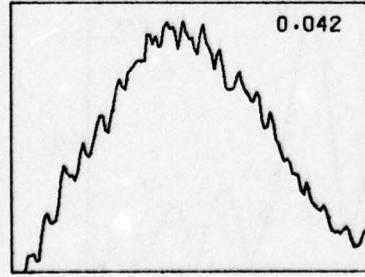
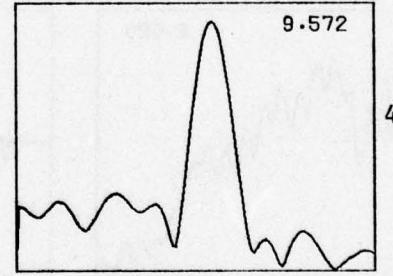
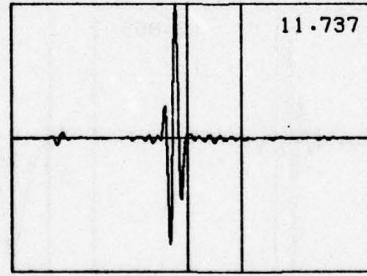
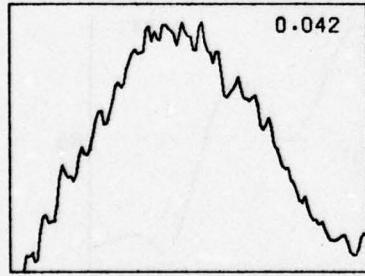
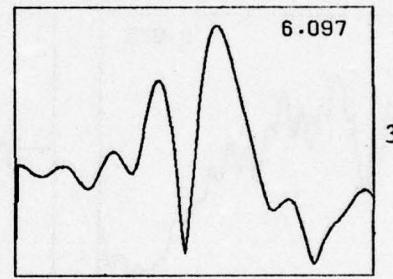
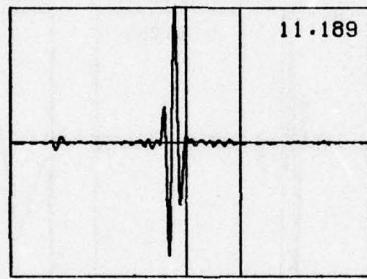
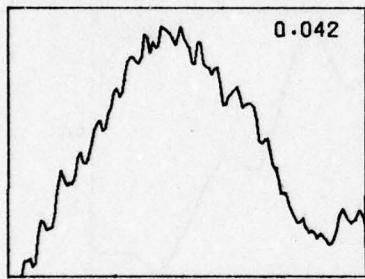
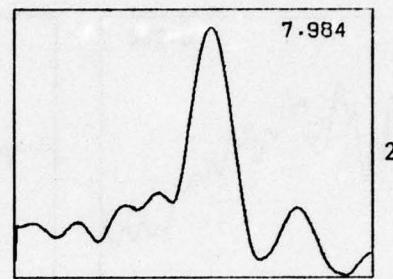
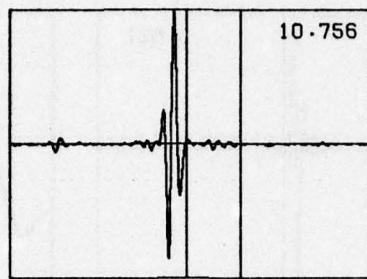
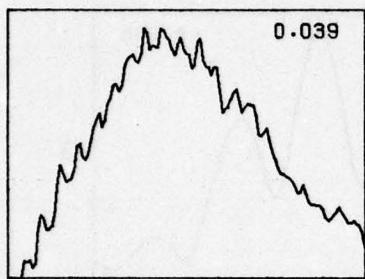
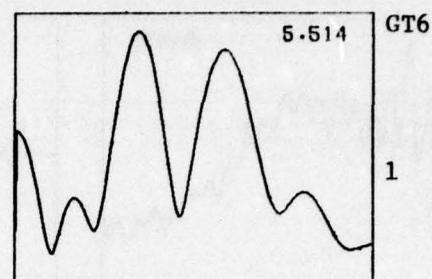
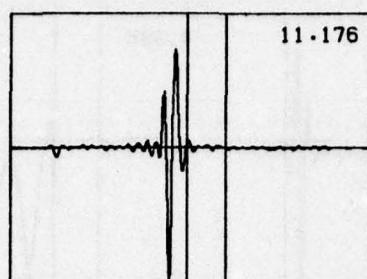
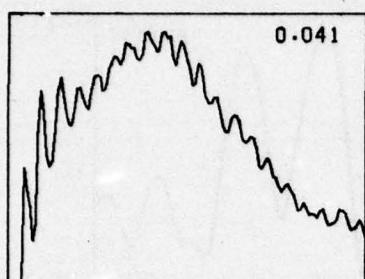
UNCLASSIFIED



Root, 6", 7%

UNCLASSIFIED

UNCLASSIFIED

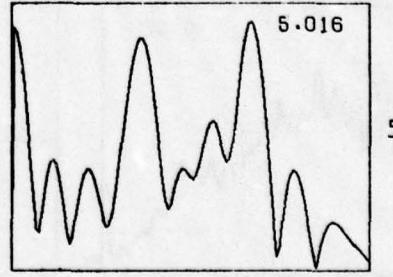
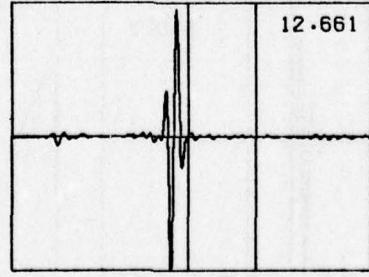
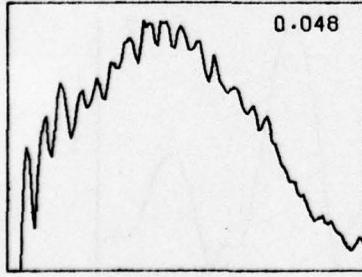
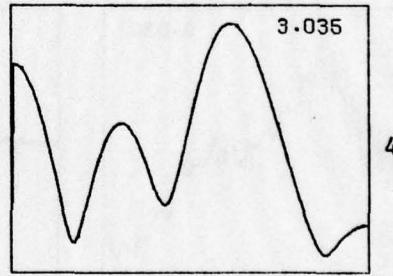
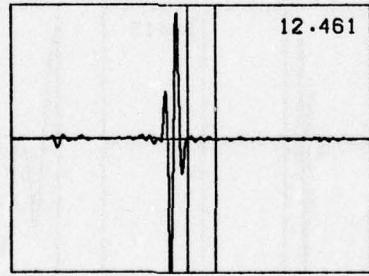
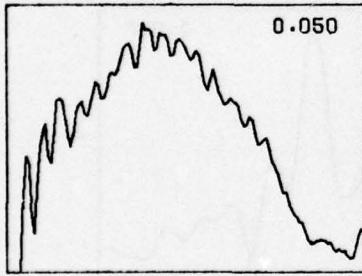
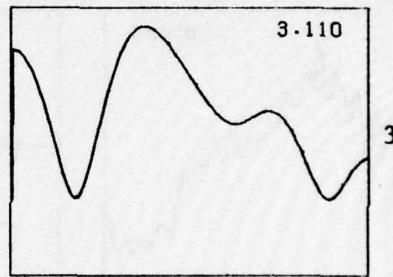
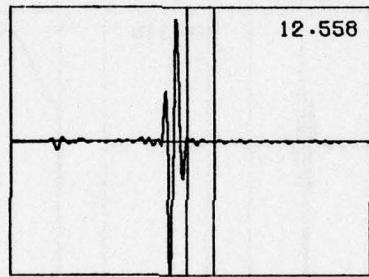
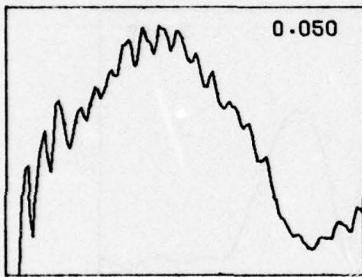
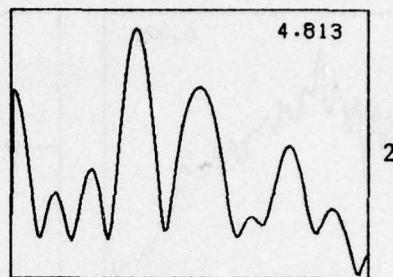
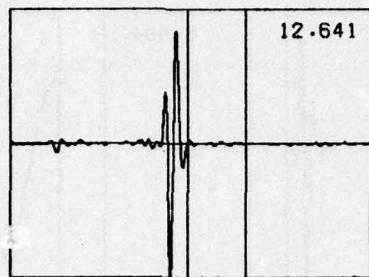
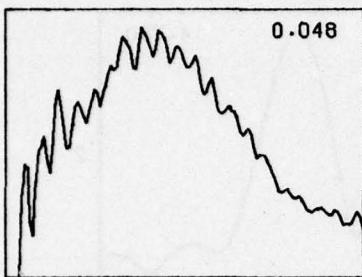
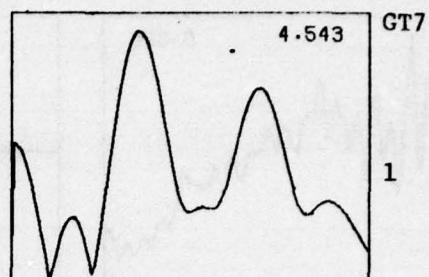
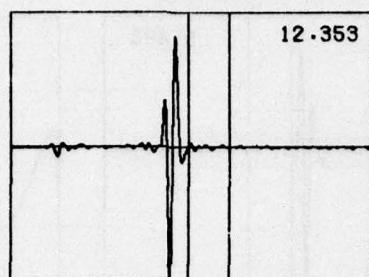
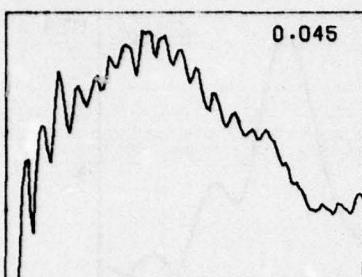


Root, 6", 17%

UNCLASSIFIED

A-58

UNCLASSIFIED

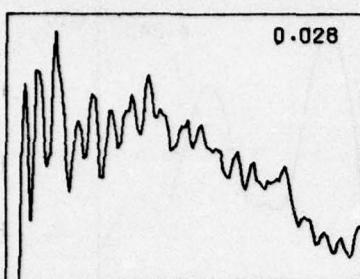


Root, 6", 18%

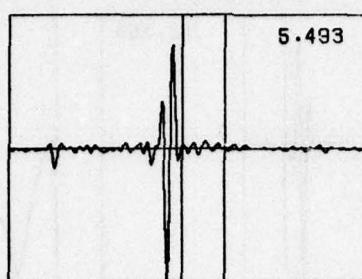
UNCLASSIFIED

A-59

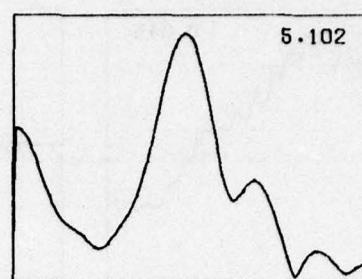
UNCLASSIFIED



0.028



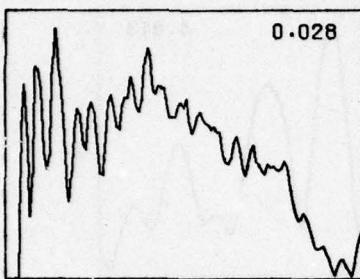
5.493



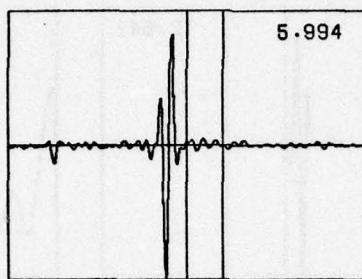
5.102

GT9

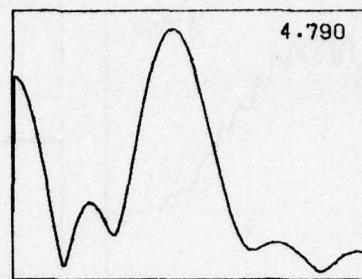
1



0.028

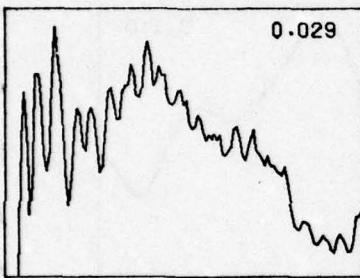


5.994

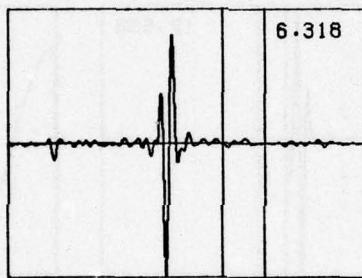


4.790

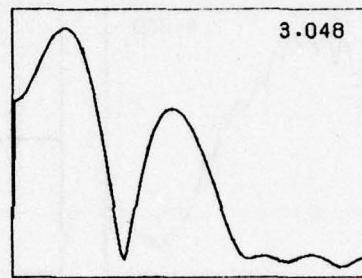
2



0.029

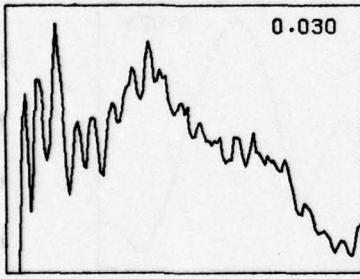


6.318

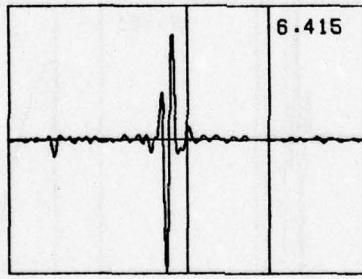


3.048

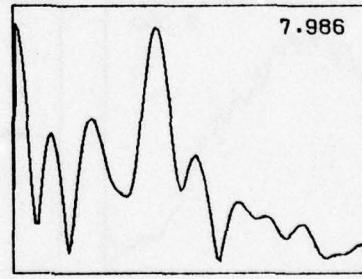
3



0.030

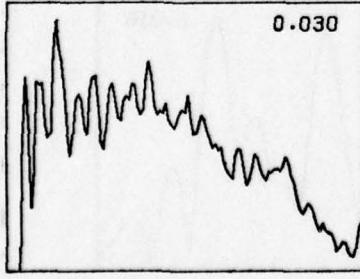


6.415

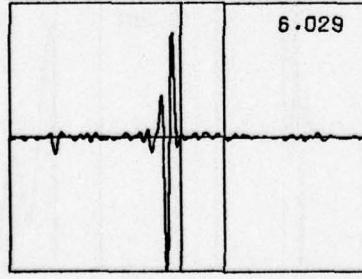


7.986

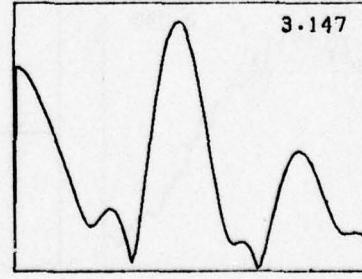
4



0.030



6.029



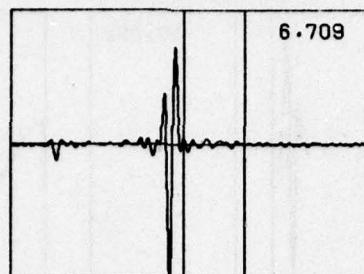
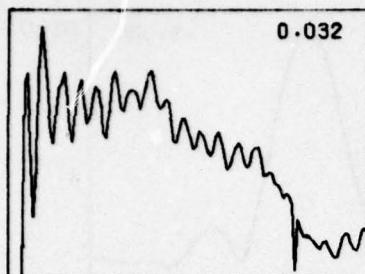
3.147

5

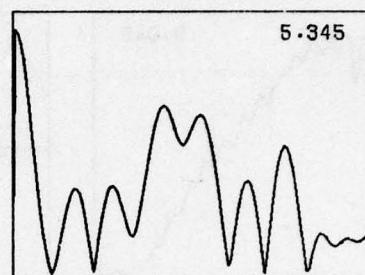
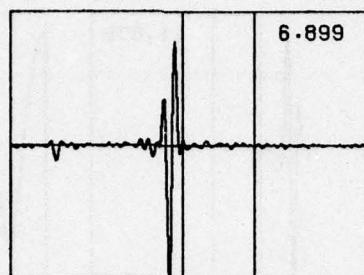
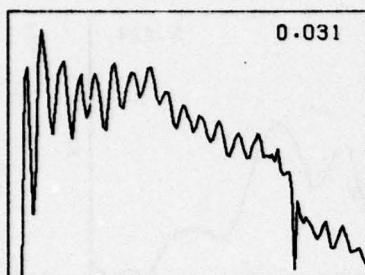
Root, 3", 12-20%

UNCLASSIFIED

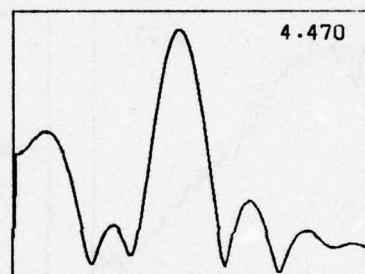
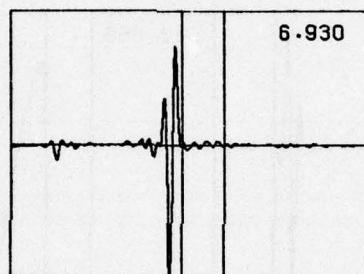
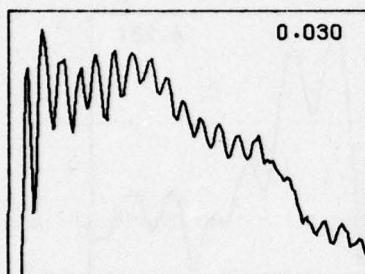
UNCLASSIFIED



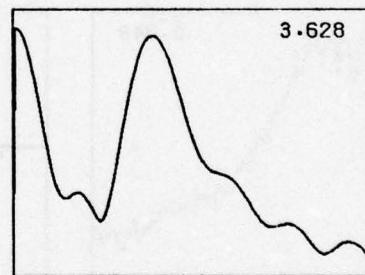
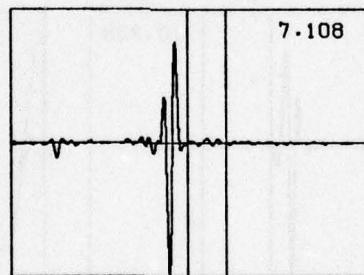
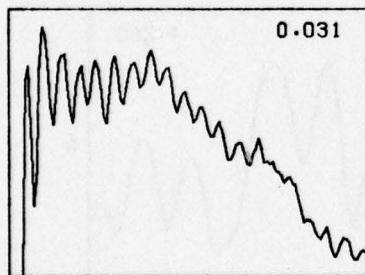
CTC



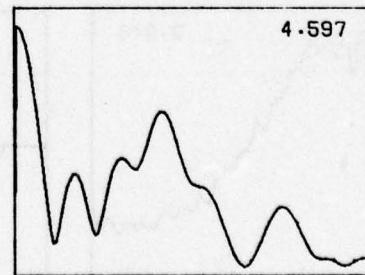
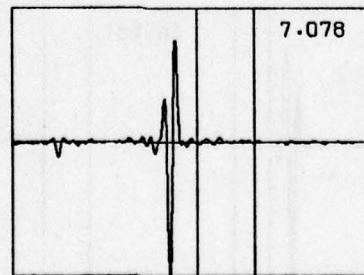
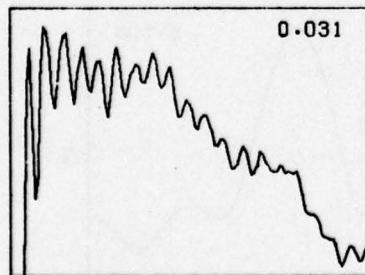
43



44



45

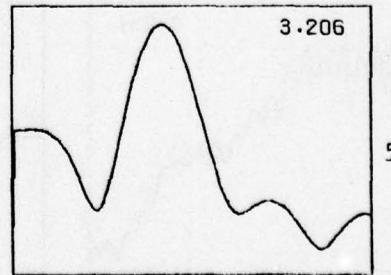
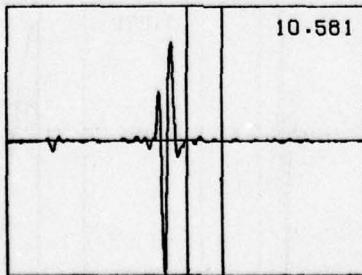
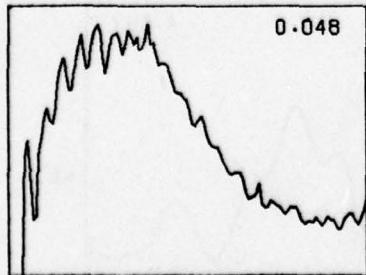
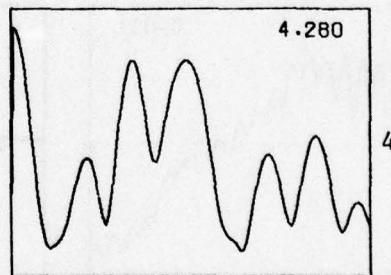
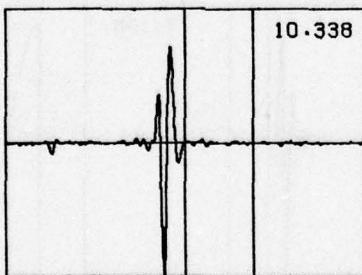
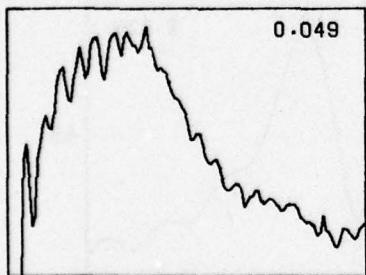
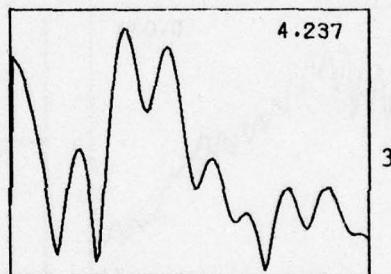
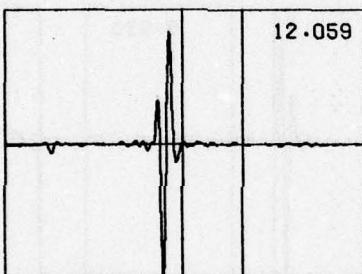
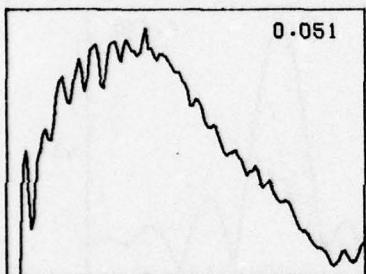
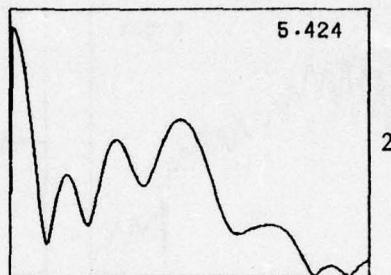
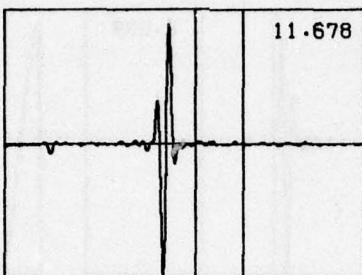
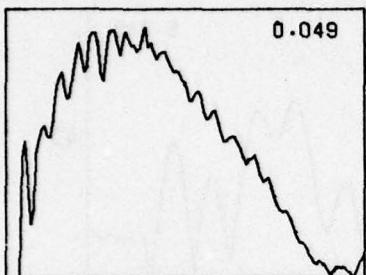
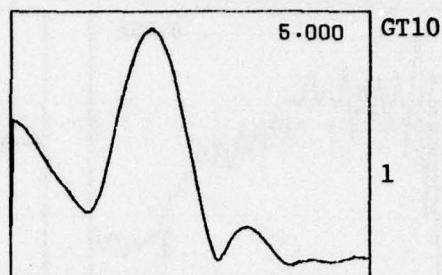
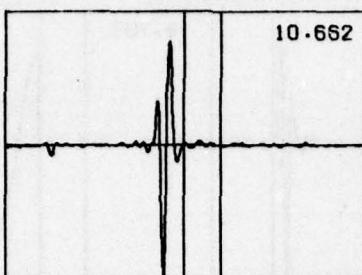
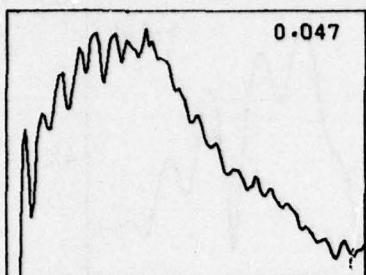


46

Root, 6", 13-16%

UNCLASSIFIED

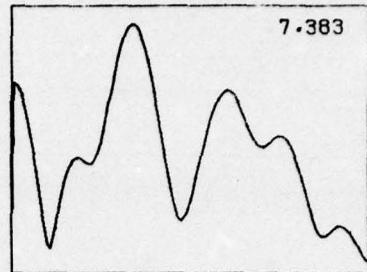
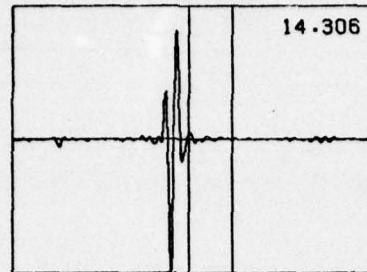
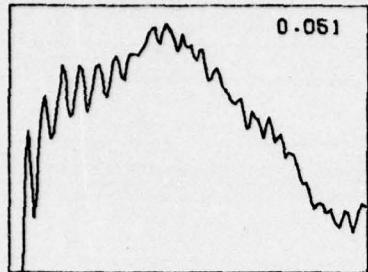
UNCLASSIFIED



Root, 6", 26-30%

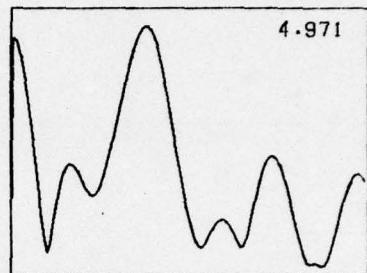
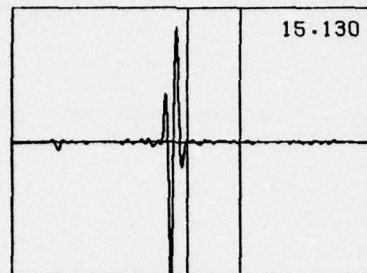
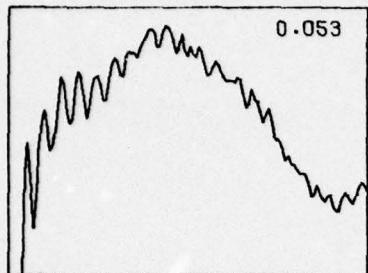
UNCLASSIFIED

UNCLASSIFIED

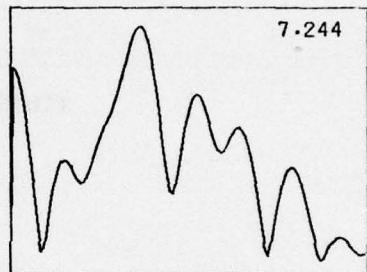
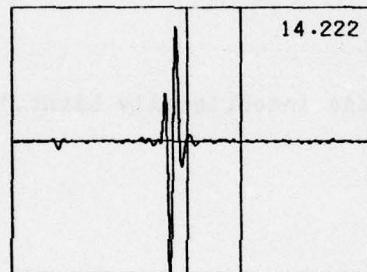
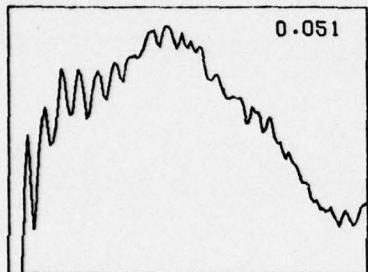


GT10

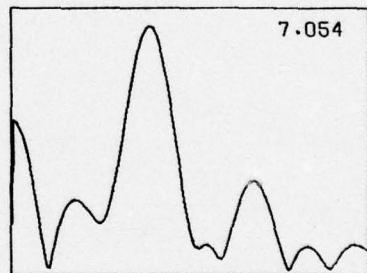
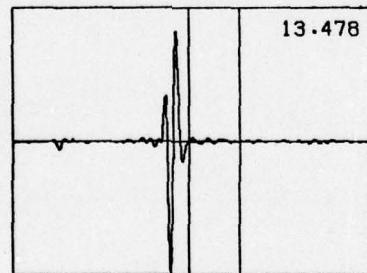
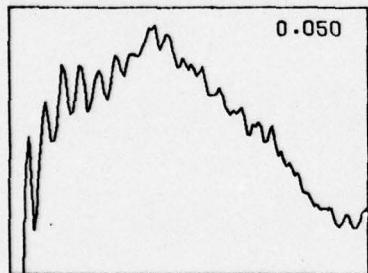
42



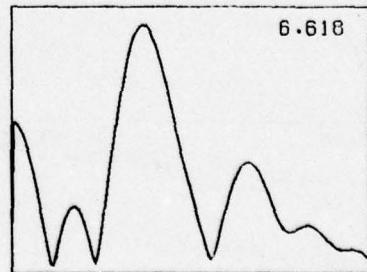
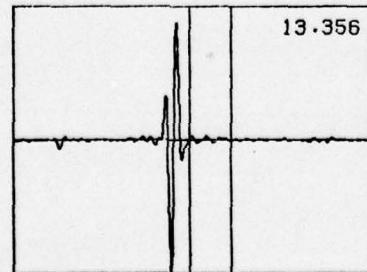
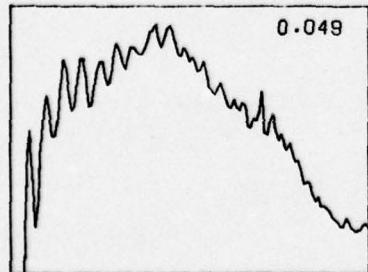
43



44



45



46

Root, 3", 30%

UNCLASSIFIED

Preceding Page BLANK - NOT FILMED

UNCLASSIFIED

APPENDIX B

**SHORT-PULSE RADAR DATA
SPECTRAL AND TEMPORAL PLOTS**

UNCLASSIFIED

UNCLASSIFIED

All of the sites for the short-pulse radar measurements were selected at random in the grounds surrounding the Georgia Tech Baker Building. The soil was dry red clay and was sandy in nature. All the mines, metal plates, and rocks were buried with their top surfaces approximately six inches beneath the soil surface. All large rocks and other debris were removed during the burying process. In some cases, the surface grass was replaced for the measurement. Only one of the three radar modules was used in the data collection; the same radar was used for all measurements. The radar antenna was placed approximately four inches above the soil surface in each case.

A matrix of measurements made with the short-pulse radar is given in Table B-1. Since the major purpose of the short-pulse measurements was to verify that this measurement system is effective for target discrimination/classification, all of the measurements were made in dry soil. All objects were buried 6 inches below the soil surface in a red clay soil. The objects buried were two types of non-metallic mines, a metallic mine*, a metal plate, and a rock about the same size as the mines. In addition, some data were taken in ground without buried objects and is labeled in Table B-1 as background data. Each object was buried in 4 different locations, and for each location, three radar measurements were taken. One measurement was taken with the radar antenna centered over the object, and measurements 4 inches on either side of the center. Thus, a total of 12 measurements per object were

*The metallic mine measurements were taken to investigate the radar signatures obtained from metallic targets. This effort was not in direct support of the non-metallic mine detection program; however, these measurements are included for the sake of completeness.

UNCLASSIFIED

UNCLASSIFIED

| Target | Position | Location 1 | Location 2 | Location 3 | Location 4 |
|-------------|----------|------------|------------|------------|------------|
| Rock | -4 | 1 | 19 | 37 | 55 |
| | 0 | 2 | 20 | 38 | 56 |
| | +4 | 3 | 21 | 39 | 57 |
| Metal Plate | -4 | 4 | 22 | 40 | 58 |
| | 0 | 5 | 23 | 41 | 59 |
| | +4 | 6 | 24 | 42 | 60 |
| Type A Mine | -4 | 7 | 25 | 43 | 61 |
| | 0 | 8 | 26 | 44 | 62 |
| | +4 | 9 | 27 | 45 | 63 |
| Type C Mine | -4 | 10 | 28 | 46 | 64 |
| | 0 | 11 | 29 | 47 | 65 |
| | +4 | 12 | 30 | 48 | 66 |
| Type D Mine | -4 | 13 | 31 | 49 | 67 |
| | 0 | 14 | 32 | 50 | 68 |
| | +4 | 15 | 33 | 51 | 69 |
| Background | -4 | 16 | 34 | 52 | 70 |
| | 0 | 17 | 35 | 53 | 71 |
| | +4 | 18 | 36 | 54 | 72 |

Table B-1. Short-pulse radar matrix.

UNCLASSIFIED

UNCLASSIFIED

taken. Table B-1 also indicates the data run numbers assigned in the Georgia Tech data files.

The format of the data plots is shown in Figures B-1 and B-2. The plots on each page are arranged in two columns and three rows, each row being the data for one of the three positions over or near the target. The first plot in each row is the measured time response. This data is the sampled video signal out of the short-pulse radar. Most of the ground return has been eliminated by circuitry in the radar system. The left most extremity of the plot represents the radar return just below the ground surface. The time scale on the plot is 0 to 7 nanoseconds (7 milliseconds of video). The two vertical lines mark the extent of the target signature and were positioned manually.

The second plot on each row is the spectrum of the gated time signature obtained by use of the Fast Fourier Transform. The frequency scale used is from 0 Hz to 3.3 GHz. This is the target signature used for classification and discrimination. The number in the upper right-hand corner of each plot is the value of the vertical scale and is included to accommodate amplitude comparisons. The integer numbers in the right column are the data file numbers listed in Table B-1.

UNCLASSIFIED

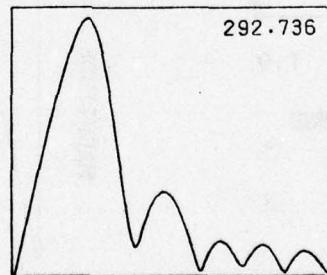
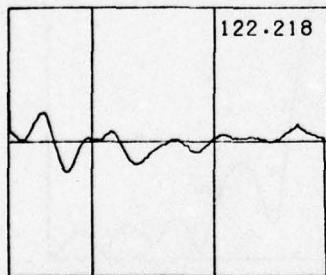
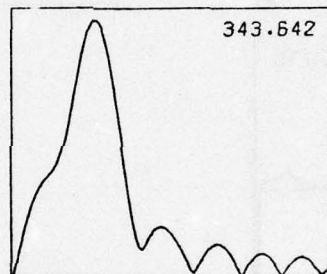
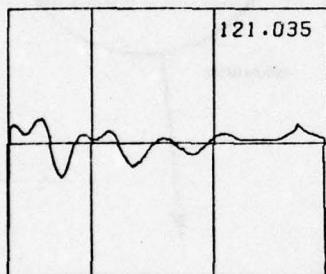
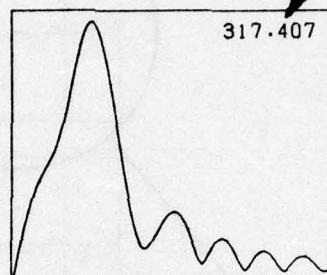
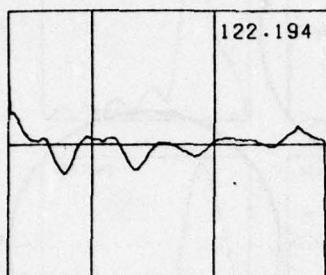
B-4

UNCLASSIFIED

TEMPORAL RESPONSE
(VIDEO)

GATED SPECTRAL
RESPONSE

VALUE ASSIGNED
TO VERTICAL
SCALE OF PLOT



1

2

3

DATA FILE
NUMBER

UNCLASSIFIED

Figure B-1. Data display format.

UNCLASSIFIED

UNCLASSIFIED

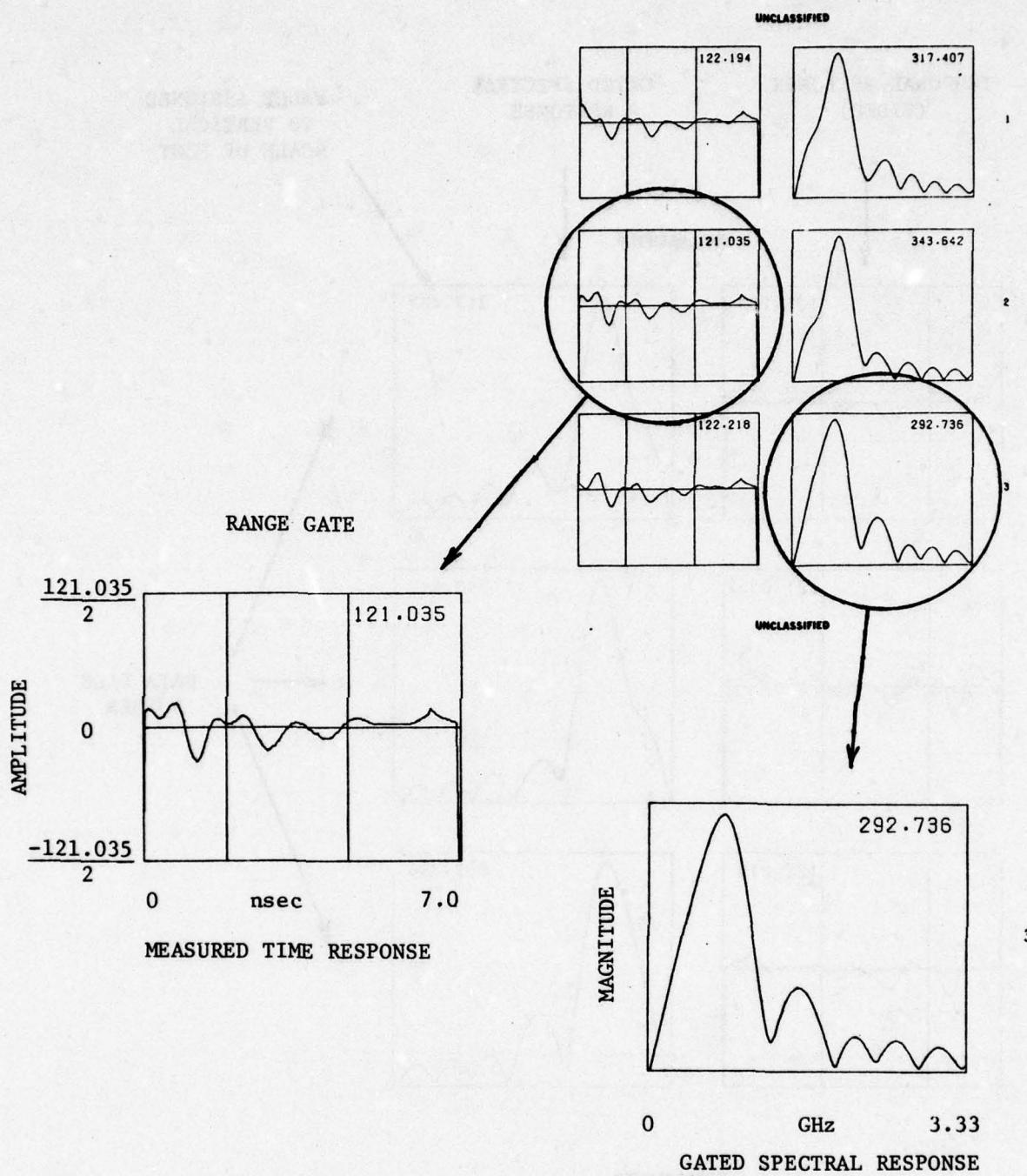
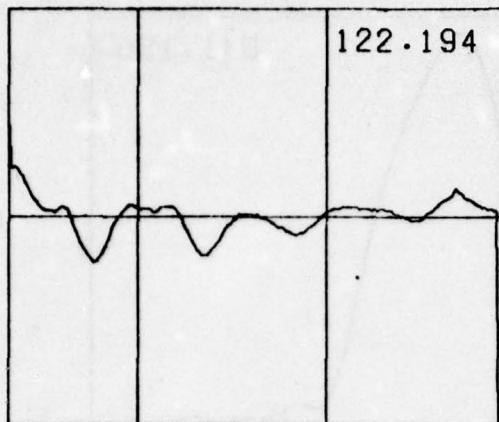


Figure B-2. Data characteristics.

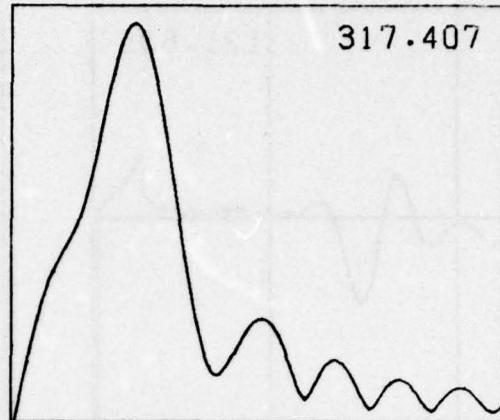
UNCLASSIFIED

B-6

UNCLASSIFIED

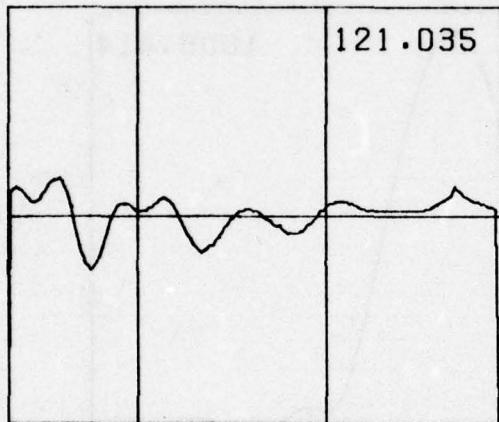


122.194

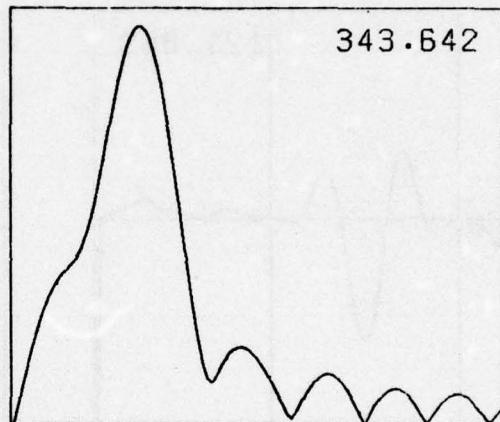


317.407

1

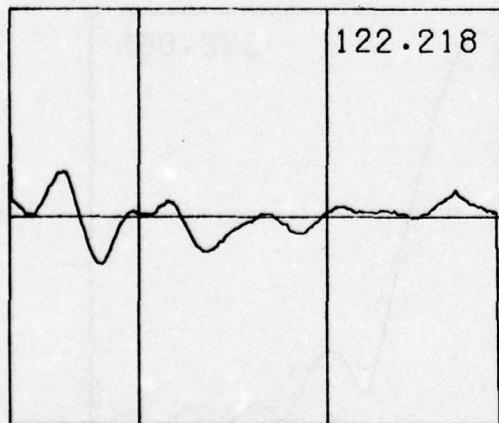


121.035

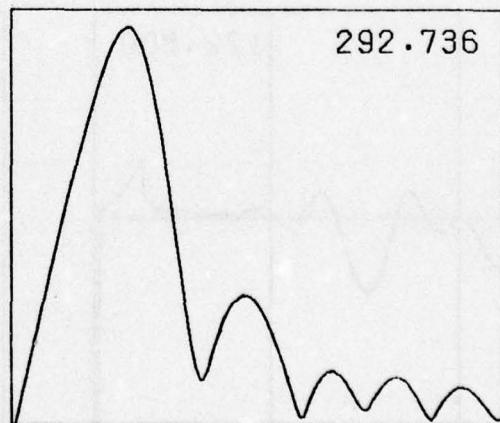


343.642

2



122.218

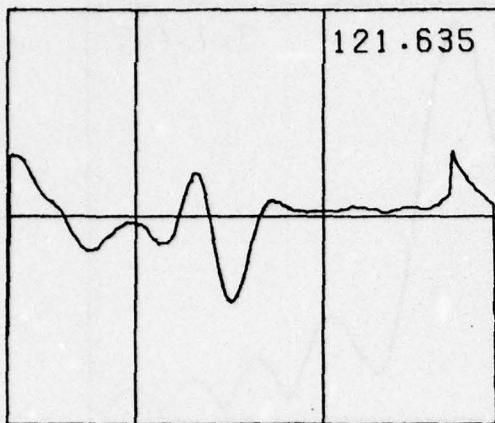


292.736

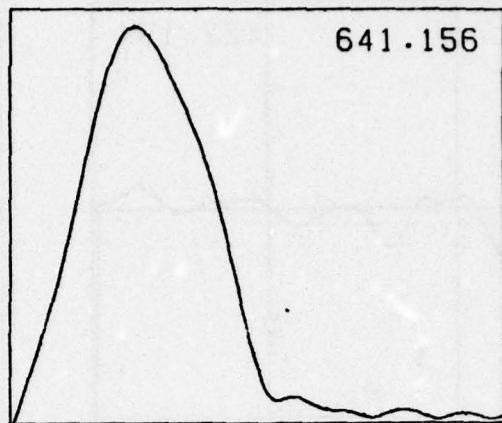
3

UNCLASSIFIED

UNCLASSIFIED

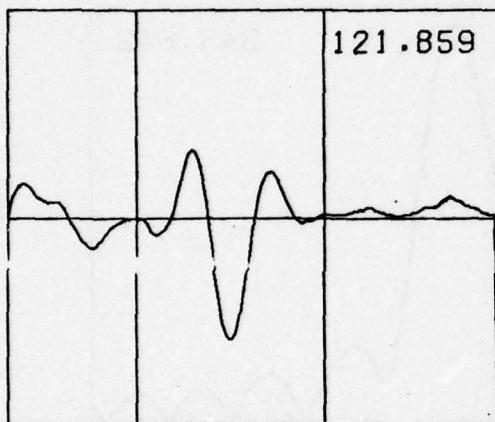


121.635

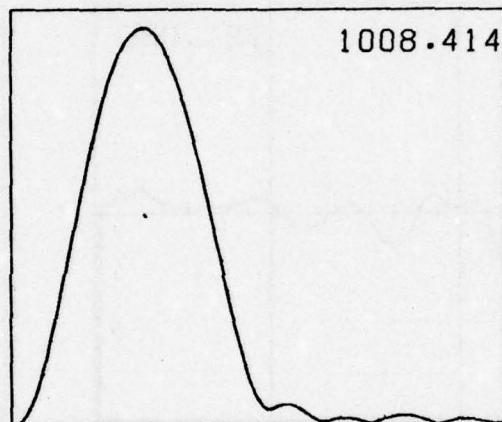


641.156

4

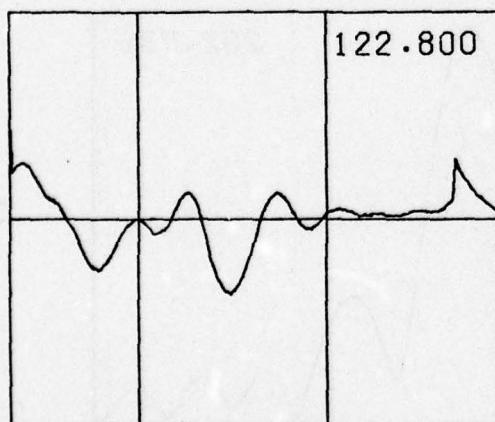


121.859

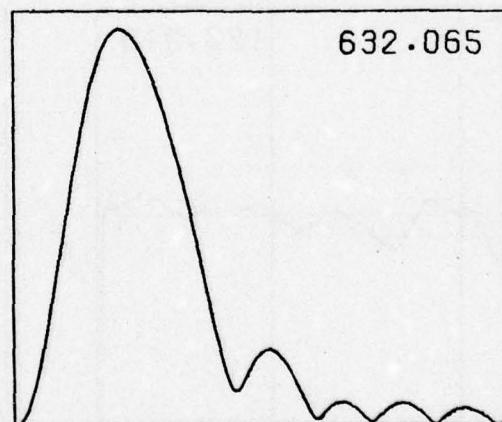


1008.414

5



122.800



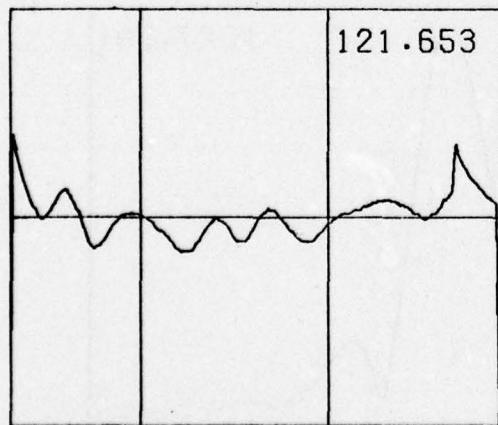
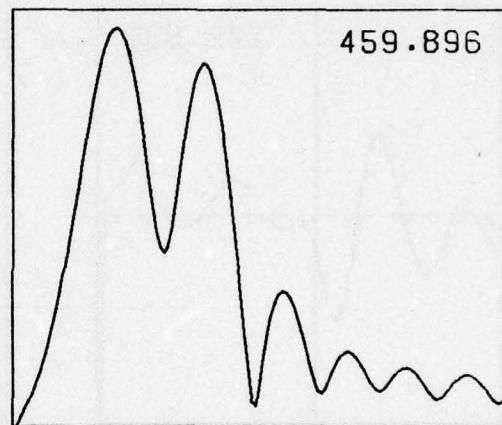
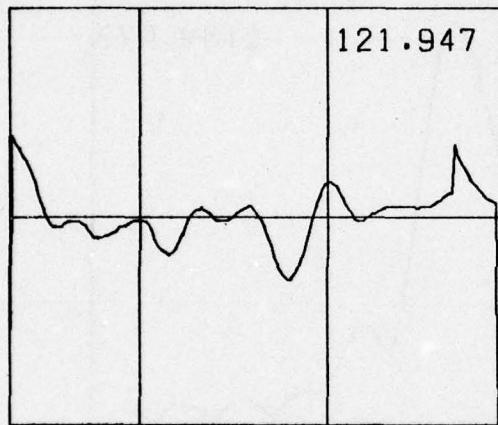
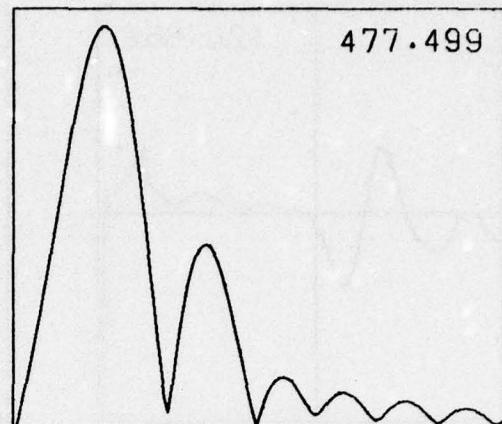
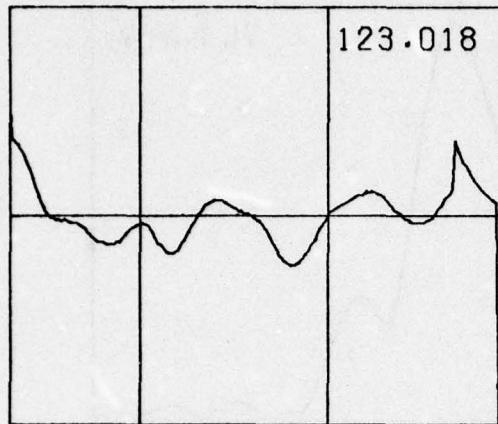
632.065

6

UNCLASSIFIED

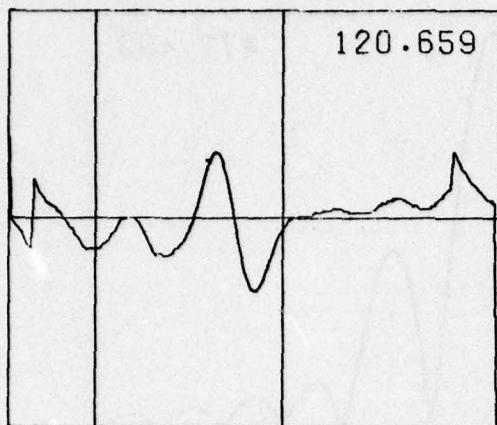
B-8

UNCLASSIFIED



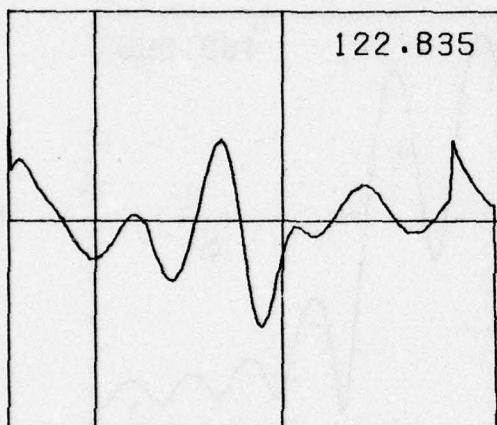
UNCLASSIFIED

UNCLASSIFIED



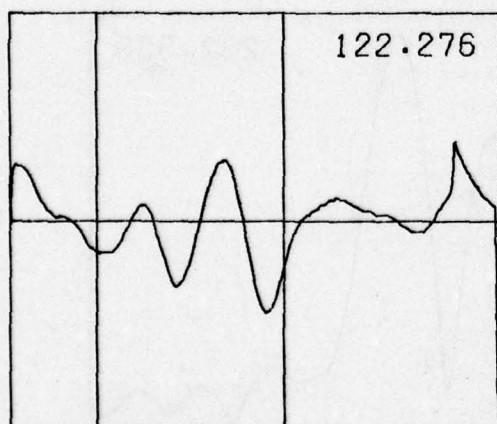
763.787

10



1139.079

11

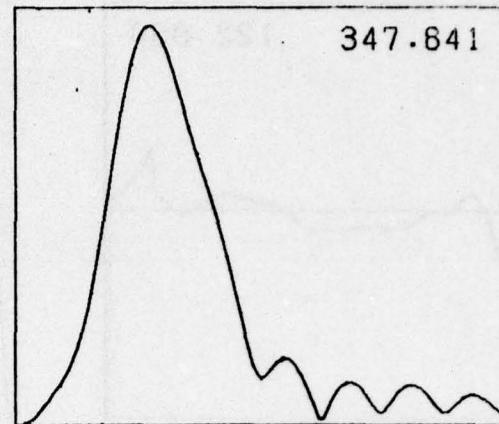
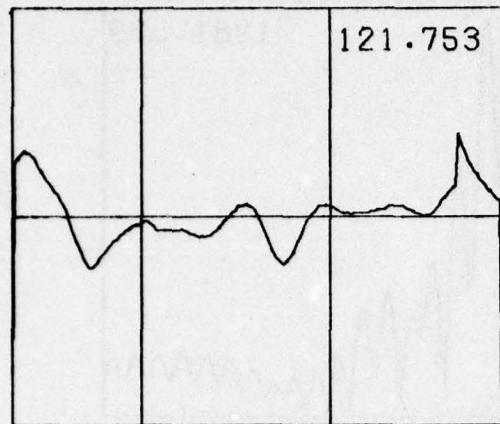


1027.591

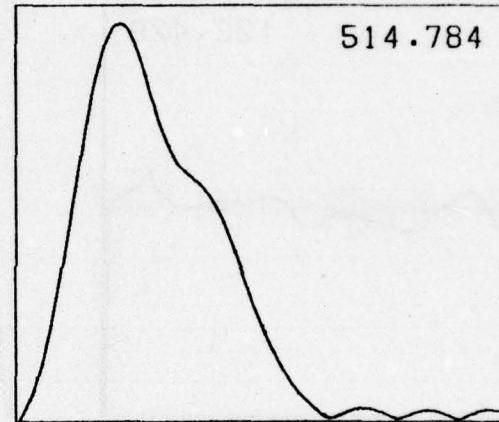
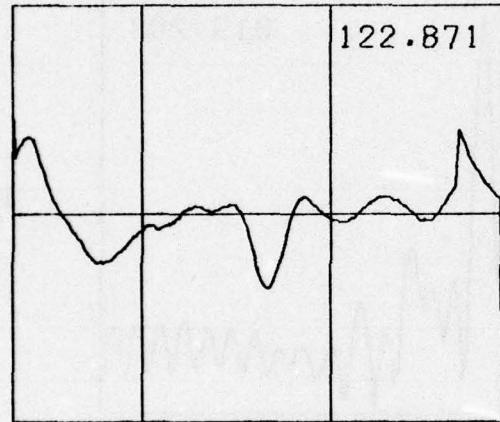
12

UNCLASSIFIED

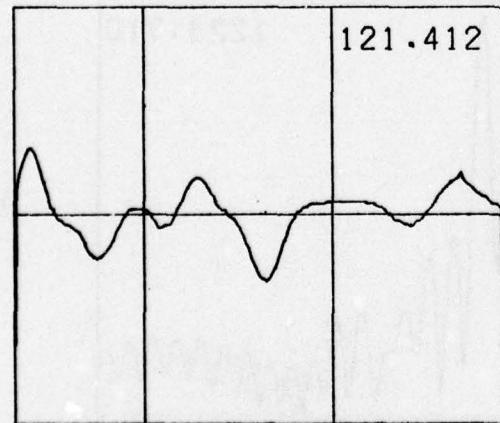
UNCLASSIFIED



13



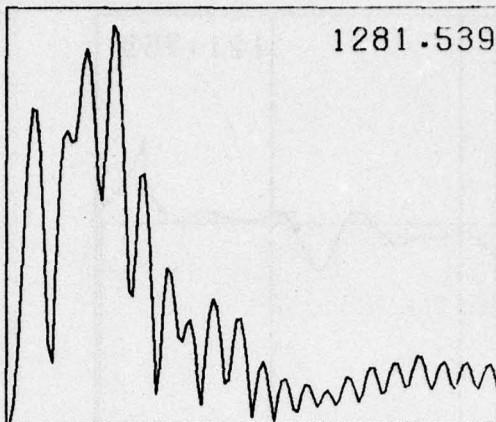
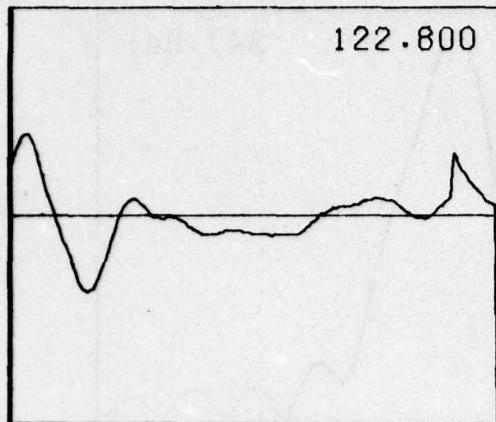
14



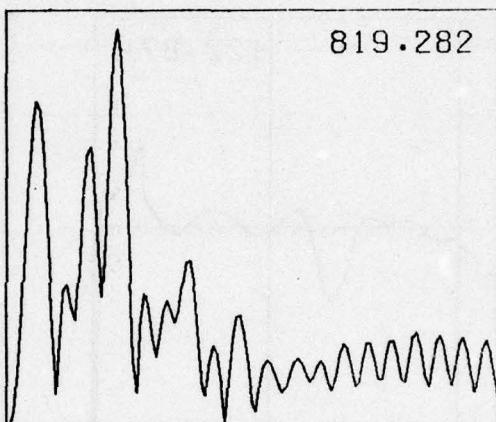
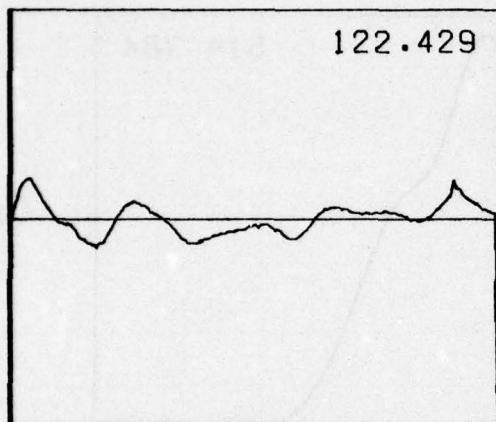
15

UNCLASSIFIED

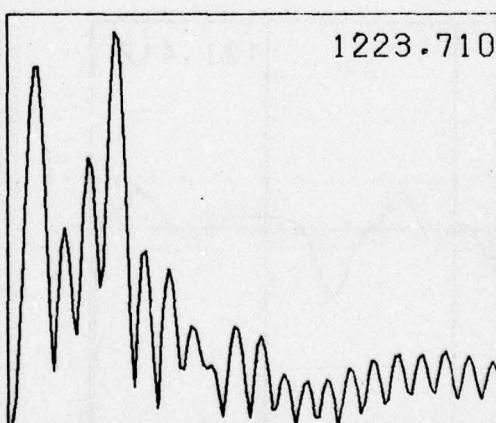
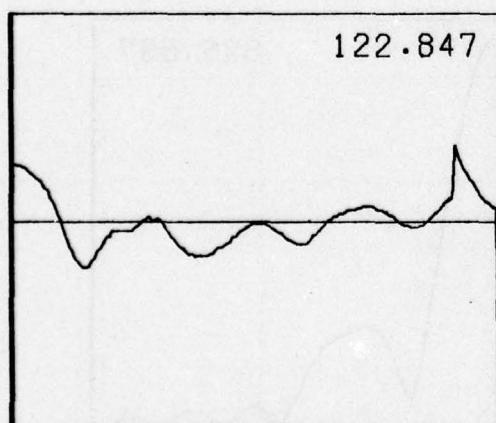
UNCLASSIFIED



16



17

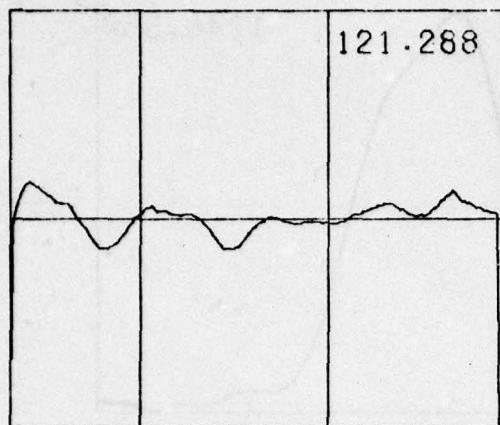


18

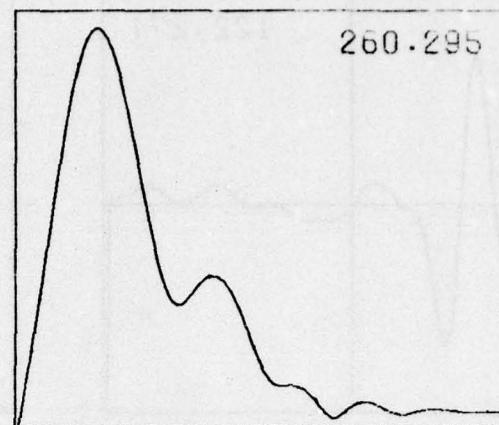
UNCLASSIFIED

B-12

UNCLASSIFIED

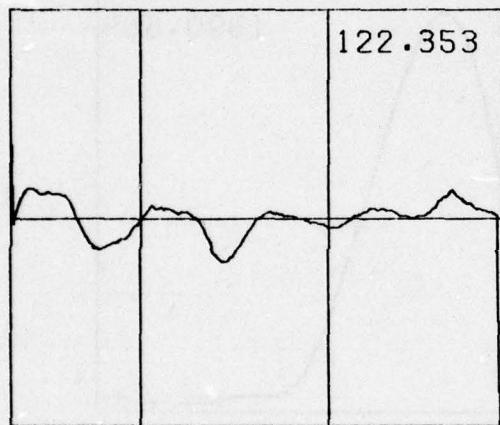


121.288

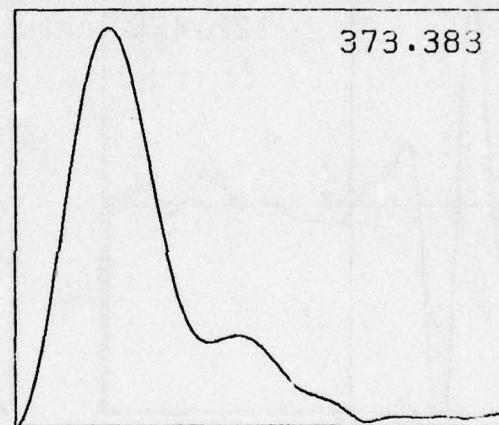


260.295

19

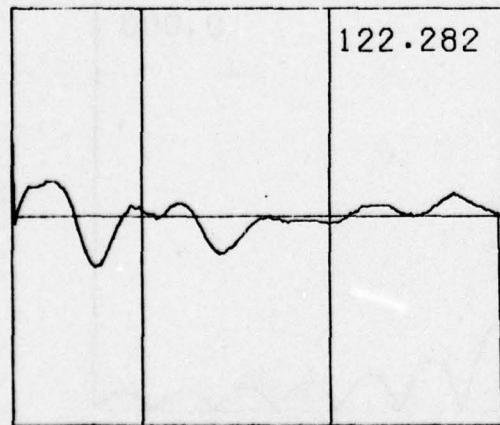


122.353

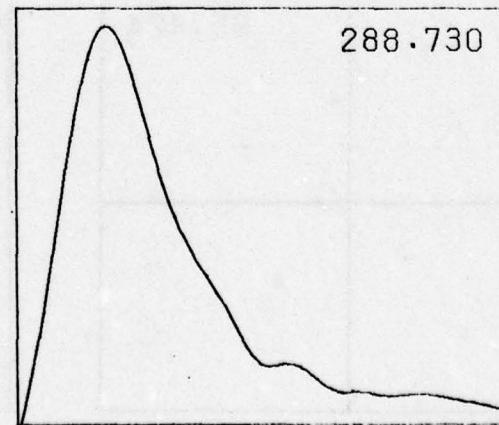


373.383

20



122.282



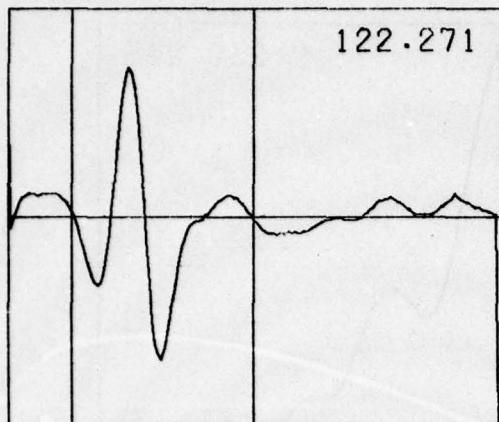
288.730

21

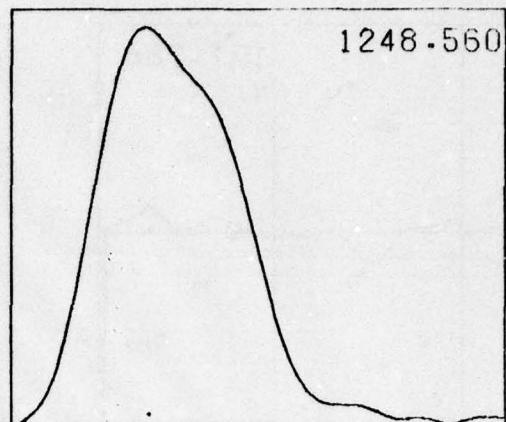
UNCLASSIFIED

B-13

UNCLASSIFIED

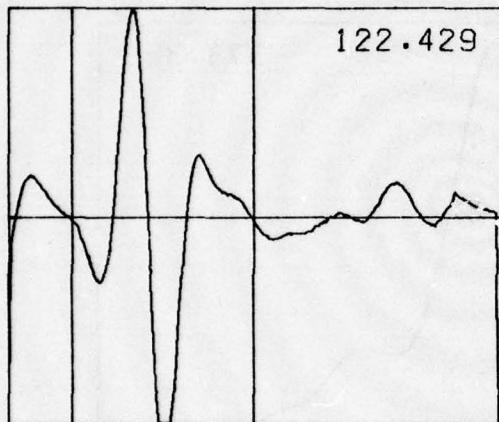


122.271

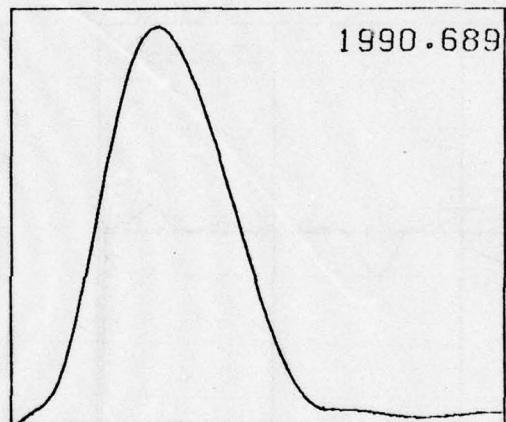


1248.560

22

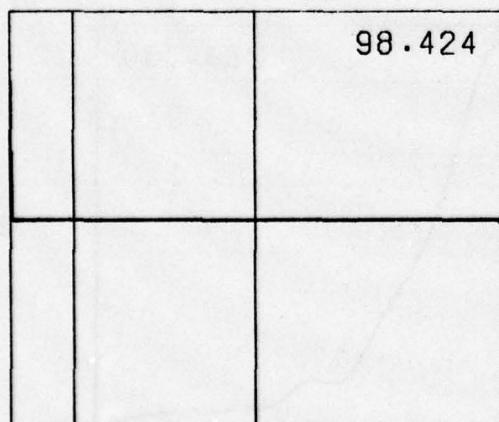


122.429

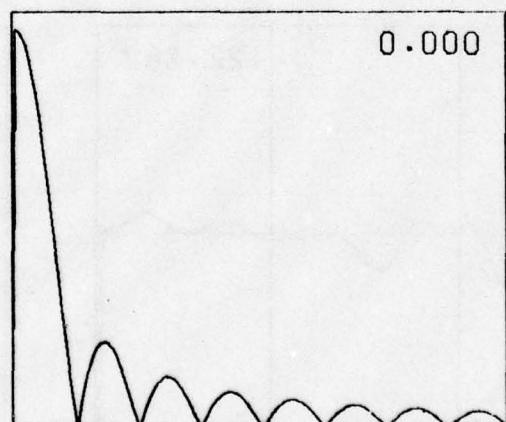


1990.689

23



98.424



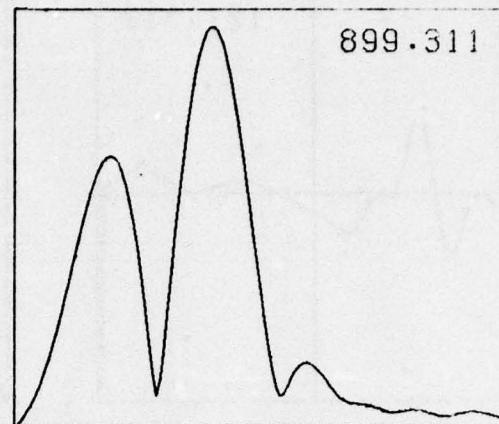
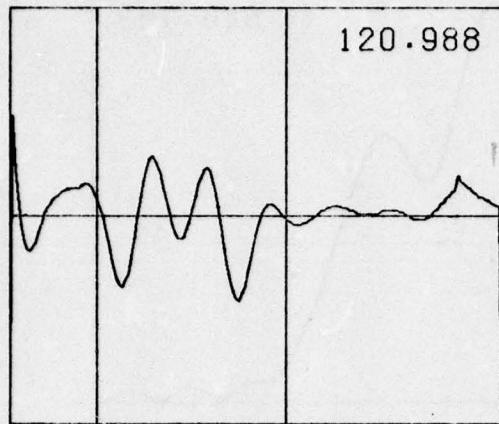
0.000

24

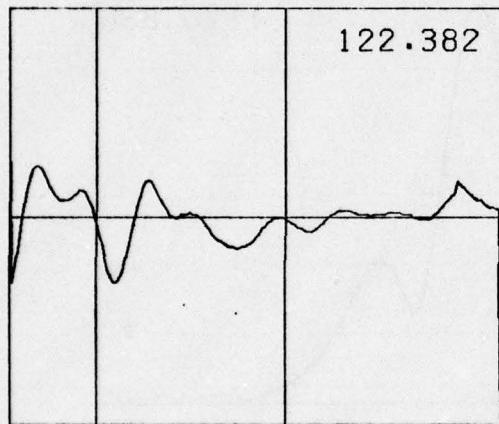
UNCLASSIFIED

B-14

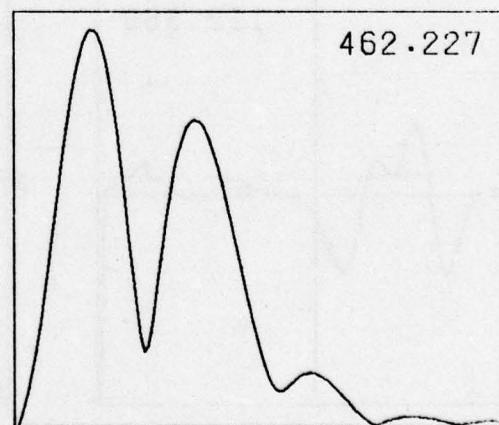
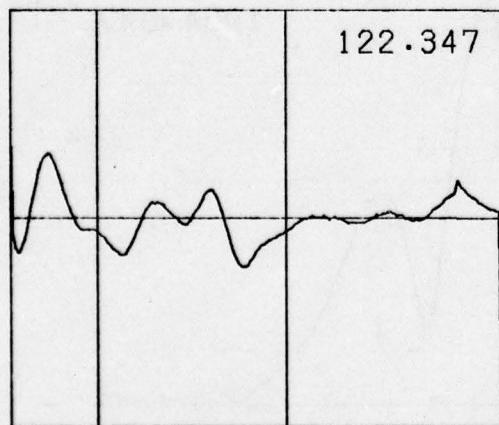
UNCLASSIFIED



25



26

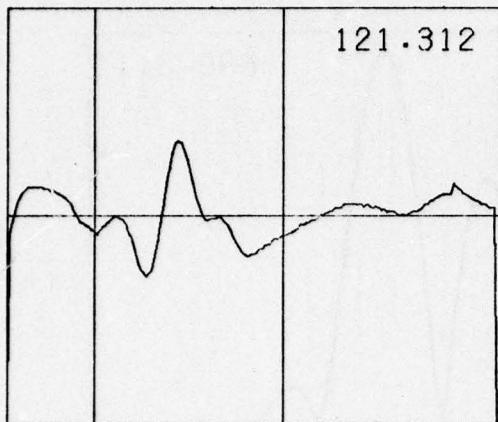


27

UNCLASSIFIED

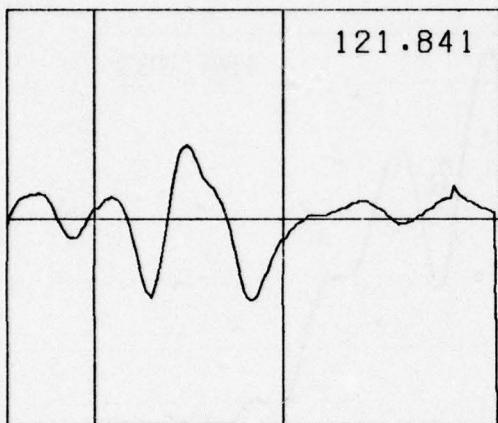
B-15

UNCLASSIFIED



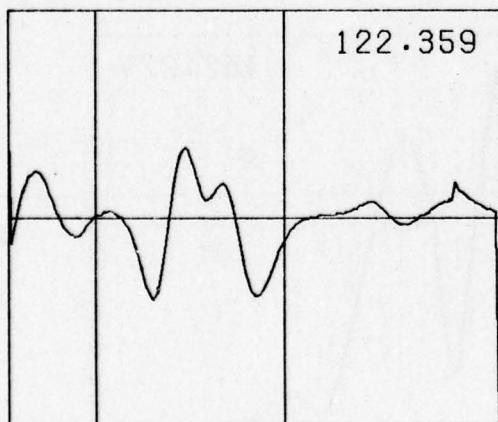
646.763

28



1120.836

29



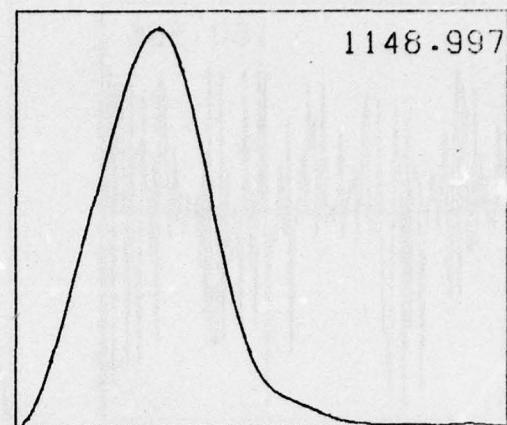
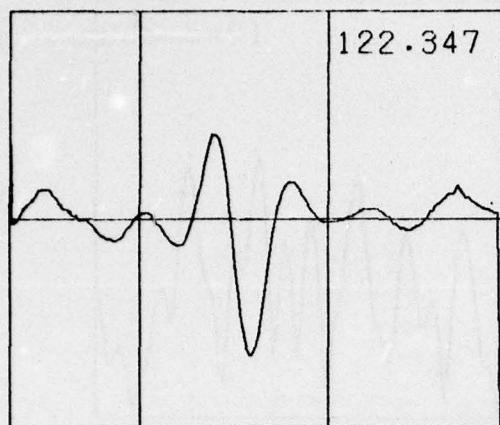
1004.037

30

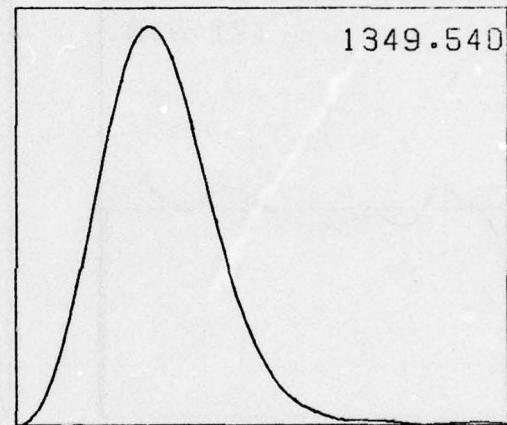
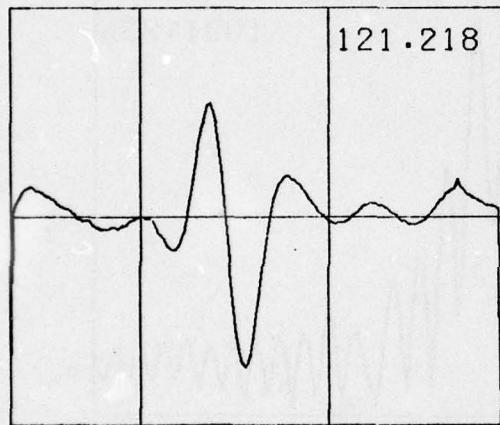
UNCLASSIFIED

B-16

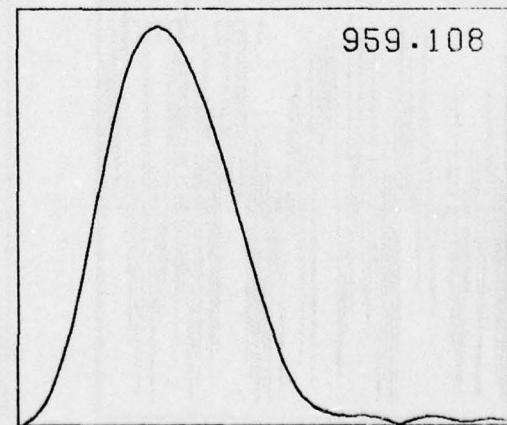
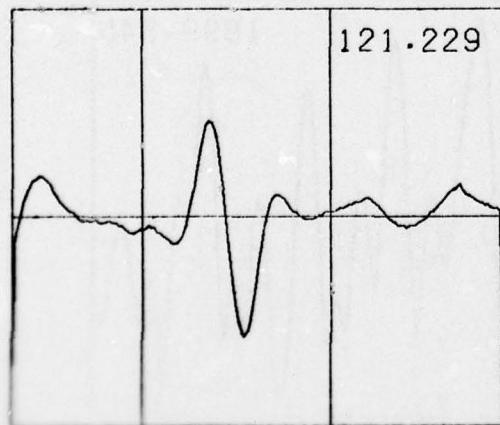
UNCLASSIFIED



31



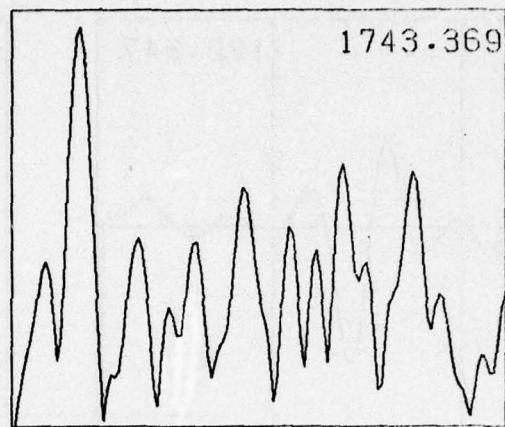
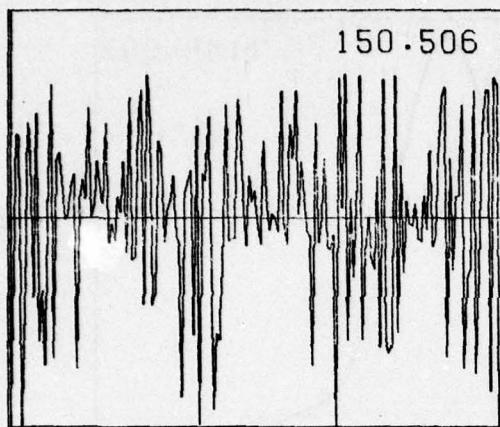
32



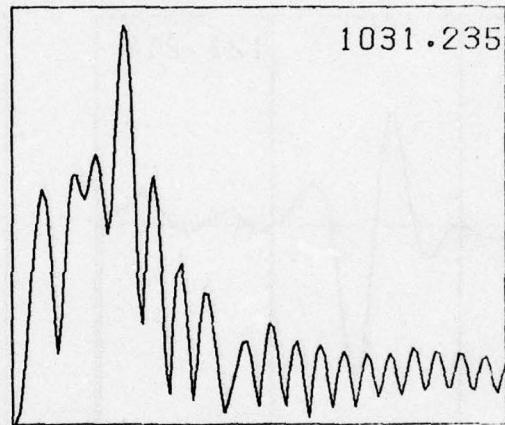
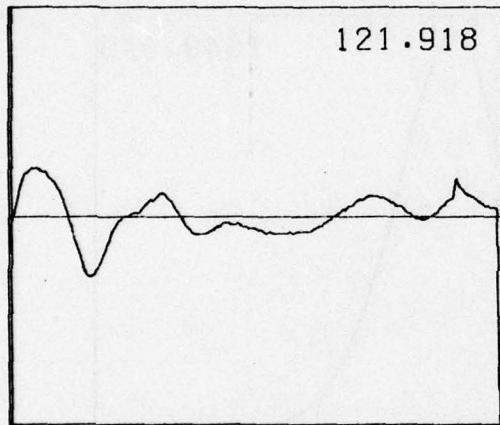
33

UNCLASSIFIED

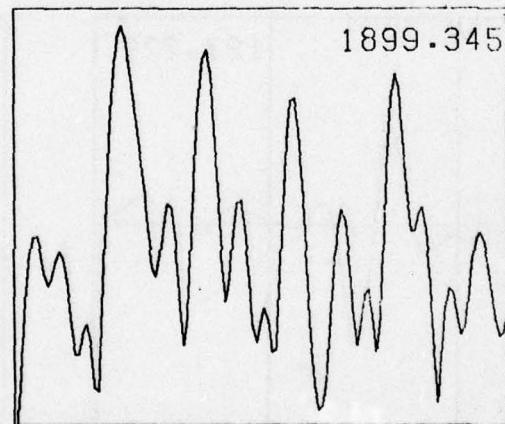
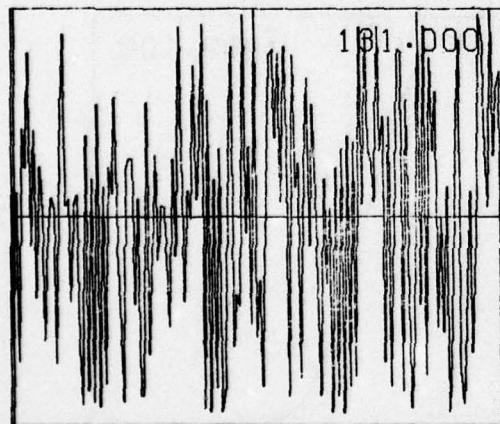
UNCLASSIFIED



34



35

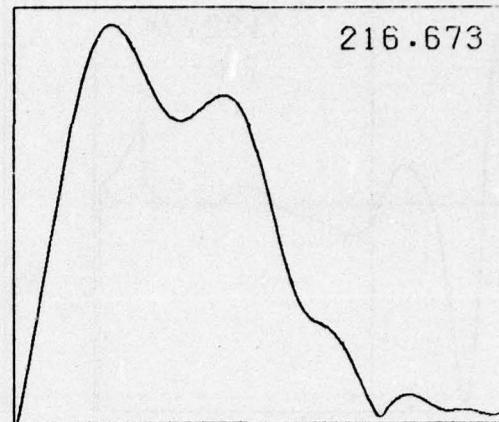
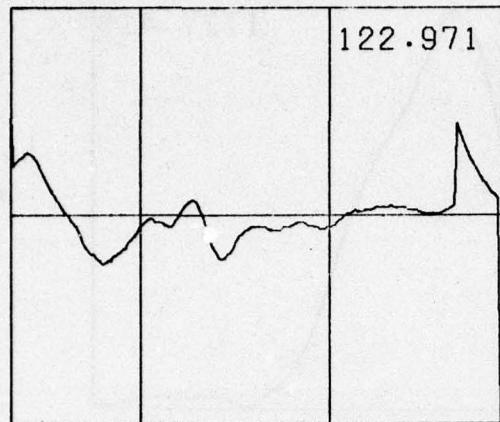


36

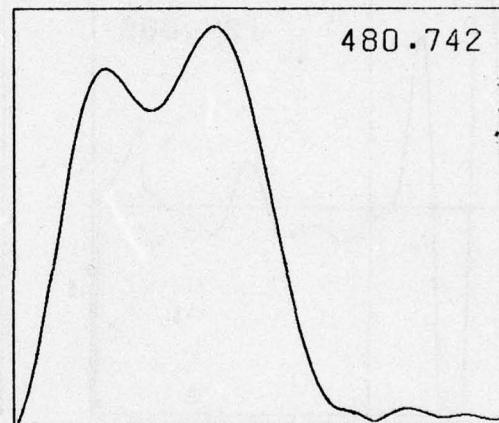
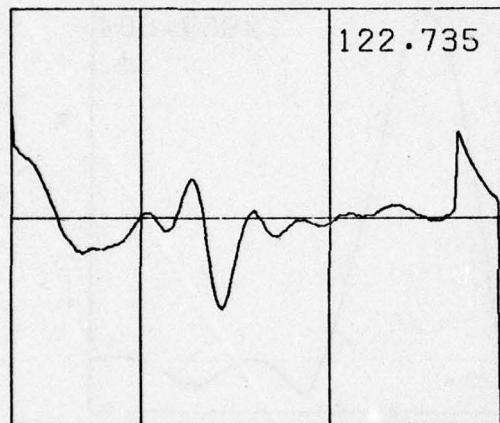
UNCLASSIFIED

B-18

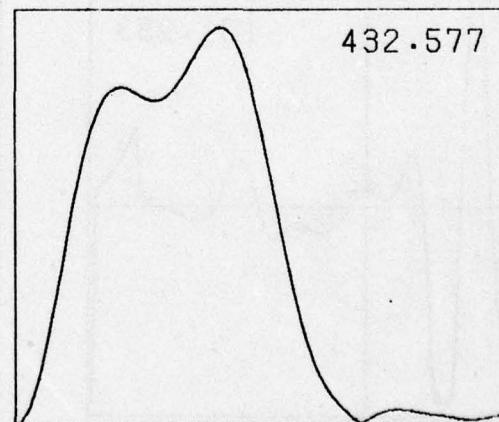
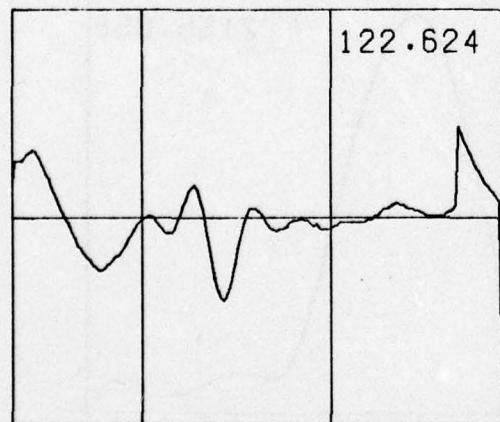
UNCLASSIFIED



37



38

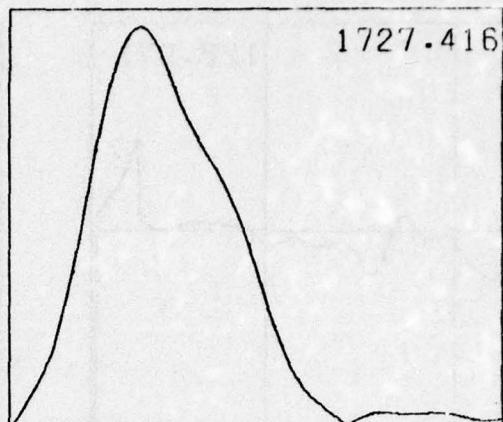
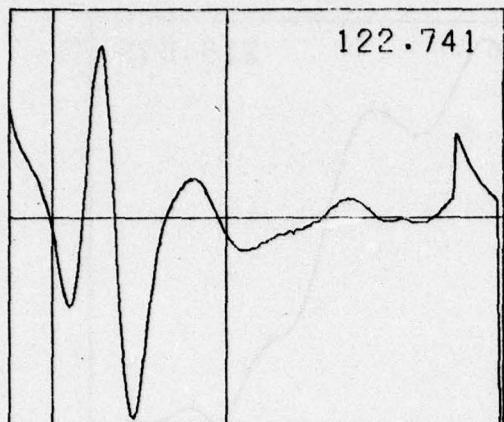


39

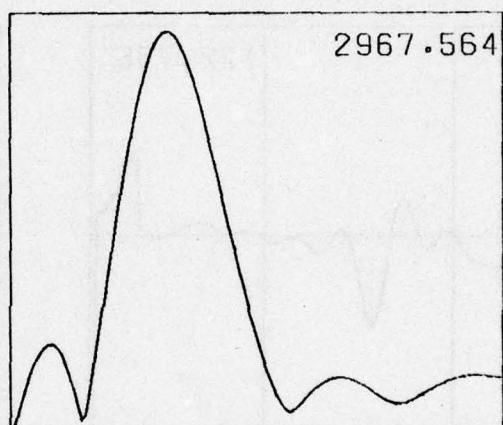
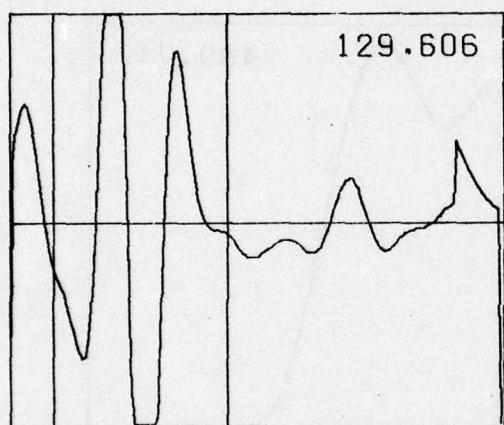
UNCLASSIFIED

B-19

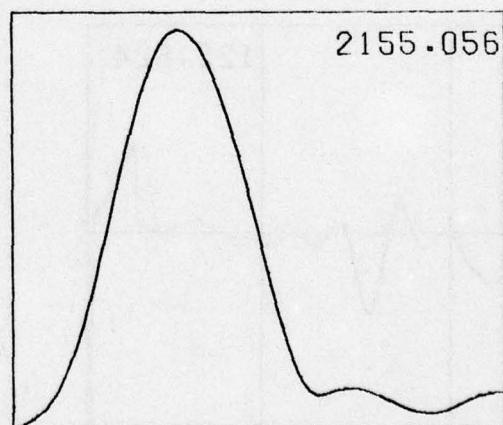
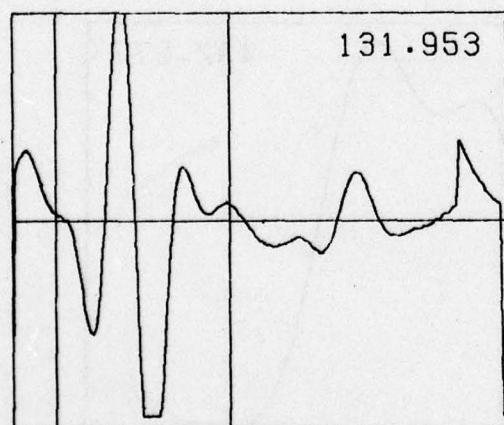
UNCLASSIFIED



40



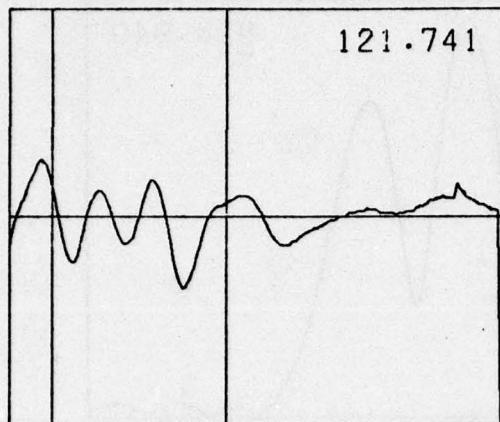
41



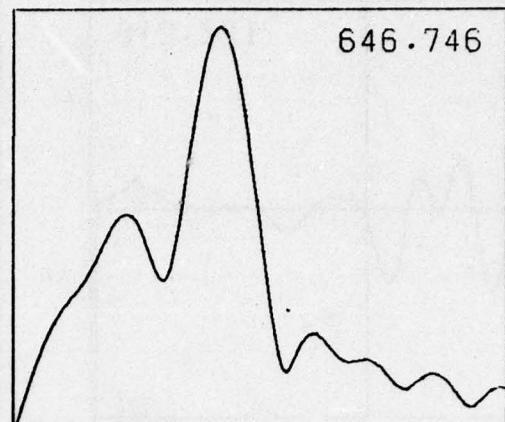
42

UNCLASSIFIED

UNCLASSIFIED

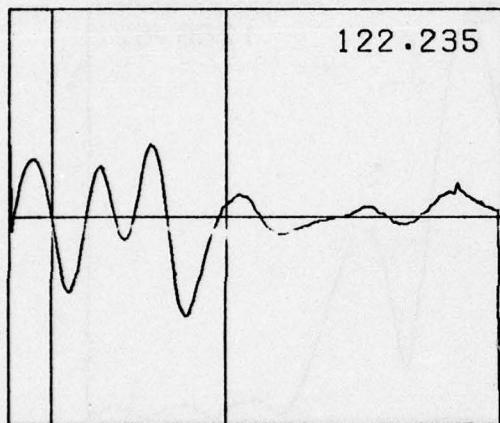


121.741

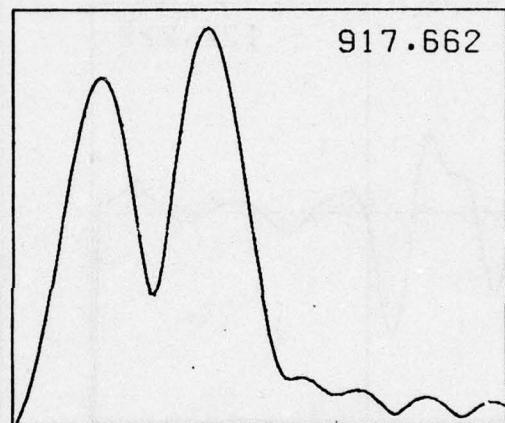


646.746

43

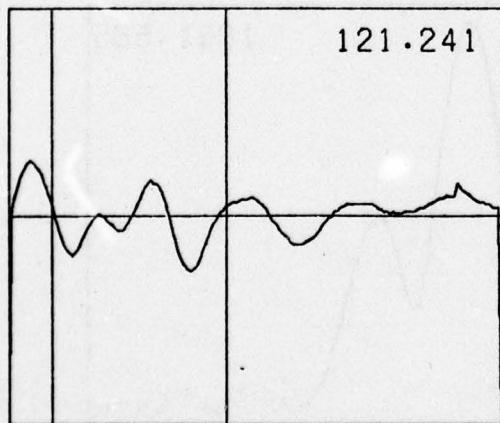


122.235

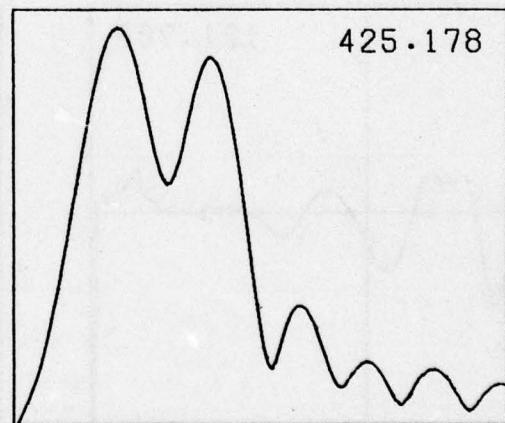


917.662

44



121.241



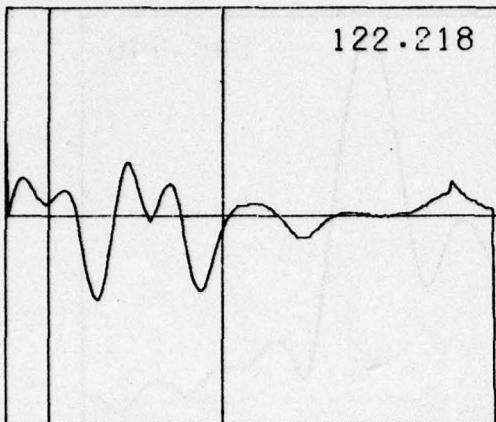
425.178

45

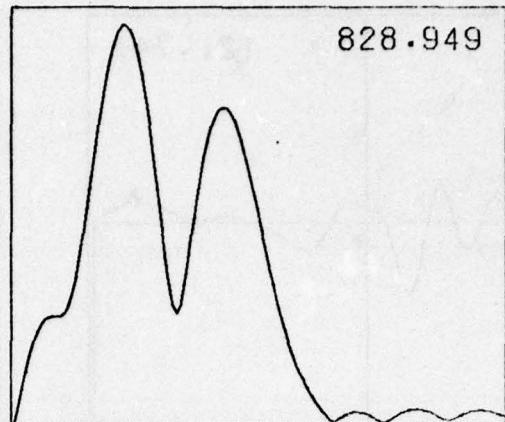
UNCLASSIFIED

B-21

UNCLASSIFIED

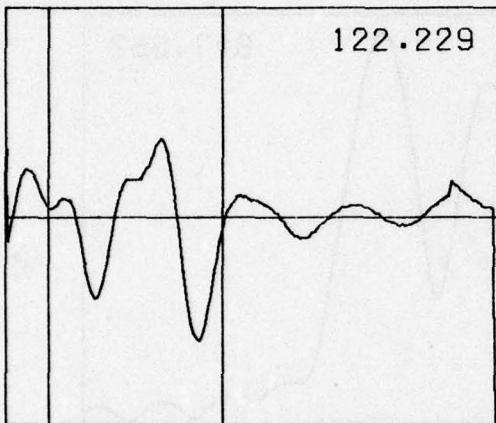


122.218

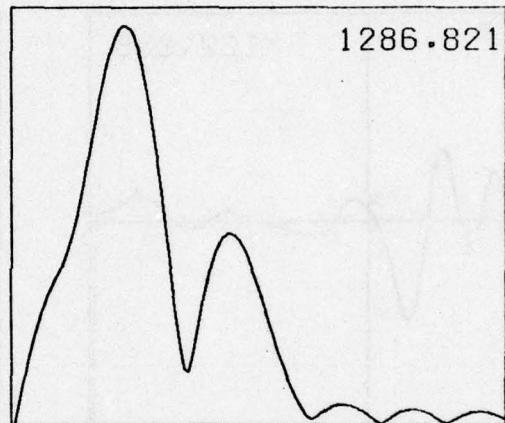


828.949

46

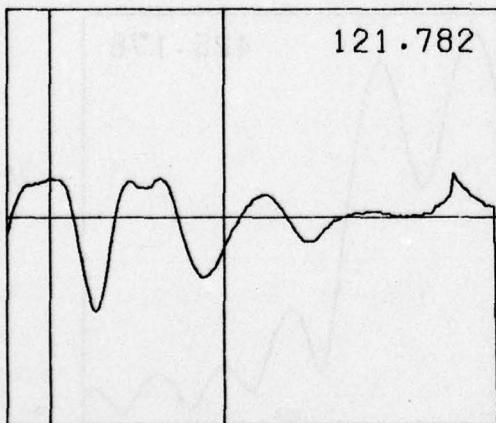


122.229

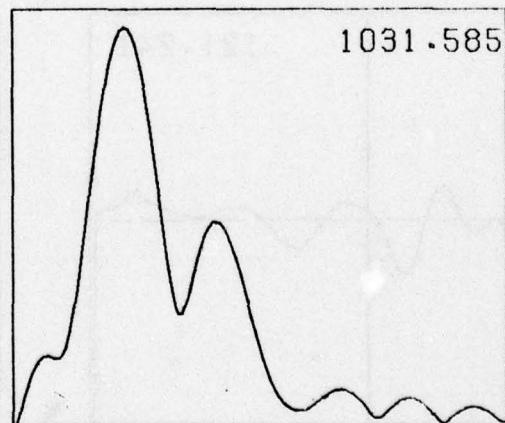


1286.821

47



121.782



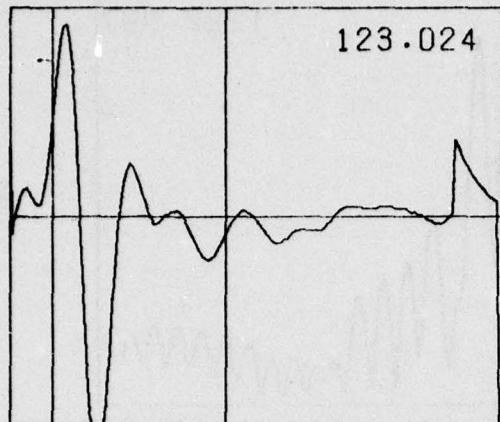
1031.585

48

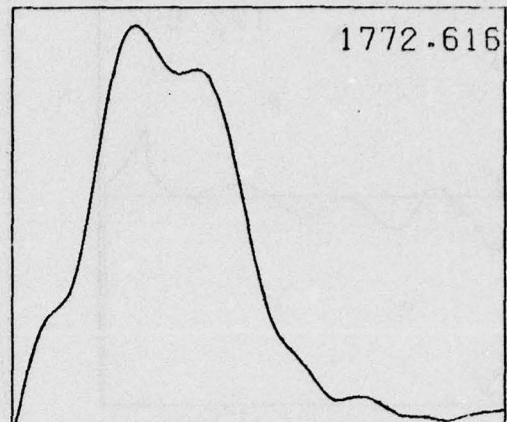
UNCLASSIFIED

B-22

UNCLASSIFIED

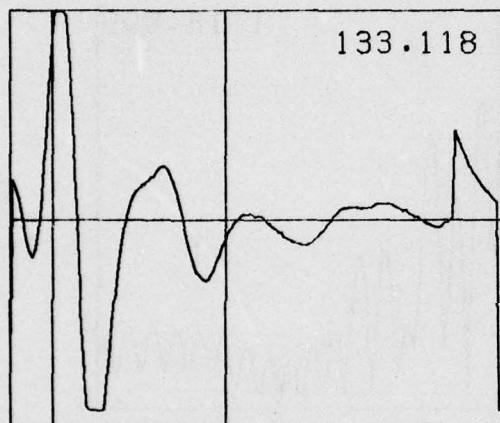


123.024

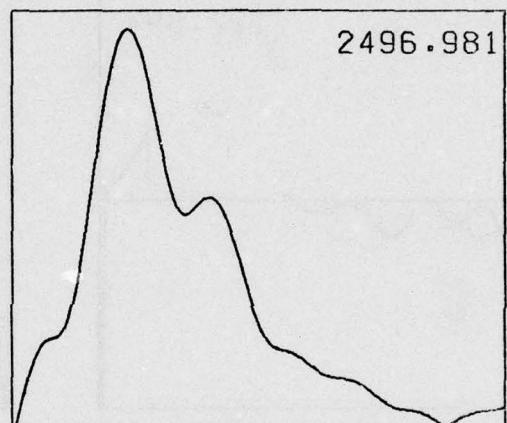


1772.616

49

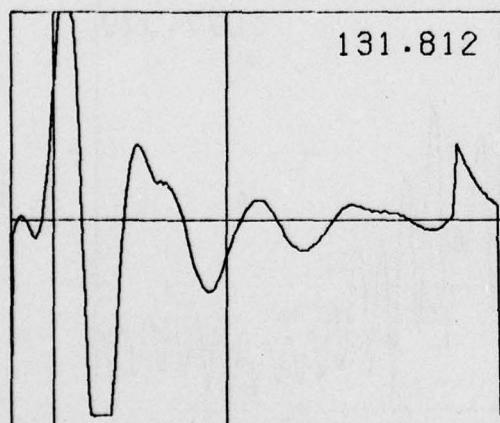


133.118

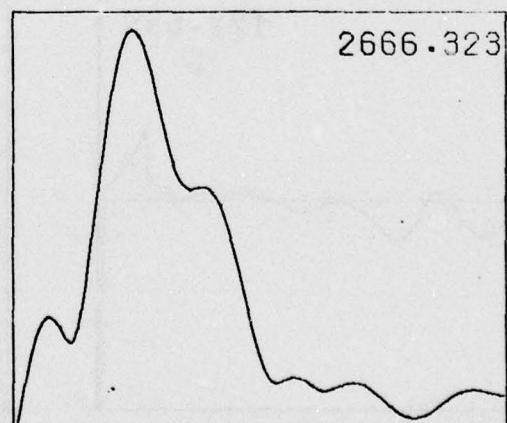


2496.981

50



131.812



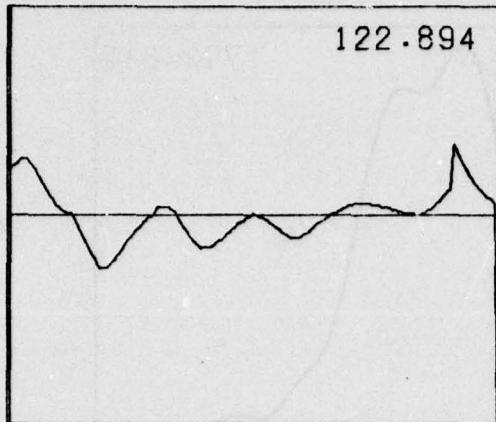
2666.323

51

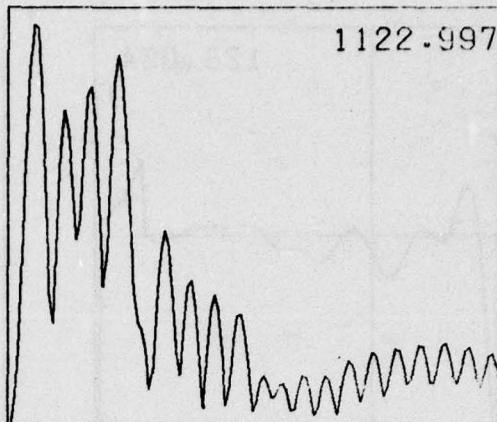
UNCLASSIFIED

B-23

UNCLASSIFIED

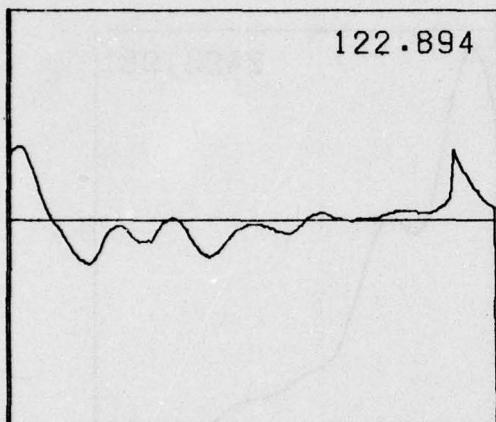


122.894

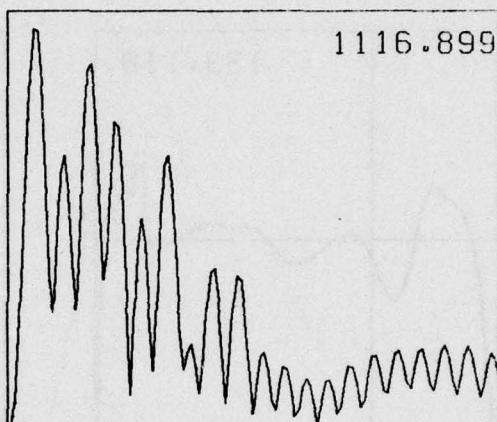


1122.997

52

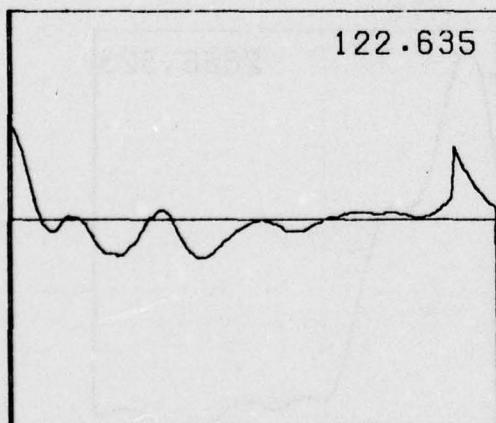


122.894

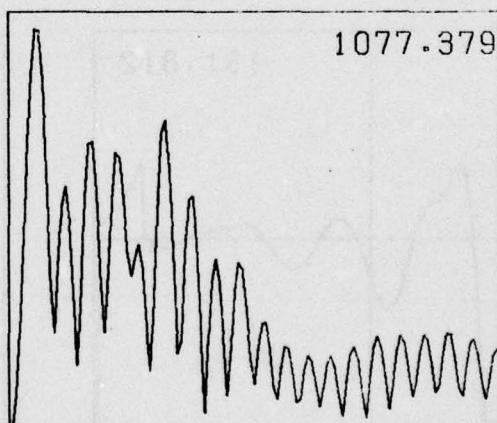


1116.899

53



122.635



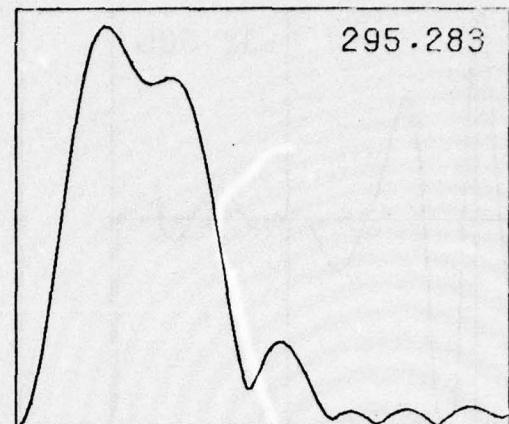
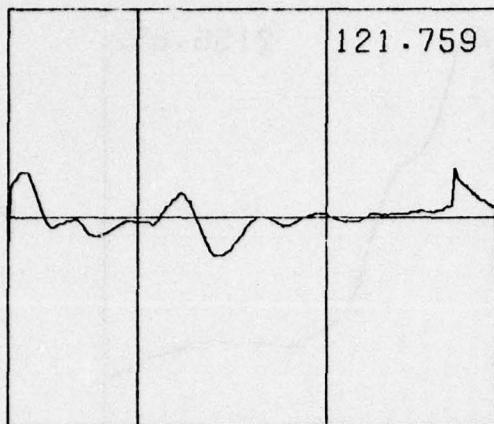
1077.379

54

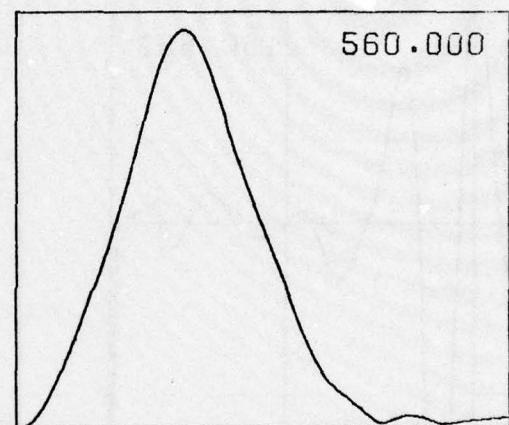
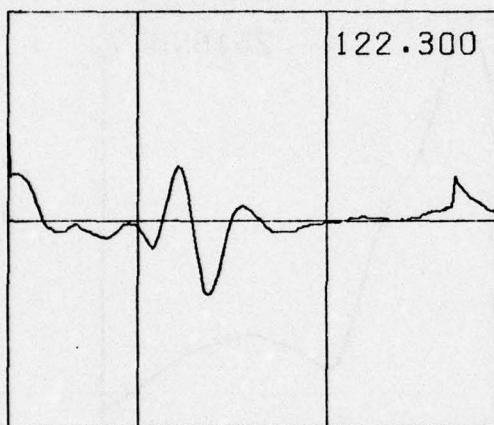
UNCLASSIFIED

B-24

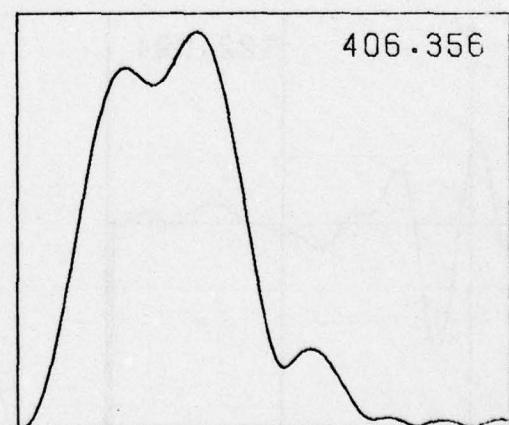
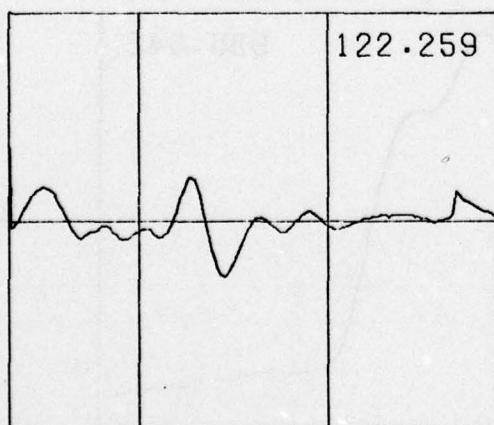
UNCLASSIFIED



55



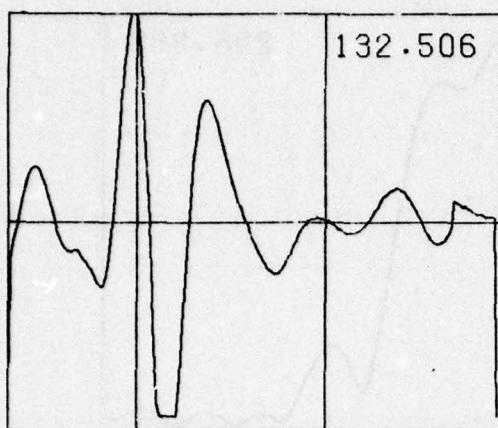
56



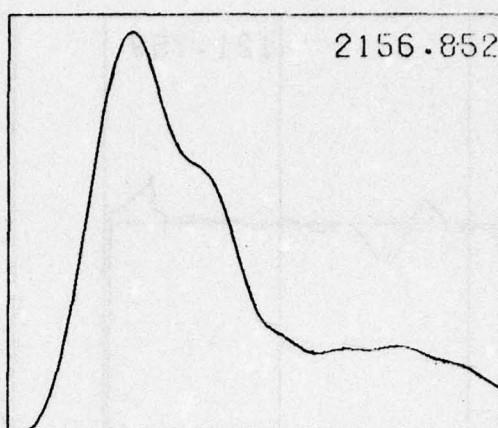
57

UNCLASSIFIED

UNCLASSIFIED

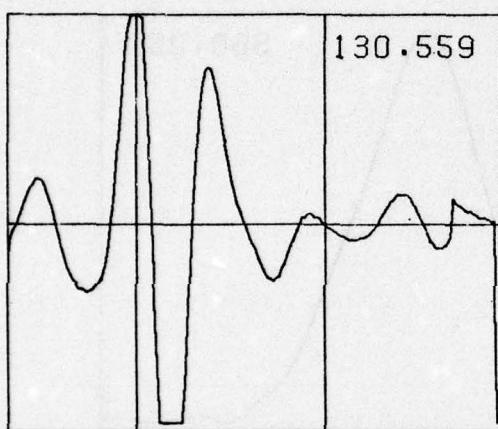


132.506

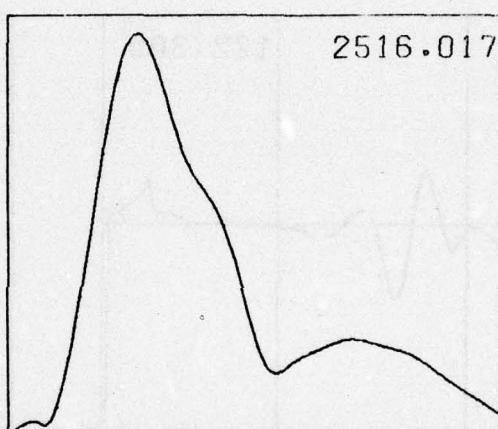


2156.852

58

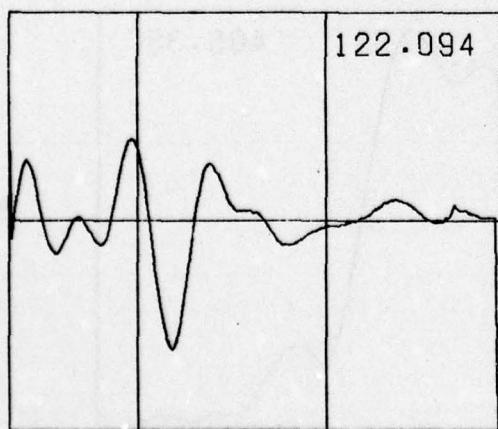


130.559

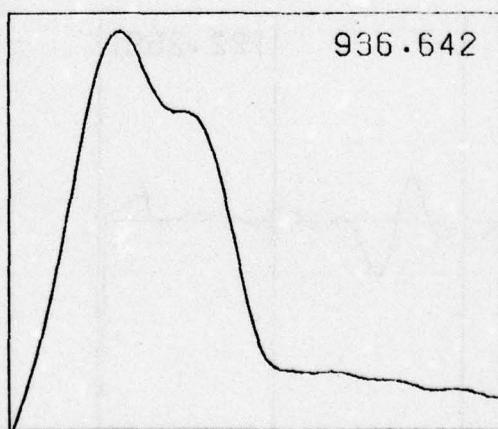


2516.017

59



122.094



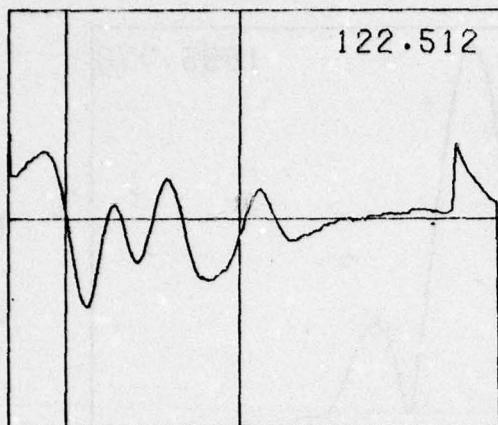
936.642

60

UNCLASSIFIED

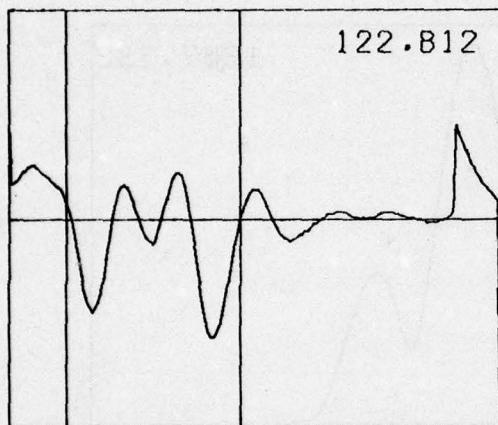
B-26

UNCLASSIFIED



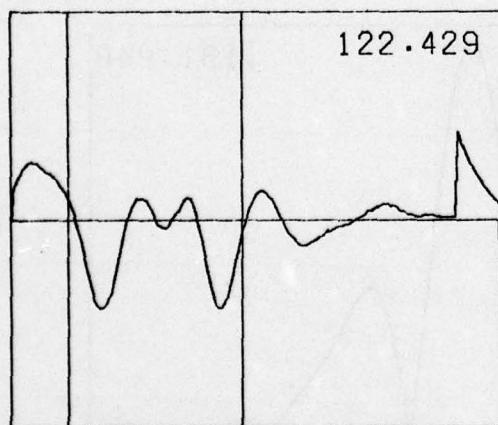
601.602

61



959.191

62



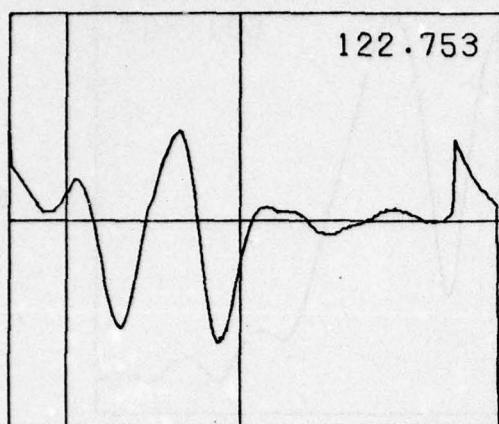
793.112

63

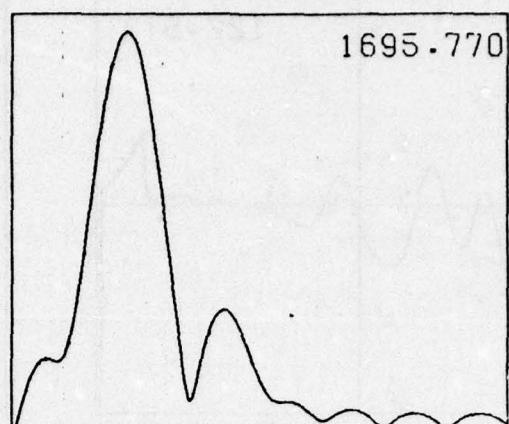
UNCLASSIFIED

B-27

UNCLASSIFIED

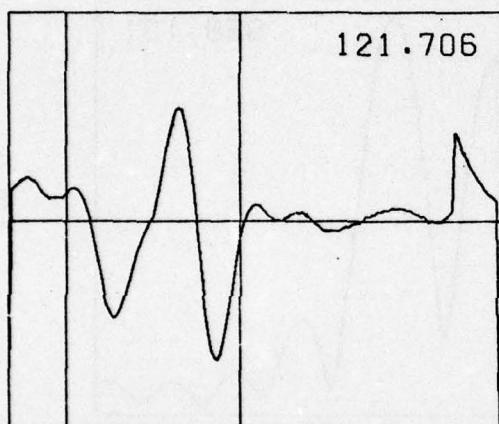


122.753

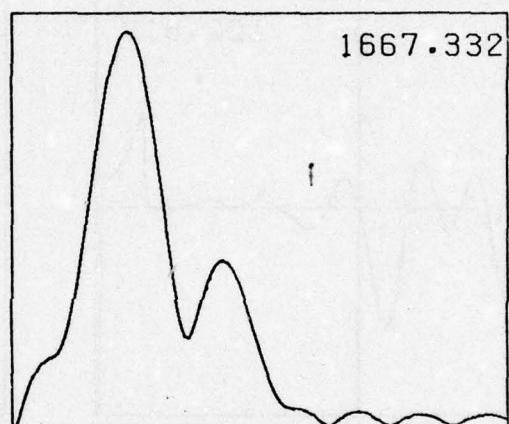


1695.770

64

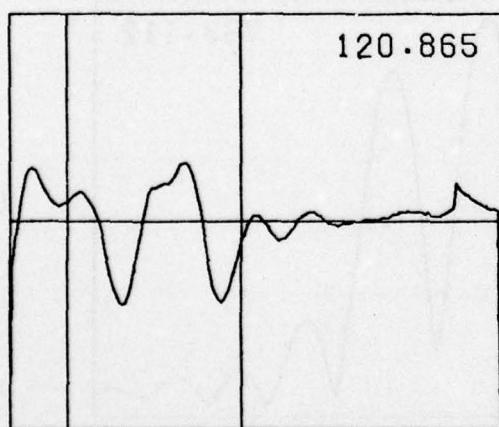


121.706

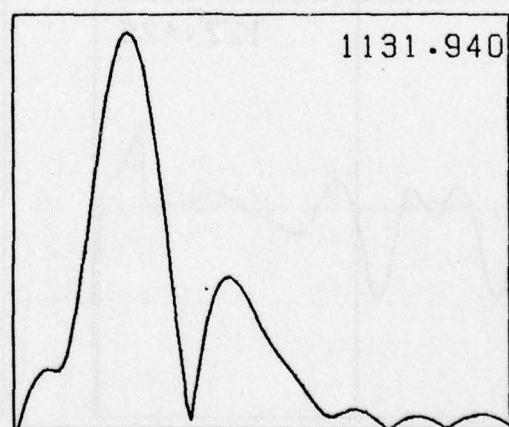


1667.332

65



120.865



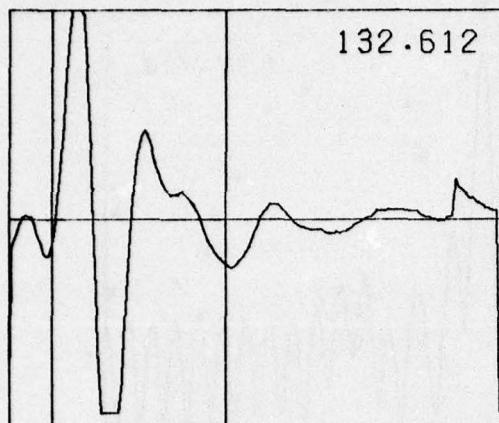
1131.940

66

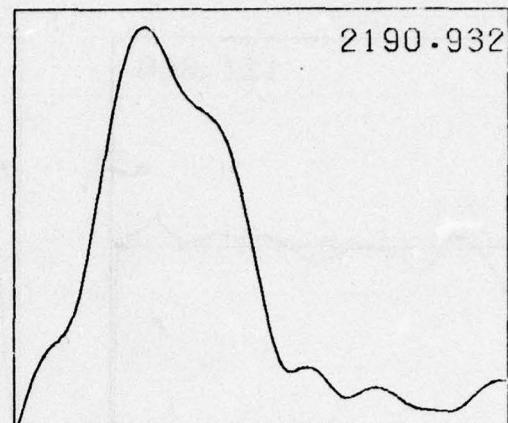
UNCLASSIFIED

B-28

UNCLASSIFIED

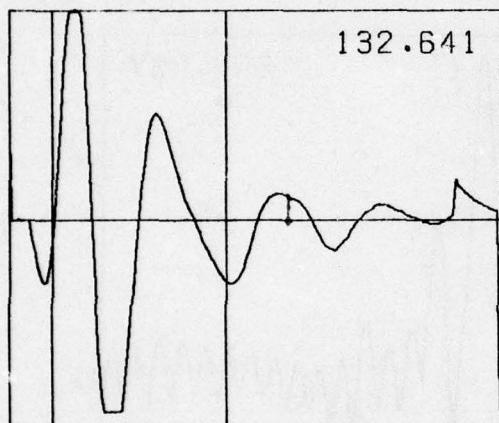


132.612

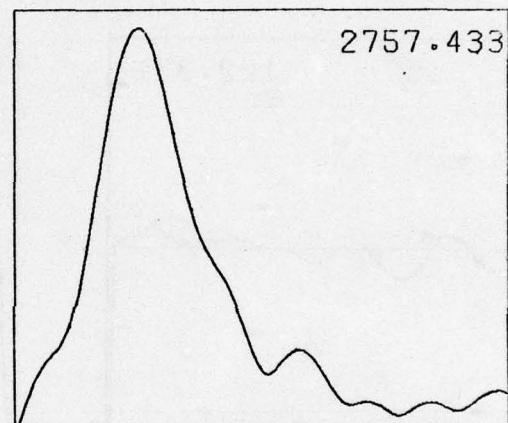


2190.932

67

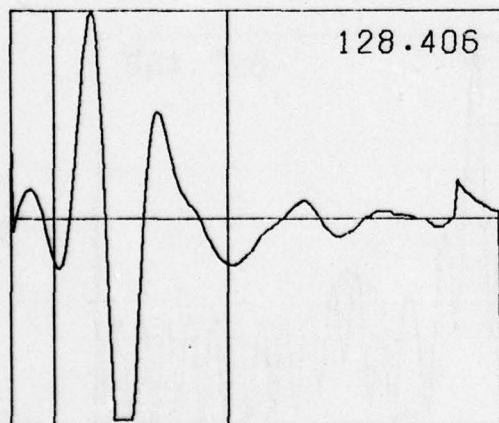


132.641



2757.433

68



128.406



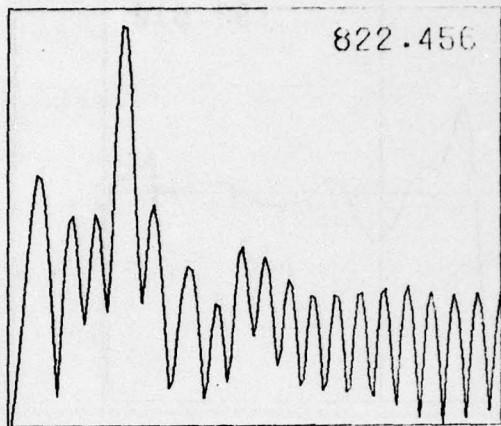
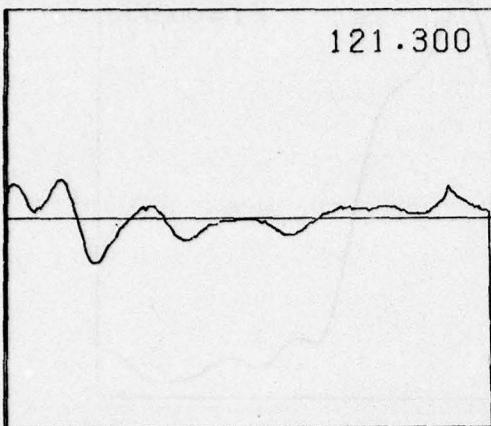
2300.470

69

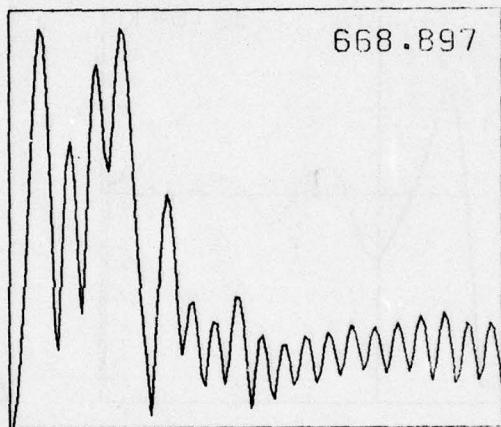
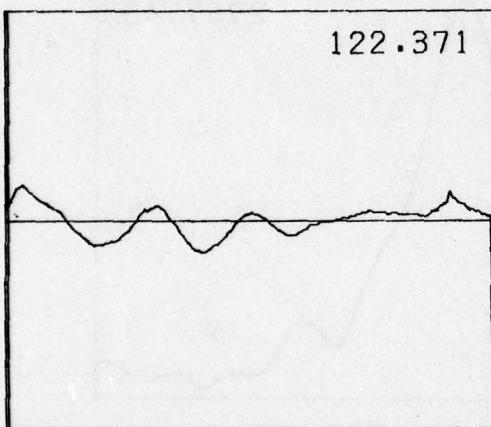
UNCLASSIFIED

B-29

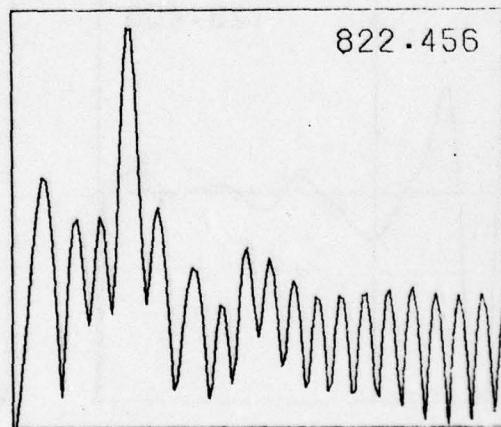
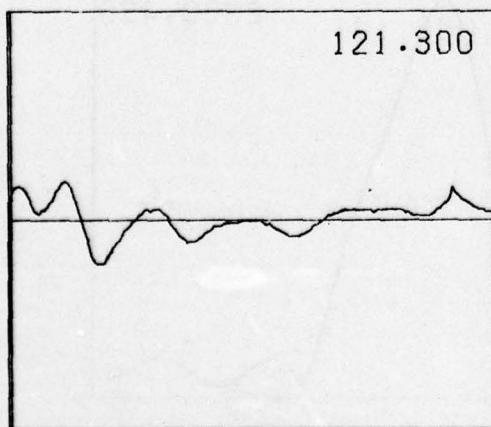
UNCLASSIFIED



70



71



72

UNCLASSIFIED

B-30

AD-A054 427

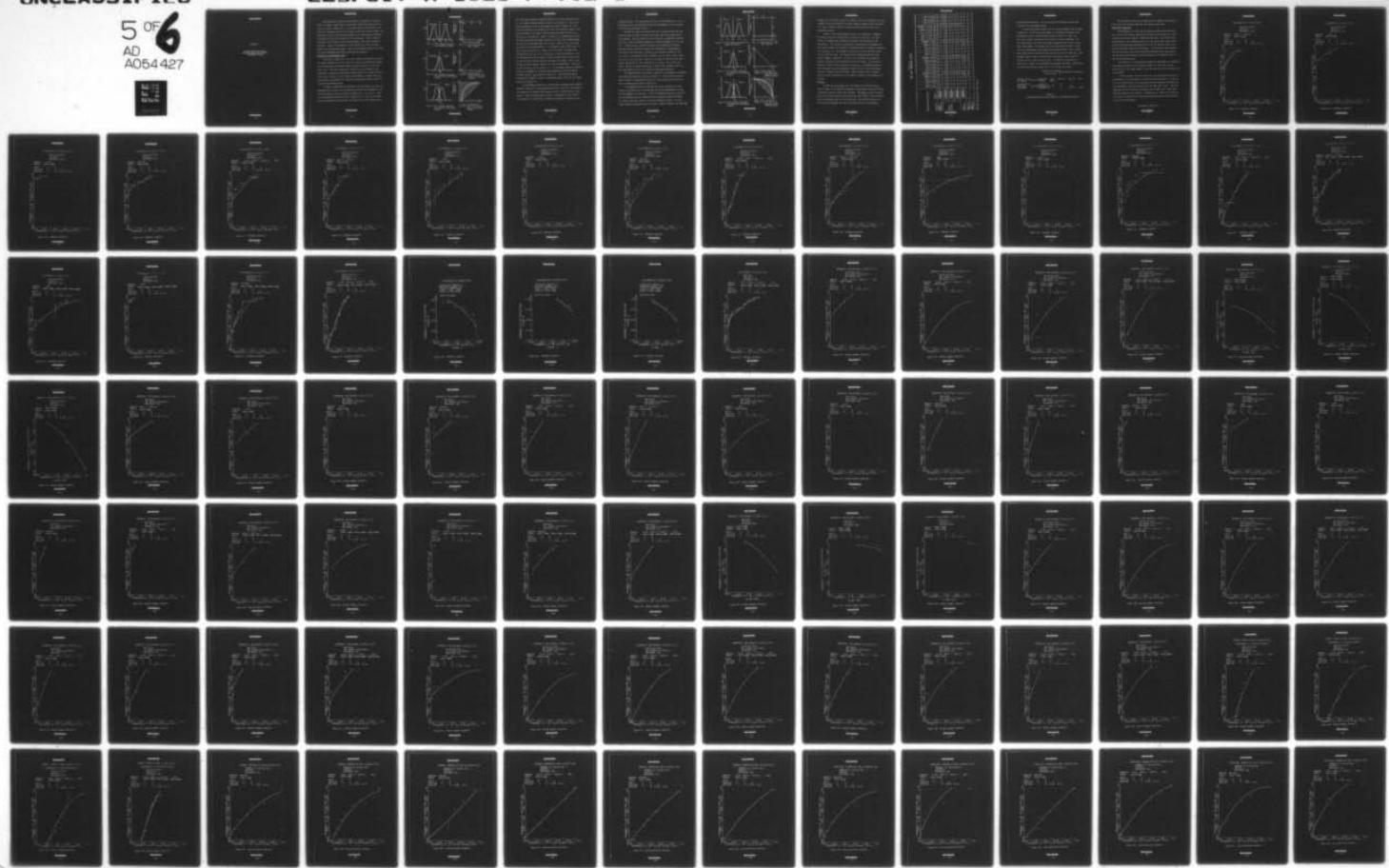
GEORGIA INST OF TECH ATLANTA ENGINEERING EXPERIMENT --ETC F/G 17/9
RADAR DETECTION, DISCRIMINATION, AND CLASSIFICATION OF BURIED N--ETC(U)
FEB 78 J D ECHARD, J A SCHEER, E O RAUSCH DAAG53-76-C-0112

UNCLASSIFIED

EES/GIT-A-1828-F-VOL-1

NL

5 of 6
AD
A054427



UNCLASSIFIED

APPENDIX C

**NBS AND SHORT-PULSE RADAR
DISCRIMINATION/CLASSIFICATION
PERFORMANCE CURVES**

UNCLASSIFIED

UNCLASSIFIED

Discrimination is defined as the process of deciding if a potential target is indeed a target (mine) or some other target-like object such as a rock, root, piece of metal, etc. On the other hand, classification is the process of deciding to which class of mines a particular target belongs. The performance curves of both the discrimination and classification processors considered in Section V are presented in this Appendix. First, a general discussion of the format in which the performance curves are presented is discussed. Limits of performance are also considered to give the reader insight into the measured results. Then, the performance curves for the NBS data and the MERADCOM short-pulse radar data are presented.

DESCRIPTION OF PERFORMANCE CURVES

The curves in Figures C-1, C-4, and C-6 show the probability of detection versus probability of false alarm for a range of postulated discriminator processors whose performance range from ideal (perfect) to very poor (worst case). Here the probability of detection, P_D , is defined as the probability of having the discriminator decide "mine" for a return resulting from a type A, type B, or type C mine; the probability of false alarm, P_{FA} , is defined as the probability of having the discriminator decide "mine" for returns from non-mine targets.

In order to demonstrate the meaning of the performance curve only two dimensions will be used. Let the mines and non-mines be represented by two continuous density functions as shown in Figures C-1, C-3, and C-5. Then, the corresponding probability curves, Figures C-2, C-4, and C-6, are generated by sweeping the decision line from right to left, and integrating the

UNCLASSIFIED

UNCLASSIFIED

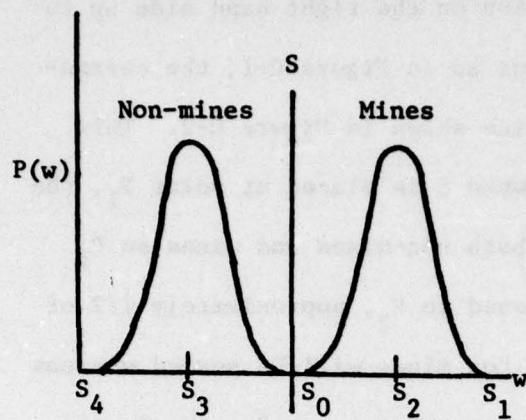


Fig. C-1 Prob. density functions for separated classes.

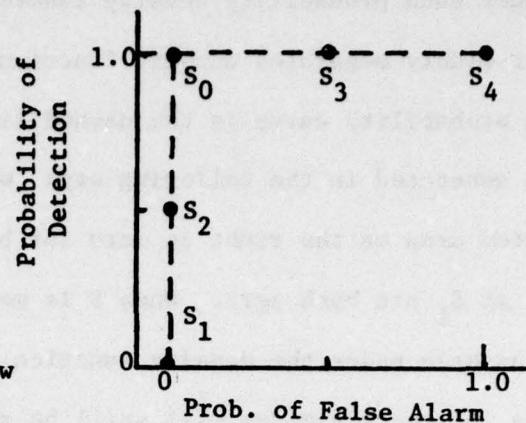


Fig. C-2 Prob. plot for separated classes

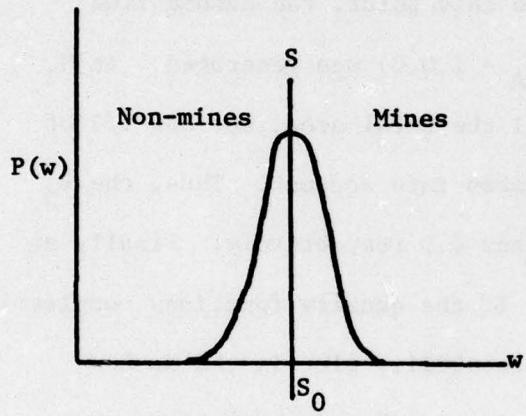


Fig. C-3 Prob. density functions for completely overlapping classes.

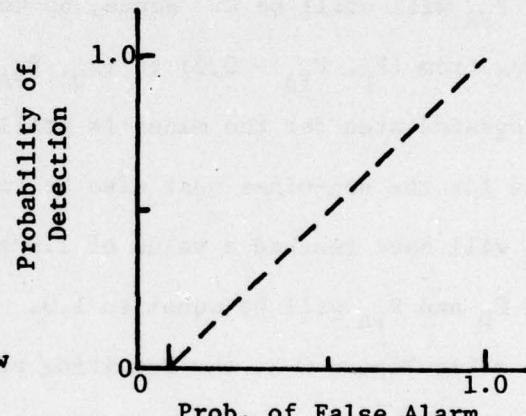


Fig. C-4 Prob. plot for completely overlapping classes.

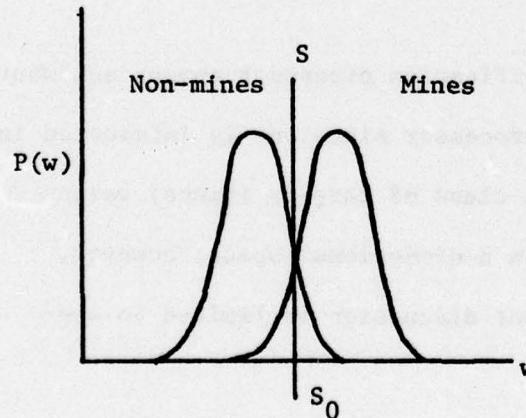


Fig. C-5 Prob. density functions for partially overlapping classes.

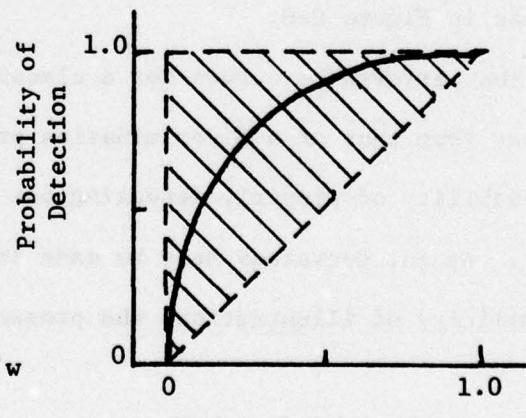


Fig. C-6 Prob. plot for partially overlapping classes.

UNCLASSIFIED

UNCLASSIFIED

area under each probability density function on the right hand side up to S_o . For widely separated density functions as in Figure C-1, the corresponding probability curve is the dashed line shown in Figure C-2. This line is generated in the following way: when S is placed at point S_1 , the integrated area on the right is zero for both non-mines and mines so P_D and P_{FA} at S_1 are both zero. When S is moved to S_2 , approximately 1/2 of the total area under the density function for mines will be summed whereas the area for the non-mines will still be zero. Hence, at S_2 , the P_D and P_{FA} become 0.5 and 0 respectively. At the point S_o the P_D will now be 1.0 but the P_{FA} will still be 0. Hence, up to this point, the dashed line extending from $(P_D, P_{FA} = 0,0)$ to $(P_D, P_{FA} = 1.0,0)$ was generated. At S_3 the integrated area for the mines is still the total area, but now 1/2 of the area for the non-mines must also be taken into account. Thus, the P_D and P_{FA} will have reached a value of 1.0 and 0.5 respectively. Finally at S_4 both P_D and P_{FA} will be equal to 1.0. If the density functions completely overlap as in Figure C-3, the resulting probability plot is the dashed straight line $P_D = P_{FA}$ as shown in Figure C-4. Other distributions as illustrated in Figure C-5 result in performances which fall into the shaded region as in Figure C-6.

The performance curves for a classification processor appear somewhat different from that of a discrimination processor since one is interested in the probability of properly detecting one class of targets (mines) versus another. Again, decisions must be made in n-dimensional space; however, for simplicity of illustration, the present discussion is limited to one-

UNCLASSIFIED

UNCLASSIFIED

dimensional space. The probability of class 1 versus probability of class 2 performance curves are generated in much the same manner as the discrimination processor performance curves.

The decision line is now swept from left to right and only the area under the class 1 density function on the right side of the decision line is integrated. The area under the class 2 function is computed on the left side of S_0 . The resulting performances are shown in Figures C-8, C-10, and C-12. To indicate the correlation between the distributions of density functions and the probability curves, the probabilities corresponding to the decision line positions S_1 through S_4 were marked in Figures C-7 and C-8. Thus, if the decision line S is moved to S_1 , the P_D for class 1 will be 1.0, but the P_D for class 2 will be 0, because the area under the class 2 density function on the left hand side of S_1 is zero. At S_2 , the P_D for class 1 will be 1.0 again, but the P_D for class 2 will be equal to 0.5, etc. This performance curve is for a perfectly performing classifier.

The dashed straight line shown in Figure C-10 corresponds to completely overlapping distributions as shown in Figure C-9. Distributions which partially overlap as illustrated in Figure C-11 give probabilities which fall into the shaded region shown in Figure C-12.

The foregoing discussion indicates the nature and form of the performance curves which are to be expected when actual measured data is used in the probability calculations. It must be emphasized that the actual sample distributions were not approximated with continuous density functions. As a result, the plots consist of discrete probability points. In other words, instead of integrating the area under a density function, the individual

UNCLASSIFIED

UNCLASSIFIED

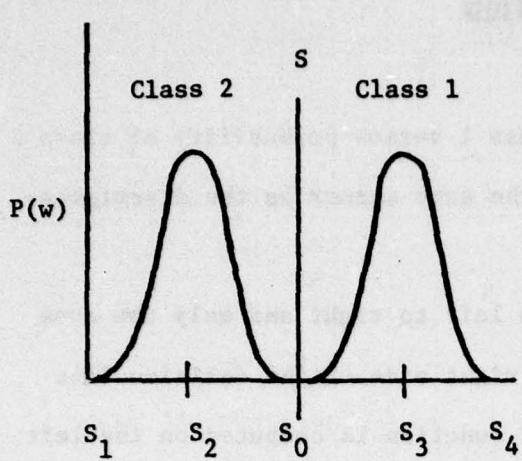


Figure C-7 Prob. density functions for separated classes.

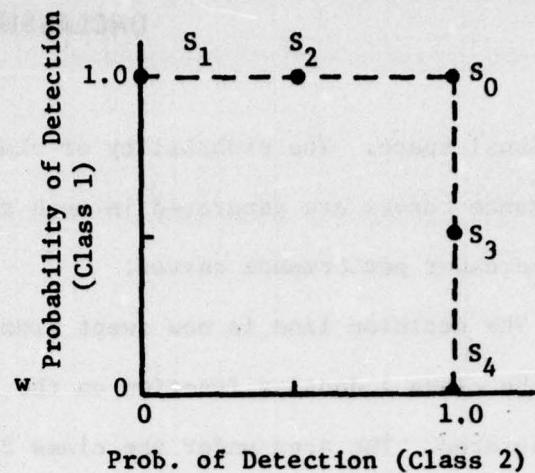


Fig. C-8 Prob. plot for separated classes.

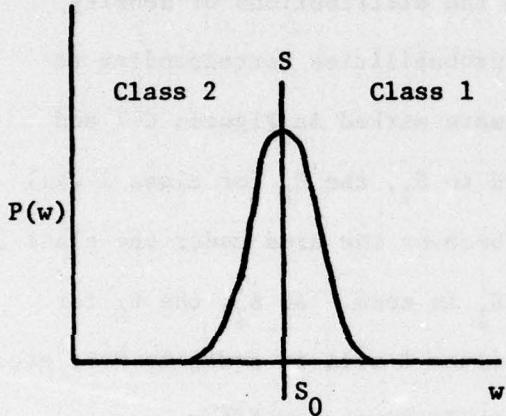


Figure C-9 Prob. density functions for completely overlapping classes.

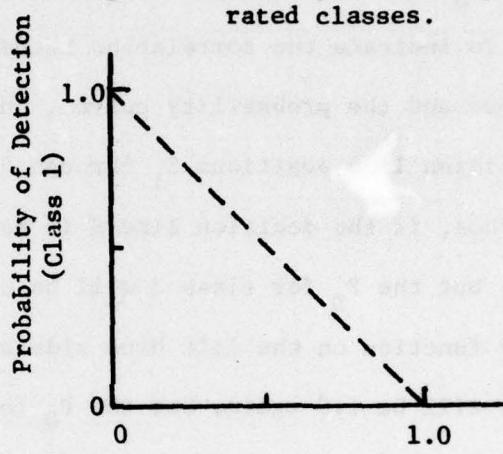


Figure C-10 Prob. plot for completely overlapping classes.

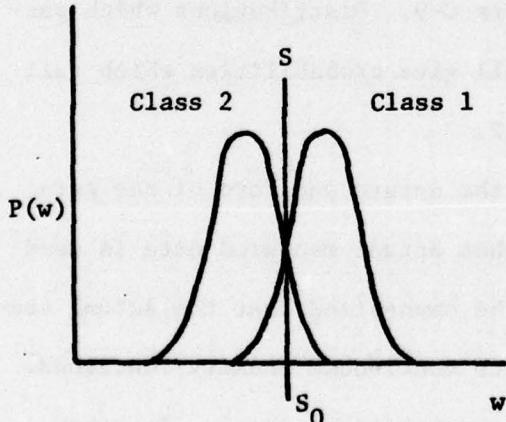


Figure C-11 Prob. density functions for partially overlapping classes.

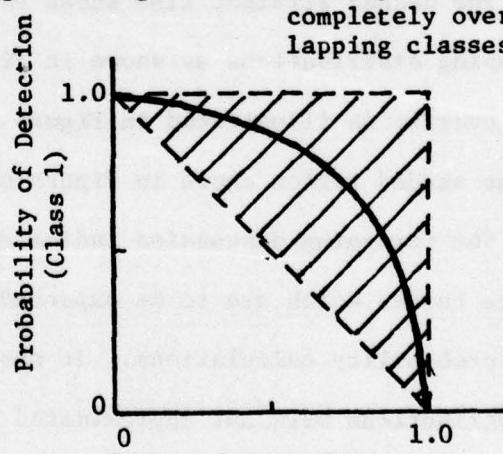


Figure C-12 Prob. plot for partially overlapping classes.

UNCLASSIFIED

UNCLASSIFIED

samples for a particular class to the right or left of the decision line were counted and the sum divided by the total number of samples within the respective class. Whenever feasible a quadratic polynomial was fitted to the probability points.

Because of the limited amount of data, the collection of signatures was used not only for a learning set but also for a test set. For this reason, two methods were considered to estimate the performance of the learning set. The FLD and SP classifiers utilized only those samples that were used to design the classifier, resulting perhaps in optimistic estimates for P_D and P_{FA} (i.e., the estimate for P_D may be too high and the estimate for P_{FA} may be too low). The "leave one out" method was applied to the nearest neighbor classifier. It uses $n-1$ of n available data samples to design a classifier, then classifies the left-out sample. This process is repeated n times to give estimates for P_D and P_{FA} . This method generally gives estimates which are pessimistic because not all of the data samples are used to design a given classifier. Both estimates tend to converge toward the true probabilities as the number of samples in the learning sets increase.

NBS DATA

The NBS data performance plots are indexed in the matrix outline shown in Table C-1 to facilitate comparison of performance between different classifiers, features, mines, and non-mines. The numbers within the matrix refer to the figure where the particular plot can be found. The performance plots are numbered Figures C-13 through C-98. The vertical column on the left hand side indicates the type of classifier and the corresponding

UNCLASSIFIED

NBS DATA PROCESSING MATRIX

NBS Data Processing Matrix

| CLASSIFIER | TYPE OF DATA | INTUITIVE OBSERVABLES RAW DATA | C-13 | C-14 | C-15 | C-16 | C-17 | C-18 | C-19 | C-20 | C-21 | C-22 | C-23 | C-24 | C-25 | C-26 | C-27 | C-28 | C-29 | C-30 | C-31 | C-32 | C-33 | C-34 | C-35 | |
|------------------------------|-----------------------------------|-----------------------------------|---------------------|-----------------------------------|------|------|------|------|------|------|------|------|------|------|------|------|------|------|------|------|------|------|------|------|------|------|
| FISHER'S LINEAR DISCRIMINANT | INTUITIVE OBSERVABLES RAW DATA | TYPE A VS. ROCKS | C-44 | C-45 | C-46 | C-47 | C-48 | C-49 | C-50 | C-51 | C-52 | C-53 | C-54 | C-55 | C-56 | C-57 | C-58 | C-59 | C-60 | C-61 | C-62 | C-63 | C-64 | C-65 | C-66 | |
| NEAREST NEIGHBOR | INTUITIVE OBSERVABLES RAW DATA | TYPE A VS. ROCKS | 3 | INTUITIVE OBSERVABLES RAW DATA | C-37 | | | | | | | | | | | | | | | | | | | | | C-36 |
| | INTUITIVE OBSERVABLES RAW DATA | TYPE A VS. ROCKS | 5 | INTUITIVE OBSERVABLES RAW DATA | C-67 | | | | | | | | | | | | | | | | | | | | | C-39 |
| | INTUITIVE OBSERVABLES RAW DATA | TYPE A VS. ROCKS | 7 | INTUITIVE OBSERVABLES RAW DATA | C-71 | | | | | | | | | | | | | | | | | | | | | C-43 |
| | INTUITIVE OBSERVABLES RAW DATA | TYPE A VS. ROCKS | SPACE PARTITION | INTUITIVE OBSERVABLES RAW DATA | C-75 | | | | | | | | | | | | | | | | | | | | | C-40 |
| | INTUITIVE OBSERVABLES RAW DATA | TYPE A VS. ROCKS | CROSS CORRELATION | INTUITIVE OBSERVABLES RAW DATA | C-79 | | | | | | | | | | | | | | | | | | | | | C-41 |
| | INTUITIVE OBSERVABLES RAW DATA | TYPE A VS. ROCKS | IMPULSE CORRELATION | INTUITIVE OBSERVABLES RAW DATA | C-83 | | | | | | | | | | | | | | | | | | | | | C-42 |
| | INTUITIVE OBSERVABLES RAW DATA | TYPE A VS. ROCKS | | C-84 | | | | | | | | | | | | | | | | | | | | | C-43 | |
| | INTUITIVE OBSERVABLES RAW DATA | TYPE A VS. ROCKS | | C-85 | | | | | | | | | | | | | | | | | | | | | C-44 | |
| | INTUITIVE OBSERVABLES RAW DATA | TYPE A VS. ROCKS | | C-86 | | | | | | | | | | | | | | | | | | | | | C-45 | |
| | INTUITIVE OBSERVABLES RAW DATA | TYPE A VS. ROCKS | | C-91 | | | | | | | | | | | | | | | | | | | | | C-46 | |
| | INTUITIVE OBSERVABLES RAW DATA | TYPE A VS. ROCKS | | C-92 | | | | | | | | | | | | | | | | | | | | | C-47 | |
| | INTUITIVE OBSERVABLES RAW DATA | TYPE A VS. ROCKS | | C-93 | | | | | | | | | | | | | | | | | | | | | C-48 | |
| | INTUITIVE OBSERVABLES RAW DATA | TYPE A VS. ROCKS | | C-94 | | | | | | | | | | | | | | | | | | | | | C-49 | |
| | INTUITIVE OBSERVABLES RAW DATA | TYPE A VS. ROCKS | | C-95 | | | | | | | | | | | | | | | | | | | | | C-50 | |

UNCLASSIFIED

*NON-MINE INCLUDES ROCKS, ROOT AND PLATE

UNCLASSIFIED

algorithms that were used. The top row shows the classes that were used to generate the performance curves.

A typical descriptive title block for each performance curve is shown in Table C-2. At the top of each figure is a classifier descriptor which corresponds to one of the descriptors listed in Table C-1. Next is a list of the objects included in each of the two classes considered. The last three lines in the title block give information on the object and the object environment. For example, the title block shown in Table C-2 indicates that measurements from targets and non-mines buried at both 3 inches and 6 inches below the ground surface were used as the two class data. Measurements taken 4 inches on either side of the object center as well as directly over the object were also used. In addition, measurements of objects for a variety of surrounding soil moistures were used: specifically, for soils with moisture content of 7%, 17%, 12-20%, and 13-16%.

| Contents of the Two Classes | → | FLD/BAYES CLASSIFIER | Intuitive Data | | Classifier Description | |
|---------------------------------------|---|--|----------------|-------------|------------------------|--|
| Non-mine Target | | Plate Type C | Rock (1) | Rock (2) | Root | |
| Information on Object and Environment | → | Depth ("") 3 Location ("") +4 Moisture (%) 7 | 6 0 17 | -4 12-20 | 13-16 | |

Table C-2
A Typical Descriptive Title Block for the Performance Curves

UNCLASSIFIED

UNCLASSIFIED

The performance curves for the NBS data are followed by performance plots for the short-pulse radar data that begins on Page C-99.

SHORT-PULSE RADAR DATA

The motivation for collection and processing short-pulse radar data was to verify the previous computerized analysis which was based on CW measurements over a broad range of frequencies (NBS data). By virtue of the wide spectrum of the transmitted pulse, the short-pulse radar system represents the analog hardware implementation of the FFT technique used to synthesize time domain data with the NBS data. The short-pulse radar temporal data was processed by the same discrimination/classification algorithms as the NBS data and performance curves were generated for comparison with the NBS data performance plots.

The results of the discriminator/classifier performance are organized and displayed in matrix form as shown in Table C-3. Each entry in the matrix refers to the figure number in this Appendix where the performance plot can be found.

As will be noted, this matrix does not cover discriminator/classifier performances to the same extent as the previous NBS data matrix. A comparison of the NBS and short-pulse radar gated spectral responses indicated very close agreement in spectral signatures for the same type of mine. This fact suggested that the performance associated with the NBS and the short-pulse radar data might be quite similar. Consequently, to conserve our resources, we elected to use only the NN classification algorithm which had previously given the best performance.

(continued on Page C-97)

UNCLASSIFIED
C-10

UNCLASSIFIED

FLD/BAYES CLASSIFIER

INTUITIVE DATA
VERSION 2
REFERENCE 336

NONMINE ROCK(1) ROCK(2)
TARGET TYPE A MINE

| | | | | |
|----------|----|----|-------|-------|
| DEPTH | 3 | 6 | | |
| LOCATION | +4 | 0 | -4 | |
| MOISTURE | 7 | 17 | 12-20 | 13-16 |

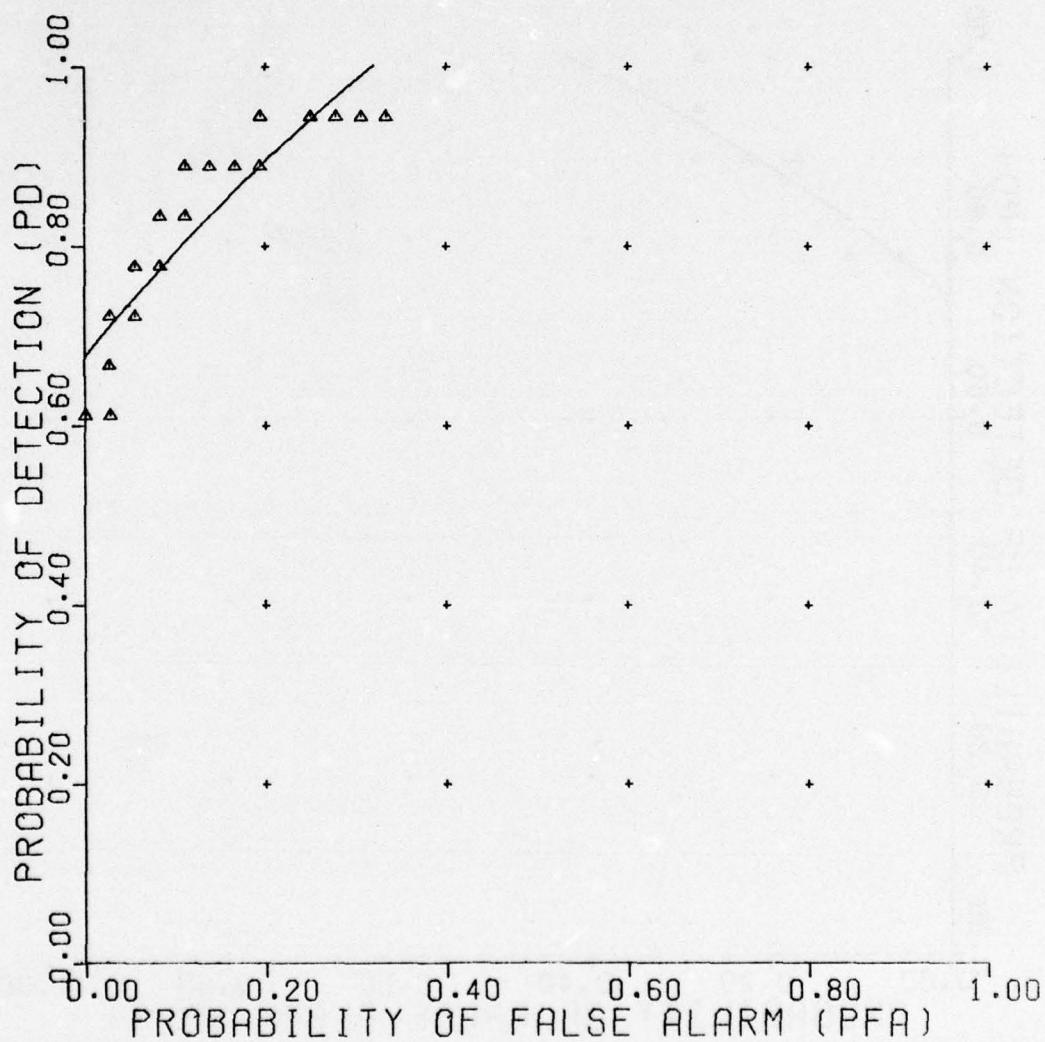


Figure C-13. FLD/Bayes classifier.

UNCLASSIFIED

UNCLASSIFIED

FLD/BAYES CLASSIFIER

INTUITIVE DATA
VERSION 2
REFERENCE 337

NONMINE ROOT
TARGET TYPE A MINE

| | | | | |
|----------|----|----|-------|-------|
| DEPTH | 3 | 6 | | |
| LOCATION | +4 | 0 | -4 | |
| MOISTURE | 7 | 17 | 12-20 | 13-16 |

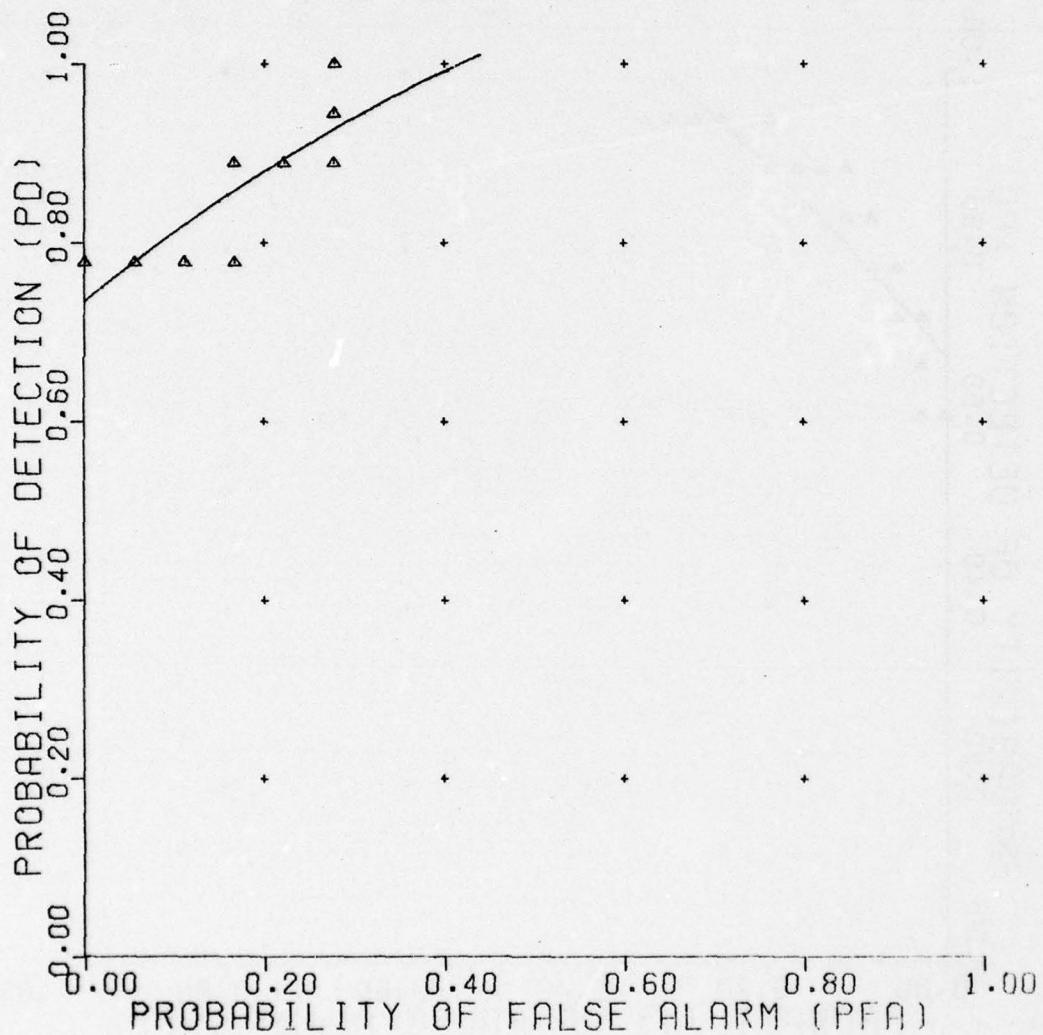


Figure C-14. FLD/Bayes classifier.

UNCLASSIFIED

UNCLASSIFIED

FLD/BAYES CLASSIFIER

INTUITIVE DATA
VERSION 2
REFERENCE 338

NONMINE PLATE
TARGET TYPE A MINE

| DEPTH | 3 | 6 |
|----------|-------|-------|
| LOCATION | +4 | 0 |
| MOISTURE | 7 | 17 |
| | 12-20 | 13-16 |

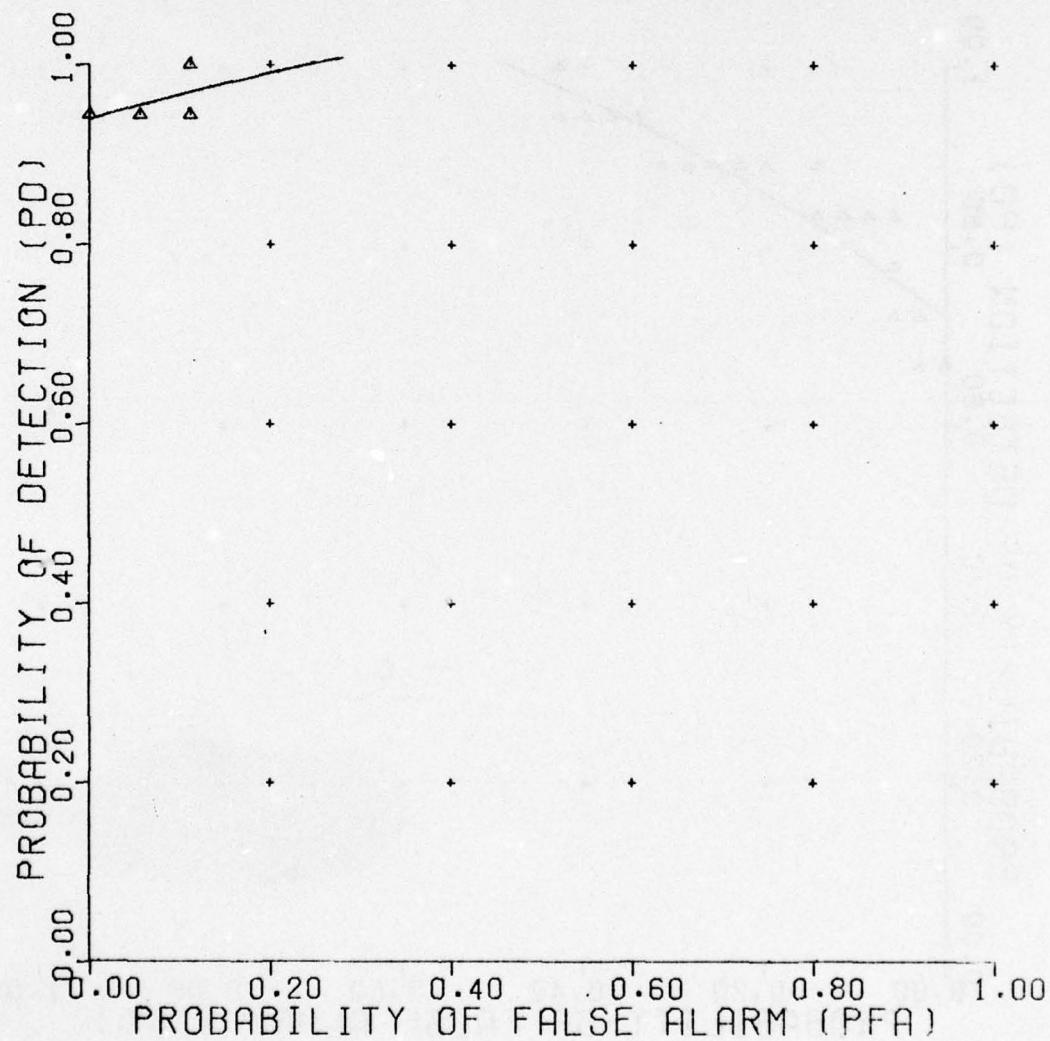


Figure C-15. FLD/Bayer classifier.

UNCLASSIFIED

UNCLASSIFIED

FLD/BAYES CLASSIFIER

INTUITIVE DATA
VERSION 2
REFERENCE 339

NONMINE BACKGND
TARGET TYPE A MINE

| DEPTH | 3 | 6 |
|----------|----|----------------------|
| LOCATION | +4 | 0 |
| MOISTURE | 7 | 17 12-20 13-16 |

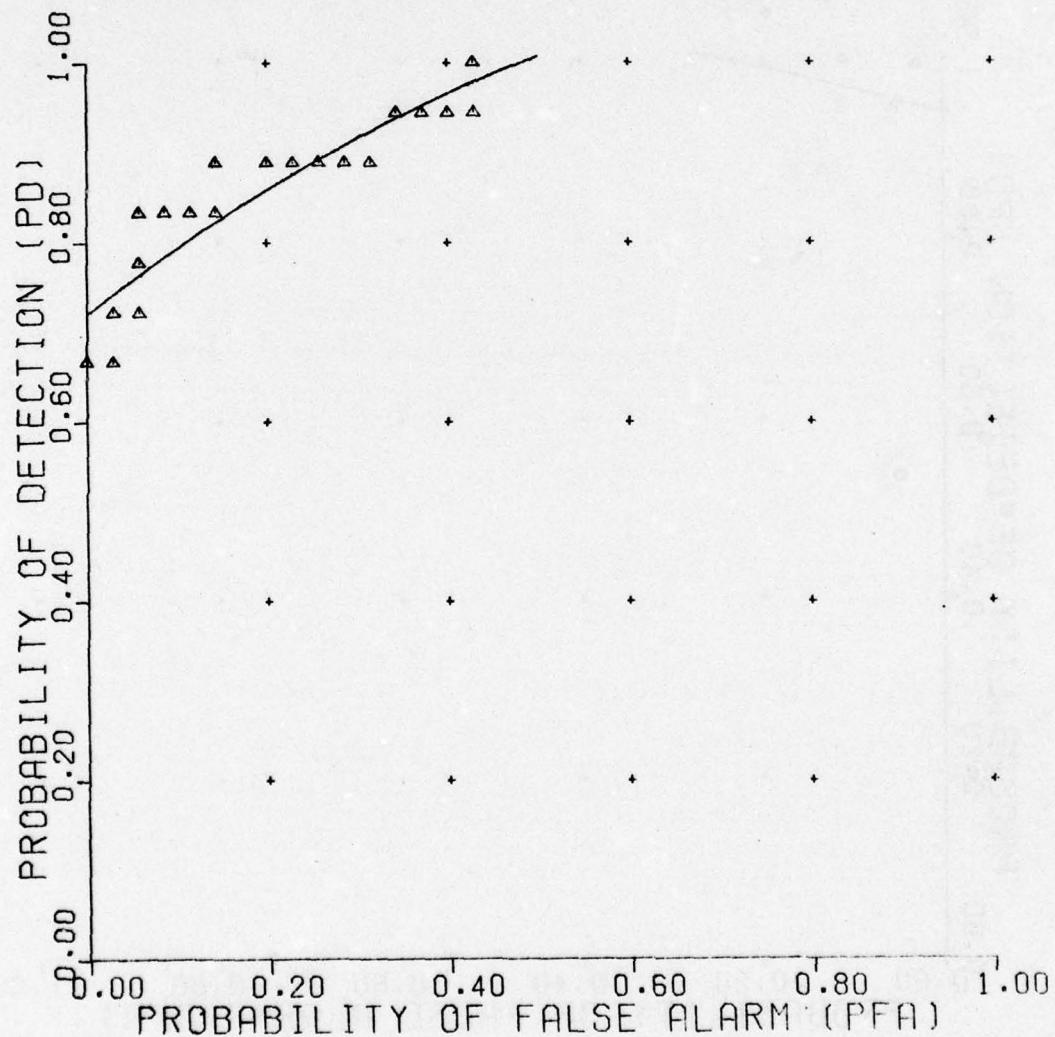


Figure C-16. FLD/Bayes classifier.

UNCLASSIFIED

UNCLASSIFIED

FLD/BAYES CLASSIFIER

INTUITIVE DATA
VERSION 2
REFERENCE 301

NONMINE PLATE ROCK(1) ROCK(2) ROOT
TARGET TYPE A MINE

| | | | |
|----------|----|----|-------|
| DEPTH | 3 | 6 | |
| LOCATION | +4 | 0 | -4 |
| MOISTURE | 7 | 17 | 12-20 |
| | | | 13-16 |

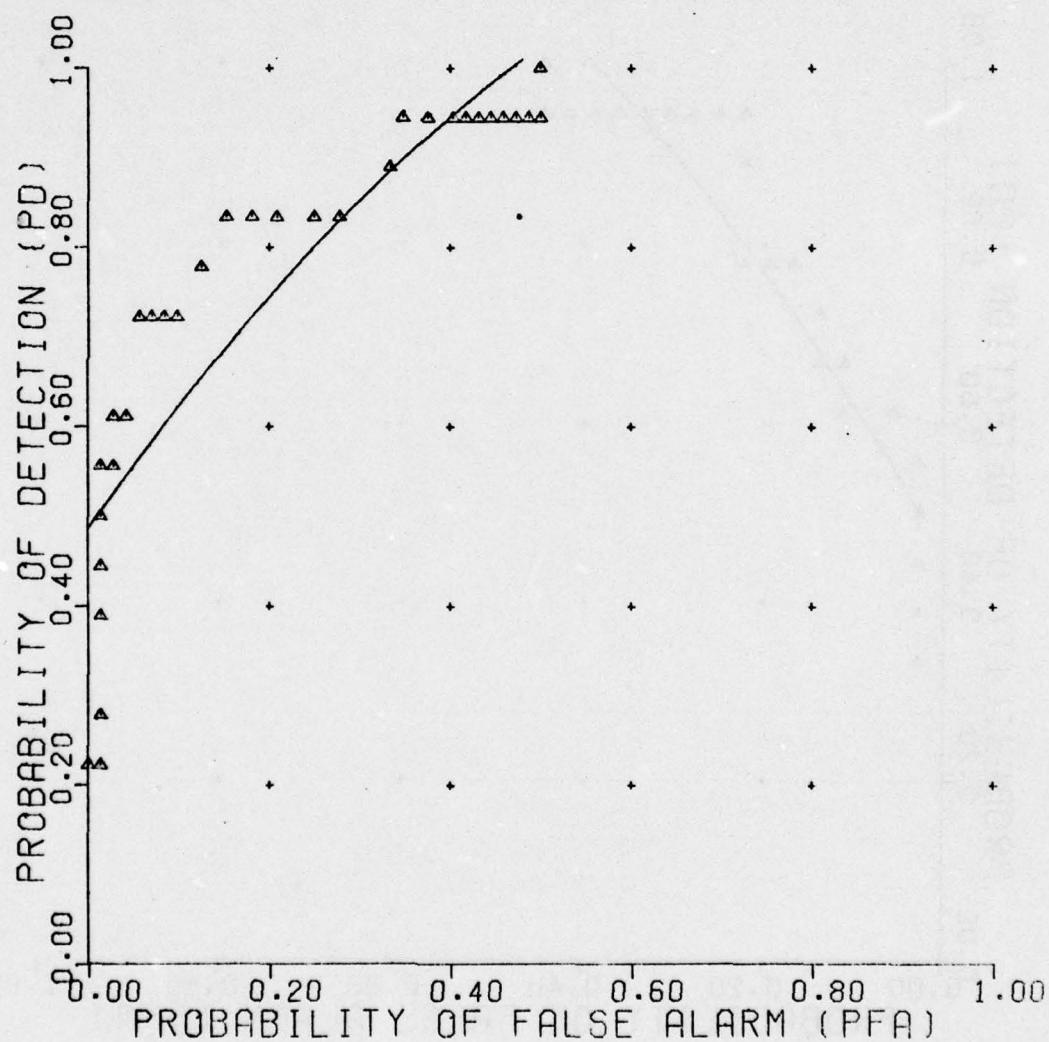


Figure C-17. FLD/Bayes classifier.

UNCLASSIFIED

UNCLASSIFIED

FLD/BAYES CLASSIFIER

INTUITIVE DATA
VERSION 2
REFERENCE 340

NONMINE ROCK(1) ROCK(2)
TARGET TYPE B MINE
DEPTH 3 6
LOCATION +4 0 -4
MOISTURE 7 17 12-20 13-16

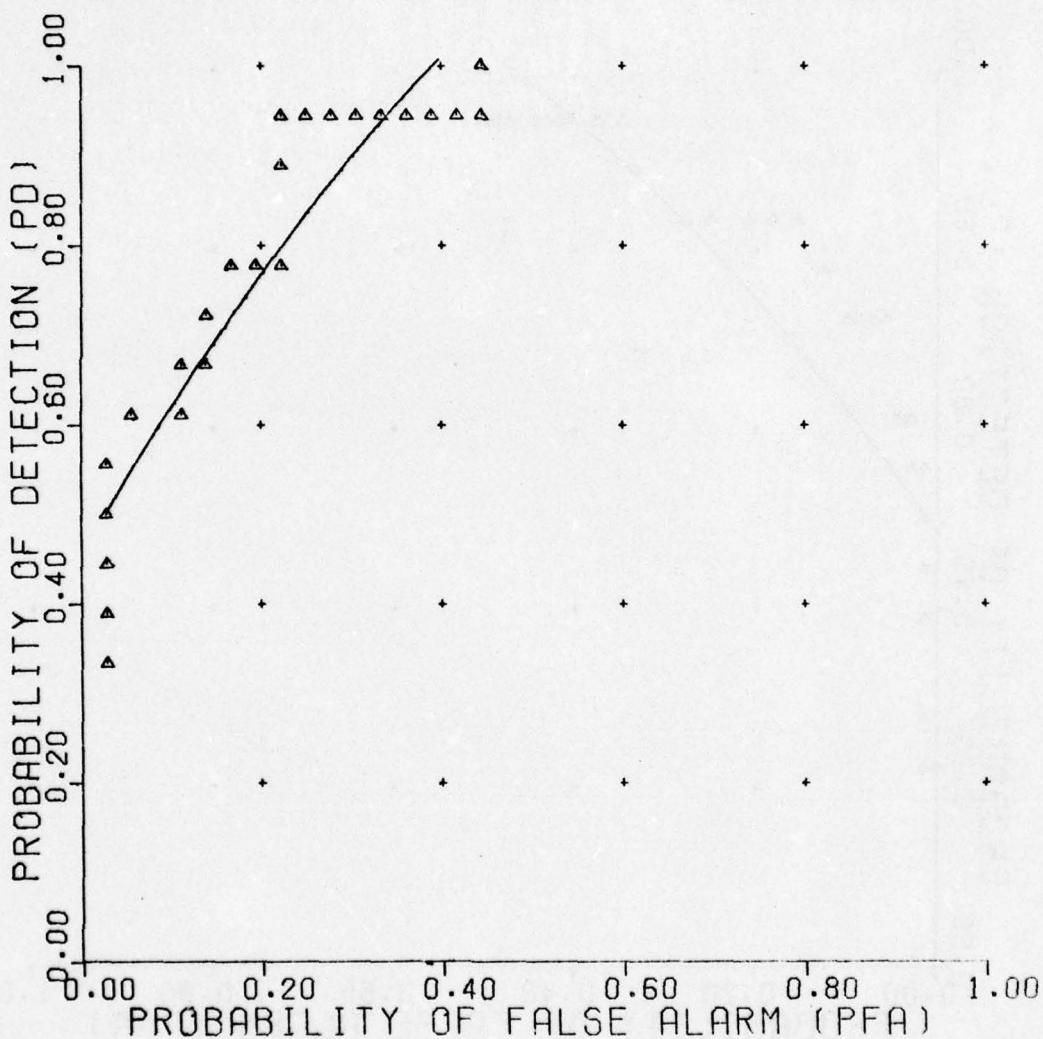


Figure C-18. FLD/Bayes classifier.

UNCLASSIFIED

UNCLASSIFIED

FLD/BAYES CLASSIFIER

INTUITIVE DATA
VERSION 2
REFERENCE 341

| | |
|----------|---------------------------------|
| NONMINE | ROOT |
| TARGET | TYPE B MINE |
| DEPTH | 3 6 |
| LOCATION | +4 0 -4 |
| MOISTURE | 7 17 12-20 13-16 |

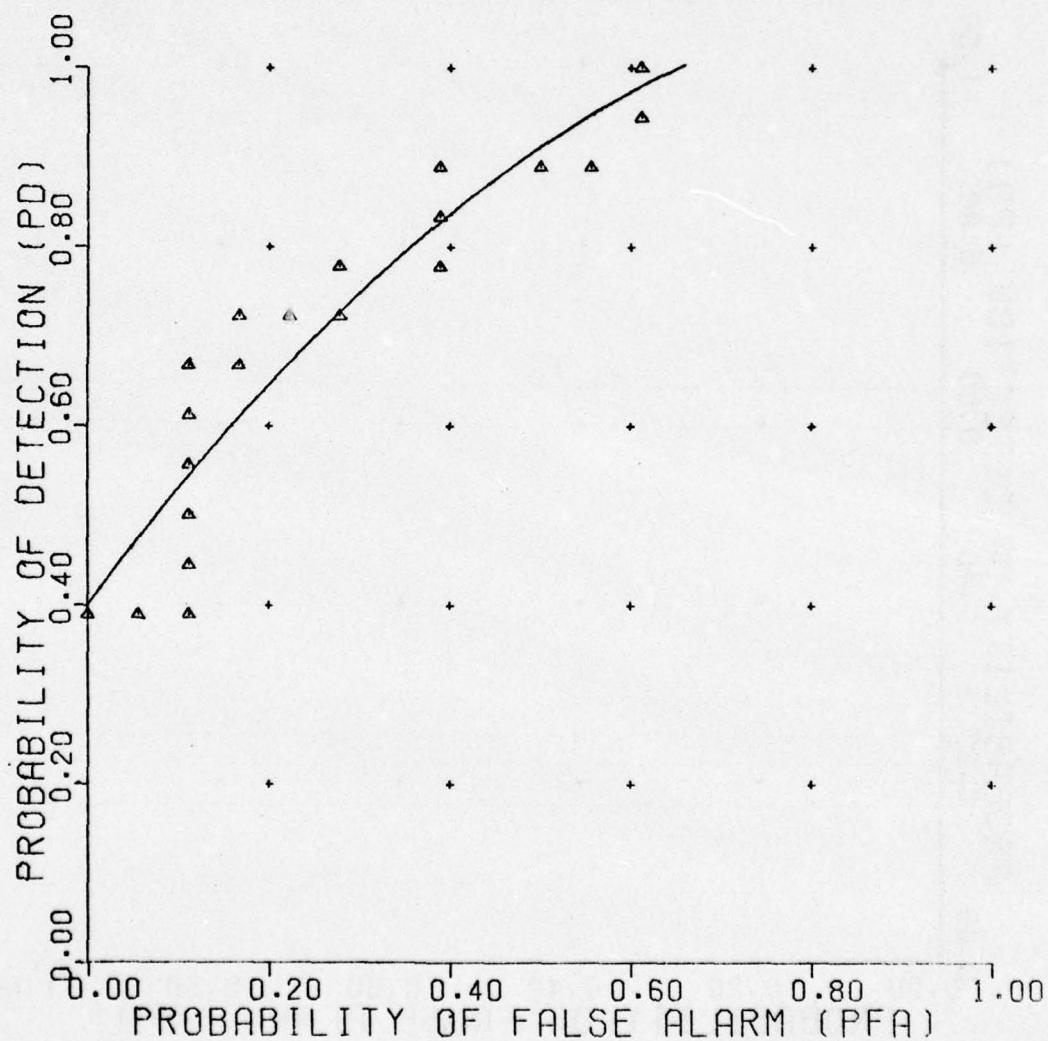


Figure C-19. FLD/Bayer classifier.

UNCLASSIFIED

UNCLASSIFIED

FLD/BAYES CLASSIFIER

INTUITIVE DATA
VERSION 2
REFERENCE 342

| | |
|----------|---------------------------------|
| NONMINE | PLATE |
| TARGET | TYPE B MINE |
| DEPTH | 3 6 |
| LOCATION | +4 0 -4 |
| MOISTURE | 7 17 12-20 13-16 |

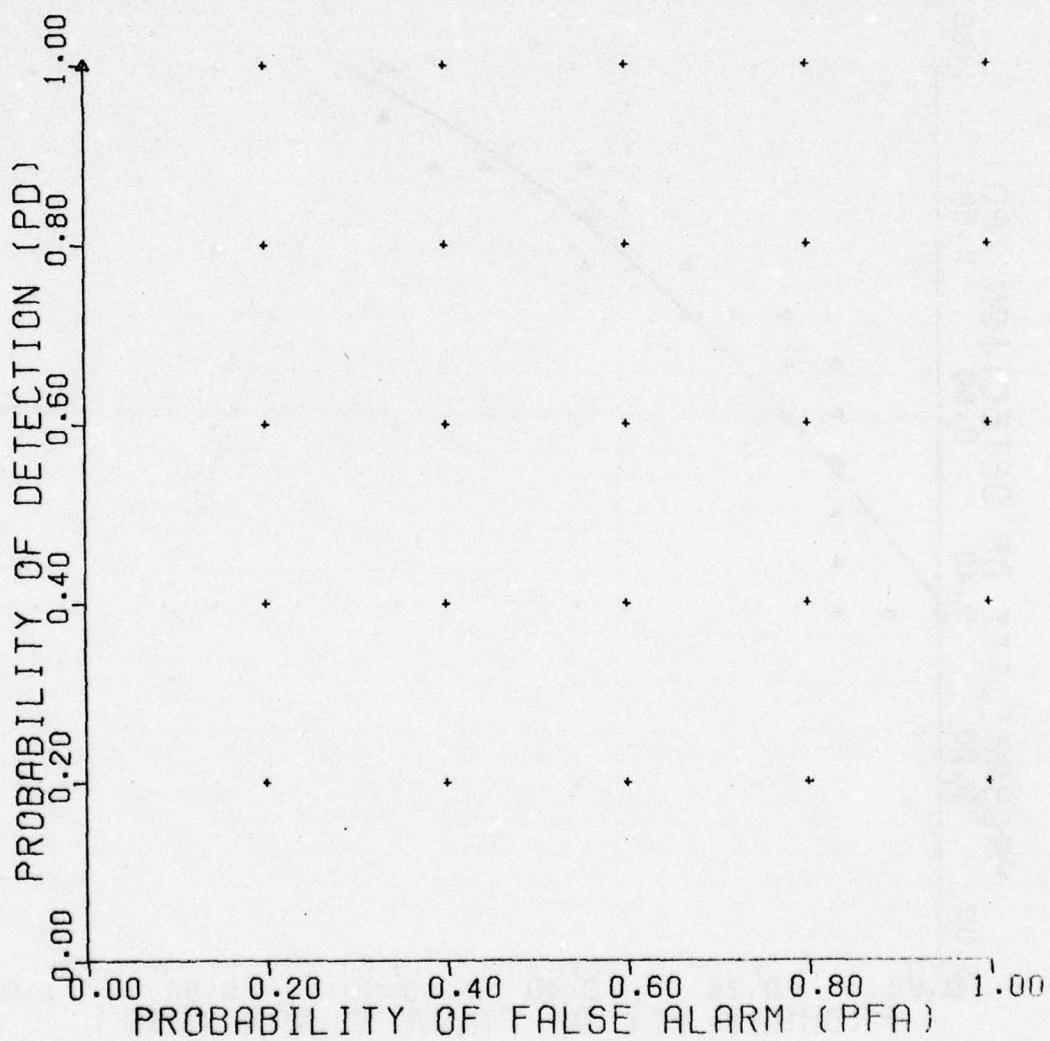


Figure C-20. FLD/Bayes classifier.

UNCLASSIFIED

UNCLASSIFIED

FLD/BAYES CLASSIFIER

INTUITIVE DATA
VERSION 2
REFERENCE 343

NONMINE BACKGND
TARGET TYPE B MINE

| | | | | |
|----------|----|----|-------|-------|
| DEPTH | 3 | 6 | | |
| LOCATION | +4 | 0 | -4 | |
| MOISTURE | 7 | 17 | 12-20 | 13-16 |

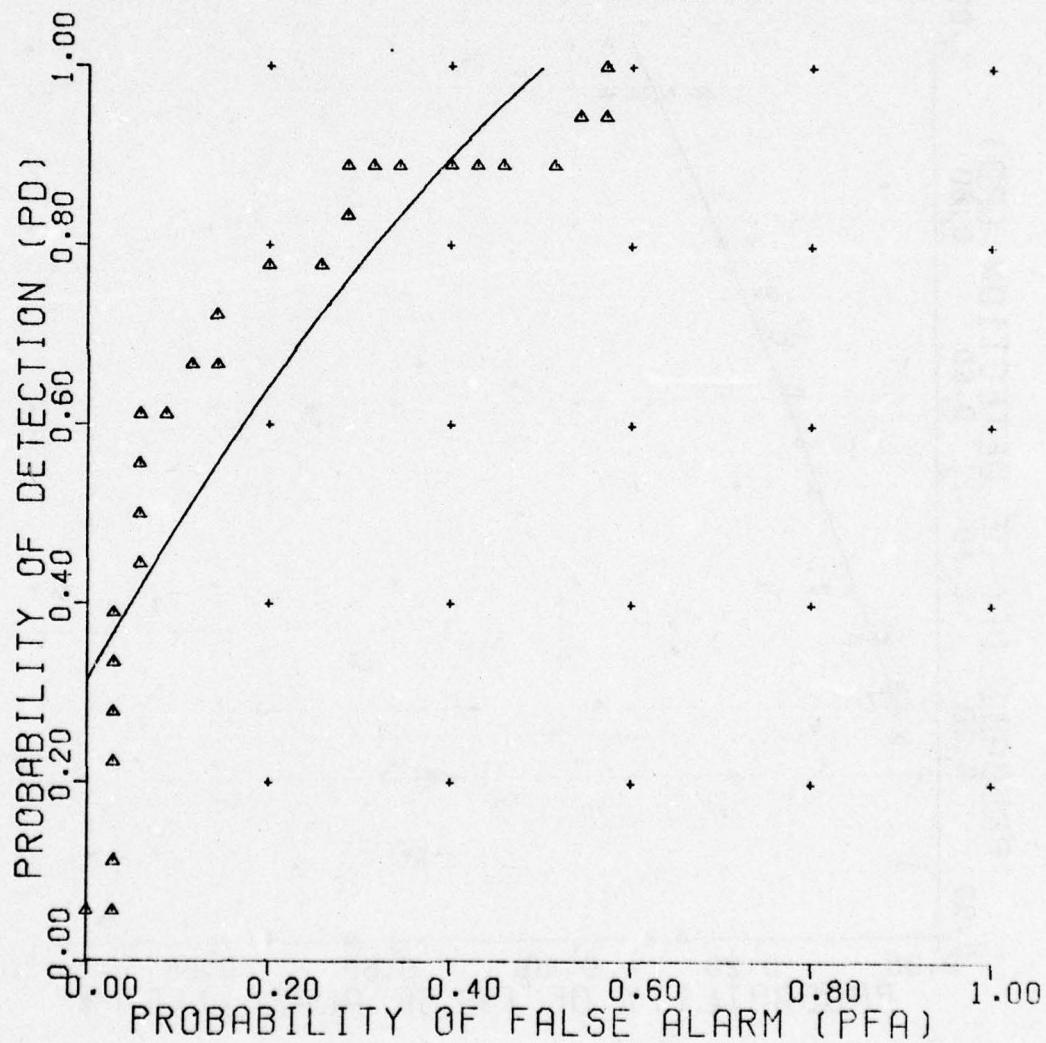


Figure C-21. FLD/Bayer classifier.

UNCLASSIFIED

UNCLASSIFIED

FLD/BAYES CLASSIFIER

INTUITIVE DATA
VERSION 2
REFERENCE 302

| NONMINE TARGET | PLATE TYPE B MINE | ROCK(1) | ROCK(2) | ROOT |
|-------------------|----------------------|---------|---------|-------|
| DEPTH | | 3 | 6 | |
| LOCATION | | +4 | 0 | -4 |
| MOISTURE | | 7 | 17 | 12-20 |
| | | | | 13-16 |

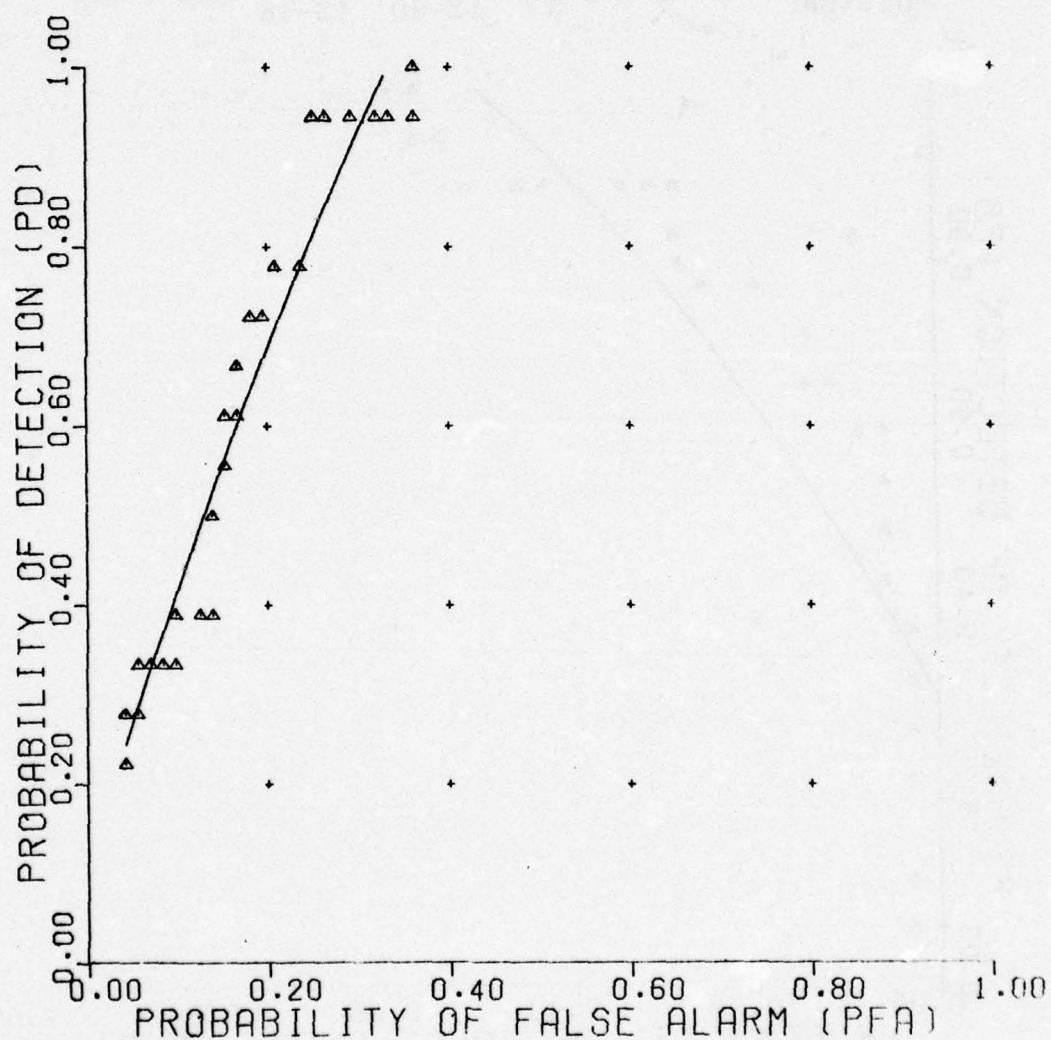


Figure C-22. FLD/Bayes classifier.

UNCLASSIFIED

UNCLASSIFIED

FLD/BAYES CLASSIFIER

INTUITIVE DATA
VERSION 2
REFERENCE 344

NONMINE ROCK(1) ROCK(2)
TARGET **TYPE B MINE**

| | | | | |
|----------|----|----|-------|-------|
| DEPTH | 3 | 6 | | |
| LOCATION | +4 | 0 | -4 | |
| MOISTURE | 7 | 17 | 12-20 | 13-16 |

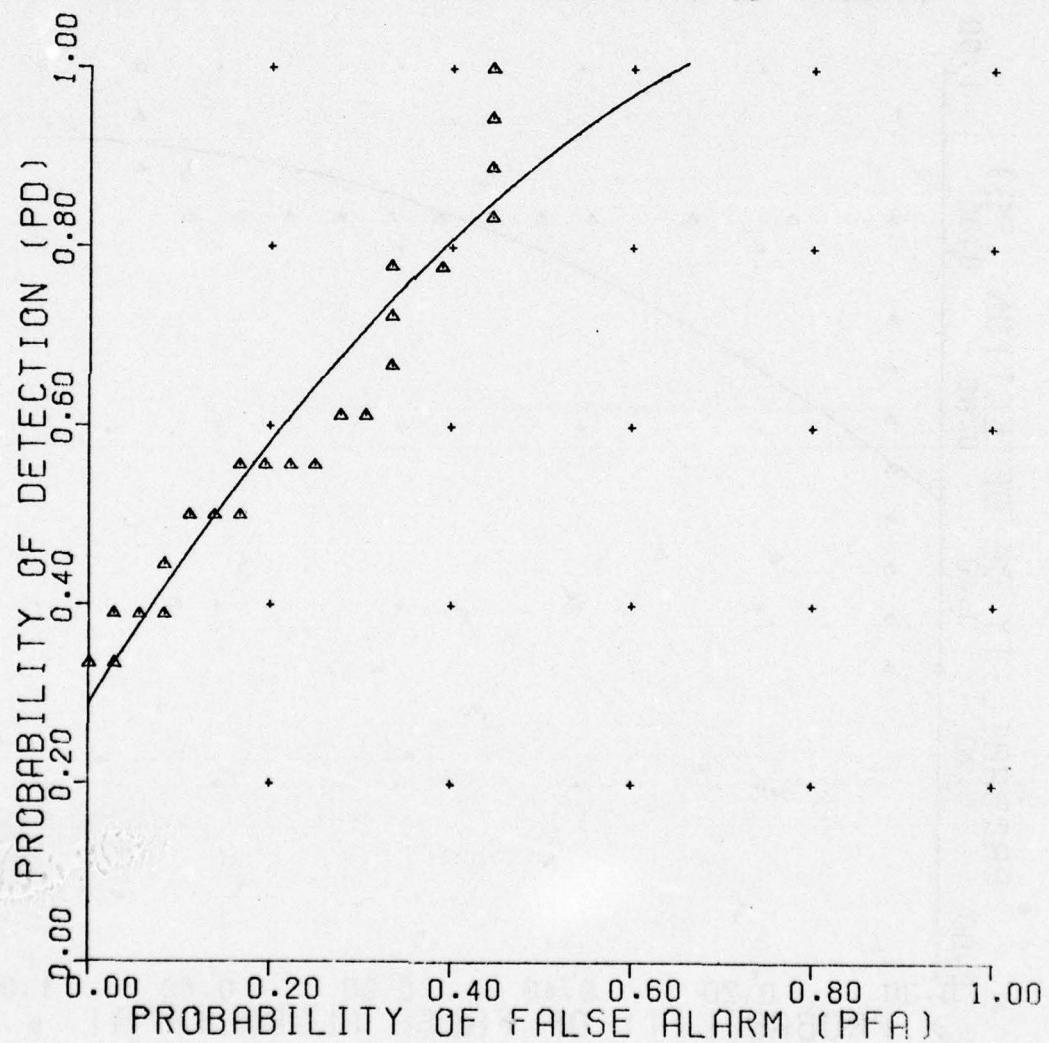


Figure C-23. FLD/Bayes classifier.

UNCLASSIFIED

UNCLASSIFIED

FLD/BAYES CLASSIFIER

INTUITIVE DATA
VERSION 2
REFERENCE 345

| NONMINE TARGET | ROOT TYPE C MINE |
|-------------------|---------------------------------|
| DEPTH | 3 6 |
| LOCATION | +4 0 -4 |
| MOISTURE | 7 17 12-20 13-16 |

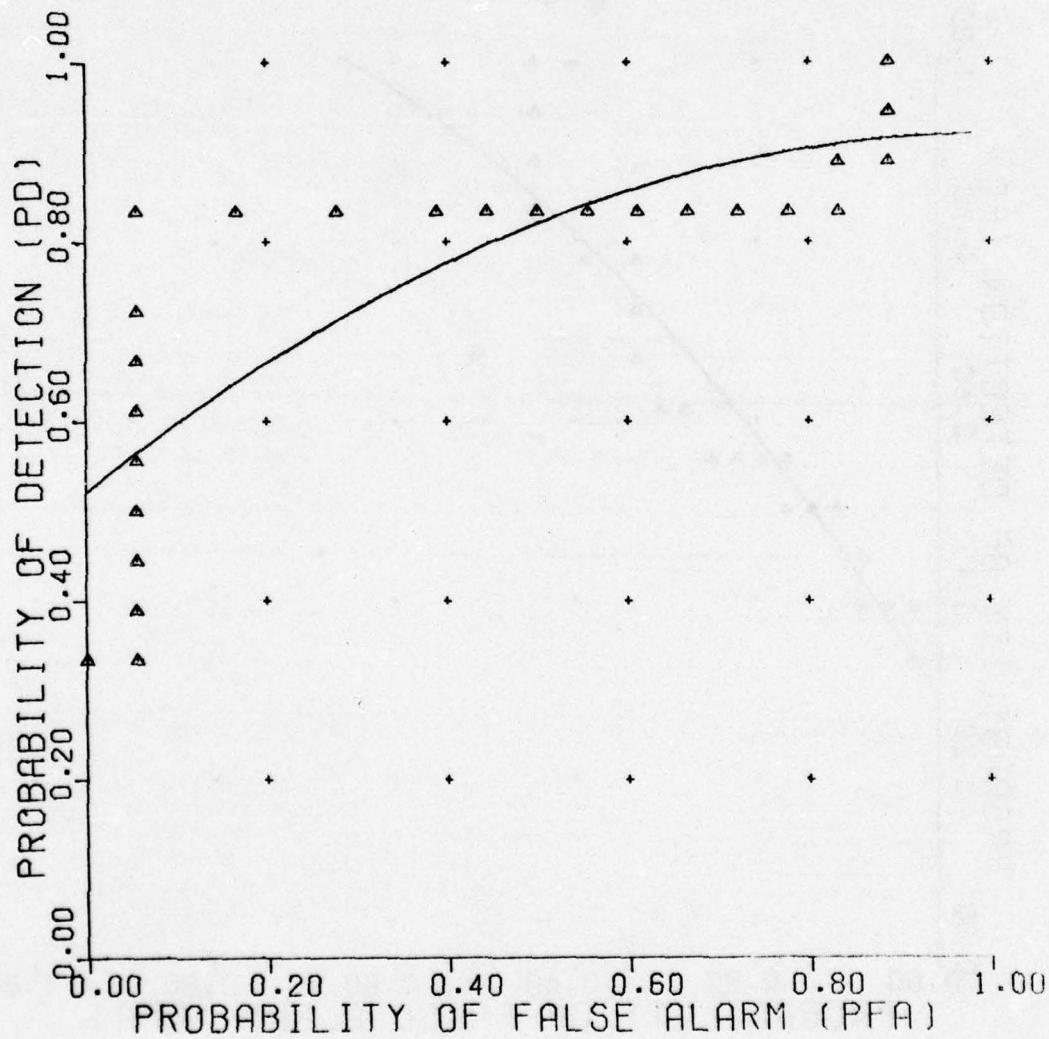


Figure C-24. FLD/Bayes classifier.

UNCLASSIFIED

UNCLASSIFIED

FLD/BAYES CLASSIFIER

INTUITIVE DATA
VERSION 2
REFERENCE 346

NONMINE PLATE
TARGET TYPE C MINE

DEPTH 3 6
LOCATION +4 0 -4
MOISTURE 7 17 12-20 13-16

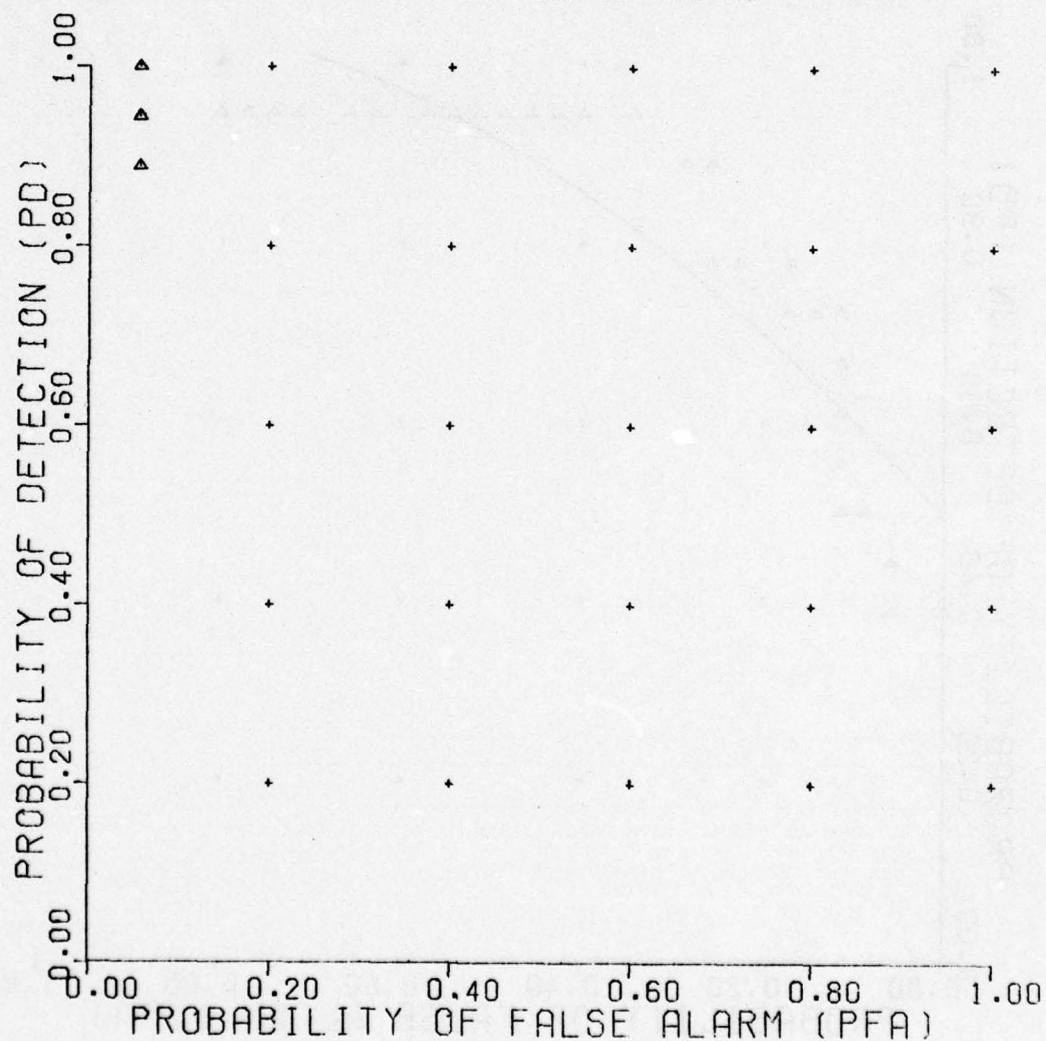


Figure C-25. FLD/Bayes classifier.

UNCLASSIFIED

UNCLASSIFIED

FLD/BAYES CLASSIFIER

INTUITIVE DATA
VERSION 2
REFERENCE 347

NONMINE BACKGND
TARGET TYPE C MINE

| | | | | |
|----------|----|----|-------|-------|
| DEPTH | 3 | 6 | | |
| LOCATION | +4 | 0 | -4 | |
| MOISTURE | 7 | 17 | 12-20 | 13-16 |

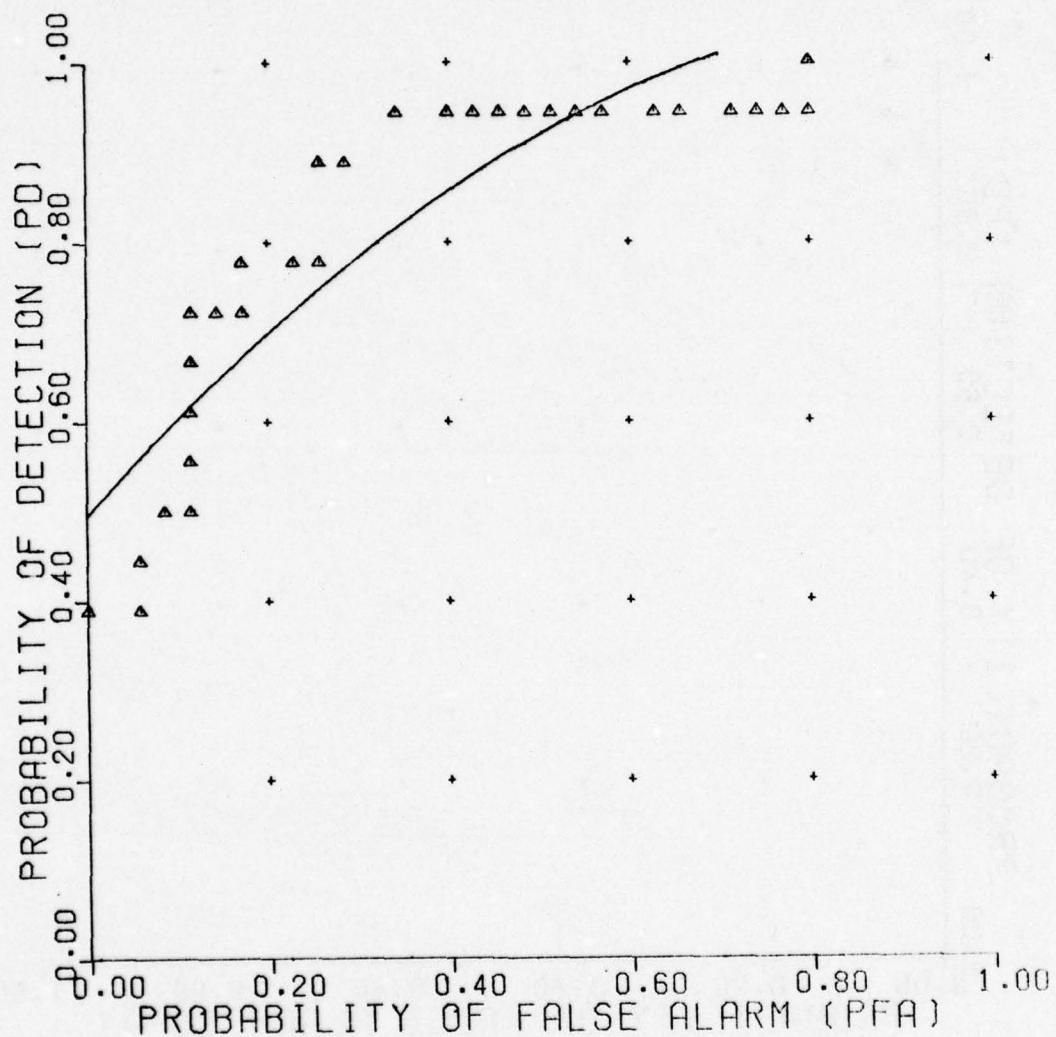


Figure C-26. FLD/Bayes classifier.

UNCLASSIFIED

UNCLASSIFIED

FLD/BAYES CLASSIFIER

INTUITIVE DATA
VERSION 2
REFERENCE 303

| NONMINE TARGET | PLATE | ROCK(1) | ROCK(2) | ROOT |
|-------------------|-------|---------|---------|-------|
| TYPE C MINE | | | | |
| DEPTH | 3 | 6 | | |
| LOCATION | +4 | 0 | -4 | |
| MOISTURE | 7 | 17 | 12-20 | 13-16 |

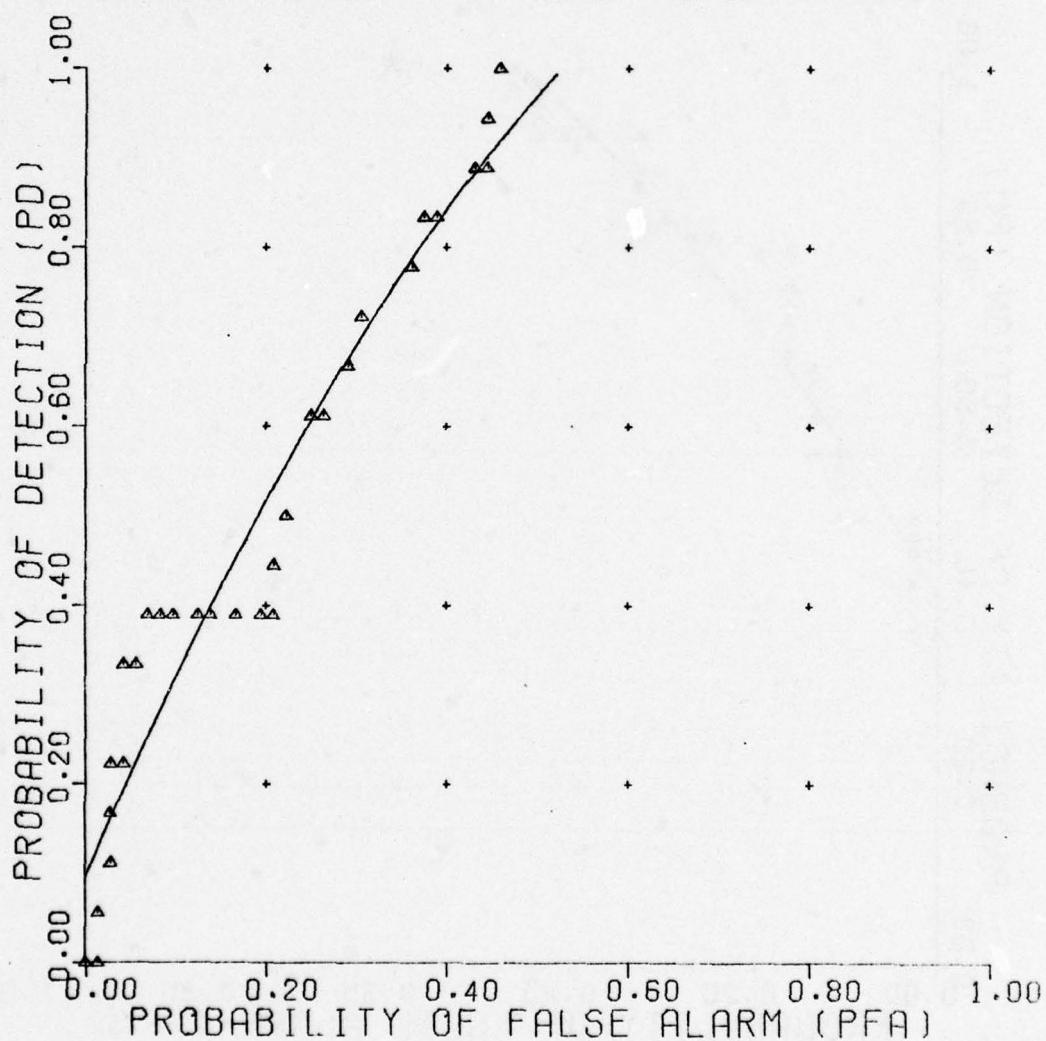


Figure C-27. FLD/Bayes classifier.

UNCLASSIFIED

UNCLASSIFIED

FLD/BAYES CLASSIFIER

INTUITIVE DATA
VERSION 2
REFERENCE 348

| NONMINE | ROCK(1) | ROCK(2) |
|----------|-------------|-------------|
| TARGET | TYPE C MINE | TYPE A MINE |
| DEPTH | 3 | 6 |
| LOCATION | +4 | 0 |
| MOISTURE | 7 | 17 |
| | | 12-20 |
| | | 13-16 |

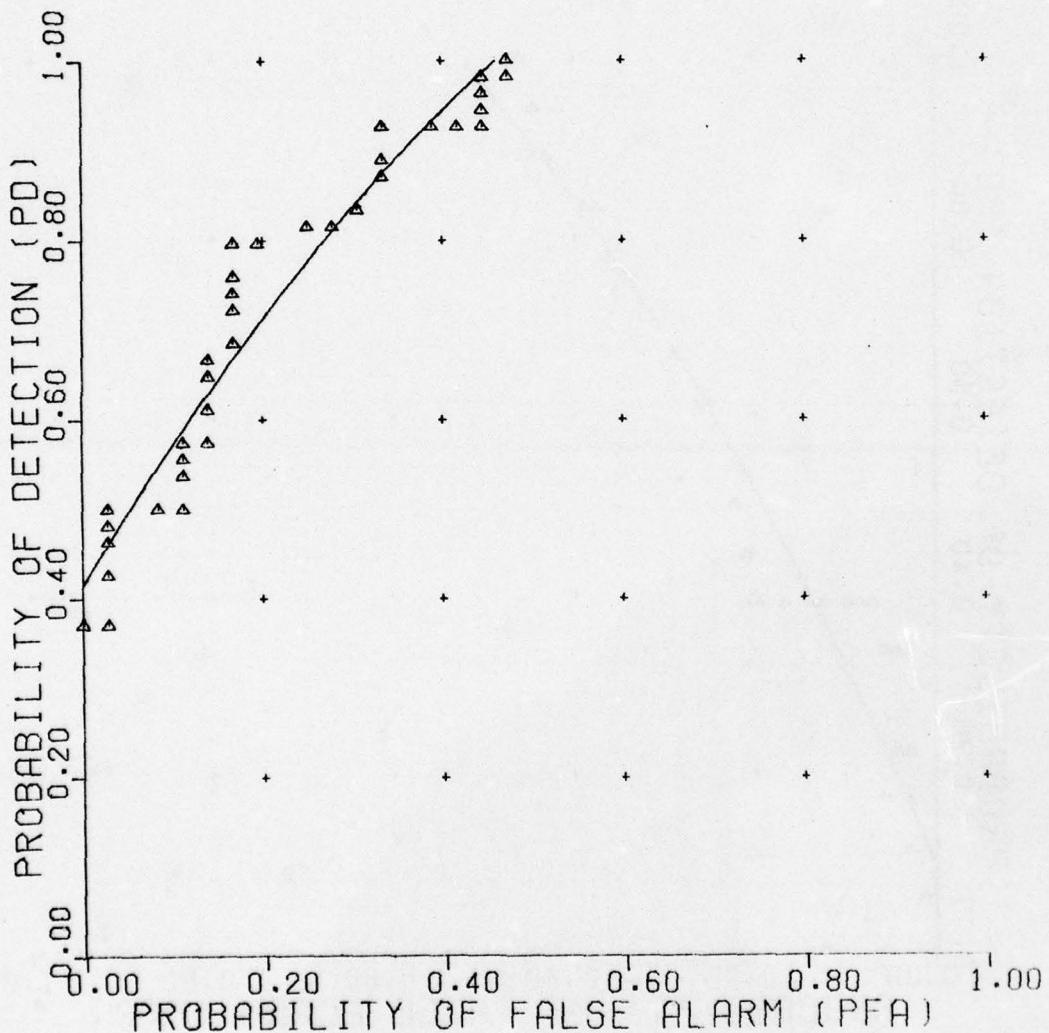


Figure C-28. FLD/Bayes classifier.

UNCLASSIFIED

UNCLASSIFIED

FLD/BAYES CLASSIFIER

INTUITIVE DATA
VERSION 2
REFERENCE 349

| NONMINE | ROOT | | |
|----------|-------------|-------------|-------------|
| TARGET | TYPE C MINE | TYPE A MINE | TYPE B MINE |
| DEPTH | 3 | 6 | |
| LOCATION | +4 | 0 | -4 |
| MOISTURE | 7 | 17 | 12-20 |

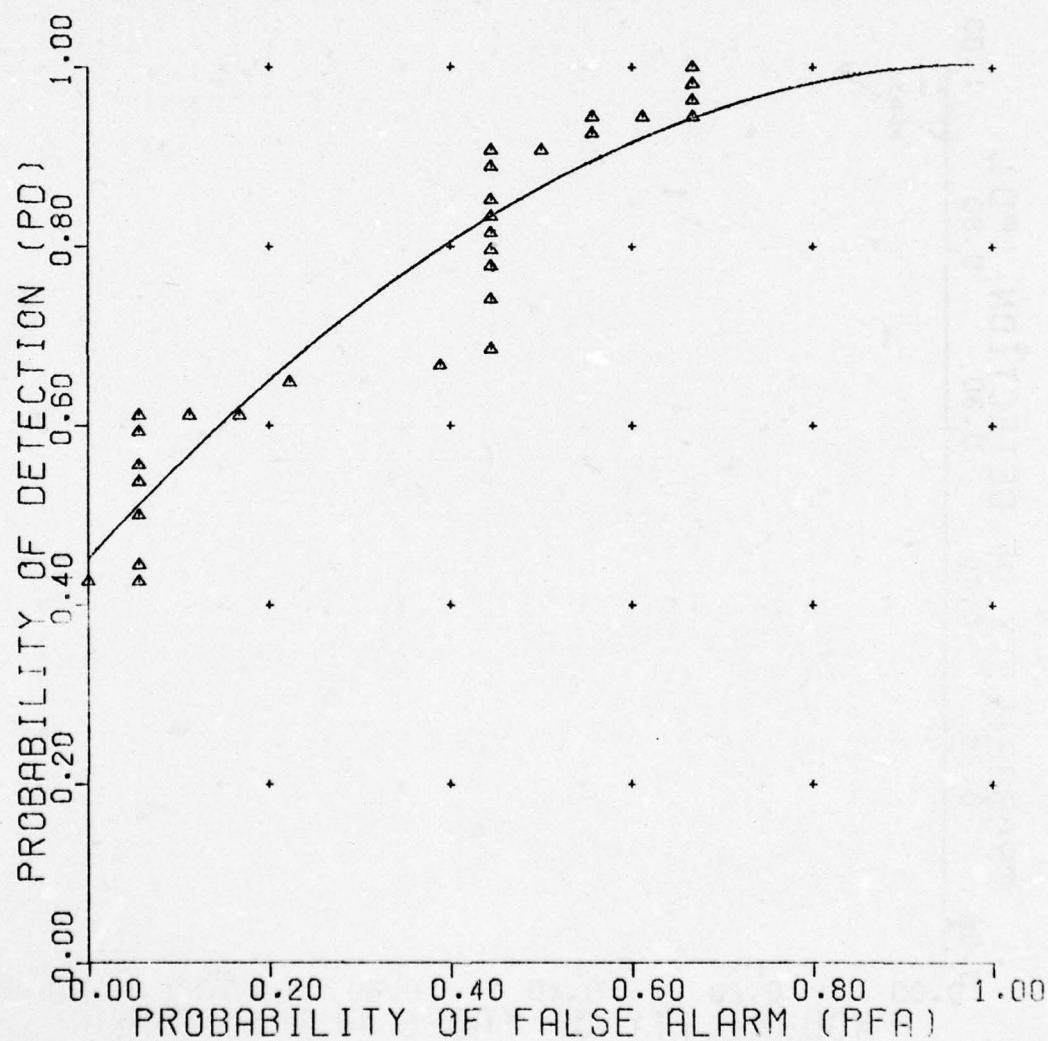


Figure C-29. FLD/Bayes classifier.

UNCLASSIFIED

UNCLASSIFIED

FLD/BAYES CLASSIFIER

INTUITIVE DATA
VERSION 2
REFERENCE 350

| NONMINE | PLATE | TYPE C MINE | TYPE A MINE | TYPE B MINE |
|----------|-------|-------------|-------------|-------------|
| TARGET | | | | |
| DEPTH | | 3 | 6 | |
| LOCATION | | +4 | 0 | -4 |
| MOISTURE | | 7 | 17 | 12-20 |

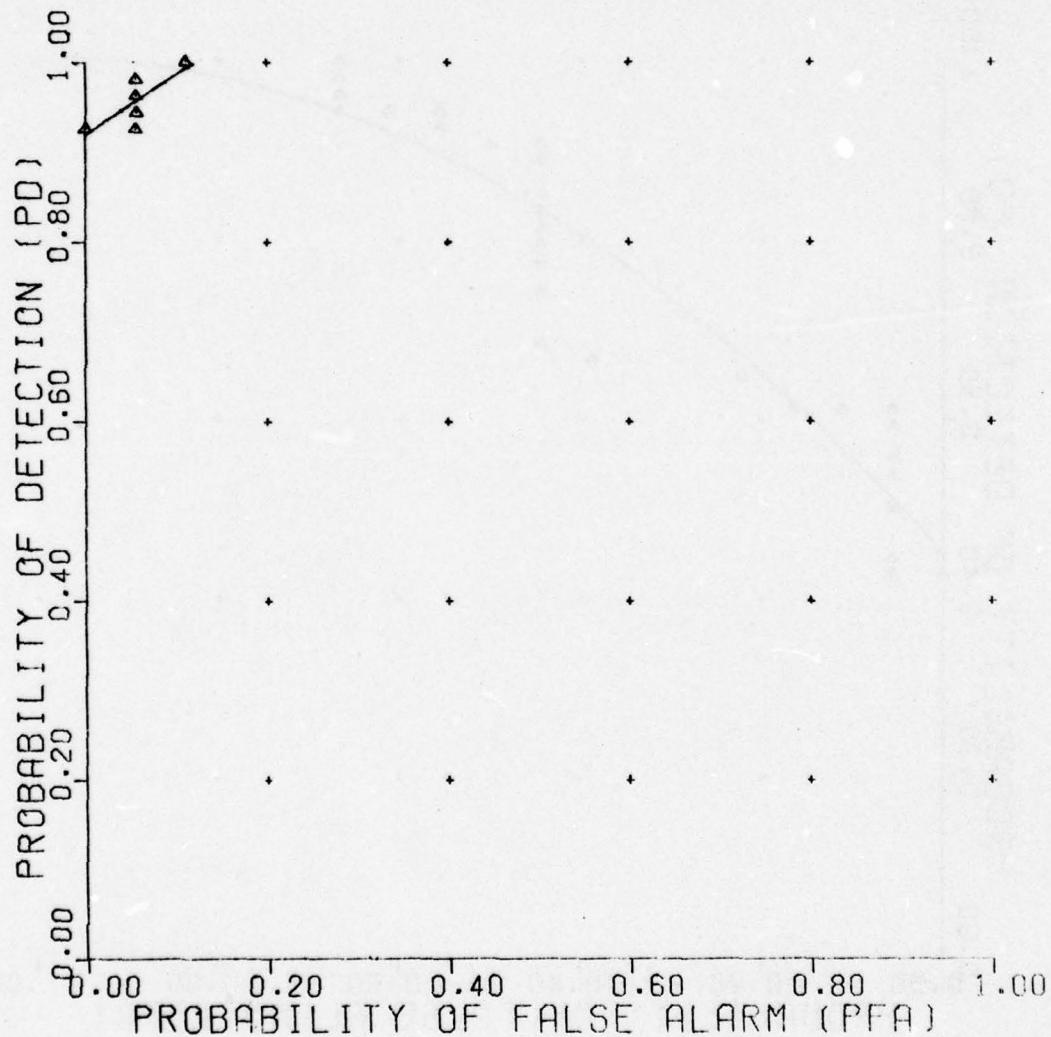


Figure C-30. FLD/Bayes classifier.

UNCLASSIFIED

UNCLASSIFIED

FLD/BAYES CLASSIFIER

INTUITIVE DATA

VERSION 2

REFERENCE 351

| NONMINE TARGET | BACKGND | TYPE C MINE | TYPE A MINE | TYPE B MINE |
|-------------------|---------|-------------|-------------|-------------|
| DEPTH | | 3 | 6 | |
| LOCATION | | +4 | 0 | -4 |
| MOISTURE | | 7 | 17 | 12-20 |

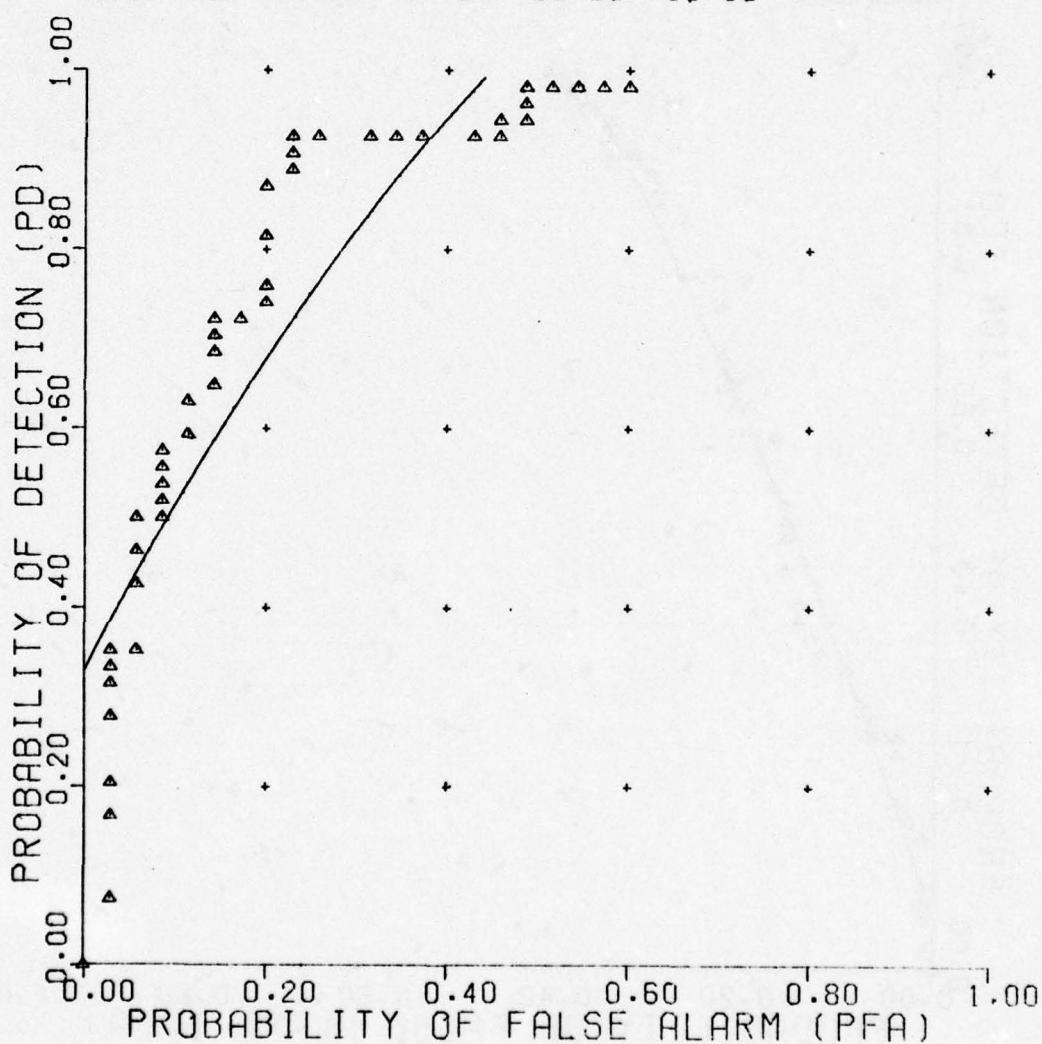


Figure C-31. FLD/Bayes classifier.

UNCLASSIFIED

UNCLASSIFIED

FLD/BAYES CLASSIFIER

INTUITIVE DATA

VERSION 2

REFERENCE 304

| NONMINE TARGET | PLATE TYPE C MINE | ROCK(1) TYPE A MINE | ROCK(2) TYPE B MINE | ROOT |
|-------------------|----------------------|------------------------|------------------------|-------|
| DEPTH | 3 | 6 | | |
| LOCATION | +4 | 0 | -4 | |
| MOISTURE | 7 | 17 | 12-20 | 13-16 |

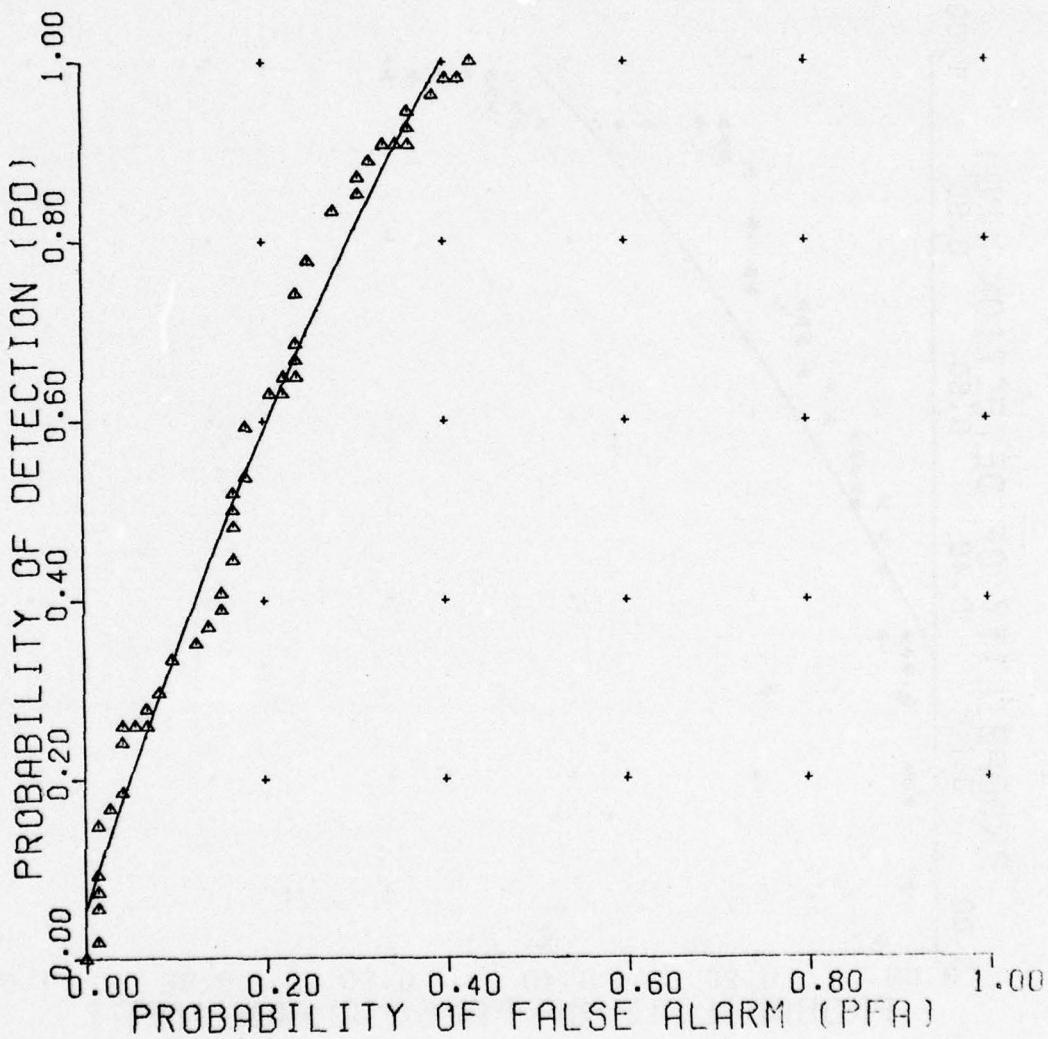


Figure C-32. FLD/Bayes classifier.

UNCLASSIFIED

UNCLASSIFIED

FLD/BAYES CLASSIFIER

CLASSIFIER VERSION= 2
REFERENCE NUMBER= 360
CLASS 1= TYPE A MINE
CLASS 2= TYPE B MINE

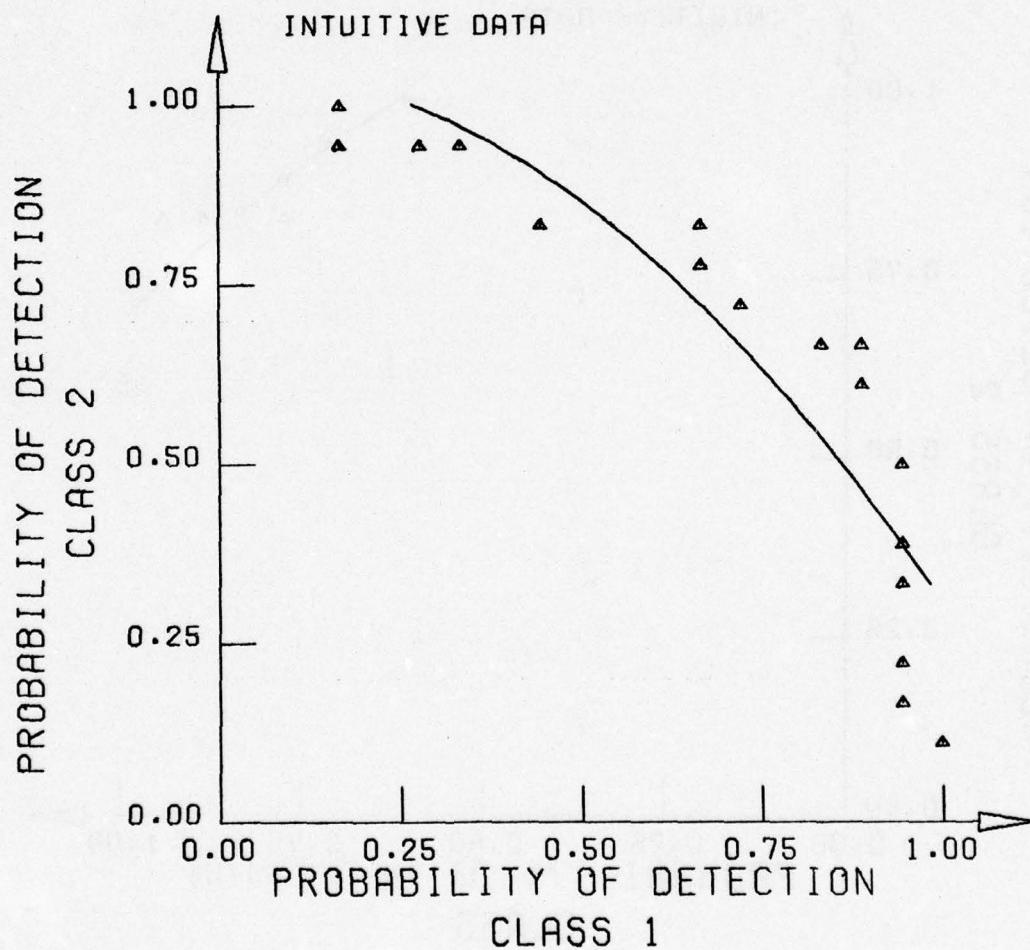


Figure C-33. FLD/Bayes classifier.

UNCLASSIFIED

UNCLASSIFIED

FLD/BAYES CLASSIFIER

CLASSIFIER VERSION= 2
REFERENCE NUMBER= 361
CLASS 1= TYPE A MINE
CLASS 2= TYPE C MINE

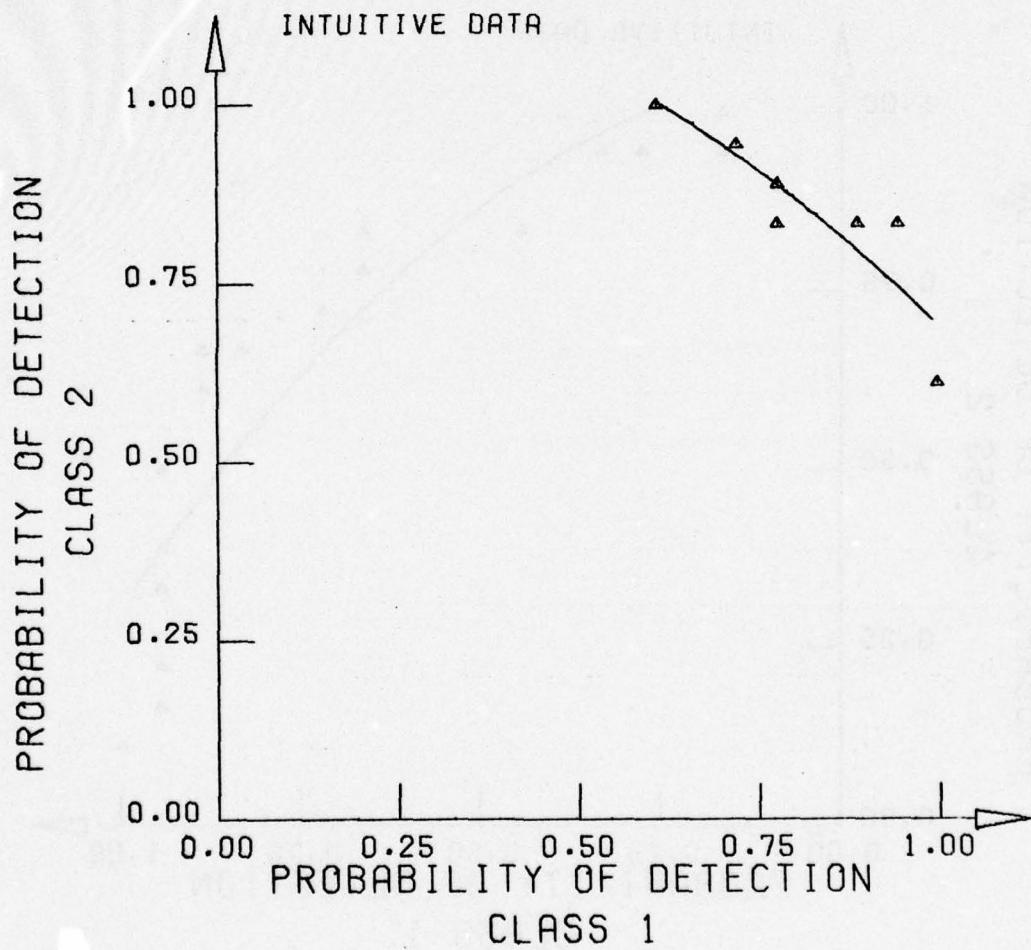


Figure C-34. FLD/Bayes classifier.

UNCLASSIFIED

UNCLASSIFIED

FLD/BAYES CLASSIFIER

CLASSIFIER VERSION= 2
REFERENCE NUMBER= 362
CLASS 1= TYPE B MINE
CLASS 2= TYPE C MINE

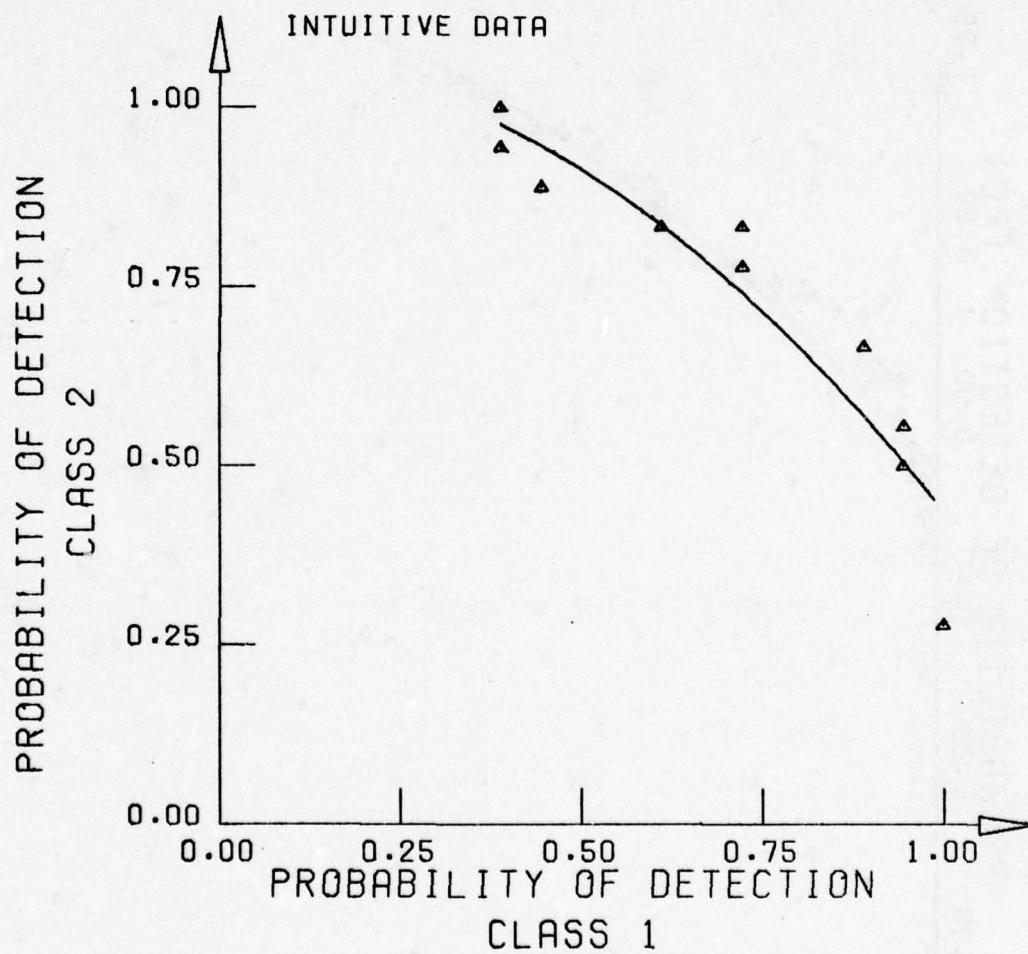


Figure C-35. FLD/Bayes classifier.

UNCLASSIFIED

UNCLASSIFIED

FLD/BAYES CLASSIFIER

RAW DATA
VERSION 0
REFERENCE 308

| NONMINE TARGET | PLATE TYPE C MINE | ROCK(1) TYPE A MINE | ROCK(2) TYPE B MINE | ROOT |
|-------------------|-------------------------|---------------------------|---------------------------|-------|
| DEPTH | 3 | 6 | | |
| LOCATION | +4 | 0 | -4 | |
| MOISTURE | 7 | 17 | 12-20 | 13-16 |

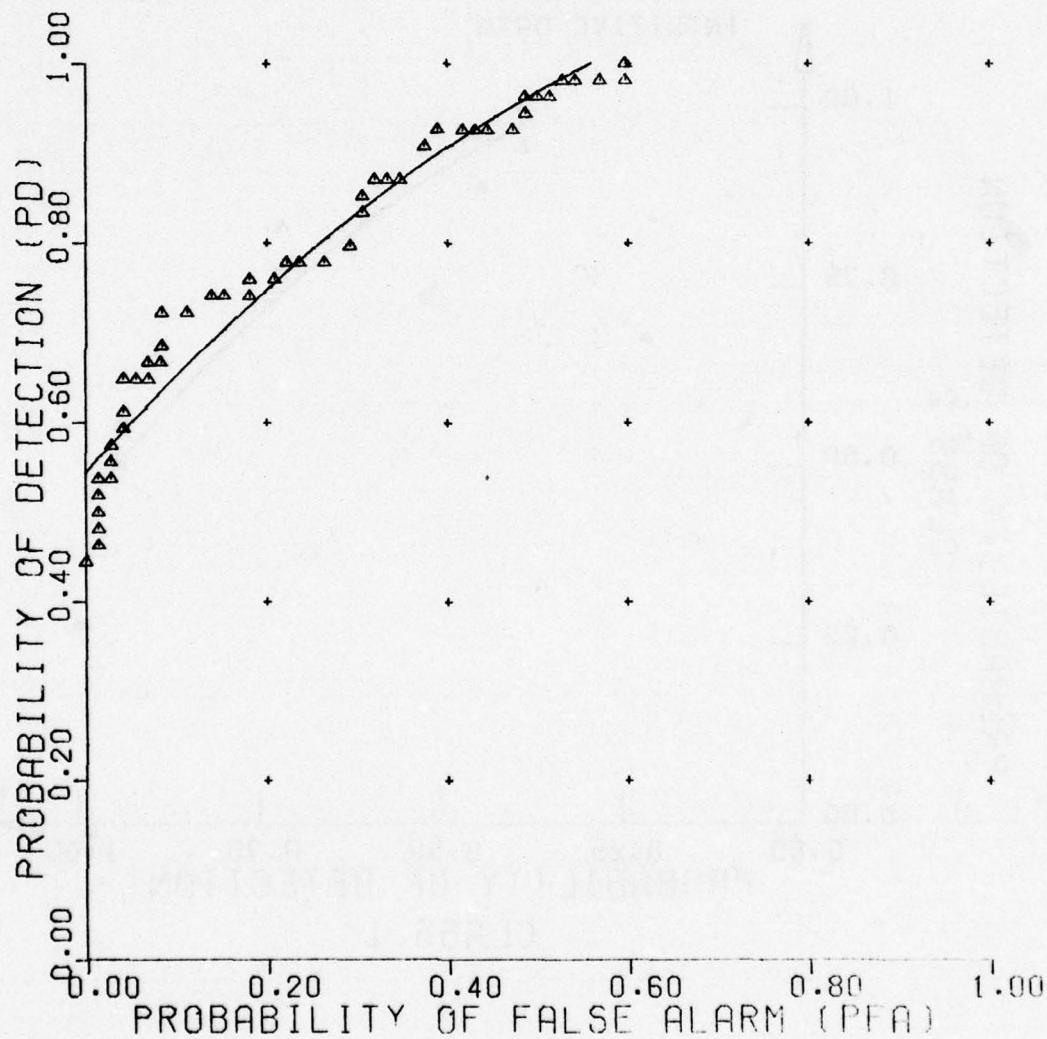


Figure C-36. FLD/Bayes classifier.

UNCLASSIFIED

UNCLASSIFIED

NEAREST NEIGHBOR CLASSIFIER

INTUITIVE DATA

NO. NEAREST NEIGHBORS 3

REFERENCE 309

| NONMINE TARGET | PLATE TYPE A MINE | ROCK(1) | ROCK(2) | ROOT |
|-------------------|----------------------|---------|---------|-------|
| DEPTH | | 3 | 6 | |
| LOCATION | | +4 | 0 | -4 |
| MOISTURE | | 7 | 17 | 12-20 |
| | | | | 13-16 |

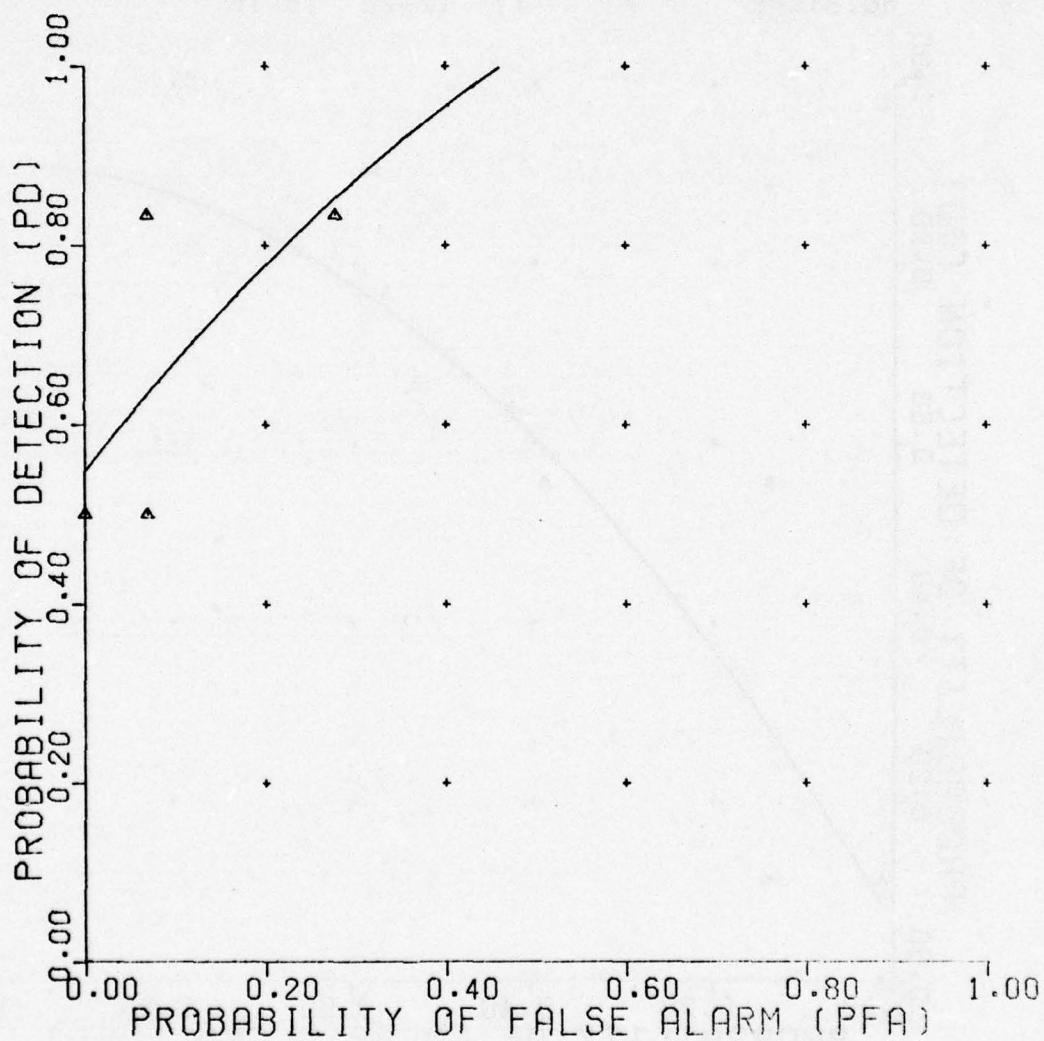


Figure C-37. Nearest neighbor classifier.

UNCLASSIFIED

UNCLASSIFIED

NEAREST NEIGHBOR CLASSIFIER

INTUITIVE DATA
NO. NEAREST NEIGHBORS 3
REFERENCE 310

| NONMINE TARGET | PLATE TYPE B MINE | ROCK(1) | ROCK(2) | ROOT |
|----------------|-------------------|---------|---------|-------|
| DEPTH | | 3 | 6 | |
| LOCATION | | +4 | 0 | -4 |
| MOISTURE | | 7 | 17 | 12-20 |
| | | | | 13-16 |

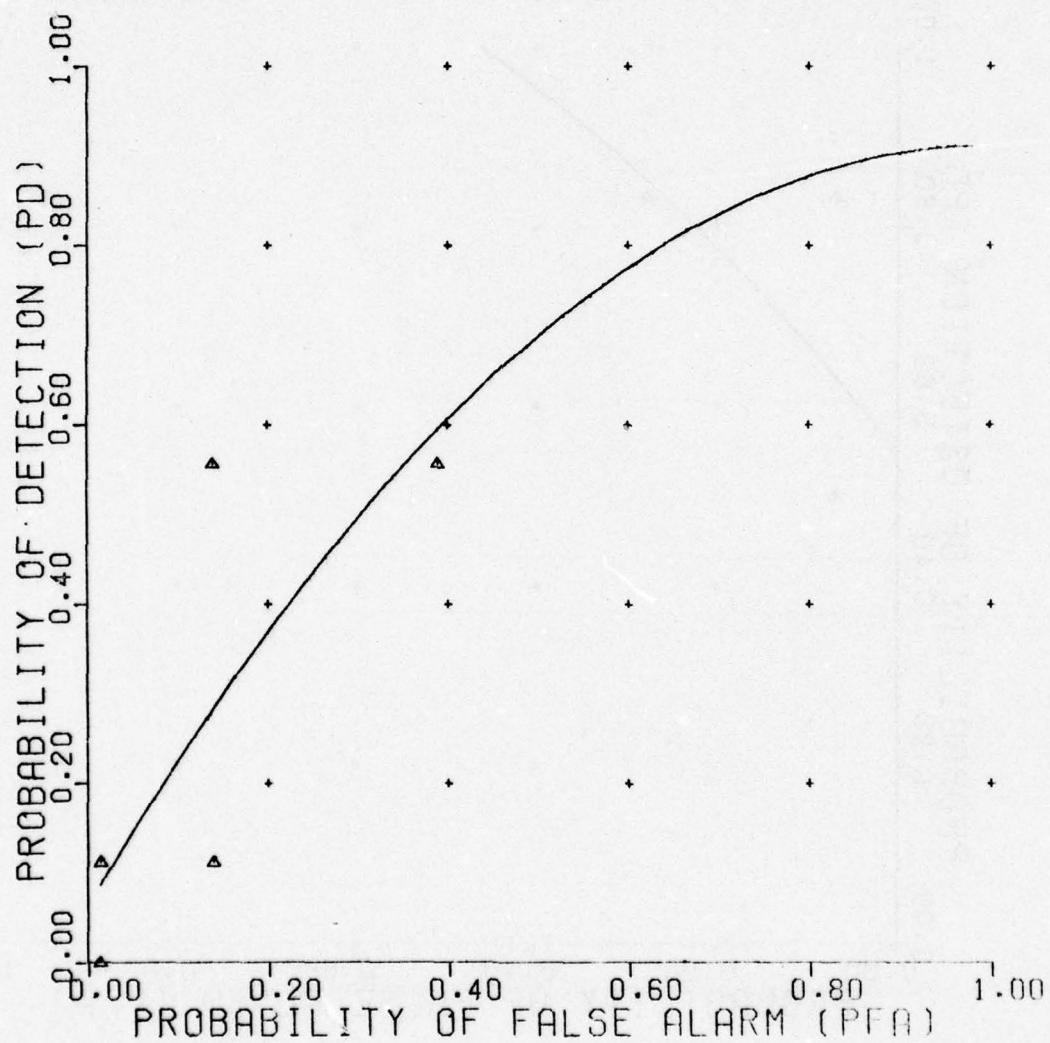


Figure C-38. Nearest neighbor classifier.

UNCLASSIFIED

UNCLASSIFIED

NEAREST NEIGHBOR CLASSIFIER

INTUITIVE DATA

NO. NEAREST NEIGHBORS 3

REFERENCE 311

| NONMINE TARGET | PLATE TYPE C MINE | ROCK(1) | ROCK(2) | ROOT |
|-------------------|----------------------|---------|---------|-------|
| DEPTH | | 3 | 6 | |
| LOCATION | +4 | | 0 | -4 |
| MOISTURE | | 7 | 17 | 12-20 |

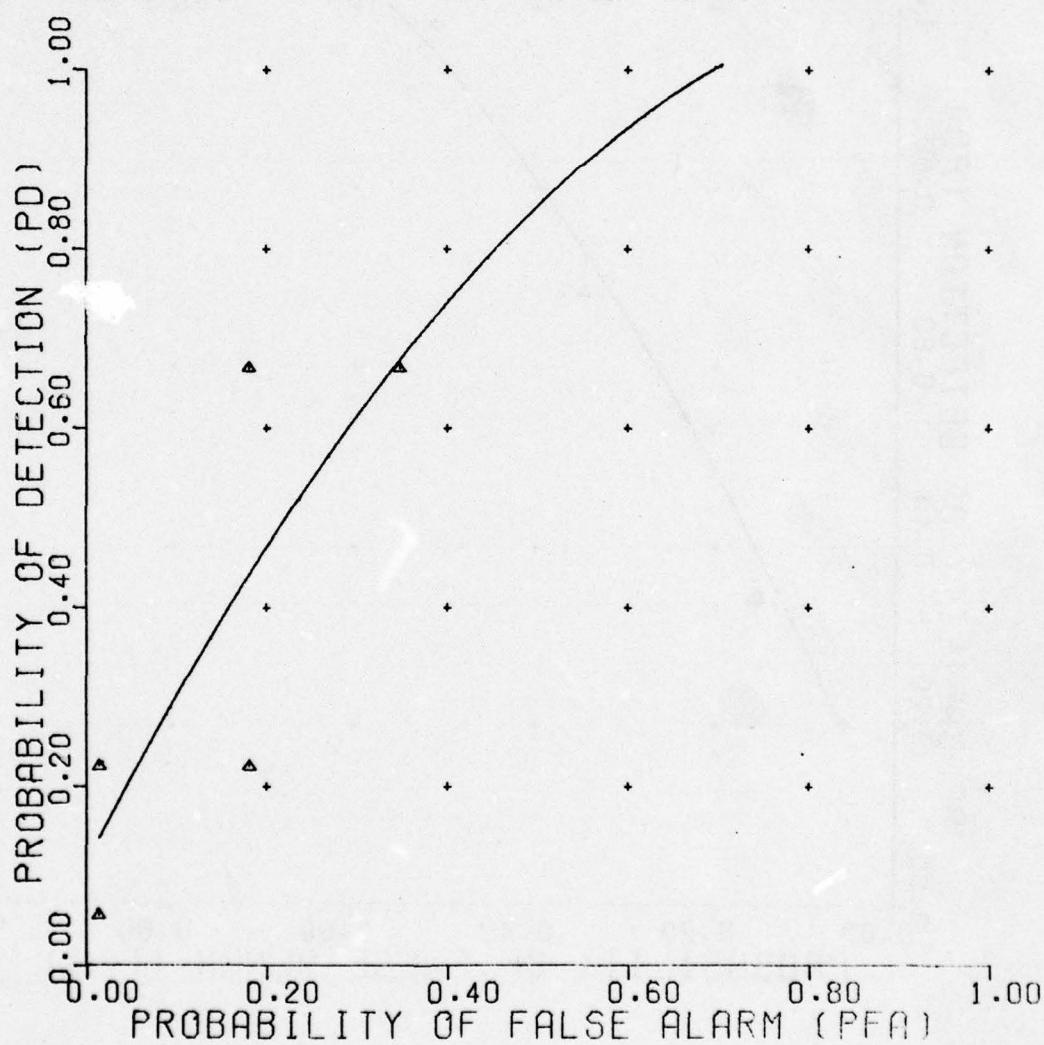


Figure C-39. Nearest neighbor classifier.

UNCLASSIFIED

UNCLASSIFIED

NEAREST NEIGHBOR CLASSIFIER

INTUITIVE DATA

NO. NEAREST NEIGHBORS 3

REFERENCE 312

| NONMINE TARGET | PLATE TYPE C MINE | ROCK(1) TYPE A MINE | ROCK(2) TYPE B MINE | ROOT TYPE B MINE |
|-------------------|----------------------|------------------------|------------------------|---------------------|
| DEPTH | 3 | 6 | | |
| LOCATION | +4 | 0 | -4 | |
| MOISTURE | 7 | 17 | 12-20 | 13-16 |

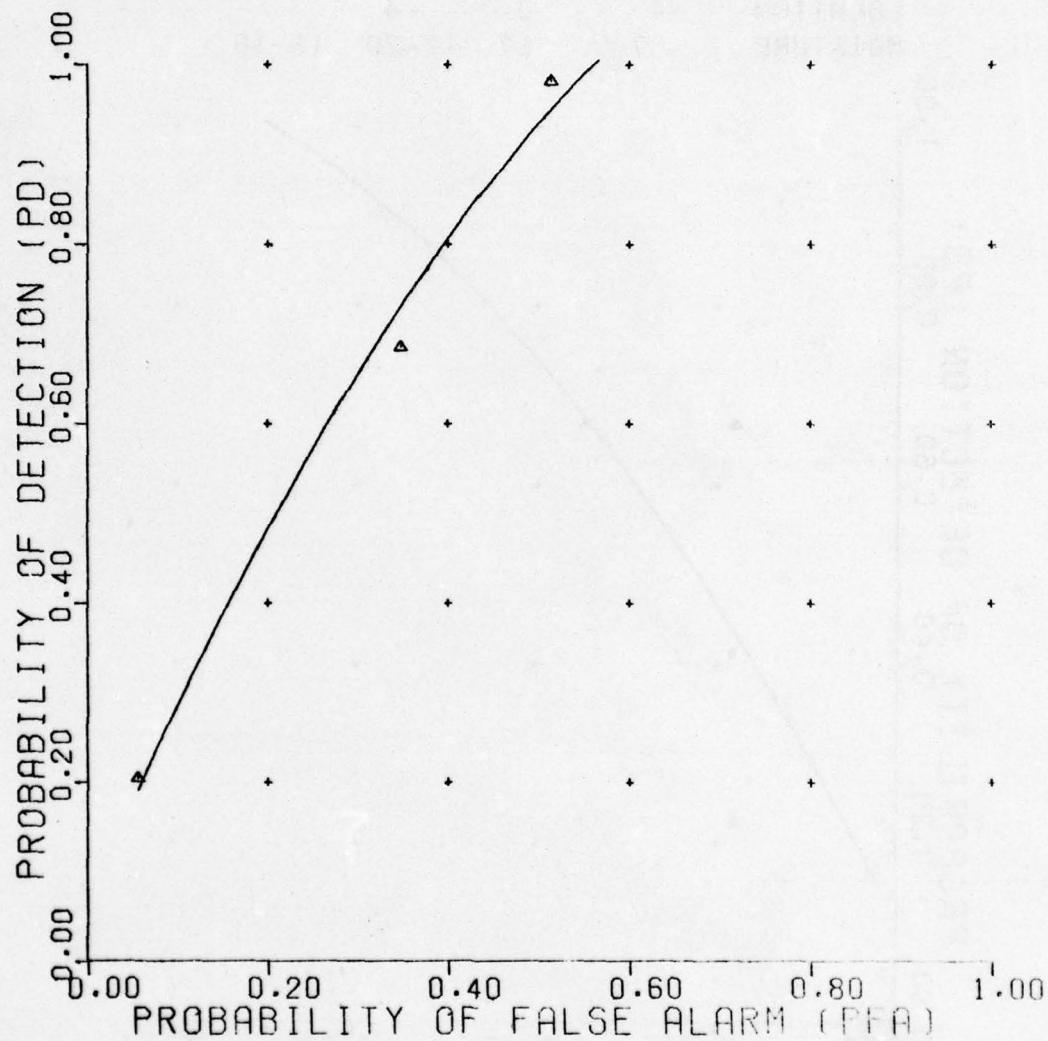


Figure C-40. Nearest neighbor classifier.

UNCLASSIFIED

UNCLASSIFIED

NEAREST NEIGHBOR CLASSIFIER

INTUITIVE DATA

VERSION 3

REFERENCE 277

TARGET2 TYPE B MINE

TARGET1 TYPE A MINE

| | | | |
|----------|----|----|-------|
| DEPTH | 3 | 6 | |
| LOCATION | +4 | 0 | -4 |
| MOISTURE | 7 | 17 | 12-20 |
| | | | 13-16 |

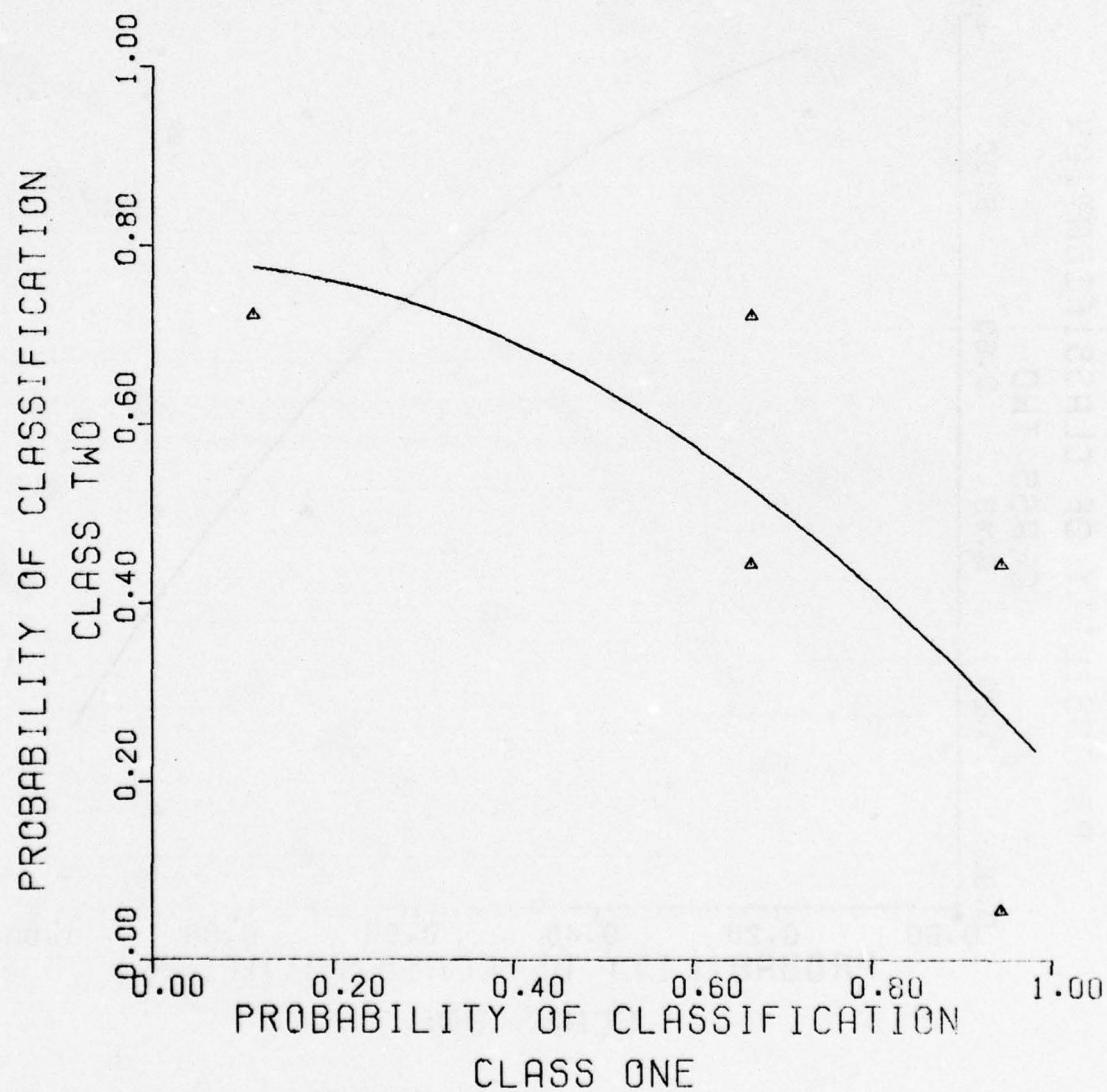


Figure C-41. Nearest neighbor classifier.

UNCLASSIFIED

UNCLASSIFIED

NEAREST NEIGHBOR CLASSIFIER

INTUITIVE DATA

VERSION 3

REFERENCE 278

TARGET2 TYPE C MINE

TARGET1 TYPE A MINE

| | | | |
|----------|----|----|-------|
| DEPTH | 3 | 6 | |
| LOCATION | +4 | 0 | -4 |
| MOISTURE | 7 | 17 | 12-20 |
| | | | 13-16 |

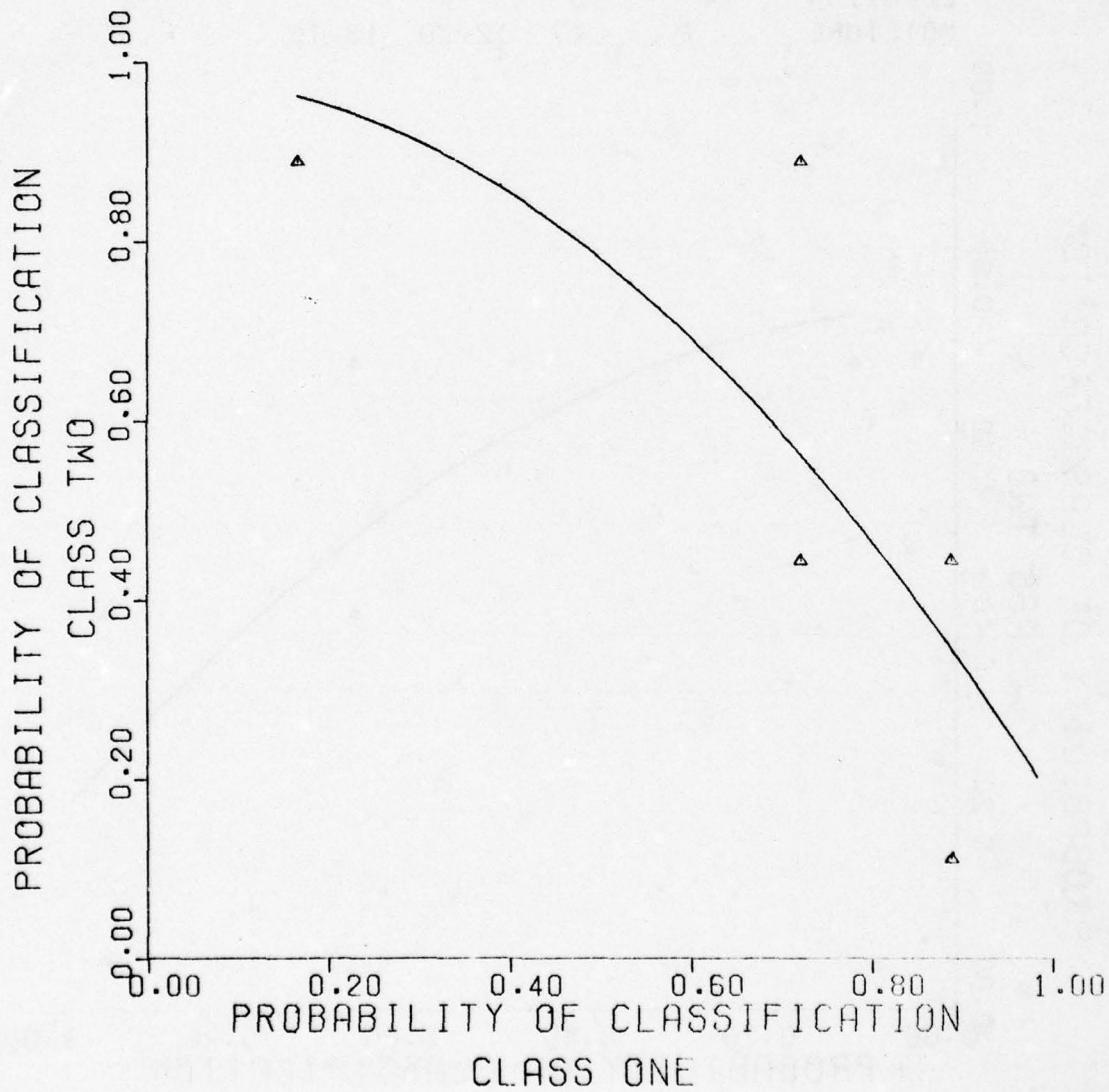


Figure C-42. Nearest neighbor classifier.

UNCLASSIFIED

UNCLASSIFIED

NEAREST NEIGHBOR CLASSIFIER

INTUITIVE DATA

VERSION 3

REFERENCE 279

TARGET2 TYPE C MINE

TARGET1 TYPE B MINE

| DEPTH | 3 | 6 |
|----------|----|----|
| LOCATION | +4 | 0 |
| MOISTURE | 7 | 17 |

-4

12-20 13-16

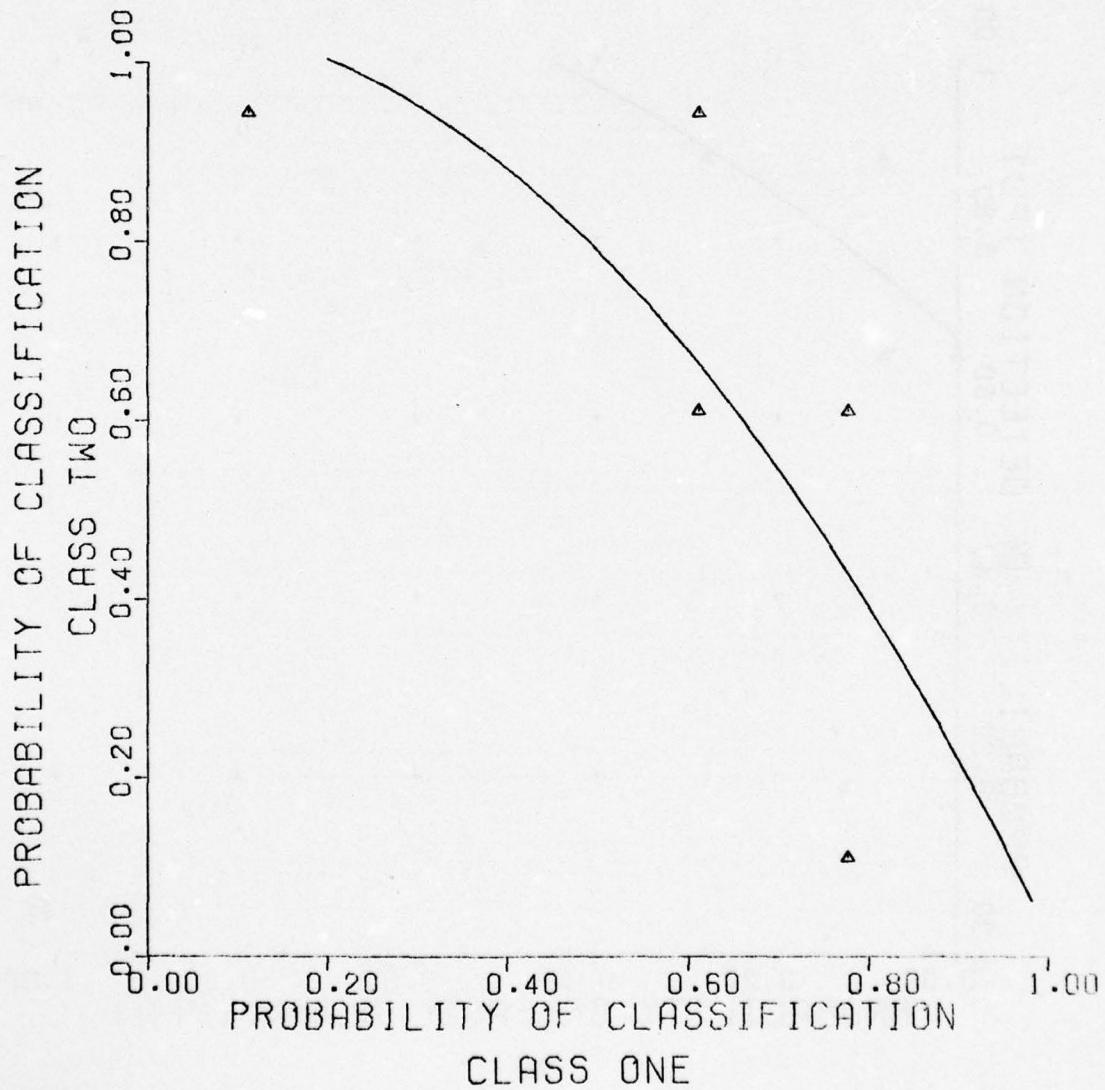


Figure C-43. Nearest neighbor classifier.

UNCLASSIFIED

UNCLASSIFIED

NEAREST NEIGHBOR CLASSIFIER

RAW DATA
NO. NEAREST NEIGHBORS 3
REFERENCE 283

NONMINE ROCK(1) ROCK(2)
TARGET TYPE A MINE
DEPTH 3 6
LOCATION +4 0 -4
MOISTURE 7 17 12-20 13-16

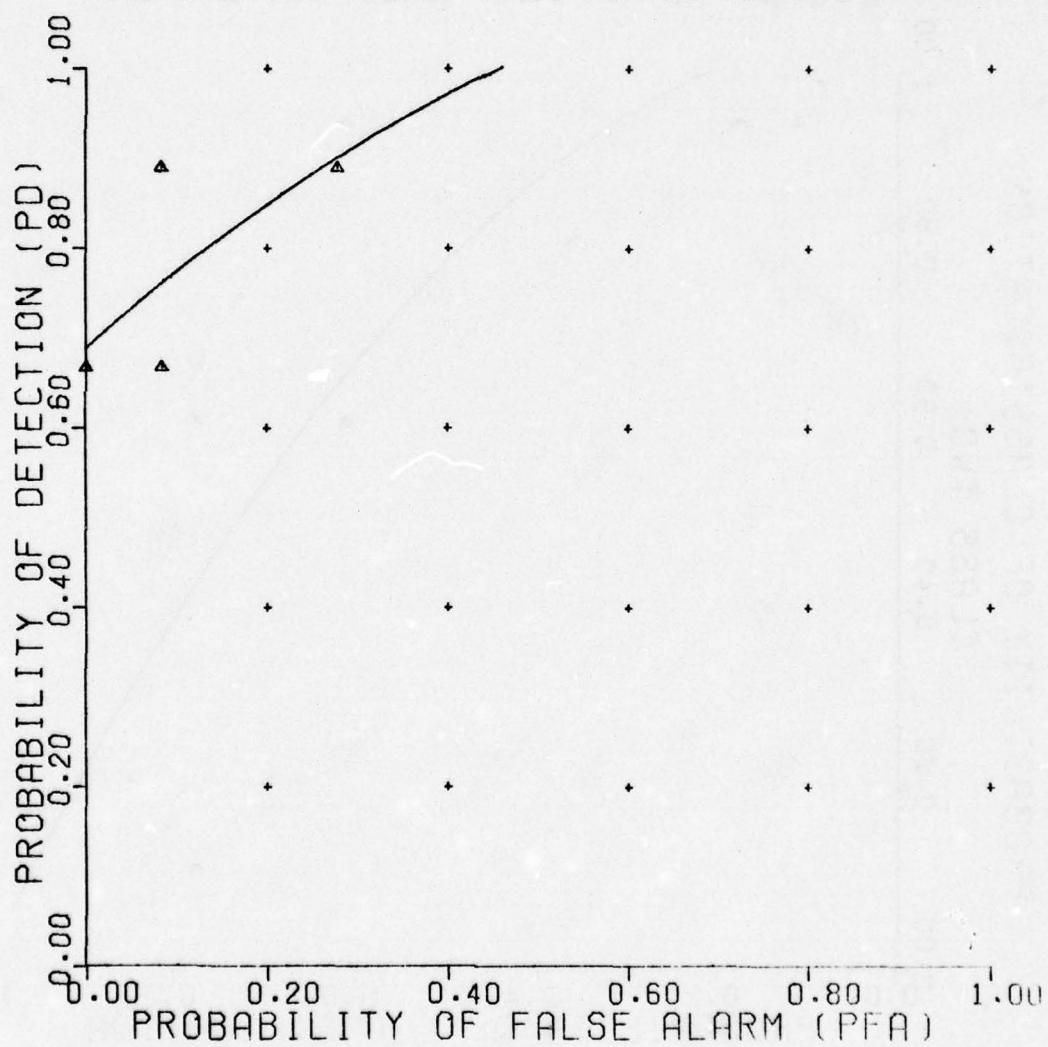


Figure C-44. Nearest neighbor classifier.

UNCLASSIFIED

UNCLASSIFIED

NEAREST NEIGHBOR CLASSIFIER

RAW DATA

NO. NEAREST NEIGHBORS 3

REFERENCE 284

| | |
|----------|---------------------------------|
| NONMINE | ROOT |
| TARGET | TYPE A MINE |
| DEPTH | 3 6 |
| LOCATION | +4 0 -4 |
| MOISTURE | 7 17 12-20 13-16 |

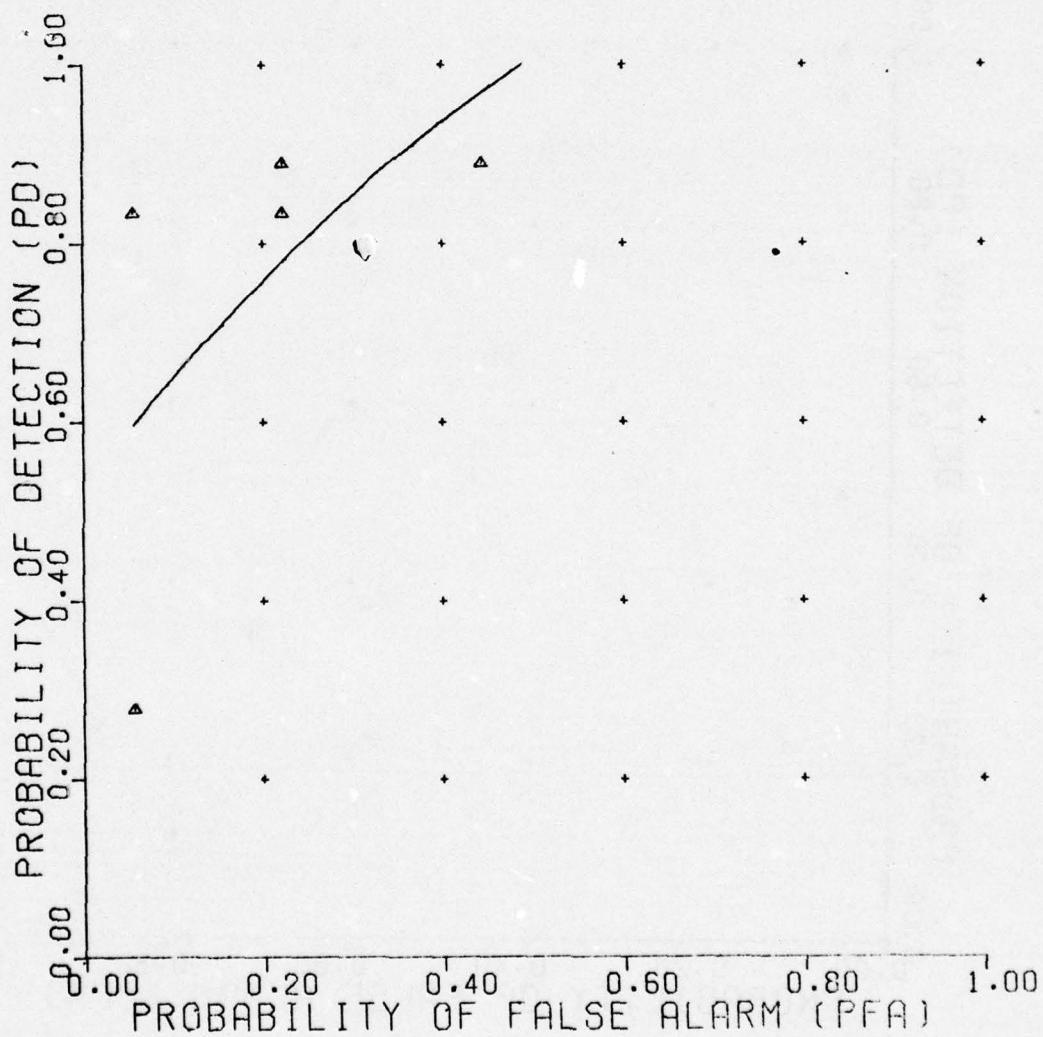


Figure C-45. Nearest neighbor classifier.

UNCLASSIFIED

UNCLASSIFIED

NEAREST NEIGHBOR CLASSIFIER

RAW DATA
NO. NEAREST NEIGHBORS 3
REFERENCE 285

| NONMINE | PLATE |
|----------|---------------------------------|
| TARGET | TYPE A MINE |
| DEPTH | 3 6 |
| LOCATION | +4 0 -4 |
| MOISTURE | 7 17 12-20 13-16 |

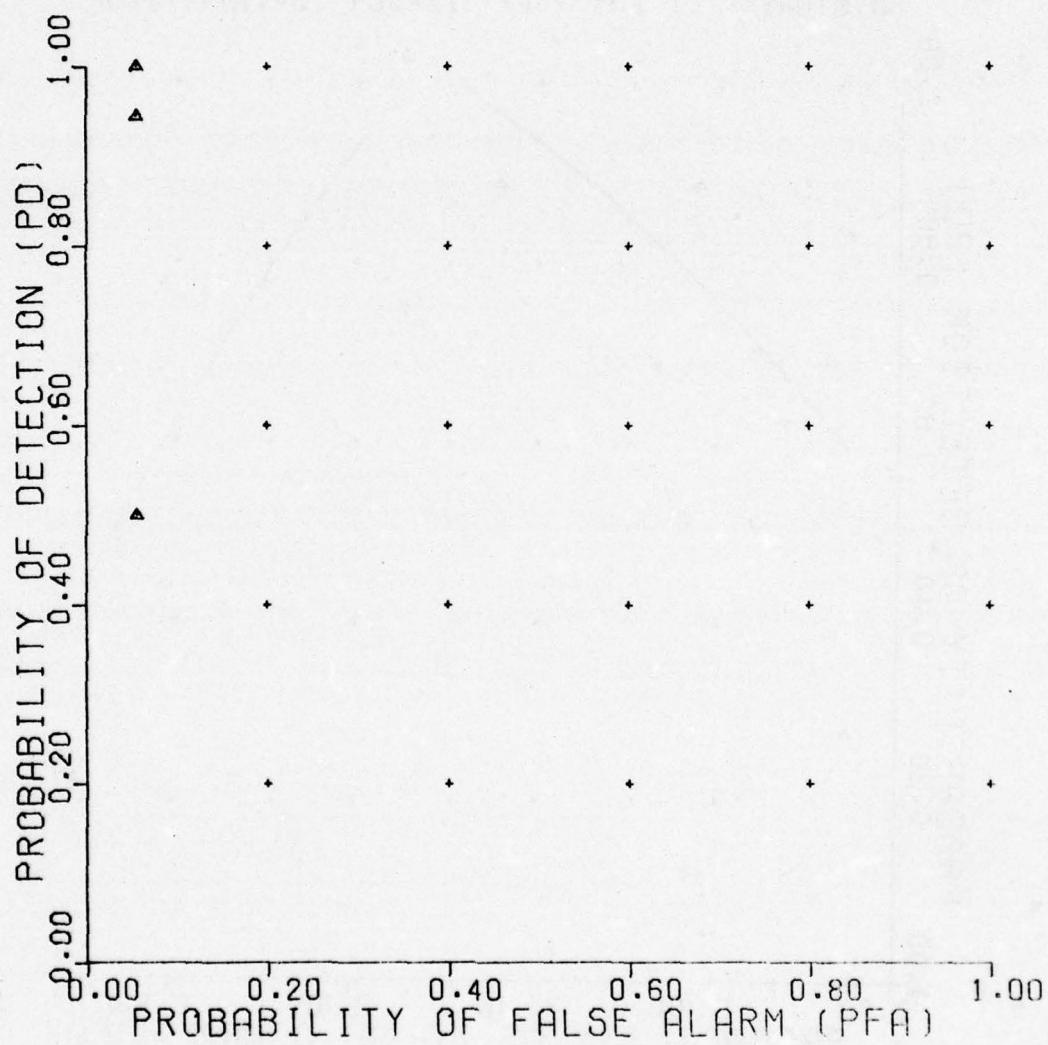


Figure C-46. Nearest neighbor classifier.

UNCLASSIFIED

UNCLASSIFIED

NEAREST NEIGHBOR CLASSIFIER

RAW DATA

NO. NEAREST NEIGHBORS 3

REFERENCE 286

NONMINE BACKGND
TARGET TYPE A MINE

| DEPTH | 3 | 6 |
|----------|-------|-------|
| LOCATION | +4 | 0 |
| MOISTURE | 7 | 17 |
| | 12-20 | 13-16 |

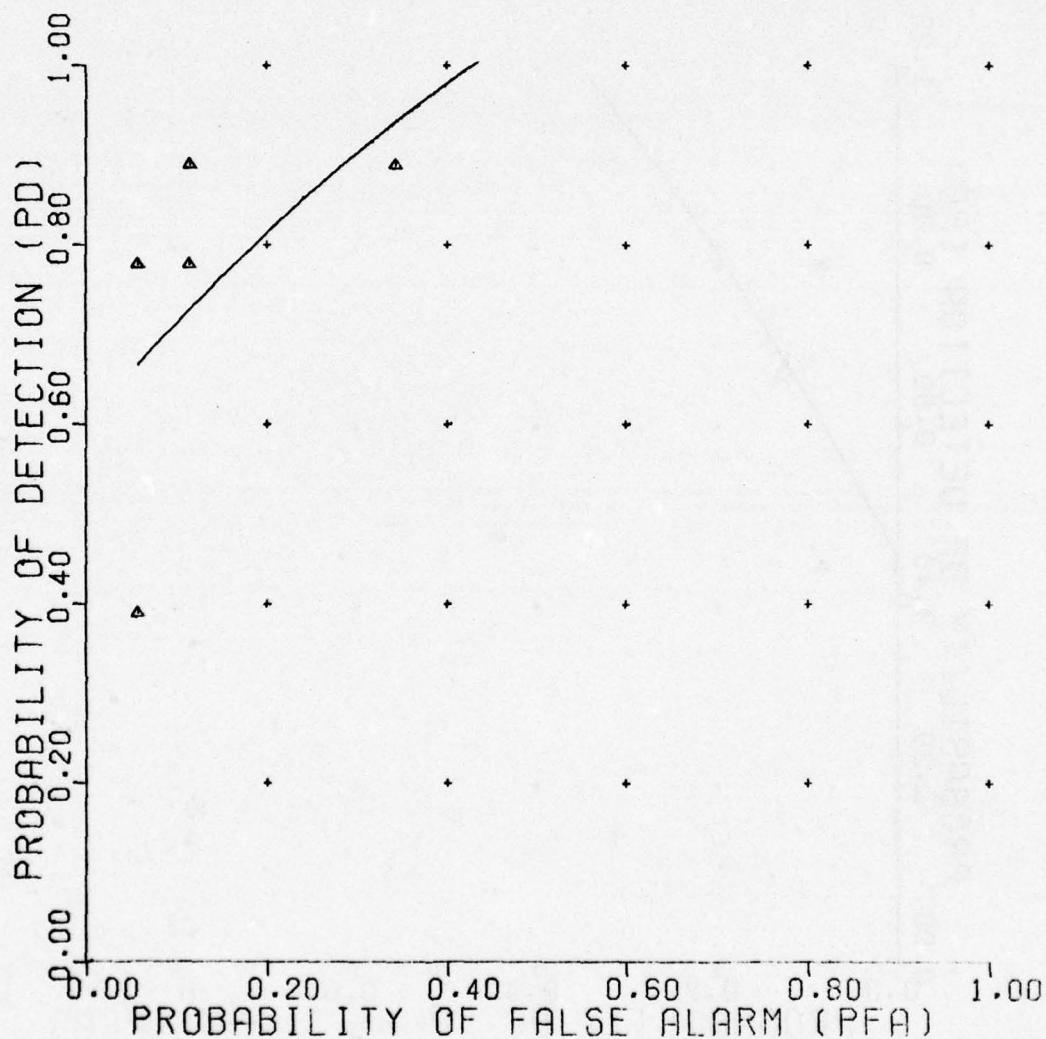


Figure C-47. Nearest neighbor classifier.

UNCLASSIFIED

UNCLASSIFIED

NEAREST NEIGHBOR CLASSIFIER

RAW DATA

NO. NEAREST NEIGHBORS 3

REFERENCE 313

| NONMINE TARGET | PLATE TYPE A MINE | ROCK(1) | ROCK(2) | ROOT |
|-------------------|----------------------|---------|---------|-------|
| DEPTH | | 3 | 6 | |
| LOCATION | | +4 | 0 | -4 |
| MOISTURE | | 7 | 17 | 12-20 |
| | | | | 13-16 |

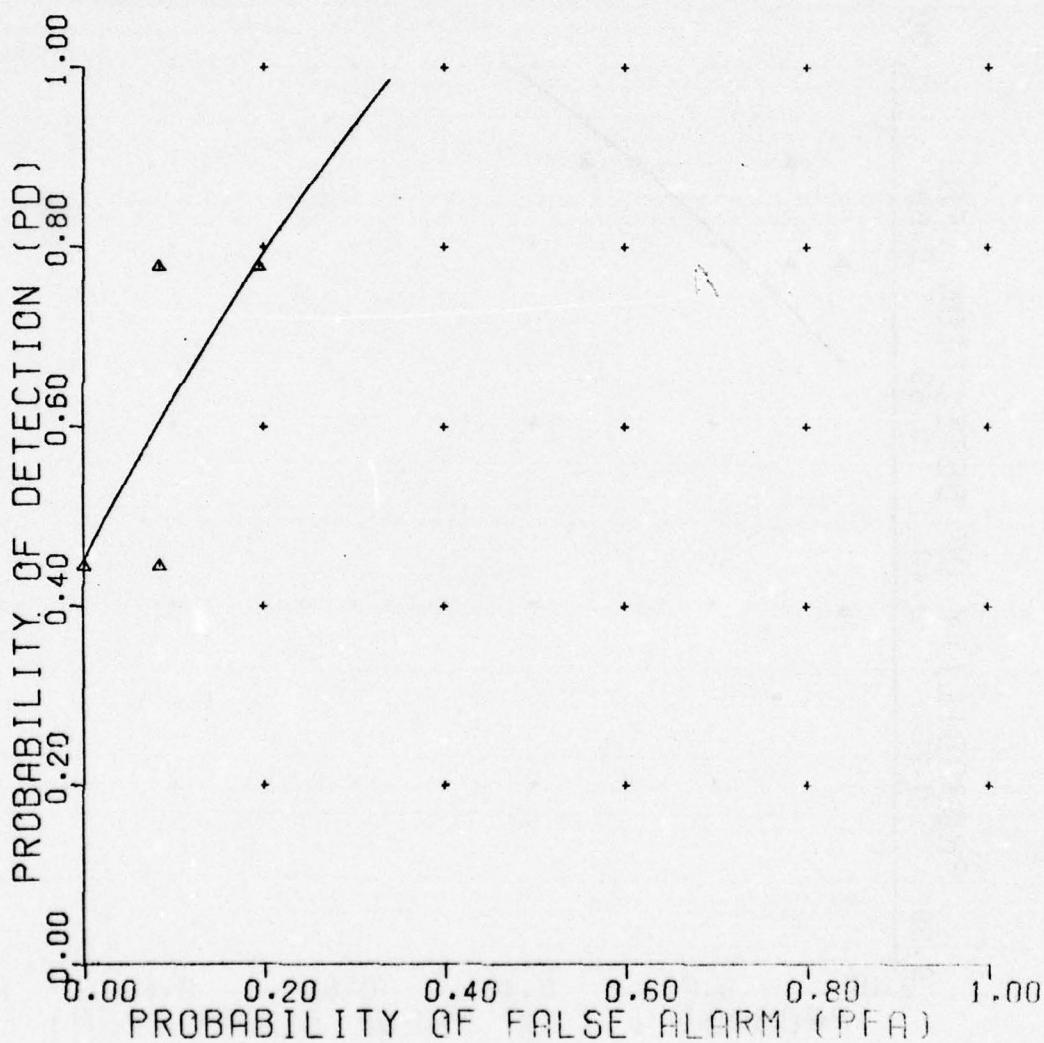


Figure C-48. Nearest neighbor classifier.

UNCLASSIFIED

UNCLASSIFIED

NEAREST NEIGHBOR CLASSIFIER

RAW DATA

NO. NEAREST NEIGHBORS 3

REFERENCE 287

NONMINE ROCK(1) ROCK(2)
TARGET TYPE B MINE

| | | | | |
|----------|----|----|-------|-------|
| DEPTH | 3 | 6 | | |
| LOCATION | +4 | 0 | | |
| MOISTURE | 7 | 17 | 12-20 | 13-16 |

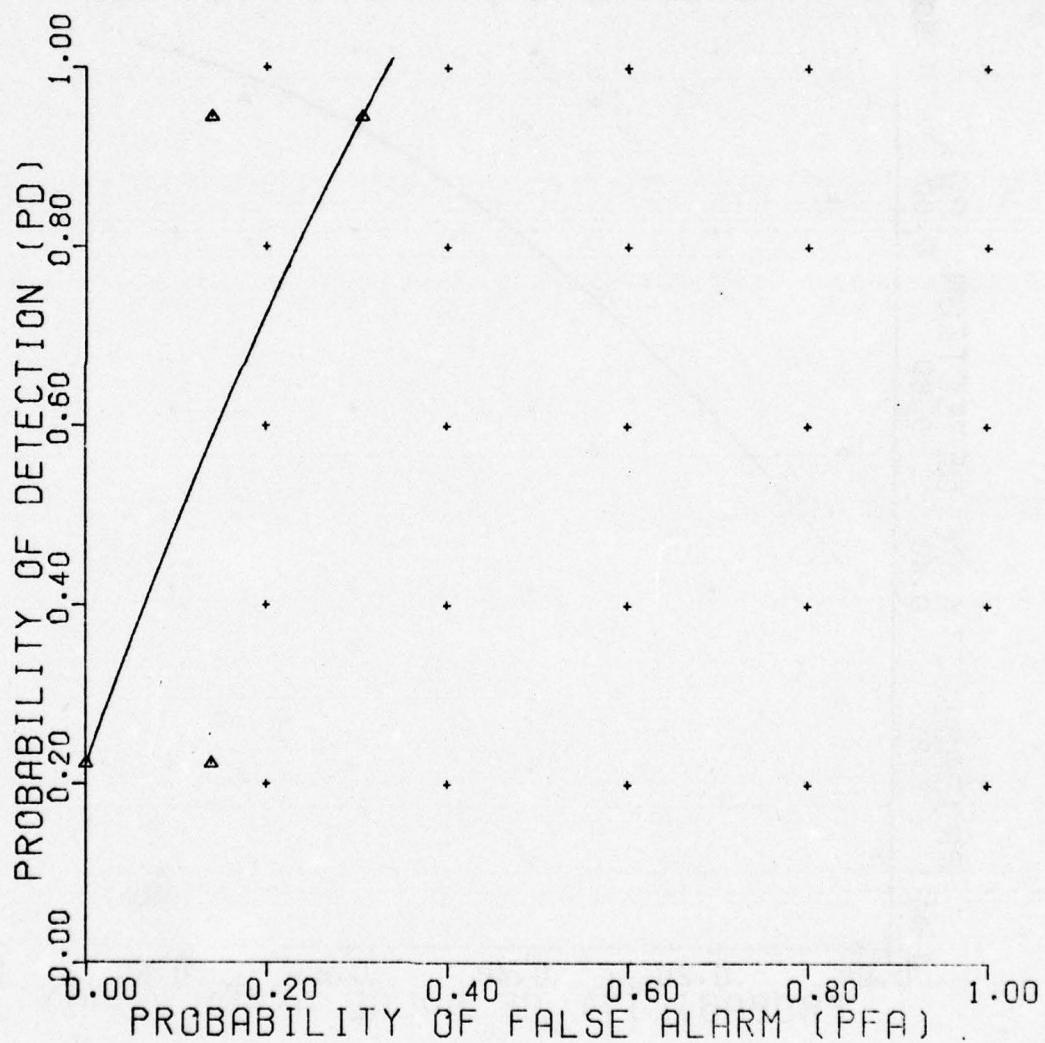


Figure C-49. Nearest neighbor classifier.

UNCLASSIFIED

UNCLASSIFIED

NEAREST NEIGHBOR CLASSIFIER

RAW DATA
NO. NEAREST NEIGHBORS 3
REFERENCE 288

| | |
|----------|---------------------------------|
| NONMINE | ROOT |
| TARGET | TYPE B MINE |
| DEPTH | 3 6 |
| LOCATION | +4 0 -4 |
| MOISTURE | 7 17 12-20 13-16 |

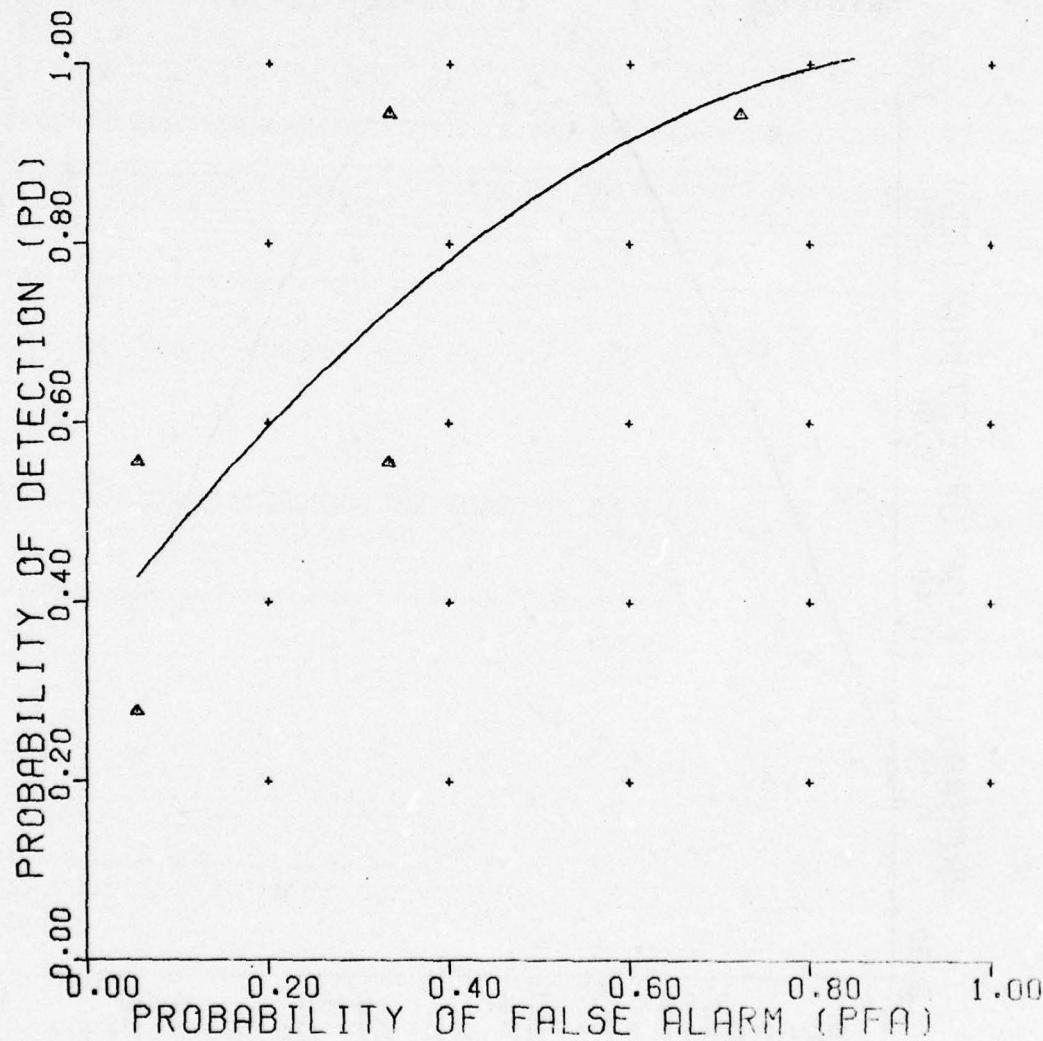


Figure C-50. Nearest neighbor classifier.

UNCLASSIFIED

UNCLASSIFIED

NEAREST NEIGHBOR CLASSIFIER

RAW DATA

NO. NEAREST NEIGHBORS 3

REFERENCE 289

| NONMINE TARGET | PLATE TYPE B MINE |
|-------------------|----------------------|-------------------|----------------------|-------------------|----------------------|-------------------|----------------------|
| DEPTH | 3 | 6 | 8 | 9 | 6 | 8 | 9 |
| LOCATION | +4 | -0 | 0 | -4 | +4 | -0 | 0 |
| MOISTURE | 7 | 17 | 12-20 | 13-16 | 7 | 17 | 12-20 |

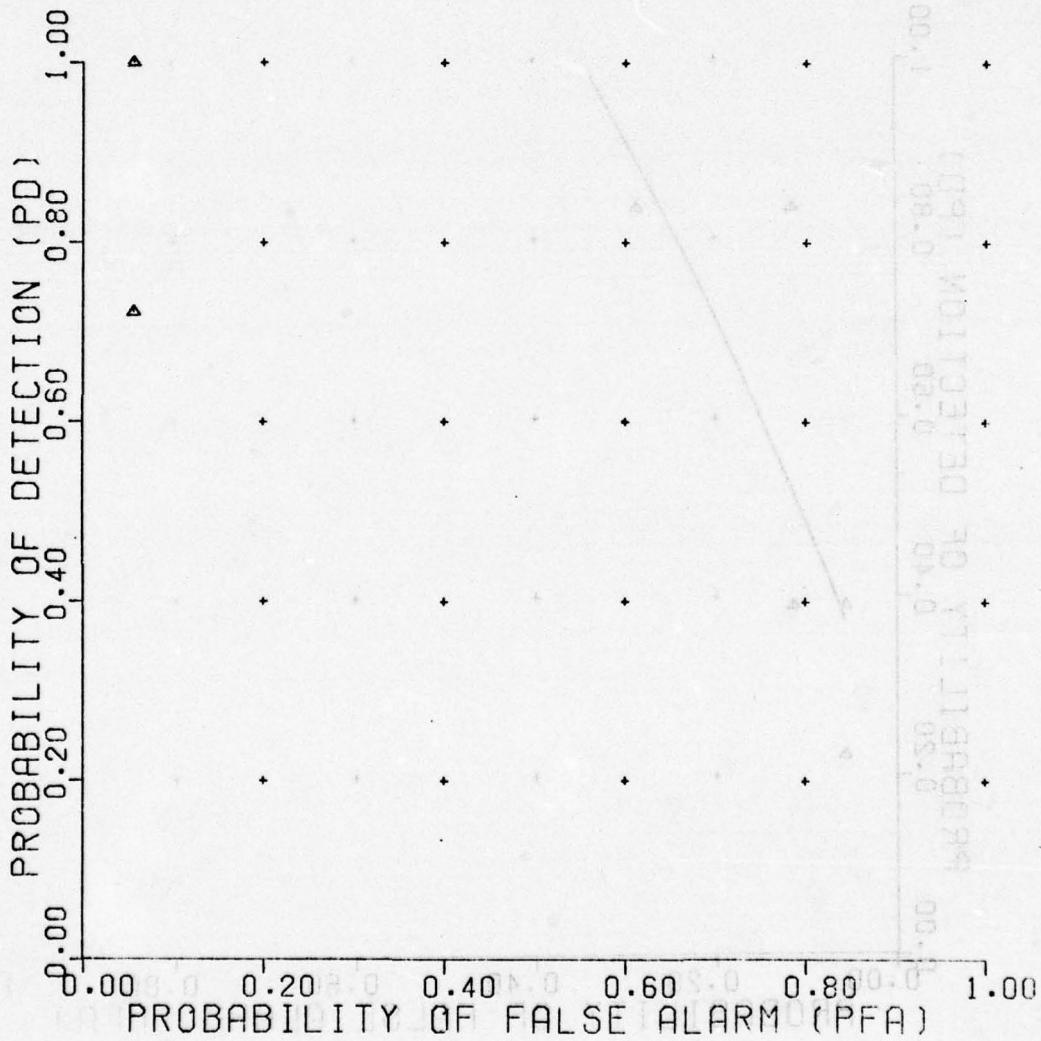


Figure C-51. Nearest neighbor classifier.

UNCLASSIFIED

UNCLASSIFIED

NEAREST NEIGHBOR CLASSIFIER

RAW DATA
NO. NEAREST NEIGHBORS 3
REFERENCE 290

| | |
|----------|---------------------------------|
| NONMINE | BACKGND |
| TARGET | TYPE B MINE |
| DEPTH | 3 6 |
| LOCATION | +4 0 -4 |
| MOISTURE | 7 17 12-20 13-16 |

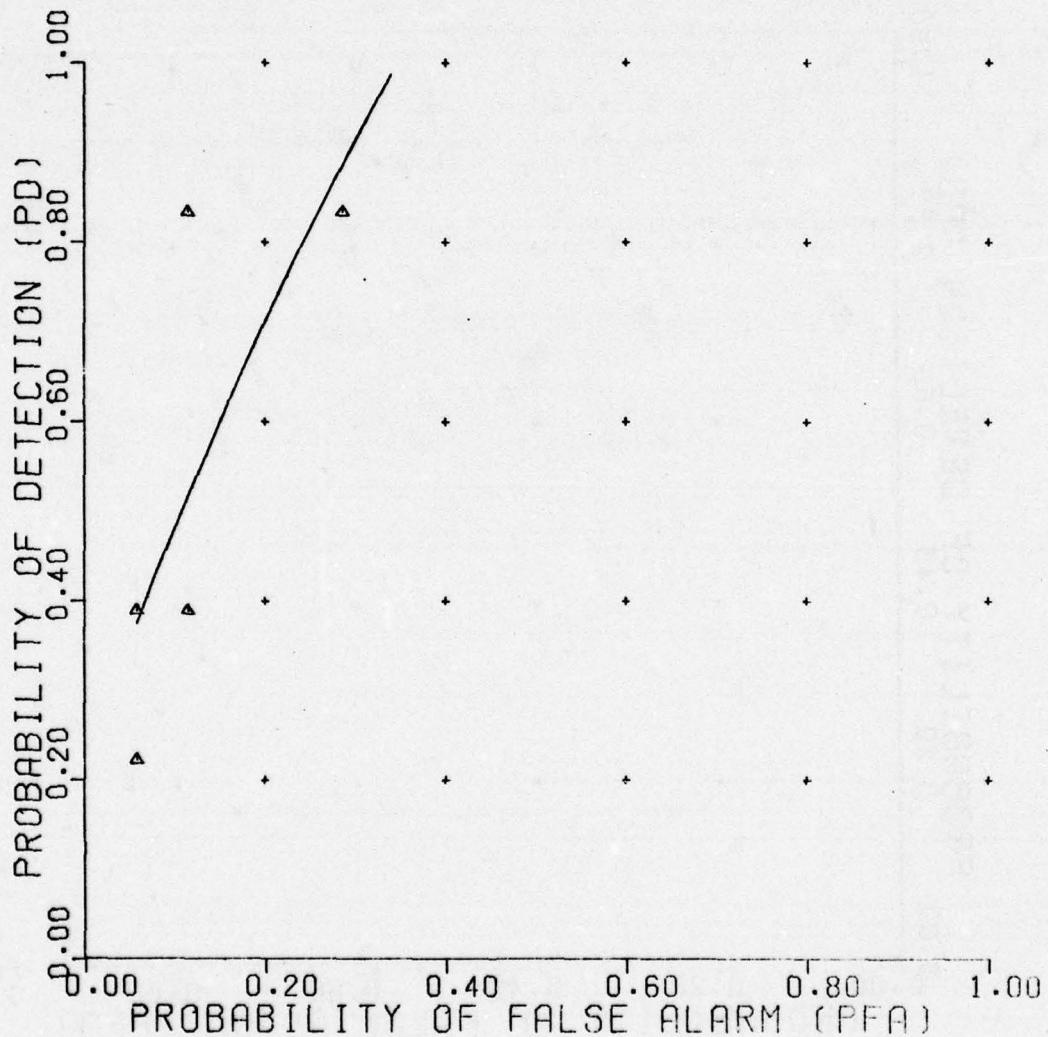


Figure C-52. Nearest neighbor classifier.

UNCLASSIFIED

UNCLASSIFIED

NEAREST NEIGHBOR CLASSIFIER

RAW DATA

NO. NEAREST NEIGHBORS 3

REFERENCE 314

| NONMINE TARGET | PLATE | ROCK(1) | ROCK(2) | ROOT |
|-------------------|-------|---------|---------|-------|
| TYPE B MINE | | | | |
| DEPTH | 3 | 6 | | |
| LOCATION | +4 | 0 | -4 | |
| MOISTURE | 7 | 17 | 12-20 | 13-16 |

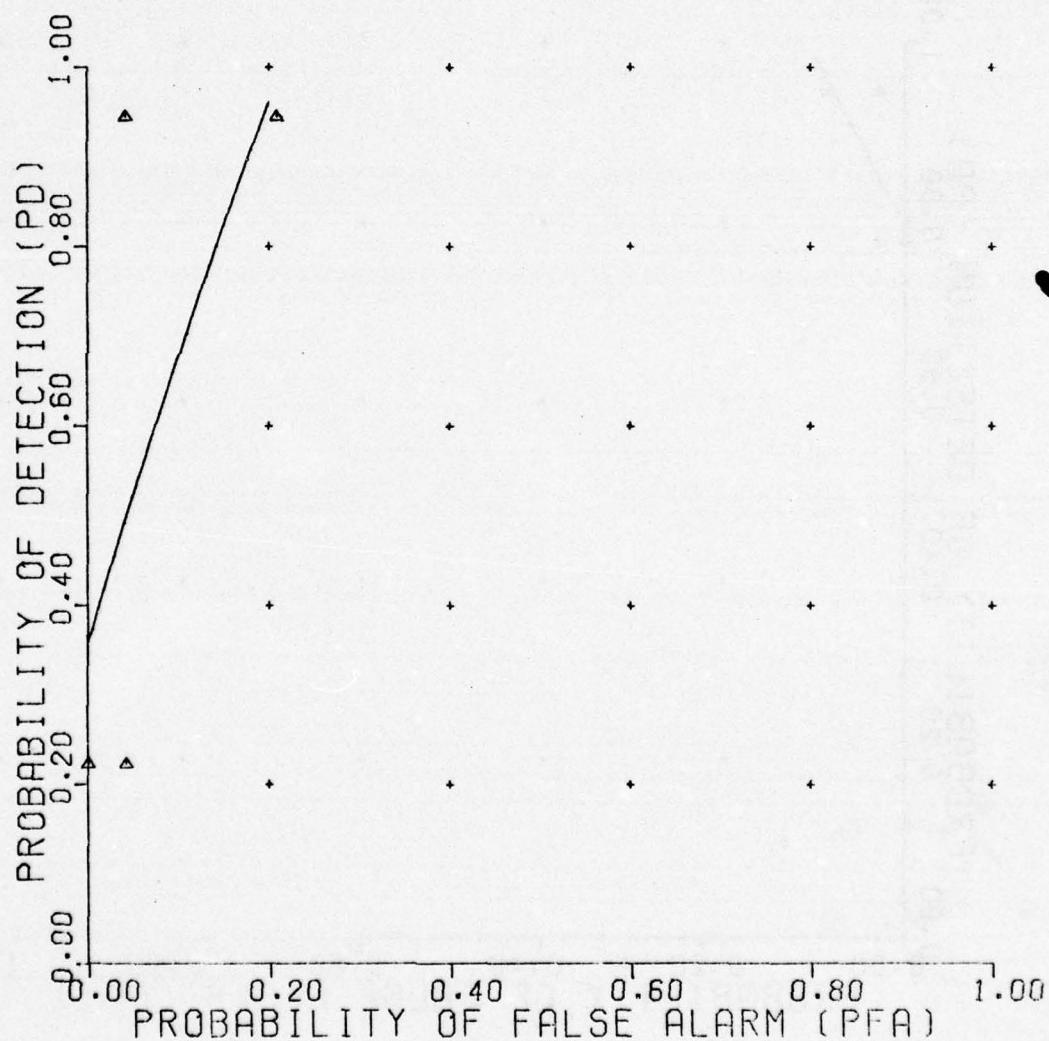


Figure C-53. Nearest neighbor classifier.

UNCLASSIFIED

UNCLASSIFIED

NEAREST NEIGHBOR CLASSIFIER

RAW DATA
NO. NEAREST NEIGHBORS 3
REFERENCE 291

NONMINE ROCK(1) ROCK(2)

TARGET TYPE C MINE

| | | | | |
|----------|----|----|-------|-------|
| DEPTH | 3 | 6 | | |
| LOCATION | +4 | 0 | -4 | |
| MOISTURE | 7 | 17 | 12-20 | 13-16 |

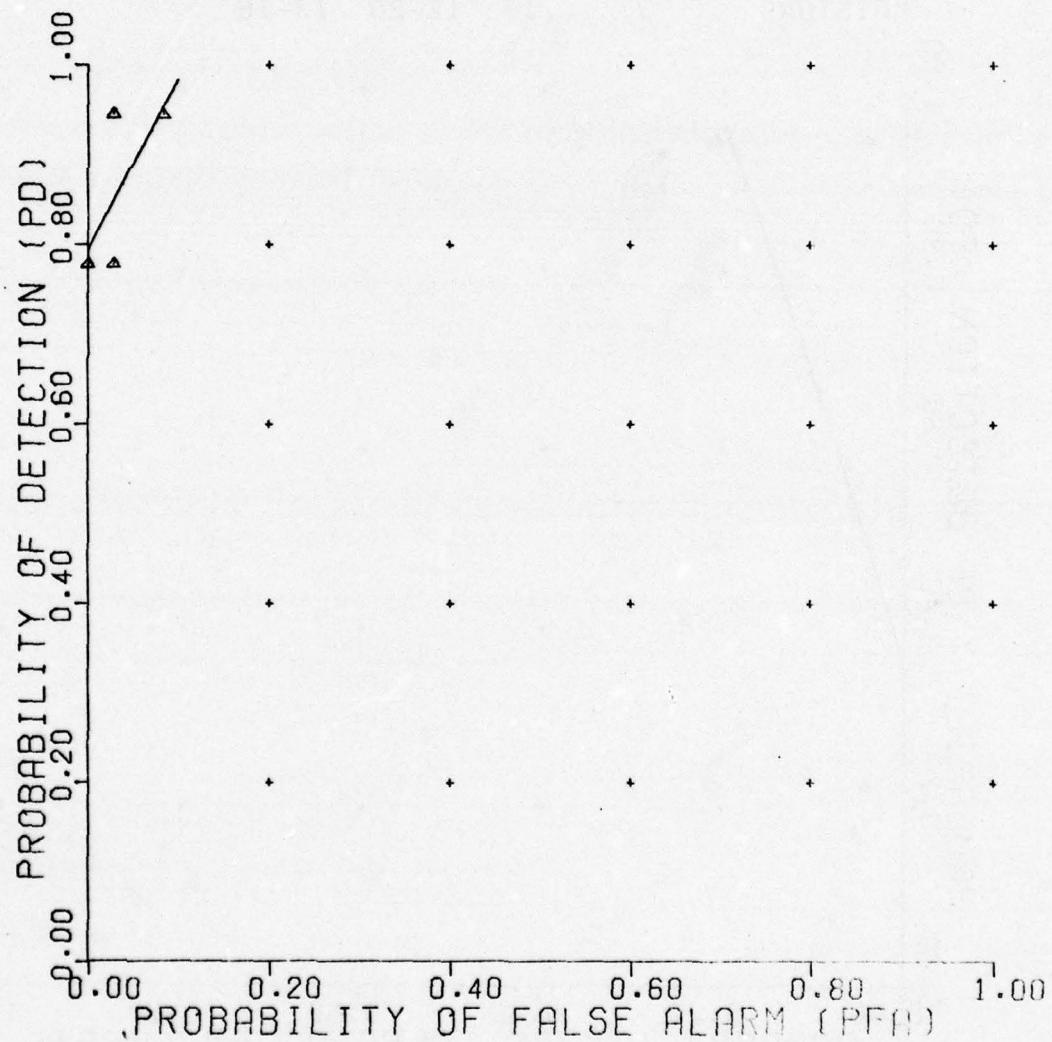


Figure C-54. Nearest neighbor classifier.

UNCLASSIFIED

UNCLASSIFIED

NEAREST NEIGHBOR CLASSIFIER

RAW DATA

NO. NEAREST NEIGHBORS 3

REFERENCE 292

| NONMINE TARGET | ROOT TYPE C MINE |
|-------------------|---------------------------------|
| DEPTH | 3 6 |
| LOCATION | +4 0 -4 |
| MOISTURE | 7 17 12-20 13-16 |

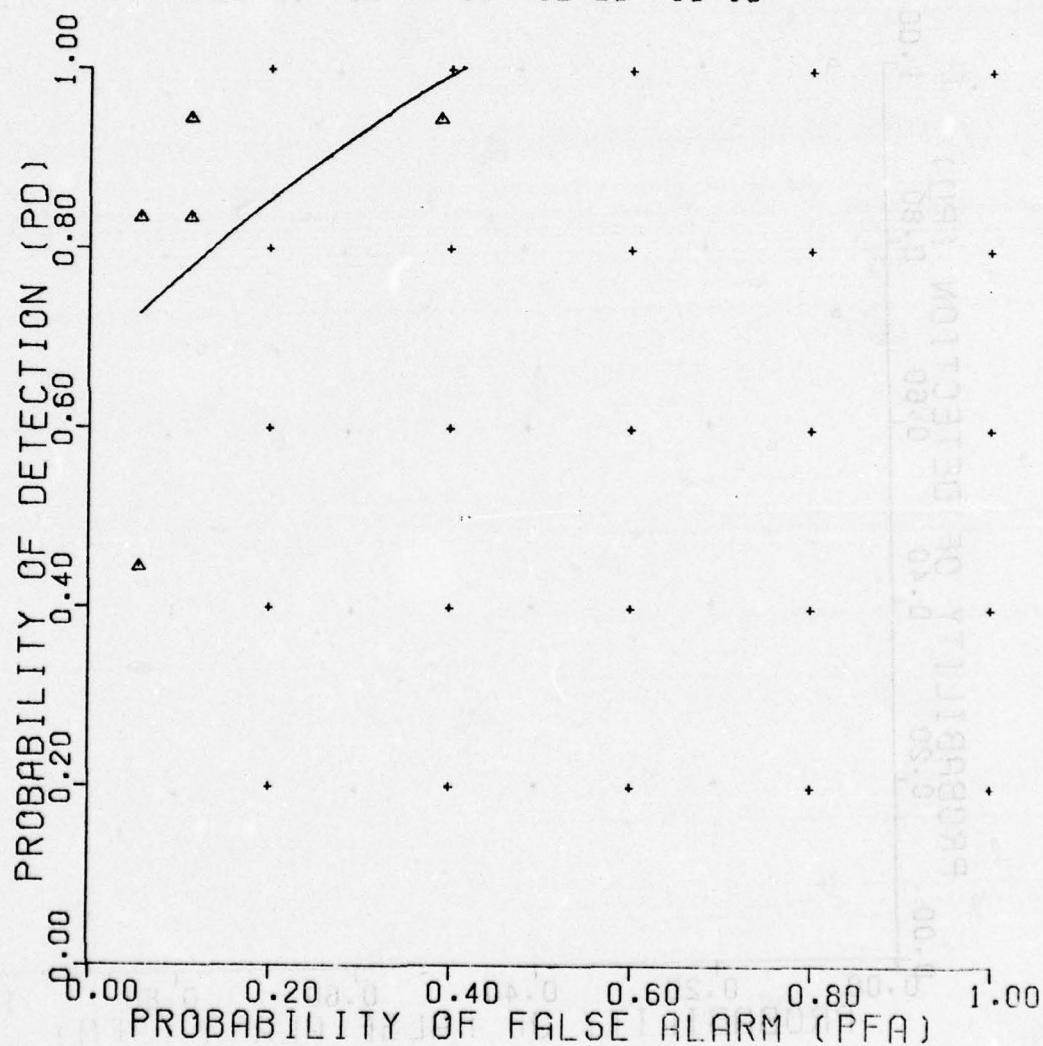


Figure C-55. Nearest neighbor classifier.

UNCLASSIFIED

UNCLASSIFIED

NEAREST NEIGHBOR CLASSIFIER

RAW DATA

NO. NEAREST NEIGHBORS 3

REFERENCE 293

| NONMINE TARGET | PLATE |
|-------------------|---------------------------------|
| | TYPE C MINE |
| DEPTH | 3 6 |
| LOCATION | +4 0 -4 |
| MOISTURE | 7 17 12-20 13-16 |

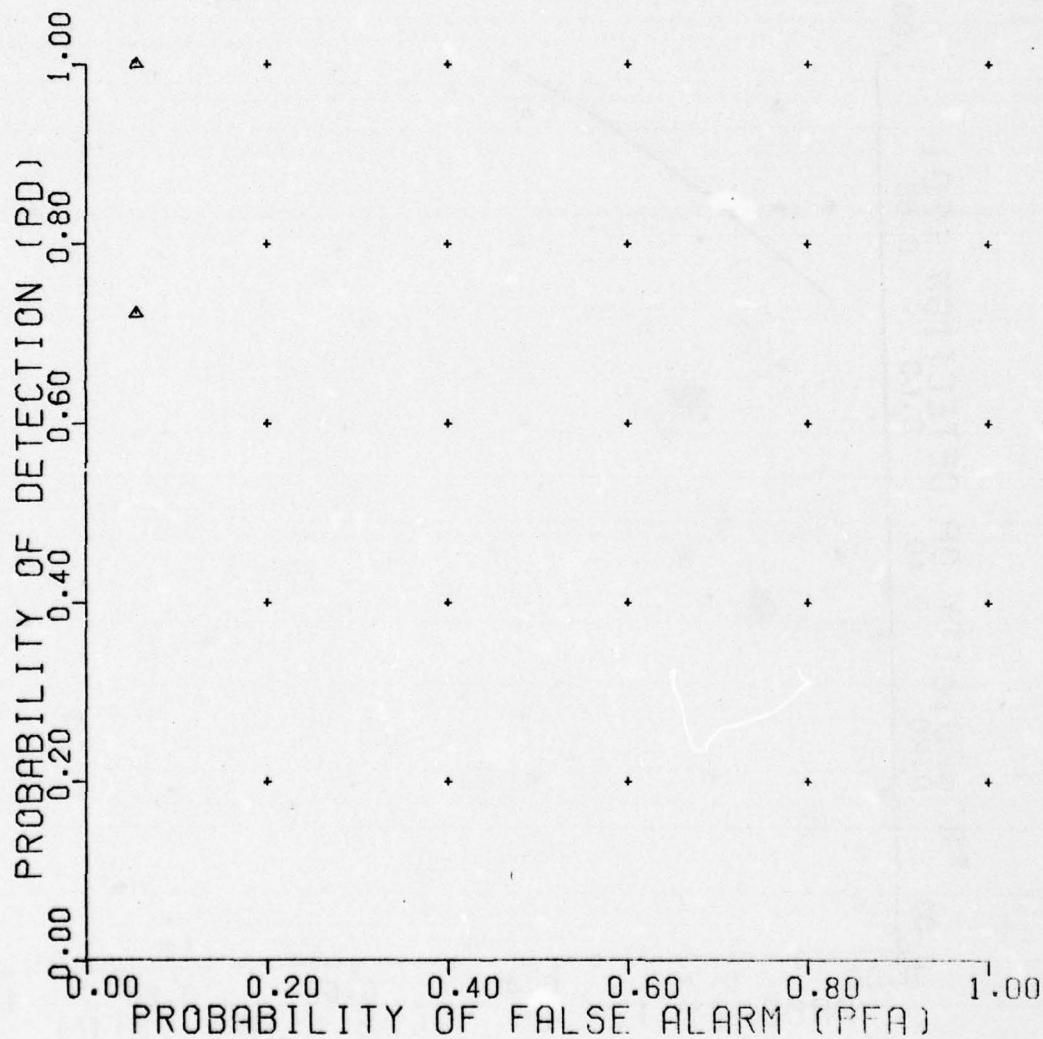


Figure C-56. Nearest neighbor classifier.

UNCLASSIFIED

UNCLASSIFIED

NEAREST NEIGHBOR CLASSIFIER

RAW DATA

NO. NEAREST NEIGHBORS 3

REFERENCE 294

NONMINE BACKGND
TARGET TYPE C MINE

| | | | | |
|----------|----|----|-------|-------|
| DEPTH | 3 | 6 | | |
| LOCATION | +4 | 0 | -4 | |
| MOISTURE | 7 | 17 | 12-20 | 13-16 |

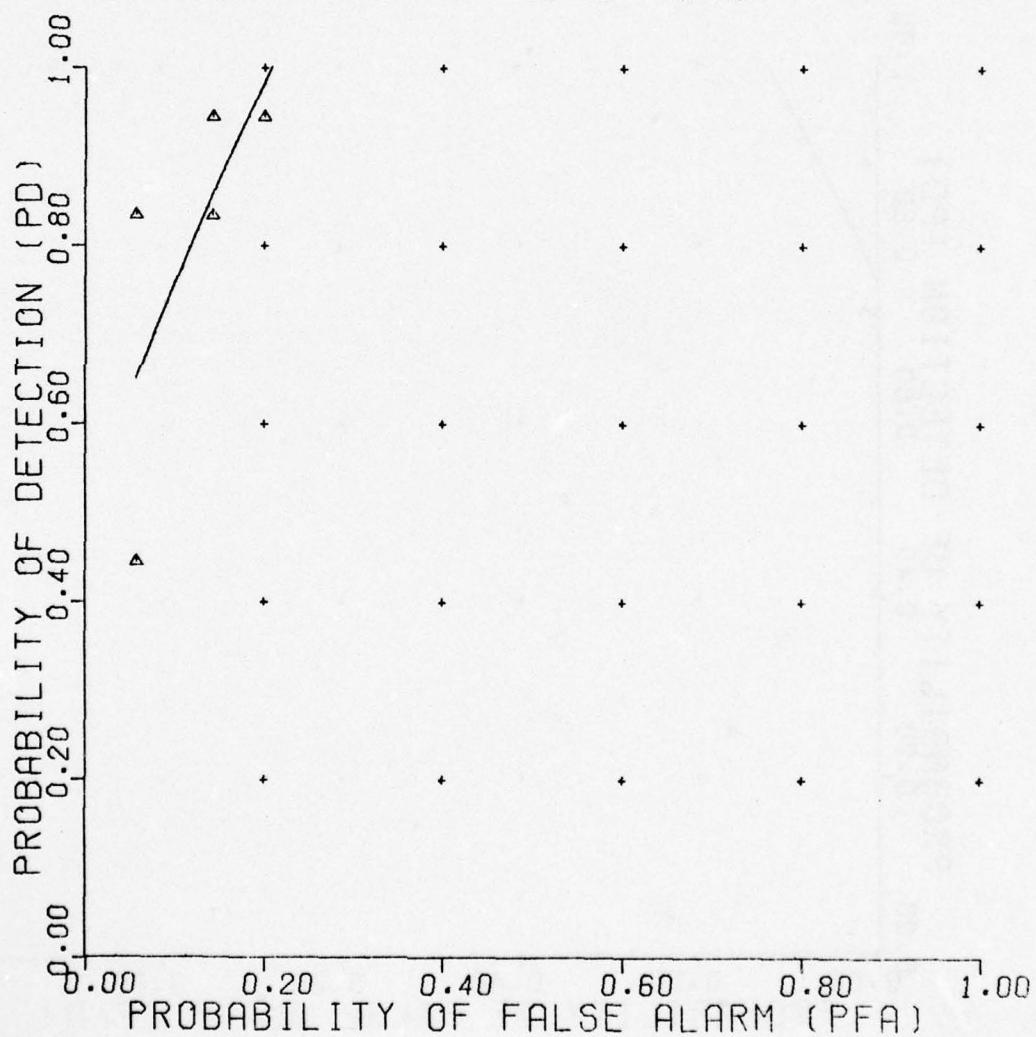


Figure C-57. Nearest neighbor classifier.

UNCLASSIFIED

UNCLASSIFIED

NEAREST NEIGHBOR CLASSIFIER

RAW DATA

NO. NEAREST NEIGHBORS 3

REFERENCE 315

| NONMINE TARGET | PLATE TYPE C MINE | ROCK(1) | ROCK(2) | ROOT |
|-------------------|----------------------|---------|---------|-------|
| DEPTH | | 3 | 6 | |
| LOCATION | | +4 | 0 | -4 |
| MOISTURE | | 7 | 17 | 12-20 |
| | | | | 13-16 |

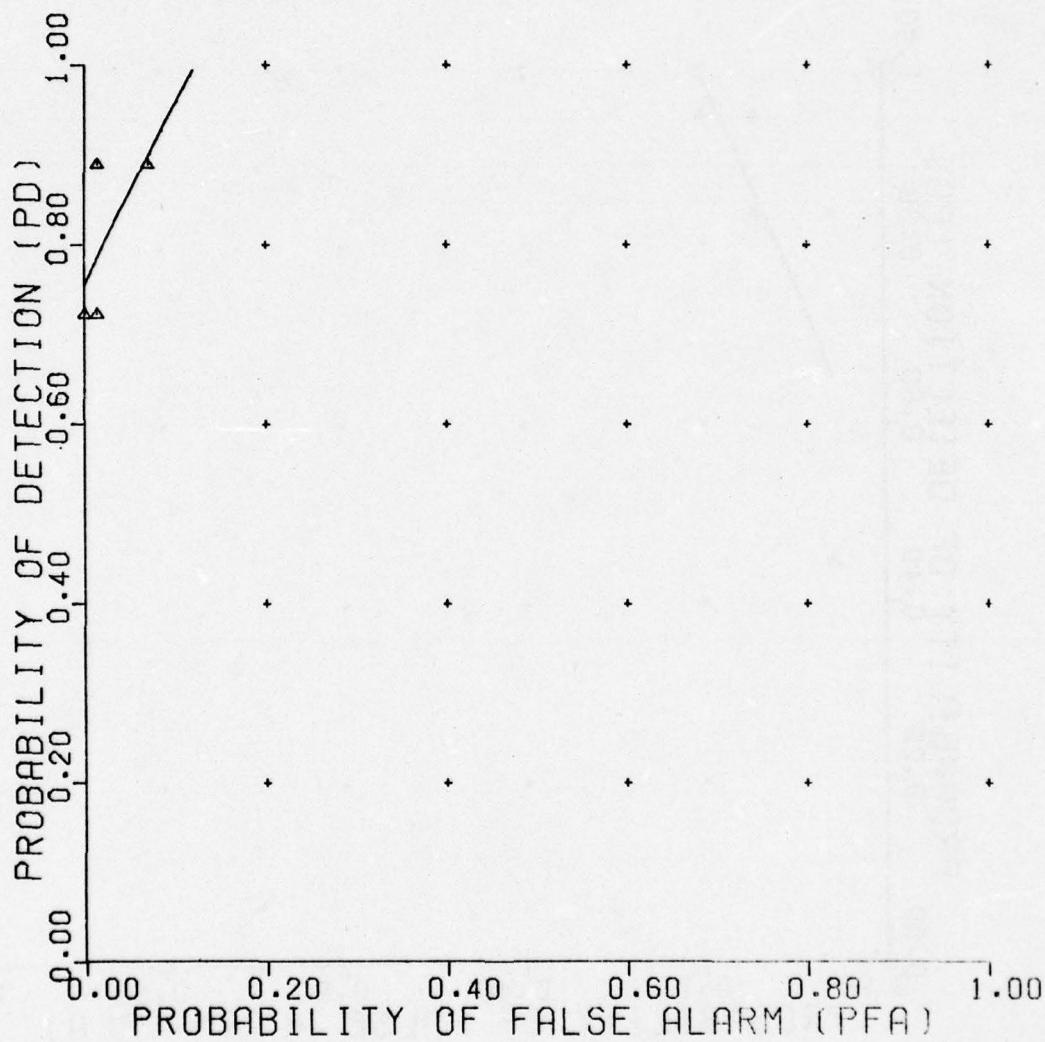


Figure C-58. Nearest neighbor classifier.

UNCLASSIFIED

UNCLASSIFIED

NEAREST NEIGHBOR CLASSIFIER

RAW DATA

NO. NEAREST NEIGHBORS 3

REFERENCE 295

| NONMINE TARGET | ROCK(1) | ROCK(2) | TYPE C MINE | TYPE A MINE | TYPE B MINE |
|-------------------|---------|---------|-------------|-------------|-------------|
| DEPTH | 3 | 6 | | | |
| LOCATION | +4 | 0 | -4 | | |
| MOISTURE | 7 | 17 | 12-20 | 13-16 | |

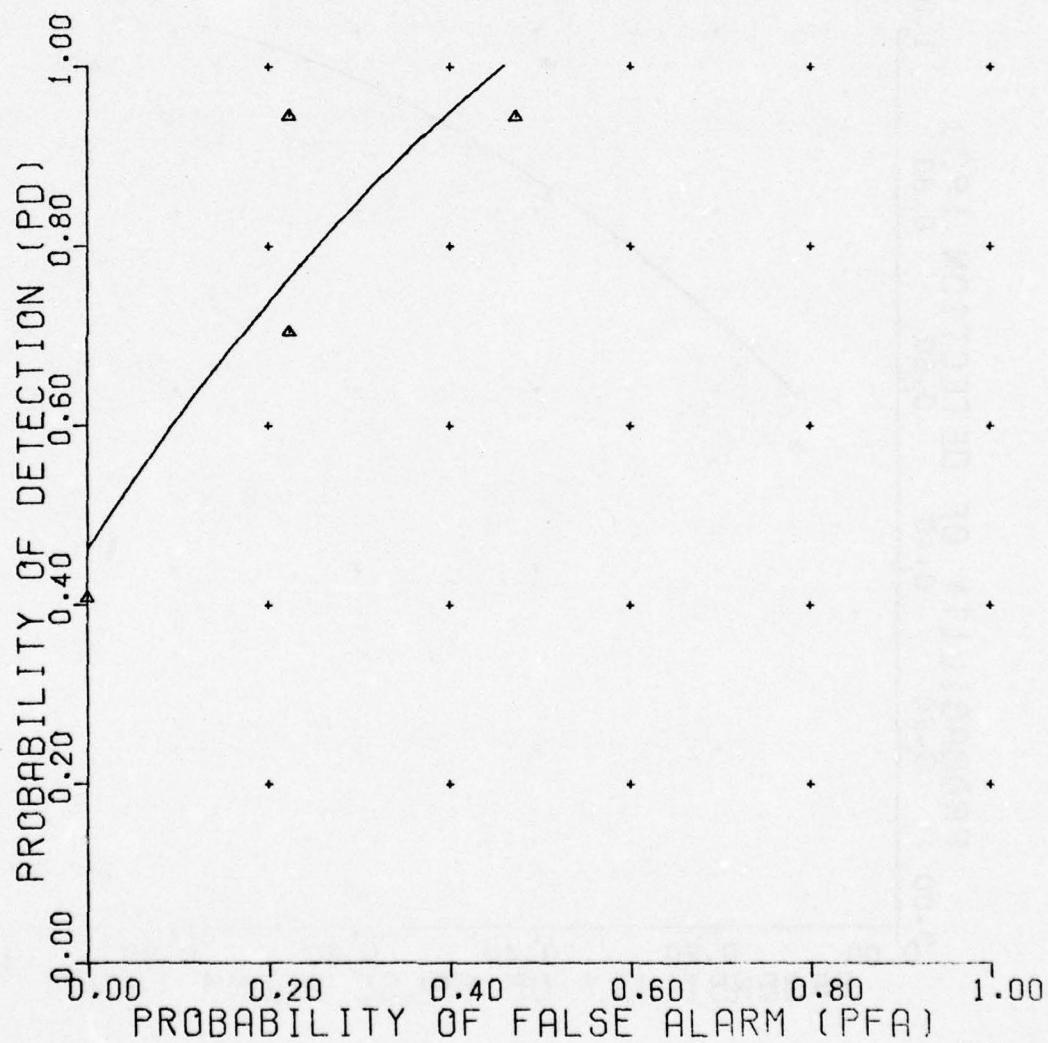


Figure C-59. Nearest neighbor classifier.

UNCLASSIFIED

UNCLASSIFIED

NEAREST NEIGHBOR CLASSIFIER

RAW DATA

NO. NEAREST NEIGHBORS 3

REFERENCE 296

| NONMINE TARGET | ROOT TYPE C MINE | TYPE A MINE | TYPE B MINE |
|-------------------|---------------------|-------------|-------------|
| DEPTH | 3 | 6 | |
| LOCATION | +4 | 0 | -4 |
| MOISTURE | 7 | 17 | 12-20 |

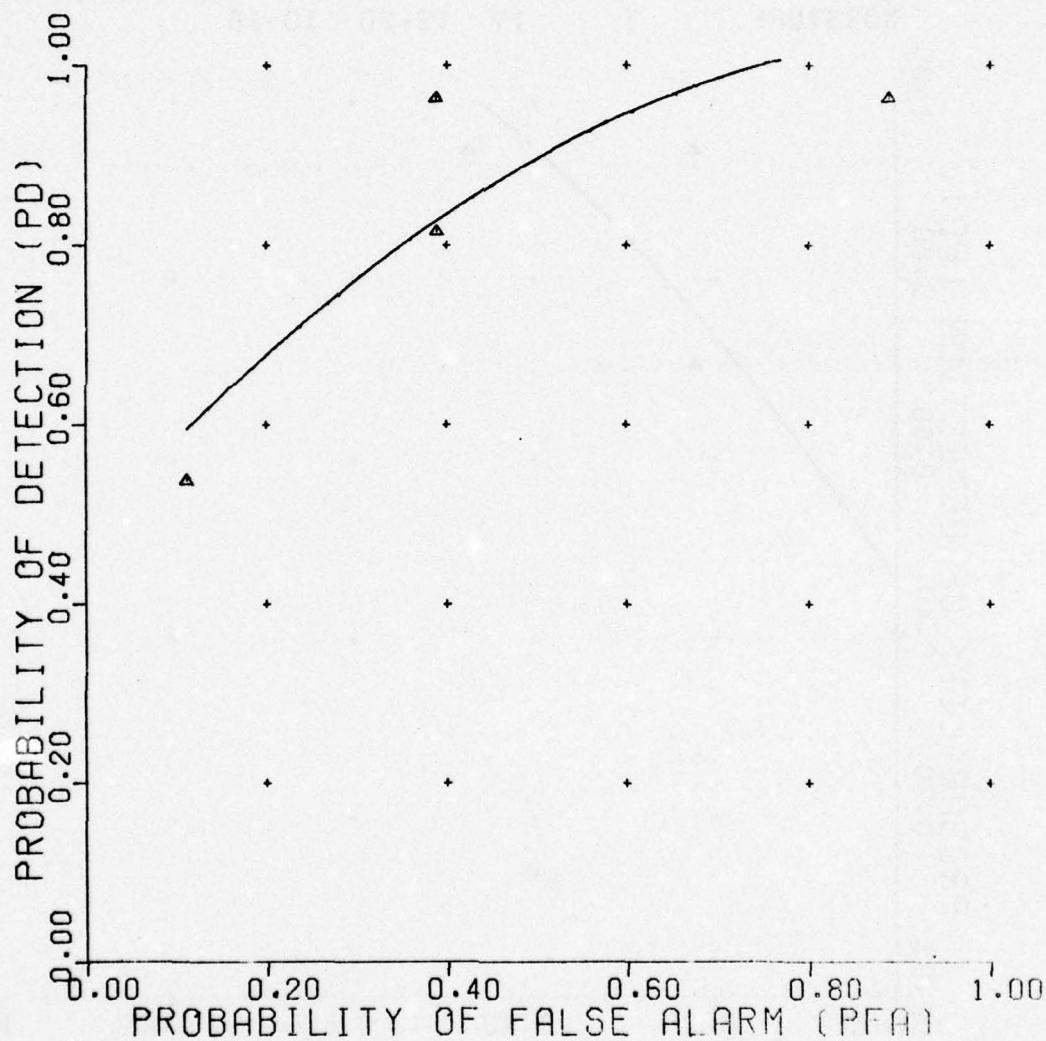


Figure C-60. Nearest neighbor classifier.

UNCLASSIFIED

UNCLASSIFIED

NEAREST NEIGHBOR CLASSIFIER

RAW DATA

NO. NEAREST NEIGHBORS 3

REFERENCE 297

| NONMINE TARGET | PLATE | TYPE C MINE | TYPE A MINE | TYPE B MINE |
|-------------------|-------|-------------|-------------|-------------|
| DEPTH | | 3 | 6 | |
| LOCATION | | +4 | 0 | -4 |
| MOISTURE | | 7 | 17 | 12-20 |
| | | | | 13-16 |

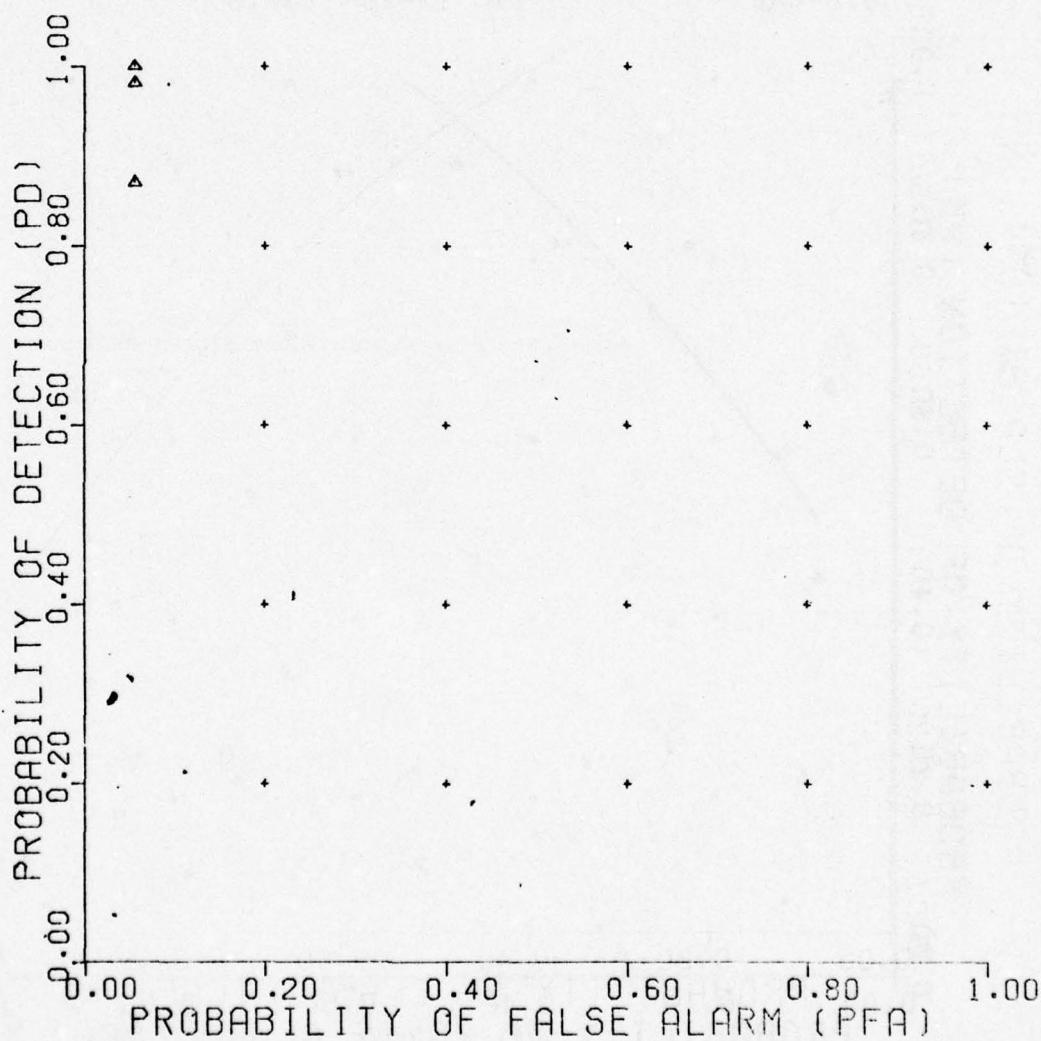


Figure C-61. Nearest neighbor classifier.

UNCLASSIFIED

UNCLASSIFIED

NEAREST NEIGHBOR CLASSIFIER

RAW DATA

NO. NEAREST NEIGHBORS 3

REFERENCE 298

| NONMINE BACKGND | TARGET | TYPE C MINE | TYPE A MINE | TYPE B MINE |
|-----------------|--------|-------------|-------------|-------------|
| DEPTH | | 3 | 6 | |
| LOCATION | | +4 | 0 | -4 |
| MOISTURE | | 7 | 17 | 12-20 |
| | | | | 13-16 |

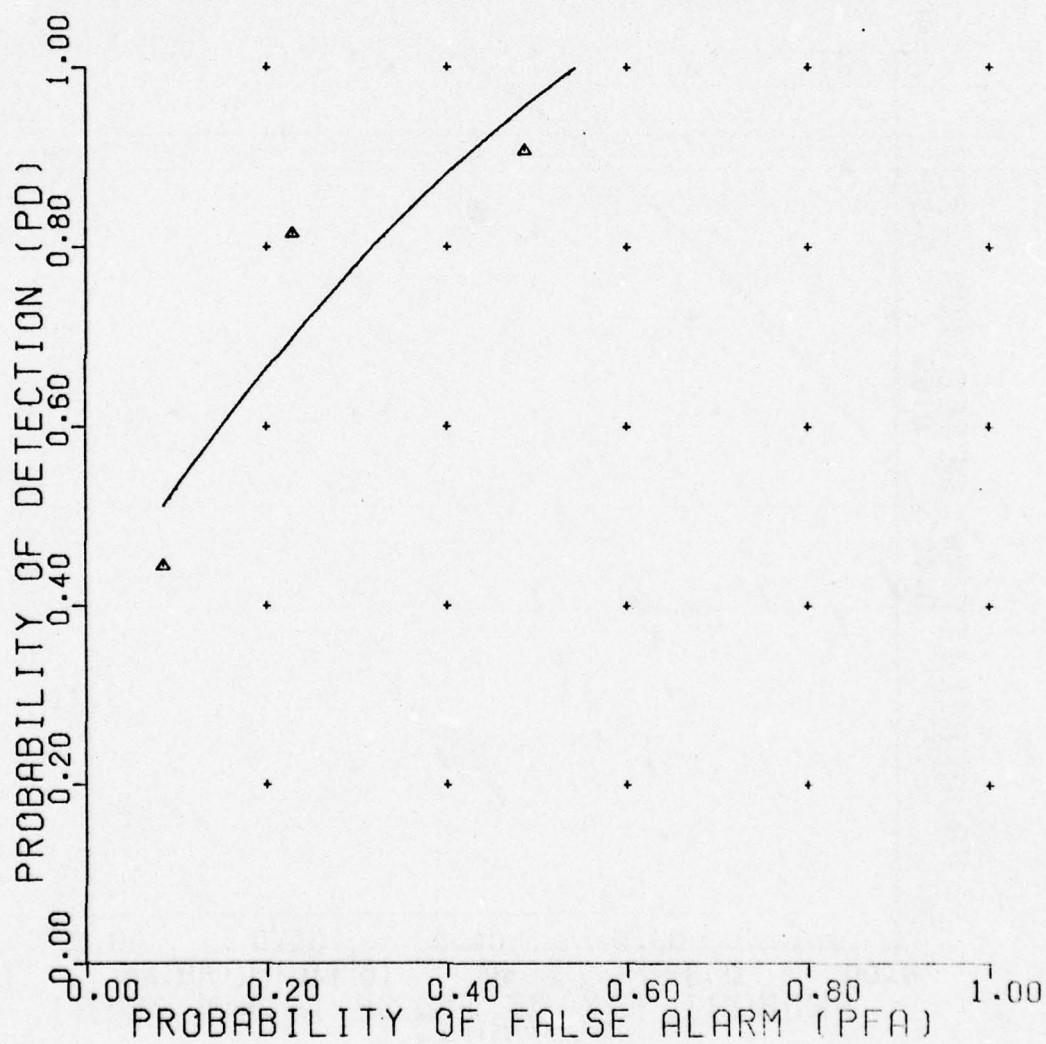


Figure C-62. Nearest neighbor classifier.

UNCLASSIFIED

UNCLASSIFIED

NEAREST NEIGHBOR CLASSIFIER

RAW DATA

NO. NEAREST NEIGHBORS 3

REFERENCE 316

| NONMINE TARGET | PLATE TYPE C MINE | ROCK(1) TYPE A MINE | ROCK(2) TYPE B MINE | ROOT |
|-------------------|----------------------|------------------------|------------------------|-------|
| DEPTH | 3 | 6 | | |
| LOCATION | +4 | 0 | -4 | |
| MOISTURE | 7 | 17 | 12-20 | 13-16 |

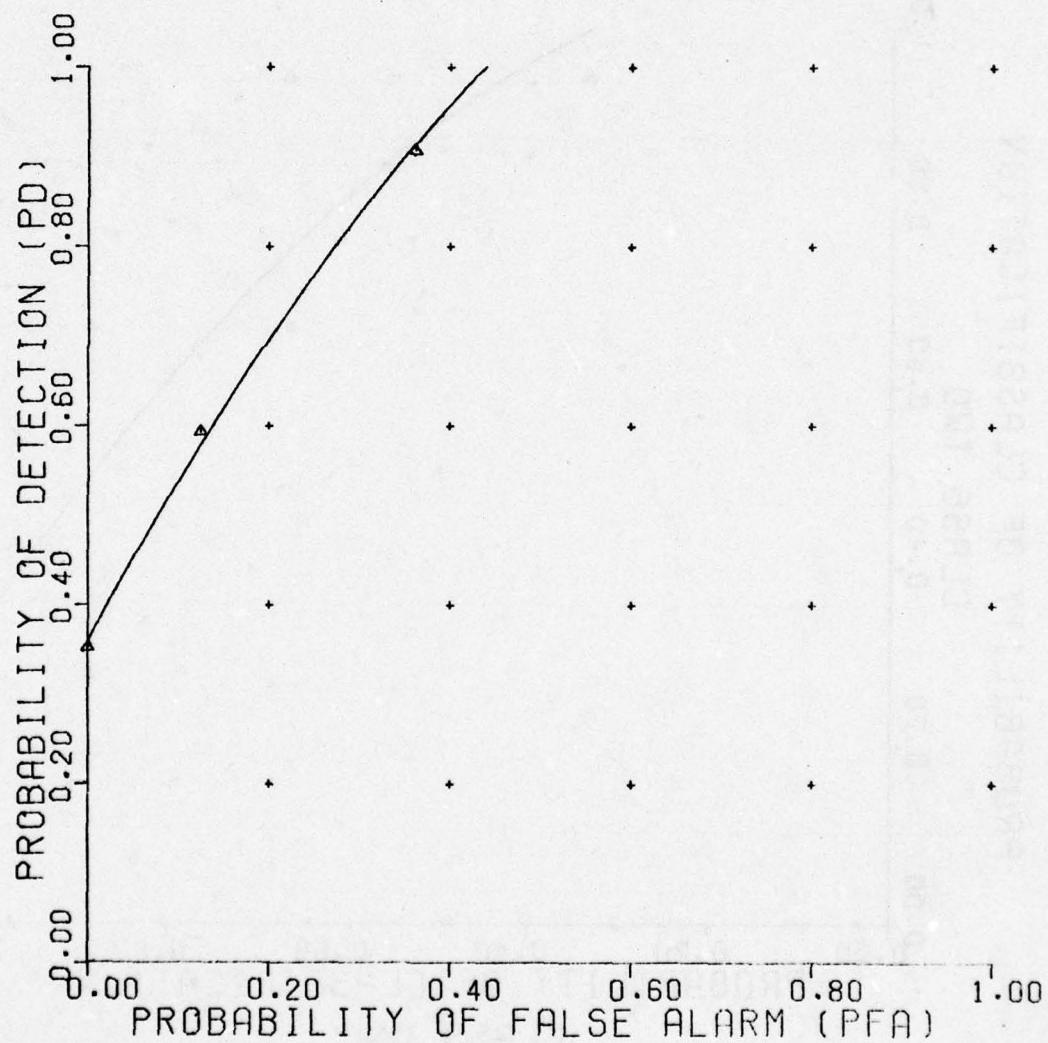


Figure C-63. Nearest neighbor classifier.

UNCLASSIFIED

UNCLASSIFIED

NEAREST NEIGHBOR CLASSIFIER

RAW DATA
VERSION 3
REFERENCE 280

TARGET2 TYPE B MINE

TARGET1 TYPE A MINE

| DEPTH | 3 | 6 |
|----------|----|----|
| LOCATION | +4 | 0 |
| MOISTURE | 7 | 17 |

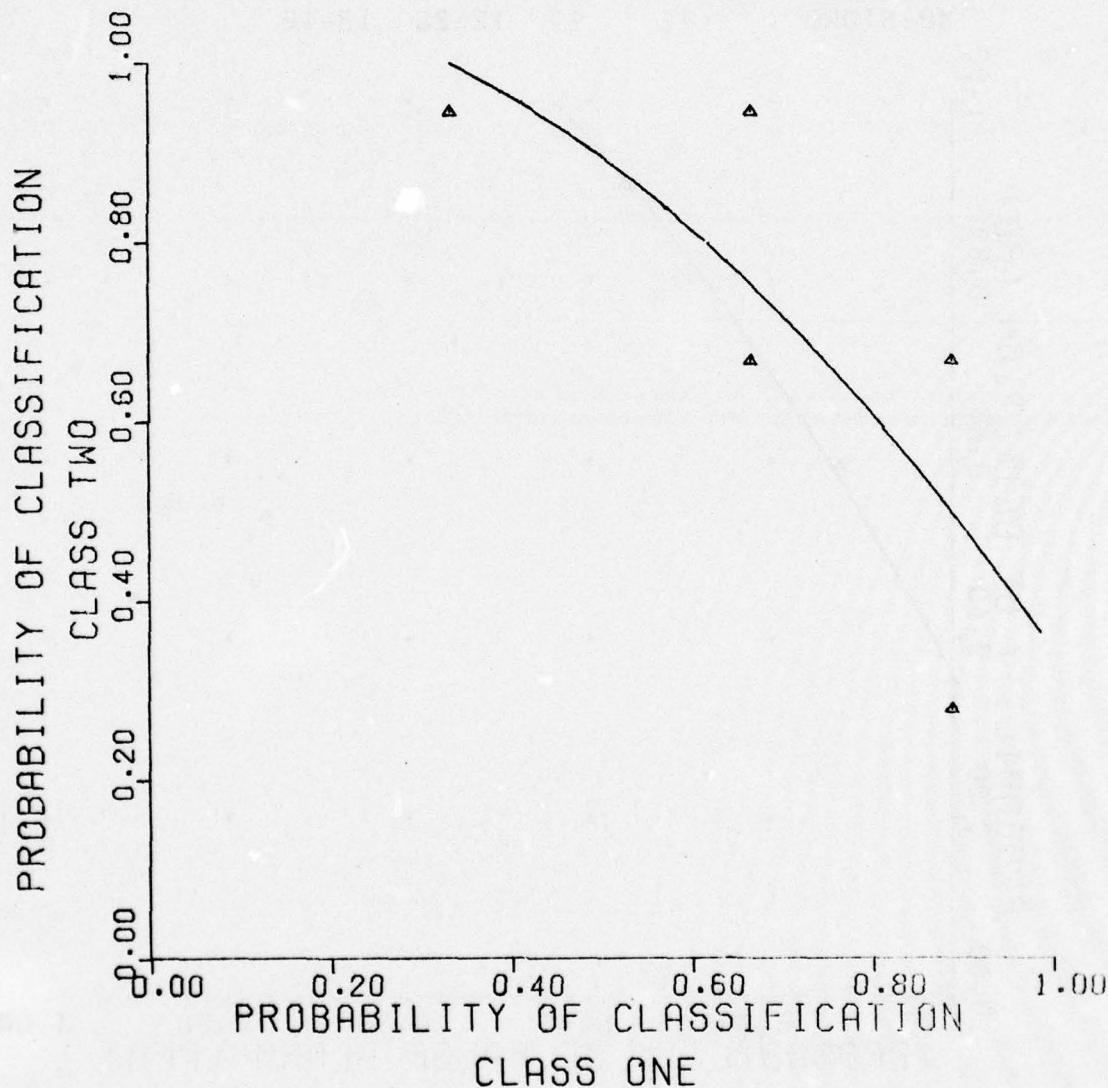


Figure C-64. Nearest neighbor classifier.

UNCLASSIFIED

UNCLASSIFIED

NEAREST NEIGHBOR CLASSIFIER

RAW DATA
VERSION 3
REFERENCE 281

TARGET2 TYPE C MINE

TARGET1 TYPE A MINE

| DEPTH | 3 | 6 |
|----------|-------|-------|
| LOCATION | +4 | 0 |
| MOISTURE | 7 | 17 |
| | 12-20 | 13-16 |

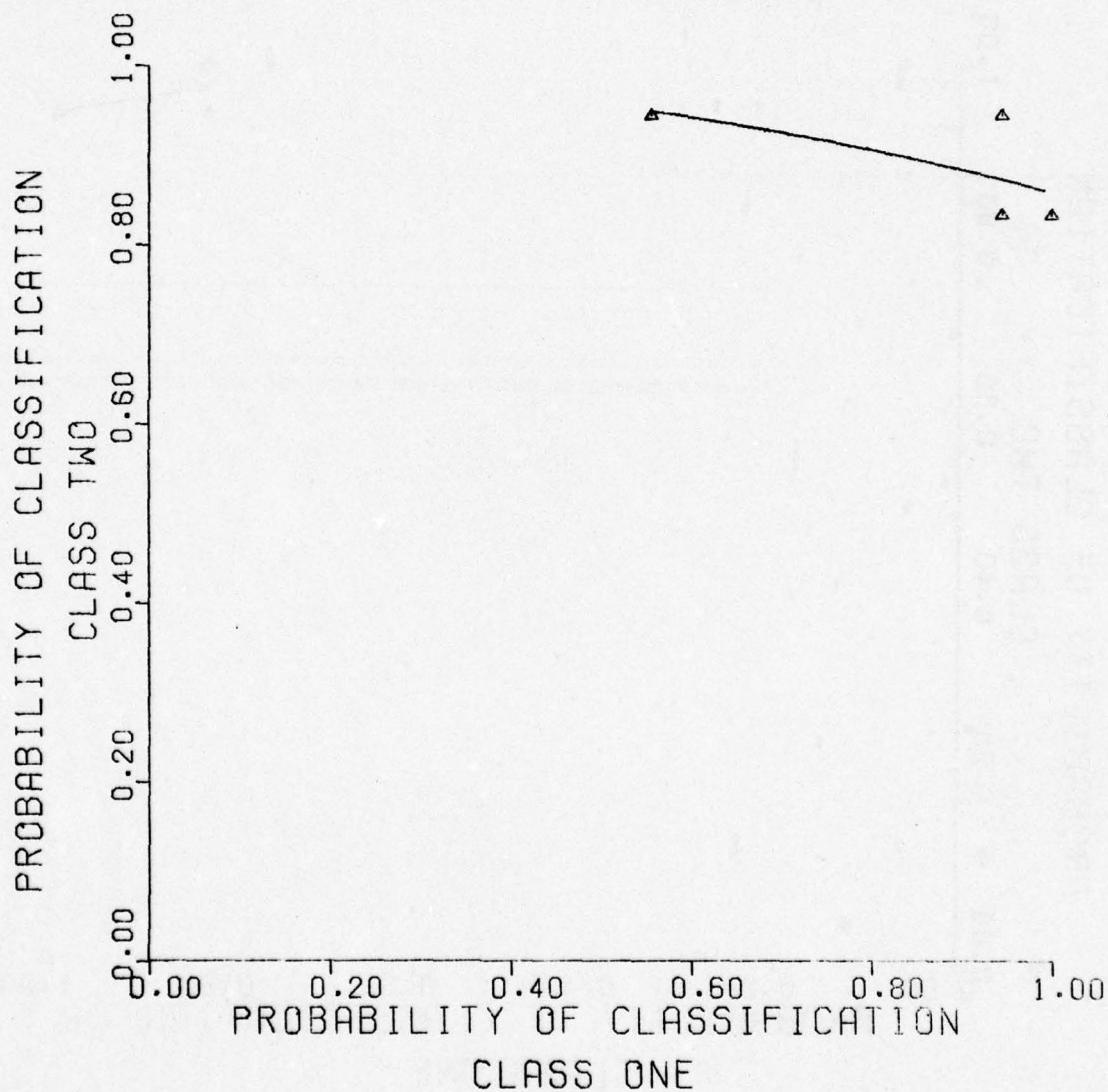


Figure C-65. Nearest neighbor classifier.

UNCLASSIFIED

UNCLASSIFIED

NEAREST NEIGHBOR CLASSIFIER

RAW DATA
VERSION 3
REFERENCE 282

TARGET2 TYPE C MINE
TARGET1 TYPE B MINE

| | | | | |
|----------|----|----|-------|-------|
| DEPTH | 3 | 6 | | |
| LOCATION | +4 | 0 | -4 | |
| MOISTURE | 7 | 17 | 12-20 | 13-16 |

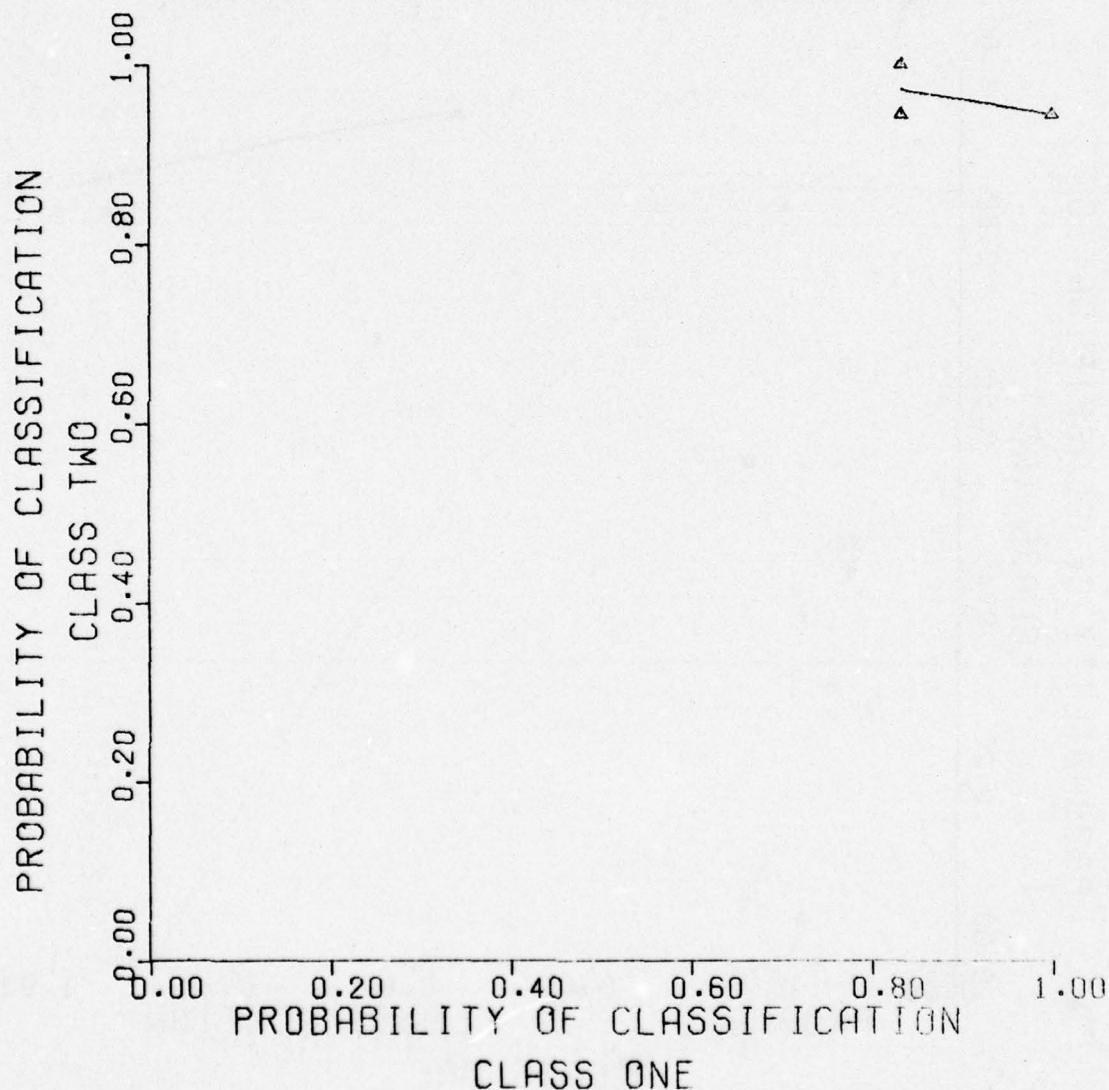


Figure C-66. Nearest neighbor classifier.

UNCLASSIFIED

UNCLASSIFIED

NEAREST NEIGHBOR CLASSIFIER

INTUITIVE DATA

NO. NEAREST NEIGHBORS 5

REFERENCE 317

| NONMINE TARGET | PLATE TYPE A MINE | ROCK(1) | ROCK(2) | ROOT |
|-------------------|----------------------|---------|---------|----------------|
| DEPTH | | 3 | 6 | |
| LOCATION | | +4 | 0 | -4 |
| MOISTURE | | 7 | 17 | 12-20 13-16 |

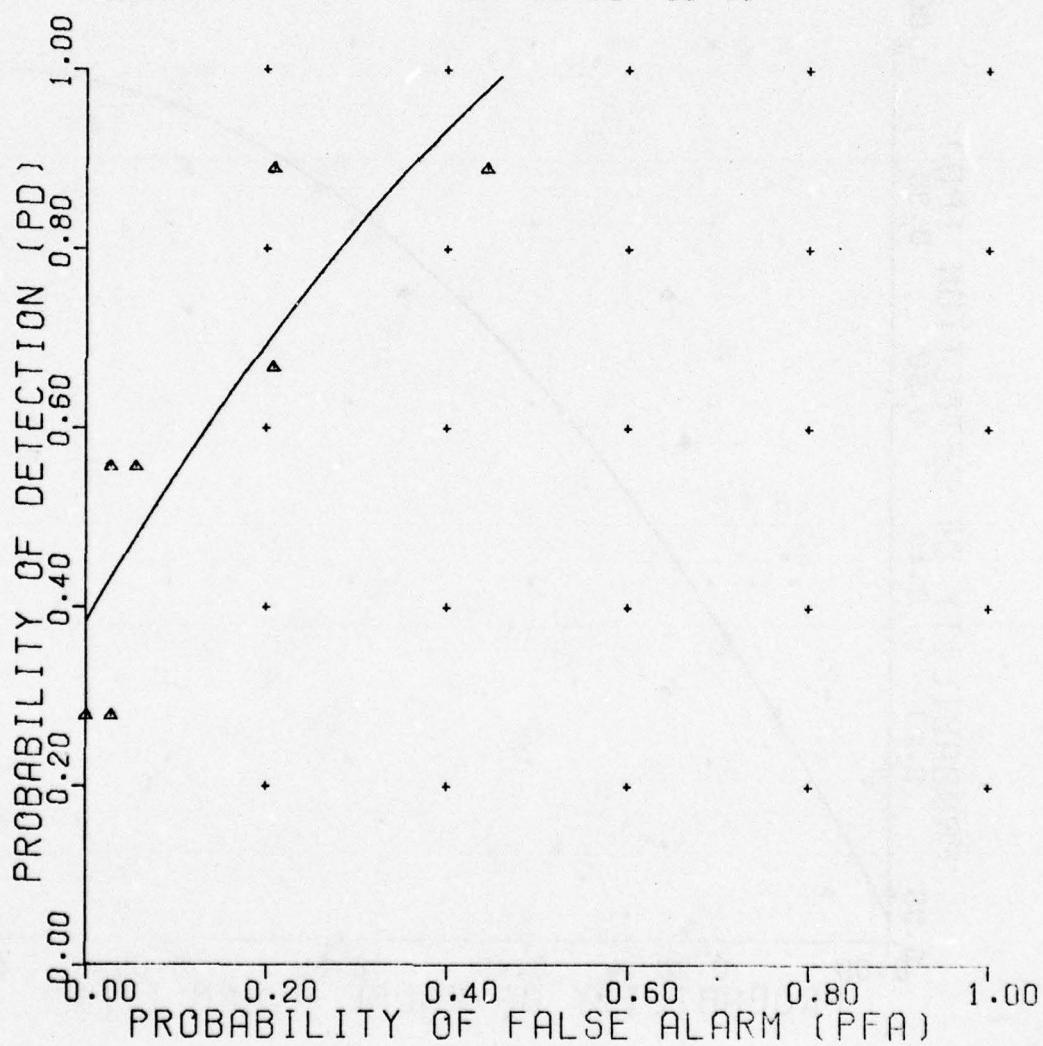


Figure C-67. Nearest neighbor classifier.

UNCLASSIFIED

UNCLASSIFIED

NEAREST NEIGHBOR CLASSIFIER

INTUITIVE DATA
NO. NEAREST NEIGHBORS 5
REFERENCE 318

| NONMINE TARGET | PLATE TYPE B MINE | ROCK(1) | ROCK(2) | ROOT |
|----------------|-------------------|---------|---------|-------|
| DEPTH | | 3 | 6 | |
| LOCATION | | +4 | 0 | -4 |
| MOISTURE | | 7 | 17 | 12-20 |
| | | | | 13-16 |

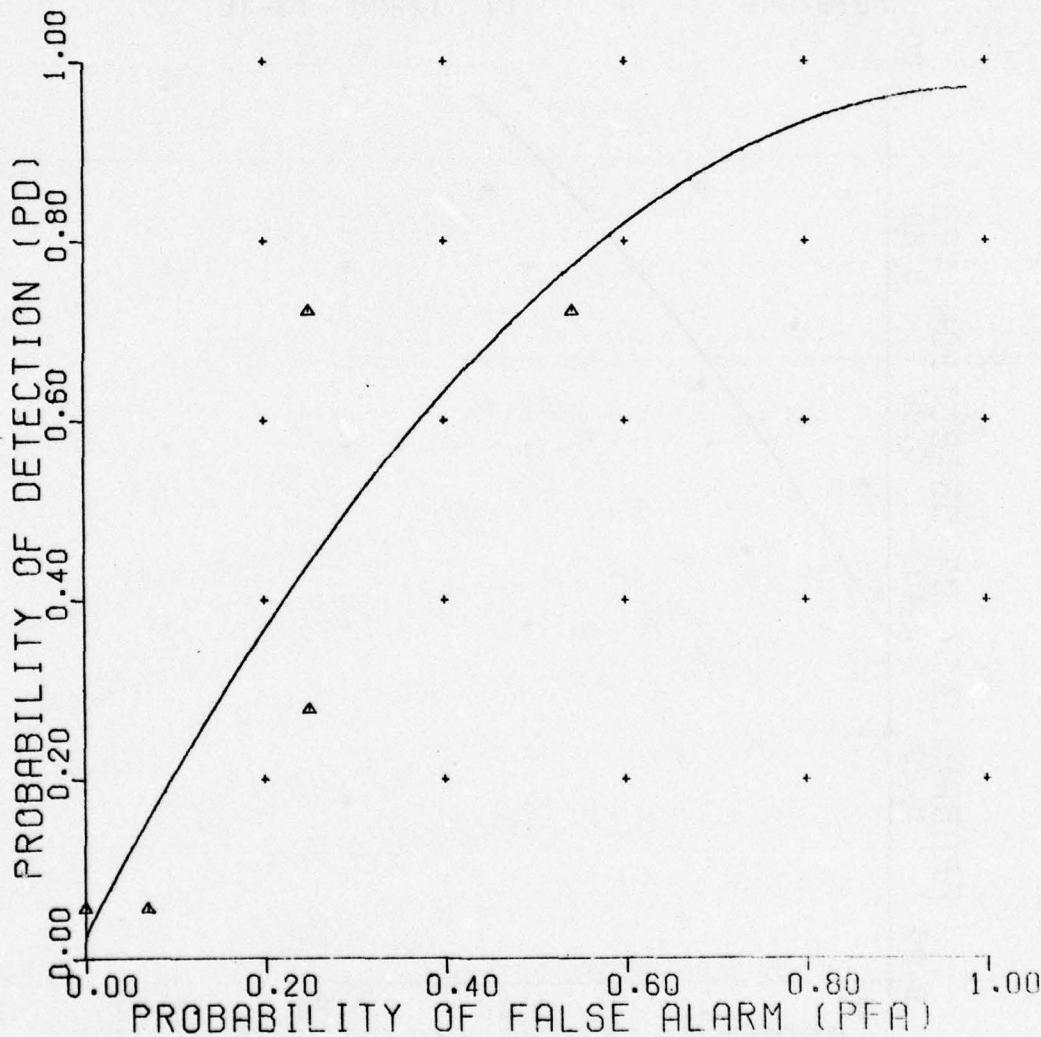


Figure C-68. Nearest neighbor classifier.

UNCLASSIFIED

UNCLASSIFIED

NEAREST NEIGHBOR CLASSIFIER

INTUITIVE DATA

NO. NEAREST NEIGHBORS 5

REFERENCE 319

| NONMINE TARGET | PLATE | ROCK(1) | ROCK(2) | ROOT |
|-------------------|-------|---------|---------|-------|
| DEPTH | 3 | 6 | | |
| LOCATION | +4 | 0 | -4 | |
| MOISTURE | 7 | 17 | 12-20 | 13-16 |

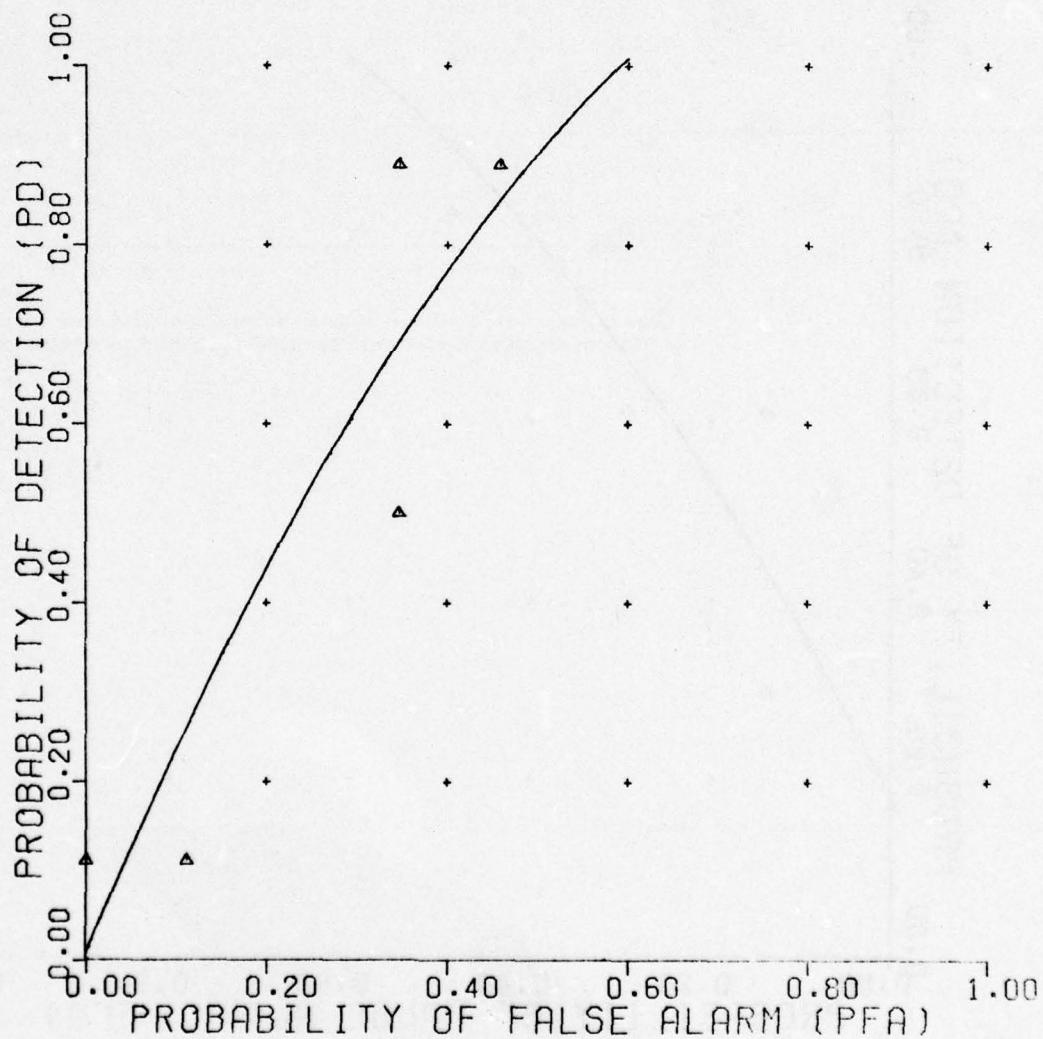


Figure C-69. Nearest neighbor classifier.

UNCLASSIFIED

UNCLASSIFIED

NEAREST NEIGHBOR CLASSIFIER

INTUITIVE DATA

NO. NEAREST NEIGHBORS 5

REFERENCE 320

| NONMINE TARGET | PLATE TYPE C MINE | ROCK(1) TYPE A MINE | ROCK(2) TYPE B MINE | ROOT |
|-------------------|----------------------|------------------------|------------------------|-------|
| DEPTH | 3 | 6 | | |
| LOCATION | +4 | 0 | -4 | |
| MOISTURE | 7 | 17 | 12-20 | 13-16 |

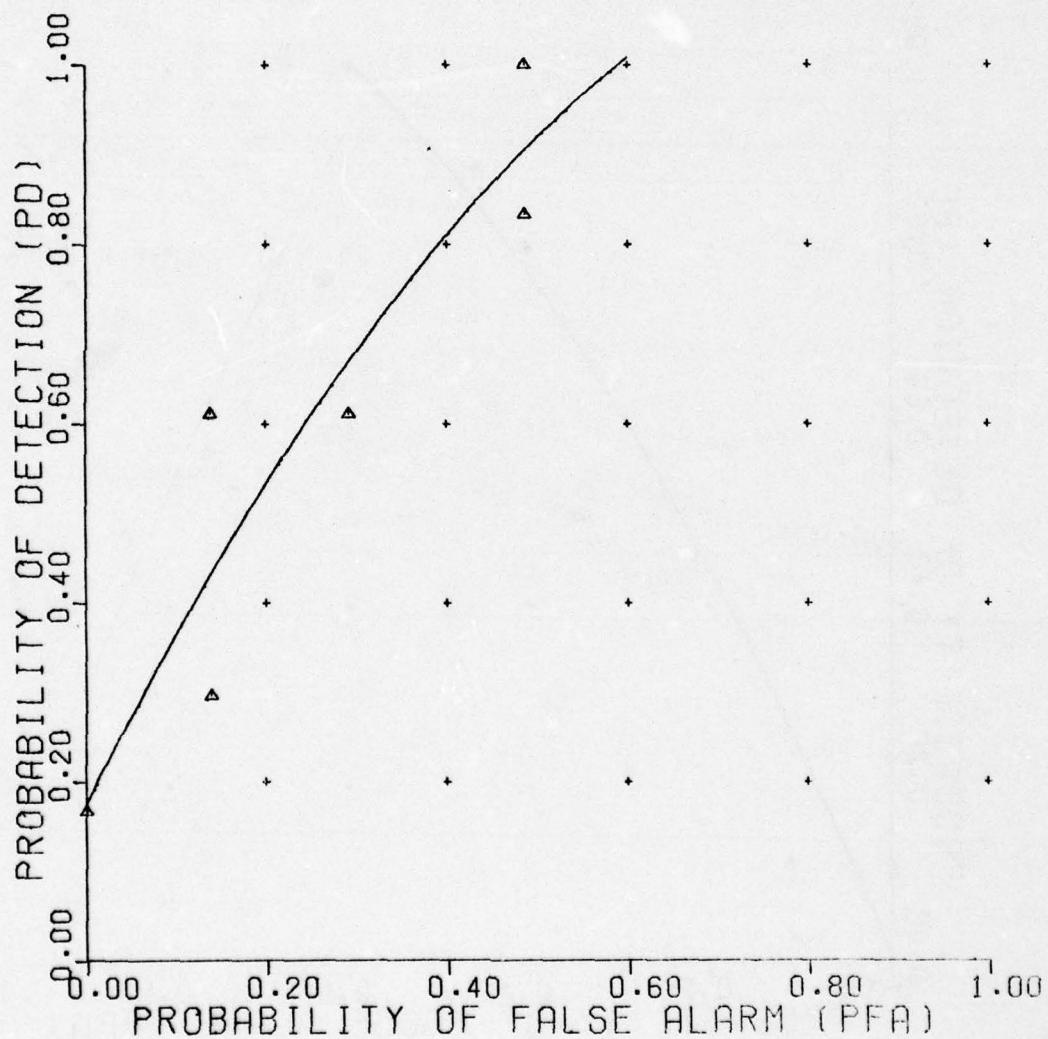


Figure C-70. Nearest neighbor classifier.

UNCLASSIFIED

UNCLASSIFIED

NEAREST NEIGHBOR CLASSIFIER

RAW DATA

NO. NEAREST NEIGHBORS 5

REFERENCE 321

| NONMINE TARGET | PLATE TYPE A | ROCK(1) MINE | ROCK(2) | ROOT |
|-------------------|-----------------|-----------------|---------|----------------|
| DEPTH | | 3 | 6 | |
| LOCATION | | +4 | 0 | -4 |
| MOISTURE | | 7 | 17 | 12-20 13-16 |

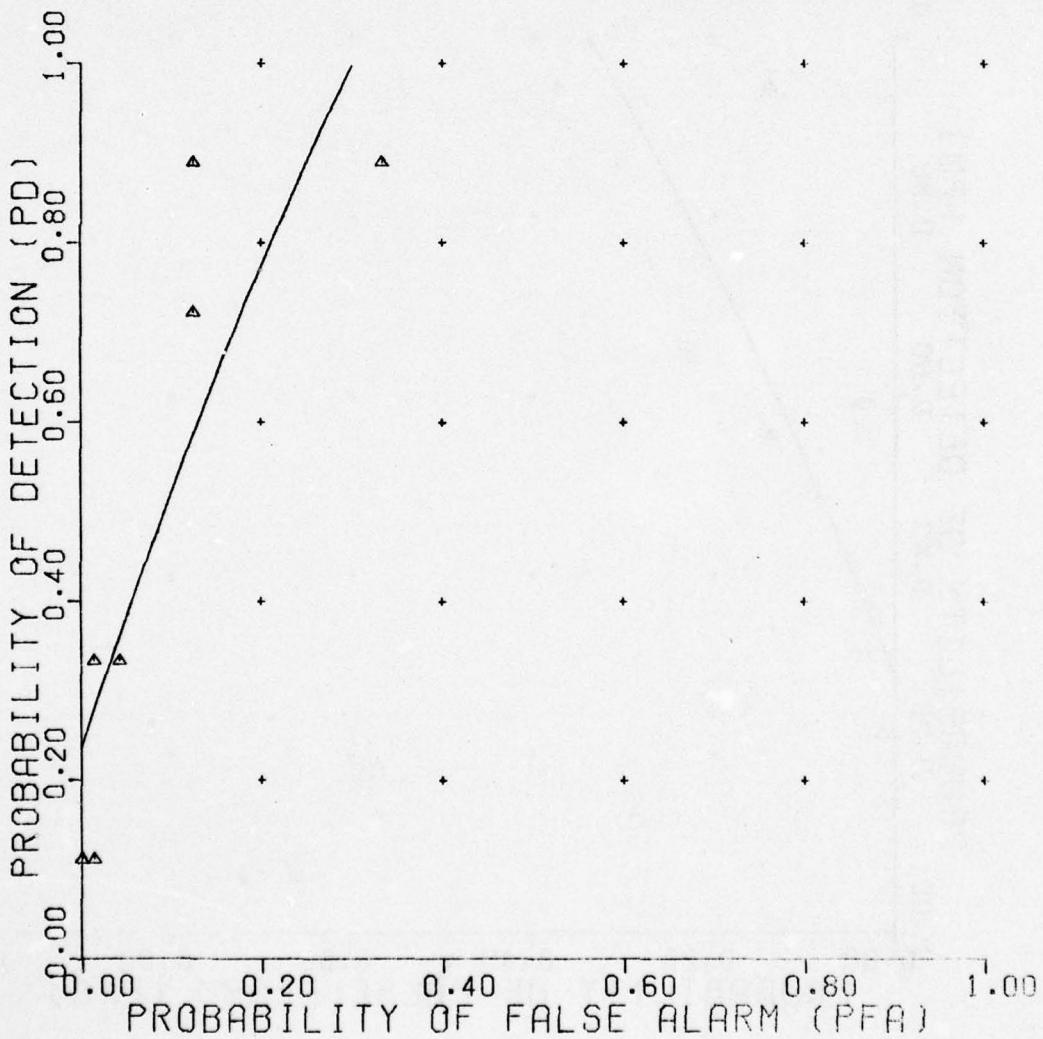


Figure C-71. Nearest neighbor classifier.

UNCLASSIFIED

UNCLASSIFIED

NEAREST NEIGHBOR CLASSIFIER

RAW DATA

NO. NEAREST NEIGHBORS 5

REFERENCE 322

| NONMINE TARGET | PLATE TYPE B MINE | ROCK(1) | ROCK(2) | ROOT |
|-------------------|----------------------|---------|---------|-------|
| DEPTH | | 3 | 6 | |
| LOCATION | | +4 | 0 | -4 |
| MOISTURE | | 7 | 17 | 12-20 |
| | | | | 13-16 |

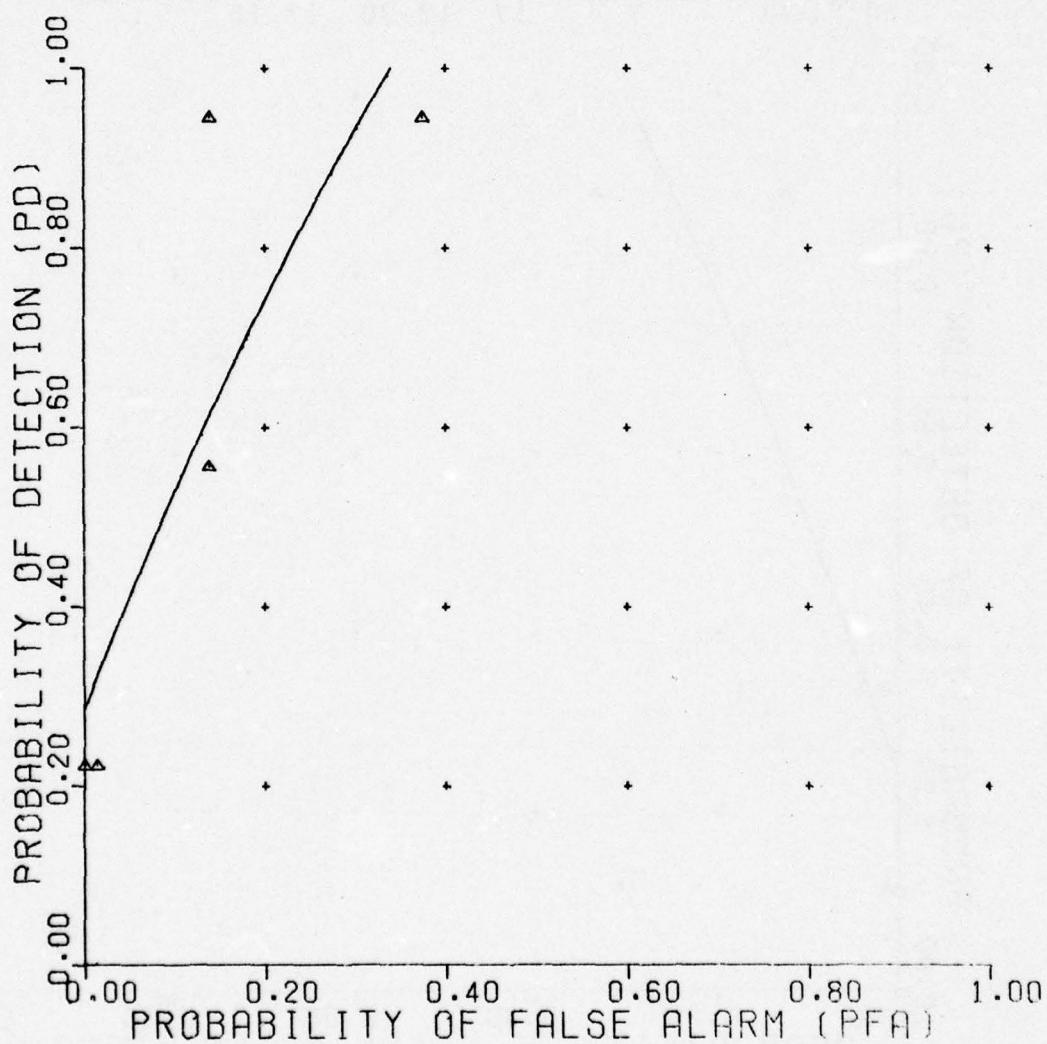


Figure C-72. Nearest neighbor classifier.

UNCLASSIFIED

UNCLASSIFIED

NEAREST NEIGHBOR CLASSIFIER

RAW DATA
NO. NEAREST NEIGHBORS 5
REFERENCE 323

| NONMINE TARGET | PLATE | ROCK(1) | ROCK(2) | ROOT |
|-------------------|-------|---------|---------|-------|
| | | 3 | 6 | |
| DEPTH | | | | |
| LOCATION | +4 | 0 | -4 | |
| MOISTURE | 7 | 17 | 12-20 | 13-16 |

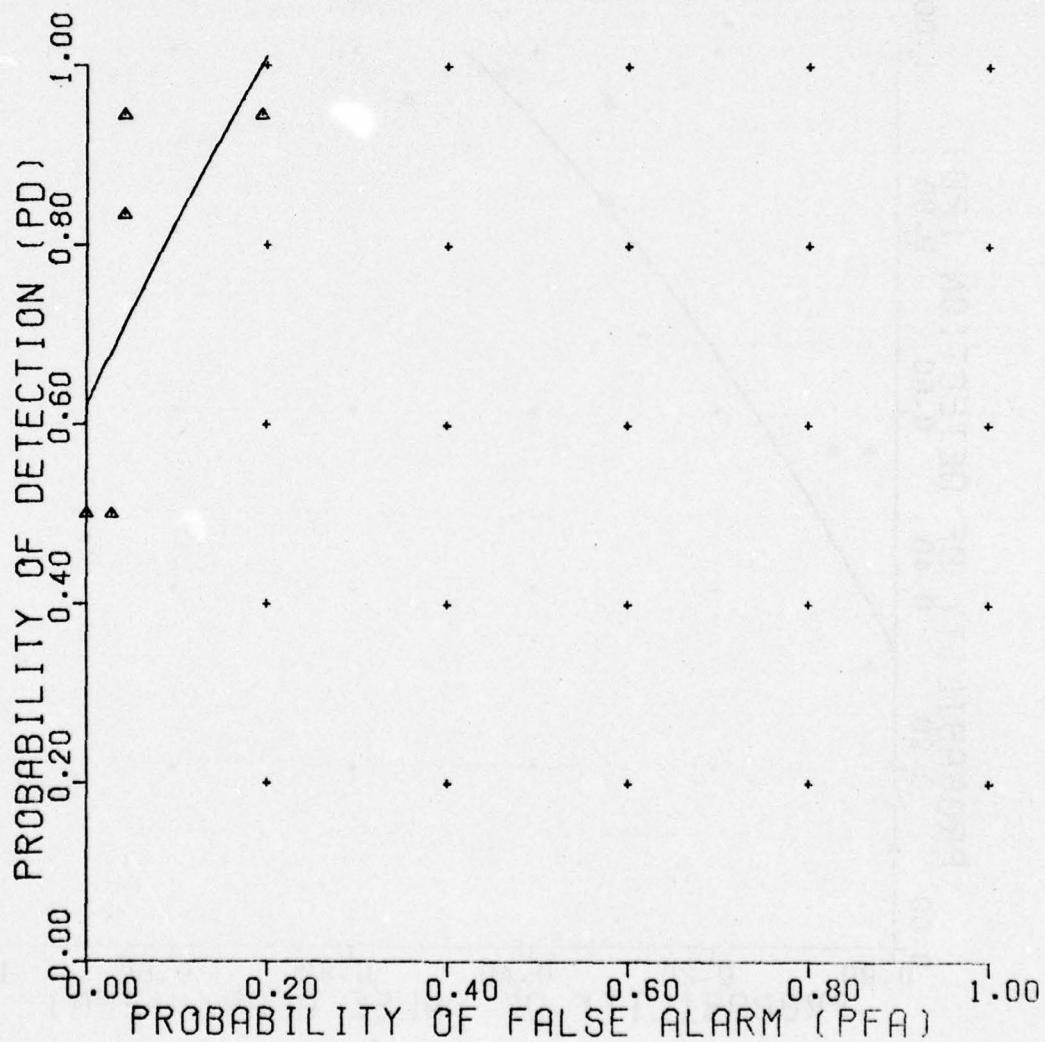


Figure C-73. Nearest neighbor classifier.

UNCLASSIFIED

UNCLASSIFIED

NEAREST NEIGHBOR CLASSIFIER

RAW DATA

NO. NEAREST NEIGHBORS 5

REFERENCE 324

| NONMINE TARGET | PLATE TYPE C MINE | ROCK(1) TYPE A MINE | ROCK(2) TYPE B MINE | ROOT |
|-------------------|-------------------------|---------------------------|---------------------------|-------|
| DEPTH | 3 | 6 | | |
| LOCATION | +4 | 0 | -4 | |
| MOISTURE | 7 | 17 | 12-20 | 13-16 |

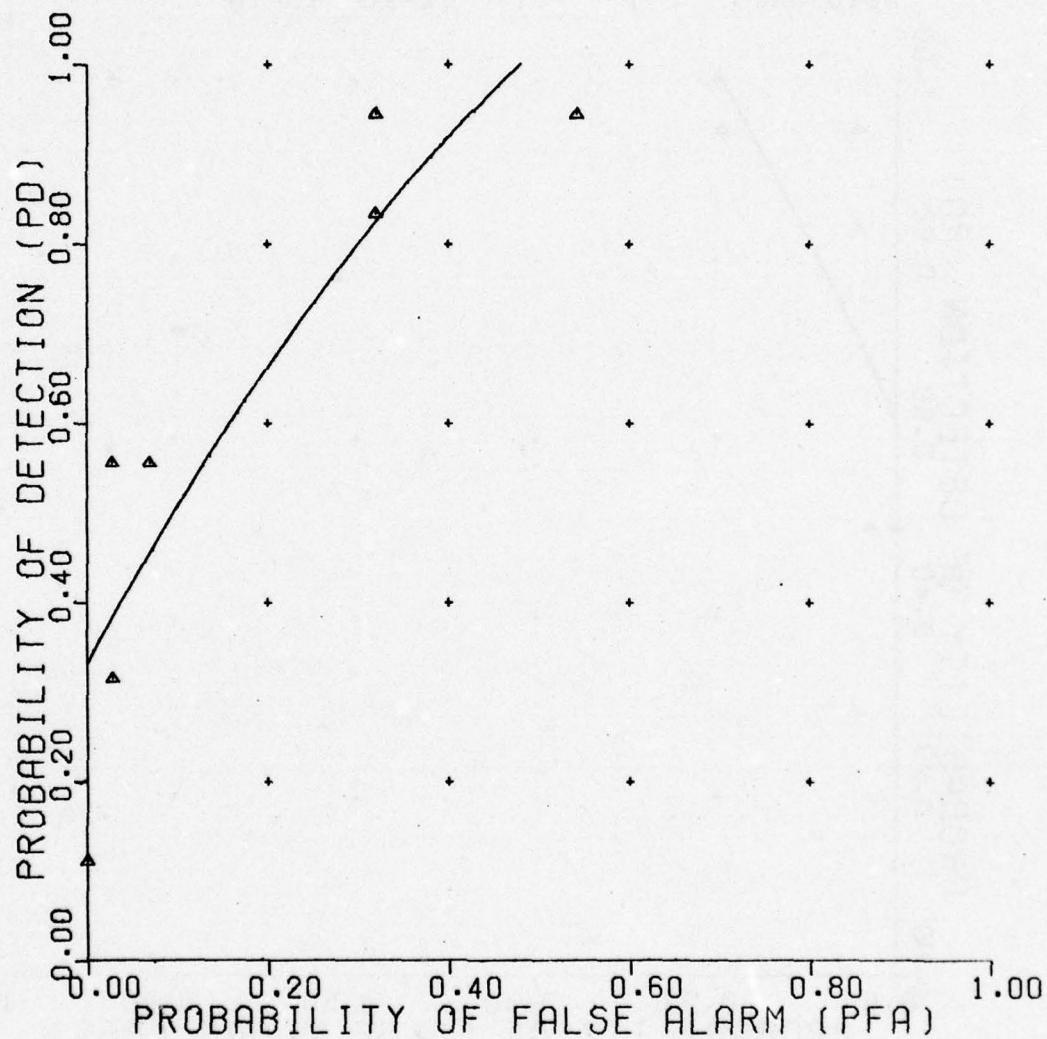


Figure C-74. Nearest neighbor classifier.

UNCLASSIFIED

UNCLASSIFIED

NEAREST NEIGHBOR CLASSIFIER

INTUITIVE DATA
NO. NEAREST NEIGHBORS 7
REFERENCE 325

| NONMINE TARGET | PLATE TYPE A MINE | ROCK(1) | ROCK(2) | ROOT |
|----------------|-------------------|---------|---------|-------|
| DEPTH | | 3 | 6 | |
| LOCATION | | +4 | 0 | -4 |
| MOISTURE | | 7 | 17 | 12-20 |
| | | | | 13-16 |

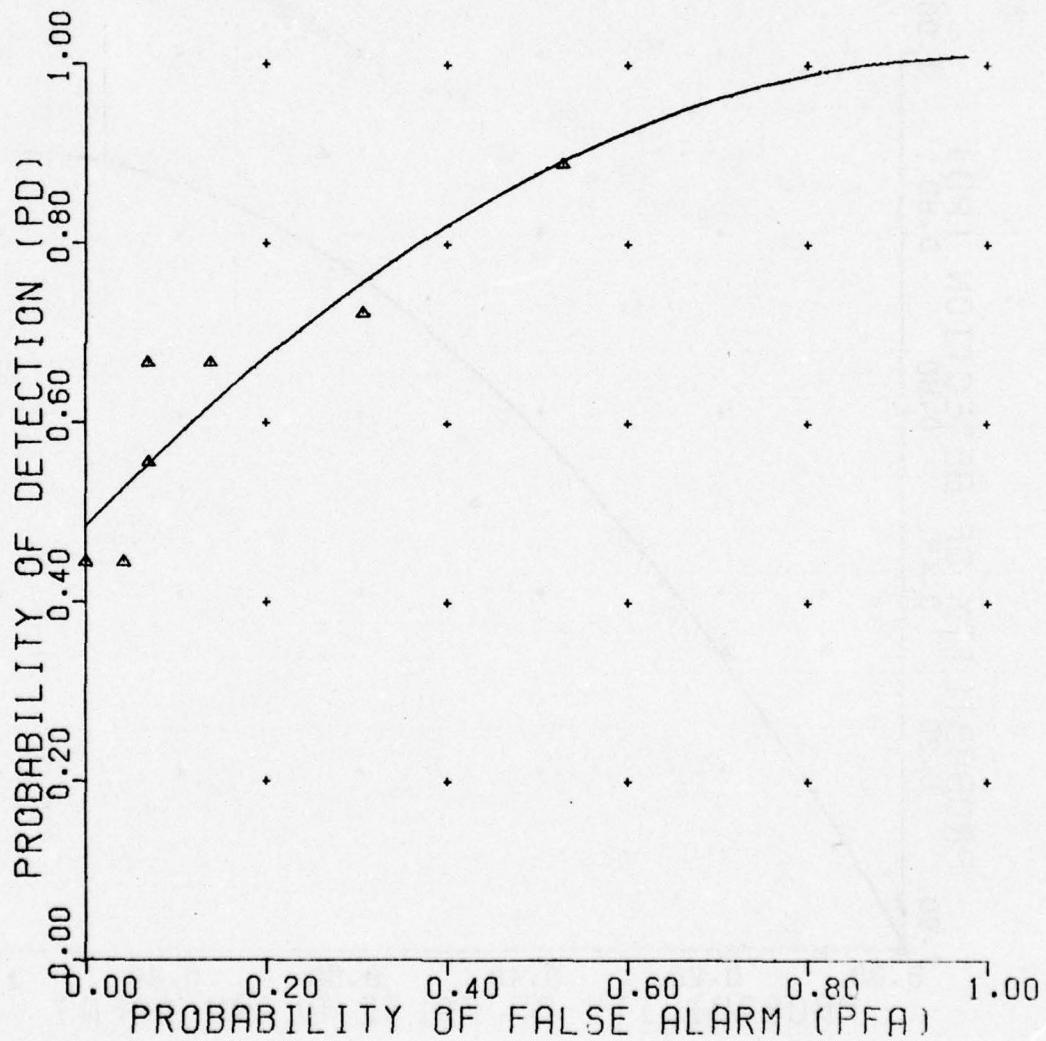


Figure C-75. Nearest neighbor classifier.

UNCLASSIFIED

UNCLASSIFIED

NEAREST NEIGHBOR CLASSIFIER

INTUITIVE DATA

NO. NEAREST NEIGHBORS 7

REFERENCE 326

| NONMINE TARGET | PLATE TYPE B MINE | ROCK(1) | ROCK(2) | ROOT |
|-------------------|----------------------|---------|---------|-------|
| DEPTH | | 3 | 6 | |
| LOCATION | | +4 | 0 | -4 |
| MOISTURE | | 7 | 17 | 12-20 |
| | | | | 13-16 |

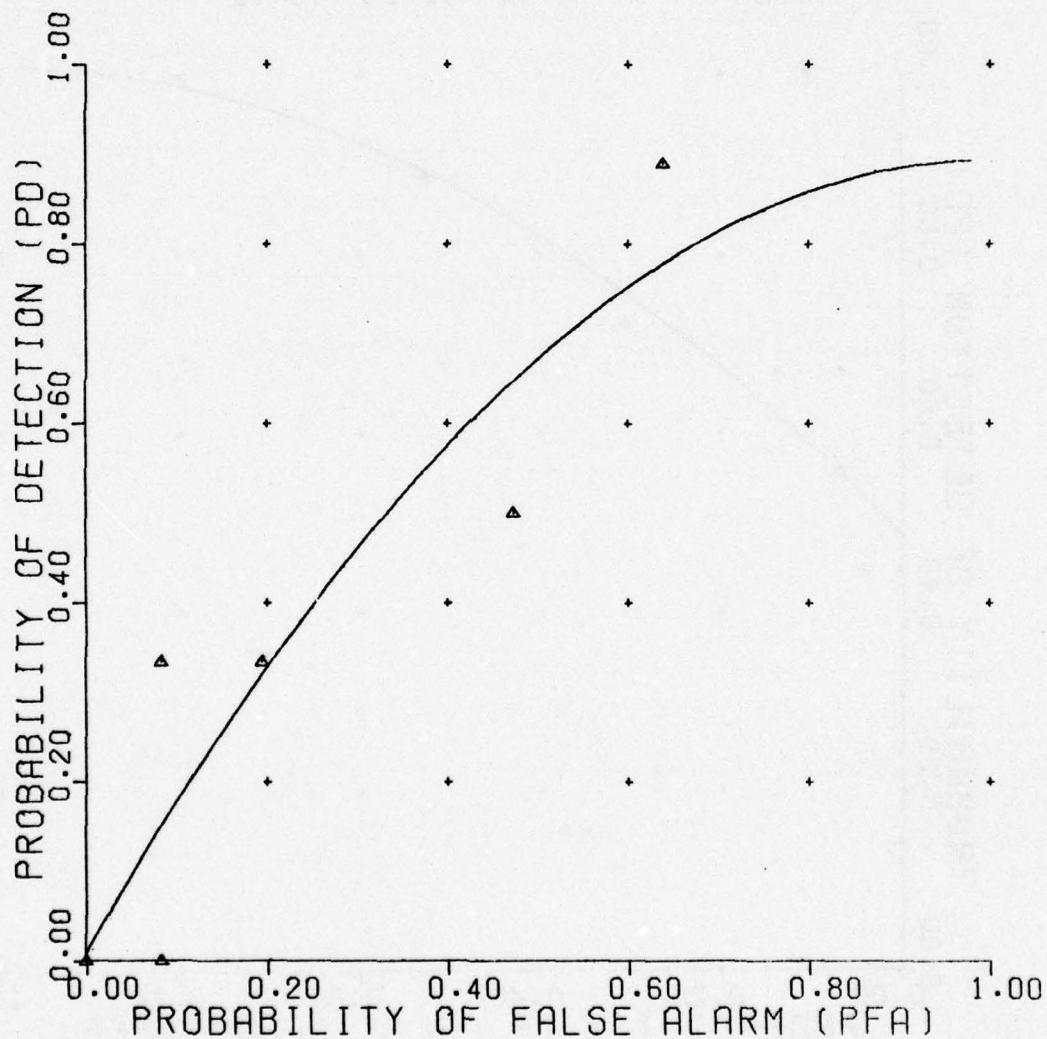


Figure C-76. Nearest neighbor classifier.

UNCLASSIFIED

UNCLASSIFIED

NEAREST NEIGHBOR CLASSIFIER

INTUITIVE DATA

NO. NEAREST NEIGHBORS 7

REFERENCE 327

| NONMINE TARGET | PLATE TYPE C MINE | ROCK(1) | ROCK(2) | ROOT |
|-------------------|----------------------|---------|---------|-------|
| DEPTH | | 3 | 6 | |
| LOCATION | | +4 | 0 | -4 |
| MOISTURE | | 7 | 17 | 12-20 |
| | | | | 13-16 |

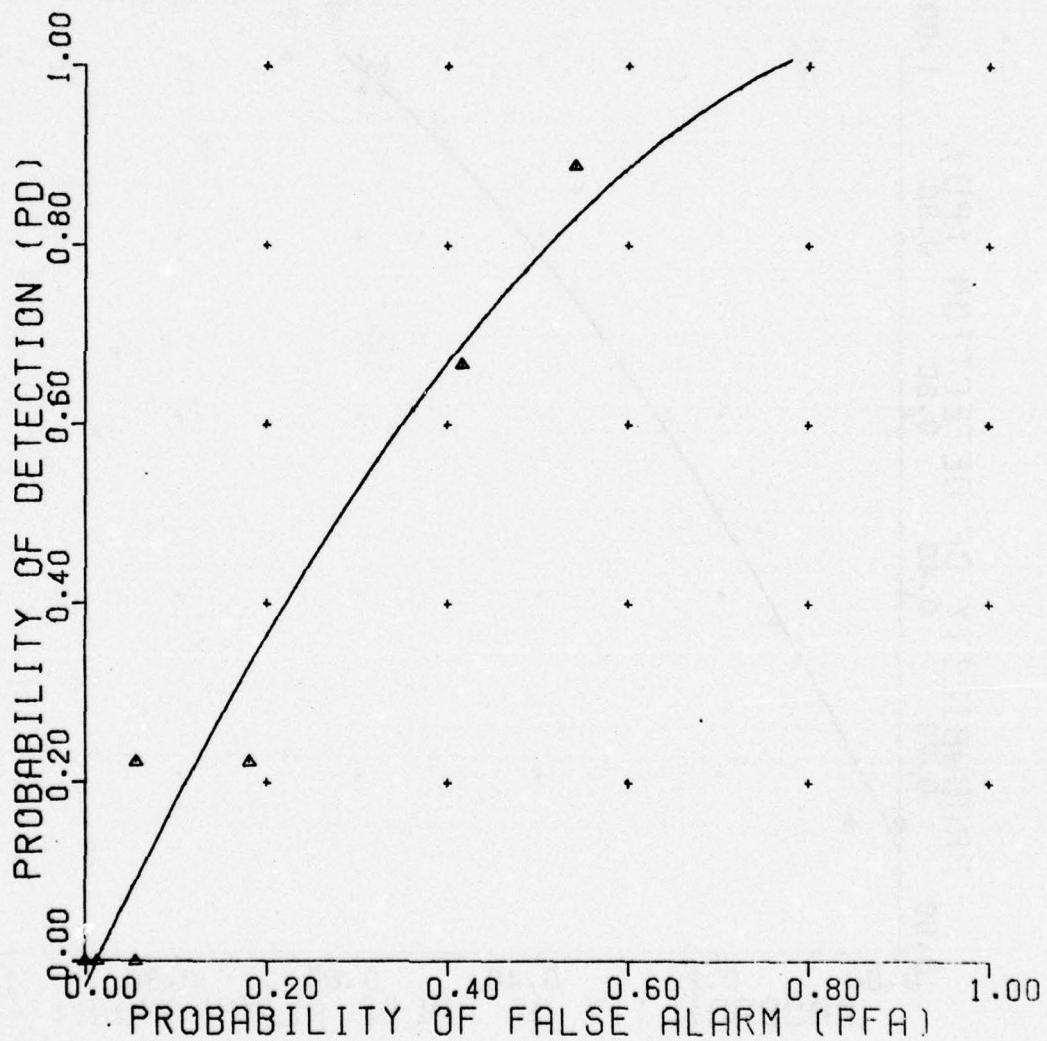


Figure C-77. Nearest neighbor classifier.

UNCLASSIFIED

UNCLASSIFIED

NEAREST NEIGHBOR CLASSIFIER

INTUITIVE DATA

NO. NEAREST NEIGHBORS 7

REFERENCE 328

| NONMINE TARGET | PLATE TYPE C MINE | ROCK(1) TYPE A MINE | ROCK(2) TYPE B MINE | ROOT |
|-------------------|----------------------|------------------------|------------------------|-------|
| DEPTH | 3 | 6 | | |
| LOCATION | +4 | 0 | -4 | |
| MOISTURE | 7 | 17 | 12-20 | 13-16 |

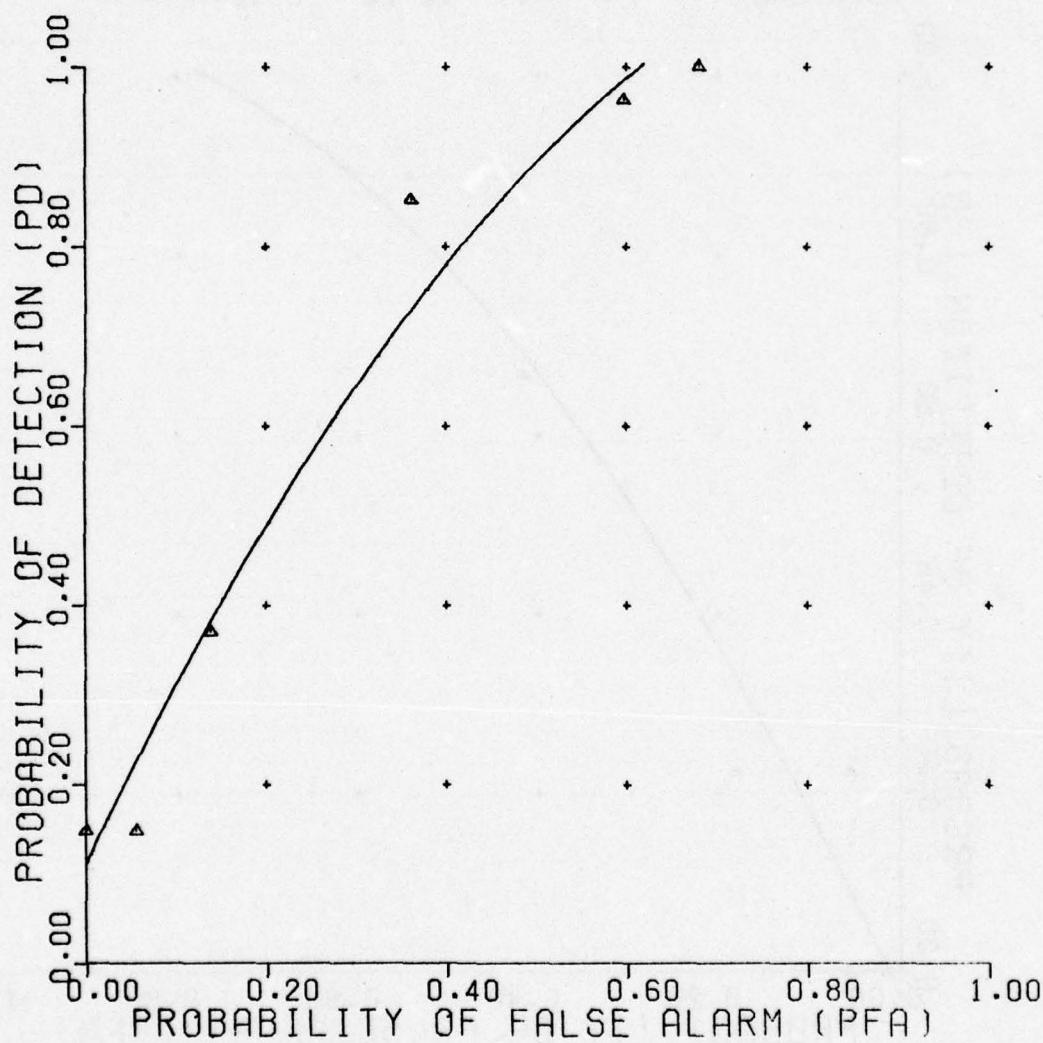


Figure C-78. Nearest neighbor classifier.

UNCLASSIFIED

UNCLASSIFIED

NEAREST NEIGHBOR CLASSIFIER

RAW DATA

NO. NEAREST NEIGHBORS 7

REFERENCE 329

| NONMINE TARGET | PLATE TYPE A MINE | ROCK(1) | ROCK(2) | ROOT |
|-------------------|----------------------|---------|---------|-------------|
| DEPTH | | 3 | 6 | |
| LOCATION | | +4 | 0 | -4 |
| MOISTURE | | 7 | 17 | 12-20 13-16 |

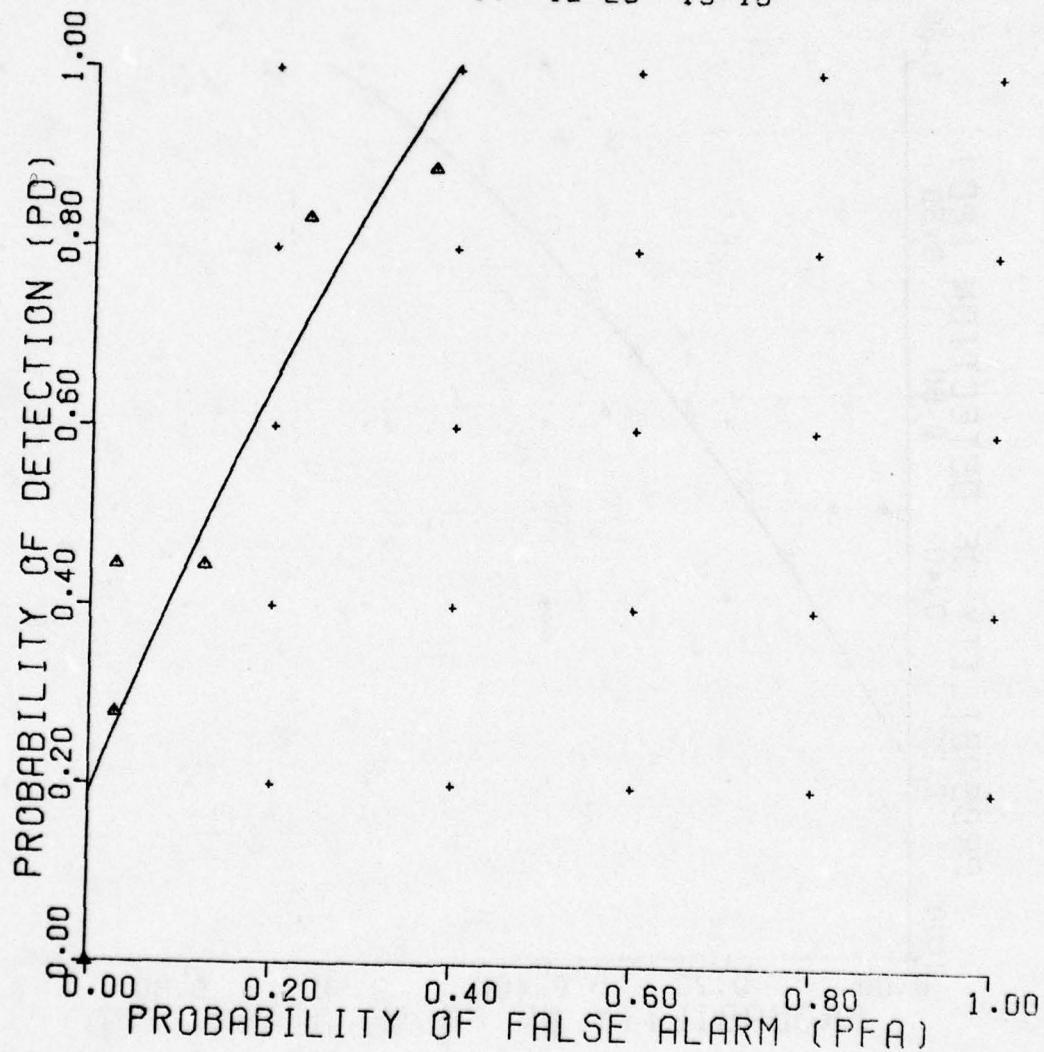


Figure C-79. Nearest neighbor classifier.

UNCLASSIFIED

UNCLASSIFIED

NEAREST NEIGHBOR CLASSIFIER

RAW DATA

NO. NEAREST NEIGHBORS 7

REFERENCE 330

| NONMINE TARGET | PLATE TYPE B MINE | ROCK(1) | ROCK(2) | ROOT |
|-------------------|----------------------|---------|---------|-------|
| DEPTH | | 3 | 6 | |
| LOCATION | | +4 | 0 | -4 |
| MOISTURE | | 7 | 17 | 12-20 |
| | | | | 13-16 |

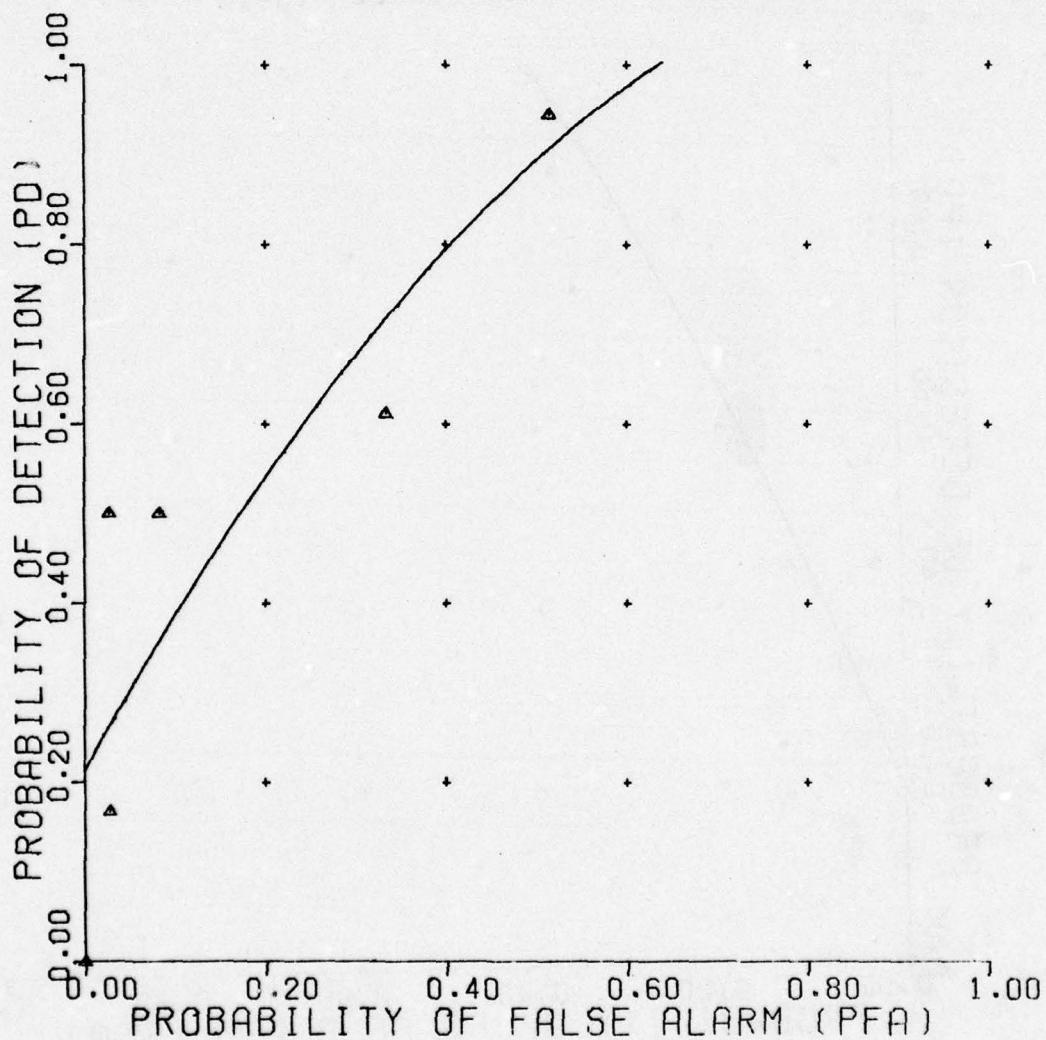


Figure C-80. Nearest neighbor classifier.

UNCLASSIFIED

UNCLASSIFIED

NEAREST NEIGHBOR CLASSIFIER

RAW DATA

NO. NEAREST NEIGHBORS 7

REFERENCE 331

| NONMINE TARGET | PLATE | ROCK(1) | ROCK(2) | ROOT |
|-------------------|-------------|---------|---------|-------|
| | TYPE C MINE | | | |
| DEPTH | 3 | 6 | | |
| LOCATION | +4 | 0 | -4 | |
| MOISTURE | 7 | 17 | 12-20 | 13-16 |

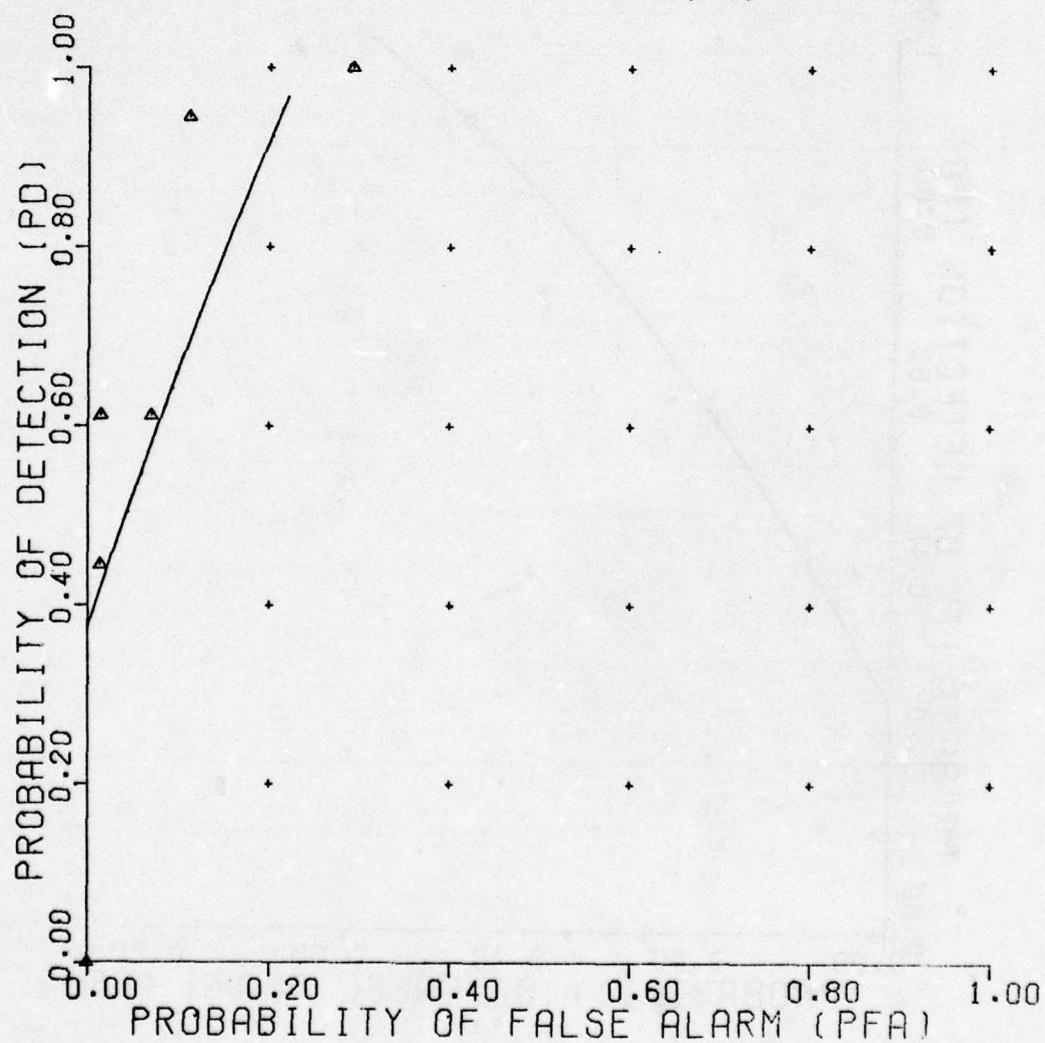


Figure C-81. Nearest neighbor classifier.

UNCLASSIFIED

UNCLASSIFIED

NEAREST NEIGHBOR CLASSIFIER

RAW DATA
NO. NEAREST NEIGHBORS 7
REFERENCE 332

| NONMINE TARGET | PLATE TYPE C MINE | ROCK(1) TYPE A MINE | ROCK(2) 12-20 | ROOT TYPE B MINE |
|----------------|-------------------|---------------------|---------------|------------------|
| DEPTH | 3 | 6 | | |
| LOCATION | +4 | 0 | -4 | |
| MOISTURE | 7 | 17 | 12-20 | 13-16 |

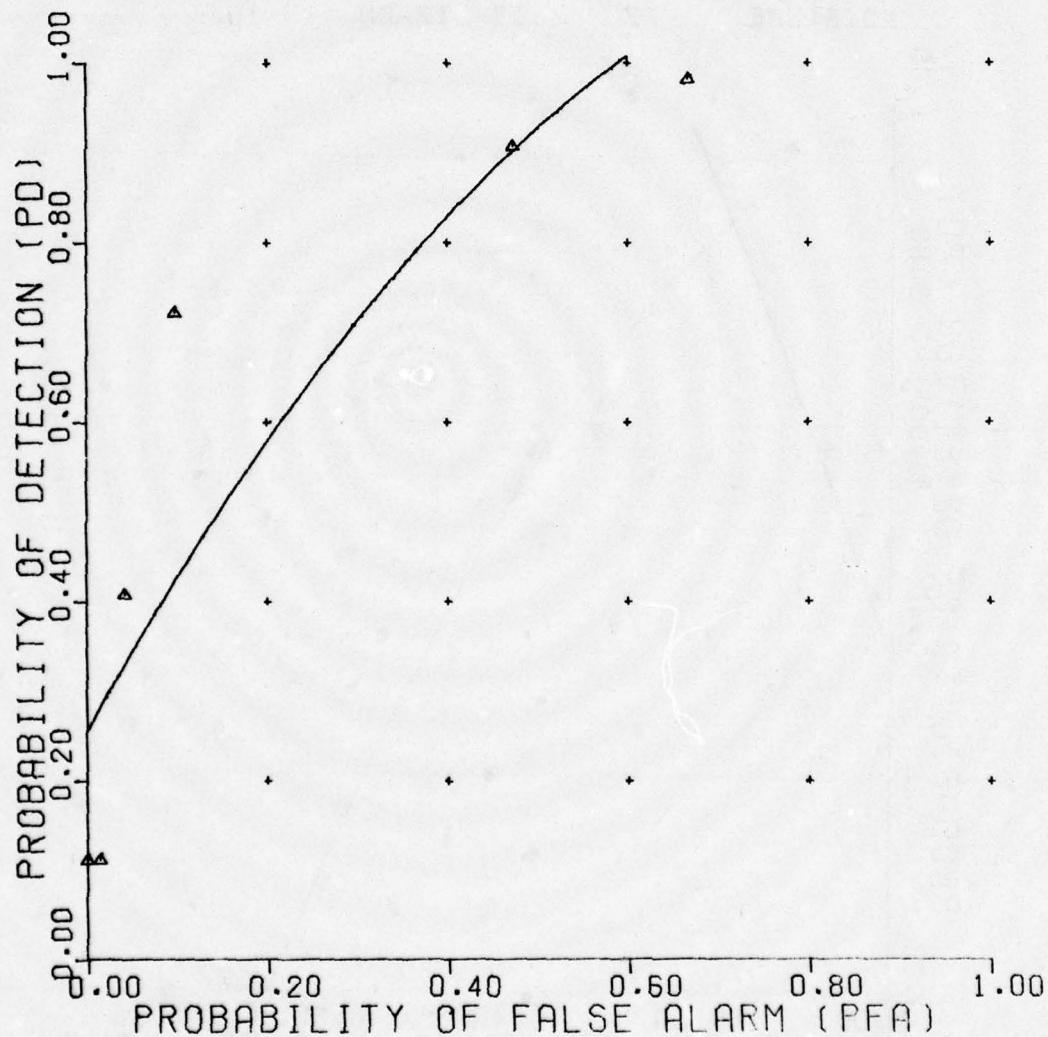


Figure C-82. Nearest neighbor classifier.

UNCLASSIFIED

UNCLASSIFIED

SPACE PARTITION CLASSIFIER
(QUADRATIC DISCRIMINANT)

INTUITIVE DATA

VERSION 2

REFERENCE 352

| NONMINE TARGET | PLATE TYPE A MINE | ROCK(1) | ROCK(2) | ROOT |
|----------------|-------------------|---------|---------|-------|
| DEPTH | | 3 | 6 | |
| LOCATION | | +4 | 0 | -4 |
| MOISTURE | | 7 | 17 | 12-20 |
| | | | | 13-16 |

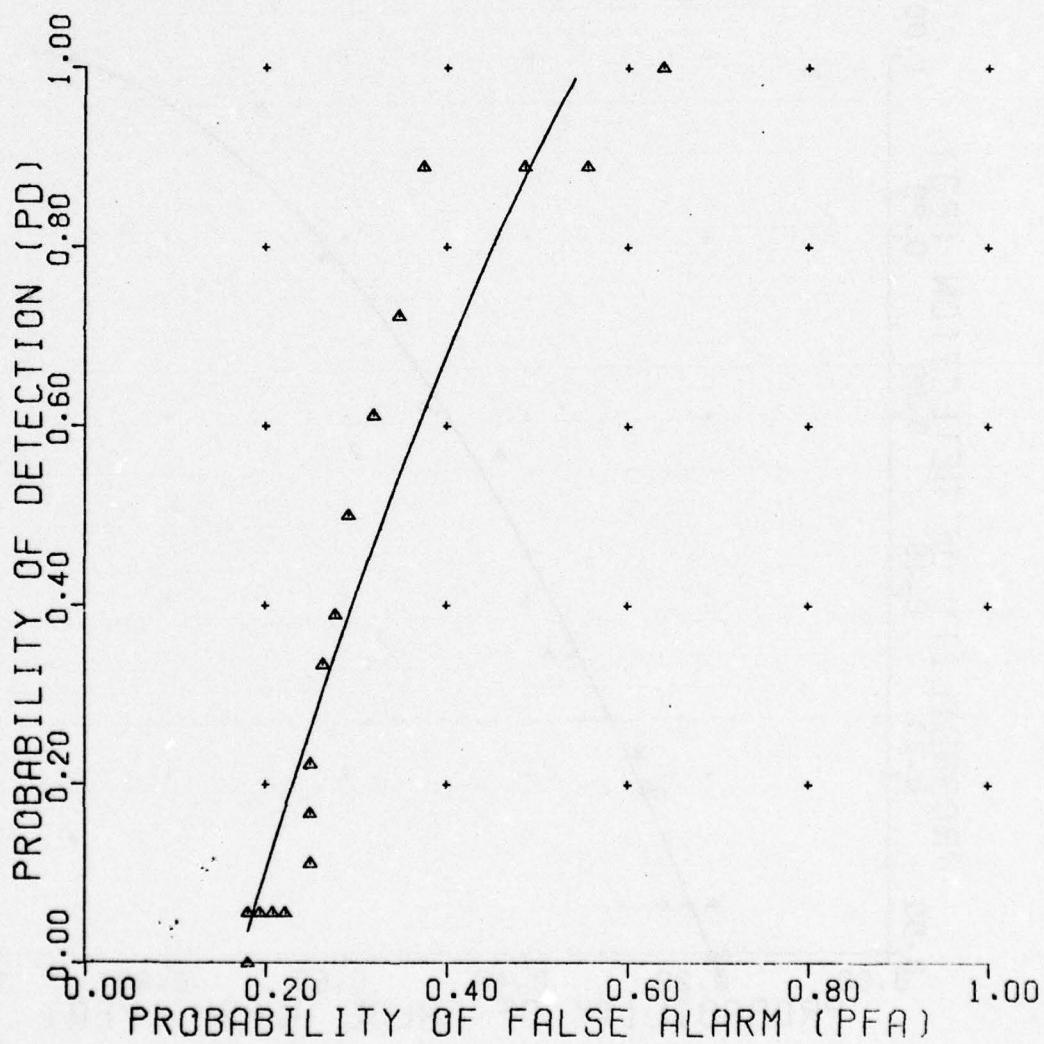


Figure C-83. Nearest neighbor classifier.

UNCLASSIFIED

UNCLASSIFIED

SPACE PARTITION CLASSIFIER
(QUADRATIC DISCRIMINANT)

INTUITIVE DATA

VERSION 2

REFERENCE 353

| | | | | |
|----------|--------|---------|---------|-------|
| NONMINE | PLATE | ROCK(1) | ROCK(2) | ROOT |
| TARGET | TYPE B | MINE | | |
| DEPTH | 3 | 6 | | |
| LOCATION | +4 | 0 | -4 | |
| MOISTURE | 7 | 17 | 12-20 | 13-16 |

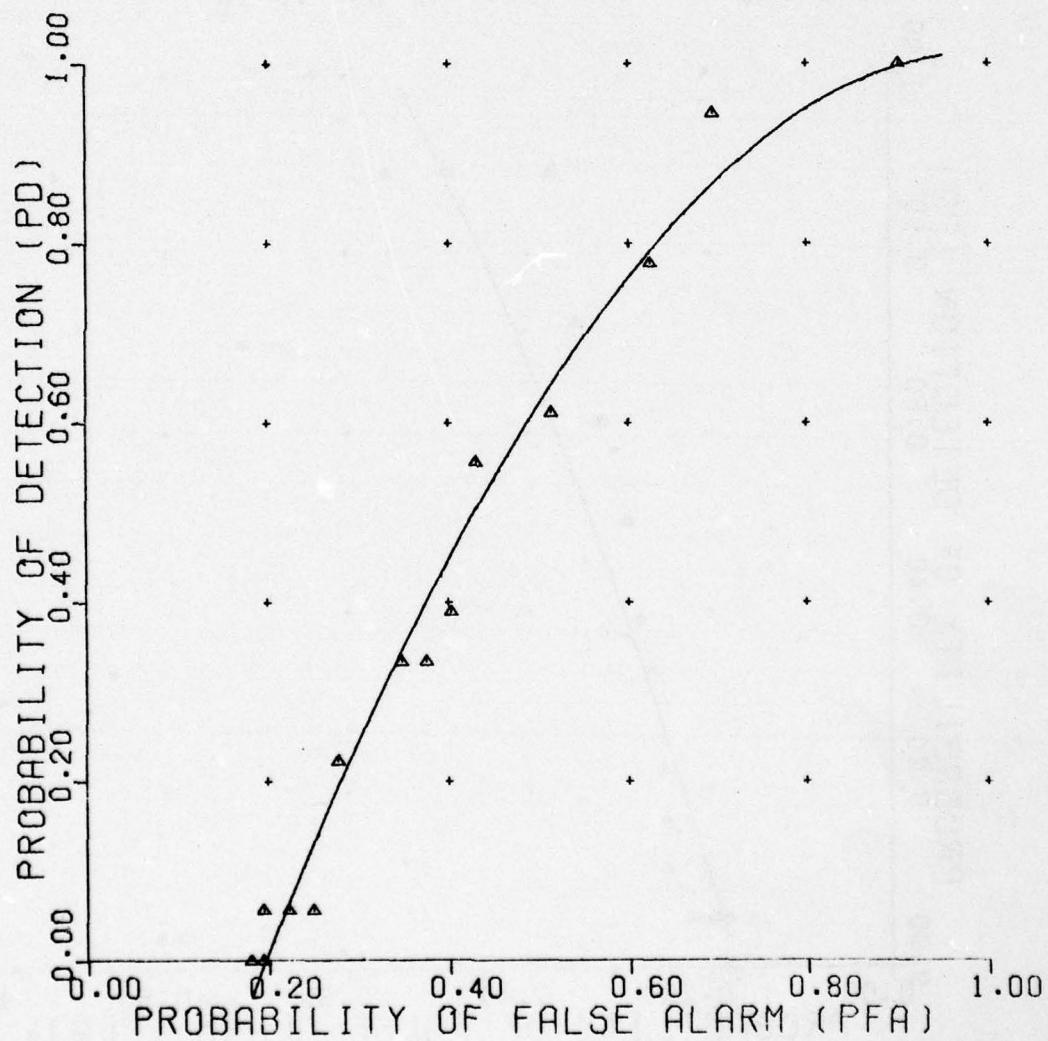


Figure C-84. Nearest neighbor classifier.

UNCLASSIFIED

UNCLASSIFIED

SPACE PARTITION CLASSIFIER
(QUADRATIC DISCRIMINANT)

INTUITIVE DATA
VERSION 2
REFERENCE 354

| NONMINE TARGET | PLATE | ROCK(1) | ROCK(2) | ROOT |
|-------------------|-------|---------|---------|-------|
| TYPE C MINE | | | | |
| DEPTH | 3 | 6 | | |
| LOCATION | +4 | 0 | -4 | |
| MOISTURE | 7 | 17 | 12-20 | 13-16 |

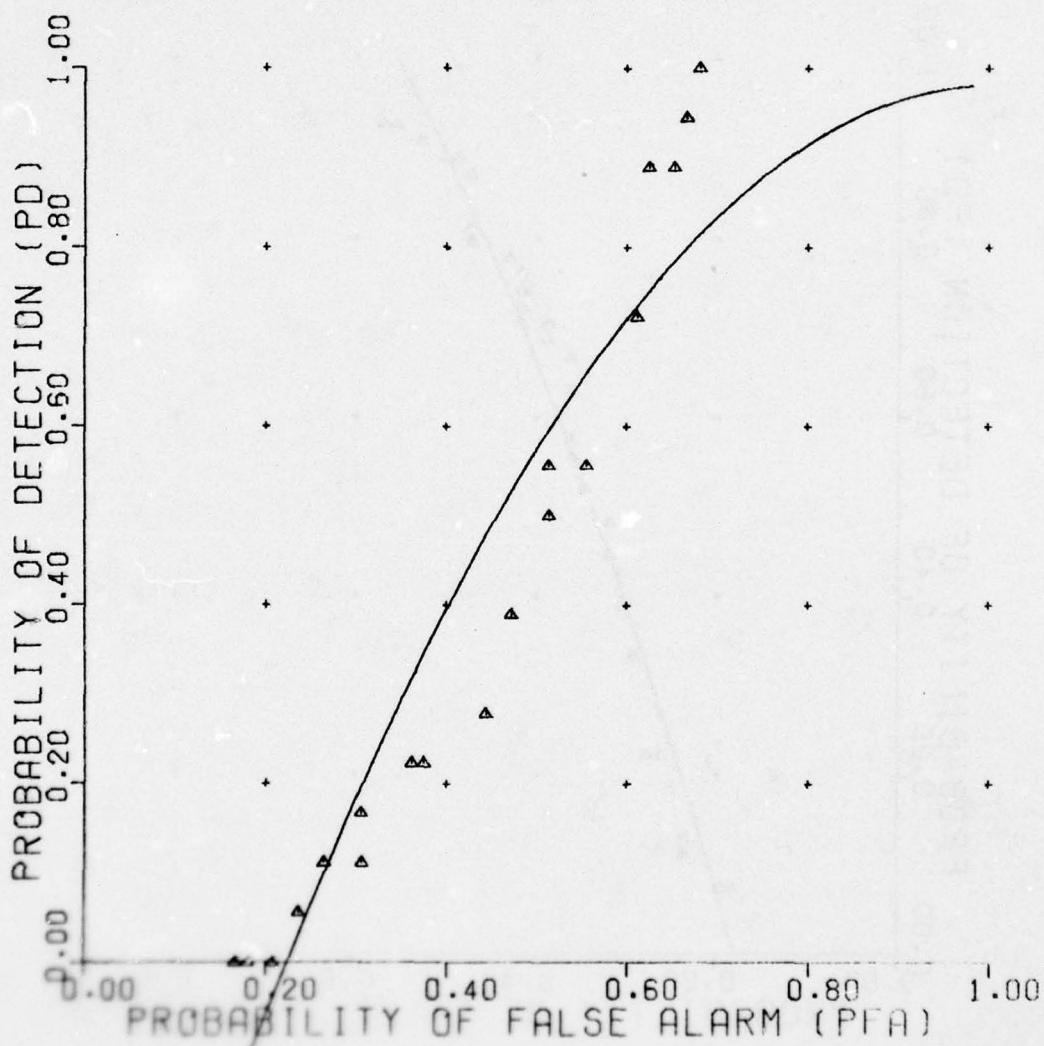


Figure C-85. Nearest neighbor classifier.

UNCLASSIFIED

UNCLASSIFIED

SPACE PARTITION CLASSIFIER
(QUADRATIC DISCRIMINANT)

INTUITIVE DATA

VERSION 2

REFERENCE 355

| NONMINE TARGET | PLATE TYPE C | ROCK(1) MINE | ROCK(2) TYPE A MINE | ROOT TYPE B MINE |
|-------------------|-----------------|-----------------|------------------------|---------------------|
| DEPTH | 3 | 6 | | |
| LOCATION | +4 | 0 | -4 | |
| MOISTURE | 7 | 17 | 12-20 | 13-16 |

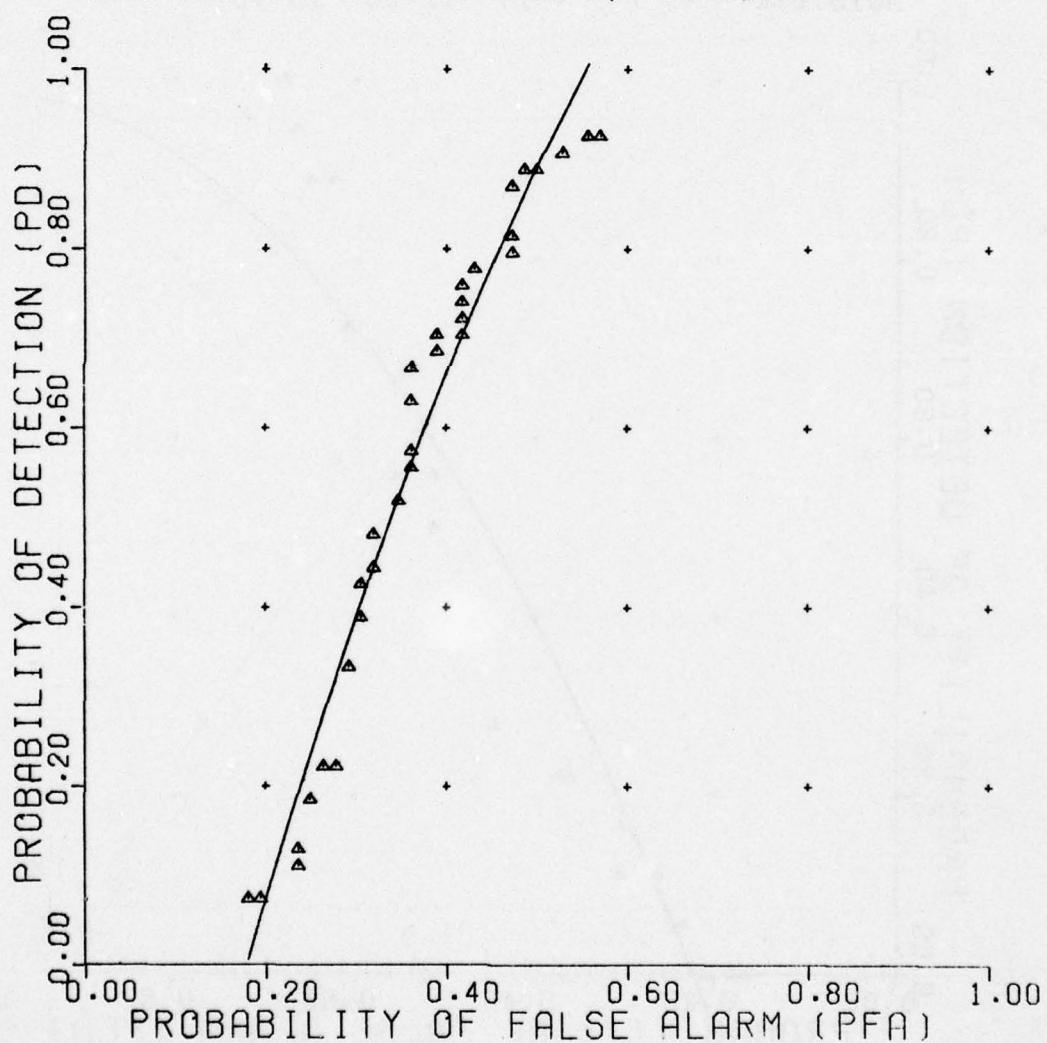


Figure C-86. Nearest neighbor classifier.

UNCLASSIFIED

UNCLASSIFIED

CROSS CORRELATION CLASSIFIER

PROBABILITY DEFINITION 1

VERSION 1

REFERENCE 210

| | |
|-------------------|---------------------------------|
| NONMINE TARGET | BACKGND TYPE A MINE |
| DEPTH | 3 6 |
| LOCATION | +4 0 -4 |
| MOISTURE | 7 17 12-20 13-16 |

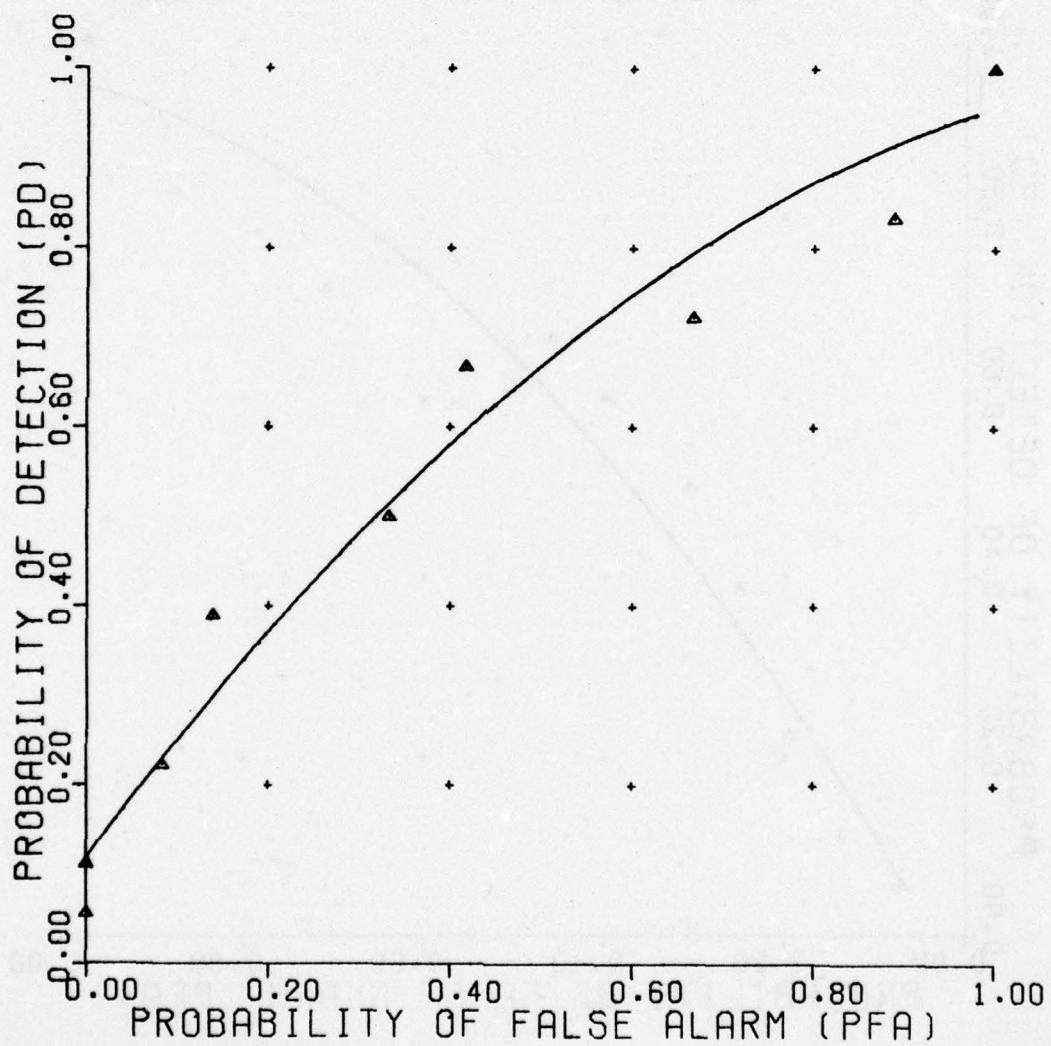


Figure C-87. Cross-correlation classifier.

UNCLASSIFIED

UNCLASSIFIED

CROSS CORRELATION CLASSIFIER

PROBABILITY DEFINITION 1

VERSION 1

REFERENCE 207

| NONMINE TARGET | PLATE TYPE A MINE | ROCK(1) | ROCK(2) | ROOT |
|-------------------|----------------------|---------|---------|-------|
| DEPTH | | 3 | 6 | |
| LOCATION | +4 | | 0 | -4 |
| MOISTURE | | 7 | 17 | 12-20 |
| | | | | 13-16 |

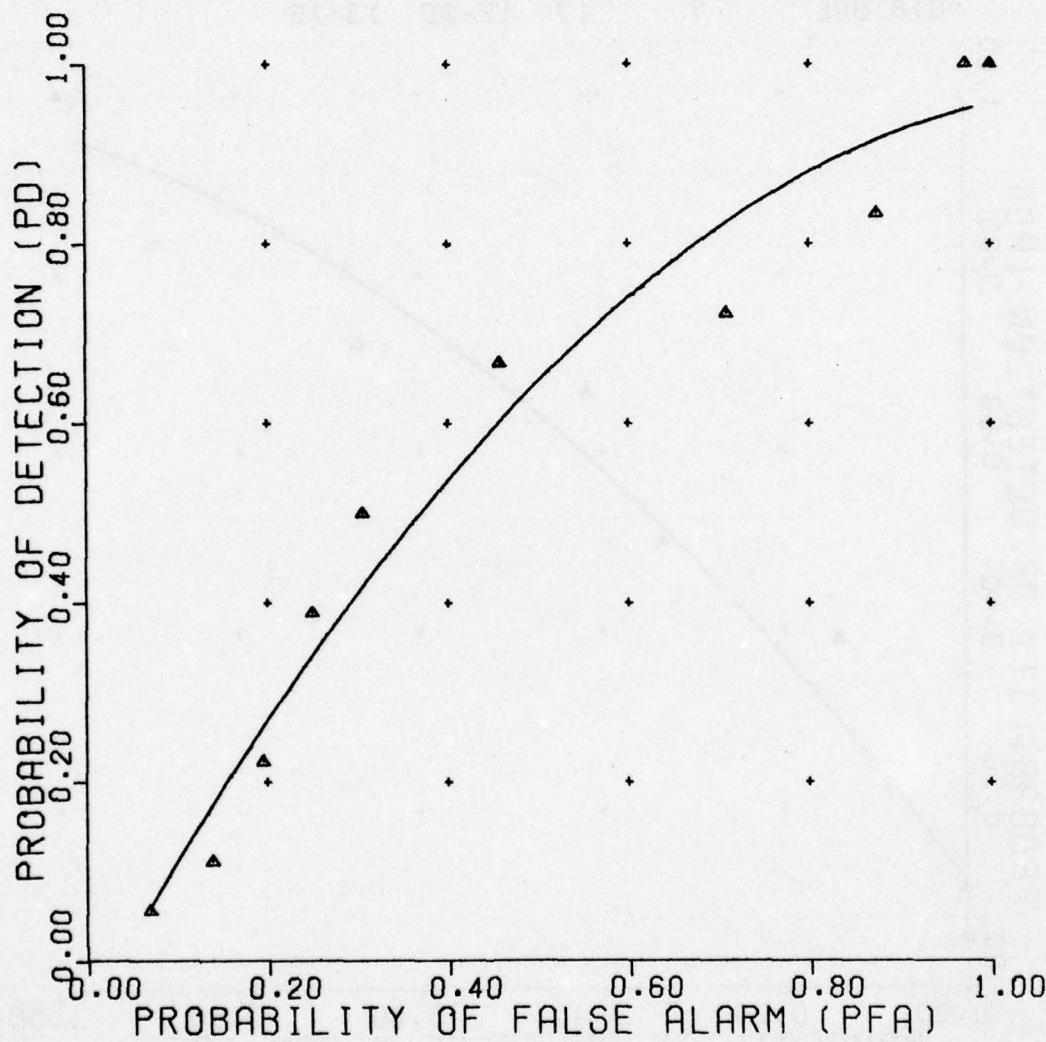


Figure C-88. Cross-correlation classifier.

UNCLASSIFIED

UNCLASSIFIED

CROSS CORRELATION CLASSIFIER

PROBABILITY DEFINITION 1

VERSION 1

REFERENCE 211

NONMINE BACKGND
TARGET TYPE B MINE

DEPTH 3 6
LOCATION +4 0 -4
MOISTURE 7 17 12-20 13-16

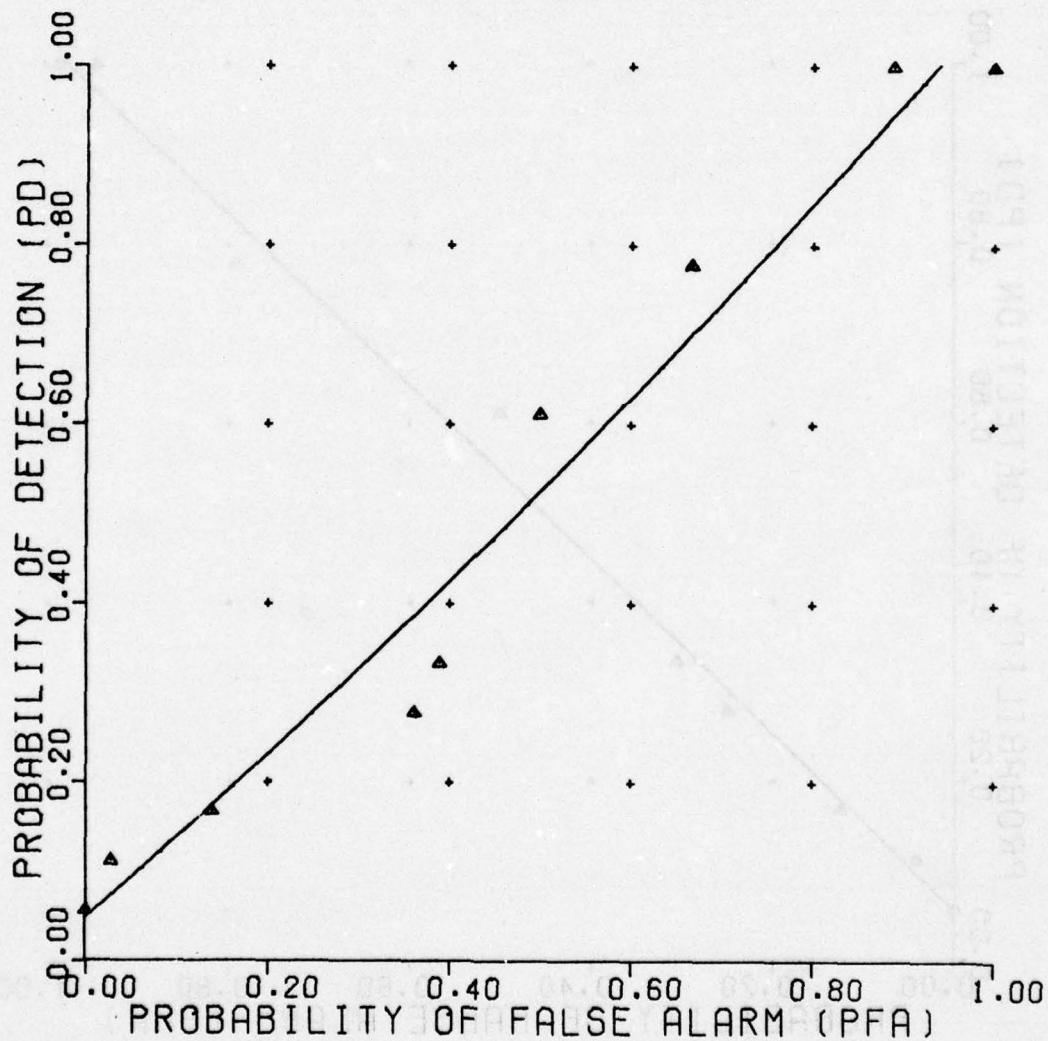


Figure C-89. Cross-correlation classifier.

UNCLASSIFIED

UNCLASSIFIED

CROSS CORRELATION CLASSIFIER

PROBABILITY DEFINITION 1

VERSION 1

REFERENCE 208

NONMINE PLATE ROCK(1) ROCK(2) ROOT
TARGET TYPE B MINE

DEPTH 3 6
LOCATION +4 0 -4
MOISTURE 7 17 12-20 13-16

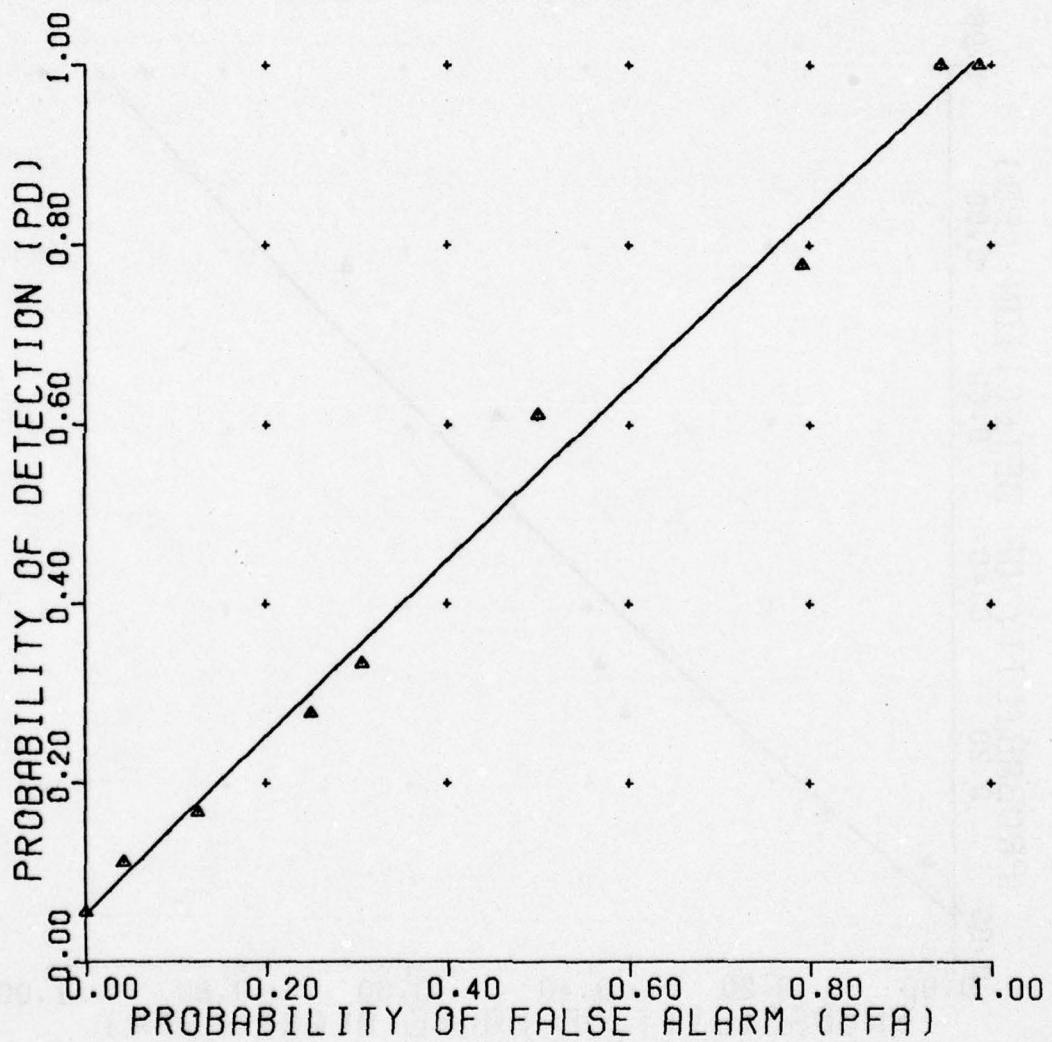


Figure C-90. Cross-correlation classifier.

UNCLASSIFIED

UNCLASSIFIED

CROSS CORRELATION CLASSIFIER

PROBABILITY DEFINITION 1

VERSION 1

REFERENCE 212

NONMINE BACKGND
TARGET TYPE C MINE

| | | | |
|----------|----|----|-------|
| DEPTH | 3 | 6 | |
| LOCATION | +4 | 0 | -4 |
| MOISTURE | 7 | 17 | 12-20 |
| | | | 13-16 |
| | | | 7 |

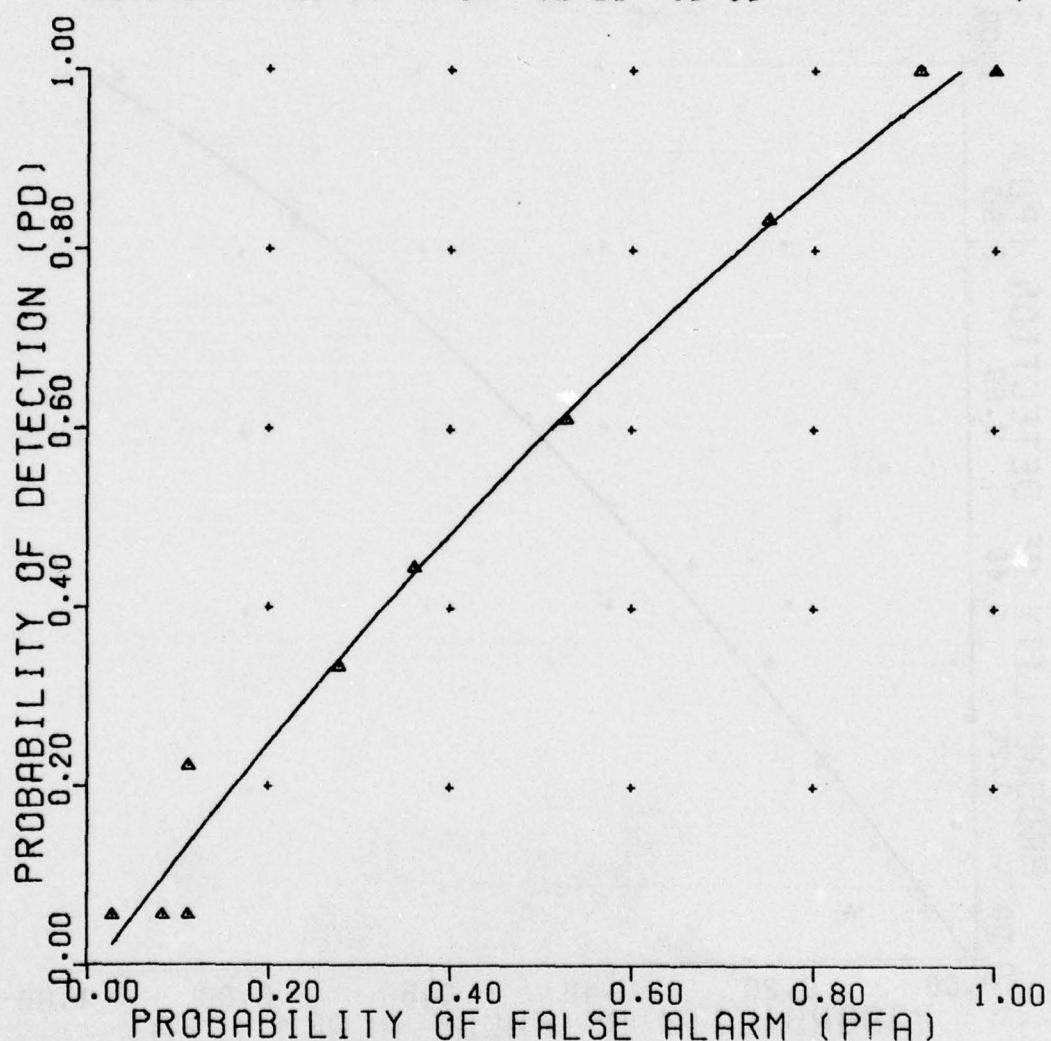


Figure C-91. Cross-correlation classifier.

UNCLASSIFIED

UNCLASSIFIED

CROSS CORRELATION CLASSIFIER

PROBABILITY DEFINITION 1

VERSION 1

REFERENCE 209

| NONMINE TARGET | PLATE | ROCK(1) | ROCK(2) | ROOT |
|-------------------|-------|---------|---------|-------|
| TYPE C MINE | | | | |
| DEPTH | 3 | 6 | | |
| LOCATION | +4 | 0 | -4 | |
| MOISTURE | 7 | 17 | 12-20 | 13-16 |

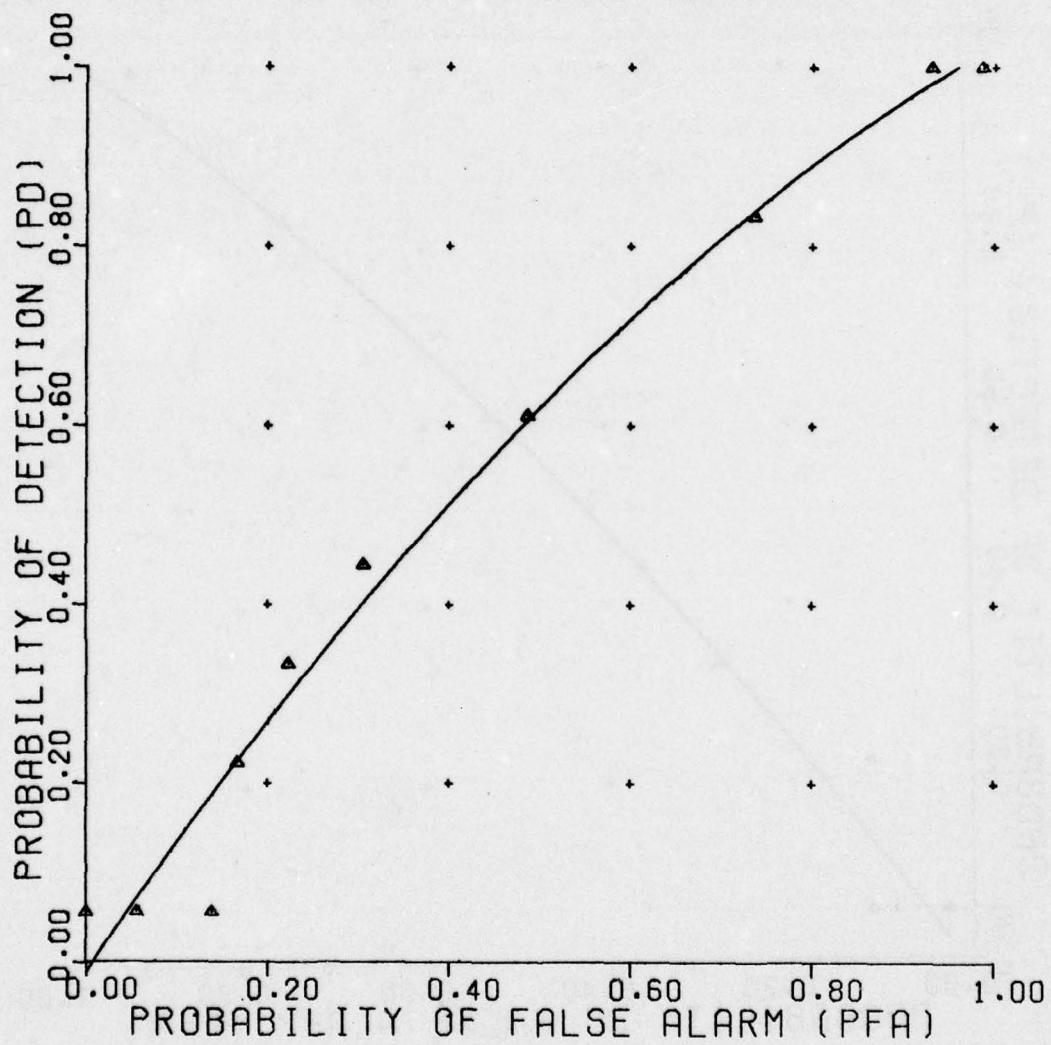


Figure C-92. Cross-correlation classifier.

UNCLASSIFIED

C-90

UNCLASSIFIED

IMPULSE CORRELATION CLASSIFIER

PROBABILITY DEFINITION 1

VERSION 1

REFERENCE 204

**NONMINE BACKGND
TARGET TYPE A MINE**

**DEPTH 3 6
LOCATION +4 0 -4
MOISTURE 7 17 12-20 13-16**

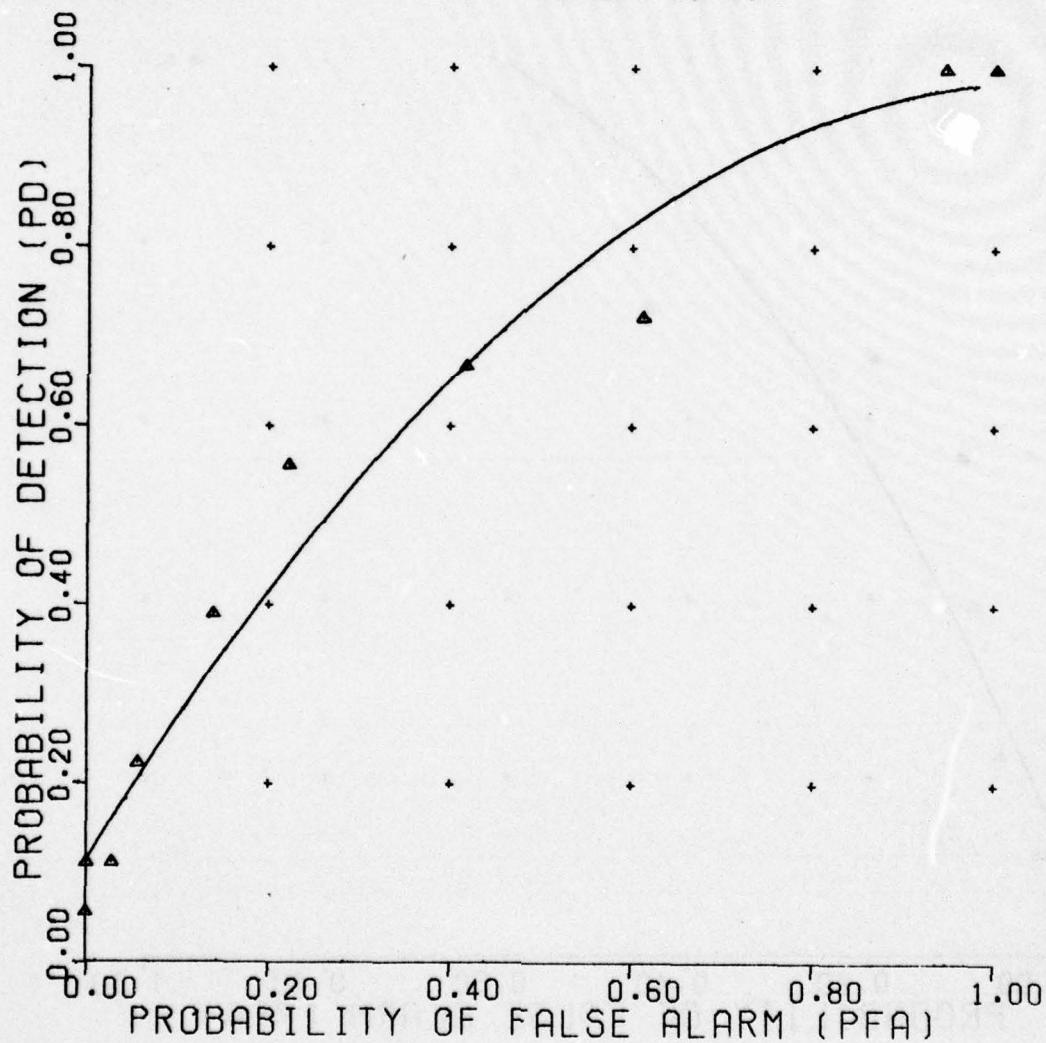


Figure C-93. Cross-correlation classifier.

UNCLASSIFIED

UNCLASSIFIED

IMPULSE CORRELATION CLASSIFIER

PROBABILITY DEFINITION 1

VERSION 1

REFERENCE 201

| NONMINE TARGET | PLATE TYPE A MINE | ROCK(1) | ROCK(2) | ROOT |
|-------------------|----------------------|---------|---------|-------|
| DEPTH | | 3 | 6 | |
| LOCATION | | +4 | 0 | -4 |
| MOISTURE | | 7 | 17 | 12-20 |
| | | | | 13-16 |

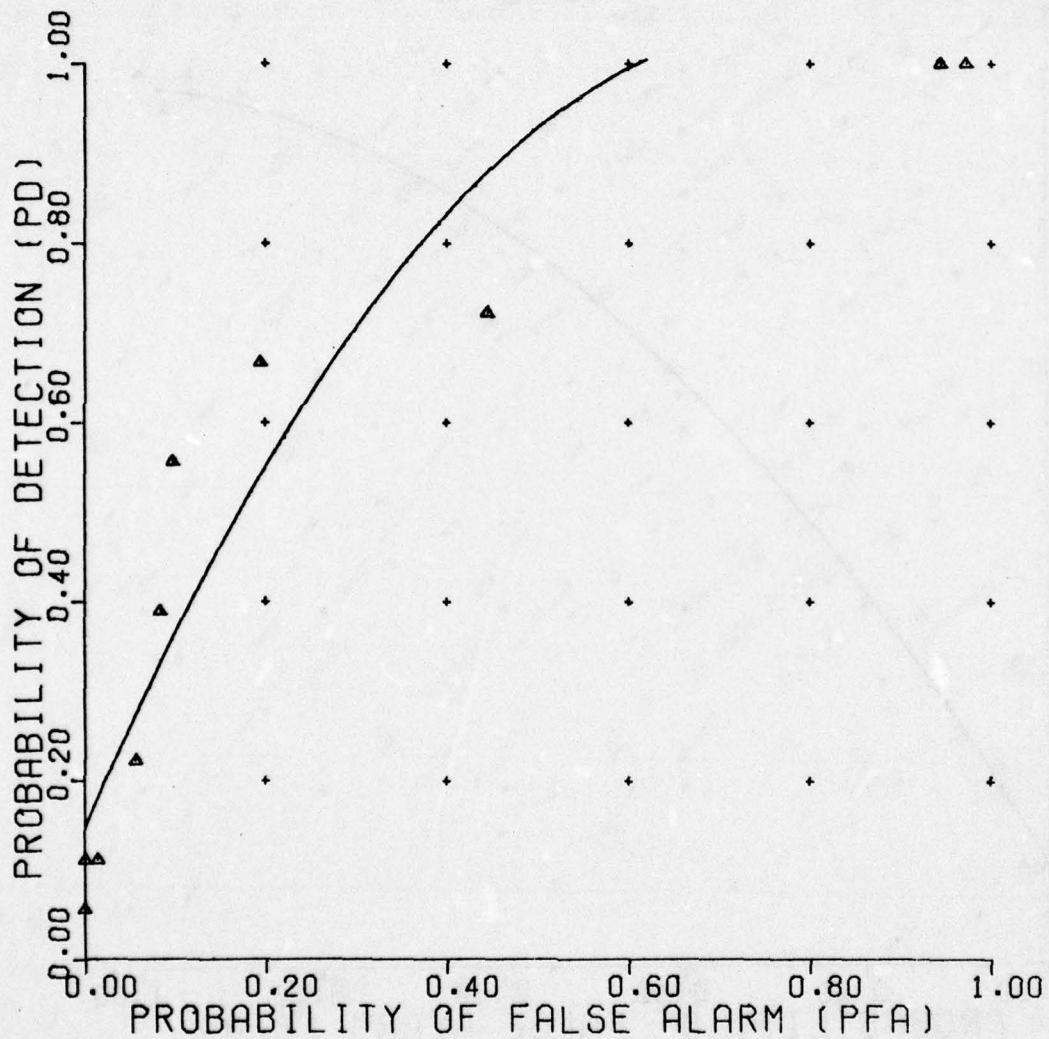


Figure C-94. Cross-correlation classifier.

UNCLASSIFIED

C-92

UNCLASSIFIED

IMPULSE CORRELATION CLASSIFIER

PROBABILITY DEFINITION 1

VERSION 1

REFERENCE 205

| | |
|----------|---|
| NONMINE | BACKGND |
| TARGET | TYPE B MINE |
| DEPTH | 3 6 |
| LOCATION | +4 0 -4 |
| MOISTURE | 7 17 12-20 13-16 |

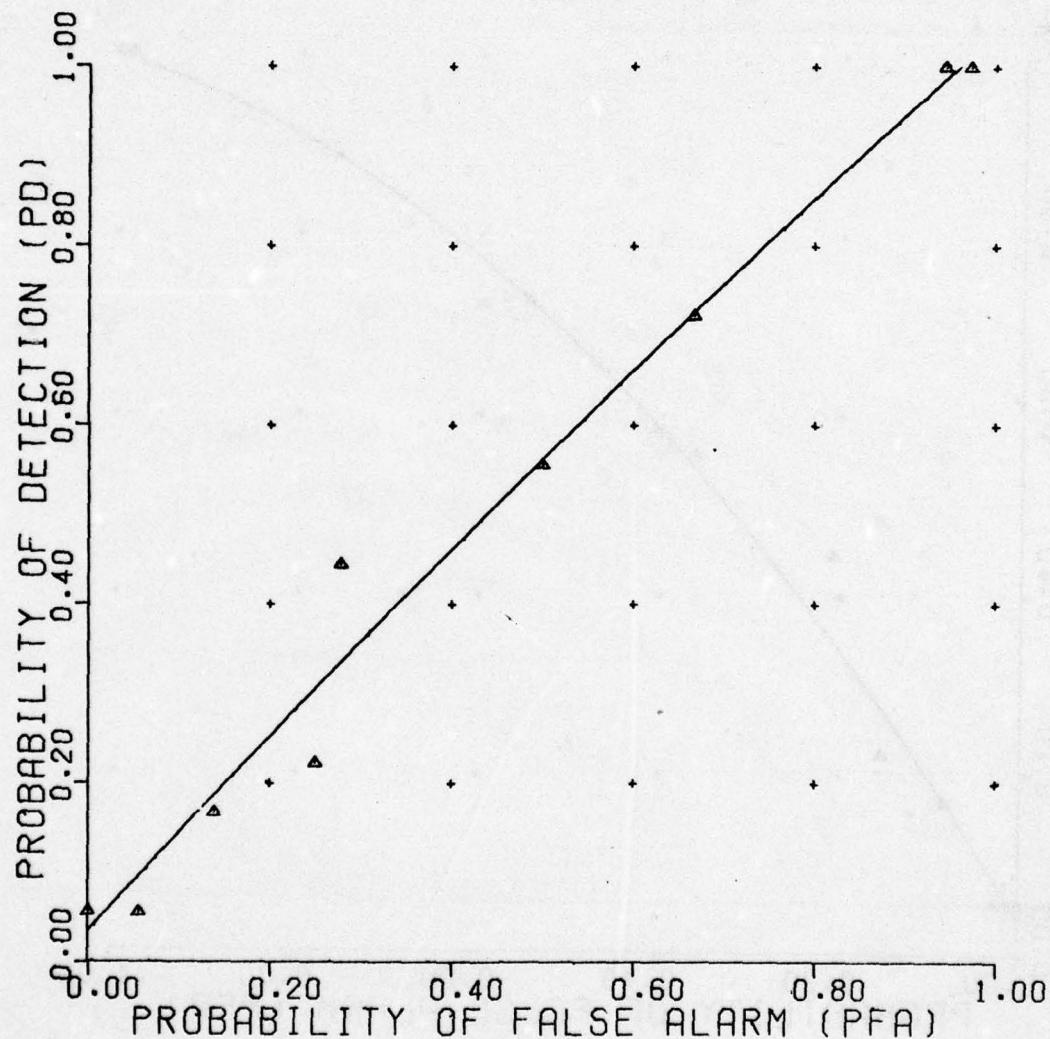


Figure C-95. Cross-correlation classifier.

UNCLASSIFIED

UNCLASSIFIED

IMPULSE CORRELATION CLASSIFIER

PROBABILITY DEFINITION 1
VERSION 1
REFERENCE 202

| | | | | |
|----------|-------------|---------|---------|-------|
| NONMINE | PLATE | ROCK(1) | ROCK(2) | ROOT |
| TARGET | TYPE B MINE | | | |
| DEPTH | 3 | 6 | | |
| LOCATION | +4 | 0 | -4 | |
| MOISTURE | 7 | 17 | 12-20 | 13-16 |

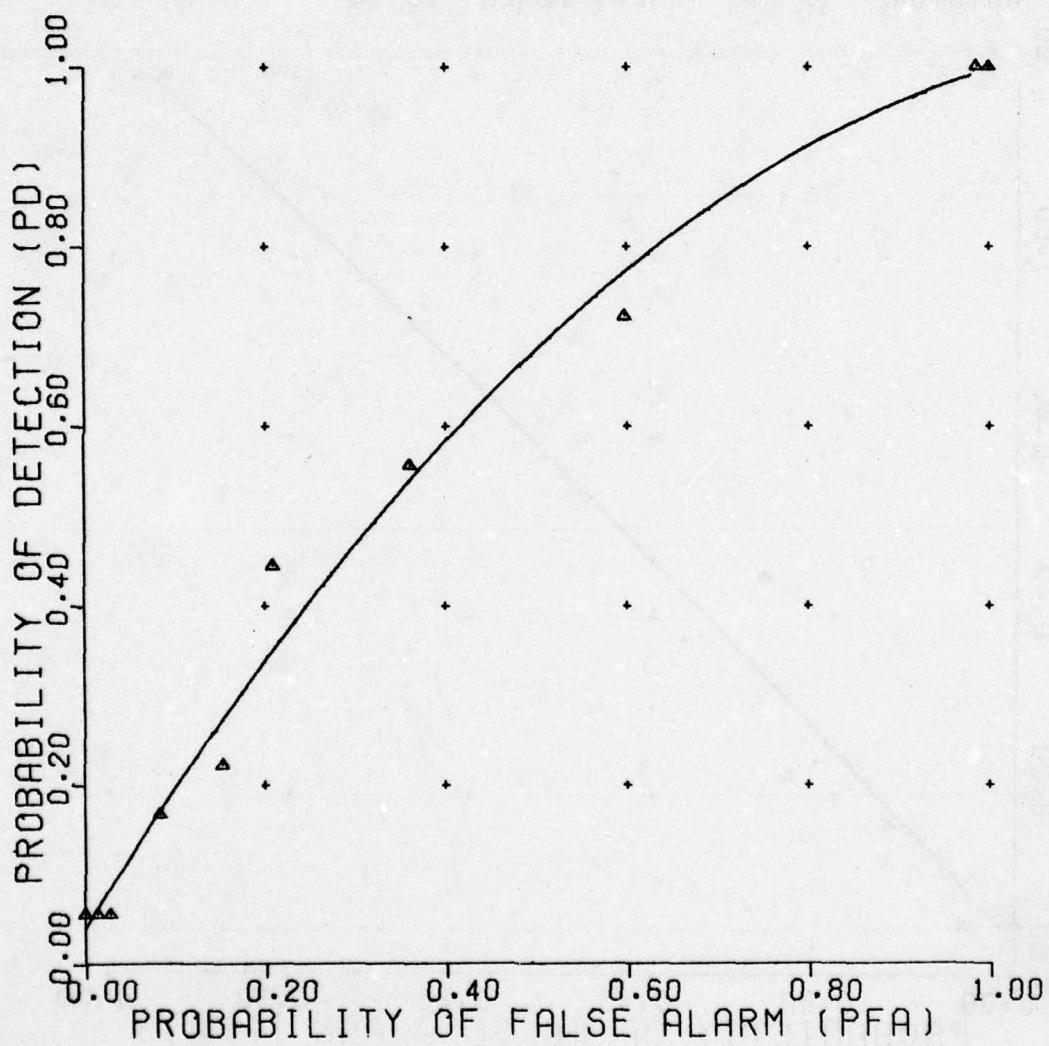


Figure C-96. Cross-correlation classifier.

UNCLASSIFIED

C-94

UNCLASSIFIED

IMPULSE CORRELATION CLASSIFIER

PROBABILITY DEFINITION 1

VERSION 1

REFERENCE 206

NONMINE BACKGND
TARGET TYPE C MINE

DEPTH 3 6
LOCATION +4 0 -4
MOISTURE 7 17 12-20 13-16

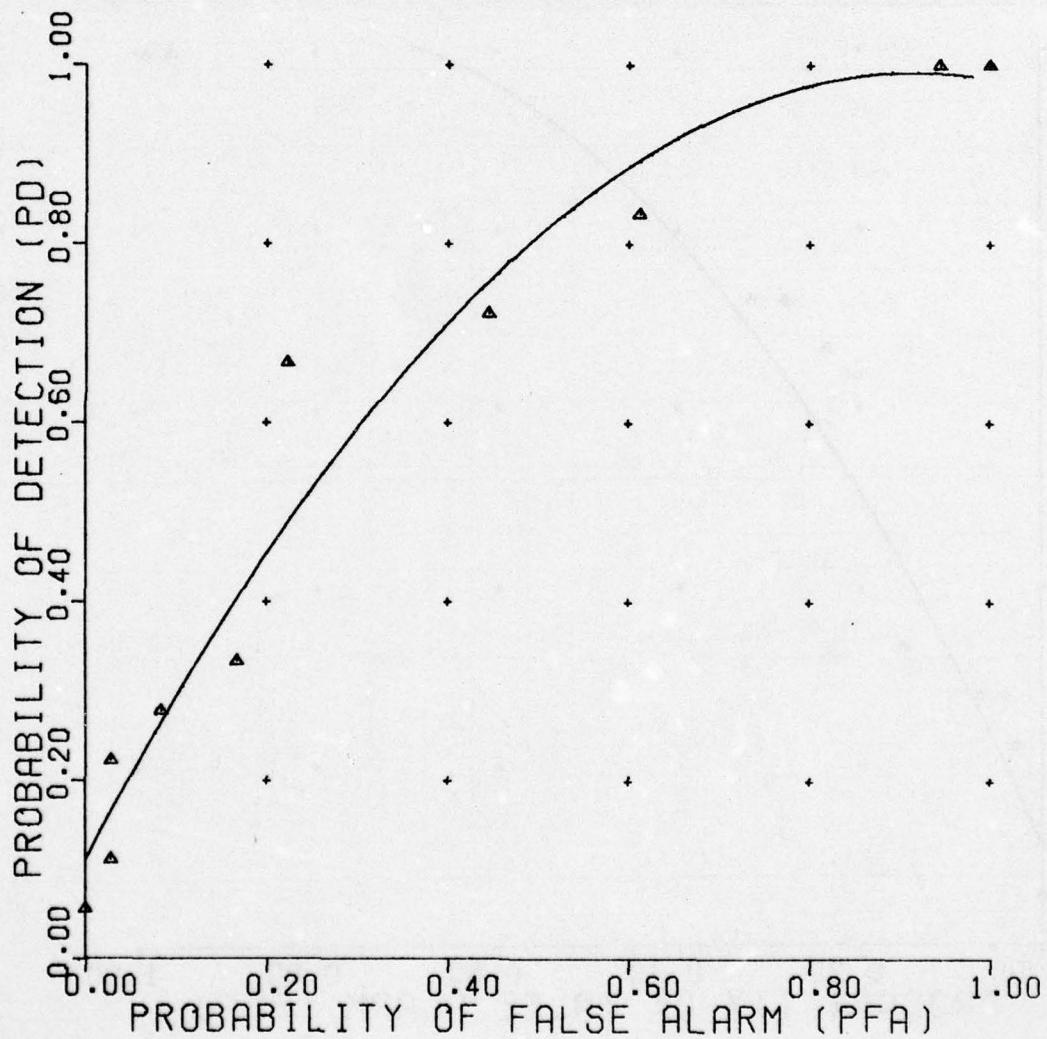


Figure C-97. Cross-correlation classifier.

UNCLASSIFIED

C-95

UNCLASSIFIED

IMPULSE CORRELATION CLASSIFIER

PROBABILITY DEFINITION 1

VERSION 1

REFERENCE 203

| NONMINE TARGET | PLATE | ROCK(1) | ROCK(2) | ROOT |
|-------------------|-------|---------|---------|------|
| | | | | |
| TYPE C MINE | | | | |

| | | | | |
|----------|----|----|-------|-------|
| DEPTH | 3 | 6 | | |
| LOCATION | +4 | 0 | -4 | |
| MOISTURE | 7 | 17 | 12-20 | 13-16 |

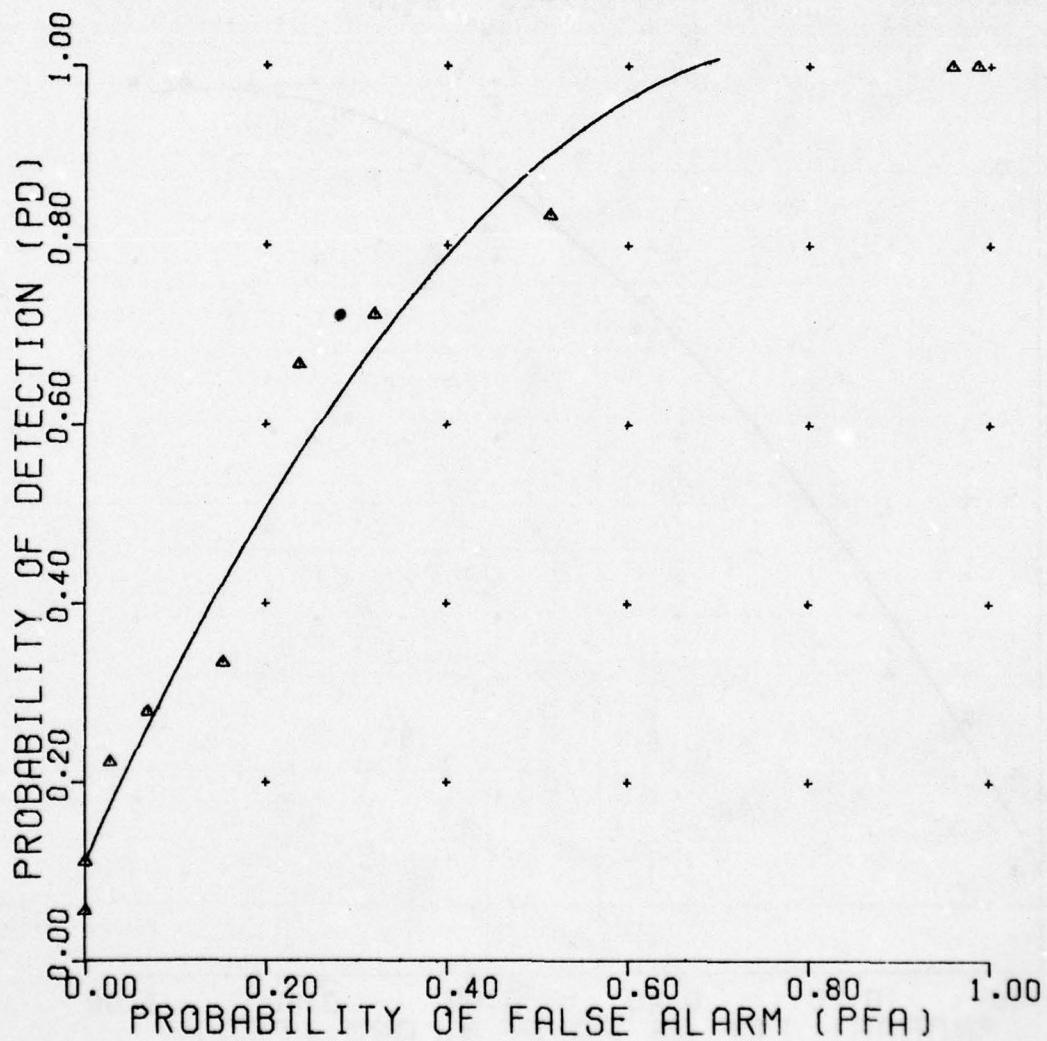


Figure C-98. Cross-correlation classifier.

UNCLASSIFIED

C-96

AD-A054 427

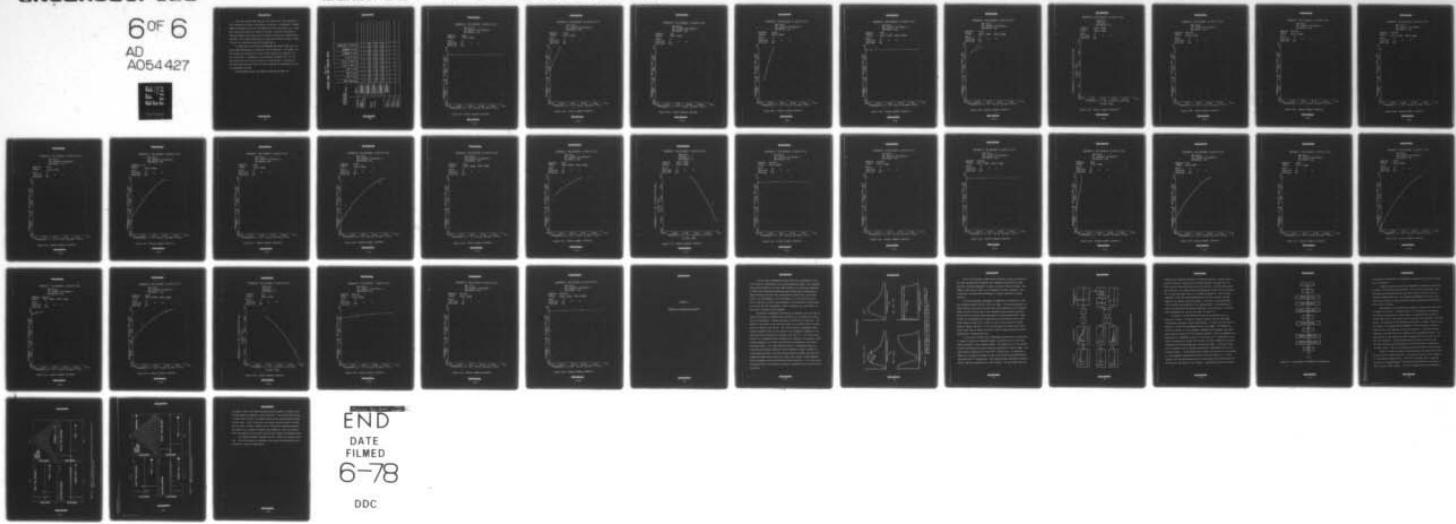
GEORGIA INST OF TECH ATLANTA ENGINEERING EXPERIMENT --ETC F/G 17/9
RADAR DETECTION, DISCRIMINATION, AND CLASSIFICATION OF BURIED N--ETC(U)
FEB 78 J D ECHARD, J A SCHEER, E O RAUSCH DAAG53-76-C-0112

UNCLASSIFIED

EES/GIT-A-1828-F-VOL-1

NL

6 OF 6
AD
A054427



END
DATE
FILED
6-78
DDC

UNCLASSIFIED

Also, short-pulse radar data was only taken in dry soil comparable to the 7% moisture soil used in the NBS data collection. In addition, a limited number of non-mine objects were included in the data collection--e.g., a rock and a metal plate buried six inches in dry soil. Soil-only data where no mine-like objects were present were also used to exercise the classification algorithm. The various combinations of mines and non-mines analyzed is shown in Table C-3, Short-Pulse Radar Performance Matrix.

It should also be noted that the MERADCOM short-pulse radar data contained fewer measurements or signatures than the NBS data. For example, the short-pulse data consisted of 12 type C mine signatures as compared to 18 for the NBS data. Consequently, the statistical confidence level for the short-pulse data is not quite as good as for the NBS data. Nevertheless, the short-pulse data does allow a relative comparison of performance for the two measurement systems.

The performance curves are numbered Figures 99 through 128.

UNCLASSIFIED

TABLE C-3
MERADCOM RADAR DATA PROCESSING MATRIX

| | | TYPE OF DATA | | | | | | | | | | | | | | | | | | | | | | | | | | | |
|------------|----------|------------------------------|---|---|---------|-----------------------|----------|-----------------|-------------------|---------------------|--------------------|------------------|------------------|-----------------|------------------|------------------|--------------------|-------------------|-----------------------|-----------------------|--------------------------|---------------------|-----------------------|-----------------------|-----------------------|-------|--|-------|--|
| | | INTUITIVE OBSERVABLES | | | | | RAW DATA | | | | | | | | | | | | | | | | | | | | | | |
| CLASSIFIER | | FISHER'S LINEAR DISCRIMINANT | | 3 | | INTUITIVE OBSERVABLES | | RAW DATA | | C-99 | | C-100 | | C-101 | | C-102 | | C-103 | | C-104 | | C-105 | | C-106 | | C-107 | | C-108 | |
| NEAREST | NEIGHBOR | 3 | 5 | 7 | NEAREST | NEIGHBOR | 7 | SPACE PARTITION | CROSS CORRELATION | IMPULSE CORRELATION | ALL MINES VS. ROCK | TYPE A VS. PLATE | TYPE C VS. PLATE | TYPE C VS. ROCK | TYPE A VS. PLATE | TYPE C VS. PLATE | ALL MINES VS. ROCK | TYPE A VS. TYPE C | TYPE A VS. BACKGROUND | TYPE C VS. BACKGROUND | ALL MINES VS. BACKGROUND | ALL MINES VS. PLATE | TYPE A VS. BACKGROUND | TYPE C VS. BACKGROUND | TYPE A VS. BACKGROUND | | | | |

UNCLASSIFIED

C-98

UNCLASSIFIED

NEAREST NEIGHBOR CLASSIFIER

RAW DATA

NO. NEAREST NEIGHBORS 3

REFERENCE 422

NONMINE
TARGET

ROCK
TYPE A MINE

DEPTH

6

LOCATION

+4

0

-4

MOISTURE

DRY

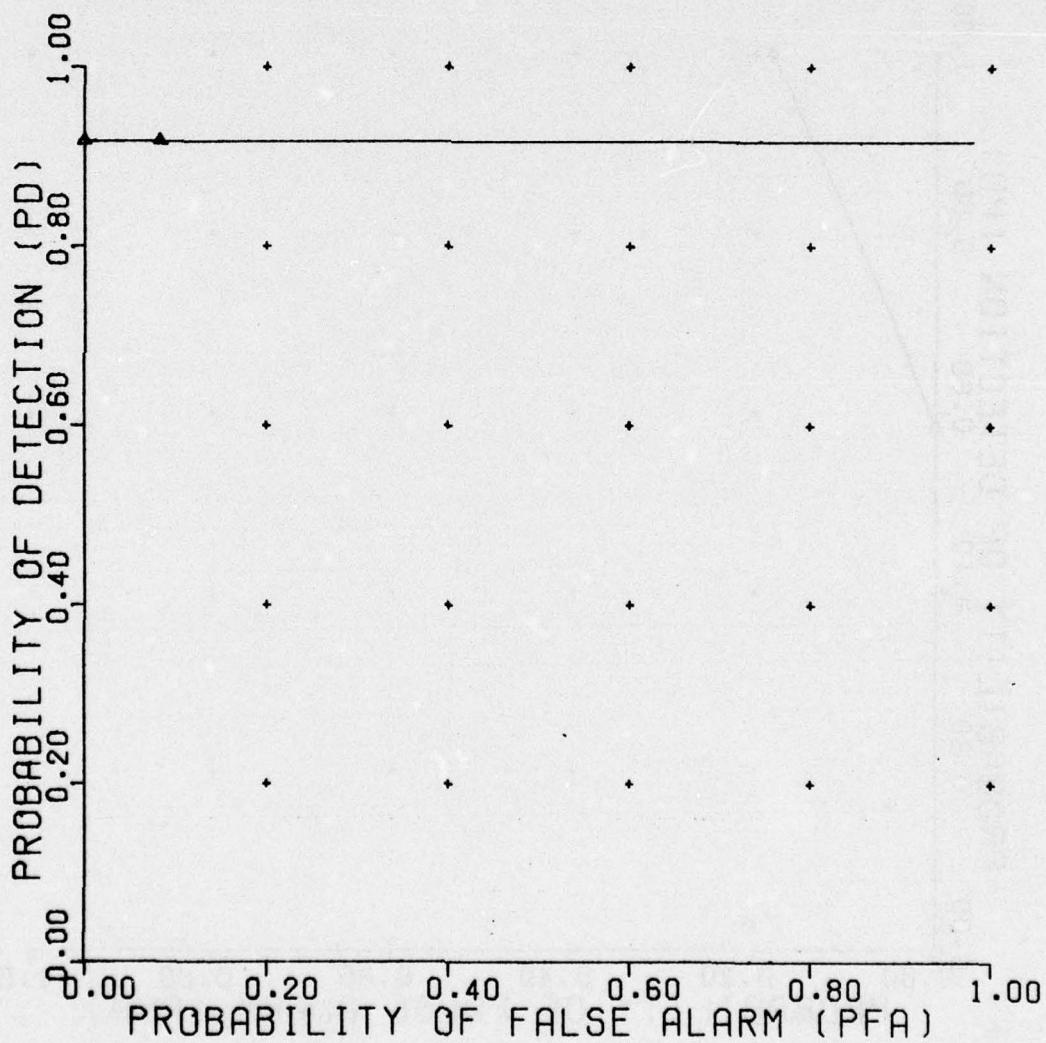


Figure C-99. Nearest neighbor classifier.

UNCLASSIFIED

UNCLASSIFIED

NEAREST NEIGHBOR CLASSIFIER

RAW DATA

NO. NEAREST NEIGHBORS 3

REFERENCE 425

| | |
|-------------------|-------------------|
| NONMINE TARGET | PLATE |
| DEPTH | 6 |
| LOCATION | +4 0 -4 |
| MOISTURE | DRY |

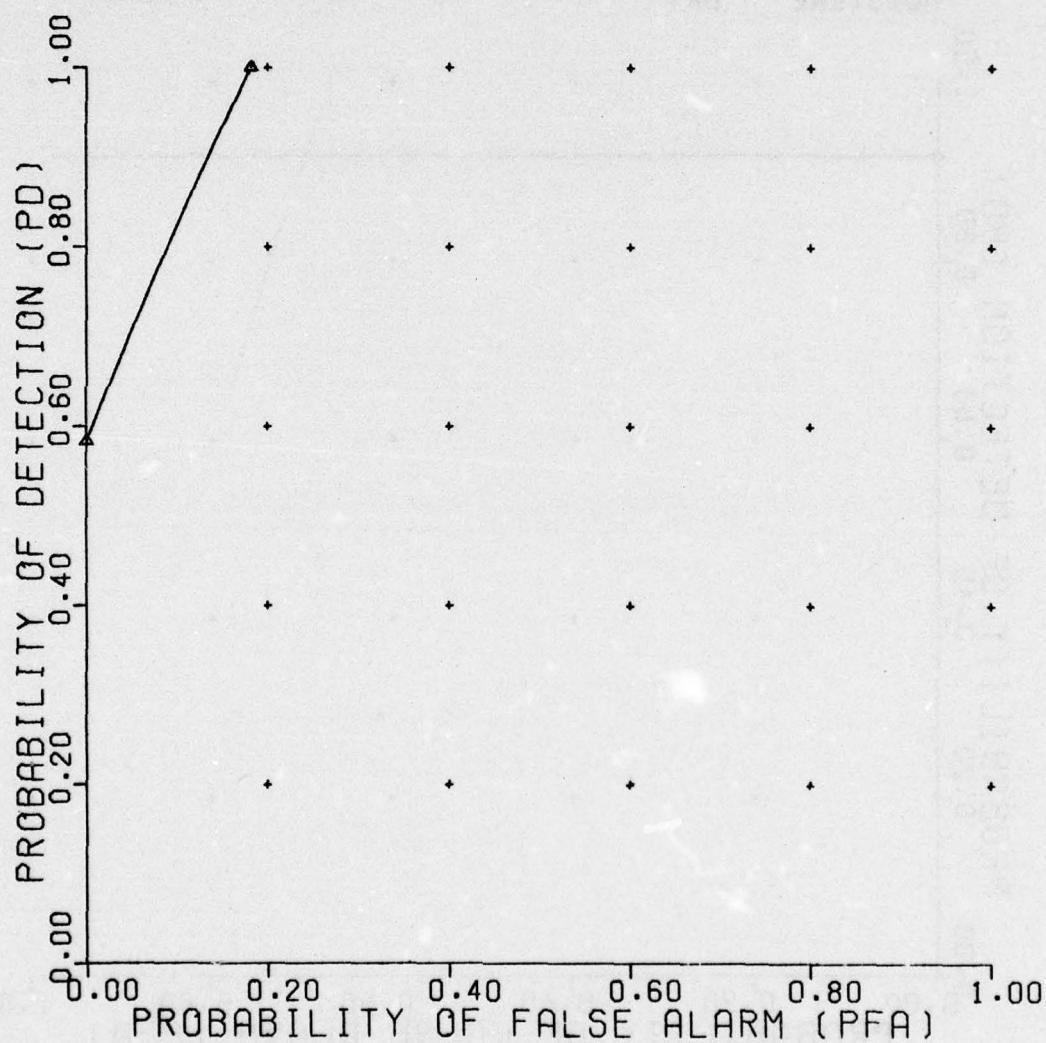


Figure C-100. Nearest neighbor classifier.

UNCLASSIFIED

UNCLASSIFIED

NEAREST NEIGHBOR CLASSIFIER

RAW DATA

NO. NEAREST NEIGHBORS 3

REFERENCE 428

| | |
|----------|-------------------|
| NONMINE | ROCK |
| TARGET | TYPE C MINE |
| DEPTH | 6 |
| LOCATION | +4 0 -4 |
| MOISTURE | DRY |

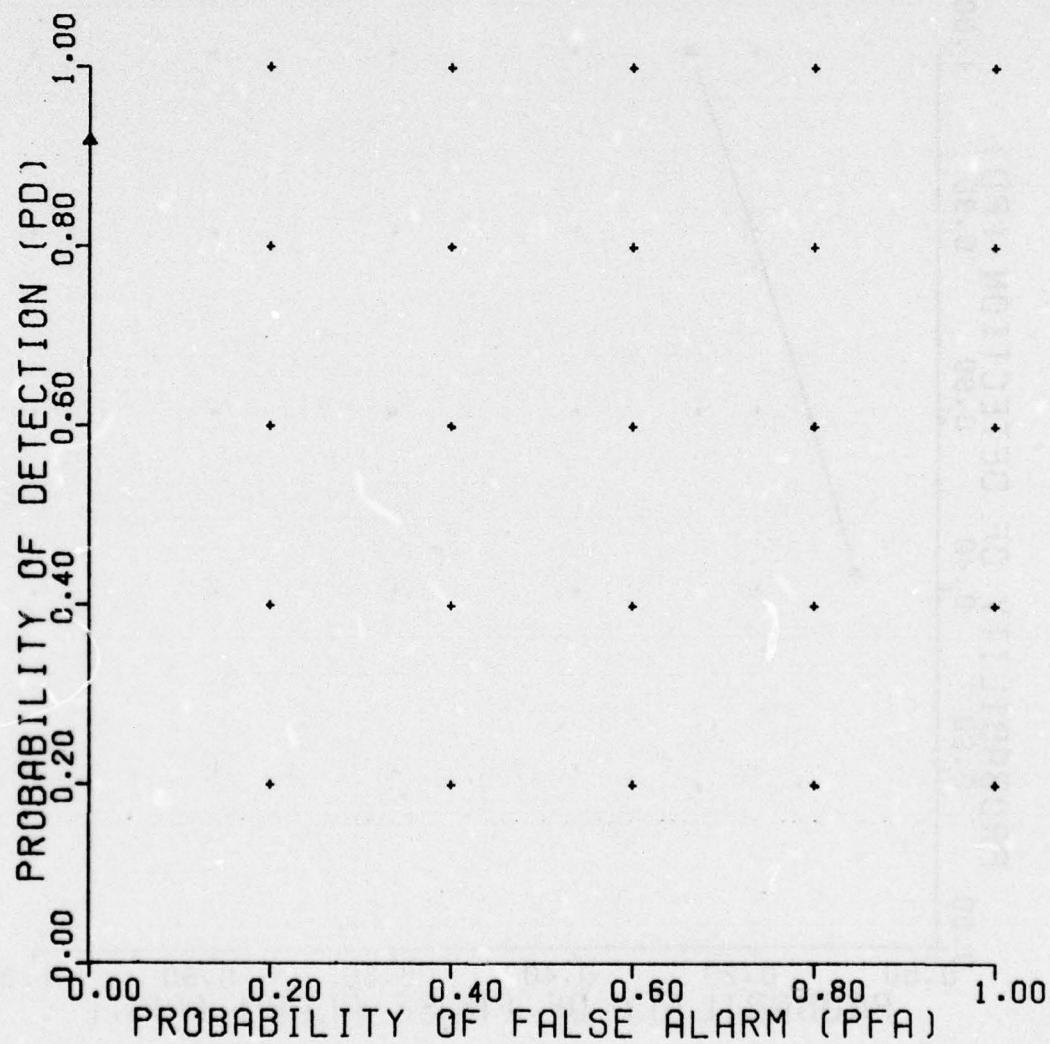


Figure C-101. Nearest neighbor classifier.

UNCLASSIFIED

UNCLASSIFIED

NEAREST NEIGHBOR CLASSIFIER

RAW DATA

NO. NEAREST NEIGHBORS 3

REFERENCE 431

| | |
|-------------------|----------------------|
| NONMINE TARGET | PLATE TYPE C MINE |
| DEPTH | 6 |
| LOCATION | +4 0 -4 |
| MOISTURE | DRY |

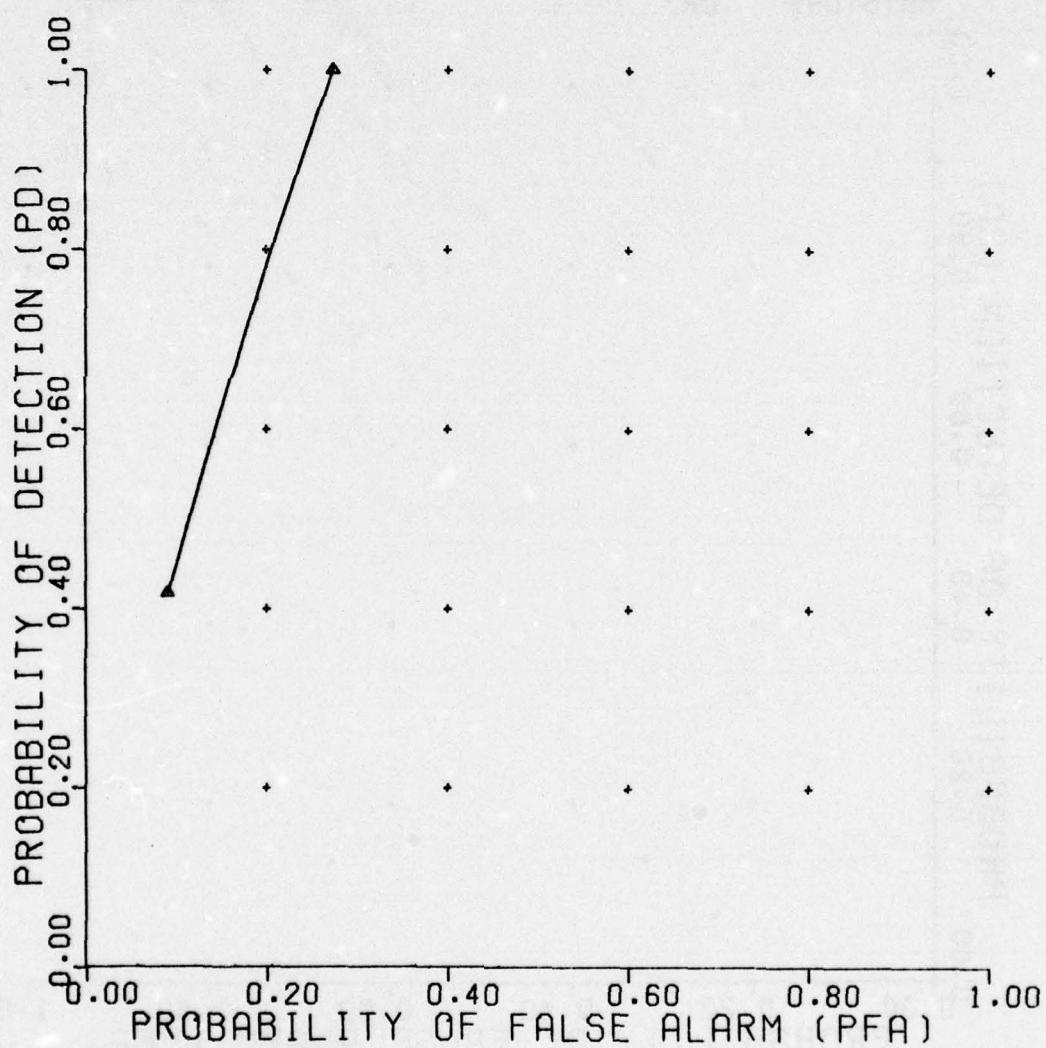


Figure C-102. Nearest neighbor classifier.

UNCLASSIFIED

UNCLASSIFIED

NEAREST NEIGHBOR CLASSIFIER

RAW DATA

NO. NEAREST NEIGHBORS 3

REFERENCE 434

NONMINE

ROCK

TARGET

TYPE C MINE TYPE A MINE

DEPTH

6

LOCATION

0

MOISTURE

-4

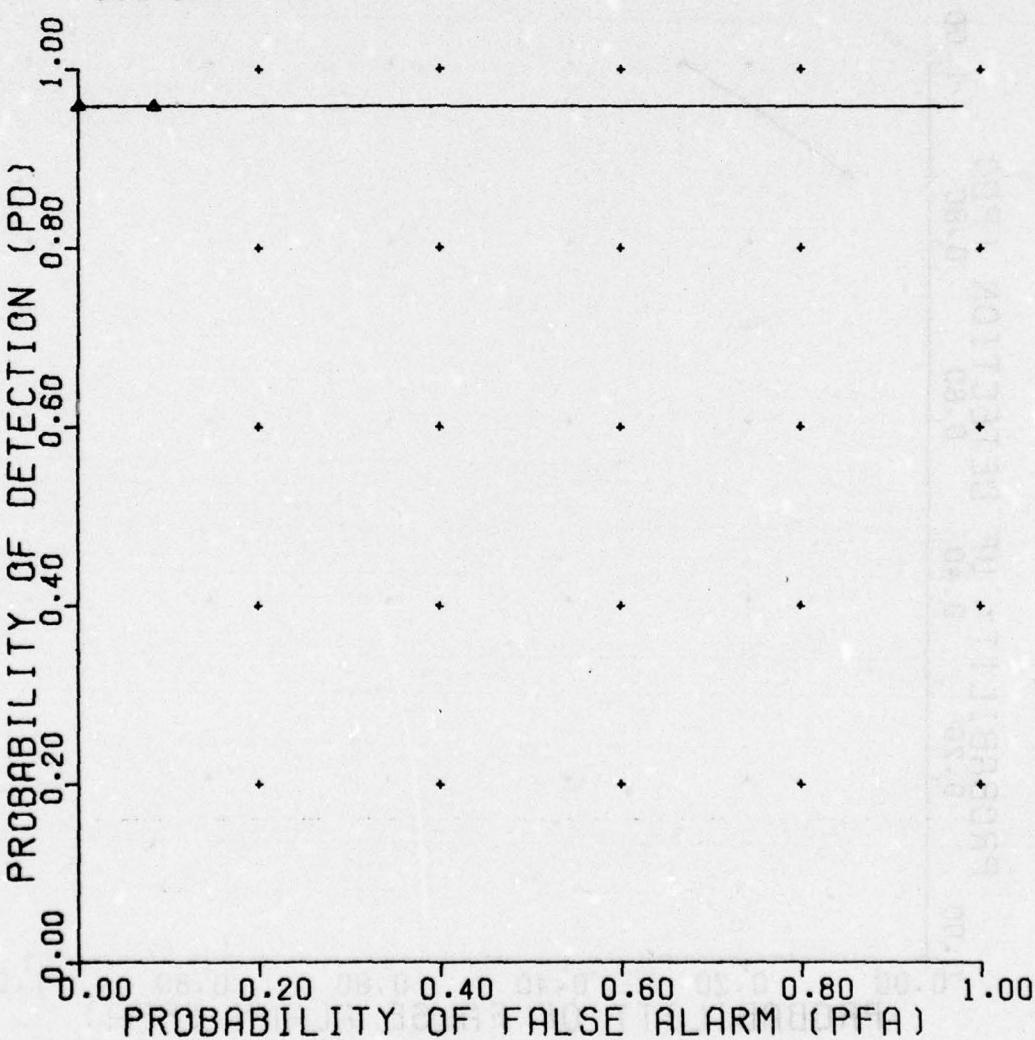


Figure C-103. Nearest neighbor classifier.

UNCLASSIFIED

UNCLASSIFIED

NEAREST NEIGHBOR CLASSIFIER

RAW DATA
NO. NEAREST NEIGHBORS 3
REFERENCE 437

| NONMINE TARGET | PLATE TYPE C MINE | TYPE A MINE |
|-------------------|----------------------|-------------|
| DEPTH | 6 | |
| LOCATION | +4 | 0 |
| MOISTURE | DRY | -4 |

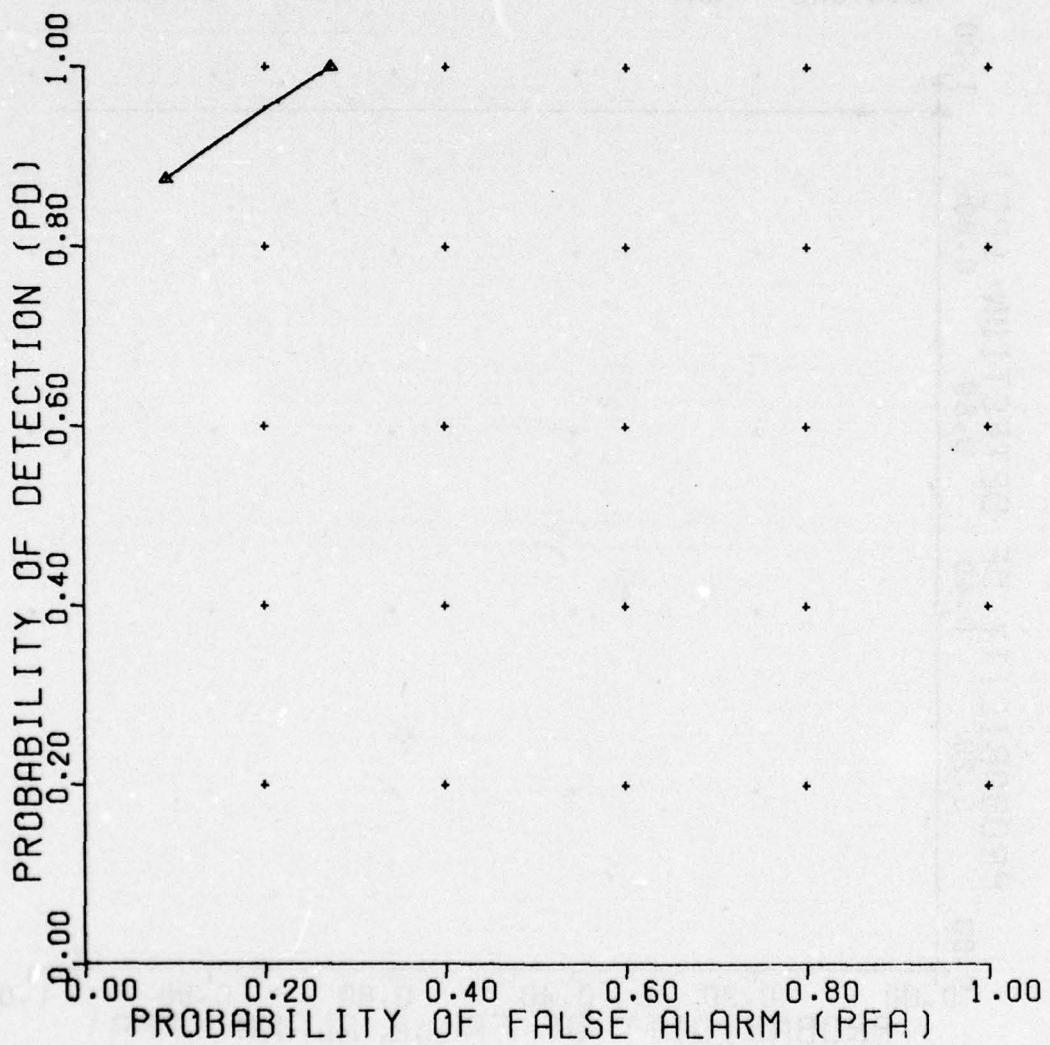


Figure C-104. Nearest neighbor classifier.

UNCLASSIFIED

UNCLASSIFIED

NEAREST NEIGHBOR CLASSIFIER

RAW DATA
VERSION 3
REFERENCE 440

| | |
|----------|-------------------|
| TARGET2 | TYPE C MINE |
| TARGET1 | TYPE A MINE |
| DEPTH | 6 |
| LOCATION | +4 0 -4 |
| MOISTURE | DRY |

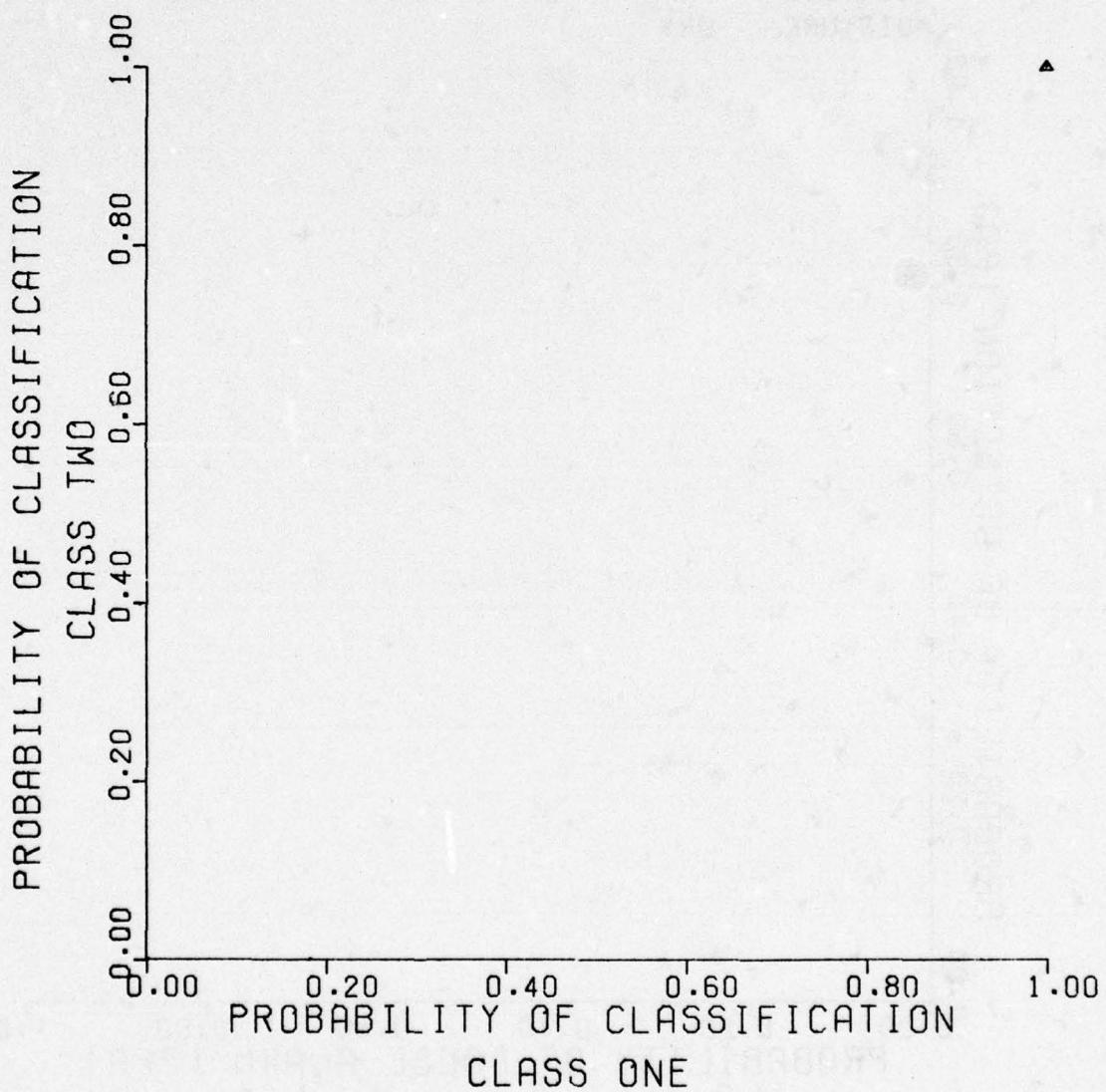


Figure C-105. Nearest neighbor classifier.

UNCLASSIFIED

UNCLASSIFIED

NEAREST NEIGHBOR CLASSIFIER

RAW DATA
NO. NEAREST NEIGHBORS 3
REFERENCE 462

NONMINE BACKGND
TARGET TYPE A MINE

DEPTH 6
LOCATION +4 0 -4
MOISTURE DRY

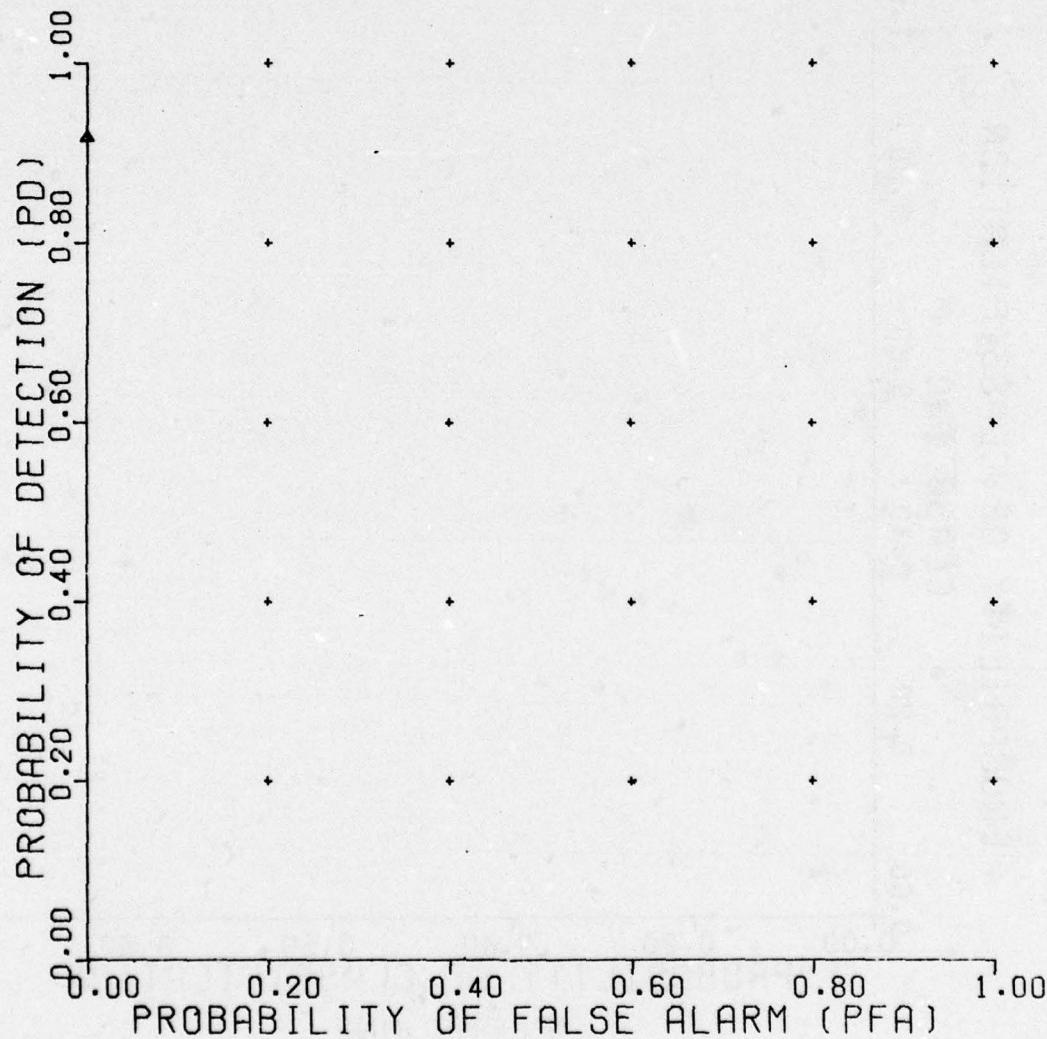


Figure C-106. Nearest neighbor classifier.

UNCLASSIFIED

UNCLASSIFIED

NEAREST NEIGHBOR CLASSIFIER

RAW DATA

NO. NEAREST NEIGHBORS 3

REFERENCE 465

NONMINE BACKGND
TARGET TYPE C MINE
DEPTH 6
LOCATION +4 0 -4
MOISTURE DRY

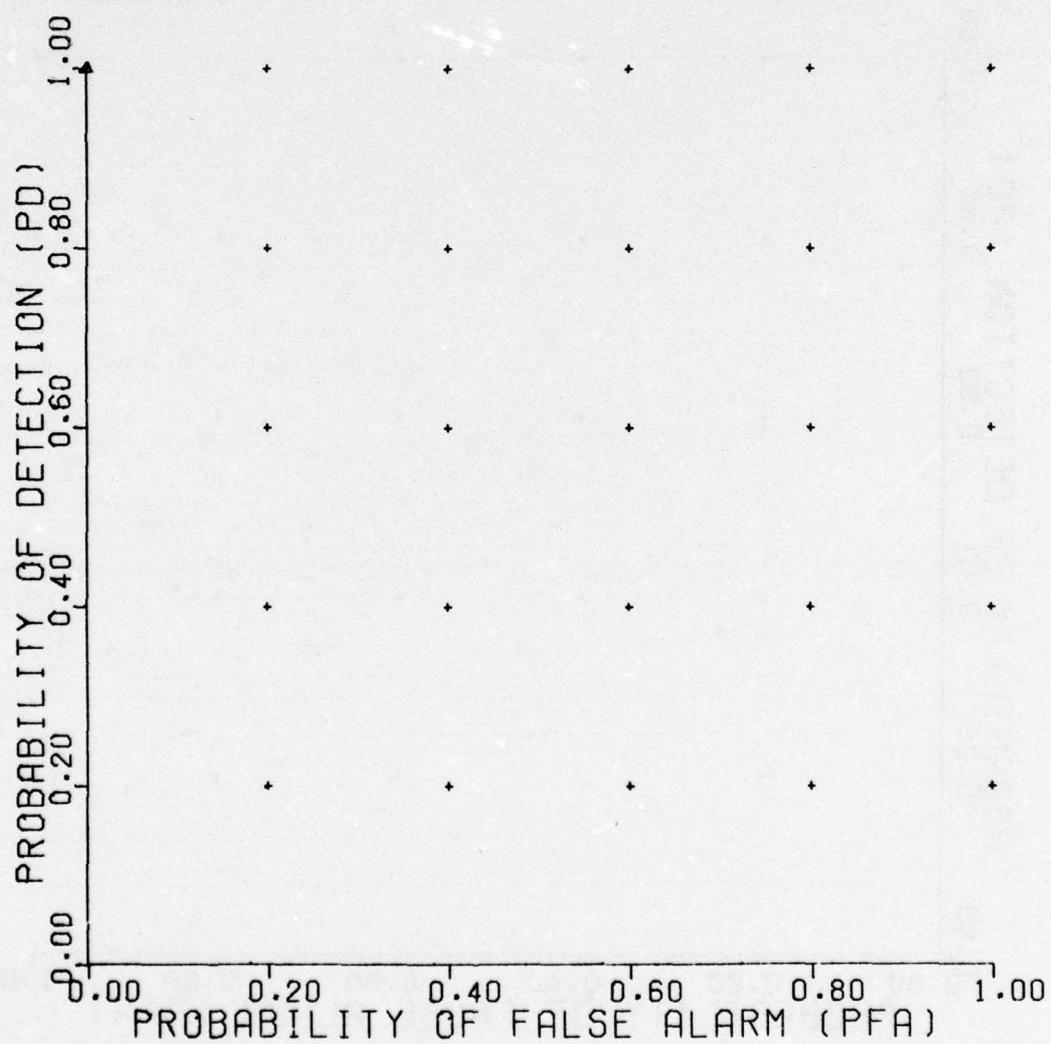


Figure C-107. Nearest neighbor classifier.

UNCLASSIFIED

UNCLASSIFIED

NEAREST NEIGHBOR CLASSIFIER

RAW DATA
NO. NEAREST NEIGHBORS 3
REFERENCE 468

| NONMINE | BACKGND |
|----------|----------------------------|
| TARGET | TYPE C MINE TYPE A MINE |
| DEPTH | 6 |
| LOCATION | +4 0 -4 |
| MOISTURE | DRY |

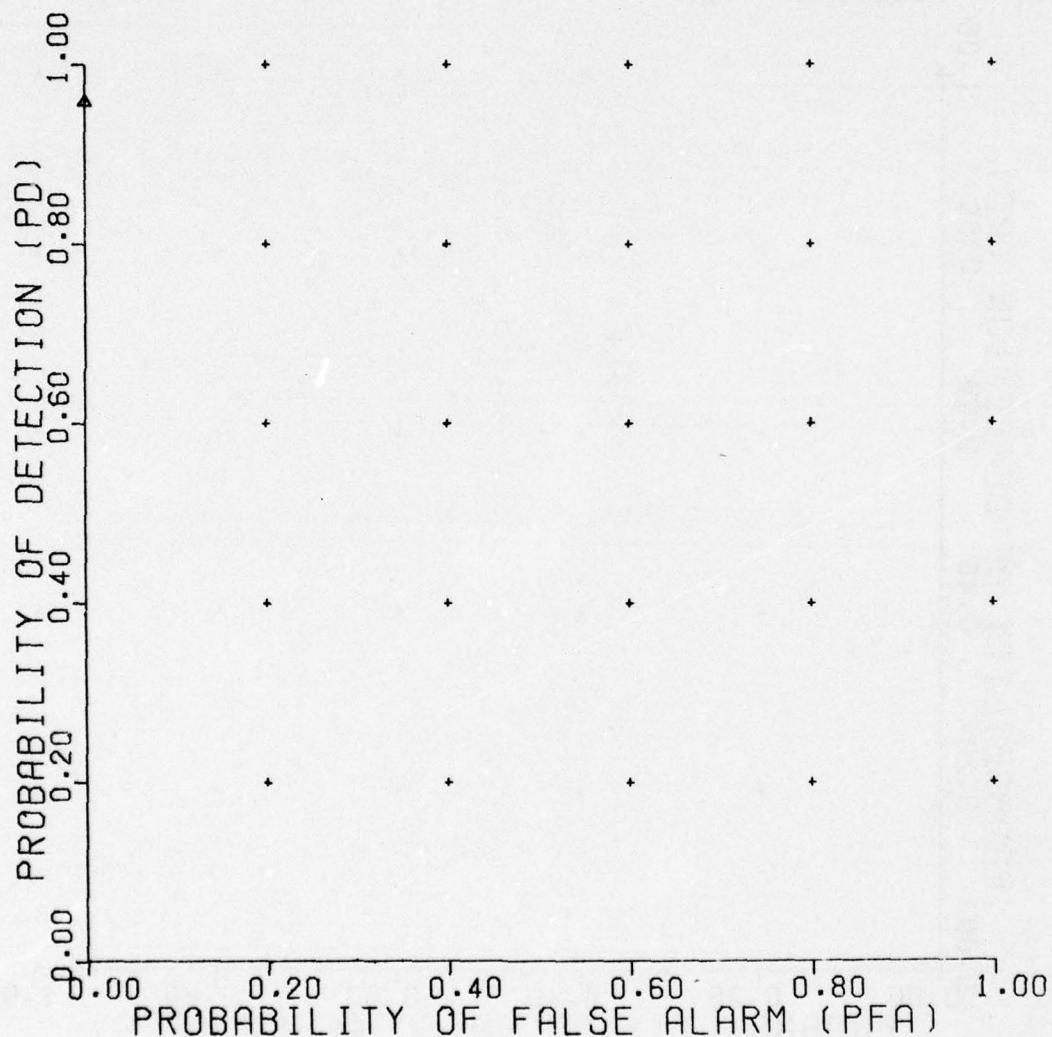


Figure C-108. Nearest neighbor classifier.

UNCLASSIFIED

UNCLASSIFIED

NEAREST NEIGHBOR CLASSIFIER

RAW DATA

NO. NEAREST NEIGHBORS 5

REFERENCE 423

NONMINE

ROCK

TARGET

TYPE A MINE

DEPTH

6

LOCATION

+4 0 -4

MOISTURE

DRY

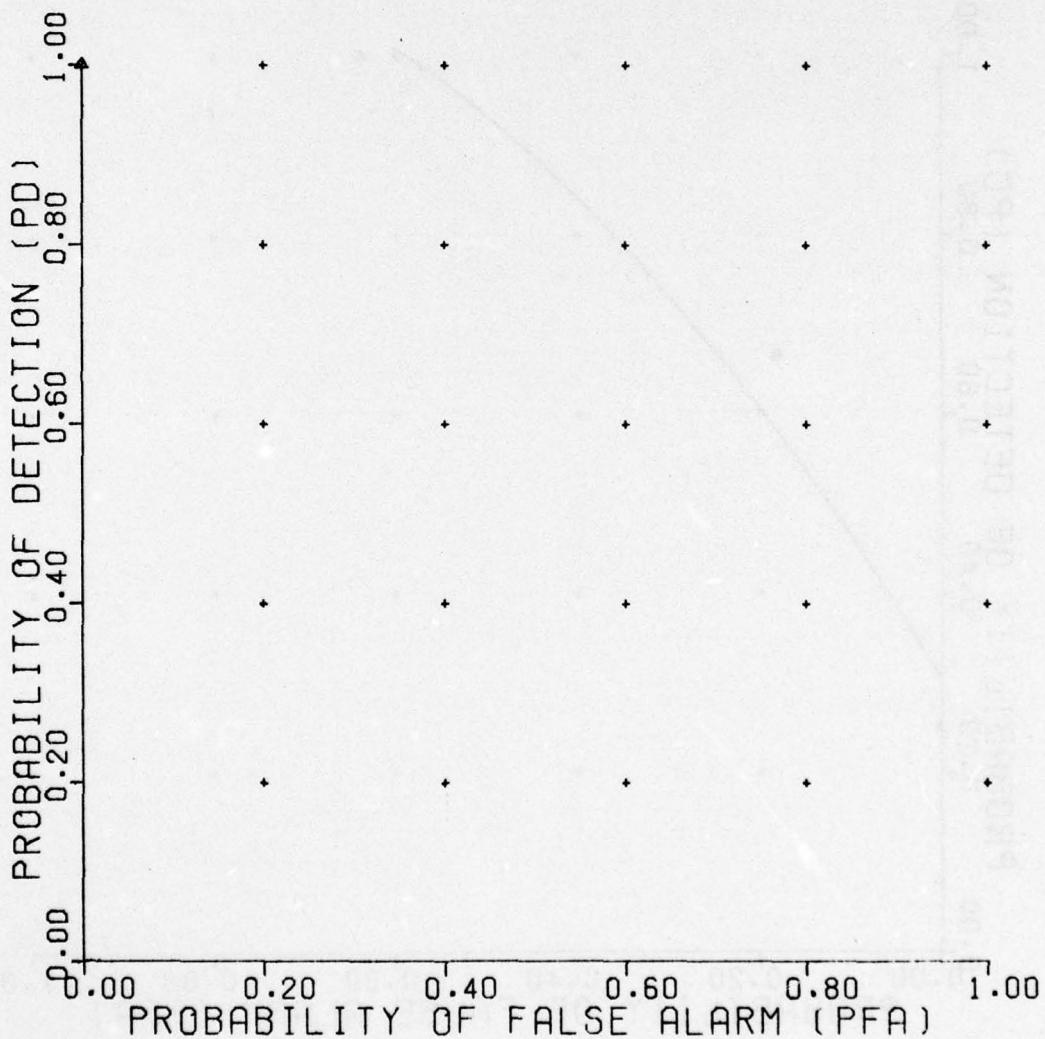


Figure C-109. Nearest neighbor classifier.

UNCLASSIFIED

UNCLASSIFIED

NEAREST NEIGHBOR CLASSIFIER

RAW DATA
NO. NEAREST NEIGHBORS 5
REFERENCE 426

NONMINE PLATE

TARGET

TYPE A MINE

DEPTH

6

LOCATION

+4

0

-4

MOISTURE

DRY

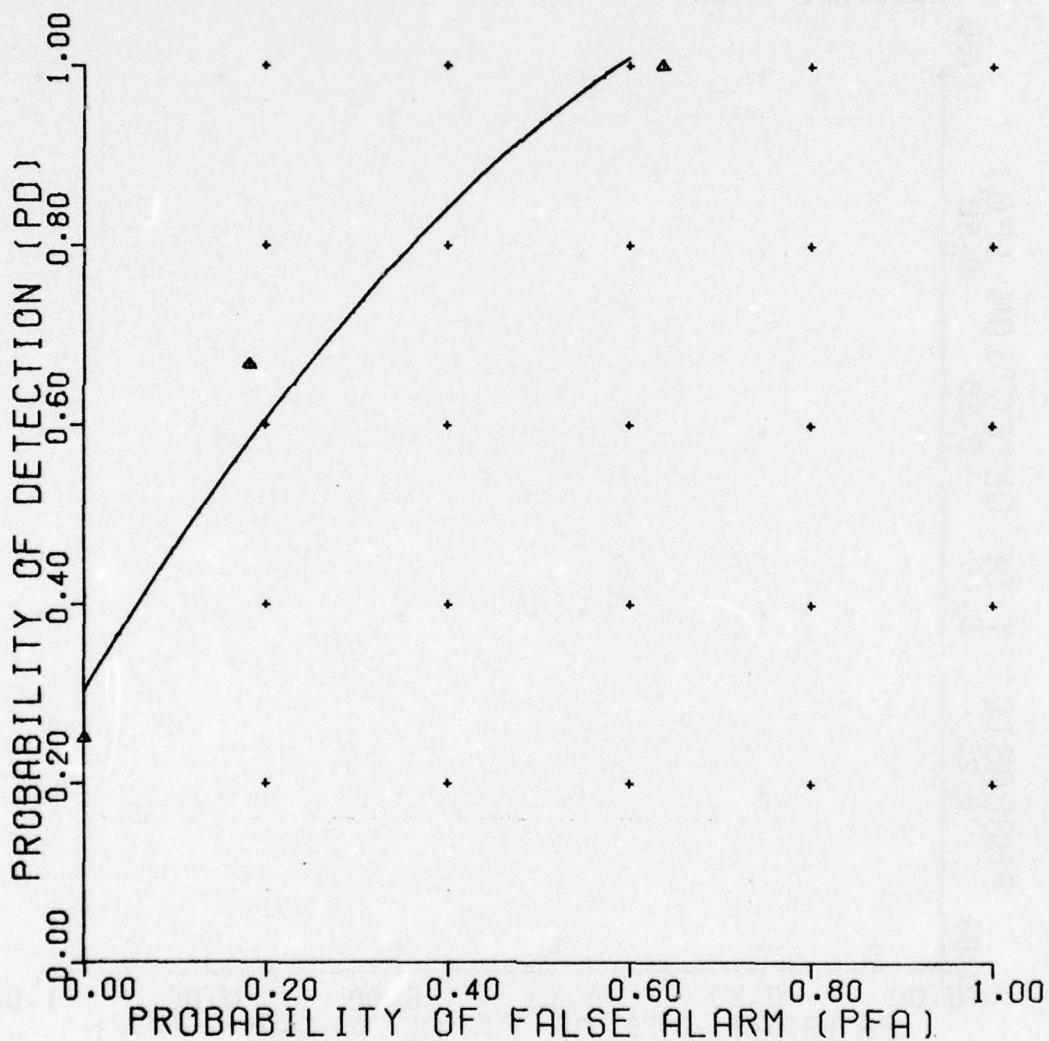


Figure C-110. Nearest neighbor classifier.

UNCLASSIFIED

UNCLASSIFIED

NEAREST NEIGHBOR CLASSIFIER

RAW DATA

NO. NEAREST NEIGHBORS 5

REFERENCE 429

| | |
|-------------------|-------------------|
| NONMINE TARGET | ROCK |
| DEPTH | 6 |
| LOCATION | +4 0 -4 |
| MOISTURE | DRY |

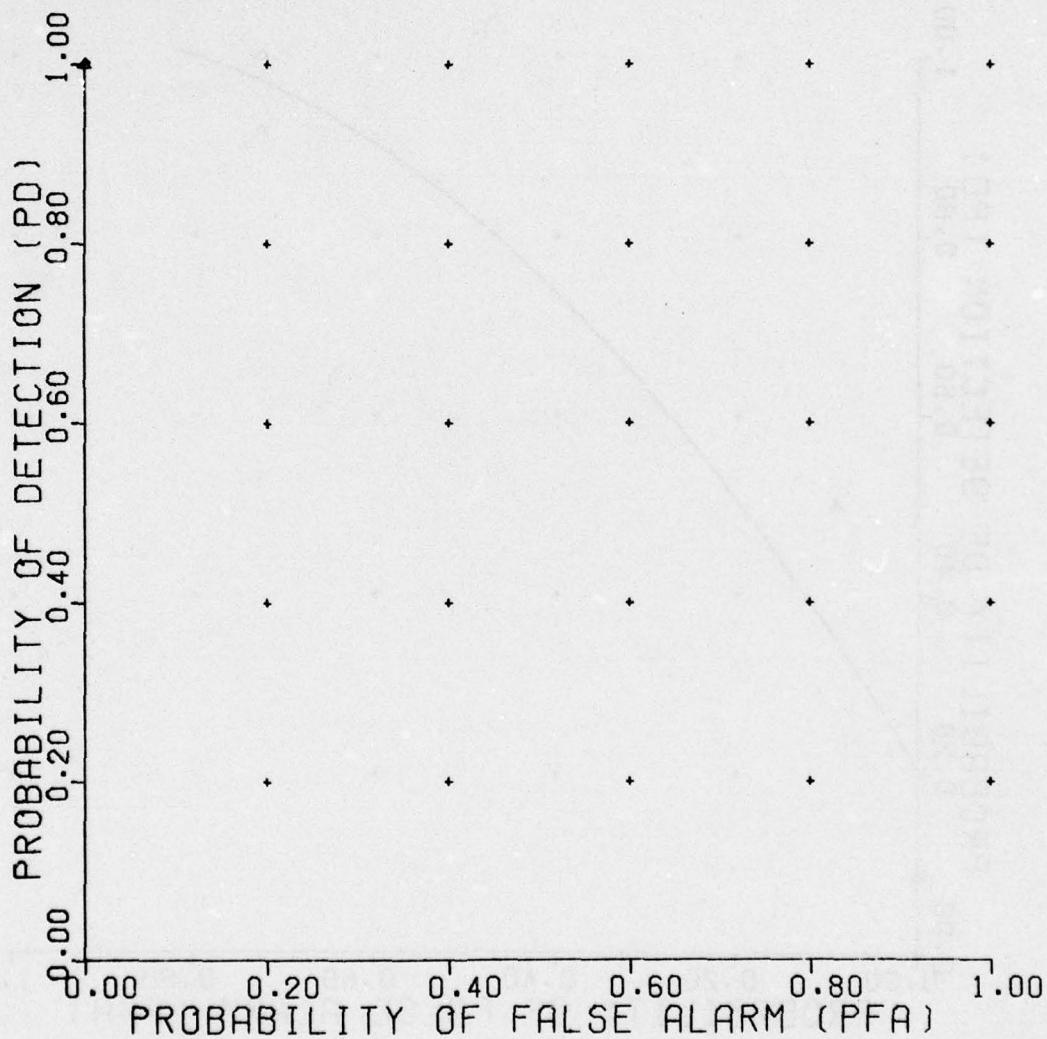


Figure C-111. Nearest neighbor classifier.

UNCLASSIFIED

C-111

UNCLASSIFIED

NEAREST NEIGHBOR CLASSIFIER

RAW DATA

NO. NEAREST NEIGHBORS 5

REFERENCE 432

| | |
|-------------------|-------------------|
| NONMINE TARGET | PLATE |
| DEPTH | 6 |
| LOCATION | +4 0 -4 |
| MOISTURE | DRY |

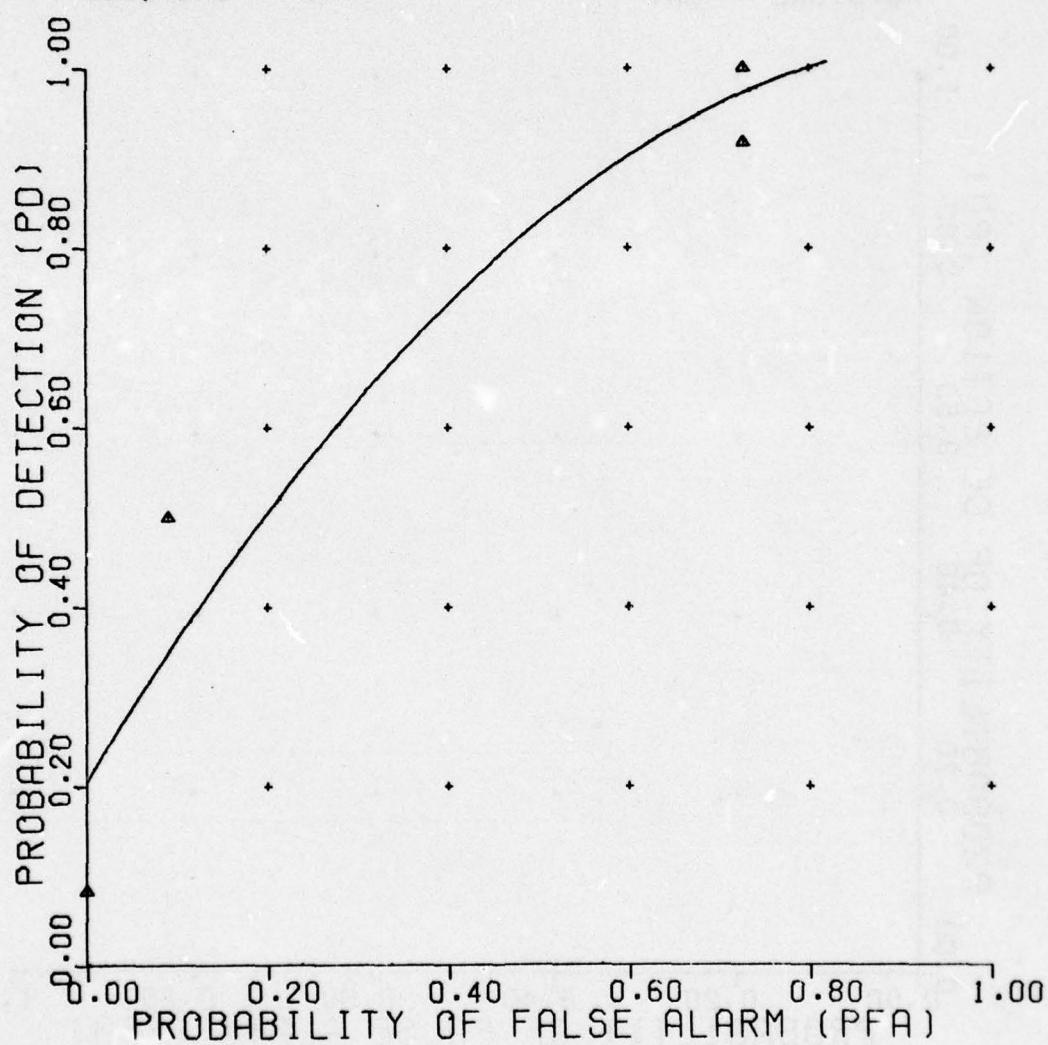


Figure C-112. Nearest neighbor classifier.

UNCLASSIFIED

UNCLASSIFIED

NEAREST NEIGHBOR CLASSIFIER

RAW DATA

NO. NEAREST NEIGHBORS 5

REFERENCE 435

| NONMINE TARGET | ROCK | TYPE C MINE | TYPE A MINE |
|-------------------|------|-------------|-------------|
| DEPTH | 6 | | |
| LOCATION | +4 | 0 | -4 |
| MOISTURE | DRY | | |

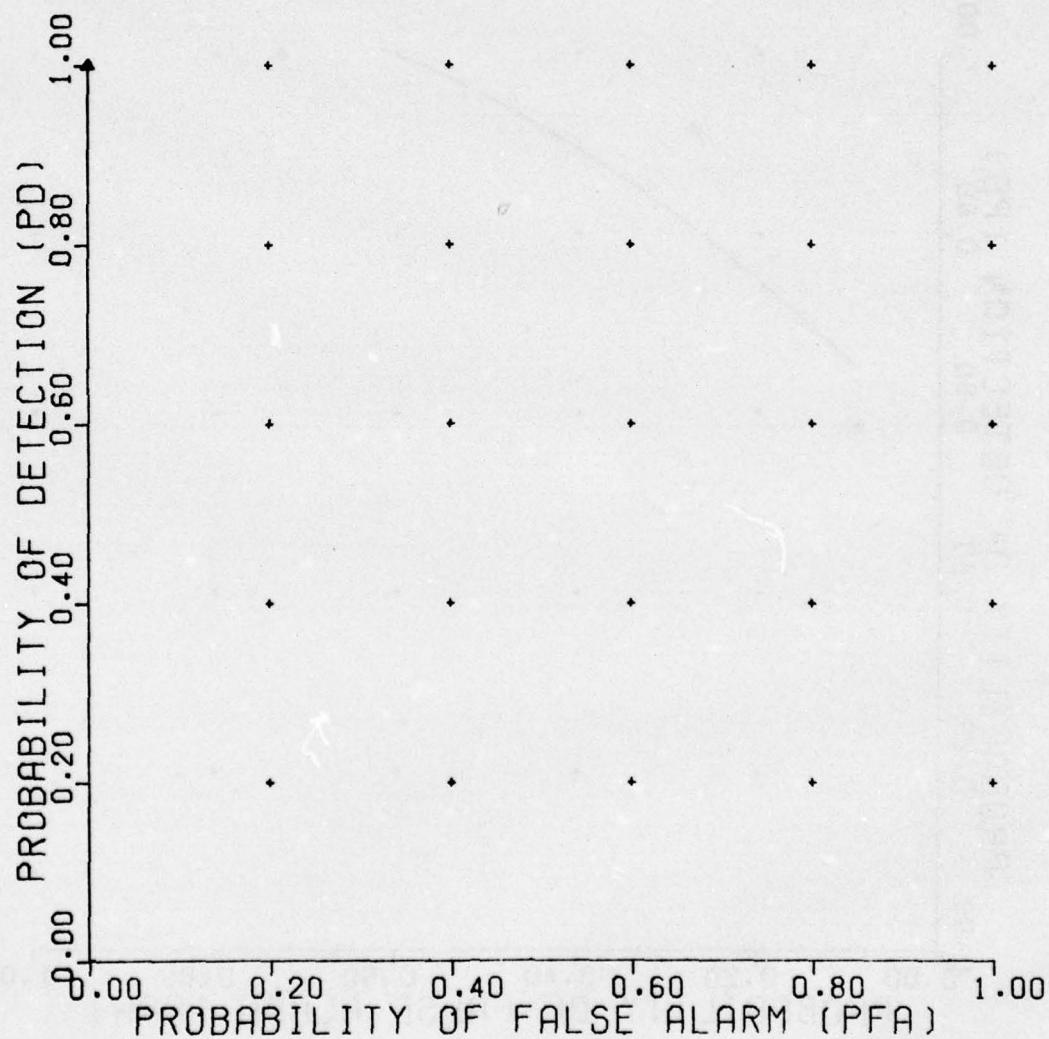


Figure C-113. Nearest neighbor classifier.

UNCLASSIFIED

C-113

UNCLASSIFIED

NEAREST NEIGHBOR CLASSIFIER

RAW DATA
NO. NEAREST NEIGHBORS 5
REFERENCE 438

| NONMINE TARGET | PLATE TYPE C MINE | TYPE A MINE |
|-------------------|----------------------|-------------|
| DEPTH | 6 | |
| LOCATION | +4 | 0 |
| MOISTURE | DRY | -4 |

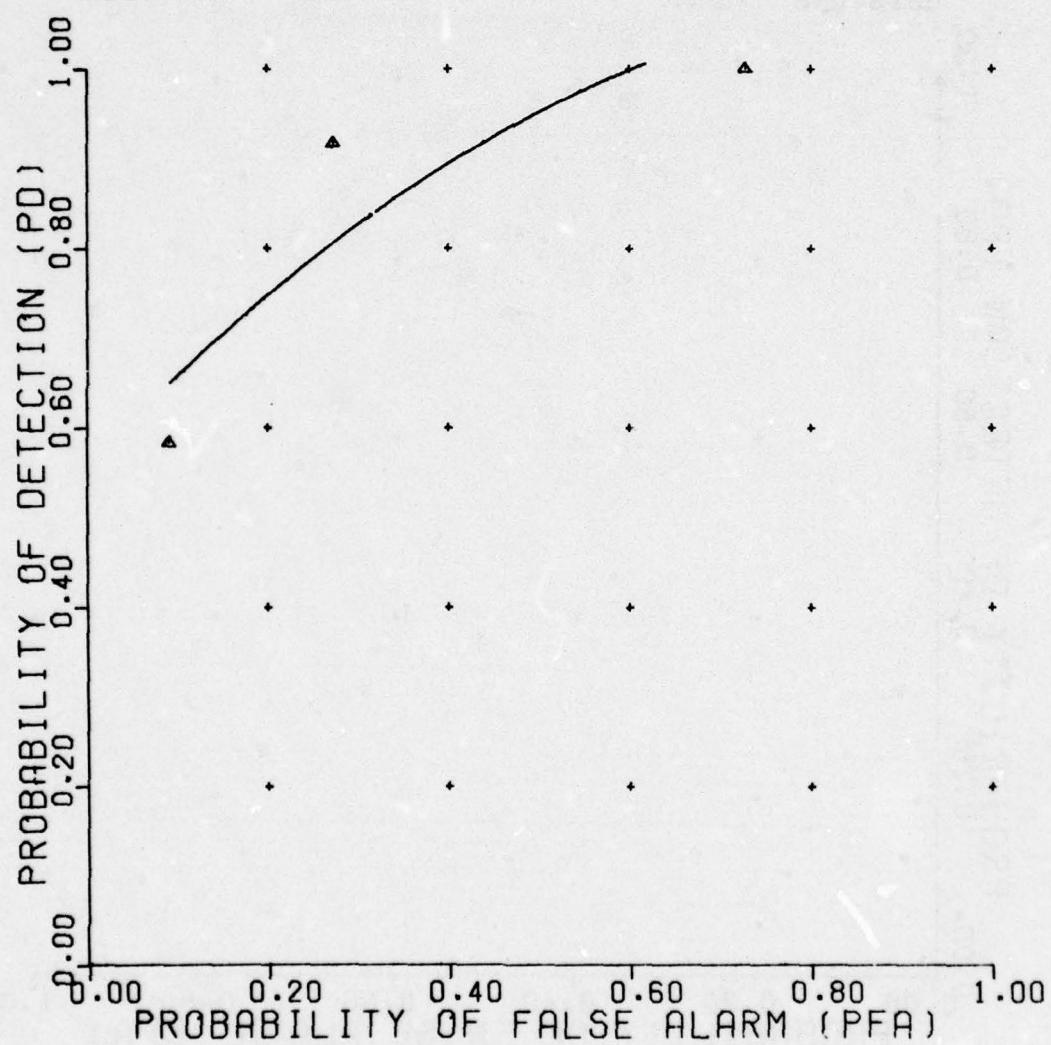


Figure C-114. Nearest neighbor classifier.

UNCLASSIFIED

UNCLASSIFIED

NEAREST NEIGHBOR CLASSIFIER

RAW DATA
VERSION 5
REFERENCE 441

| | |
|----------|-------------------|
| TARGET2 | TYPE C MINE |
| TARGET1 | TYPE A MINE |
| DEPTH | 6 |
| LOCATION | +4 0 -4 |
| MOISTURE | DRY |

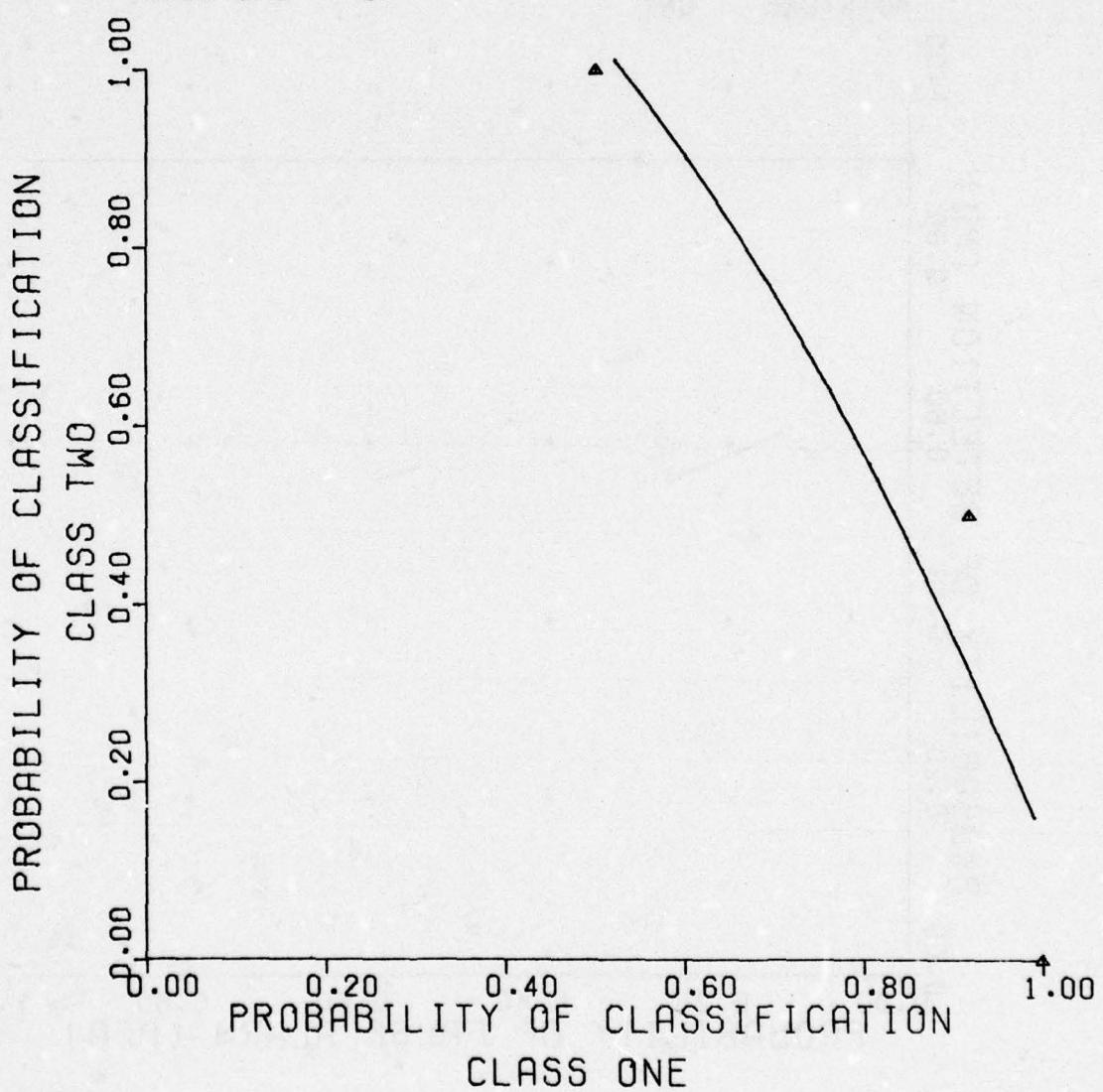


Figure C-115. Nearest neighbor classifier.

UNCLASSIFIED

UNCLASSIFIED

NEAREST NEIGHBOR CLASSIFIER

RAW DATA
NO. NEAREST NEIGHBORS 5
REFERENCE 463

NONMINE BACKGND
TARGET TYPE A MINE

DEPTH 6
LOCATION +4 0 -4
MOISTURE DRY

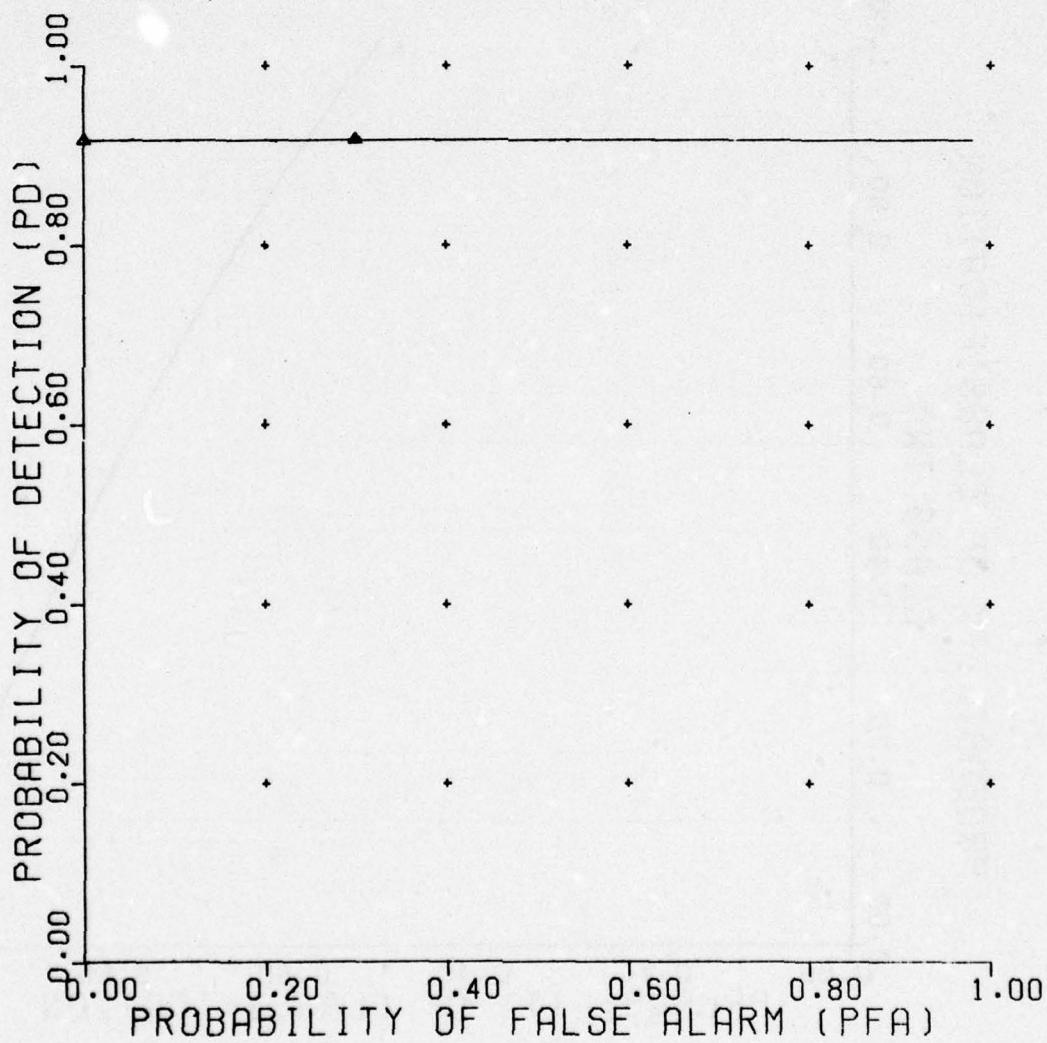


Figure C-116. Nearest neighbor classifier.

UNCLASSIFIED

UNCLASSIFIED

NEAREST NEIGHBOR CLASSIFIER

RAW DATA

NO. NEAREST NEIGHBORS 5

REFERENCE 466

NONMINE BACKGND
TARGET TYPE C MINE
DEPTH 6
LOCATION +4 0 -4
MOISTURE DRY

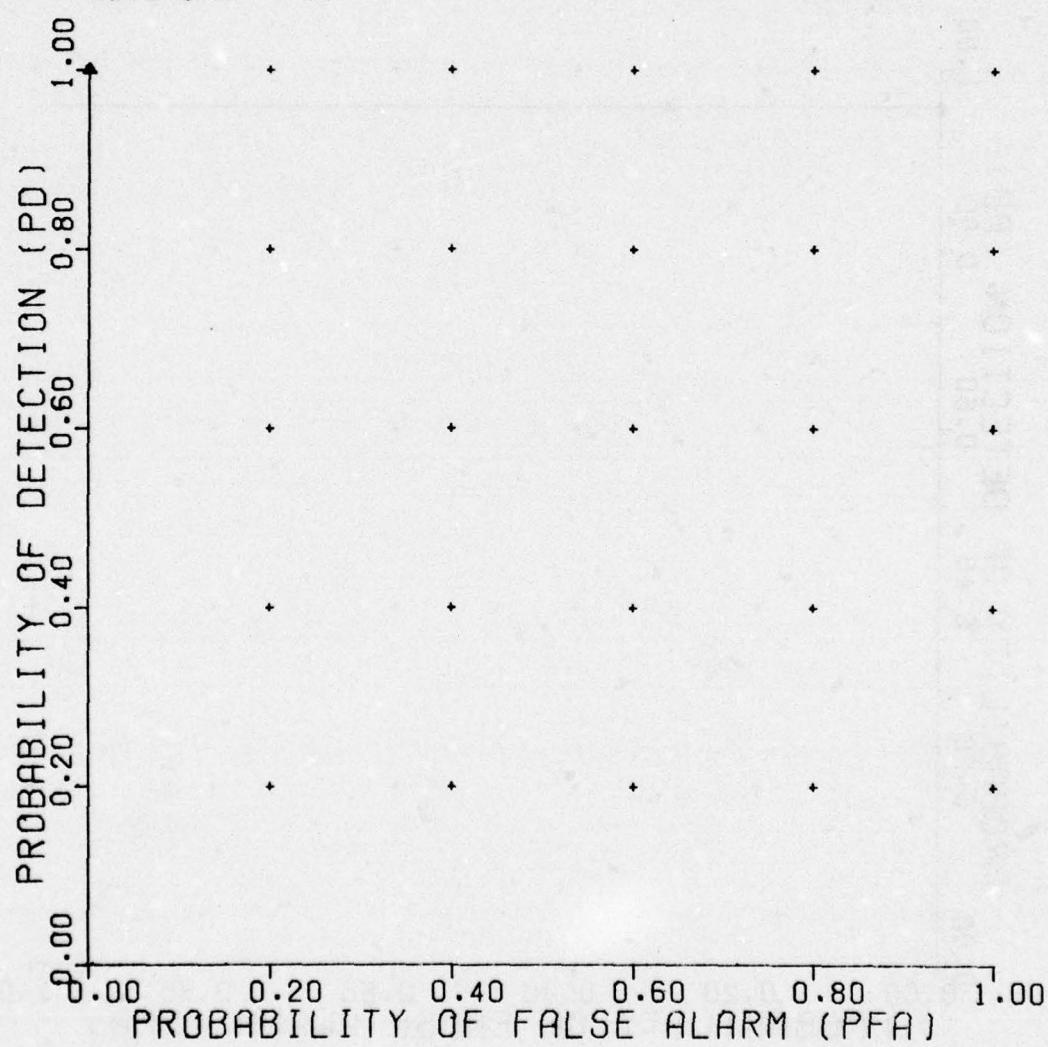


Figure C-117. Nearest neighbor classifier.

UNCLASSIFIED

UNCLASSIFIED

NEAREST NEIGHBOR CLASSIFIER

RAW DATA
NO. NEAREST NEIGHBORS 5
REFERENCE 469

| NONMINE | BACKGND |
|----------|-------------------------------|
| TARGET | TYPE C MINE TYPE A MINE |
| DEPTH | 6 |
| LOCATION | +4 0 -4 |
| MOISTURE | DRY |

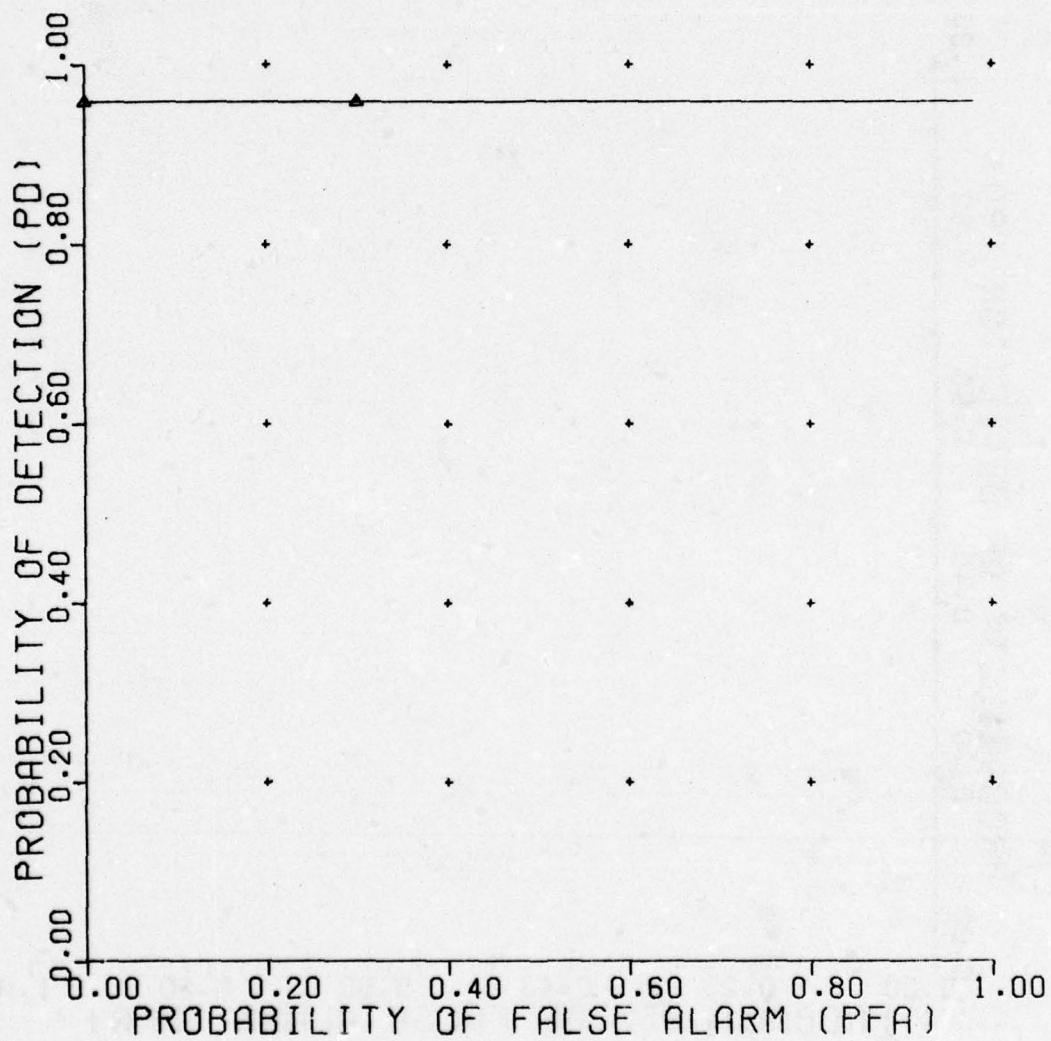


Figure C-118. Nearest neighbor classifier.

UNCLASSIFIED

UNCLASSIFIED

NEAREST NEIGHBOR CLASSIFIER

RAW DATA
NO. NEAREST NEIGHBORS 7
REFERENCE 424

NONMINE ROCK
TARGET TYPE A MINE
DEPTH 6
LOCATION +4 0 -4
MOISTURE DRY

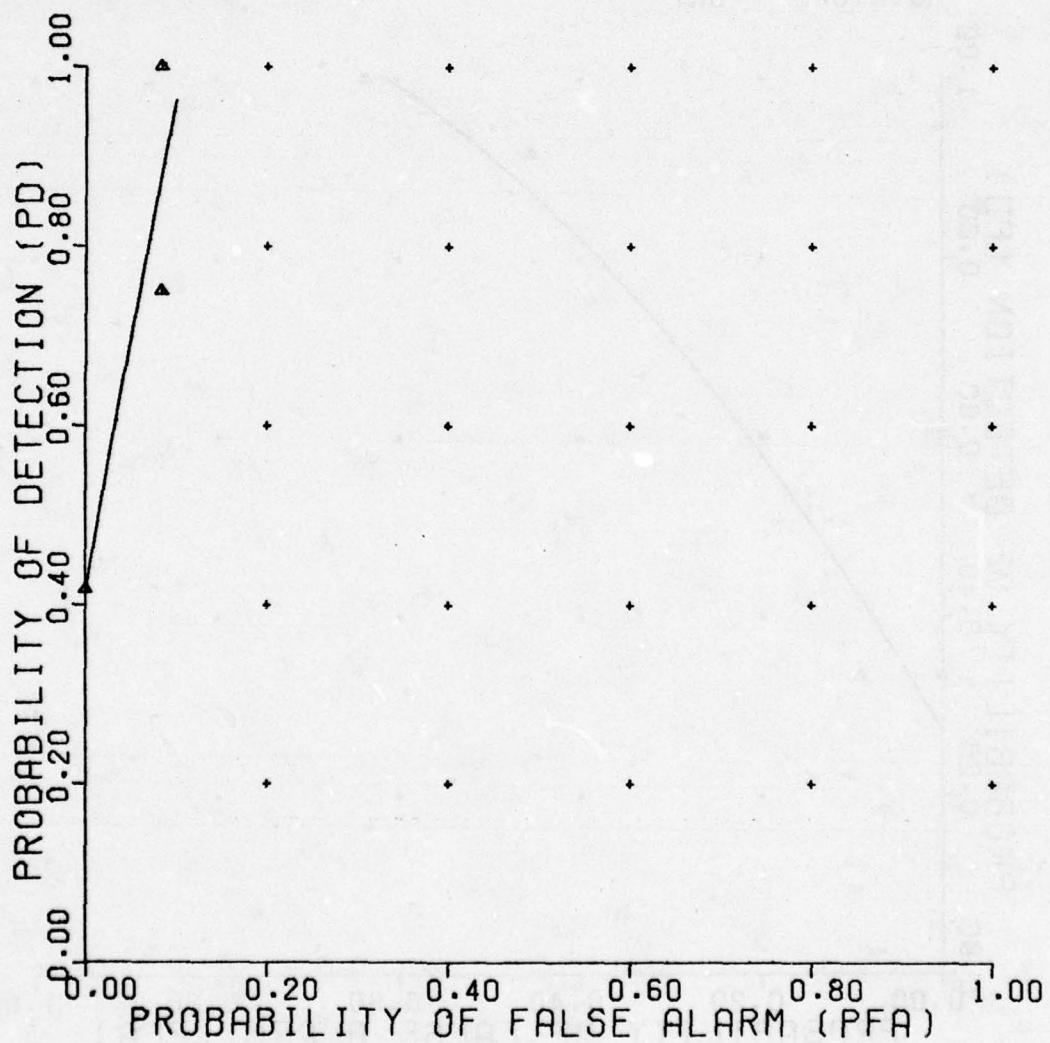


Figure C-119. Nearest neighbor classifier.

UNCLASSIFIED

UNCLASSIFIED

NEAREST NEIGHBOR CLASSIFIER

RAW DATA
NO. NEAREST NEIGHBORS 7
REFERENCE 427

NONMINE PLATE
TARGET TYPE A MINE

DEPTH 6
LOCATION +4 0 -4
MOISTURE DRY

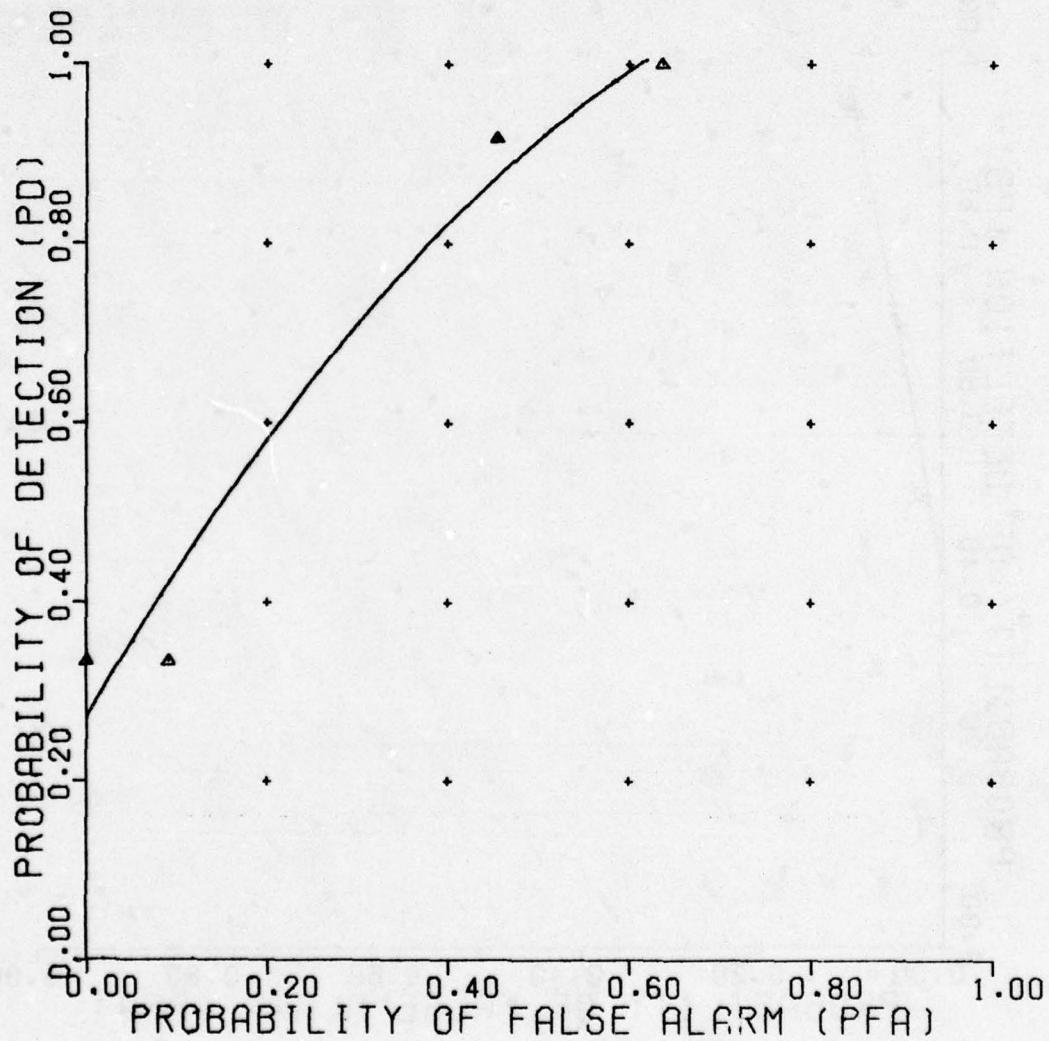


Figure C-120. Nearest neighbor classifier.

UNCLASSIFIED

UNCLASSIFIED

NEAREST NEIGHBOR CLASSIFIER

RAW DATA

NO. NEAREST NEIGHBORS 7

REFERENCE 430

| | |
|----------|-------------------|
| NONMINE | ROCK |
| TARGET | TYPE C MINE |
| DEPTH | 6 |
| LOCATION | +4 0 -4 |
| MOISTURE | DRY |

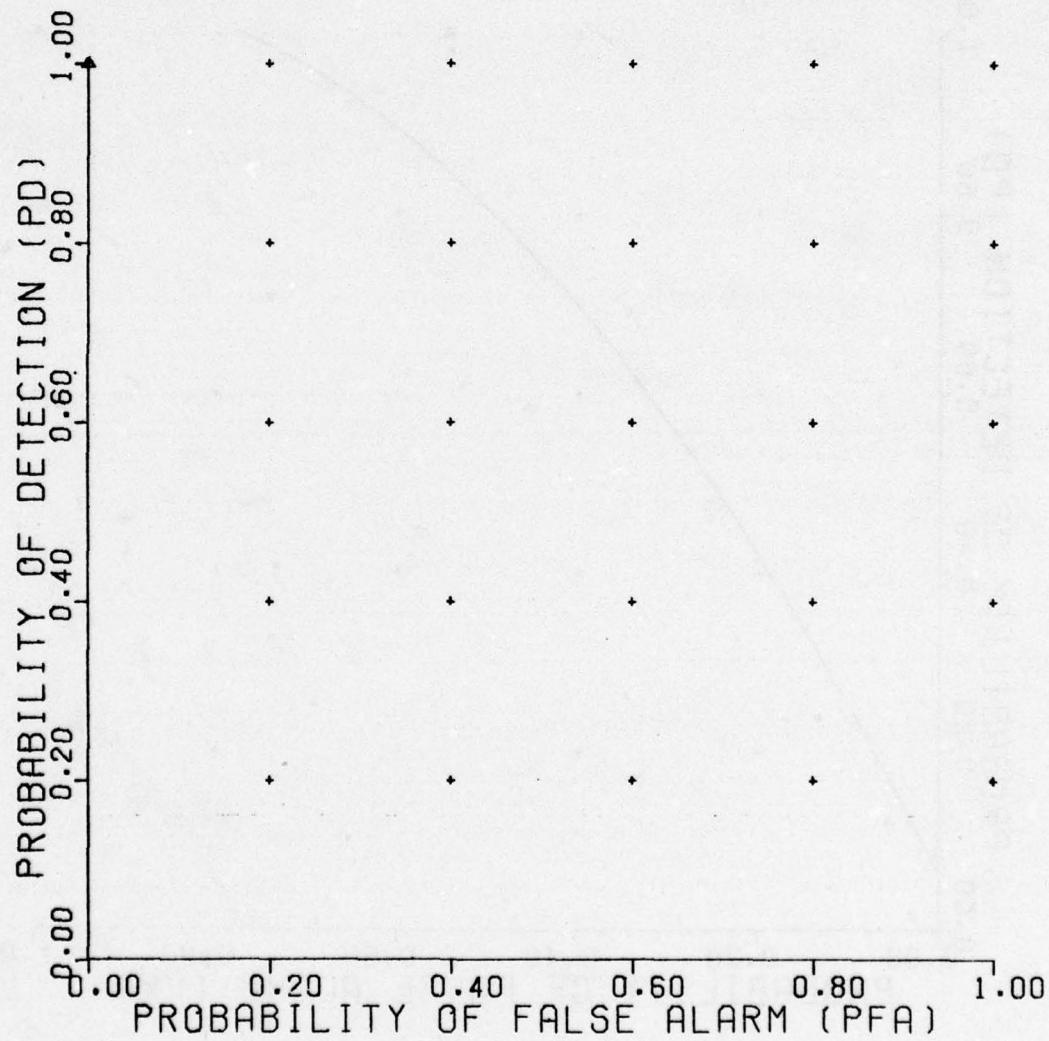


Figure C-121. Nearest neighbor classifier.

UNCLASSIFIED

UNCLASSIFIED

NEAREST NEIGHBOR CLASSIFIER

RAW DATA
NO. NEAREST NEIGHBORS 7
REFERENCE 433

NONMINE PLATE
TARGET TYPE C MINE
DEPTH 6
LOCATION +4 0 -4
MOISTURE DRY

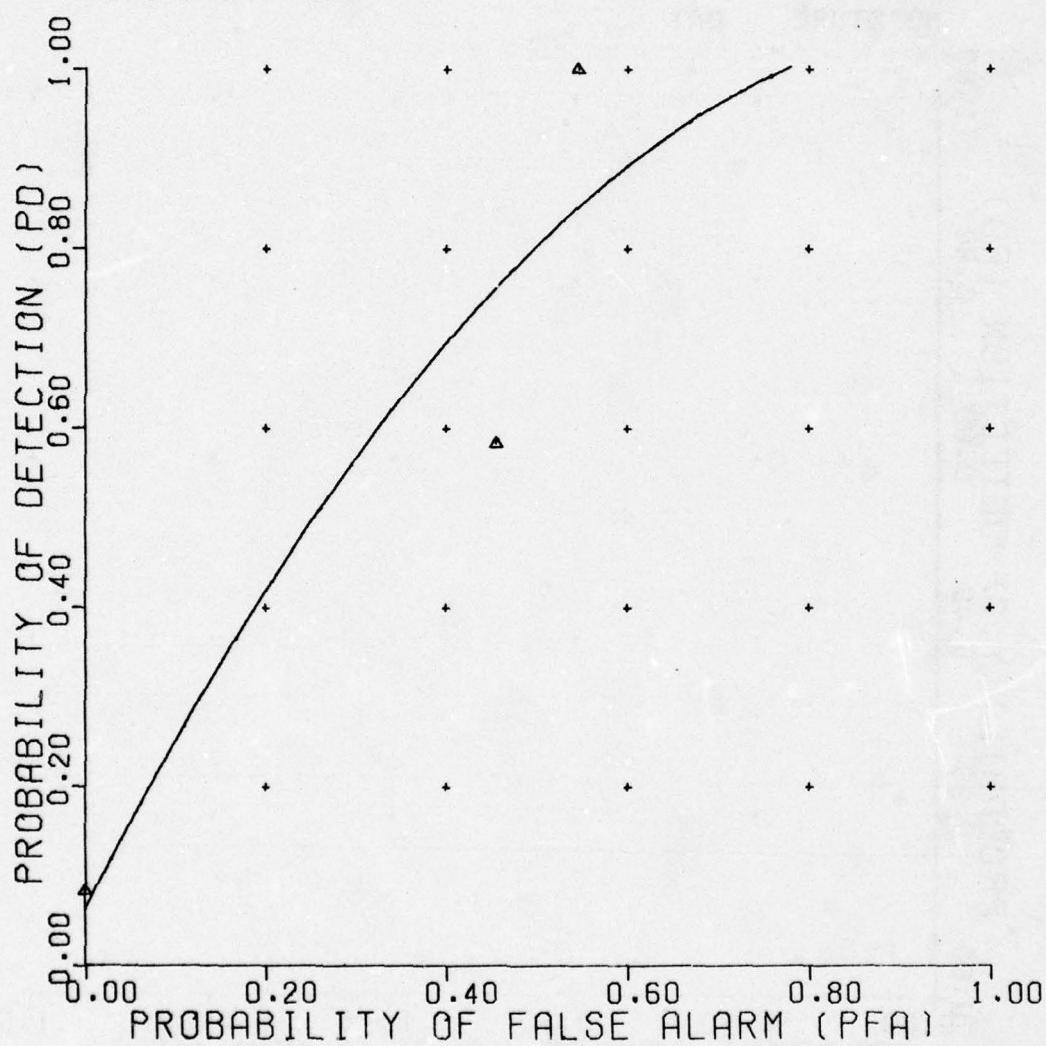


Figure C-122. Nearest neighbor classifier.

UNCLASSIFIED

UNCLASSIFIED

NEAREST NEIGHBOR CLASSIFIER

RAW DATA

NO. NEAREST NEIGHBORS 7

REFERENCE 436

| | |
|----------|----------------------------|
| NONMINE | ROCK(2) |
| TARGET | TYPE C MINE TYPE A MINE |
| DEPTH | 6 |
| LOCATION | +4 0 -4 |
| MOISTURE | DRY |

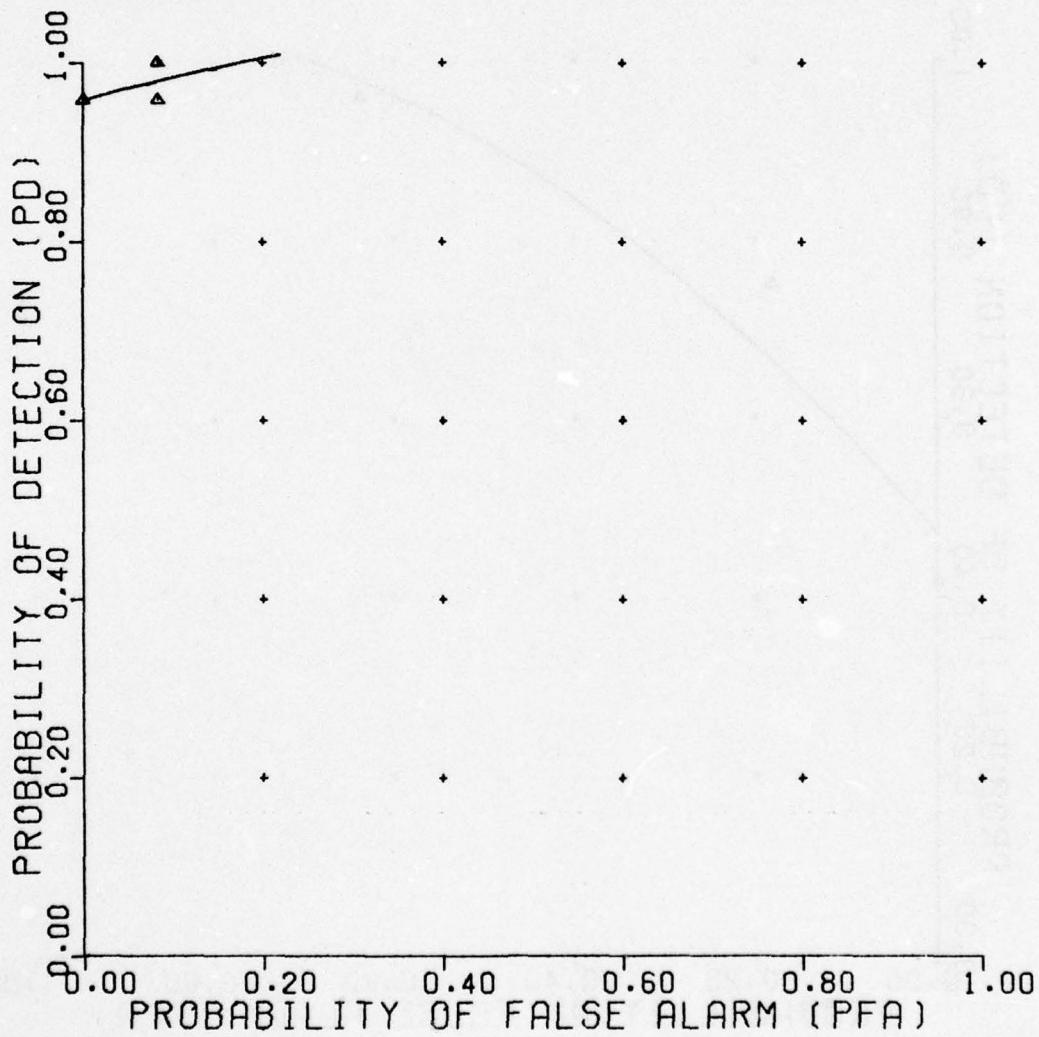


Figure C-123. Nearest neighbor classifier.

UNCLASSIFIED

UNCLASSIFIED

NEAREST NEIGHBOR CLASSIFIER

RAW DATA

NO. NEAREST NEIGHBORS 7

REFERENCE 439

| NONMINE TARGET | PLATE TYPE C MINE | TYPE A MINE |
|-------------------|----------------------|-------------|
| DEPTH | 6 | |
| LOCATION | +4 | 0 |
| MOISTURE | DRY | -4 |

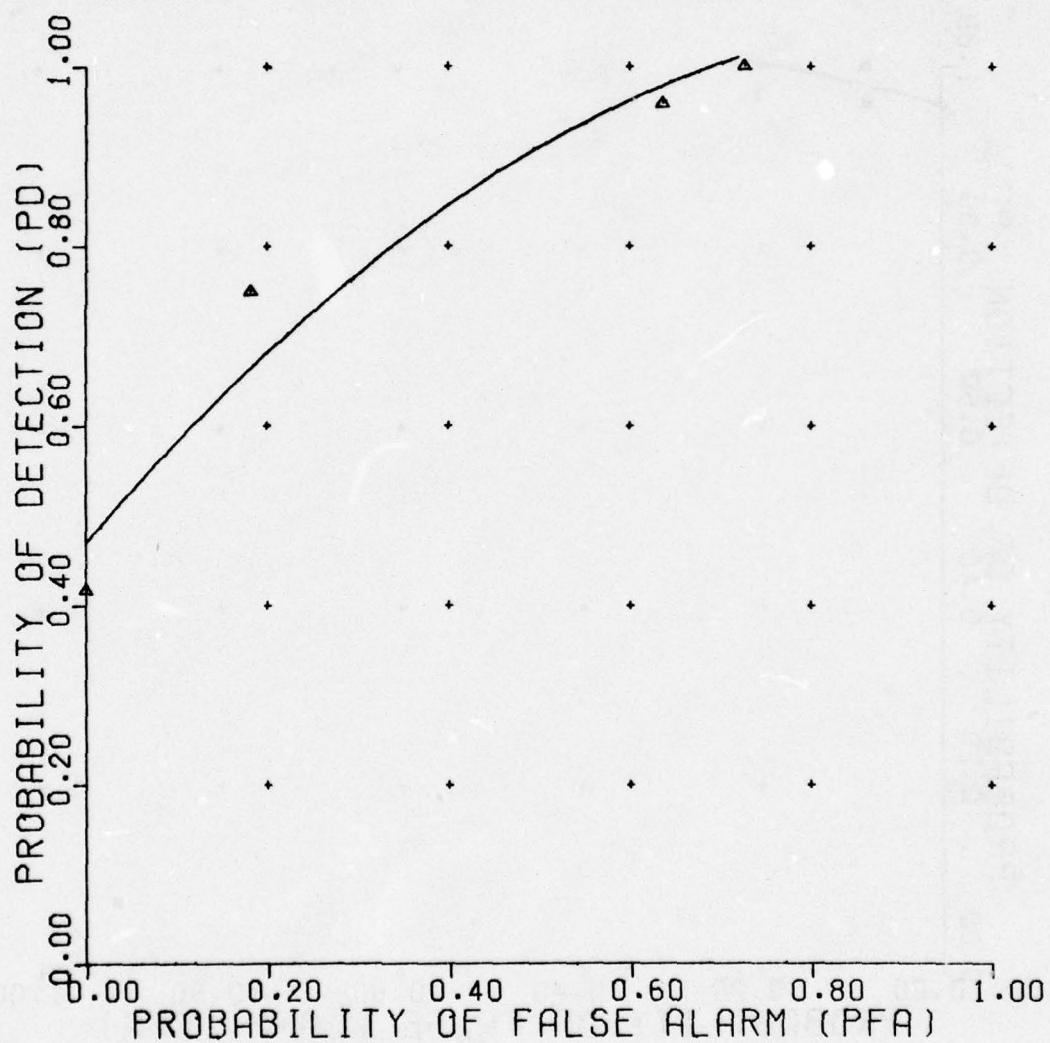


Figure C-124. Nearest neighbor classifier.

UNCLASSIFIED

C-124

UNCLASSIFIED

NEAREST NEIGHBOR CLASSIFIER

RAW DATA
VERSION 7
REFERENCE 442

TARGET2 M19
TARGET1 TYPE C MINE
DEPTH 6
LOCATION +4 0 -4
MOISTURE DRY

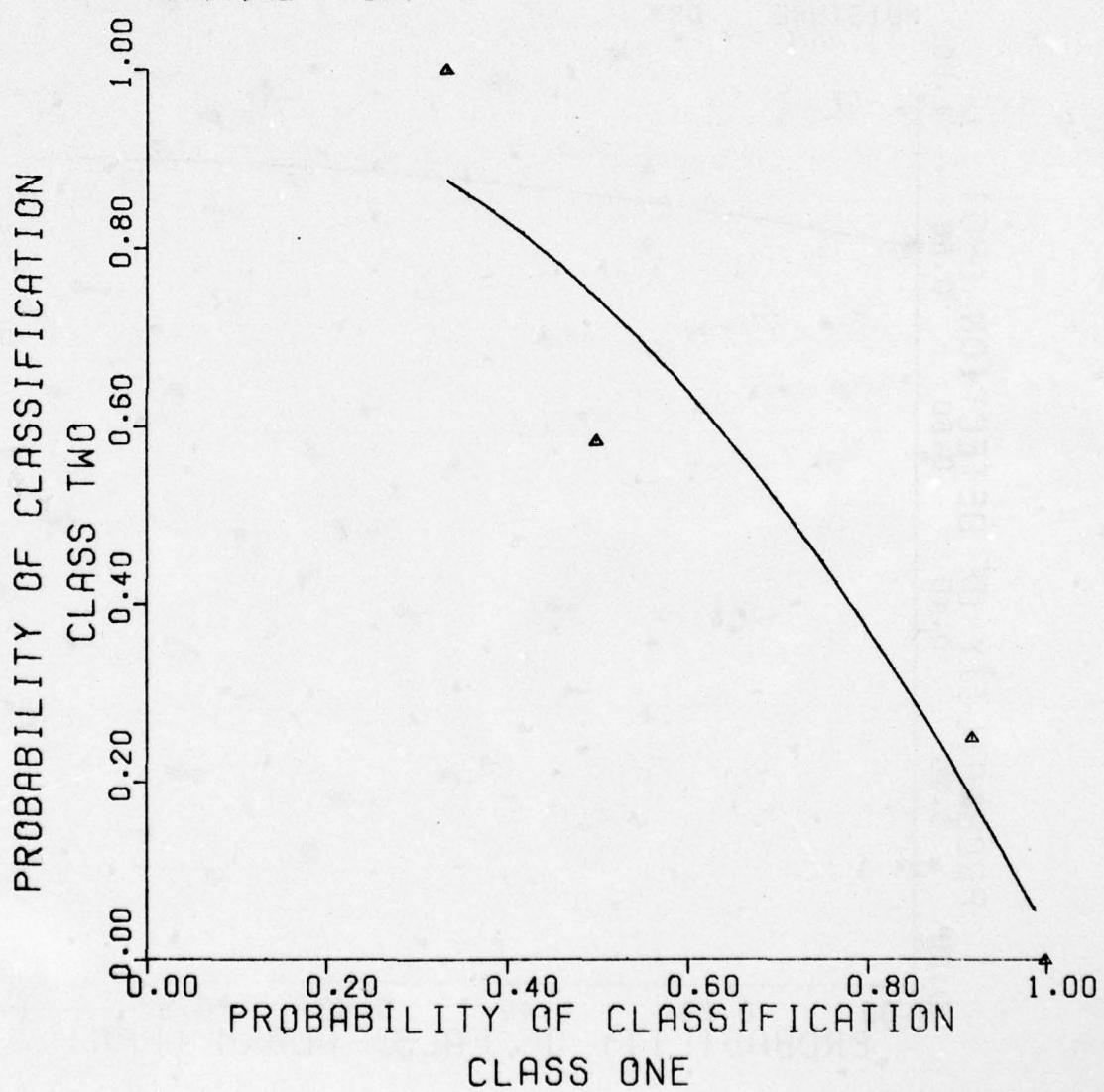


Figure C-125. Nearest neighbor classifier.

UNCLASSIFIED

UNCLASSIFIED

NEAREST NEIGHBOR CLASSIFIER

RAW DATA
NO. NEAREST NEIGHBORS 7
REFERENCE 464

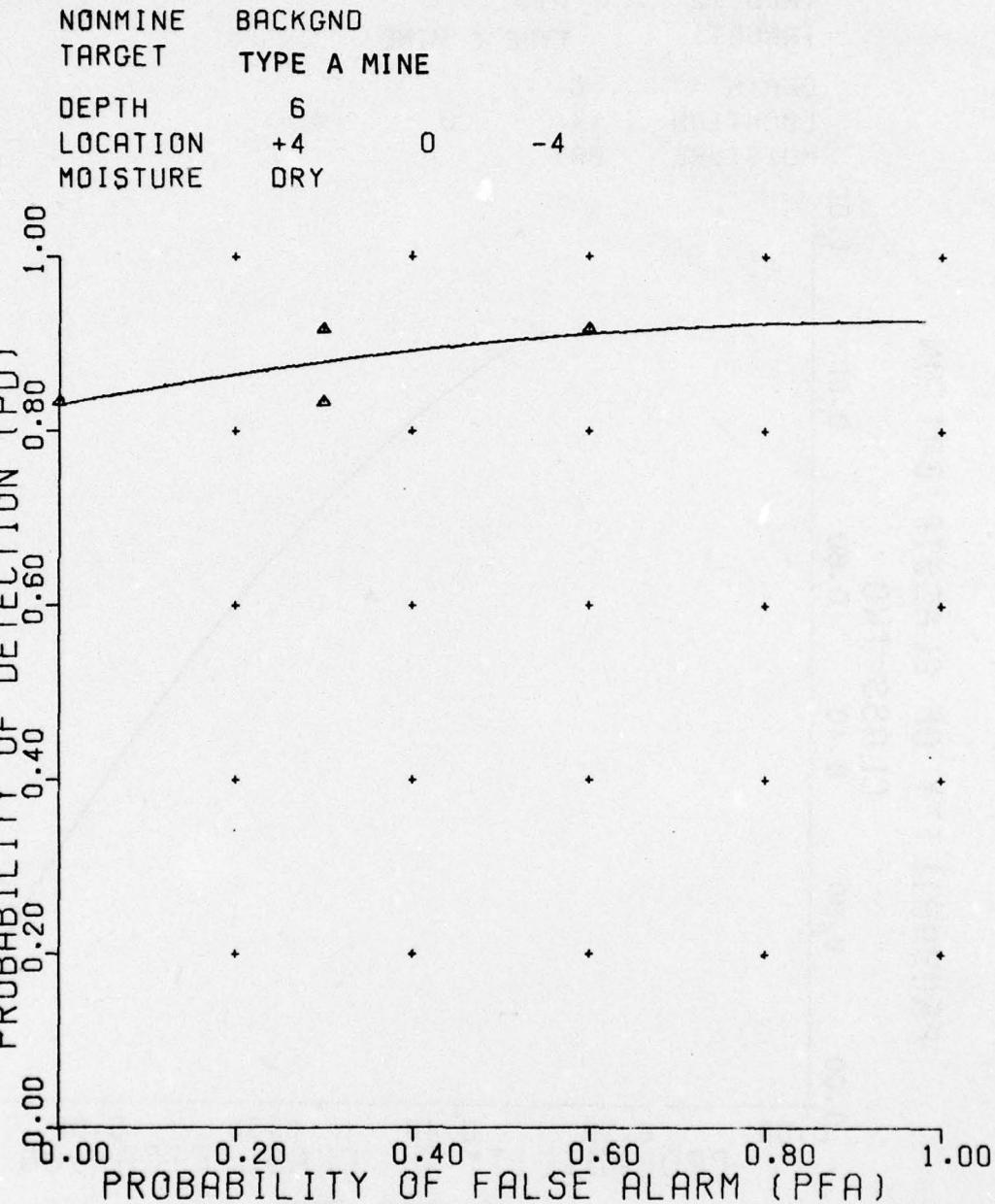


Figure C-126. Nearest neighbor classifier.

UNCLASSIFIED

C-126

UNCLASSIFIED

NEAREST NEIGHBOR CLASSIFIER

RAW DATA
NO. NEAREST NEIGHBORS 7
REFERENCE 467

NONMINE BACKGND
TARGET TYPE C MINE
DEPTH 6
LOCATION +4 0 -4
MOISTURE DRY

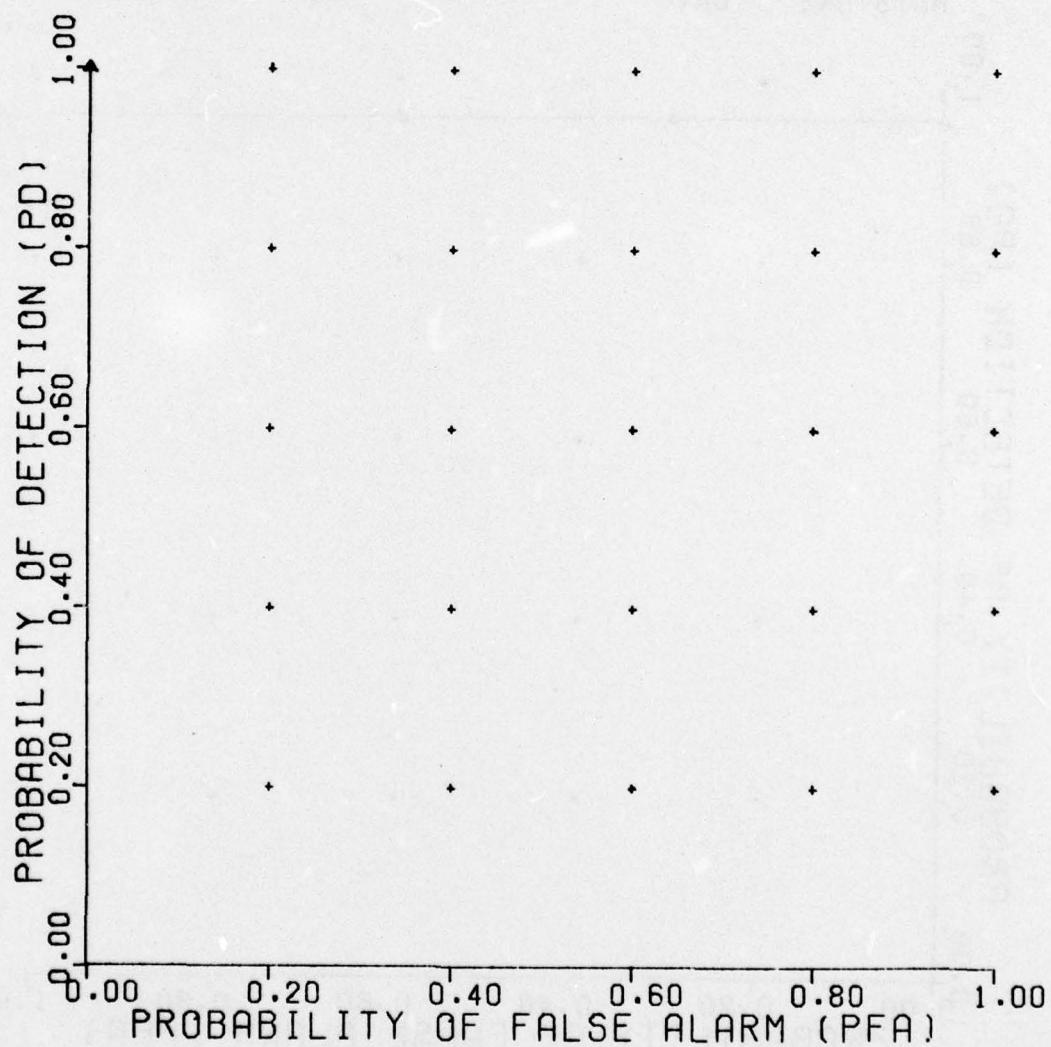


Figure C-127. Nearest neighbor classifier.

UNCLASSIFIED

UNCLASSIFIED

NEAREST NEIGHBOR CLASSIFIER

RAW DATA

NO. NEAREST NEIGHBORS 7

REFERENCE 470

| NONMINE | BACKGND |
|----------|----------------------------|
| TARGET | TYPE C MINE TYPE A MINE |
| DEPTH | 6 |
| LOCATION | +4 0 -4 |
| MOISTURE | DRY |

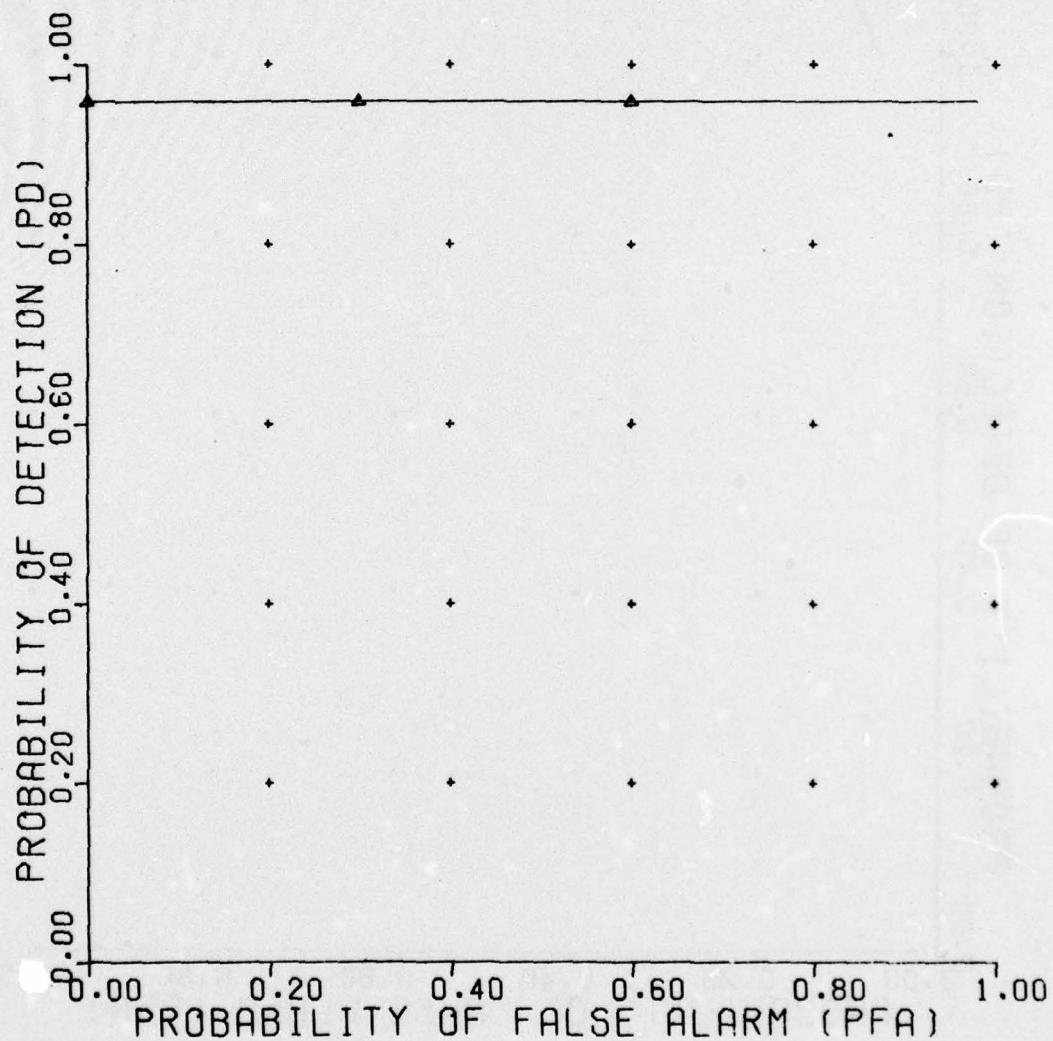


Figure C-128. Nearest neighbor classifier.

UNCLASSIFIED

UNCLASSIFIED

APPENDIX D

HOMOMORPHIC DECONVOLUTION ANALYSIS

UNCLASSIFIED

UNCLASSIFIED

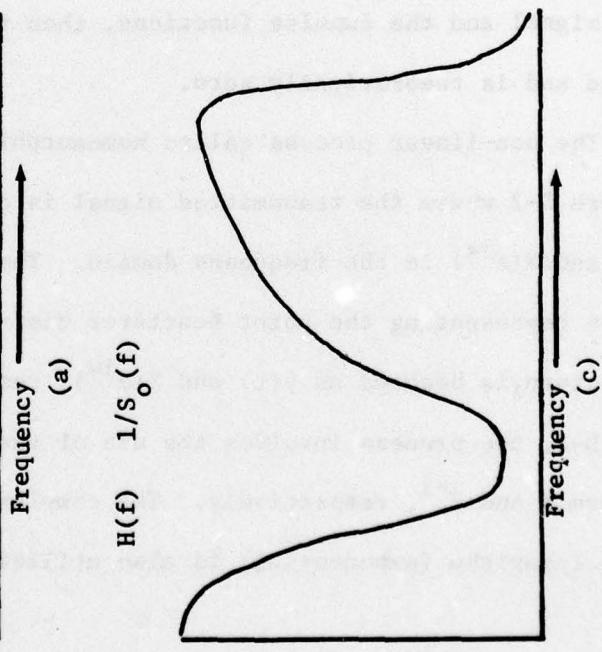
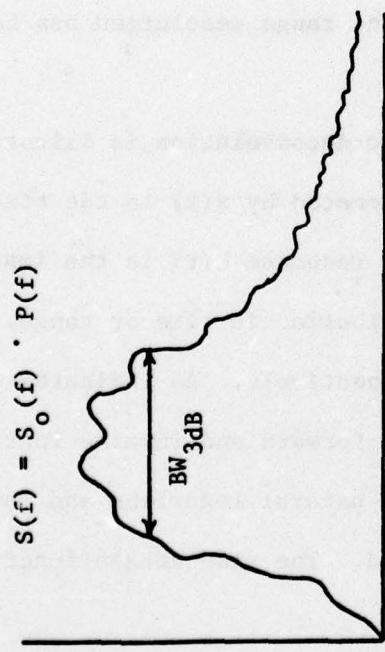
A process called homomorphic deconvolution was investigated as part of the study for applicability to the mine detection problem. This approach theoretically allows one to trade radar bandwidth for processing complexity. In other words, additional processing might synthetically provide greater range resolution than one could conventionally achieve with a given radar system. The investigation of this technique was a low priority task and was not completed; however, some preliminary conclusions were reached based on the work that was accomplished. These conclusions and a description of the process are given in this Appendix.

Functionally, homomorphic deconvolution accomplishes the same task as inverse filtering--it accentuates the extremities of the spectrum to yield a larger 3-dB bandwidth. Inverse filtering is illustrated in Figure D-1. The spectra of the signal at the input and output of the inverse filter is illustrated in Figures D-1(a) and (d). The inverse filter is designed to have a frequency response which is the inverse of the fundamental component of the input spectrum as illustrated in Figures D-1(b) and (c). In this filtering process, it is assumed that the information of interest is the smaller, faster varying component of the input spectrum which is preserved in the inverse filtering process. In a radar application where a transmitted signal is reflected from multiple surfaces or points extended in range (or depth for a mine detection radar), the slowly varying spectra component represents the transmitted signal spectra while the faster, more rapidly varying component yields information about the separation between scatterers. It is this latter information which is of interest and which is preserved in the inverse filtering process.

UNCLASSIFIED

UNCLASSIFIED

INVERSE FILTERING



$$S_o(f)$$

Frequency
(b)

$$H(f) \cdot 1/S_o(f)$$

Frequency
(a)

$$P(f) \cdot S(f) \cdot H(f)$$

Frequency
(b)

eff. BW_{3dB}

Frequency
(d)

UNCLASSIFIED

Figure D-1. Inverse filtering: (a) spectrum before filtering; (b) an estimate of the fundamental component of the spectrum; (c) the inverse filter response; and (d) the spectrum at the output of the inverse filter.

UNCLASSIFIED

One of the problems in using inverse filtering is that the portion of the input spectrum which represents the transmitted signal must be known precisely, including magnitude, in order to perform inverse filtering. The output of this type of filter is very sensitive to filter mismatch. Thus, in practice, the theoretical performance of inverse filtering is seldom achieved.

One of the purported advantages of homomorphic deconvolution is that the transmitted signal does not need to be known. The process separates the radar return spectrum into two parts--that part representing the transmitted signal and that portion which yields information about scatterer position. The equivalent operation in the time domain is called deconvolution. Radar returns can be mathematically represented by the convolution of the transmitted temporal signal with a series of point or plane scatterers represented by impulse functions. If we can successfully deconvolve the transmitted signal and the impulse functions, then the range resolution has been enhanced and is theoretically zero.

The non-linear process called homomorphic deconvolution is illustrated in Figure D-2 where the transmitted signal is denoted by $x(t)$ in the time domain and $X(e^{jw})$ in the frequency domain. The response $h(t)$ is the impulse function representing the point scatterer distribution in time or range. The radar return is denoted as $y(t)$ and $Y(e^{jw})$, respectively. As indicated in Figure D-2, the process involves the use of the forward and inverse Fourier transform F and F^{-1} , respectively. The complex natural logarithm and inverse natural logarithm (exponential) is also utilized. The time domain function

UNCLASSIFIED

UNCLASSIFIED

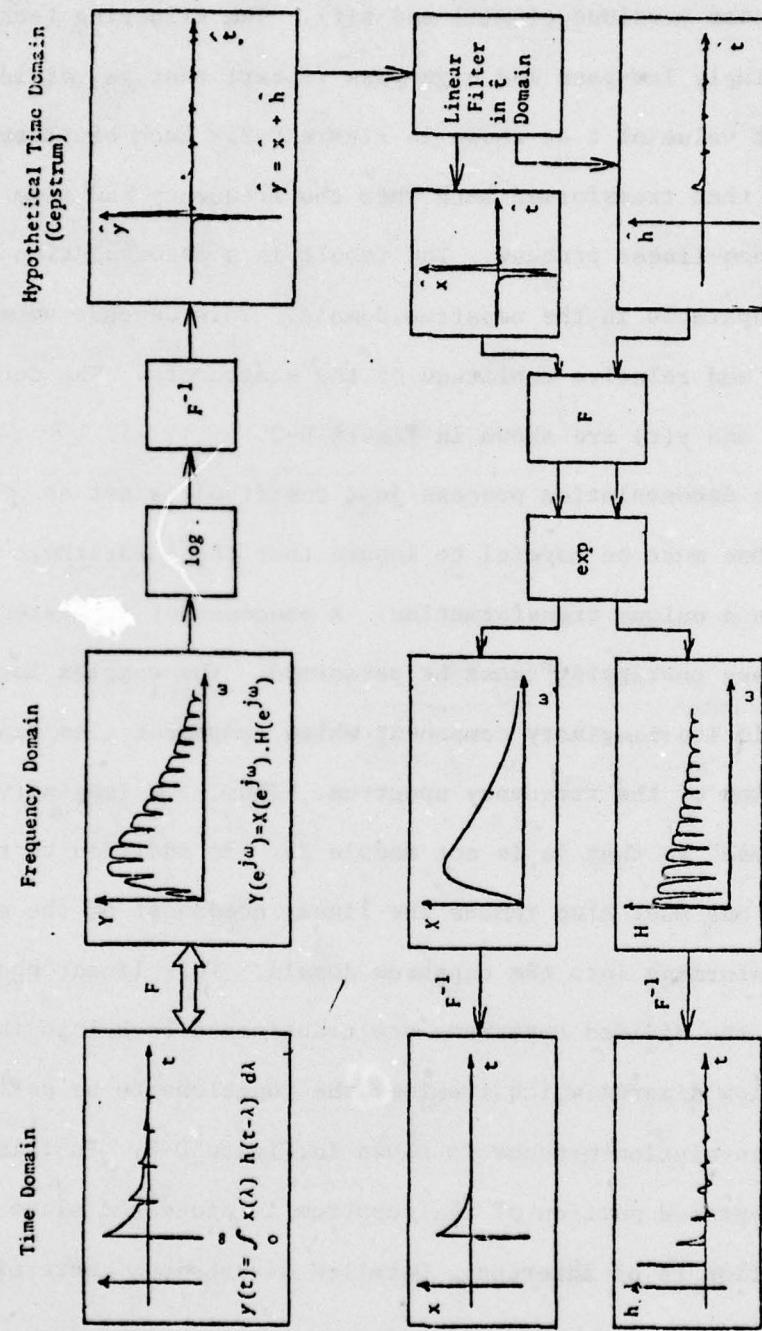


Figure D-2. The homomorphic deconvolution.

UNCLASSIFIED

UNCLASSIFIED

formed by the logarithmic process is called the cepstrum. Several types of linear filtering can be used in the cepstrum domain to separate $\hat{x}(t)$ and $\hat{h}(t)$, which are non-linear versions of $x(t)$ and $h(t)$. The filtering technique often used is to simply low-pass and high-pass filter; that is, dividing $\hat{y}(t)$ at some convenient value of t as shown in Figure D-2. Each of these components of $\hat{y}(t)$ are then transformed back into the frequency and time domains by an inverse non-linear process. The result is a deconvolution if $\hat{h}(t)$ and $\hat{x}(t)$ are separable in the cepstrum domain. This depends somewhat on the separation and relative amplitude of the scatterers. The deconvolved components $x(t)$ and $y(t)$ are shown in Figure D-2.

In practice, the deconvolution process just described is not as simple as it sounds. One must be careful to insure that the logarithmic transformation provides a unique transformation. A process not indicated in Figure D-2, called "phase unwrapping" must be performed. The complex log function is module 2π in its imaginary component which component also represents the phase variation of the frequency spectrum. Thus, the imaginary component must be "unwrapped" so that it is not module 2π . In addition to this special consideration, one must also remove the linear component of the spectrum phase before transforming into the cepstrum domain. This linear phase must be replaced after the divided cepstrums are transformed back into the frequency domain. A flow diagram which itemizes the functions to be performed in the homomorphic deconvolution process is shown in Figure D-3. In this diagram, only the high-passed portion of the cepstrum is processed since only the scatterer distribution is of interest. Detailed discussions concerning

UNCLASSIFIED

UNCLASSIFIED

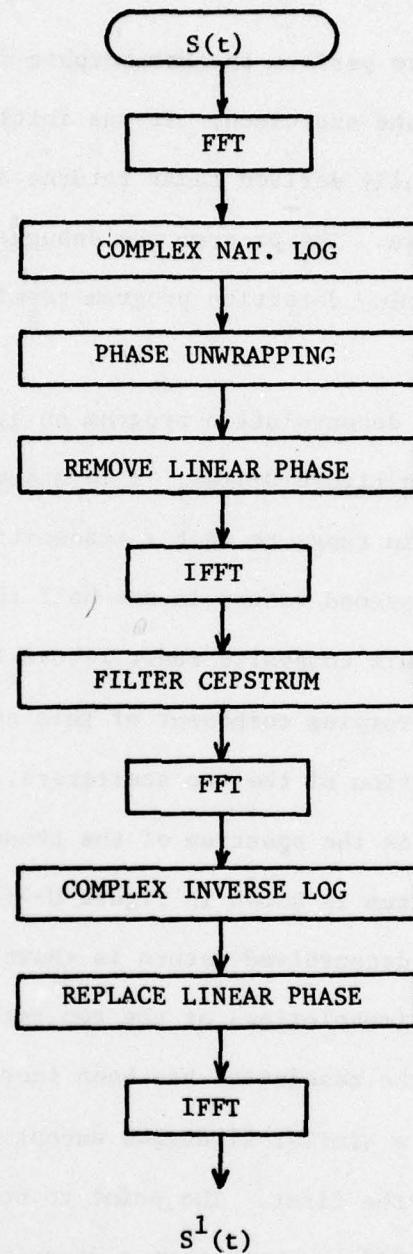


Figure D-3. Flow diagram of homomorphic deconvolution.

UNCLASSIFIED

UNCLASSIFIED

the practical considerations of homomorphic deconvolution are given in References 7 through 23.

A computer program to perform the homomorphic deconvolution described by Figure D-3 was written and exercised. It was initially intended to test the program with synthetically derived radar returns and then to use the program on measured NBS data. The program was debugged and tested on synthetic data; however, the mine detection program terminated before measured data could be utilized.

Some results of the deconvolution program on synthetic data are shown in Figures D-4 and D-5. In Figure D-4(a), it is assumed that two unequal size scatterers separated in range reflect a transmitted pulse similar to the NBS short pulse. The second return is one-half the amplitude of the first return. The spectrum of this composite radar return is shown in Figure D-4(b). The period of the rapidly varying component of this spectrum is inversely proportional to the separation of the two scatterers. The slowly varying component of the spectrum is the spectrum of the transmitted waveform. The upper portion of the cepstrum is shown in Figure D-4(c); the lower portion has been eliminated. The deconvolved return is shown in Figure D-4(d). Note that the time spread (resolution) of the two returns is smaller than in Figure D-4(a). Thus, the resolution has been increased via this process.

Figure D-5 depicts a similar situation except the second radar return is now almost as large as the first. The point to be made in this example is illustrated in Figure D-5(c). Note that a decaying train of impulses occurs in the cepstrum domain. The rate of decay depends on the relative size of the two radar returns. If the two returns are equal in amplitude,

UNCLASSIFIED

UNCLASSIFIED

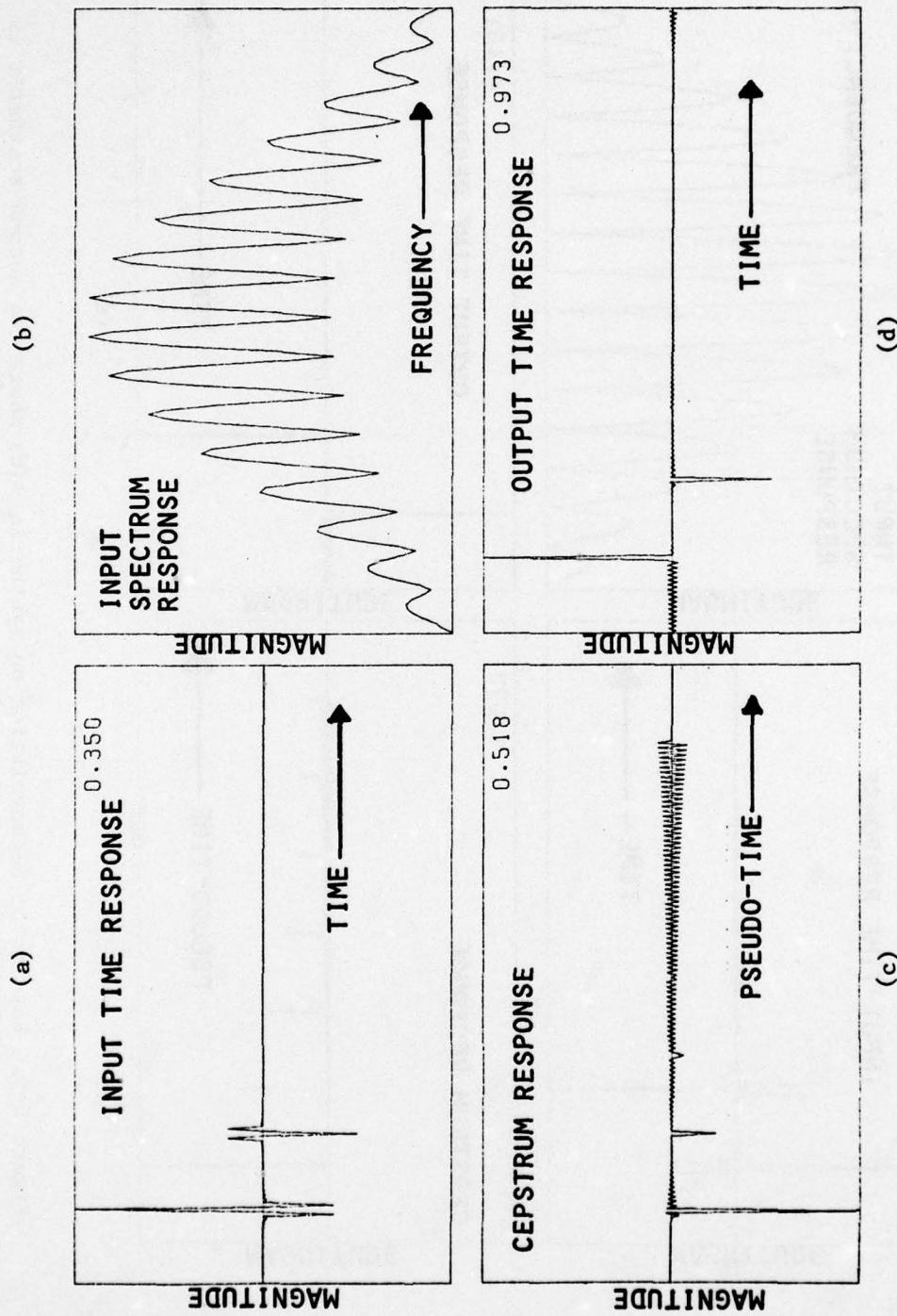


Figure D-4. Results of deconvolution on synthetic data where the second scatterer is one-half the size of the first.

UNCLASSIFIED

UNCLASSIFIED

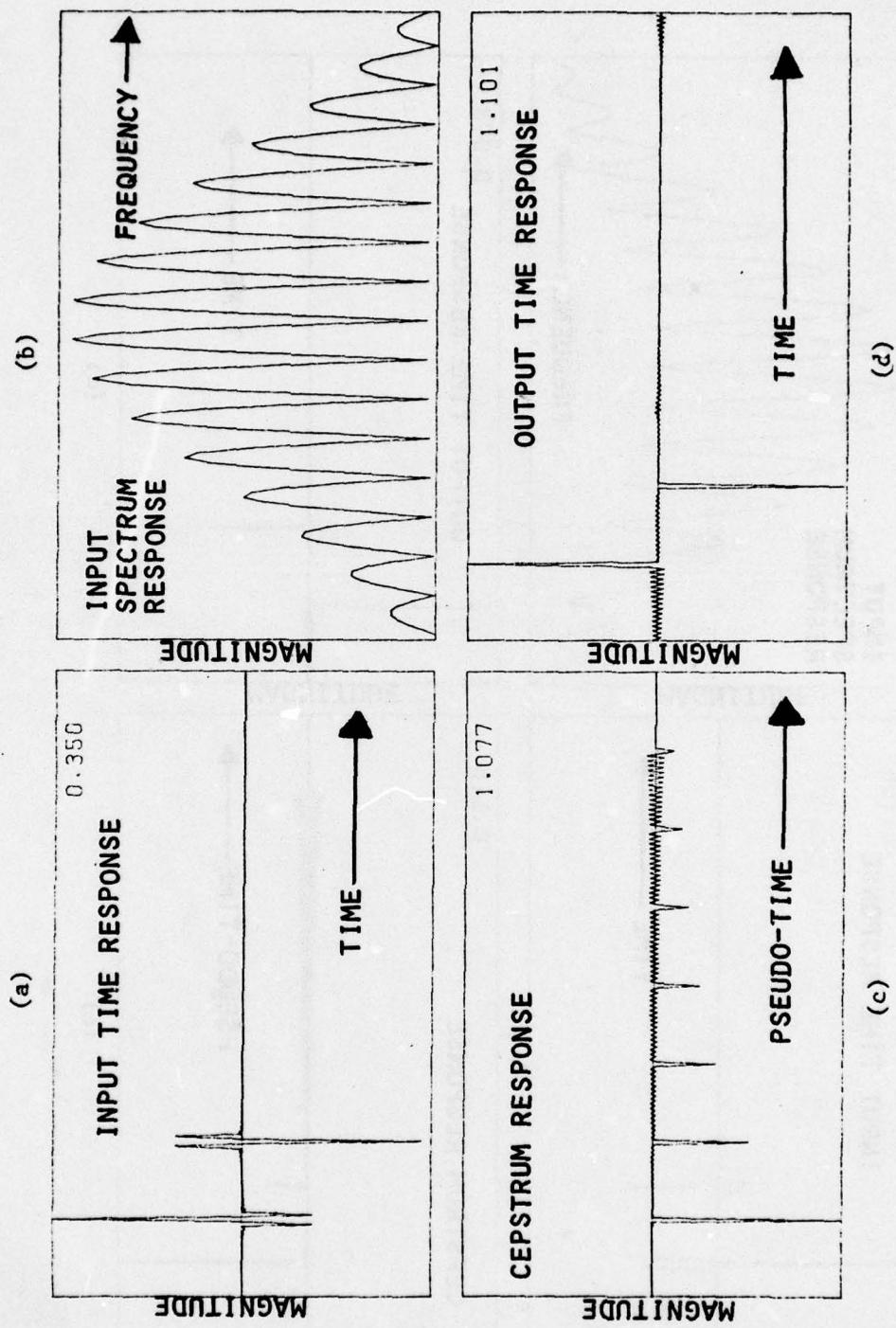


Figure D-5. Results of deconvolution on synthetic data where the second scatterer is 95% of the size of the first.

UNCLASSIFIED

UNCLASSIFIED

the impulse train in the cepstrum domain does not decay but consists of an infinite number of impulses of equal amplitude. If the second radar return is larger than the first, the impulse train in the cepstrum domain diverges without limit. Since, in practice, the second return can easily be larger than the first, one must consider ways of solving this processing problem. One approach is to weight the radar return response to force the second return to be smaller than the first and then later remove the weighting factor.

The foregoing example considered was for a simple two scatterer problem. If more scatterers are considered, the process could become more complicated in a practical application.

UNCLASSIFIED